GEOLOGICAL SURVEY RESEARCH 1967

Chapter B

GEOLOGICAL SURVEY PROFESSIONAL PAPER 575–B

Scientific notes and summaries of investigations in geology, hydrology, and related fields

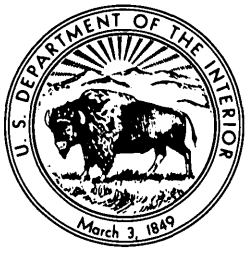

UNITED STATES GOVERNMENT PRINTING OFFICE, WASHINGTON: 1967

UNITED STATES DEPARTMENT OF THE INTERIOR

STEWART L. UDALL, Secretary

GEOLOGICAL SURVEY

William T. Pecora, Director

For sale by the Superintendent of Documents, U.S. Government Printing Office
Washington, D.C., 20402 - Price $2.25

CONTENTS

GEOLOGIC STUDIES

GEOLOGICAL SURVEY RESEARCH 1967

This collection of 49 short papers is the first published chapter of "Geological Survey Research 1967." The papers report on scientific and economic results of current work by members of the Geologic, Topographic, and Water Resources Divisions of the U.S. Geological Survey.

Chapter A, to be published later in the year, will present a summary of significant results of work done during fiscal year 1967, together with lists of investigations in progress, reports published, cooperating agencies, and Geological Survey offices.

"Geological Survey Research 1967" is the eighth volume of the annual series Geological Survey Research. The seven volumes already published are listed below, with their series designations.

Geological Survey Research 1960—Prof. Paper 400
Geological Survey Research 1961—Prof. Paper 424
Geological Survey Research 1962—Prof. Paper 450
Geological Survey Research 1963—Prof. Paper 475
Geological Survey Research 1964—Prof. Paper 501
Geological Survey Research 1965—Prof. Paper 525
Geological Survey Research 1966—Prof. Paper 550

RARE EARTHS IN PHOSPHORITES— GEOCHEMISTRY AND POTENTIAL RECOVERY

By Z. S. ALTSCHULER, SOL BERMAN, and FRANK CUTTITTA, Washington, D.C.

Abstract.—Rare earths are only trace constituents of marine apatite, but as millions of tons of such apatite are dissolved annually to make phosphoric acid, an opportunity exists for greatly increasing rare-earth output as a byproduct of fertilizer production. New, quantitative analyses of rare earths in representative apatite concentrates reveal that the potential for byproduct rare earths equals current production. The rare-earth assemblage in marine apatite is unusual, showing depletion in cerium and relative enrichment in the heavier lanthanons, a favorable distribution for rare-earth technology and utilization. Uranium, thorium, and scandium may also be recoverable from phosphoric acid.

A potential for doubling our domestic production of rare earths entirely as a byproduct of fertilizer manufacturing is demonstrated in this study of the geochemistry of marine phosphorite, the principal raw material of phosphate fertilizers. Extensive marine phosphorites, such as those mined in Florida and Idaho, comprise vast storehouses of the rare earths and several other strategic metals. These elements occur as traces in solid solution in the structure of apatite ($Ca_{10}[PO_4]_6F_2$), the essential mineral of phosphorites.[1]

The rare earths (lanthanons and yttrium) generally make up from 0.01 to 0.1 percent by weight of marine apatite. However, these traces achieve unusual significance as a mineral resource for American industry in view of the explosive increase in the use of phosphorite for ammonium- and triple-superphosphate fertilizers. These fertilizers are made mostly from "wet process" phosphoric acid and hence involve the acidulation and complete solution of apatite, the basic raw material and the rare-earth host. In effect, the costs of mining, beneficiating, processing, and completely solubilizing the rare earths in phosphorites are therefore already paid for in the normal course of phosphoric acid production.

The magnitude of the potentially extractable rare-earths byproduct may be judged from the statistics for national production of wet-process phosphoric acid. In 1964 this production amounted to 2,275,000 tons (100 percent P_2O_5) (U.S. Bur. Census, 1965). This necessitated solution of 6,000,000 tons of apatite, and liberated roughly 3,500 tons of rare earths elemental to solution. During the same year U.S. production of rare-earth oxides, primarily from bastnaesite and monazite ores, amounted to 2,300 tons (Parker, 1965).

Major deposits of marine phosphorite are presently mined in the Bone Valley Formation in central Florida and the Phosphoria Formation in Idaho and Montana, and large new reserves are being developed in northern Florida and North Carolina. The rapid expansion of rare-earth research and utilization, and the parallel surge in phosphate mining and fertilizer production, make it particularly timely to assess the amounts of total and individual rare earths available for recovery from phosphoric acid.

HISTORICAL REVIEW

The first observation of rare earths in apatite, by R. de Luna in 1866, was accompanied by a suggestion that "the crystals of apatite from Jumilla (Spain) could serve for the extraction of cerium, lanthanum, and 'didymium'." Jumilla apatite occurs in rare-earth-rich alkalic igneous rocks, in which apatite may be present in massive segregations. The Kola Peninsula (Soviet Karelia) contains the largest and best-known deposits of such apatite. Kola apatite contains several percent of rare earths, and byproduct recovery of rare earths is now practiced in the Kola-based fertilizer industry (Ryabtchikov and others, 1958). Rare-earth

[1] The occurrence of rare-earth elements in apatite is an example of diadochic (or coupled) substitutions in which the replacement of divalent calcium by a trivalent rare earth is electrostatically balanced by the replacement of another calcium by Na^{+1}, or by substitution of SiO_4^{-4} for PO_4^{-3}.

reserves in the Kola apatite deposits are estimated at 160 million tons (Bril, 1964).

Rare earths in apatites of sedimentary and biological origin were first detected by Cossa in 1878, in spectrographic studies of phosphorites, fossil bone, and coprolites from Nassau, Germany. Since then the occurrence of rare earths in apatites of diverse origins, and of wide geographic distribution, has been cited in geological, agricultural, and chemical literature. Borneman-Starynkevitch (1924) and Drobkov (1937) reported up to 0.8 percent of rare earths in individual samples of Russian phosphorites. Hill and others (1932) and Robinson (1948) give rare-earth contents of various domestic and foreign phosphorites from 0.01 to 0.15 percent. Spectrographic data on rare earths in marine and insular phosphorites from foreign and domestic sources have been widely reported (Swaine, 1962).

PRESENT STUDY

The suggestion of de Luna (1866) to extract rare earths from apatite was reiterated by Russian investigators and by McKelvey, Cathcart, and Worthing (1951) in their presentation of spectrographic data on yttrium and lanthanum in significant composites of Florida phosphorite. However, the potential for recovery of rare earths from phosphorites could not be adequately evaluated due to the lack of complete quantitative data on apatite from marine phosphorite, and the paucity of data on typical ores. Quantitative analyses that we have recently completed for geochemical study of rare earths in marine apatite have been applied to such an evaluation, and the results reveal a rare-earth resource of considerable importance. They are presented below to stimulate industrial investigation of the rare earths in individual mining properties, and in the various products of apatite solution and smelting.

DISTRIBUTION OF RARE EARTHS IN MARINE APATITE

Preparation and analysis of samples

Marine sedimentary apatite typically occurs as microcrystalline ovules and nodules, of sand and pebble size, in extensive sands, clays, and carbonate rocks, that are designated "phosphorites" if rich in apatite. Analyses were made on apatite concentrates that were separated by heavy liquids from marine phosphorites from Florida, Idaho, and Morocco, and then powdered and further purified of mineral inclusions by heavy-liquid and magnetic extraction. The samples are thus comparable to (although slightly purer than) the flotation concentrates used as feed for phosphoric acid manufacturing. In contrast to most phosphorite analyses that have been made of total rock, our results give rare-earth contents inherent to the apatite, and therefore apply directly to studies of the rare-earth geochemistry or recovery. The rare earths were determined by a combination of chemical and spectrographic procedures. They were made soluble in perchloric-nitric acid and concentrated by triple oxalate precipitation, using calcium as a carrier. The rare earths were then freed from calcium by a triple ammonium hydroxide precipitation, with fixed amounts of aluminum as a carrier. The individual rare-earth elements in the precipitate were then quantitatively determined by optical emission spectroscopy, using a powder d-c arc technique (Bastron and others, 1960).

Analytical data

Table 1 presents the analytical results for three apatite concentrates separated from phosphorite of the Bone Valley Formation of Florida. One of these is a quantitatively composited sample of material beneficiated during a week of mining, and represents some tens of thousands of tons of raw phosphorite. These quantitative data are supported, in their order of magnitude, by several dozen semiquantitative spectrographic analyses on other purified apatite composites from various mines in the Bone Valley Formation (Altschuler, unpub. data). Scandium was also separated and analyzed with the rare earths (table 1), as its recovery, along with these elements, may be industrially feasible.

TABLE 1.—*Quantitative spectrographic analysis of rare earths and scandium in three apatite samples from the Bone Valley Formation of Florida, in weight percent*

[Analyst: Sol Berman]

Element	Range	Average
La	0.018 –0.0081	0.015
Ce	.017 – .0074	.012
Pr	.004 – .0017	.003
Nd	.010 – .0037	.007
Sm	.005 – .0011	.003
Eu	.0007– .0001	.0004
Gd	.002 – .0008	.0014
Tb	.0006– .0003	.0004
Dy	.0021– .0007	.0016
Ho	.0005– .0002	.0004
Er	.0026– .0013	.0021
Tm	.0002– .0001	.0002
Yb	.001 – .0004	.0008
Lu	.0003– .0002	.0003
Total lanthanons		0.0476
Y	0.016 –0.005	.011
Total rare earths		0.0586
Sc	0.0006–0.0002	.0003

Relative distribution and geochemistry of lanthanons

The analyses in table 1 reveal unusual, and possibly unique, fractionation of rare earths in apatite of marine origin. Most major rocks, including marine limestone, deep-sea clays, and manganese nodules, reflect the crustal abundance pattern for rare-earth distribution (Goldberg and others, 1963; Wildeman and Haskin, 1965). Although minor departures are known and may be geochemically significant, rare-earth distribution in most rocks is in accord with the well-known Oddo-Harkins "law," showing cerium to be much more abundant than lanthanum (table 2). In marine apatite, however, cerium is markedly depleted, being less abundant than lanthanum, and commonly less abundant than neodymium. Moreover, the heavier lanthanons are slightly enriched over their proportions in terrigenous sediments (fig. 1). We have found this abundance pattern to be consistent in marine apatite from the Bone Valley Formation (3 analyses), the Phosphoria Formation (1 analysis), and the Moroccan deposits (2 analyses). This fractionation parallels that of rare earths in sea water,[2] and probably reflects precipitation from the marine environment (fig. 1). The relative enrichment of the less abundant, heavy lanthanons in marine apatite has important technological implications which are discussed later in this report, and important geochemical implications which will be discussed in a later publication.

The cerium deficiency that characterizes marine apatite is not shown by igneous apatite (Denisov and others, 1961; Lyakovitch and Barinski, 1961) or by subaerially precipitated apatite of ground water or guano origins (Altschuler, Berman, and Cuttitta, unpub. data). Thus rare-earth distribution in apatite may distinguish marine from terrestrial or igneous apatite, and may provide a test of the theory of precipitation of marine apatite from upwelling ocean waters.

In view of the economic and geologic implications of the unusual rare-earth distribution in marine apatite, it must be noted that our data appear to conflict with a large body of rare-earth analyses on phosphorite. Complete rare-earth determinations are available on 67 organic-rich and pyritic bone beds of the Maikop sediments (Kochenov and Zinovieff, 1960), on 23 phosphorites from Kara Tau and eastern

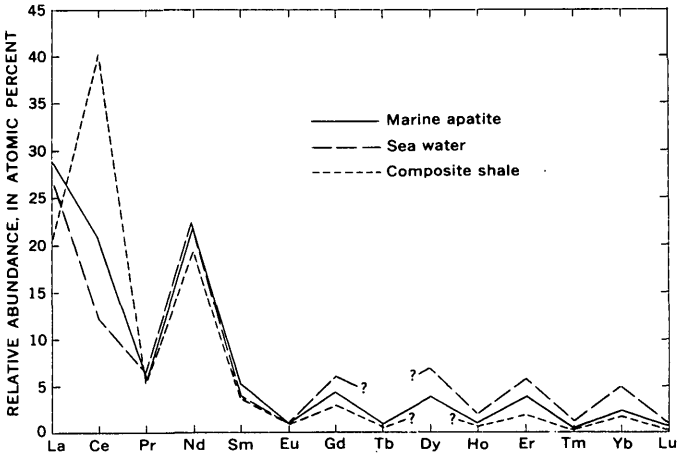

FIGURE 1.—Abundance of lanthanons in marine apatite, sea water, and terriginous sediments. Apatite is an average of 3 samples from the Bone Valley Formation of Florida, 1 from the Phosphoria Formation in Idaho, and 2 from Khouribga, Morocco (this report); sea water is 1 sample from coastal California (Goldberg and others, 1963); and shale is a composite of 40 samples of shale from North America (Wildeman and Haskin, 1965).

Europe (Semenov and others, 1962), 13 phosphorites from Bulgaria (Alexiev and Arnaudov, 1965), and 1 continental-shelf phosphorite from southern California (Goldberg and others, 1963). Except for 3 of the Bulgarian phosphorites and 1 earlier Florida sample (Waring and Mela, 1963) none of these has the cerium deficiency we have found to characterize marine apatite.

Two probable causes for these differences are: (1) Other investigations were made on whole-rock samples, and the rare earths determined thus include contributions from nonphosphatic clastic and chemical constituents. This suggestion is supported by the similarity of the rare-earth analyses on phosphorites (that is, whole rock) to published rare-earth analyses of shales; in contrast there is a close similarity of the rare-earth assemblage in purified apatite to that in sea water (see table 2). (2) Significant differences in depositional environment may create pronounced variations in solubility and fixation of the individual rare earths. This is particularly applicable to the highly reduced organic- and pyrite-rich bone beds such as those of the Maikop sediments, which were deposited in a hyposaline, euxinic basin (Blokh and Kochenov, 1964; Kholodov, 1963). These bone beds are unusually rich in scandium (0.001–0.015 percent, Borisenko, 1961) and rare earths (0.08–1.34 percent, Kochenov and Zinovieff, 1960), particularly of the cerium group. Undoubtedly many other causal factors will be revealed with more study, but it should

[2] Only 1 complete analysis of rare earths in sea water is published (from coastal California waters, Goldberg and others, 1963). Though this analysis confirms determinations for Ce and La by Goldschmidt (1937), preliminary data by D. W. Hayes, J. F. Slowey, and D. W. Hood, Texas A. and M. Univ., (unpub. data, 1966) and Spirn (1965) are not in complete accord. Discussions of rare earths in sea water are therefore tentative.

be emphasized that definitive information for recovery or geochemical study can be obtained only from individual mineral concentrates.

TABLE 2.—*Relative atomic abundance of lanthanons in marine apatite, sea water, phosphorite, and shale (normalized to lanthanum)*

	Marine apatite (concentrated from phosphorite)			Sea water	Phosphorite (whole rock)			Shale	
	1	2	3	4	5	6	7	8	9
La	1.0	1.0	1.0	1.0	1.0	1.0	1.0	1.0	1.0
Ce	.81	.64	.54	.44	2.05	1.43	1.81	2.59	1.94
Pr	.21	.21	.12	.22	.45	.22	.25	.30	.26
Nd	.47	1.39	.69	.74	1.43	.82	.98	.72	.92
Sm	.18	.24	.10	.14	.31	.20	.18	.32	.17
Eu	.03	.04	.03	.04	.04	.01	.04	.05	.05
Gd	.10	.27	.14	.18	.33	.12	.24	.30	.14
Tb	.03	.04	.03	------	.04	.06	.03	.05	.03
Dy	.10	.23	.08	.22	.20	.15	.19	.21	------
Ho	.03	.07	.03	.06	.04	.06	.05	.06	.03
Er	.14	.18	.07	.17	.12	.09	.14	.11	.09
Tm	.01	.08	.02	.04	.02	.06	.02	.01	.01
Yb	.05	.17	.07	.14	.13	.18	.10	.12	.07
Lu	.02	.02	.01	.03	.02	.05	.02	.03	.01

1. Bone Valley Formation, Florida, average of 3 samples (this report).
2. Moroccan phosphate, Khouribga, Morocco, average of 2 samples (this report).
3. Phosphoria Formation, averaged duplicate analysis of 1 sample (this report).
4. Sea water, coastal California (Goldberg and others, 1963).
5. Eastern Europe and Kazakhstan, average of 23 samples (Semenov and others, 1962).
6. Bulgaria, average of 13 samples (Alexiev and Arnaudov, 1965).
7. Phosphate nodule, coastal California (Goldberg and others, 1963).
8. Average of 3 composite samples of 50 Paleozoic shales of Europe and Japan, and 10 Mesozoic shales of Japan (Minami, 1935).
9. Composite of 40 American shales (Wildeman and Haskin, 1965).

POTENTIAL FOR RARE-EARTH RECOVERY

Florida land-pebble phosphate field

The potential for annual byproduct recovery of the rare earths can be evaluated by applying the data on the grade of apatite (table 1) to the yearly production statistics for wet process phosphoric acid (table 3). The only available complete rare-earth analyses on separated apatite from typical domestic ores are those for Florida phosphorite. The Florida industry thus serves as a test case. This is appropriate as more than 2,000,000 of the 2,275,000 tons of wet-process phosphoric acid produced in the United States during 1964 were made from rock of the Bone Valley Formation. For several reasons the tonnages shown must be construed as orders of magnitude of potential recovery rather than a precise evaluation. For example, the most recent phosphoric acid production statistics are those for 1964, whereas production has been steadily increasing since then. Also, the averages for the individual rare earths are based on three samples, and the computed grade for the entire Bone Valley Formation, or for the holdings of a particular mining company, would undoubtedly change with more data. The tonnage evaluation (table 3) is deemed correct, however, as the determinations on the composite sample of large tonnage gave the highest values.

TABLE 3.—*Rare earths and scandium made available for recovery in wet-process phosphoric acid manufacture*

[On basis of 1964 production]

		Phosphoric acid production	
		Florida phosphate field	Northwestern phosphate field
H_3PO_4 (100 percent P_2O_5)---short tons		[1] 2,000,000	275,000
Apatite dissolved [2]---do		5,260,000	725,000
Element	Percent in apatite [3]	Short tons dissolved	
FLORIDA PHOSPHATE ROCK			
La	0.015		789
Ce	.012		631
Pr	.003		158
Nd	.007		368
Sm	.003		158
Eu	.0004		21
Gd	.0014		74
Tb	.0004		21
Dy	.0016		84
Ho	.0004		21
Er	.0021		110
Tm	.0002		11
Yb	.0008		42
Lu	.0003		16
Total lanthanons	0.0476		2,504
Y	.011		579
Total rare earths	0.0586		3,083
Sc	.0003		16
NORTHWESTERN PHOSPHATE ROCK			
Total rare earths	0.04		300
Sc	.00009		<1
TOTAL			
Rare earths	----------		3,383
Sc	----------		17

[1] Compiled from unpublished data of Business and Defense Services Administration and U.S. Bureau of Mines.
[2] Converted from H_3PO_4 produced. Based on analyses of apatite from Bone Valley Formation, Florida (Altschuler and others, 1953).
[3] Florida phosphate, see table 1; Northwestern phosphate: rare earths, see text; Sc, Altschuler, Berman, and Cuttitta unpublished data).

National potential

To assess the national potential the rare earths liberated in phosphoric acid produced from the Phosphoria Formation, or Northwestern phosphate deposits, must be considered in addition to the Florida deposits. In view of the vastness of the Northwestern field, the paucity of complete rare-earth analyses on separated apatites or large-scale composites, and the possible regional variations in rare-earth contents, the potential for recovery from this district is difficult to estimate.

Several sources of information may be utilized to appraise the rare-earth contents of the Northwestern phosphorites. Analyses of three high-grade samples

of mined rock published by the U.S. Department of Agriculture give 0.056, 0.098, and 0.155 percent RE_2O_3 (rare-earth oxides) (Hill and others, 1932; Robinson, 1948). Some of these values may be atypically high for use as an average. A significant group of 14 analyses on samples representing individual beds of Northwestern phosphate rock shows a range of 0.02 to 0.06 percent RE_2O_3 (V. E. McKelvey, U.S. Geol. Survey, unpub. data). Our own complete analysis of an apatite concentrate from Idaho phosphorite yielded 0.03 percent RE with a distribution somewhat like that in table 1. A large number of semiquantitative spectrographic determinations obtained on apatite samples in the U.S. Geological Survey laboratories (Altschuler, unpub. data) confirm a range of 0.02 to 0.06 percent RE_2O_3 in apatite from the Phosphoria Formation. Accordingly, a median RE_2O_3 content of 0.04 in apatite of the Northwestern field is tentatively assumed in estimating potential recovery and reserves of rare earths (tables 3, 4).

It is important to note that mining and beneficiation losses are accounted for in the above evaluations, as these are based on actual phosphoric acid production.

Near-future potential

A projection of recent growth in wet-process phosphoric acid production indicates a virtual doubling of the 1964 output by 1970. The annual rate of growth has been 12 percent in 1962, 23 percent in 1963, and 16 percent in 1964 (U.S. Bur. Census, 1965). Moreover, planned expansions and current new plant construction indicate a continuing high rate of growth (Horner, 1965). Although an increasing part of our phosphoric acid will come from the Northwestern and North Carolina phosphate fields, whose rare-earth content is not adequately known, the bulk of the output in 1970 will derive from the Bone Valley Formation. Thus, by extrapolation based on phosphoric acid production, a quantity of recoverable rare earths in the neighborhood of 6,000–7,000 tons annually by 1970 may reasonably be predicted.

RESERVES AND RESOURCES

Reserves of rare earths in phosphorites should be appraised in terms of phosphorite mineable at present, and future phosphorite reserves or resources; the latter category is too low in grade or amenability, for mining at present. Utilizing the previously derived contents of rare earths for the Bone Valley and the Phosphoria apatites, an analysis of rare-earth reserves, restricted solely to currently mined rock, yields a potential resource of approximately 1.6 million tons of rare earths (table 4). The appreciable new reserves of marine phosphorite in the developing North Carolina field and northern Florida fields (roughly 400 million tons of P_2O_5, J. B. Cathcart, U.S. Geol. Survey, preliminary estimate) suggest a total domestic resource of rare earths in phosphorite in the realm of 2 million tons, available under present conditions. The ubiquity of rare earths in marine apatite supports this estimate. These orders of magnitude of established reserves in the ground (1.6 million tons RE now available from the Florida "Land Pebble" and the Northwestern fields, and a total of 2 million tons RE soon to be available) appreciably exceed reserves actually obtainable. Obviously, obtainable reserves should be restricted to rock mined only for phosphoric acid production.

During 1964 phosphoric acid production by wet process amounted to 27.3 percent of the total phosphate commodity production (R. W. Lewis, U.S. Bur. Mines, oral commun., 1965). Calculated on this basis, and allowing for losses during mining and beneficiation, the reserves of obtainable byproduct rare earths would be roughly 25 percent of the available (minable) reserves, or approximately 400,000 tons of rare earths. Considered in the light of the dramatic growth rate in wet-process phosporic acid production, obtainable reserves could be about half of available reserves by 1970, or approximately 800,000 tons of rare earths, from the Florida and Northwestern fields alone, and possibly 1 million tons from all domestic sources.

FAVORABILITY OF PHOSPHORITES FOR RECOVERY OF RARER LANTHANONS

Much of the new impetus to rare-earth mining stems from new uses which have spurred demands for less abundant members of the series and have even dictated new recovery operations solely for the purpose of segregating these rarer and more costly elements. Such demands are illustrated by the new market for cracking catalysts using samarium and praesodymium, by the use of europium in color television and home lighting phosphors, and by the use of neodymium as an activator in laser materials.

The versatility in fundamental properties of the rare earths makes them especially valuable in reactor and medical technology. Those with low-neutron cross section (Y, Ce, La) are ideal diluents for reactor fuels. Those with high-neutron cross section (Gd, Dy, Sm, Eu) are useful in shielding alloys and control rods. A number of short-lived radioactive isotopes (Gd 153, Tm 170, Tm 171, Lu 177) are of pos-

TABLE 4.—*Phosphate and rare-earth resources in currently mined domestic phosphorites*

Area and formation	Reserves minable at present					Resources minable under changed conditions					Total resources		
	P_2O_5 [1]	Apatite [2]	Total lanthanons	Y	Total RE	P_2O_5 [2]	Apatite [2]	Total lanthanons	Y	Total RE	Total lanthanons	Y	Total RE
	Millions of short tons		Thousands of short tons			Millions of short tons		Thousands of short tons			Thousands short tons		
Florida land-pebble field (Bone Valley Formation) [3]	360	950	450	100	550	670	1,800	850	200	1,050	1,300	300	1,600
Northwestern field (Phosphoria Formation) [4]	970	2,560	-------	-------	1,020	6,400	16,800	-------	-------	6,700	-------	-------	7,740
Total	1,300	3,500	-------	-------	1,600	7,100	18,600	-------	-------	7,750	-------	-------	9,300

[1] McKelvey and others (1953).
[2] Apatite converted from P_2O_5 on basis of 38 percent P_2O_5 in the carbonate fluorapatite. (Altschuler and others, 1958)
[3] RE tonnages for Florida calculated on basis of 0.047 percent Ln and 0.011 percent Y in apatite.
[4] RE tonnages for Northwestern field calculated on basis of 0.04 percent RE in apatite.

sible interest as sources of radioactivity, thermal energy, or power. Thulium is noteworthy, as its radioactive isotopes are sufficiently long-lived for such critical uses as heart machines and space exploration, and Tm 170 has low volatility and lacks alpha activity, and is thus free of obvious biological hazard. Moreover, thulium isotopes can be produced directly from natural raw materials: Tm 170 (half-life 128 days) from monoisotopic natural Tm 169, and Tm 171 (half-life 1.9 years) from Er 170 (15 percent of naturally occurring erbium).

The marine phosphorites are particularly attractive raw materials for this new technology. Compared to conventional rare-earth sources they are unusually enriched in yttrium, and in the middle and higher atomic weight rare earths. The latter enrichment is due principally to marine apatites' deficiency in cerium, the normally preponderant lanthanon. The enrichment in heavier elements is clearly shown by comparing the distributions of lanthanons in marine phosphorites, monazites, and bastnaesite ores. It is expressed in the following table in terms of the aggregate percentage of the total lanthanon suite (RE less Y) contributed by the first four lanthanons (lanthanum through neodymium). The remaining lanthanons (samarium through lutetium) thus typically aggregate in phosphorites to 25 percent, in monazites to 10 percent, and in bastnaesites to 5 percent (table 5). This distribution is further illustrated by three elements of immediate interest, europium, gadolinium, and thulium (table 5).

TABLE 5.—*Distribution of rare earths in phosphorites, monazites, and bastnaesites, in relative weight percent*

Element	Phosphorites [1]	Monazite [2]	Bastnaesites [3]
La, Ce, Pr, Nd	70–80	85–95	95+
Eu	.5–1.0+	.0x–.1	.1±
Gd	1.–6.	1.0–4.	.1–.5
Tm	.3–.6	.1	

[1] This report.
[2] Vainshtein and others (1956); Murata and others (1957); Fleischer (unpub. compilation).
[3] Murata and others (1957); Fleischer (unpub. compilation).

Approximately 21 tons of europium, 74 tons of gadolinium, and 11 tons of thulium were available for recovery during the production of wet-process phosphoric acid from Florida rock in 1964 (table 3). Thus the marine origin of phosphorite adds an additional economic and industrial significance to the extraction of rare earths from it.

ECONOMIC VALUE OF RECOVERABLE RARE EARTHS IN PHOSPHORITES

The monetary value of the recoverable rare-earth byproduct in phosphorites is difficult to assess, as such major new sources may influence prices markedly. Calculated at the current price of $1.50 per pound of mixed rare-earth oxides (Chemical and Engineering News, 1965), the gross value of the potentially recoverable rare-earth product from Florida alone during 1964 (about 3,100 tons, see table 3), would have been $9.3 million. Estimated expansion of phosphoric acid production by 1970 in Florida would increase this considerably.

The potential value of the rare-earth byproduct is orders of magnitude higher, however, when reckoned on the basis of individual rare-earth elements. For example, the current price for purified europium oxide, even after appreciable reduction in response to greatly increased production, is $600 per pound. Cerium oxide currently sells for $5.00 a pound, yttrium oxide for $50 a pound, and a pound of thulium oxide may cost $1,500. The acceleration in national needs for individual rare earths, coupled with the favorable capacity of phosphorites to meet these needs, suggests that some of our future market for individual rare earths could be served by the phosphoric acid industry.

The prospect of rare-earth recovery from phosphoric acid offers additional benefit to the American chemical industry. Several major purchasers of rare-earth ores for production of rare-earth compounds are also major producers of phosphoric acid.

POSSIBLE EXTRACTIVE PROCESSES

The realization of this byproduct potential for rare-earth production is clearly dependent on a program of extraction research. The essentials of a recovery technology are now available in established practices in the fields of concentration-separation chemistry, liquid extraction, ion exchange, and gas chromatography (Eyring, 1964). These practices must be adapted, however, to the specific technology of the American phosphoric acid industry, which is based on sulfuric acid attack. Elsewhere, nitric and hydrochloric acids are also used.

The following discussion is not intended as an exhaustive or definitive treatment of the recovery problem. It outlines several areas of research which are technically feasible and may be auspicious commercially.

Liquid-liquid extraction

A major recovery-separation route of potential industrial importance is selective liquid-liquid extraction of rare earths from acid solution with immiscible solvent systems containing either phosphorus-based or nonphosphorus-based organoextractants. The countercurrent extraction of rare-earth nitrates, chlorides, and sulfates into a tri-n-butyl phosphate (TBP) phase is well understood operationally (Peppard and others, 1952; Peppard, 1964; Weaver and others, 1953) and has been applied successfully on a large scale (Bochinski and others, 1958). Rare earths have also been segregated with a variety of primary amines, oximes, and aldehydes (Dryssen, 1956; Weaves, 1964). These should be studied for their effectiveness in phosphoric acid solutions.

Successful extraction of uranium from phosphoric acid, incident to triple-superphosphate and sodium phosphate production, was practiced industrially in the United States The uranium recovery was based on countercurrent extraction with an alkyl pyrophosphate (octyl pyrophosphoric acid, OPPA) from original ores containing only 0.01 percent uranium (Long and others, 1956).

Research on use of organophosphorus compounds for liquid-liquid extraction of the rare earths from phosphoric acid is also attractive for possible recovery of other rare-metal byproducts. The chemical similarity of scandium and thorium to the rare earths extends to their complexing behavior in acid media with these organophosphates Interest in cheap, low-grade sources of uranium for long-term supply creates still another incentive for coupling the recovery of other metals in phosphorites to that of rare earths. The quantity of these metals made available for byproduct recovery in phosphoric acid is outlined in table 6, in terms of 1964 production from Florida. The figures might double by 1970.

TABLE 6.—*Tonnage of scandium, thorium, and uranium available for recovery in 1964 production of wet-process phosphoric acid from Florida phosphorite*

Element	Percent in apatite	Short tons dissolved [1]
Sc	[2] 0.0003	16
Th	[3] .0005	26
U	[3] .01	500

[1] Based on U.S. Bur. Census (1965) statistics for H_3PO_4 production.
[2] Table 1, this report.
[3] Altschuler and others (1958).

Selective precipitation

The successful extraction of rare earths during phosphoric acid production in the Soviet Union attests to the availability of selective precipitation processes based on nitric acid solution of the ores (Ryabtchikov and others, 1958). Rare-earth phosphates in the filtrate are collected through precipitation by partial neutralization with ammonia, urea, or calcium oxide (Mazgaj, 1957). Processes have also been developed for rare-earth recovery after sulfuric acid solution of the ores for normal superphosphate production (Bril, 1964).

Extraction from caustic solutions

The caustic treatment of phosphate rock or phosphoric acid solutions for production of sodium phosphates may also permit rare-earth recovery. Caustic metathesis (<70 percent NaOH$\approx$140°C) is an established means of obtaining rare earths as hydroxides from the decomposition of phosphates. The reaction product is extracted with hot water and the residue (rare-earth hydroxides, and phosphates) separated by filtration from the trisodium phosphate (Poirier and others, 1958; Kaplan and Uspenskaya, 1958). As caustic attack of apatite yields a relatively high-grade raffinate at an early processing stage, it may have additional significance for separation of individual rare-earth metals either by liquid-liquid extraction of the hydroxides solubilized in nitric acid, or by ion exchange of the sulfates.

Ion exchange, gas chromatography, physical methods

A number of techniques are available for concentrating individual or groups of rare-earth elements.

Some of these warrant research for gross recovery of rare earths during phosphoric acid or ammonium phosphate manufacturing. They may be based on (1) basicity differences amenable to fractional precipitation, ion exchange (Spedding and others, 1951; Powell and Spedding, 1959), or solvent extractions; (2) thermal stability of organometallic compounds, as in gas chromatography; (3) physical separations such as those involving differences in volatility (as in, rare-earth halides at elevated temperatures), in speed of ion migration, or in magnetic attraction.

The recently reported gas-chromatographic separation of 13 lanthanons, yttrium, and scandium using 2,2,6,6-tetramethyl heptanedione (Hthd) (Eisentraut and Siever, 1965) is an interesting example of combined physical and chemical techniques. Heptanedione chelates are volatile, thermally stable, anhydrous, and unsolvated. Differences among rare earth-Hthd volatilites permit fraction sublimation at atmospheric pressure using helium as a carrier. Reported data justify serious research efforts in the application of such techniques to industrial recovery of rare earths from phosphoric acid solutions.

REFERENCES

Alexiev, E., and Arnaudov, B., 1965, Rare earths, uranium and thorium in certain Bulgarian phosphorites: Trudy vurkhu geolog. na Bulgariia, v. 5, p. 69–78. [In Bulgarian]

Altschuler, Z. S., Clarke, R. S., and Young, E. J., 1958, The geochemistry of uranium in apatite and phosphorite: U.S. Geol. Survey Prof. Paper 314–D, p. 45–90.

Bastron, Harry, Barnett, P. R., and Murata, K. J., 1960, Methods for the quantitative spectrochemical analysis of rocks, minerals, ores, and other materials by a powder d–c arc technique: U.S. Geol. Survey Bull. 1084–G, p. 165–182.

Blokh, A. M., and Kochenov, A. B., 1964, Element admixture in bones of fossil fish: Geol. mestorozhd. redkii elementov, v. 24, p. 1–100. [In Russian]

Bochinski, Julius, Smutz, Morton, and Spedding, F. H., 1958, Separation of monazite rare earths by solvent extraction: Indus. Eng. Chemistry, v. 50, p. 157–160.

Borisenko, L. F., 1961, Occurrence of scandium in bone remnants of fishes of Tertiary age: Trudy Instit. Mineralog. Geokym. i Kristallokhim. Redkikh Elementov, no. 7, p. 65–70. [In Russian]

Borneman-Starynkevitch, I. D., 1924, On the presence of rare earths in apatites: Comptes rendus del'Acad. des Sciences del 'U.R.S.S., A., p. 39–41. [In Russian]

Bril, K. J., 1964, Mass extraction and separation, *in* Eyring, LeRoy (ed.), Progress in the science and technology of the rare earths: New York, Macmillan Co., v. 1, p. 30–61.

Chemical and Engineering News, 1965, Rare earths—the lean and hungry industry: v. 43, no. 19, May 10, p. 78–92.

Cossa, 1878, "Sur la diffusion du cérium, du lanthane et du didyme" extract of a letter from Cossa to M. Sella, presented by M. Fremy: Acad. Sciences [Paris] Comptes rendus, v. 87, p. 378–388.

de Luna, R., 1866, Sur un gisement de phosphate de chaux naturel: Acad. Sciences [Paris] Comptes rendus, v. 63, p. 220–221.

Denisov, A. P., Dudkin, O. B., Elina, N. A., Kravchenko-Berezhnoi, R. A., and Polezhalva, S. M., 1961, Dependence of the physical properties of apatite on the admixture of rare earths and strontium: Geochemistry, no. 8, p. 718–730.

Drobkov, A. A., 1937, The influence of rare earths on plant growth: Comptes rendus de l'Acad. des Sciences del 'U.R.S.S., v. XVII, p. 265–267.

Dryssen, D., 1956, Studies on the extraction of metal complexes, XXXII and XXXI: Acta Chem. Scand., v. 10, p. 341–359.

Eisentraut, K. J., and Siever, R. E., 1965, Volatile rare earth chelates: Am. Chem. Soc. Jour., v. 87, no. 22, p. 5254–5256.

Eyring, LeRoy (ed.), 1964, Progress in the science and technology of the rare earths: New York, McMillan Co., v. 1, 532 p.

Goldberg, E. D., Koide, Minoiu, Schmitt, R. A., and Smith, H. V., 1963, Rare earth distribution in the marine environment: Jour. Geophys. Research, v. 68, p. 4209–4217.

Goldschmidt, V. M., 1937, The principles of distribution of chemical elements in minerals and rocks: Jour. Chem. Soc. for 1937, p. 655–673.

Hill, W. L., Marshall, H. L., and Jacob, K. D., 1932, Minor metallic constituents of phosphate rock: Indus. Eng. Chemistry, v. 24, p. 1306–1312.

Horner, C. K., 1965, Inorganic chemicals, *in* Facts and figures for the chemical process industries: Chem. and Eng. News, v. 43, no. 36, Sept. 6, p. 100–107.

Kaplan, G. E., and Uspenskaya, T. A., 1958, Investigations on alkaline methods for monazite and zircon processing: Internat. Conf. Peaceful Uses Atomic Energy, 2d, Geneva, Proc., v. 3, p. 378–382.

Kholodov, V. N., 1963, On rare and radioactive elements in phosphorites: Akad. Nauk Instit. Miner. Geokim. i Cristallokhim. Redkikh Elementov, Trudy, v. 17, p. 67–108. [In Russian]

Kochenov, A. V., and Zinovieff, V. V., 1960, Distribution of rare earth elements in phosphatic fish rests from the Maikop sediments: Geochemistry, no. 8, p. 714–725.

Long, R. S., Ellis, D. A., and Bailes, R. H., 1956, Recovery of uranium from phosphates by solvent extraction: Internat. Conf. Peaceful Uses Atomic Energy, 1st, Geneva, Proc., v. 8, p. 77–80.

Lyakovitch, V. V., and Barinski, R. L., 1961, Peculiarities of the rare earth composition of accessory minerals in granitoids: Geochemistry, no. 6, p. 467–479.

Mazgaj, W. Y., 1957, Separation of the rare earths contained in phosphate concentrate: Chem. Tech. [Berlin], v. 9, p. 350–353.

McKelvey, V. E., Cathcart, J. B., Altschuler, Z. S., Swanson, Roger, and Buck, K. L., 1953, Domestic phosphate deposits, *in* Soil and fertilizer phosphorus in crop nutrition: Agronomy Monograph IV, New York, Academic Press, p. 347–376.

McKelvey, V. E., Cathcart, J. B., and Worthing, H. W., 1951, Preliminary note on the minor metal content of Florida phosphate rock: U.S. Geol. Survey Trace Elements Memo. Report 236. (AEC Tech. Inf. Serv.) 6 p.

Minami, E., 1935, Gehalte an seltenen Erden in europaischen und japanischen Tonschiefern: Nachr. Gesell. Wiss. Göttingen, ser. IV, N.F., 1, no. 14, p. 155–170.

Murata, K. J., Rose, H. J., Carron, M. K., and Glass, J. J., 1957, Systematic variation of rare earth elements in cerium-earth minerals: Geochim. et Cosmochim. Acta, v. 11, p. 141–161.

Parker, J. G., 1965, Rare earth minerals and metals, 1964, preprint, 10 p.: from U.S. Bur. Mines Minerals Yearbook, 1964.

Peppard, D. F., 1964, Fractionation of rare earths by liquid-liquid extraction using phosphorus-based extractants, *in* Eyring, LeRoy (ed.), Progress in the science and technology of the rare earths: New York, Macmillan Company, v. 1, p. 89–109.

Peppard, D. F., Faris, J. P., Gray, P. R., and Wilson, G. W., 1952, Studies of the solvent extraction behavior of the transition elements; I. Fractionation of the trivalent rare earths: U.S. Atomic Energy Comm. Rept. AECD-3327, 48 p.

Poirier, B. H., Calkins, G. D., Lutz, G. A., and Bearse, A. E., 1958, Ion exchange separation of uranium from thorium: Indus. Eng. Chemistry, v. 50, p. 613–616.

Powell, J. E., and Spedding, F. H., 1959, The separation of the rare earths by ion exchange: Am. Inst. Mining Metall. Petroleum Engineers Trans., v. 215, p. 457–463.

Robinson, W. O., 1948, The presence and determination of molybdenum and rare earths in phosphate rock: Soil Sci., v. 66, p. 317–322.

Ryabtchikov, D. I., Senyavin, M. M., and Sklyarenko, Y. S., 1958, Separation of individual rare earth elements: Internat. Conf. Peaceful Uses Atomic Energy, 2d, Geneva, Proc., v. 4, p. 333–340.

Semenov, E. I., Kholodov, V. N., and Barinskii, R. L., 1962, Rare earths in phosphorites: Geochemistry, no. 5, p. 501–507.

Spedding, F. H., Filmer, E. I., Powell, J. E., Butler, T. A., and Jaffee, I. S., 1951, Separation of the rare earths by ion exchange; VI. Conditions for effecting separations with Nalcite HCR: Am. Chem. Soc. Jour., v. 73, p. 4840–4847.

Spirn, R. V., 1965, Rare earth distributions in the marine environment: Massachusetts Inst. Technology, Dept. Geology and Geophysics, Ph. D. thesis, 165 p.

Swaine, D. J., 1962, The trace element content of fertilizers: Herpenden, England, Commonwealth Bur. Soils, Tech. Comm. no. 52, 306 p.

U.S. Bureau of the Census, 1965, Current industrial reports: Inorganic chemicals and gases: Series M28A (64)–13, 31 p.

Vainshtein, Tugarinov, and Turanskaya, 1956, Regularities of the distribution of rare earths in certain minerals: Geochemistry, no. 2, p. 36–56.

Waring, C. L., and Mela, Henry, 1953, Methods for determination of small amounts of rare earths and thorium in phosphate rocks: Anal. Chemistry, v. 25, p. 432–435.

Weaver, Boyd, 1964, Liquid-liquid extraction of the rare earths, *in* Eyring, LeRoy (ed), Progress in the science and technology of the rare earths: New York, Macmillan Co., v. 1, p. 85–88.

Weaver, Boyd, Kappelman, P. A., and Topp, A. C., 1953, Quantity separation of rare earths by liquid-liquid extraction: Am. Chem. Soc. Jour., v. 75, p. 3943–3945.

Wildeman, T. R., and Haskin, L., 1965, Rare earth elements in ocean sediments: Jour. Geophys. Research, v. 70, no. 12, p. 2905–2910.

SILVER AND MERCURY GEOCHEMICAL ANOMALIES IN THE COMSTOCK, TONOPAH, AND SILVER REEF DISTRICTS, NEVADA-UTAH

By H. R. CORNWALL,[1] H. W. LAKIN,[2] H. M. NAKAGAWA,[2] and H. K. STAGER,[1]
[1] Menlo Park, Calif.: [2] Denver, Colo.

Abstract.—Approximately 450 samples of residual soil, rock from mine workings, and bedrock were collected in two bonanza silver-gold districts (Comstock and Tonopah) in Nevada, and in one silver sandstone district (Silver Reef) in Utah, and analyzed for Ag, Hg, and Au by colorimetric and atomic-absorption methods. Geochemical anomalies for silver clearly delineate areas of principal silver mines in all the districts, and mercury anomalies show the same pattern at Tonopah and Silver Reef. In the Comstock district, however, mercury values are highest outside the main silver-gold mining area; this suggests horizontal zoning from a central silver-gold area outward to a mercury area. If similar zoning occurs in the vertical plane, several mercury anomalies may be underlain by silver-gold mineralization. Areas where further exploration might be warranted are also indicated at Tonopah and Silver Reef.

Fresh and altered rocks from outcrops, mine workings and dumps, and residual soils were systematically collected and analyzed for trace amounts of gold, silver, and mercury at two gold-silver bonanza disdistricts (Comstock and Tonopah) in Nevada and a silver-bearing sandstone district in southwest Utah (Silver Reef). The results for each area are described separately below.

Representative samples of surface bedrock and soil, and wallrock in mine workings were collected in each area, but those from mine dumps were selected from materials that appeared to be favorable hosts for silver and gold. Mine workings and dumps were sampled only at Comstock and Tonopah, and the results of this sampling are grouped in one category in figures 1-4. In each district approximately half the samples are from mine workings. Figures 1 and 3 show that most of the samples in this category are high in silver content; it should be kept in mind, however, that half these samples are truly representative, and half are selective. All the samples except two at Tonopah are very low in gold content.

The samples were analyzed for silver and mercury in a mobile camper laboratory at field sites. Silver was measured indirectly by its catalytic action on the persulfate oxidation of manganous ion to permanganate ion (Nakagawa and Lakin, 1965). The intensity of the permanganate color in sample solutions was compared with standard solutions containing known amounts of silver. Mercury was determined by the atomic absorption of its vapor in an instrument designed for field use by Vaughn and McCarthy (1964).

Analysis of separate splits of these samples was made in the laboratory in Denver, and these results generally showed higher silver and mercury contents than the field results. Finer and more uniform grinding of the Denver laboratory splits is probably the principal reason for this difference.

The gold determinations were made on the laboratory splits by a colorimetric method (Lakin and Nakagawa, 1965).

COMSTOCK MINING DISTRICT, NEVADA

The famous Comstock mining district includes, from north to south, the Virginia City, Gold Hill, and Silver City districts, and also the Flowery district 3 miles east of Virginia City. Total recorded production has amounted to $398 million, according to Couch and Carpenter (1943, p. 92-94, 134–138). Lincoln (1923, p. 225–226) reported that from 1859 to 1921 the production in this area, exclusive of the Silver City district, was 12,399,366 tons of ore that contained gold valued at $164,023,917 and silver valued at $222,315,814 for a total of $386,339,731.

The geology of the Comstock district was described by Becker (1882), Bastin (1923), Gianella (1936), Calkins (1944), and Thompson (1956). Volcanic rocks of Tertiary age cover most of the district (figs. 1 and 2). The most widespread units are the Alta

U.S. GEOL. SURVEY PROF. PAPER 575-B, PAGES B10–B20

and overlying Kate Peak Formations, composed of a series of andesitic flows, pyroclastic rocks, and intrusive rocks. Tertiary rhyolitic welded tuff, Cretaceous granodiorite, and Triassic(?) metamorphosed volcanic and sedimentary rocks underlie the Alta Formation, and small bodies of granodiorite and andesite porphyry have intruded it and older rocks. Younger Tertiary and Quarternary andesite and basalt flows overlie the Tertiary units. Normal faults, striking northwest to northeast, have moderately disrupted the gently to moderately dipping volcanic rocks. The largest of these is the Comstock fault, which dips 45° E., with the east side displaced downward more than 2,000 feet.

The main gold-silver ore bodies occur in intensely altered andesite of the Alta Formation along the hanging wall of the Comstock fault for a distance of 3 miles in the Virginia City area, and along a southeast-trending normal fault at the south end of the district (fig. 1). The ore minerals argentite, electrum, native gold, native silver, and minor polybasite, as well as pyrite, sphalerite, chalcopyrite, and galena, occur in quartz and calcite veins and as replacements of altered wallrocks along veins. The average value of the ore mined between 1859 and 1921 was $31 per ton, but the largest bonanza ore body averaged $93 per ton (Lincoln, 1923, p. 227).

Widespread bleaching of the andesites of the Alta and Kate Peak Formations has resulted from alteration by hydrothermal solutions and possibly also from weathering of propylitized areas peppered with pyrite. In the present investigation these altered rocks were sampled at nearly 100 localities both in and outside the mining areas (figs. 1 and 2). A few samples of fresh andesite were also collected for comparison

All but one of the samples of altered material from dumps and mine workings in the mining areas contain 1 part per million or more of silver, and 16 of the 18 samples contain more than 5 ppm. Mercury exceeded 300 parts per billion in 11 of the 18 samples.

The silver content of 18 samples outside the mining district is greater than the background values, which are 0.10 ppm or less for silver and 100 ppb or less for mercury. These samples obtained 6 miles northwest of Virginia City contain more than 0.3 ppm of silver, and one of these contains more than 500 ppb of mercury. Five samples from scattered localities due north of the Comstock district, more or less along the extension of the Comstock fault, also contain silver in excess of 0.3 ppm, and 10 samples in this area contain 0.1–0.3 ppm of silver. Mercury values are particularly high in the same area and also in a sample from the extreme northwest corner of the map. The two samples 6 miles north of Virginia City that contain more than 3,000 ppb of mercury are from the Castle Peak mine, which produced over 2,500 flasks of mercury. The two clusters of samples containing anomalous mercury, that occur 1 to 3 miles south of the area shown at north edge of figure 2 are in an area that has been rather intensively prospected for mercury, but no workable ore has been discovered (Thompson, 1956, p. 72). In this area andesite flows of the Kate Peak Formation have been intensely altered to opal, quartz, clay, and alunite.

The distribution of mercury anomalies in the area of figure 2 indicates that mercury is more abundant outside the area of principal gold-silver deposits. This pattern suggests a lateral zoning from higher temperature gold–silver–base-metal mineralization to lower temperature mercury mineralization. There might also be similar vertical zoning from mercury at the surface to gold-silver at depth.

Two particularly promising areas for possible gold-silver mineralization at shallow to moderate depth are the clusters of mercury anomalies at the sample localities 2 miles and 4½ miles north of the center of Virginia City. These anomalies occur in altered andesite of the Alta Formation, or of the Kate Peak Formation near its contact with the underlying Alta; both sample sites are on the northward extension of the Comstock fault. Furthermore, we find that these areas apparently have not been thoroughly explored by trenches, pits, or diamond-drill holes.

Other promising areas for gold-silver metallization at depth are the mercury anomalies at the Castle Peak mine and in the two clusters of samples in the area 1–3 miles south of the north edge of figure 2. The silver anomaly in the area shown near the west edge of figure 1 might also warrant some exploratory work.

All the samples from the area of figure 1 were also analyzed for gold; every sample contained 0.05 ppm or less of Au except two in the Flowery district that ran 0.15 ppm of Au.

TONOPAH MINING DISTRICT, NEVADA

Tonopah, one of the largest and most famous silver-gold districts of the United States, was discovered in 1900. Between 1901 and 1946 the total production was $150,085,000 from 8,396,000 tons of ore, averaging $17.87 per ton (Kral, 1951, p. 171). The geology of the district was first described by Spurr (1905), also by Burgess (1909), Bastin and Laney (1918), and most recently by Nolan (1935), who mapped and studied the underground workings

241-334 O—67——2

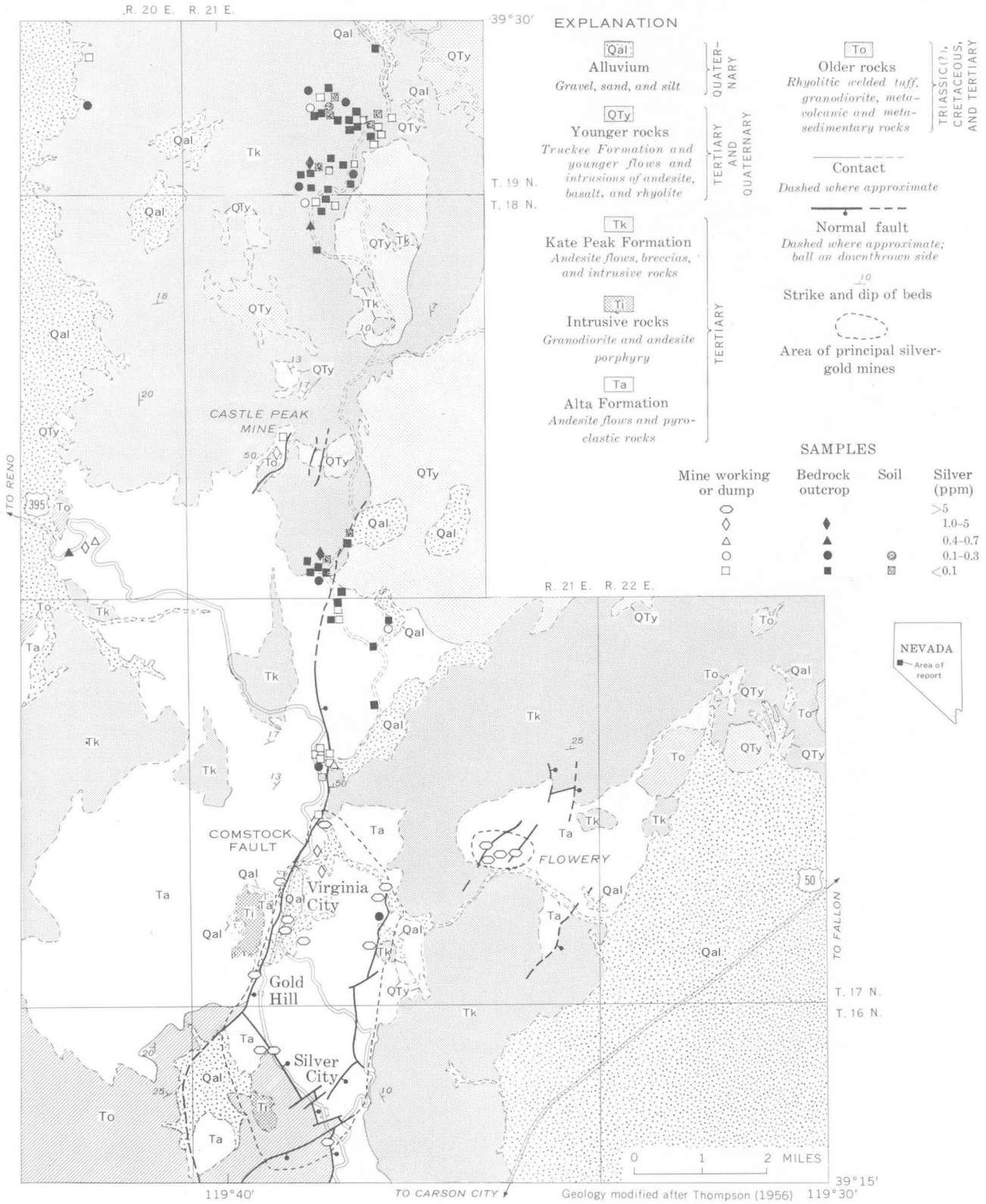

FIGURE 1.—Geochemical map of silver distribution in the Comstock mining district, Nevada.

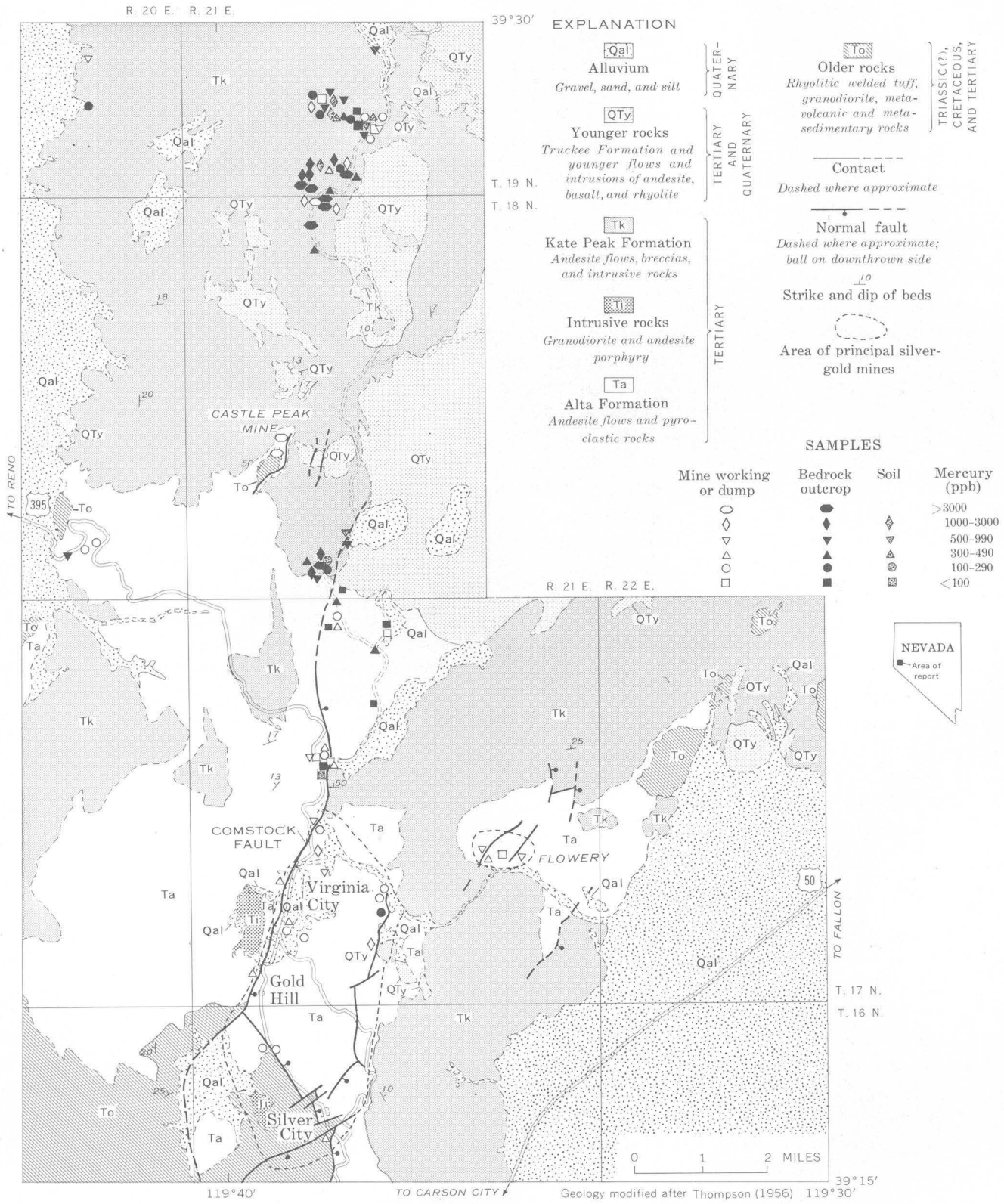

FIGURE 2.—Geochemical map of mercury distribution in the Comstock mining district, Nevada.

The ore bodies occur in the Mizpah Trachyte, a group of andesitic flows that are part of a Tertiary volcanic sequence of andesitic to rhyolitic tuffs, flows, plugs, and tuffaceous sedimentary rocks. According to Nolan (1935, p. 41-47) the ore bodies are replacement veins of quartz, carbonates, barite, electrum, argentite, polybasite, and other silver and base-metal sulfides that occur along faults and fractures. Locally, near the center of the mineralized area, cerargyrite, iodyrite, and embolite are abundant in a zone of supergene enrichment.

Individual ore shoots range from a few feet to 1,500 feet in length, 1–40 feet in width, and are restricted to a domed shell 300–600 feet thick of altered and fractured rock that nearly reaches the surface in the center of the district. Several faults containing the principal ore veins are also within and generally parallel to this domed shell. The Mizpah Trachyte, which is the host rock for the ore bodies, has been albitized and further altered to quartz sericite and adularia in the central part of the district. Beyond the central area, chlorite-carbonate alteration predominates. The ore ratio of silver to gold varies from 85:1 in the central area to more than 100:1 in peripheral areas (Nolan, 1935, p. 45). The features described above are believed to be related to an igneous intrusion, below the central area, that produced the crescent-shaped faults by forceful intrusion and supplied heat and solutions that altered the andesite and deposited the ore minerals.

One hundred and forty three samples, including some soils, and some material from dumps and mine workings, were collected in the Tonopah district and analyzed for silver and mercury. The analytical results are given in figures 3 and 4, which also show what types of samples were taken and the general geologic setting for each sample within the district.

The 18 samples from mine dumps in the main part of the district are all high in silver content; all but 2 contain more than 4 ppm. Mercury is anomalously high in 12 of these samples, 9 of which contain 500 ppb or more. The background for silver in the Tonopah district appears to be 0.05 ppm or less, and for mercury, 20–60 ppb.

Another very promising area of anomalous silver and mercury values was found 3/4 to 1¾ miles north of the center of Tonopah. Soils and dumps in this area contain, for the most part, more than 1 ppm of silver, and 6 samples near and north of the King Tonopah mine (figs. 3 and 4) have a high mercury content (300–>1,000 ppb). This is an area of intense alteration in the Mizpah Trachyte similar to that at Tonopah (quartz-sericite-adularia). The area was drilled by the Calumet and Hecla Co. in the 1940's, and they intersected quartz veins containing gold and silver. The silver and mercury anomalies found in that area in the present investigation indicate a need for more exploratory work.

In addition, samples were taken along normal faults north and east of Tonopah as well as in a large area of Mizpah Trachyte east of Tonopah. Leakage from hidden ore bodies at depth might provide surface anomalies locally along these faults. Such an anomaly was found at the King Tonopah mine. Silver values are also high in 3 samples, 1¼ miles northeast of Tonopah, just north of an area shown as alluvium and mine tailings in figure 3. Exploration might be warranted there also. Results of sampling in the rest of the area were rather discouraging, particularly for mercury.

The Tonopah samples were also analyzed for gold, and all contain 0.05 ppm or less except 2 from dumps of the Mizpah and Silver Top shafts in Tonopah that contain 0.07 and 3.8 ppm, respectively, and one from a dump 1 mile north of Tonopah, just west of the road shown on figures 3 and 4, that contains 2.5 ppm. These samples are also high in silver content (12, 8, 120 ppm, respectively) and 2 of the 3 are high in mercury content (6,500, 1,800, 170 ppb).

SILVER REEF MINING DISTRICT, UTAH

The Silver Reef district, also known as the Harrisburg or Leeds district, was discovered in 1869. Between 1875 and 1909, 7,200,000 ounces of silver was recovered (Butler, 1920) from deposits in the Springdale Sandstone Member of the Moenave Formation. The Springdale is locally known as the "Silver Reef sandstone" (Proctor, 1953). The stratigraphic nomenclature used in this paper is based on recent work by Averitt and others (1955), and Wilson (1965).

The Moenave and Kayenta Formations of Late Triassic(?) age, and the underlying Chinle Formation of Late Triassic age are folded into a major anticline with a subsidiary anticline and syncline plunging northeastward down the nose of the major structure. A northeast-trending normal fault, and a thrust fault with minimum eastward displacement of 1,500 feet (Proctor, 1953) repeat the silver-bearing Springdale Sandstone Member three times across the nose of the anticline. Quaternary alluvium and basalt locally overlie these units (figs. 5 and 6).

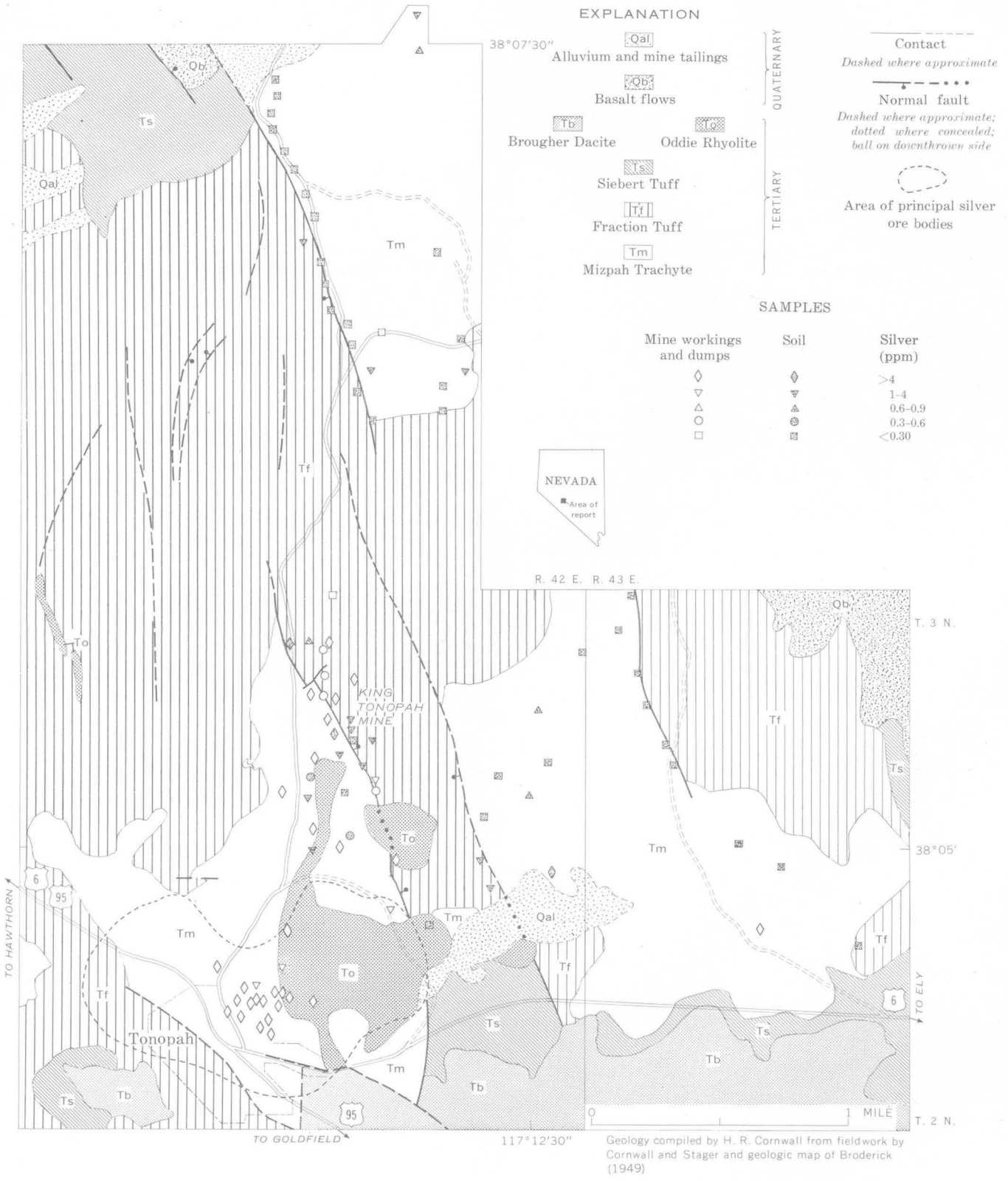

FIGURE 3.—Geochemical map of silver distribution in the Tonopah mining district, Nevada.

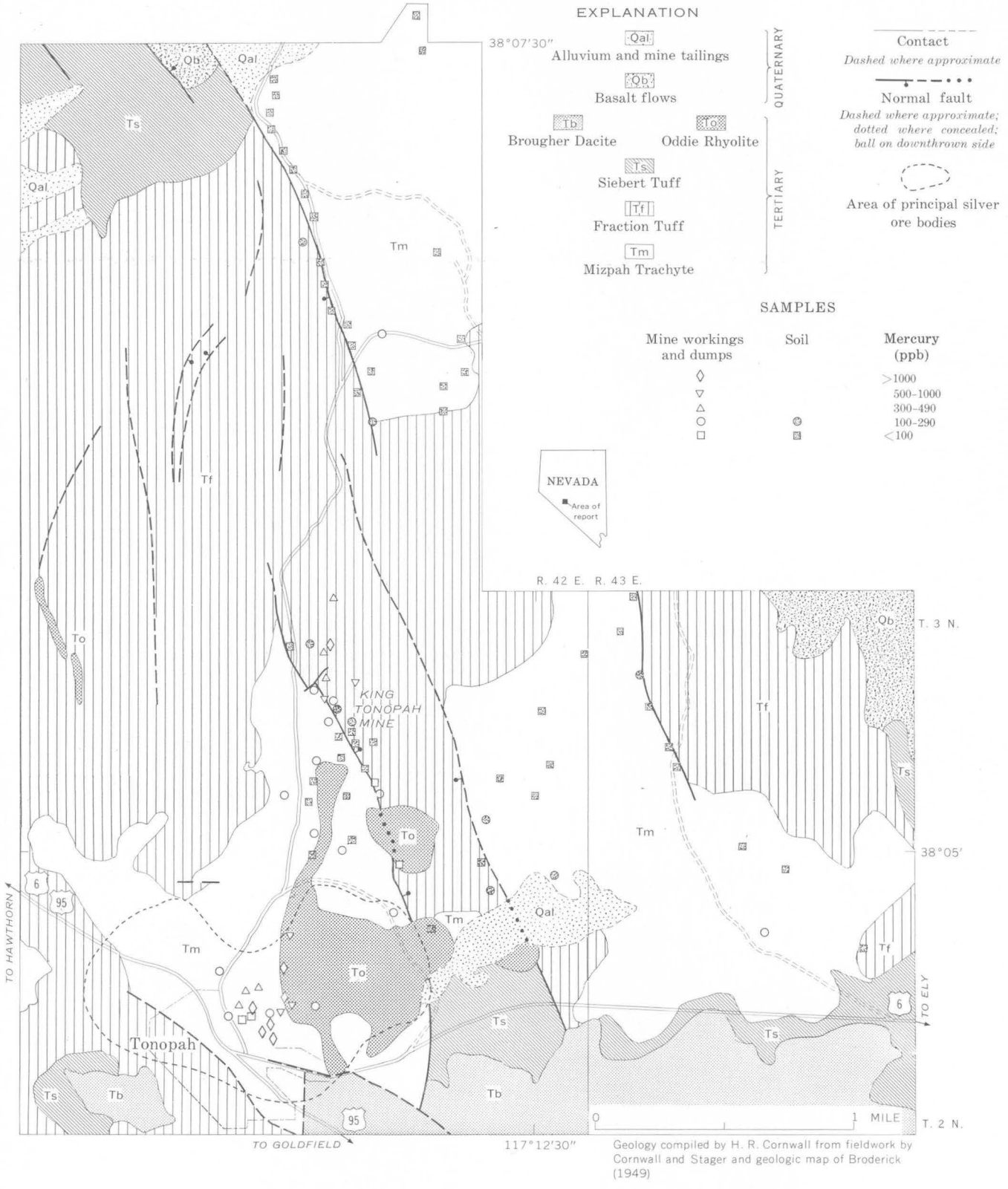

FIGURE 4.—Geochemical map of mercury distribution in the Tonopah mining district, Nevada.

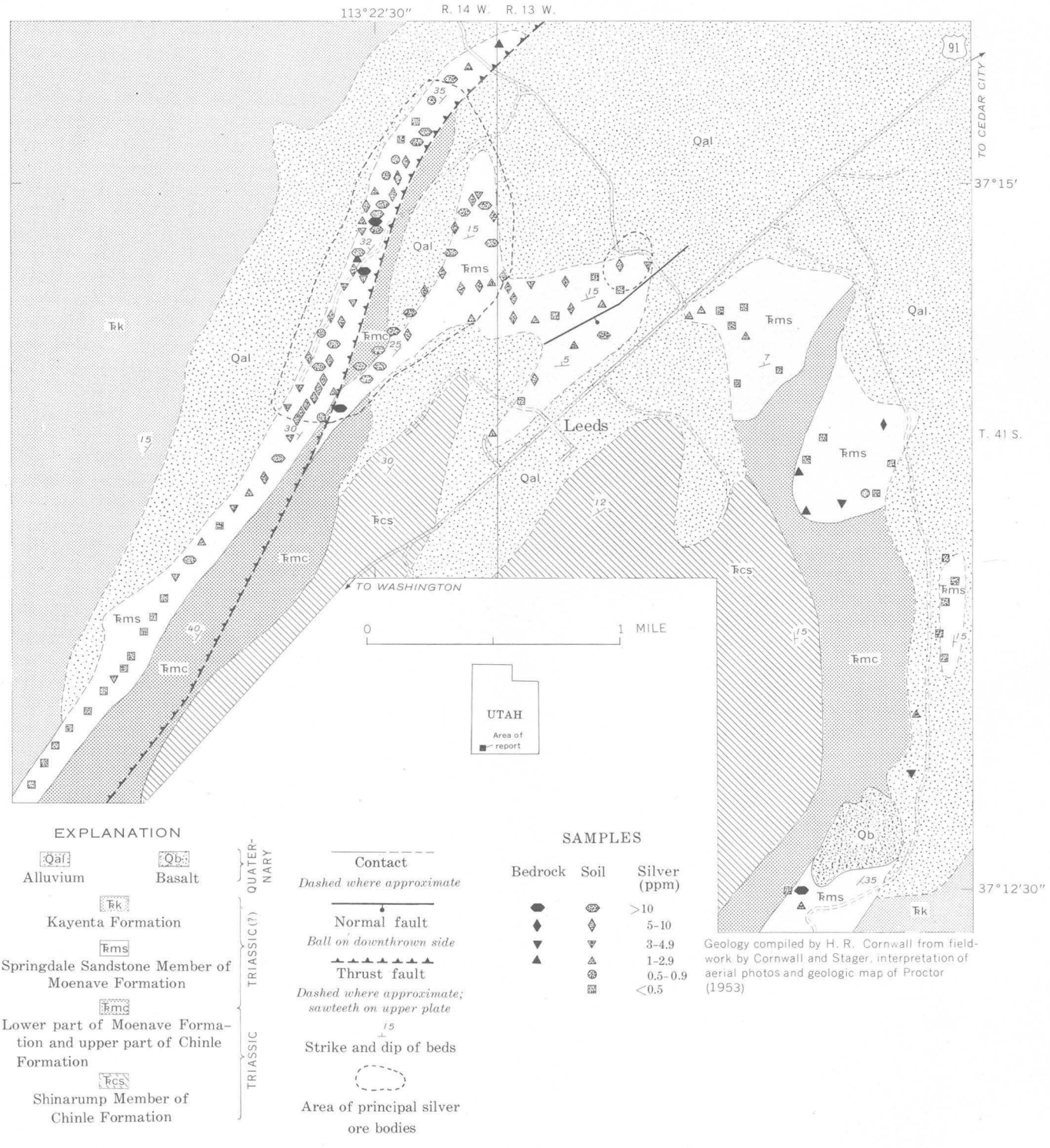

FIGURE 5.—Geochemical map of the silver distribution in the Silver Reef mining district, Utah.

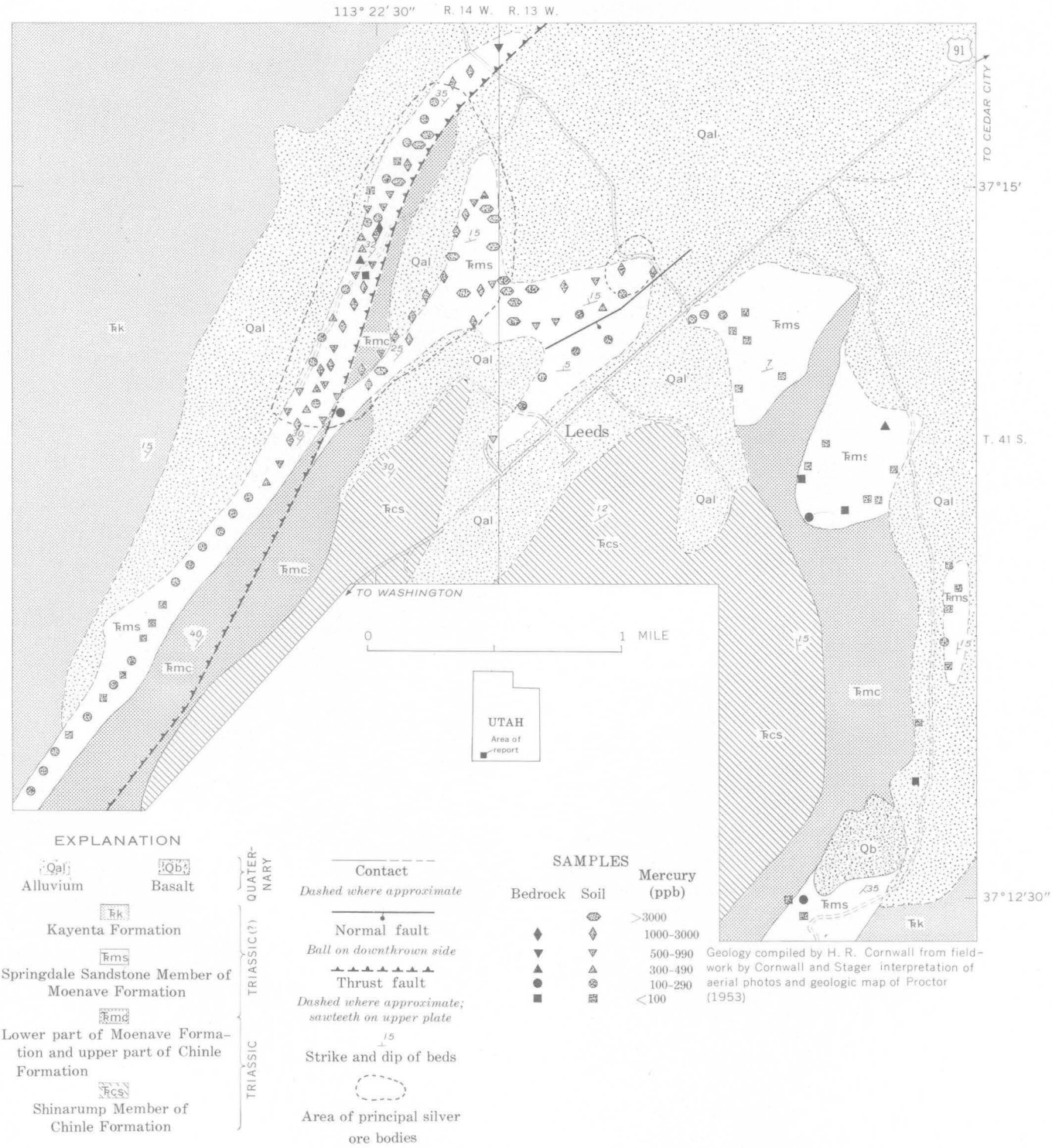

FIGURE 6.—Geochemical map of the mercury distribution in the Silver Reef mining district, Utah.

The silver deposits occur in a white to light-brown, fine-grained sandstone, 30 to 60 feet thick, with interbedded lenses of dark gray, green, or maroon shale commonly less than 1 foot thick. Beds containing clay galls, and fossil reeds and rushes are also present.

The silver deposits are irregular, generally elongate bodies, a few feet to several hundred feet long, and 1 inch to 20 feet thick. The ore mined averaged 20 to 30 oz. of silver per ton. The silver minerals cerargyrite (AgCl), plus a little reported argentite, occur as disseminated grains replacing the matrix of the sandstone, as thin seams along bedding-plane joints, and as replacements of fossil plants. The copper carbonates azurite and malachite are present, and locally are abundant; small amounts of vanadium-uranium minerals have also been found.

The sandstone and included lenticular ore bodies dip 15° to 35° north to northwest on the northwest part of the nose and flank of a large anticline.

A total of 167 samples, predominantly of residual soil (figs. 5, 6), were collected in the district. Residual soil near the base of the scarp slope of the silver-bearing Springdale Sandstone Member was sampled at regular intervals for a distance of approximately 10 miles. Residual soil samples were also obtained for a distance of approximately 3 miles, mainly in the area of principal silver ore bodies, along the base of the dip slope of the sandstone.

The area of principal silver ore bodies is clearly delineated by anomalous high values of both silver and mercury. The background value for silver appears to be 0.5 ppm or less, and values greater than 1 ppm are anomalous. In the area of known silver ore bodies, most of the samples range from 3 to more than 10 ppm of silver, whereas outside the area the majority of the samples contain less than 1 ppm. The background value for mercury is 20–200 ppb. In the area of known silver ore bodies, most of the samples contain more than 300 ppb of mercury, and the majority contain more than 1,000 ppb.

Anomalous silver values extend for nearly 1 mile southwest of the area of known silver ore bodies, and mercury values are high for half this distance. This might be a favorable area for finding new ore bodies. Half a mile north of Leeds, northwest of the normal fault shown in figures 5 and 6, is another favorable area in which silver has not heretofore been mined and where anomalous silver and mercury values were obtained from the majority of 10 soils samples.

At 32 of the sample sites along the scarp slope of the Springdale Member, paired samples of residual soil and sandstone ledge were taken. In two-thirds of the localities silver and mercury values are comparable in soil and bedrock. Only one of these sites, located 1,000 ft. southwest of the area of principal silver ore bodies shown in figures 5 and 6, has anomalously high values. At 8 localities, however, where silver values are anomalously high in the soils, ranging from 2 to 10 ppm, mercury values are also high in the soils (240–2,000 ppb), but low in the rocks (20–100 ppb). In 5 of these samples the rocks also have high silver values (1–14 ppm).

These results suggest that mercury values in areas of silver mineralization are apt to be higher in residual soils than in the parent rock. The reason for this is not clear, but possibly the erratic distribution of silver-rich, and presumably also mercury-rich, lenses in the sandstone ledge makes representative sampling difficult. Residual soils might more accurately represent the silver and mercury content of the weathered sandstone face. Friedrich and Hawkes (1966) have reported a somewhat similar situation in the Pachuca-Real del Monte district, Hidalgo, Mexico. They state that residual soils above a system of well-mineralized silver veins contain 250–1,900 ppb of mercury as contrasted to a background of 50 ppb, whereas wallrock immediately adjoining mercury-rich silver ore showed no enrichment in mercury.

Gold was determined in 122 of the Silver Reef samples. Ninety-nine contain 0.05 ppm or less. Nineteen have 0.07 ppm; three have 0.10 ppm, one has 0.35 ppm. All but 4 of the higher values are in soil samples, and all but 6, including the highest one, came from the area of principal silver ore bodies.

REFERENCES

Averitt, Paul, Detterman, J. S., Harshbarger, J. W., Repenning, C. A., Wilson, R. F., 1955, Revisions in correlation and nomenclature of Triassic and Jurassic formations in southwestern Utah and northern Arizona: Am. Assoc. Petroleum Geologists Bull., v. 39, p. 2515–2524.

Bastin, E. S., 1923, Bonanza ores of the Comstock lode, Virginia City, Nevada: U.S. Geol. Survey Bull. 735–C, p. 41–63.

Bastin, E. S., and Laney, F. B., 1918, The genesis of the ores at Tonopah, Nevada: U.S. Geol. Survey Prof. Paper 104, 50 p.

Becker, G. F., 1882, Geology of the Comstock lode and Washoe district: U.S. Geol. Survey Mon. 3, 422 p.

Broderick, A. T., 1949, Geology of the southern part of the San Antonio Mountains, Nevada: Yale Univ. Ph. D. thesis, 81 p.

Burgess, J. A., 1909, The geology of the producing part of the Tonopah mining district: Econ. Geology, v. 4, p. 681–712.

Butler, B. S., 1920, Silver Reef (Harrisburg, Leeds) district, *in* Butler, B. S., and others, The ore deposits of Utah: U.S. Geol. Survey Prof. Paper 111, p. 582–594.

Calkins, F. C., 1944, Outline of the geology of the Comstock lode district, Nevada: U.S. Geol. Survey Prelim. Rept., 35 p.

Couch, B. F., and Carpenter, J. A., 1943, Nevada's metal and mineral production (1859–1940 inclusive): Nevada Bur. Mines Bull. 38, 159 p.

Friedrich, G. H., and Hawkes, H. E., 1966, Mercury as an ore guide in the Pachuca-Real del Monte district, Hidalgo, Mexico: Econ. Geology, v. 61, p. 744–753.

Gianella, V. P., 1936, Geology of the Silver City district and the southern portion of the Comstock lode, Nevada: Nevada Bur. Mines Bull. 29 (Nevada Univ. Bull., v. 30, no. 9), 105 p.

Kral, V. E., 1951, Mineral resources of Nye County, Nevada: Nevada Bur. Mines Bull. 50, 220 p.

Lakin, H. W., and Nakagawa, H. M., 1965, A spectrophotometric method for the determination of traces of gold in geologic materials, *in* Geological Survey Research 1965: U.S. Geol. Survey Prof. Paper 525–C, p. C168–C171.

Lincoln, F. C., 1923, Mining districts and mineral resources of Nevada: Reno, Nev., Nevada Newsletter Pub. Co., 295 p.

Nakagawa, H. M., and Lakin, H. W., 1965, A field method for the determination of silver in soils and rocks, *in* Geological Survey Research 1965: U.S. Geol. Survey Prof. Paper 525–C, p. C172–C175.

Nolan, T. B., 1935, The underground geology of the Tonopah mining district, Nevada: Nevada Bur. Mines Bull. 23 (Nevada Univ. Bull., v. 29, no. 5), 49 p.

Proctor, P. D., 1953, Geology of the Silver Reef (Harrisburg) mining district, Washington County, Utah: Utah Geol. and Mineralog. Survey Bull. 44, 169 p.

Spurr, J. E., 1905, Geology of the Tonopah mining district, Nevada: U.S. Geol. Survey Prof. Paper 42, 295 p.

Thompson, G. A., 1956, Geology of the Virginia City quadrangle, Nevada: U.S. Geol. Survey Bull. 1042–C, p. 45–77.

Vaughn, W. W., and McCarthy, J. H., Jr., 1964, An instrumental technique for the determination of submicrogram concentrations of mercury in soils, rocks, and gas, *in* Geological Survey Research 1964: U.S. Geol. Survey Prof. Paper 501–D, p. D123–D127.

Wilson, R. F., 1965, Triassic and Jurassic strata of southwestern Utah, *in* Geology and resources of south-central Utah: Guidebook to the geology of Utah, Utah Geol. Soc. and Intermountain Assoc. Petroleum Geologists, no. 19, p. 31–46.

MINERALIZED VEINS AT BLACK MOUNTAIN, WESTERN SEWARD PENINSULA, ALASKA

By C. L. SAINSBURY and JOHN C. HAMILTON, Denver, Colo.

Abstract.—Veins at Black Mountain contain anomalous amounts of Sn, Pb, Zn, and Ag and trace amounts of Be, Cu, Bi, and Mo, elements characteristic of tin deposits. The veins are associated with a small stock of biotite granite of Late Cretaceous(?) age, and occur for the most part in limestone altered to calc-silicate rock near the stock. By analogy with ore-bearing veins at the Lost River tin mine, 20 miles to the west, where the higher levels of a tin ore shoot contain only small amounts of Sn and other rare metals, the veins at Black Mountain may contain an ore shoot at depth.

A small biotite granite stock intruded and metamorphosed older slates, phyllites, and argillaceous limestones at Black Mountain in the Seward Peninsula tin belt. Pyrite and arsenopyrite were noted in rocks of the contact aureole by Steidtmann and Cathcart (1922, p. 116), but no valuable ore minerals were known until 1963 when Sainsbury (U.S. Geol. Survey, 1964, p. A5) found cassiterite and wolframite with topaz and fluorite in altered granite during a reconnaissance traverse of the mountain. Several veins and mineralized faults were found during geologic mapping in 1966, and are shown on figure 1. The mineralized structures are called veins if there is only minor offset of beds, and mineralized faults if offset is appreciable and introduced minerals are confined to only a part of the fault. Some of the veins can be traced for several thousand feet, and more work is warranted to determine the tenor of the veins at depth.

The ore deposits herein discussed are on the public domain. They are accessible by bush plane, or by boat and foot traverse, from Teller or Nome, respectively 20 and 80 miles to the southeast of the deposits. Small, high-performance bush planes can land on a small airstrip on a flat bench about 1.5 miles east of the deposits (fig. 1).

GEOLOGY

The small stock of Late Cretaceous(?) biotite granite crops out on the south side of Black Mountain, where it intrudes a pre-Ordovician slate altered to biotite-andalusite hornfels (fig. 1). Above the granite and slate, pre-Ordovician thin-bedded argillaceous limestone has been altered to calc-silicate rock. Near the granite, the calc-silicate rock is composed mainly of garnet, vesuvianite, and tourmaline with minor amounts of other contact minerals, and generally is greenish gray on weathered surface. Farther from the granite, the calc-silicate rock is composed of wollastonite and other light-colored calc-silicate minerals, and contains pods and lenses of recrystallized limestone. Southeast of the granite, limestone and dolomite of Ordovician age are thrust over the older limestone. The slate locally is intruded by irregular bodies of medium- to coarse-grained gabbro also of pre-Ordovician age, but no gabbro intrudes the argillaceous limestone or calc-silicate rock.

The granite was intruded forcibly; it occupies the center of a domal uplift with the slate generally dipping away from the granite. This fact, and the clustering of normal faults around the area of the stock, indicates a genetic relation of intrusion, doming, and normal faulting. The faults mapped form three distinct sets: one set strikes about N. 20°–45° E.; a second set strikes N. 20°–50° W., and a third set strikes generally east. Some faults of all sets are altered locally by hydrothermal solutions, and one such altered fault cuts the granite (Helen fault, fig. 1).

Sainsbury (1965) gives a description of the rock units shown on figure 1, as well as the tectonic history of the general area.

MINERALIZED VEINS

Mineralized veins occur in a faulted area about 1 mile square just north of the granite stock (figs. 1, 3). Two mineralized faults (Winkley and Helen faults, fig. 1) contain anomalous amounts of tin. The Winkley fault is a normal fault striking northwestward and dipping steeply southwestward. The miner-

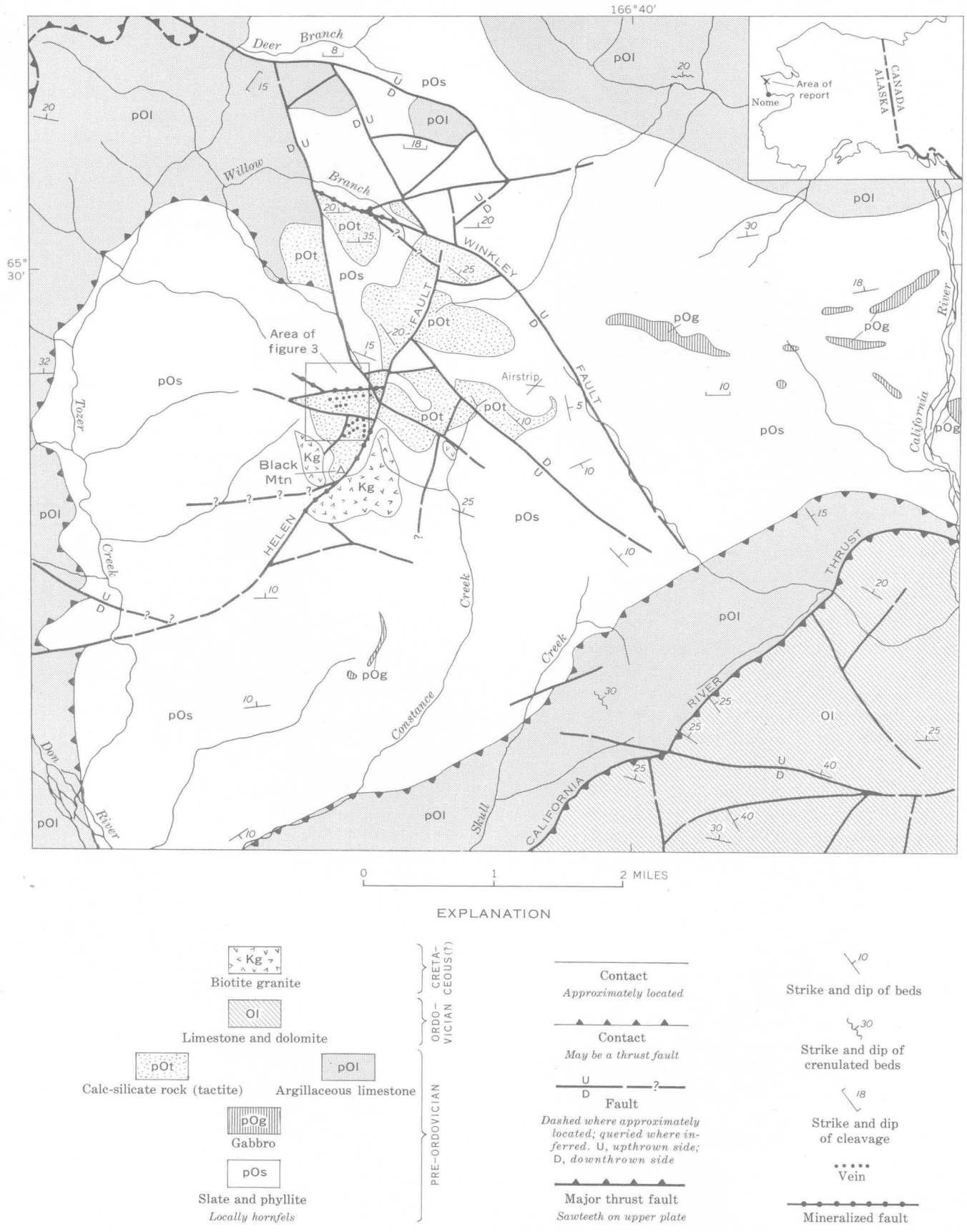

FIGURE 1.—Geologic map of the Black Mountain area, western Seward Peninsula, Alaska.

alized segment lies along the fault in the valley of Willow Branch of Tozer Creek, where the fault forms a distinct bench about 100 feet above the creek level. North of the fault, the bedrock is contorted slate; on the south side, the bedrock is light-colored calc-silicate rock containing lenses of recrystallized limestone. For a distance of about 2,500 feet along the fault, ore solutions have converted the calc-silicate rock to dark garnet-rich tactite containing several percent of sulfide minerals, including ferroan sphalerite (marmatite), pyrite, arsenopyrite, and a sooty-black unidentified material. Gangue minerals younger than the light-colored calc-silicate rock are fluorite and fine-grained silica. On the north side, where the bedrock is slate, the vein material consists of white quartz, tawny fine-grained silica, and cassiterite (sparse).

The distribution of sulfide-bearing tactite float, as well as scattered outcrops of tactite, shows that ore solutions spread outward from the fault and irregularly replaced the calc-silicate rock updip, as shown on figure 2. An analysis of a random chip sample (66–ASn–485) of the sulfide-bearing tactite is shown in table 1, and the sampled locality is shown on figure 2. The mineralized part of the Winkley fault is favorably located for drilling, for water is available in Willow Branch, and inclined holes of moderate length can test the downdip extension of the fault.

The Helen fault (fig. 1) strikes about N. 20° E., dips steeply northwest, and probably cuts the granite along the northwest border. The granite contact follows the line of the fault, as does altered granite containing float of cassiterite and wolframite-bearing topaz-fluorite veins, suggesting that the fault controls the granite contact. The fault plane, however, was covered by frost-broken rubble and snow, which prevented conclusive determination of the relation between faulting and granite. Mineralized segments of the fault are marked by distinct linear depressions with associated clay minerals and iron stains.

At the northeast end of the granite, near the Helen fault, quartz-topaz greisen containing cassiterite, pyrite, pyrrhotite, sphalerite, and galena has replaced the granite irregularly. This greisen may be related to ore solutions rising through shattered wallrocks along the fault. At the head of the valley of the unnamed south fork of Willow Branch, the Helen fault contains lenses of both white quartz and rusty fine-grained silica. The quartz does not contain observable cassiterite or sulfide minerals, but it does contain trace amounts of gold and silver. No samples for analysis were collected along the Helen fault, but cassiterite and sulfide minerals are megascopically visible in altered rock along it.

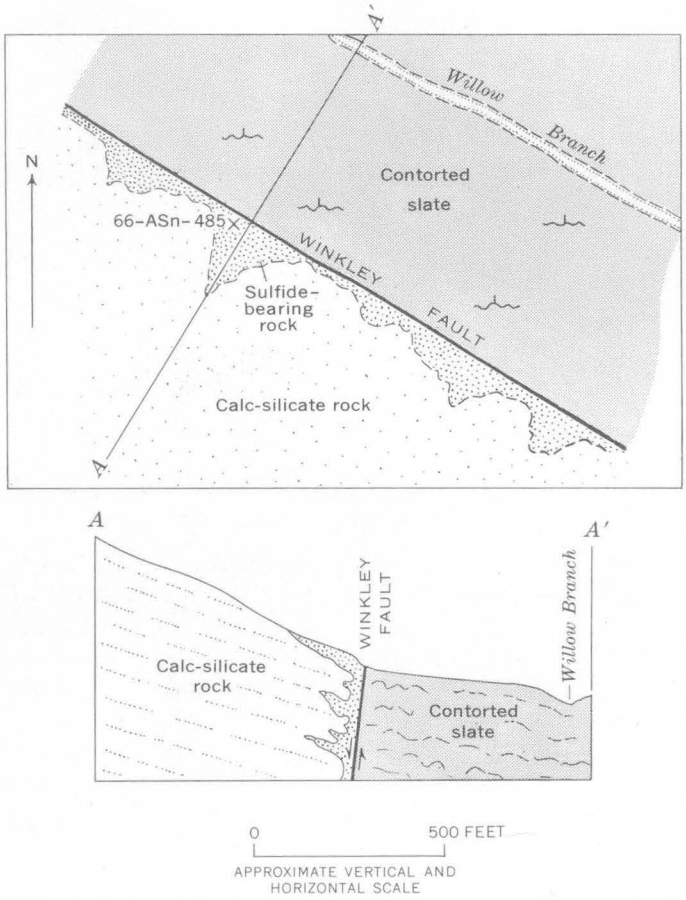

FIGURE 2.—Schematic drawing of the relation between sulfide-bearing calc-silicate rock and the Winkley fault, Black Mountain, Alaska. Wavy-line symbols in the contorted strata show the strike and the direction of dip of crenulated beds.

The shorter veins are confined to the outcrop area of the calc-silicate rock on the top of a tablelike area just north of the granite of Black Mountain (figs. 1, 3). Several veins were found, and others probably exist. They are grouped in two areas separated by a small knoll on which are several rock pinnacles 6 to 10 feet high. A schematic map of the veins, with sample locations, is shown on figure 3. The main vein (vein X) can be traced at least 5,000 feet; it consists of an east part striking about east, and a west part that trends about N. 70° W. downward off the hilltop. In the east part, where one wall of the vein is calc-silicate rock and the other slate or siltstone, fluorite is abundant, whereas quartz and minor fluorite form the gangue in the west half where hornfels forms both walls. The vein outcrops are marked only by frost-broken fragments of iron-stained vein material, some of which contain radiating needles of wollastonite(?) or diaspore(?). Small specks of cassiterite(?) and a very dusky purple sulfide mineral are noticeable in the northwest part of the vein. Owing to the scattering

TABLE 1.—*Semiquantitative spectrographic analyses, in weight percent, of random chip samples of float vein material, Black Mountain, Alaska*

[Analyst: J. C. Hamilton, U.S. Geol. Survey]

Sample No.	66-ASn-308	66-ASn-308A	66-ASn-471	66-ASn-485
Lab. No.	ABG-756	ABG-757	ABG-763	ABG-764
Map reference	Fig. 3	Fig. 3	Fig. 3	Fig. 2
Sn	0.003	0	0.007	0.07
Be	.00015	0	.0003	.00015
Cu	.003	.0001	.003	.03
Pb	.003	0	.03	.03
Zn	0	0	.03	3.0
Mo	0	0	.0003	0
Bi	0	0	0	.007
Ag	.00015	0	0	.0015
Sb	.15	0	0	0
Sr	.003	2	.003	.03

NOTE.—0 indicates below detection limits, which are as follows: Sn, 0.001; Be, 0.0001; Cu, 0.0001; Pb, 0.001; Zn, 0.02; Mo, 0.0003; Bi, 0.001; Ag, 0.0001; Sb, 0.02; and Sr, 0.0005.

of vein float by frost action, the width of float varies from a few feet to 12 feet, and the true thickness of the vein cannot be determined. The same is true for the other veins. A semiquantitative spectrographic analysis of a random chip sample of float vein material in which sulfide minerals are megascopically detectable is shown in table 1 (66–ASn–471).

A second vein trending about N. 80° E. lies a few hundred feet south of the main vein, and can be traced about 2,000 feet. The float consists of iron-strained vein material containing fluorite, fine-grained silica, and altered calc-silicate rock.

The veins in the southern part of figure 3 lie just north of the contact zone of the granite; they are more numerous but not as persistent along the strike nor as well mineralized as are those previously discussed. These veins are confined to calc-silicate rock and comprise two distinct sets which strike about N. 80° E., and north. The float vein material consists of porous iron-stained silica, fluorite, and carbonate. The longest north-trending vein can be traced for a distance of about 1,500 feet, and the longest N. 50° E. trending vein is 800 feet long. Several smaller veins, principally belonging to the set striking N. 50° E., were found, and others probably exist. Spectrographic analyses of two chip samples of vein float are shown in table 1; in one, only Sr is anomalously abundant. The veins probably do not exceed a few feet in thickness, but judged from their lateral continuity they probably extend to some depth.

ECONOMIC IMPORTANCE

With the possible exception of the mineralized part of the Winkley Fault, none of the surface exposures of the veins herein discussed contain minable amounts of ore minerals. However, the same elements which are characteristic of the tin lodes at Lost River (Sn, Be, Cu, Pb, Zn, Bi, Ag, and Mo) occur in the veins at Black Mountain, and fluorite is a common gangue mineral at both places. At the Lost River mine, 20 miles to the west, a strong downward zonation is characterized by surface exposures of barren lodes with only anomalous amounts of metals and commercial ore at a depth of a few hundred feet (Sainsbury, 1965). This change from barren lodes to commercial ore occurs at depths that do not exceed the projected depth to granite in the Black Mountain area.

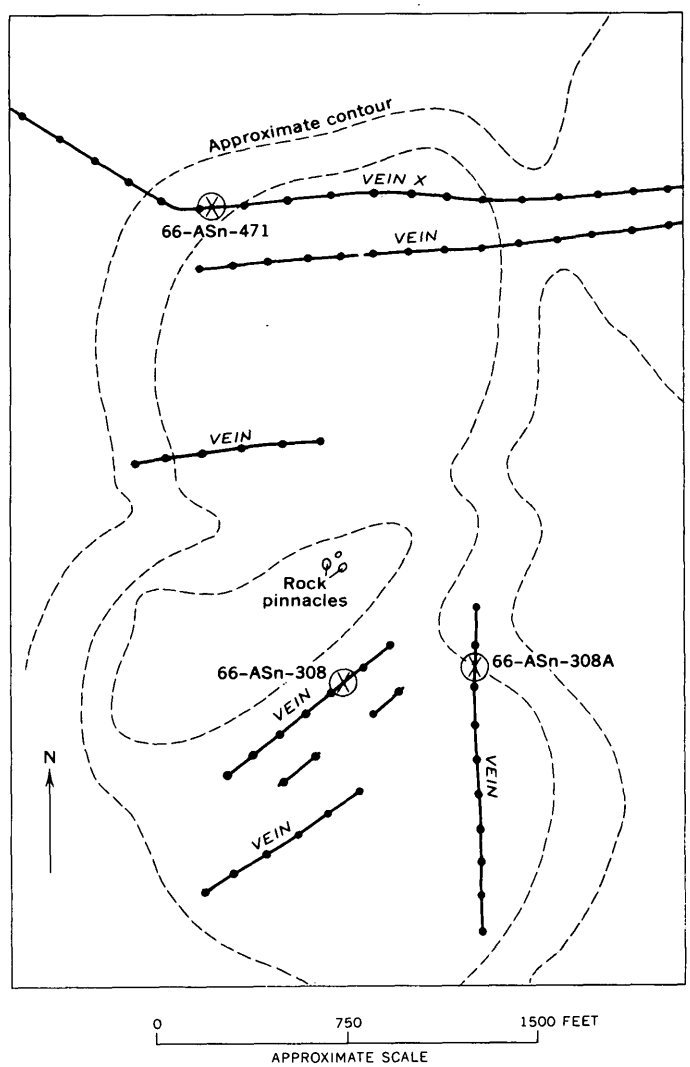

FIGURE 3.—Sketch map of known veins north of the granite at Black Mountain, Alaska. Sample numbers (66–ASn–308) and localities (X) are shown. Contour interval is approximately 50 feet.

REFERENCES

Sainsbury, C. L., 1965, Geology and ore deposits of the central York Mountains, western Seward Peninsula, Alaska: U.S. Geol. Survey open-file rept., and Stanford University, Ph. D. thesis, 146 p.

Steidtmann, Edward, and Cathcart, S. H., 1922, Geology of the York tin deposits, Alaska: U.S. Geol. Survey Bull. 733, 130 p.

U.S. Geological Survey, 1964, Geological Survey Research 1964: U.S. Geol. Survey Prof. Paper 501–A, 367 p.

MONOGRAPTUS HERCYNICUS NEVADENSIS N. SUBSP., FROM THE DEVONIAN IN NEVADA

By WILLIAM B. N. BERRY, Berkeley, Calif.

Abstract.—A new subspecies of *Monograptus hercynicus*, *M. hercynicus nevadensis*, is described from two localities in Nevada. One locality, near Carlin, is in Western assemblage rocks; the other, in Coal Canyon in the Simpson Park Mountains, is in Eastern assemblage rocks. The new subspecies has a greater width than European members of the species but is generally similar in other characteristics. The graptolite is indicative of a probable Siegenian age for the beds from which it came, and necessitates reconsideration of denoting the Silurian-Devonian boundary on the basis of the last appearance of monograptids.

Recently, great interest in *Monograptus hercynicus* has arisen because the species is considered to have a possible age range of late Gedinnian into Siegenian (Jaeger, 1962; Solle, 1963). It may well be restricted to the Siegenian (Jaeger, written commun. 1966). Inasmuch as these stages are commonly included in the Devonian System, the denoting of the Silurian-Devonian boundary on the basis of the last appearance of monograptids now must be reconsidered. The definition of the Silurian-Devonian boundary is still in debate. Holland (1965) has summarized several opinions on its position. The writer suggests that, inasmuch as the Gedinnian and Siegenian Stages have long been included in the Devonian, they remain within that system.

Although *M. hercynicus* was originally described in 1899 by Perner from Bohemia, it had long been overlooked until studies by Jaeger (1959, 1962, 1964) focused attention on it. Jaeger's work has resulted in worldwide interest in *M. hercynicus* and allied species. It has been recognized by Jaeger (1959, 1962, 1964) in Thuringia, the Kellerwald, Marburg, and West Sudeten in Germany; Spassov (1963) described it in Bulgaria; Obut (1960) noted its presence in central Asia; Hollard and Willefert (1961) recorded it from Morocco; Legrand (1961) described it from the Chaînes d'Ougarta in Algeria; and Greiling and Puschmann (1965) listed it from a locality near Barcelona, Spain. The species has been found by Johnson (1965) in the stratigraphic section in Coal Canyon in the Windmill window, Simpson Park Mountains, Nev. (fig. 1, Horse Creek Valley quadrangle, NW¼SE¼ sec. 17, T. 25 N., R. 49 E.). It has also been collected by J. F. Smith, Jr., K. B. Ketner, and R. J. Ross, Jr., of the U.S. Geological Survey, near Carlin, Nev. (fig. 1; Carlin quadrangle, W½ sec. 34, T. 32 N., R. 52 E.). Specimens from these two Nevada localities are described below.

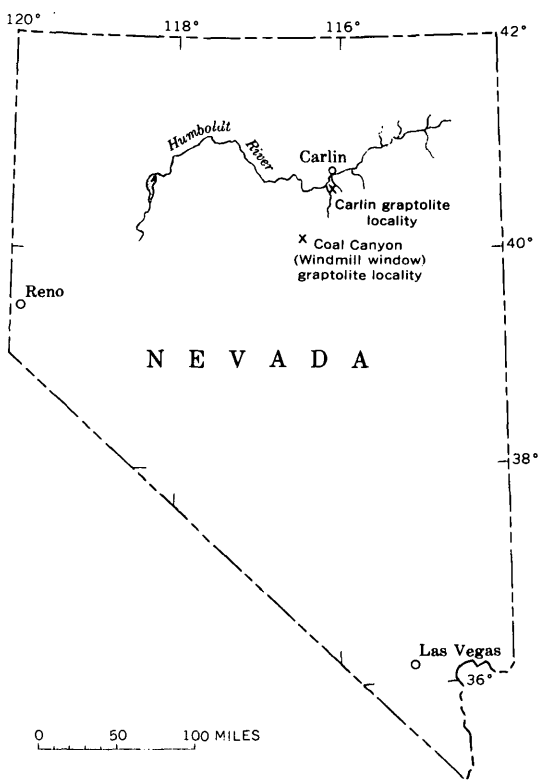

FIGURE 1.—Index map showing the position of the two localities at which *Monograptus hercynicus nevadensis* was found.

U.S. GEOL. SURVEY PROF. PAPER 575-B, PAGES B26-B31

The specimens of the subspecies of *M. hercynicus* described herein were collected in Nevada from both Eastern (primarily carbonate), and Western (primarily chert and argillite) assemblage rocks. The similarity of the specimens from the two localities suggests that free communication existed between these areas when the graptolite-bearing deposits were forming.

Acknowledgments.—The author is indebted to Dr. Hermann Jaeger, Humboldt University, Berlin, for examining some of the specimens described and for critically reviewing the manuscript and to Dr. R. L. Ethington, University of Missouri, for information concerning the conodonts found near the graptolites at the Carlin, Nev., locality. Thanks are also due his colleagues on the U.S. Geological Survey for sending the specimens to him and for their suggestions concerning the manuscript.

AGE OF *MONOGRAPTUS HERCYNICUS* IN NEVADA

Although *Monograptus hercynicus* is known to occur in Europe in beds of possible late Gedinnian and Siegenian age (Jaeger, 1962), the evidence bearing on the age of the beds that contain the Nevada subspecies needs evaluation. Inasmuch as the Gedinnian and Siegenian Stages have been recognized in Europe on the basis of shelly fossils, the age range of *M. hercynicus* in North America must be based on an analysis of the shelly fossils that occur with it. Johnson (1965, p. 370–371 and fig. 4) has provided such an analysis of the shelly faunas that occur below and above the graptolite-bearing beds in his Windmill Limestone at Coal Canyon, where he grouped the brachiopods from his Windmill Limestone into the *Quadrithyris* zone, and considered the *Quadrithyris* zone as correlative with the Gedinnian or Siegenian. Johnson has continued his study of these brachiopods and is now of the opinion that they indicate correlation only with the Siegenian (written comm., 1966). Johnson's studies of the brachiopods occurring with the Nevada subspecies of *M. hercynicus* at Coal Canyon indicate that the Nevada subspecies of *M. hercynicus* falls within the age range of this species established in Europe.

The evidence concerning the age of the Nevada subspecies of *M. hercynicus* at Carlin is not as precise as at Coal Canyon. According to J. F. Smith (written comm., 1966), "The locality is in W½ sec. 34, T. 32 N., R. 52 E.," and "the rock there is almost black to pale brown siltstone, some of which is very carbonaceous. It is in a formation that makes up part of the upper plate of the Roberts thrust." Smith also indicates that the monograptid-bearing beds are in the lower part of a formation that includes most of the Devonian; fossils suggestive of a Late Devonian age had been found in the same unit several miles away from the monograptid locality. R. J. Ross, Jr. (written comm., 1964) has noted that conodonts considered indicative of a Devonian age had been obtained from not more than 10 feet stratigraphically above the monograptids. R. L. Ethington, who had collected some of the conodonts and examined the fauna, states (written comm., 1966) that "the conodont fauna consists almost exclusively of *Icriodus latericrescens* with an occasional specimen of a new species of *Spathognathodus*" and indicates that the age suggested by the conodont fauna was consistent with that of the graptolites, namely, late Gedinnian or Siegenian. The evidence from the Carlin occurrence thus tends to substantiate the age of the Nevada subspecies of *M. hercynicus* as documented by Johnson.

Johnson (1965, p. 370–372) discussed correlation of the *Quadrithyris* zone, pointing out that it had been recognized in the lower part of the McMonnigal Limestone of Kay and Crawford (1964, p. 440) at Ikes Canyon in the Toquima Range. Johnson (1965, p. 370 and fig. 3) also indicated that his Windmill Limestone was the lateral equivalent of a part of the Lone Mountain Dolomite and pointed out that the *Quadrithyris* zone fauna had closest affinities with those from Asiatic Russia and the Urals.

SYSTEMATIC PALEONTOLOGY

Class GRAPTOLITHINA Bronn, 1846
Order GRAPTOLOIDEA Lapworth, 1875
Suborder MONOGRAPTINA Lapworth, 1880
Family MONOGRAPTIDAE Lapworth, 1873
Genus *MONOGRAPTUS* Geinitz, 1852
Monograptus hercynicus Perner, 1899

The species *M. hercynicus* has been fully described by Jaeger (1959, p. 87–92; table 1, figs. 1, 10, table 2, table 3, fig. 1, Abh. 15 a–h), who noted that the most characteristic features of this species were the unique trumpet shape of the sicula, the thecal hooks, and the near-vertical form of a major portion of the free ventral wall of most of the thecae. The Nevada specimens have all these features and clearly fall within the species *M. hercynicus*. However, they have somewhat wider rhabdosomes than the European *M. hercynicus* and appear to constitute a distinct subspecies.

Monograptus hercynicus subsp. *nevadensis* n. subsp.

Figure 2, *a* - *i*

Description.—The rhabdosomes are straight for the greater part of their length, except that they commonly have a slight to moderate ventral curvature from the level of the sicula apex up to about 6 to 8 mm from

a

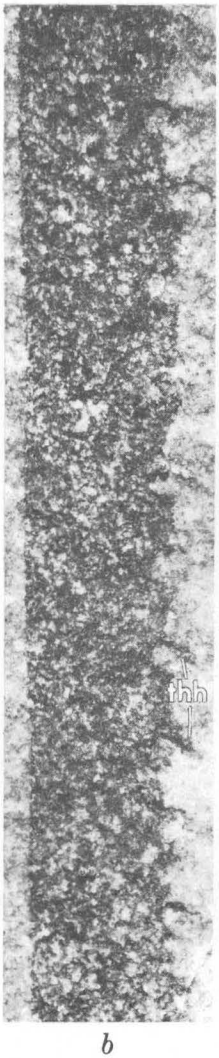

b

c

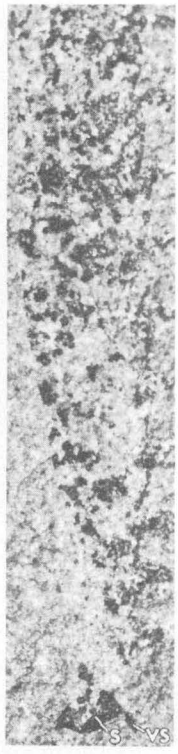

d

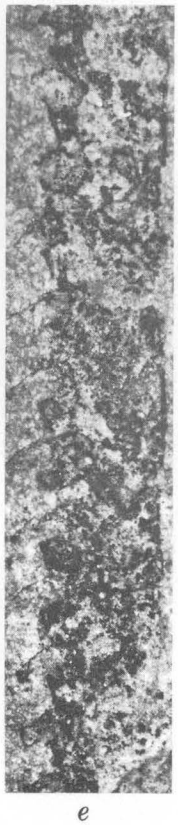

e

f

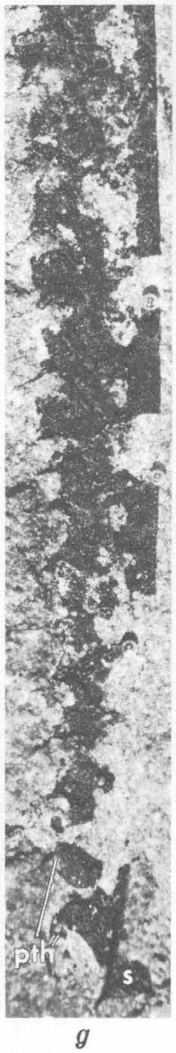

g

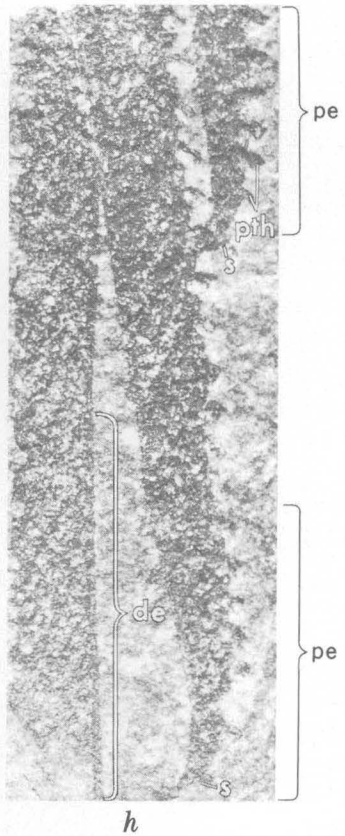

h

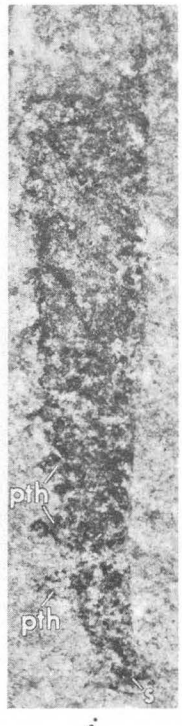

i

that level (fig. 2, *h*, *i*). A slight to moderate dorsal flexure commonly occurs throughout the length of the sicula (fig. 2, *a*, *c*, *i*). All of the rhabodosomes studied are incomplete or immature; the longest of them measured 4 to 5 cm.

The rhabdosomes widen from about 0.7–0.8 mm (without thecal hook) and 1.2–1.4 mm (with thecal hook) at the first theca (th 1) to 1.3–1.5 mm (without thecal hook) and 1.5–1.8 mm (with thecal hook) at 5 mm from that level, to 1.5–1.8 mm (without thecal hook) and 1.9–2.1 mm (with thecal hook) at 10 mm from that level to a maximum of 1.8–2.2 mm (without thecal hook) and 2.4–2.6 mm (with thecal hook) at 12 to 15 mm from that level. The commonest maximum width is 2.0 mm without thecal hook and 2.5 mm with thecal hook.

Five to 5½ thecae occur in the proximal 5 mm of the rhabdosome and 9½ to 11 in its proximal 10 mm. Seven to 8½ thecae are present in 10 mm in the distal portions of the rhabdosome of the Coal Canyon specimens, and 8¼ to 9 in the distal portions of the rhabdosome of the Carlin specimens. In all rhabdosomes, the thecae are more markedly hooked in the proximal portion of the rhabdosome than in the distal portion (see figs. 2*g*, *e*, *h*). Marked thecal hooks may be present in only the proximal 2 or 3 thecae in some specimens (see figs. 2*c*, *g*, *i*), but may be present in as many as 15 to 18 thecae in others (see fig. 2*h*). Commonly, however, the initial 5 to 7 thecae are markedly hooked and the more distal ones less so. The general shape of the proximal thecae is similar to that of the thecae in *Monograptus uncinatus* (see figs. 2*a*, *g*, *h*, *i*). The hooked portion of these thecae is a tube that is approximately 0.2 mm wide and 0.3 to 0.4 mm high. The distal thecae are somewhat different in shape (see figs. 2*b*, *e*, *f*) in that the tubular hooked part of the theca is reduced to scarcely 0.1 mm in width and in height. The hooked part in the distal thecae of some specimens has been drawn out to such an extent that it appears as a small spine projecting from the ventral thecal wall (see figs. 2*c*, *f*). In most highly compressed specimens the tiny hooks appear as small flanges projecting from the ventral side of the rhabdosome. In addition to the small size of the thecal hook, the distal thecae have a relatively unique shape, inasmuch as the greater part of the free ventral wall is vertical and approximately parallel with the rhabdosome axis. The free portion of the ventral wall (see figs. 2*b*, *c*, *f*, *g*, *h*) appears to be vertical at the ventral rhabdosome margin. It then curves abruptly inward, making a near-90° angle before curving around to form the thecal hook. The marked depression formed beneath the thecal hook in the distal thecae (see figs. 2*b*, *c*) is 0.3 to 0.45 mm deep and 0.3 to 0.4 mm high. The vertical portion of the free ventral wall in the distal thecae is 0.75 to 0.95 mm long. The interthecal septum is approximately S-shaped with the inner part almost normal to the rhabdosome axis. The greater part of the septum makes a 30° to 40° angle with the rhabdosome axis.

The sicula of the Nevada specimens, as is true of the European members of this species, has a shape similar to that of the bell of a trumpet (fig. 2 *a*, *c*, *d*, *g*, *h*, *i*). The shape of the sicula, characterized by a marked rate of widening in the apertural region, is a diagnostic feature. The siculae of the Nevada specimens range from 1.5 to 2.1 mm in length and 1.0 to 1.3 mm in width at the aperture. Most of the siculae are 1.8 to 2.0 mm long and 1.0 to 1.1 mm wide. The sicula apex commonly attains the level of the second thecal aperture. The sicula aperture appears to have short spines projecting from both its dorsal and ventral sides. The virgella spine from the margin on the ventral side commonly appears to be the more robust, measuring 0.2 to 0.4 mm in length (see fig. 2*d*).

Discussion.—The Nevada specimens are wider than the European specimens described by Jaeger (1959, p. 87–92). The European forms have a maximum width of 1.8 to 2.0 mm (with thecal hook), whereas the Nevada specimens are fully ½ mm wider in maximum width. In all other features, however, the Nevada specimens appear to fall within the range in variation of the European material as discussed by Jaeger (1959, p. 87–92). The differences between the Nevada and European specimens are indeed relatively slight but may be considered to be those of geographic

FIGURE 2.—*Monograptus hercynicus nevadensis* n. subsp.

a. Proximal end of rhabdosome showing shape of sicula (s) and first theca (th 1). × 10. USNM 155931. Windmill Limestone, Coal Canyon.

b. Distal portion of rhabdosome showing nature of thecae and thecal hooks (thh). × 10. USNM 155932. Windmill Limestone, Coal Canyon.

c. Nearly complete rhabdosome; s, sicula; pth, proximal thecae. × 5. USNM 155933. Unnamed unit, Carlin. USGS Silurian-Devonian Loc. D62.

d. Proximal end of rhabdosome showing sicula (s) shape and virgella spine (vs). × 10. USNM 155934. Unnamed unit, Carlin. USGS Silurian-Devonian Loc. D62.

e. Medial part of rhabdosome showing change in thecal form from the proximal (bottom of photo) to the distal (top of photo) thecae. × 10. USNM 155935. Unnamed unit, Carlin. USGS Silurian-Devonian Loc. D62.

f. Distal part of rhabdosome. × 5. USNM 155936. Windmill Limestone, Coal Canyon.

g. Proximal end of rhabdosome shown in *c* illustrating shape of sicula (s) and proximal thecae (pth). × 10.

h. Distal end (de) of one rhabdosome and proximal ends (pe) of two others showing sicula (s) and proximal thecae (pth). × 5. USNM 155937. Windmill Limestone, Coal Canyon.

i. Proximal end of rhabdosome showing shape of sicula (s) and proximal thecae (pth). × 10. USNM 155938. Windmill Limestone, Coal Canyon.

(and perhaps some slight temporal) difference. Because of the apparent geographic separation, the Nevada specimens are considered to comprise a subspecies within the species of *M. hercynicus*. Jaeger (written comm., 1962) noted that central Asian specimens of *M. hercynicus* he had examined were wider than the European ones and similar in width to those from Nevada. If other characteristics are similar, the Asian and Nevada forms might fall within the same subspecies, thus emphasizing the closeness of the faunal affinities between Asia and the Western United States during the early Siegenian revealed by Johnson's (1965, p. 370) analysis of the brachiopods.

The Nevada specimens are relatively similar in most characteristics to the African ones described by Legrand (1961) from the Chaînes d'Ougarta and by Hollard and Willefert (1961) from the Erfoud region near Tafilalt in Morocco. The Moroccan specimens are, however, thinner than either the European or Nevada ones as they are but 1.7 mm in maximum width (with thecal hook). Both sets of African specimens have more closely spaced thecae in the proximal region (12 in 10 mm) than do those from either Europe or Nevada.

Abraded and otherwise poorly preserved specimens of *M. hercynicus* may be relatively difficult to identify. If the thecal hooks in the distal thecae particularly become indistinct, the medial and distal portions of the rhabdosomes may appear similar to those in *M. vomerinus*. If the thecal hooks are preserved in such a way that they are readily seen and the ventral portions of the thecal walls are not, then the forms may be mistaken for some monograptid with small hooked thecae such as *M. riccartonensis*. The sicula shape is perhaps the most important feature and must be seen to identify *M. hercynicus* correctly in poorly preserved material.

Although the specimens from Carlin and Coal Canyon may be grouped within a single subspecies, some slight differences exist between the two groups. These may be the result of local environmental differences between the two areas. They could also reflect, at least in part, some slight difference in time of existence of the two groups. The Coal Canyon specimens, as a group, have slightly wider rhabdosomes than the Carlin ones, although many specimens in the two groups have rhabdosomes of the same width. A few of the Carlin specimens appear to have a maximum rhabdosome width of 2.0 mm (with thecal hooks). These are fragments of rhabdosomes and may reflect only a slow rate of widening. The Carlin specimens commonly have slightly more closely spaced thecae in 10 mm (most have 8 ¾ to 9) in the distal portions of the rhabdosomes than do the Coal Canyon ones, which commonly have 7 ½ to 8 ½ in the same region. The two groups of specimens are similar in other features.

REFERENCES

Greiling, Lothar, and Puschmann, Horst, 1965, Die Wende Silurium/Devon am St. Creu d'Olorde bei Barcelona (Katalonien) [The Silurian-Devonian boundary at St. Creu d'Olorde near Barcelona (Catalonia)]: Senck. leth., v. 46, p. 453–457.

Holland, C. H., 1965, The Siluro-Devonian boundary: Geol. Mag., v. 102, p. 213–221.

Hollard, Henri, and Willefert, Solange, 1961, Presence de *Monograptus hercynicus* Perner dans le Silurien du Tafilalt (Maroc) [Presence of *Monograptus hercynicus* Perner in the Silurian at Tafilalt (Morocco)]: Compte Rendu Somm. des Seances de la Soc. Geol. de France, no. 2, p. 42–43.

Jaeger, Hermann, 1959, Graptolithen und Stratigraphie des jungsten Thuringer Silurs [Graptolites and stratigraphy of the youngest Thuringian Silurian]: Abh. Deutsch. Akad. Wiss. Berlin, Klasse Chem., Geol., Biol., no. 2, 197 p., 14 pls.

———1962, Das Silur (Gotlandium) in Thüringen und am Ostrand des Rheinischen Schiefergebirges (Kellerwald, Marburg, Giessen) [The Silurian (Gotlandian) in Thuringia and the east end of the Rhenish Schiefergebirge (Kellerwald, Marburg, Giessen)]: Internat. Arbeitstagung über die Silur/Devon Grenze und die Stratigraphie von Silur und Devon, 2d, Bonn-Bruxelles, 1960, Symposiums Band, Stuttgart, p. 108–135.

———1964, *Monograptus hercynicus* in den Westsudeten und das Alter der Westsudeten-Hauptfaltung [*Monograptus hercynicus* in the West Sudeten and the age of the west Sudeten major faulting]: Pt. 1, Geologie, v. 13, no. 3, p. 249–277, Pt. 2, no. 4, p. 377–394.

Johnson, J. G., 1965, Lower Devonian stratigraphy and correlation, northern Simpson Park range, Nevada: Canadian Petroleum Geol. Bull., v. 13, p. 365–381.

Kay, Marshall, and Crawford, J. P., 1964, Paleozoic facies from the miogeosynclinal to the eugeosynclinal belt in thrust slices, central Nevada: Geol. Soc. America Bull., v. 75, p. 425–454.

Legrand, Phillip, 1961, Decouverte de *Monograptus hercynicus* (Perner) dans les Chaînes d'Ougarta (Algerie) [Discovery of *Monograptus hercynicus* (Perner) in the Chaines d'Ougarta (Algeria)]: Geol. Soc. France Bull., 7th ser., v. III, p. 201–205.

Obut, A. M., 1960, Zonale Einteilung des Silurs in der UdSSR nach Graptolithen [Graptolite zonal division of the Silurian in the USSR]: Prager Arbeitstagung über die Stratigraphie des Silurs und des Devons (1958), Prague, p. 269–275.

Solle, Gerhard, 1963, *Hysterolites hystericus* (Schlotheim) (Brachiopoda; Unterdevon), die Einstufung der oberen

Graptolithen-Schiefer in Thüringen und die stratigraphische Stellung der Zone des *Monograptus hercynicus* [*Hysterolites hystericus* (Schlotheim) (Brachiopoda; Lower Devonian) its position in the upper graptolite shales in Thuringia and the stratigraphic position of the zone of *Monograptus hercynicus*]: Geol. Jahrb., v. 81, p. 171–220.

Spassov, Christo, 1963, Das Oberludlow mit *Monograptus hercynicus* und dessen grenze mit dem Devon bei Stanjovci, Bezirk Pernik [The upper Ludlow with *Monograptus hercynicus* and its boundary with the Devonian at Stanjovci, Bezirk Pernik]: Bulgarian Geol. Soc. Rev., v. 24, pt. 2, p. 119–141.

PALEOGEOGRAPHIC SIGNIFICANCE OF TWO MIDDLE MIOCENE BASALT FLOWS, SOUTHEASTERN CALIENTE RANGE, CALIFORNIA

By H. EDWARD CLIFTON, Menlo Park, Calif.

Abstract.—Two basalt flows interbedded with marine-nonmarine transitional deposits of middle Miocene age in the southeastern Caliente Range provide information about the paleogeographic setting and the depositional environment of the sediments. The distribution, thickness, and internal structures of the flows indicate their source, their direction of flow, and the location at which one flow advanced across the strand line. Except at this location both flows seem to be subaerial even though they lie in many places upon sandstone of marginal marine origin. The sandstone is a very near shore, and perhaps a littoral, facies.

Pronounced interfingering of marine, continental, and transitional deposits characterizes the sedimentary rocks of middle Miocene age in the southeastern Caliente Range of southwestern California (fig. 1). The upper part of this sequence contains three basalt flows that Eaton (1939, p. 269) termed the "Triple" basalts. The lower two of these flows extend laterally across the transitional zone from a dominantly continental sequence into a sequence composed mostly of marine strata. These two flows are similar in composition and distribution, and probably erupted from the same feeder system. The third flow, the uppermost of Eaton's Triple basalts, is missing over much of the area, and has not been studied in detail.

The lower two flows of the Triple basalts not only provide time lines for the study of sedimentary facies relationships, but also contain clues as to the local paleogeography at the time of their eruption. Study of these flows has established their source area, the direction of flow, and the location at which one flow crossed the strand line. These data facilitate interpretation of facies changes and directional structures in adjacent sediments.

GEOLOGIC SETTING

The sedimentary rocks that enclose the lower two basalt flows change laterally, northwest to southeast (fig. 1), from marine siltstone (Saltos Shale Member of the Monterey Shale of Hill and others, 1958, p. 2989), through a marginal marine sandstone (Branch Canyon Formation of Hill and others, 1958, p. 2991), into continental sandstone and red mudstone (Caliente Formation of Hill and others, 1958, p. 2993) (Vedder and Repenning, 1965). These units interfinger in beds several feet thick.

The strata lie on the south limb of the southeast-plunging Wells Ranch syncline (Eaton and others, 1941, p. 235). The north limb of the syncline is mostly covered by Quaternary alluvium of the Carrizo Plain, and middle Miocene sedimentary rocks and basalt crop out on this limb only near the nose of the syncline or as small, isolated, structurally complex inliers surrounded by alluvium (fig. 1). Neither of the lower two flows of Eaton's (1939) Triple basalts occurs near the nose of the syncline, and the identity of the poorly exposed basalt within the inliers is unknown (J. G. Vedder, oral commun., 1964). The lower two flows, therefore, are exposed in a homocline that dips 40°–55° to the northeast under the alluvium of the Carrizo Plain.

The sequence of Triple basalts is overlain by continental deposits of the upper Caliente Formation. This part of the Caliente Formation contains several other basalt flows, the uppermost and largest of which is the "Main" basalt of Eaton (1939) of Clarendonian (late Miocene to early Pliocene) age (Repenning and Vedder, 1961, p. C238).

To facilitate discussion of the rock units used throughout this report, the informal terms "Triple" basalts and "Main" basalt applied by Eaton (1939) to the volcanic rocks, and the formal stratigraphic names applied by Hill and others (1958) to the sedimentary rocks, have been retained in this report.

U.S. GEOL. SURVEY PROF. PAPER 575-B, PAGES B32-B39

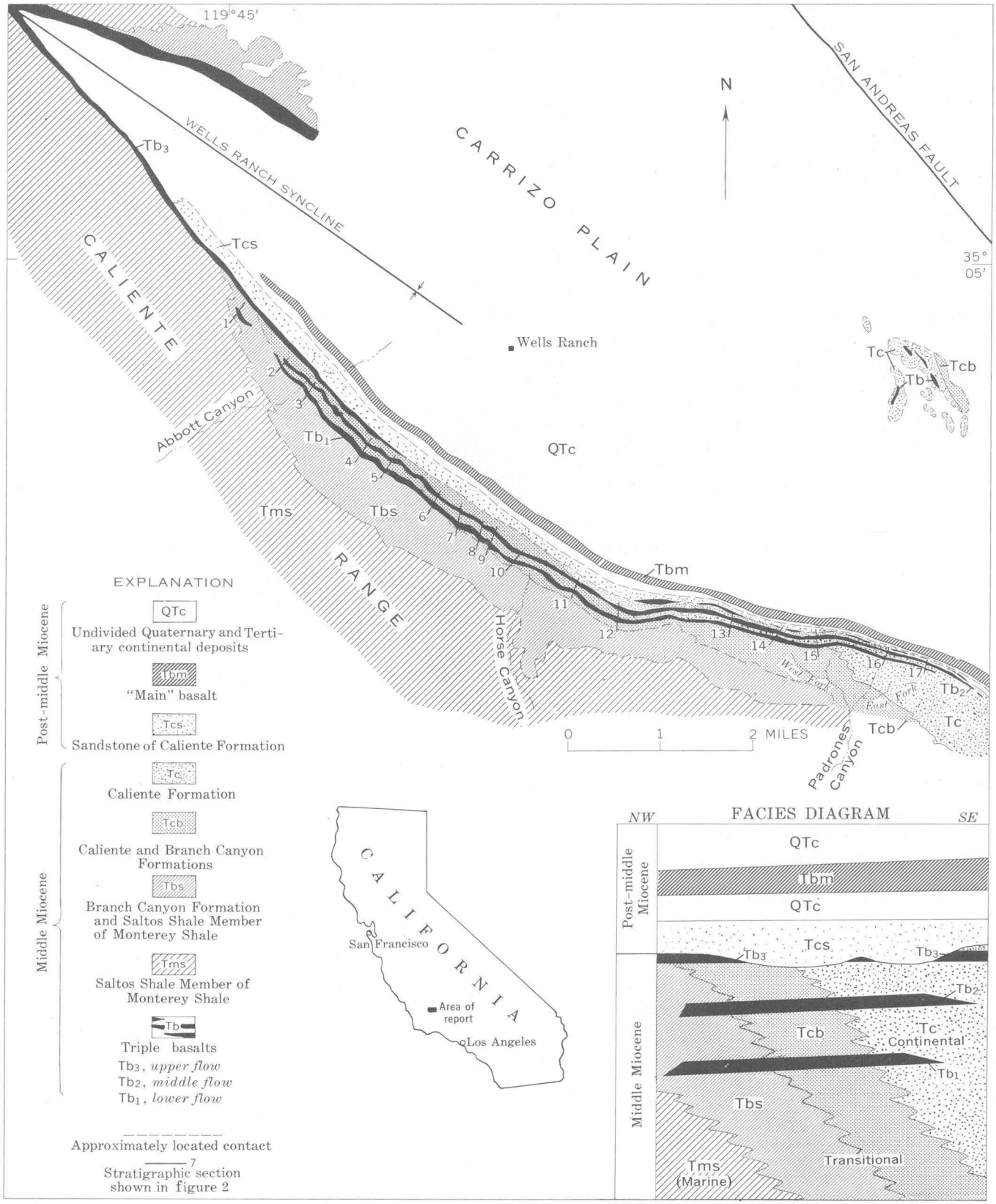

FIGURE 1.—Middle Miocene and post-middle Miocene rocks in the southeastern Caliente Range, Calif. (modified after Vedder and Repenning, 1965). Stratigraphic nomenclature is that of Eaton (1939) and Hill and others (1958).

DISTRIBUTION AND THICKNESS

The middle and lower flows of the Triple basalts extend continuously from the East Fork of Padrones Canyon to the western wall of Abbott Canyon (fig. 1), a distance of more than 8 miles (Eaton, 1939; Vedder and Repenning, 1965). On the southeast, the lower flow pinches out in an area of poor exposures in the East Fork of Padrones Canyon, and the middle flow can be traced with certainty only a short distance farther eastward. On the northwest, the lower flow crops out intermittently nearly a mile northwest of Abbott Canyon (figs. 1 and 2), whereas the middle flow is not present beyond the western slope of the ridge west of Abbott Canyon.

The two flows lie in contact with either the Caliente or Branch Canyon Formations; they are nowhere in contact with the Saltos Shale (fig. 2). In the southeast both flows are enclosed within continental sandstone or mudstone of the Caliente Formation. To the northwest, both are overlain mostly by the Branch Canyon Formation, but whereas the middle flow overlies sandstone of the Branch Canyon Formation, the lower flow rests mostly upon red and green mudstone of the Caliente Formation (fig. 2).

The thicknesses of the flows vary similarly (fig. 2). Both flows are thickest (100–140 ft) near the West Fork of Padrones Canyon, and thin rather abruptly to the southeast. Northwestward, they gradually thin to a minimum of 25–30 feet near section 9; just west of this point the thickness of the flows increases to 60–80 feet and remains nearly constant westward to the vicinity of Abbott Canyon. The thickness of the

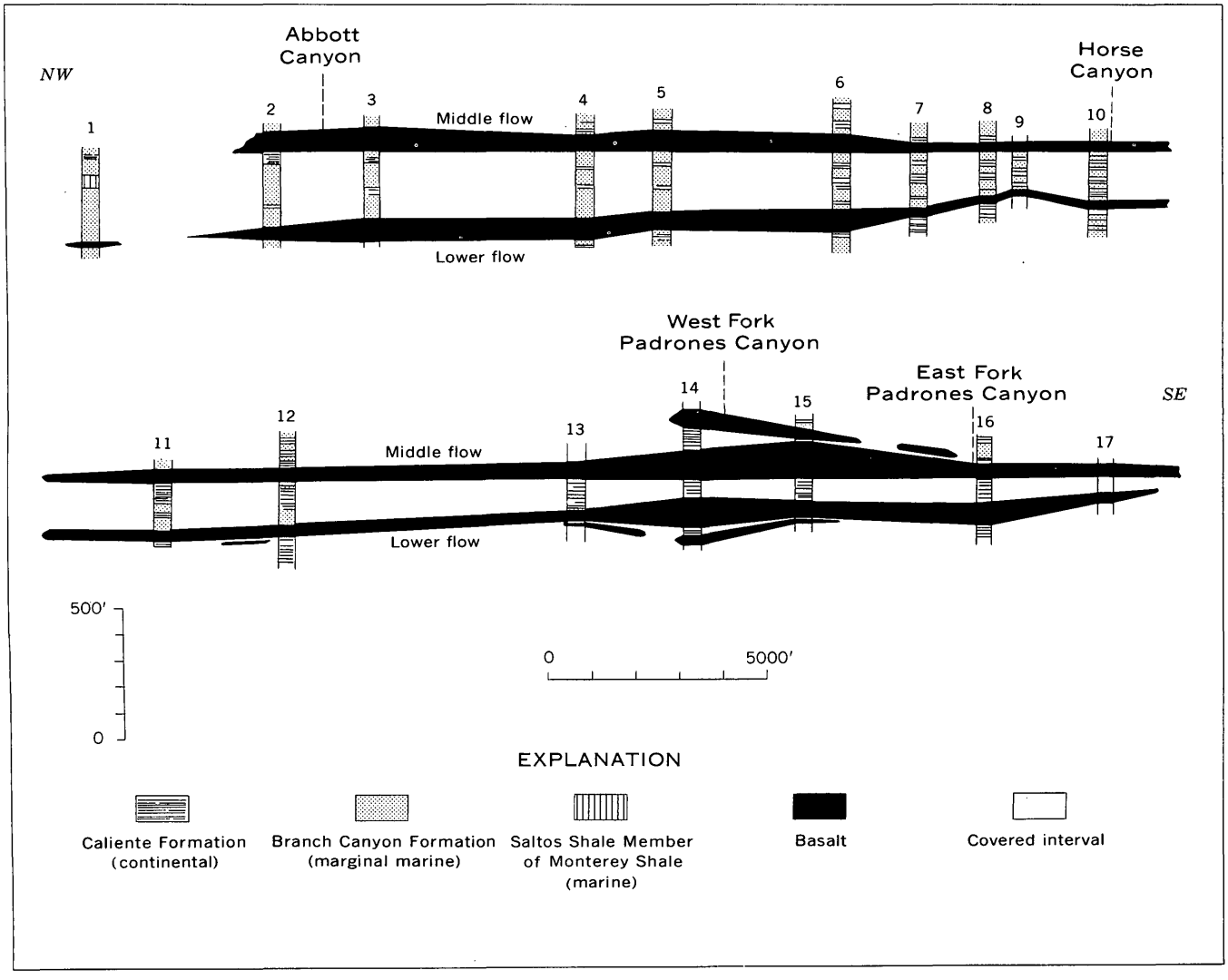

FIGURE 2.—Stratigraphic cross section along the strike of the lower two flows of the Triple basalts of Eaton (1939). Location of numbered stratigraphic sections is shown on figure 1.

sedimentary rocks between the flows follows a somewhat reciprocal pattern, being smallest on the southeast and increasing northwestward, although it, too, decreases locally near section 9.

In the vicinity west of the fork of Padrones Canyon, the flows are accompanied by two less extensive ones (fig. 2, not shown in fig. 1 because of the small map scale). A basalt flow, as much as 40 feet thick, lies beneath the lowest flow of the Triple basalts and is separated from it by a lens of basaltic sandstone. Another flow, as much as 60 feet thick, overlies continental sediments above the middle flow. Both of the smaller flows are discontinuous and of limited extent; the lower one crops out intermittently for nearly 3 miles and the uppermost for more than 1 mile.

In the west fork of Padrones Canyon, basaltic dikes as much as 3 feet thick intrude the sedimentary rocks beneath the Triple basalts. The dikes are nearly vertical and strike north. They are petrographically similar to the flows, and, although not in contact with them, probably are part of the system that fed the flows.

DESCRIPTION

The flows appear from a distance as dark-gray streaks intercalated with cream-colored sandstone beds of the Branch Canyon Formation and pastel mudstones and sandstones of the Caliente Formation. The basalt is relatively resistant to erosion in the southeastern part of the area, but relatively unresistant in the northwestern part.

The flows typically are dark gray and speckled near the top and bottom by white amygdules. The basalt weathers to a monotonous hackly surface which is interrupted by zones as much as 20 feet wide containing resistant basalt spheroids which range from a few inches to several feet in diameter (fig. 3). Except for the spheroidal masses, the outcrops generally are covered with a thin layer of basaltic debris. The flows commonly have a partly stratified aspect resulting from platy partings and alternating layers of different resistance to weathering (fig. 4).

The lower contact of the flows is generally planar, although in a few places the basalt seems to have sunk into the underlying sediment or to have been injected at the base by small amounts of sediment. Such features are analogous to the load casts and flame structures of sedimentary rocks. Where red mudstone underlies the flow, the color of the mudstone is intensified along the contact. In most places where sandstone underlies the flow the uppermost few inches are generally red or purple, but in the northwestern part of the area most of the sandstone under the middle flow is uncolored.

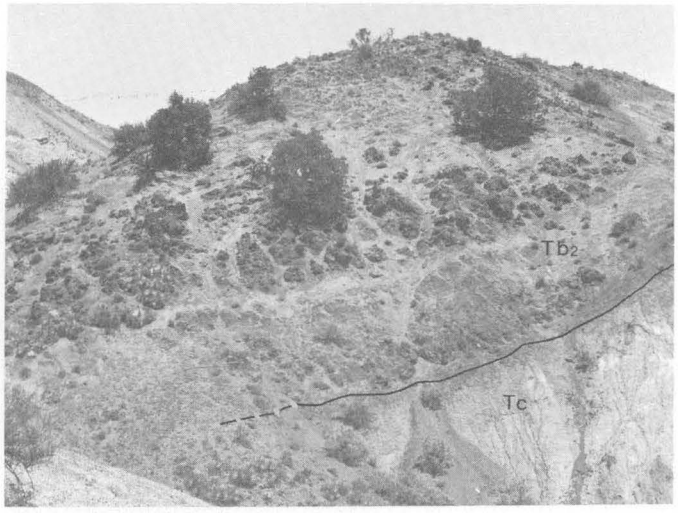

FIGURE 3.—Middle flow of the Triple basalts near section 15 (figs. 1 and 2). Note resistant spheroids in central part of flow. Tb_2, middle basalt flow of the Triple basalts; Tc, Caliente Formation.

The tops of the flows show evidence of erosion. Overlying mudstone contains coarse angular basalt rubble in the lower foot or so. Where sandstone overlies a flow, the rubble is absent and the sandstone lies directly on the flow, filling irregular cracks and pockets. Isolated basalt fragments are common, however, in such sandstone.

COMPOSITION AND TEXTURE

Originally the flows consisted of 5–20 percent euhedral phenocrysts and granules of high-magnesium olivine, 10–15 percent plagioclase phenocrysts (An_{55}-An_{60}), 25–45 percent plagioclase microlites (An_{50}-An_{55}), 0–25 percent titaniferous subcalcic ($2V=30°$–$40°$) augite, 5–10 percent opaque iron-titanium oxides, 0–55 percent dark-brown glass, and 0–10 percent interstitial voids.

The original mineralogy of the flows is considerably altered. A clay mineral of the montmorillonite group in most places forms pseudomorphs after the olivine. Plagioclase commonly is partly to completely altered to celadonite, which also occurs interstitially, probably as a void-filling. The glass is devitrified to a slightly birefringent, very fine grained aggregate. Calcite commonly replaces olivine, plagioclase, and glass near the base of the flows and, particularly, at the western terminus of the middle flow. Augite, in contrast to the other primary minerals, shows no sign of replacement or alteration.

The texture of the basalt depends upon its location within the flow. The texture is hyalophitic at the bottom and top of the flow. Here, devitrified glass encloses small olivine and plagioclase microlites, and augite is absent, as it is wherever the basalt has been

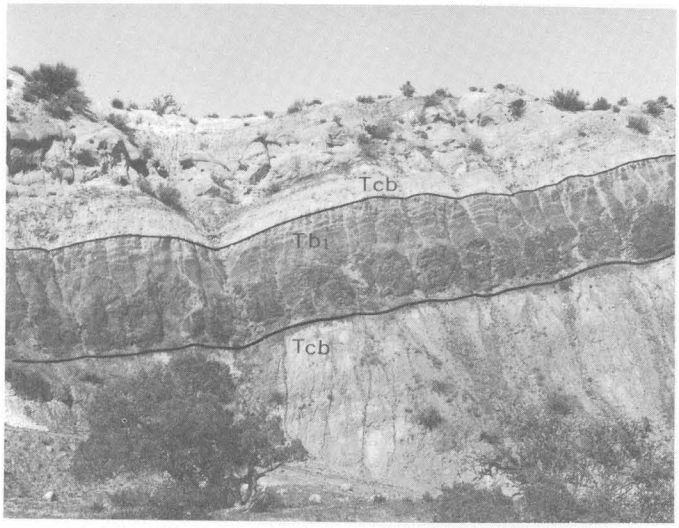

FIGURE 4.—Lower flow of the Triple basalts near section 10 (figs. 1 and 2). Note banding in upper part of flow. Tb_1, basalt flow; Tcb, Caliente and Branch Canyon Formations.

chilled. Augite first occurs as microlites in the basal 6 inches or upper 3 feet of the flow, and increases in abundance within a foot or so toward the center of the flow to form a subophitic or ophitic texture. The distribution of augite—particularly its absence from the chilled basalt at the western end of the middle flow—indicates that it did not begin to crystallize until movement had ceased.

STRUCTURES

The flows contain these primary structures: vesicles, pipe vesicles, contraction joints, indistinct flow banding, and locally, pillows.

Most vesicles now are amygdules consisting of either calcite or montmorillonitic clay minerals, although a few consist of calcite rimmed by radially fibrous clay minerals. Most amygdules are about half an inch across, although some are as much as 2 inches long. Their shapes range from spheroids to irregular knobby masses; knobby amygdules are equally abundant in the tops and bottoms of the flows. In general, the amygdaloidal zones extend for 2 to 3 feet below the top of a flow and for half a foot to 1 foot above the base. Locally, amygdaloidal layers several inches thick also occur in the flow interior, but such layers lack lateral persistence. Some larger cavities, as much as several inches long, are partly filled with drusy quartz or calcite, but they occur only locally.

A few pipe vesicles, vertical tubes half an inch to 1 inch in diameter and as much as several feet long, occur in the lower half of the flows. The tubes are either empty or filled with disintegrated basalt. The tops of the tubes commonly are bent in the direction of flow.

Contraction joints a quarter of an inch to 1 inch wide, filled with a friable mixture of calcite and montmorillonitic clay minerals, are abundant in the lower part of the flows. Most of these joints curve upward randomly and join an anastomosing network of similar joints in the flow interior. Similar fractures in the upper part of the flow tend to parallel the upper flow surface. Basalt in contact with the joints is finer grained than that several inches away, indicating formation of the joints before complete crystallization. The joints are not uniformly deflected from the base, however; therefore, they probably developed after flowage had ceased.

An indistinct horizontal banding appears in the basalt at many places (fig. 4). The banding, which reflects variation in the degree of alteration and weathering of the basalt, results from alternating zones of different resistance that may be due to unequal volatile concentrations in zones of internal shear during flowage.

Well-shaped pillows occur only at the western terminus of the middle flow, and are described in detail later since they relate to the movement of the flow across the strand line. Other structures, similar to poorly defined, possibly incipient, pillows, occur in numerous places near the base of the flows. They are outlined by spheroidal clusters of amygdules or by anastomosing contraction joints. They are probably not pillows, however, for the basalt in the amygdaloidal clusters is texturally similar to the nonvesicular rim; this similarity suggests that internal volatile concentration, not external chilling, caused the structure. Resistant spheroids that are common on exposures of the basalt have a pillowlike appearance but probably are weathering phenomena. They are distinctly less altered than the surrounding rock but show no textural difference.

SOURCE OF FLOWS

Much evidence indicates that both flows originated near the present West Fork of Padrones Canyon (sections 14 and 15, figs. 1 and 2). Here the flows reach their greatest thickness and are associated with small local flows. Nearby subjacent dikes of similar basaltic composition suggest a feeder system. In addition, the partly volcaniclastic rocks between the flows imply nearby volcanism.

A lens of basaltic sandstone as much as 50 feet thick separates the lower flow of the Triple basalts from the thin, local, flow beneath it. More than half of this sandstone consists of altered basalt clasts

ranging in size from fine sand to blocks several inches across. Basalt in sand-size grains is much more glassy and vesicular than in the flows and commonly contains grains of detrital quartz. Nearly all the basaltic grains are intensely oxidized and appear bright red in transmitted light. The grains probably formed while the basalt was still fluid, for many have an opaque, unvesiculated rim that completely envelops them. Moreover, some seem to have been deformed while pliable, because stretched vesicles conform with the shapes of the grains (fig. 5). Olivine phenocrysts, now replaced by a tan clay mineral of low birefringence and refractive index, have "charred," nearly opaque rims which suggest strong oxidation prior to and during eruption. These features indicate that the basaltic grains are lapilli ejected under hot, oxidizing conditions. Their concentration in these beds indicates that the vent was nearby.

The lapilli have been reworked, for they are mixed with a considerable amount of nonvolcanic detritus, and the larger basalt fragments probably were derived from erosion of the lower local flow. Broken oyster shells, probably derived from nearby marine deposits, are scattered through the sandstone, which also has yielded a jaw fragment of a Miocene felid (C. A. Repenning, oral commun., 1965).

A different type of pyroclastic material also occurs in this vicinity. Both the middle and lower flows of the Triple basalts are locally overlain by bentonitic mudstone as much as 2 feet thick. Glass shards in the mudstone, altered to a montmorillonitic clay, attest to its pyroclastic origin. The mudstone also contains vesicular basaltic clasts as much as several inches across that contain much altered basaltic glass. Plagioclase microlites in the glass are much smaller than those in the flows. Chilled rinds enveloping these fragments indicate that they, too, are ejecta, and their presence in a volcanic ash bed suggests direct pyroclastic activity.

In summary, the lower and middle flows of the Triple basalts emanated from a source very near the West Fork of Padrones Canyon. This interpretation differs from that of Eaton and others (1941, p. 225), who surmised that the flows "originated several miles northeast of the present Wells Ranch" (fig. 1).

DIRECTION OF FLOW

Evidence of flow direction (Waters, 1960) is meager. The best indication occurs in the lowermost part of the flows, where amygdules locally are inclined with respect to the flow base. Where oriented, they consistently are elongate in a generally west-southwest direction and plunge toward the east. Such inclination generally is toward the source (Waters, 1960, p. 360) and in this area indicates flowage to the west and southwest (fig. 6), with a hint of fanning from a postulated vent just north of the present West Fork of Padrones Canyon. The only other indication of flow direction, the westward deflection of pipe vesicles (Waters, 1960, p. 358), supports the idea of lava flowage toward the west.

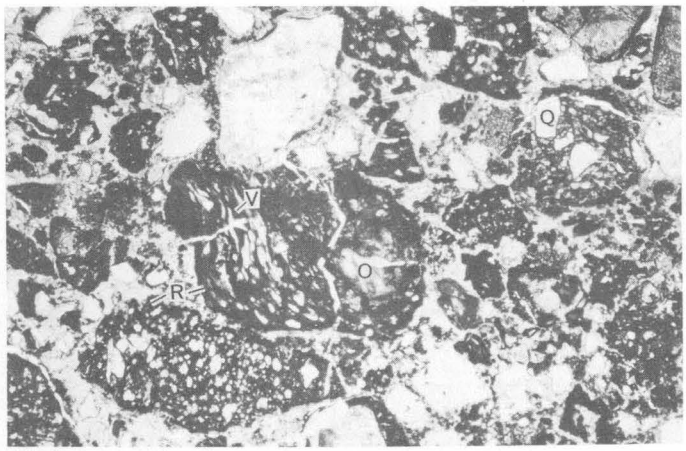

FIGURE 5.—Photomicrograph of basaltic sandstone below the lower flow of the Triple basalts near section 14. Note deformed vehicles (V), detrital quartz in basaltic grains (Q), chilled rim on basaltic grain (R), and opaquely rimmed relict olivine phenocrysts (O). × 25.

Paleocurrent data from a fluviatile sandstone (Tcs on fig. 1) in the upper part of the Caliente Formation substantiate this interpretation of local paleoslope. The sandstone disconformably overlies the middle Miocene strata that contain the basalt flows. It has yielded no diagnostic fossils but grades upward into strata that bear fossil vertebrates of Clarendonian age (Repenning and Vedder, 1961, p. C238). Therefore, the age of the sandstone is probably late Miocene (Mitchell and Repenning, 1963, p. 15; Evernden and others, 1964, fig. 1), and the hiatus separating it from middle Miocene strata is likely minor. Pebble imbrication (fig. 6) in this sandstone as well as a consistent westward decrease in clast size, indicate a paleoslope direction similar to that suggested by the structures in the basalts and establish a local paleoslope toward the west-southwest.

POSITION OF THE STRAND LINE

The lower flow of the Triple basalts lacks pillows or breccia indicative of subaqueous flow and seems everywhere to be subaerial. So, for nearly its full extent, does the middle flow, even though it rests upon sandstone of the Branch Canyon Formation for more than half its length (fig. 2). Near Abbott Canyon, however, the middle flow contains many features that

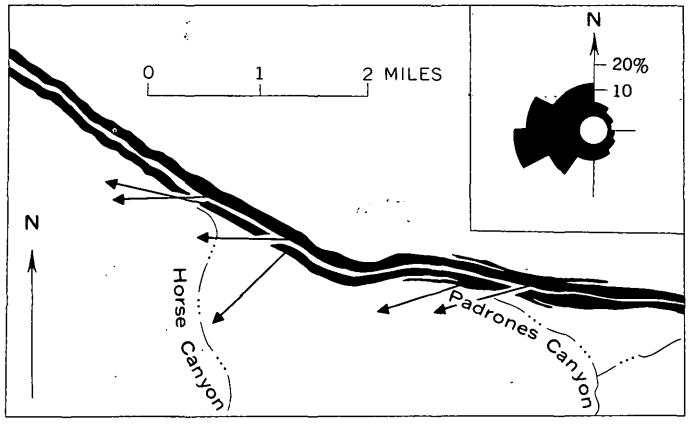

FIGURE 6.—Direction of flow (arrows) of the lower two flows of the Triple basalts as indicated by amygdule orientation. Rose diagram (inset) shows direction of currents that deposited sandstone of the Caliente Formation (Tcs, fig. 1), based on measurements of pebble imbrication in 98 beds.

suggest that it here crossed the strand line (fig. 7): pillows near the bottom and top of the flow, breccia at its base, and numerous geodes as much as 3 inches across that are partly filled with quartz or calcite. The basalt adjacent to the geodes is chilled, indicating that they were large primary cavities, probably formed by expanding steam.

Pillows near the bottom of the middle flow are exposed under a veneer of basaltic debris on the ridgetop west of Abbott Canyon (sec. 2). The pillows are isolated, generally less than a foot across, and flattened parallel to bedding. Many contain a geode or large amygdule in their upper part. Each pillow has a yellowish chilled margin about a quarter of an inch thick. The matrix between the pillows contains much more altered glass than the basalt in the pillow interiors. The matrix may be basalt breccia, but samples sufficiently large to demonstrate fragmentation could not be obtained because of thorough decomposition of the material.

A cluster of pillows also occurs in the upper 8 feet of the flow about 500 feet west of this ridge top, at a point where the flow thickness abruptly decreases toward the west (fig. 2). These pillows, as much as 3 feet in diameter, are larger than those at the base. Individual pillows are separated by an envelope of sandstone, and the basalt in contact with the sandstone is chilled. A few yards west of the pillows, the upper surface of the flow is quite irregular and suggests invasion into loose wet sand, possibly heaped onto the front of the advancing lava.

The flow at this point rests on sandstone that contains impressions of marine mollusks, and the lowermost foot of basalt is brecciated. Westward the basalt continues to thin (fig. 2) and grades laterally from a thin, glassy basalt flow with a brecciated base, through basaltic breccia, into basaltic sandstone. The basaltic sandstone bed, little more than a foot thick, becomes progressively diluted by terrigenous material and can be traced as a distinct bed for only about 100 feet.

In summary, indications of lava passage into the marine environment exist only in the middle flow at its western end. The lava appears to have crossed the strand line at a point near the ridgetop west of Abbott Canyon. Sand-encased pillows at the top of the flow suggest that the flow plowed under wet sand as it advanced into the water.

CONCLUSIONS

The lower and middle flows of the Triple basalts erupted near the West Fork of Padrones Canyon and flowed toward the west-southwest. Directional properties of slightly younger fluviatile sandstone indicate a similar local paleoslope. The depositional strike of sediments deposited in this area during the middle Miocene, which can be considered to be normal to this paleoslope, serves as a base relative to which features of the sediment such as directional structures and facies change can be interpreted. The middle flow crossed the strand line near the terminus of the flow just west of Abbott Canyon; otherwise neither flow

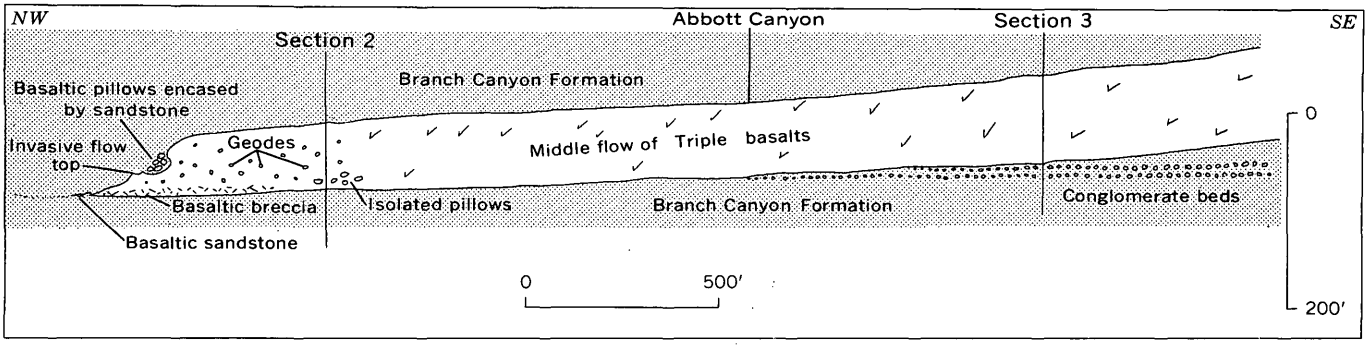

FIGURE 7.—Features at the western end of the middle flow of Eaton's (1939) Triple basalts. For location see figure 1.

shows evidence of having flowed into water. The middle flow extensively overlies sandstone of the Branch Canyon Formation, as does the lower flow locally; much of the marginal marine sandstone of the Branch Canyon Formation is therefore thought to have been subaerially exposed during at least part of middle Miocene time.

REFERENCES

Eaton, J. E., 1939, Geology and oil possibilities of Caliente Range, Cuyama Valley, and Carrizo Plain, California: California Jour. Mines and Geology, v. 35, no. 3, p. 255–274.

Eaton, J. E., Grant, U. S., and Allen, H. B., 1941, Miocene of Caliente Range and environs, California: Am. Assoc. Petroleum Geologists Bull., v. 25, no. 2, p. 193–262.

Evernden, J. F., Savage, D. E., Curtis, G. H., and James, G. T., 1964, Potassium-argon dates and the Cenozoic mammalian chronology of North America: Am. Jour. Sci., v. 262, p. 145–198.

Hill, M. L., Carlson, S. A., and Dibblee, T. W., Jr., 1958, Stratigraphy of Cuyama Valley-Caliente Range area, California: Am. Assoc. Petroleum Geologists Bull., v. 42, no. 12, p. 2973–3000.

Mitchell, E. D., Jr., and Repenning, C. A., 1963, The chronologic and geographic range of desmostylians: Los Angeles County Museum Contr. in Sci., no. 78, 20 p.

Repenning, C. A., and Vedder, J. G., 1961, Continental vertebrates and their stratigraphic correlation with marine mollusks, eastern Caliente Range, California: Art. 235 *in* U.S. Geol. Survey Prof. Paper 424–C, p. C235–C239.

Vedder, J. G., and Repenning, C. A., 1965, Geologic map of the southeastern Caliente Range, San Luis Obispo County, California: U.S. Geol. Survey Oil and Gas Inv. Map OM–217, scale 1:24,000.

Waters, A. C., 1960, Determining direction of flow in basalts: Am. Jour. Sci., v. 258–A (Bradley Volume), p. 350–366.

MICROFOSSIL EVIDENCE FOR CORRELATION OF PALEOCENE STRATA IN BALLARD COUNTY, KENTUCKY, WITH THE LOWER PART OF THE PORTERS CREEK CLAY

By S. M. HERRICK and ROBERT H. TSCHUDY, Atlanta, Ga., Denver, Colo.

Work done in cooperation with the Kentucky Geological Survey

Abstract.—Foraminiferal and palynological evidence suggests an early Porters Creek age for deposits in northern Ballard County, Ky. Comparison with microfaunas described from localities in the Gulf Coast and Mississippi embayment regions indicates an horizon above the Clayton and in the basal part of the Porters Creek that is equivalent to Plummer's "transition zone" (Paleocene of Texas) and to Kellough's *Polymorphina cushmani* zonule in the basal part of the Wills Point Formation (Paleocene of Texas).

The purpose of this paper is (1) to record the presence of certain Foraminifera and palynomorphs (pollen, spores, acritarchs, and dinoflagellates) from an exposure in northern Ballard County, Ky., (2) comparing these Foraminifera and palynomorphs with previously described assemblages from other parts of the Gulf Coast and the Mississippi embayment region, and (3) to suggest the nature of the environment under which the sediments yielding these fossils were deposited.

Two samples were collected by W. W. Olive, of the U.S. Geological Survey, in Ballard County, Ky., from an exposure of Paleocene deposits on the bank of the Ohio River (fig. 1), 0.5 mile below the landing at Olmsted, Ill. (Kentucky coordinates S1,030,700–323,120). Sample Od–2, taken from an altitude of 295 feet, was a dark-greenish-gray, silty, micaceous, sparsely glauconitic clay that yielded palynomorphs. Sample Od–1, taken from an altitude of 286 feet, was much sandier and more abundantly glauconitic and phosphatic, and it yielded both Foraminifera and palynomorphs. Other fossils observed in the samples were some unidentified fish teeth. U.S. Geological Survey paleobotanical locality numbers D–3691 and D–3692 were assigned to samples Od–2 and Od–1, respectively.

C. L. Cooper apparently was the first to publish on the Foraminifera from the northern part of the Mississippi embayment. Cooper (1944) described and illustrated a fauna derived from cuttings from a well drilled in 1938 near Cache, Alexander County, Ill. These fossils, with some taxonomic changes by the authors, are listed under locality 2 in table 1. On the basis of the species identified from these well cuttings, Cooper concluded that this fauna was of Porters Creek age.

Pryor and Ross (1962, p. 24) assigned an 18-foot clay bed of a measured geologic section in Pulaski County, in southern Illinois, to the Clayton Formation on the basis of the foraminifer, *Globigerinoides daubjergensis*. However, this fossil occurs throughout the Paleocene of the Atlantic and Gulf Coasts (Loeblich and Tappan, 1957, p. 185); consequently, it is not diagnostic of the lower unit (Clayton or Kincaid) of the Paleocene of North America. Pryor and Ross noted that material from about 4 to 11 inches from the base of the 18-foot clay bed was very sandy. On the basis of field evidence, W. W. Olive (written commun., 1965) considers this basal sandy horizon of Pryor and Ross to be the probable equivalent of a 4-foot fossiliferous sandy clay containing the 286-foot horizon herein discussed.

Browne and Herrick (1963) described and illustrated a Paleocene foraminiferal fauna from an outcrop near Reidland, McCracken County, Ky., and concluded that this fauna was of probable Porters Creek age.

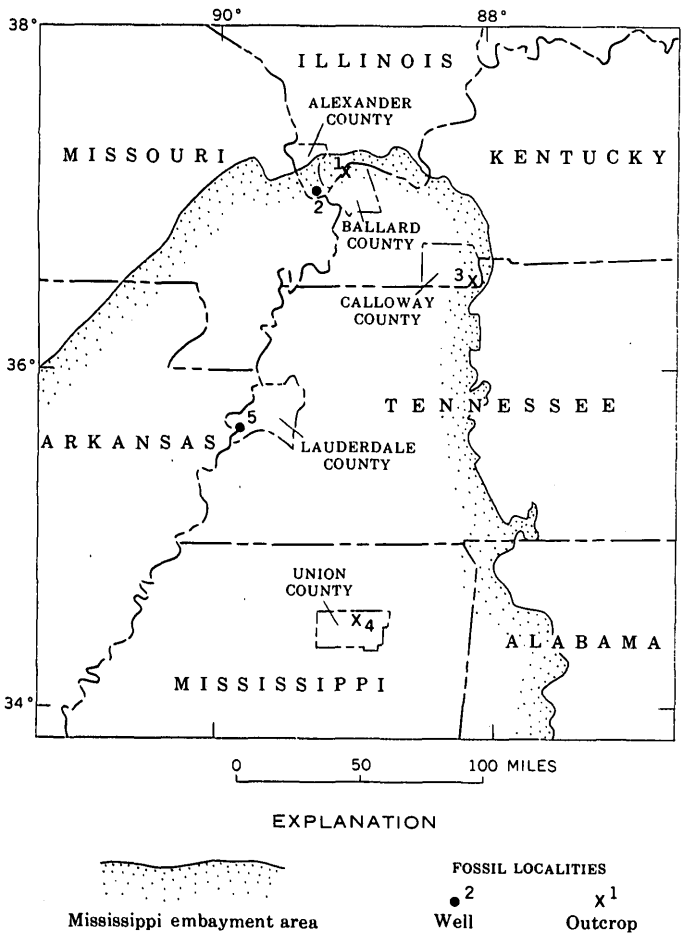

FIGURE 1.—Location of fossil localities referred to in text.

Although there is almost a complete lack of published information on palynology of Paleocene rocks of the Mississippi embayment region, an exception is a paper by Jones (1962) in which some of the palynological characteristics of the Porters Creek Clay and the Wilcox Group in south-central Arkansas are discussed. In a 70-foot Porters Creek sequence, Jones found taxodiaceous pollen to be the dominant form present. He reported also the presence of the genus *Aquilapollenites*. This genus, until recently, had not been found in rocks of the northeastern part of the embayment. Jones noted the similarity of some of his fossils to Paleocene fossils from other regions, but no closer age determinations were drawn.

AGE IMPLICATIONS

Foraminifera

In using Foraminifera as age indicators, known ranges for the individual species are usually satisfactory in an analysis of this kind. In this paper, the Foraminifera listed in table 1 were compared with the same species as previously reported by Plummer (1926). The Foraminifera from the 286-foot horizon of locality 1 were considerably leached but were sufficiently well preserved to permit identification of approximately 45 species.

With the exception of *Vaginulina gracilis*, which according to Plummer (1926, p. 23-24) characterizes the lower part (Kincaid) of the Paleocene in Texas, the species listed in table 1 are of Porters Creek age.

TABLE 1.—*Paleocene Foraminifera from Kentucky and Illinois*

	Locality 1 [1] (Ballard County, Ky.)	Locality 2 [2] (Alexander County, Ill.)
Clavulinoides midwayensis Cushman	X	
Robulus degolyeri (Plummer)	X	
R. inornatus (d'Orbigny)		X
R. magnificus Toulmin		X
R. midwayensis (Plummer)	X	X
R. pseudomamilligerus (Plummer)	X	
Marginulina earlandi (Plummer)	X	
Dentalina aculeata d'Orbigny	X	
D. colei Cushman and Dusenbury		X
D. delicatula Cushman	X	
D. pauperata d'Orbigny		X
D. plummerae Cushman	X	
D. vertebralis (Batsch) var. *albatrossi*? (Cushman)	X	
Nodosaria affinis Reuss	X	X
N. latejugata Gümbel	X	X
N. ? cf. *N. longiscata* d'Orbigny	X	
N. ? *spinocostata* Cooper	X	X
Chrysalgonium eocenicum Cushman and Todd	X	
C. granti (Plummer)	X	X
Pseudonodosaria laevigata (d'Orbigny) var. *occidentalis* Cushman	X	
Vaginulina gracilis Plummer	X	X
V. midwayana Fox and Ross	X	X
Lagena laevis (Montagu)		X
Guttulina problema d'Orbigny	X	X
Globulina gibba d'Orbigny	X	
Polymorphina cushmani Plummer	X	X
P. subrhombica Reuss	X	
Bullopora ? *laevis* (Sollas)	X	
Spirobolivina scanica (Brötzen)	X	
Rectoguembelina alabamensis Cushman		X
Siphogenerinoides eleganta (Plummer)	X	X
Buliminella elegantissima (d'Orbigny)	X	
B. cacumenata Cushman and Parker	X	
Bolivina midwayensis Cushman	X	
Pleurostomella paleocenica Cushman	X	
Stilosomella midwayensis (Cushman and Todd)	X	X
S. paleocenica (Cushman and Todd)	X	X
S. plummerae (Cushman)	X	X
Gyroidinoides aequilateralis (Plummer)	X	
Eponides plummerae Cushman	X	
Pulsiphonina prima (Plummer)	X	X
Epistominella cf. *E. vitrea* Parker [3]	X	
Alabamina wilcoxensis Toulmin	X	X
Pullenia quinqueloba (Reuss) var. *angusta* Cushman and Todd	X	
Globigerina triloculinoides Plummer	X	X
Globigerinoides daubjergensis (Bronnimann)	X	
Globorotalia compressa (Plummer)	X	X
Anomalinoides acuta (Plummer)	X	X
A. midwayensis (Plummer)	X	X
Cibicides vulgaris (Plummer)	X	X
Cibicidoides alleni (Plummer)		X

[1] Identified by S. M. Herrick, (this paper); sample Od-1 (286-foot level).
[2] Identified by Cooper (1944, pls. 54, 55), with some taxonomic changes (this paper).
[3] Identified by Ruth Todd (this paper), U.S. Geological Survey, Washington, D.C.

Elsewhere in the Mississippi embayment these species occur in the upper and lower units of the Midway Group, are confined to the upper unit of the Midway, or occur in formations that are geologically younger than Midway. Of the species listed in table 1, four are considered here as significant indicators of the geologic age of these deposits. These include *Robulus pseudomamilligerous*, *Polymorphina cushmani*, *Cibicides vulgaris*, and *Cibicidoides alleni*. All four are regarded by Plummer (1926, p. 98, 125, 145) as indicative of the "transition zone," an horizon she places between the upper (Wills Point Formation) and lower (Kincaid Formation) units of the Texas Paleocene. Kellough (1959, fig. 7) gives the Foraminifera composing this unique fauna the name "*Polymorphina cushmani* zonule" and places it in the basal part of the Wills Point of the Paleocene section as exposed along Tehuacana Creek, Limestone County, Tex.

The three species, *Vaginulina gracilis*, *Nodosaria ? spinocostrata*, and *Epistominella* cf. *E. vitrea* probably should be added to this group. Regarding *V. gracilis* as an indicator of her "transition zone," Plummer (1926, p. 111) states, "In the areas where a narrow zone of transition lies between the basal and upper beds, *V. gracilis* dies out through these few feet of section as the upper form, *V. midwayana* becomes more and more abundant . . ." In the 286-foot horizon *V. gracilis* occus rarely, whereas *V. midwayana* is rather numerous—a condition similar to that reported by Plummer (1926, p. 21, 111) in the region north and northeast of the Mexia area, Texas, where this faunal transition prevails in the Texas Paleocene section. *Nodosaria ? spinocostrata*, its stratigraphic range yet to be established, was described by Cooper (1944, p. 349) as a new species. This species may represent a variant of *Stilostomella midwayensis*. However, until appropriate comparisons have been made, this species is here regarded as distinct and as a possible indicator of early Porters Creek age in the northern part of the embayment. *Epistominella vitrea* was described by Haynes (1956, p. 88) from the upper Paleocene (Thanet beds) of East Kent, England. Its presence in the "transition zone" of the Paleocene sequence in Ballard County, Ky., is interesting, though its stratigraphic significance in this part of the embayment remains to be determined. On the basis of this foraminiferal comparison, the age of the 286-foot horizon in Ballard County, Ky., is early Porters Creek.

Plant fossils

So that the fossil pollen and spores in the two Ballard County samples similarly might be used for correlation purposes, the U.S. Geological Survey palynological laboratory in Denver, Colo., determined the microfloral content of "control" samples collected from well-dated sections of the Clayton Formation and of the Porters Creek Clay.

The control samples of the Clayton were collected in the S½NW¼ sec. 8, T. 6 S., R 3 E., from an exposure in the southwest wall of a tributary to Guyton Creek in Union County, Miss. This exposure, which is shown as locality 4 in figure 1, is along a county road 1.5 miles south-southwest of the town of Cotton Plant and is in an area mapped geologically by Conant (1942) as Clayton. The samples yielding abundant and well-preserved microfossils were given U.S. Geological Survey paleobotanical location numbers D1966A, B, C, and F.

Although sampled in several places, the Porters Creek Clay generally yielded only a few very small palynomorphs or only finely divided organic remains. However, a sample (OHA–2) suitable for use as a control was obtained from the channel of McCollough Fork, 300 feet north of the Kentucky-Tennessee State line, Hazel quadrangle, Calloway County, Ky. (Kentucky coordinates S1,263,500–70,250). This sample was given U.S. Geological Survey paleobotanical locality number D–3285, and the site of collection is shown on figure 1 as locality 3.

Table 2 lists the percentage occurrence of groups of plant microfossils in the Clayton and Porters Creek control samples and in the two samples from the Ballard County exposure (D–3691, D–3692). The Ballard County samples contained corroded but nevertheless easily recognizable pollen grains and a few spores intermixed with well-preserved marine dinoflagellates and acritarchs. These assemblages were in contrast to the assemblages from Clayton control samples which yielded, in addition, an abundance of bisaccate conifer pollen that is poorly represented in the Ballard County samples.

As shown in table 2, the percentage of several microfossil groups in the control samples from the Clayton Formation and Porters Creek Clay differed markedly. Compared to the sample from the Porters Creek, the composited sample from the Clayton contained much smaller percentages of monosulcate, tricolpate, and tricolporate pollen and much larger percentages of bisaccate conifer and taxodiaceous pollen. Moreover, the composited sample from the Clayton contained 160 code species,[1] whereas the Porters Creek control sample and the two Ballard County samples together contained 106. Only 4 of the code

[1] Many of the species have not been named formally. For the present both those named and not named have been given temporary code designations and a "type" specimen of each has been placed on file in the U.S. Geological Survey paleobotanical laboratory in Denver, Colo.

TABLE 2.—*Comparison of percentages of total pollen and spores found in control samples and in samples from Ballard County, Ky.*

[Percentages computed from specimen counts by R. H. Tschudy, U.S. Geological Survey]

Plant microfossil groups	Locality 4 (Union County, Miss.)	Locality 3 (Calloway County, Ky.)	Locality 1 (Ballard County, Ky.)	
	Clayton Formation control samples composited	Porters Creek Clay control sample	Od-1 (286-ft altitude)	Od-2 (295-ft altitude)
	D1966	D3285	D3692	D3691
Monolete spores	1.2			
Trilete spores	3.9	2.0	3.5	1.5
Monosulcate pollen	5.4	12.0	13.0	8.5
Triporate pollen	37.4	33.0	35.5	42.0
Arcoid triporate pollen	1.5	2.0	3.5	.5
Tricolpate pollen	9.2	22.5	17.0	14.5
Tricolporate pollen	9.7	17.0	15.0	16.5
Brevitricolporate pollen	1.9	.5	.5	.5
Bisaccate conifer pollen	15.0	1.5	2.5	2.0
Taxodiaceous pollen	6.0	3.0	3.0	2.5
Other pollen and spores	8.8	6.5	6.5	11.5
	100.0	100.0	100.0	100.0
Total count exclusive of dinoflagellates and acritarchs	600	400	200	200

species found in the Porters Creek samples were not found in the Clayton, and more than 50 code species found in the Clayton were not found in the Porters Creek. Furthermore, the 4 samples from the Clayton contained an average of 66 code species, the single sample from the Porters Creek contained 54, and of the two Ballard County samples one contained 54 and the other 41. Thus the available evidence indicates a decline in the number of different species living in the Mississippi embayment area from Clayton to Porters Creek time. This decline accords with other evidence that a decrease in the number of plant species in the embayment area began with the end of the Cretaceous and continued through the Paleocene.

Recently, a sidewall core sample was obtained from the upper part of the Porters Creek sequence in a hole drilled for the U.S. Geological Survey in Lauderdale County, Tenn., (locality 5, fig. 1). The Porters Creek sequence, according to the authors' interpretation of the electric log, extends from depths of about 1,720 feet to about 2,350 feet. The sidewall core sample, which was from a silty layer at a depth of 1,803 feet, yielded, specimens of *Thomsonipollis* and *Aquilapollenites*. The former is present in the upper Paleocene Naborton Formation of Louisiana and commonly is found in samples of upper Paleocene and lower Eocene sediments in the northern part of the embayment region. *Aquilapollenites* previously had been reported by Jones (1962) from the Porters Creek of Arkansas. This genus occurs commonly in Upper Cretaceous rocks of the Rocky Mountain region, but has not been found in the Cretaceous or lower Tertiary rocks of the Mississippi embayment region other than from these two localities. It appears unlikely that specimens of *Aquilapollenites* from the 1,803-foot level in the Lauderdale County well were redeposited. Several clumps made up of dozens of specimens were found, indicating deposition of whole anthers rather than disseminated pollen grains. During redeposition these anthers certainly would have been broken apart. The presence of *Aquilapollenites* in Jones' (1962) Porters Creek material suggests that his samples were from the upper part of the Porters Creek Clay.

The samples from the Ballard County exposure clearly pertain to the Porters Creek rather than to the Clayton, and the absence of late Paleocene genera such as *Aquilapollenites* and *Thomsonipollis* point to a lower Porters Creek stratigraphic position. The foraminiferal evidence obtained from the 286-foot level not only confirms this hypothesis but also provides a tie with Plummer's "transition zone" between the Kincaid and Wills Point Formation of the Paleocene of Texas.

ENVIRONMENT OF DEPOSITION

From the Foraminifera and lithology of the 286-foot horizon, the ecologic environment under which this material was deposited doubtlessly involved a rather warm, shallow-water shelf or epeiric sea. This is deduced from the sandy nature of the clay containing the Foraminifera as well as by the relative scarcity of pelagic Foraminifera, the latter as noted by Plummer (1926, p. 12) and substantiated by the foraminiferal species listed in table 1.

In addition to the Porters Creek Clay samples discussed herein, at least 10 other Porters Creek Clay samples from the northern embayment region have been examined. These yielded only finely divided organic fragments and a few small pollen grains. All the organic matter was nearly the same size, ranging from about 5 to about 20 microns in diameter. This suggests winnowing, and deposition of the small-sized organic fraction along with clay at a distance from the margins of the basin. The three Porters Creek samples reported herein all yielded good suites of plant microfossils, although many were somewhat corroded. Large-sized spores and pollen were few but conspicuous by their scarcity. This, with the sandy nature of the clay, suggests a nearer shore deposition

site than that of the more winnowed nearly barren other Porters Creek samples.

The presence in both the Clayton and Porters Creek samples of acritarchs and dinoflagellates indigenous to a marine basin indicates marine deposition. Large-sized and abundant pollen and spores in Clayton samples indicate nearshore deposition. With the exception of the sidewall core sample from the Lauderdale County well (which yielded no marine forms), the Porters Creek samples yielded a larger number and higher proportion of marine forms than did the Clayton.

CONCLUSIONS

Correlation of the Ballard County exposure with the Porters Creek Clay rather than with the Clayton Formation is indicated by both the foraminiferal and palynological assemblages. Furthermore, correlation with Plummer's "transition zone" between the Kincaid and Wills Point Formations and with Kellough's *Polymorphina cushmani* zonule in the basal Wills Point of the Texas Paleocene is based on foraminiferal similarities. The lack of upper Paleocene genera such as *Aquilapollenites* and *Thomsonipollis* in the Ballard County exposure indicates correlation with the lower and not the upper part of the Porters Creek. The sandiness and the relative scarcity of pelagic Foraminifera at the 286-foot horizon of the Ballard County exposure suggest that the depositional environment was a shallow-water, shelf epeiric sea.

REFERENCES

Browne, R. G., and Herrick, S. M., 1963, Smaller Paleocene Foraminifera from Reidland, Kentucky: Bull. Am. Paleontology, v. 46, no. 210, p. 247–284, pls. 53–57, 2 figs.

Conant, L. C., 1942, Union County mineral resources: Mississippi Geol. Survey Bull. 45, 158 p.

Cooper, C. L., 1944, Smaller Foraminifera from the Porters Creek Formation (Paleocene) of Illinois: Jour. Paleontology, v. 18, no. 4, p. 343–354, pls. 54, 55, 2 figs.

Haynes, J., 1956, Certain smaller British Paleocene Foraminifera: Cushman Lab. Foraminifera Research Contr., v. 7, pt. 3, p. 79–101, 2 figs., pls. 16–18.

Jones, E .L., 1962, Palynology of the Midway-Wilcox boundary in south-central Arkansas: Gulf Coast Assoc. Geol. Socs. Trans., v. 12, p. 285–294.

Kellough, G. R., 1959, Biostratigraphic and paleoecologic study of Midway Foraminifera along Tehuacana Creek, Limestone County, Texas: Gulf Coast Assoc. Geol. Socs., Trans., v. 9, p. 147–160, 10 figs. 1 pl.

Loeblich, A. R., and Tappan, Helen, 1957, Planktonic Foraminifera of Paleocene and early Eocene age from the Gulf and Atlantic Coastal Plains: U.S. Natl. Museum Bull. 215, p. 173–198, 2 figs., pls. 40, 41, 44–51, 55–58, 60, 61, 64.

Plummer, H. J., 1926, Foraminifera of the Midway Formation in Texas: Texas Univ. Bull. 2644, 206 p., 15 pls., 13 figs.

Pryor, W. A., and Ross, C. A., 1962, Geology of the Illinois parts of the Cairo, LaCenter, and Thebes quadrangles: Illinois Geol. Survey Circ. 332, p. 1–39, 8 figs., 16 tables.

PALYNOLOGICAL EVIDENCE FOR DEVONIAN AGE OF THE NATION RIVER FORMATION, EAST-CENTRAL ALASKA

By RICHARD A. SCOTT and L. IMOGENE DOHER, Denver, Colo.

Abstract.—The Nation River Formation of Alaska has been considered to be of Pennsylvanian or Early Permian age. Fossil spores from the upper part of the formation at its type area show that it is not as young as Pennsylvanian and that it is most probably Late Devonian in age.

The term Nation River Formation was applied by Mertie (1930, p. 113) to a portion of the rocks along and near the Yukon River originally called the Nation River series by Brooks and Kindle (1908, p. 294). Mertie (1930) considered the Nation River Formation to be of Pennsylvanian age despite a tentative assignment of Late Devonian or Early Mississippian age made by David White (*in* Mertie, 1930) on the basis of poorly preserved plant megafossils. Churkin and Brabb (1965) assigned a Late Devonian age to the Nation River Formation, partly on the basis of plant spores identified by Scott.

Laudon and others (1966) have questioned on nonpaleontological grounds the assignment of the Nation River Formation to the Late Devonian rather than to the Pennsylvanian or Early Permian. They consider that serious structural and stratigraphic problems are raised if this formation is of Devonian age. Some of the geologic problems will be discussed elsewhere by Brabb; the evidence furnished by plant spores regarding the age of the Nation River Formation is summarized here.

Several samples collected by Earl E. Brabb and Michael Churkin, Jr. from the Nation River Formation have yielded spores. In this preliminary report, material from only three samples is considered; these are from near the top of the Nation River Formation in its type area opposite the mouth of the Nation River, about 175 miles east of Fairbanks (fig. 1). These samples are from a locality designated by USGS paleobotany locality numbers D1940A, B, and C. The locality is in the Charley River A–2 quadrangle, NW¼ sec. 17, T. 4 N., R. 30 E., lat 65°10.8′ N., long 141°41.8′ W. Sample 1940C is from the top few inches of the Nation River Formation of Mertie (1930), Brabb and Churkin (1964), and Churkin and Brabb (1965); samples D1940A and B are from the upper 75 feet of the formation. These samples occur in the upper part of the "Permian" section of Laudon and others (1966, fig. 5). No significant differences were observed in the spore content of the three samples, which are from the youngest beds in the formation.

Forms included in more than 20 genera of spores have been recognized thus far in the 3 samples studied, despite certain deficiencies in preservation. Most of these genera are listed in table 1 and illustrated in part in figures 2 and 3. The outstanding feature of this spore assemblage from the Nation River Formation is the presence of spores with prominent spines

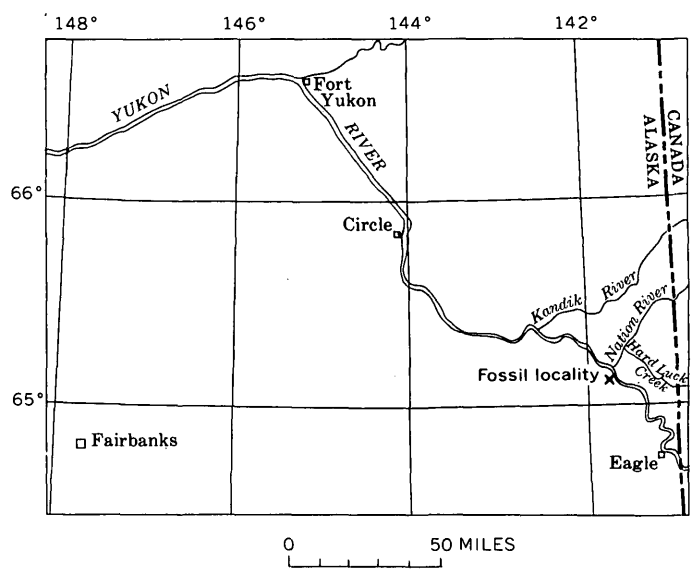

FIGURE 1.—Location of spore-bearing beds in the Nation River Formation, east-central Alaska.

having bifurcate tips. The spores include several species assignable to the genera *Hystricosporites* McGregor and *Ancyrospora* Richardson (fig. 2*e*, *f*). These spores with anchor-shaped processes are common in the assemblage.

TABLE 1.—*Partial list of spore genera from the Nation River Formation*

Acanthotriletes (Naumova) Potonié and Kremp 1954
Ancyrospora Richardson 1960
Archaeoperisaccus Naumova 1953
Archaeozonotriletes (Naumova) Allen 1965
Auroraspora Hoffmeister, Staplin, and Malloy 1955
Calamospora Schopf, Wilson, and Bentall 1944
Camptozonotriletes Staplin 1960
Convolutispora Hoffmeister, Staplin, and Malloy 1955
Corystisporites Richardson 1965
Cristatisporites Potonié and Kremp 1954
Diaphanospora Balmé and Hassell 1962
Foveosporites Balmé 1957
Hymenozonotriletes Naumova 1953
Hystricosporites McGregor 1960
Leiotriletes (Naumova) Potonié and Kremp 1954
Leiozonotriletes Hacquebard 1957
Lophozonotriletes (Naumova) Potonié and Kremp 1954
Lycospora (Schopf, Wilson, and Bentall) Potonié and Kremp 1954
Pustulatisporites (Potonié and Kremp) Imgrund 1960
Raistrickia (Schopf, Wilson, and Bentall) Potonié and Kremp 1954
Retusotriletes (Naumova) Richardson 1965.
Samarisporites Richardson 1965

The occurrence of spores with bifurcate spines is a consistent feature of Middle and Late Devonian spore assemblages from widely distributed areas. They are known, for example, from Australia (Balmé and Hassell, 1962), Scotland (Richardson, 1962), Spitsbergen (Allen, 1965), Russia (see Richardson, 1965, p. 595), Canada (McGregor and Owens, 1966), and Ohio (Winslow, 1962).

The common occurrence of spores with bifurcate spines in the Nation River Formation is well substantiated evidence that the formation cannot be as young as Pennsylvanian or Early Permian, as suggested by Laudon and others (1966), unless the contained spore assemblage was eroded from Devonian rocks and redeposited with the Nation River sediments. That this is unlikely is shown by the large number of other genera (table 1), all consistent with a pre-Pennsylvanian age, that are present with the spores having bifurcated spines. No spores belonging to taxa limited to strata younger than Devonian were found in the samples; no evidence for reworking was seen.

Preliminary comparison of the Nation River spores with published assemblages indicates that the Nation River Formation is most probably of Late Devonian age rather than Middle Devonian or Early Mississippian. The number and variety of spores with bifurcated spines from the Nation River Formation is characteristic of Middle and Late Devonian rather than Mississippian assemblages. In the few instances where these spores range into the Mississippian (Playford, 1962; Winslow, 1962) they typically are limited in variety and number, bearing out the observation of Richardson (1965) that spores with bifurcate processes show a rapid decline in importance in the Lower Carboniferous. Despite some obvious similarities, such as the presence in the Nation River assemblage of *Pustulatisporites pretiosus* Playford (fig. 2*b*), described from the Mississippian Horton Group of Canada (Playford, 1963, p. 19), clear differences exist between the Alaskan assemblage and those from the Horton Group. Significant compositional differences also exist between the Nation River spores and the Lower Carboniferous assemblages described by Playford (1962, 1963) from Spitsbergen.

Comparison of the Nation River assemblage has been facilitated by the recent publication of illustrations of Devonian spores of eastern and northern Canada by McGregor and Owens (1966). They show from the Upper Devonian of northern Canada a variety of types of *Hystricosporites* and *Ancyrospora*, genera with bifurcate spines, comparable to the variety found in the Nation River Formation. A species of *Archaeoperisaccus* Naumova, cf. *A. timanicus* Pashkevich (McGregor and Owens, 1966, pl. 18, figs. 4, 5), from the Griper Bay Formation (Frasnian) on Melville Island, appears identical with a species of *Archaeoperisaccus* in the Nation River Formation (fig. 3*l*). *Foveosporites pertusus* Vigran is present among the spores from the Nation River Formation (fig. 3*f*). McGregor and Owens figure (1966, pl. 27, fig. 1) a similar spore from the Griper Bay Formation which they designate as *?Foveosporites pertusus* Vigran. Although there are some differences, these and other similarities suggest relationships with the Late Devonian assemblages from Canada for the Nation River spores.

Some of the Nation River spore genera are also represented in the Middle Devonian of Scotland (Richardson, 1965), where the proliferation of spores with bifurcated tips is notable. One genus, *Corystisporites* Richardson, based on material from the

FIGURE 2.—Spores from the Nation River Formation, east-central Alaska. *a–c*, × 500; *d–h*, × 250. Numbers are USGS paleobotany locality and slide numbers.

a. *Acanthotriletes* sp. Locality D1940A, slide 26.
b. *Pustulatisporites pretiosus* Playford. D1940A, slide 21.
c. *Cristatisporites* sp. D1940A, slide 21.
d. *Hymenozonotriletes* sp. D1940C, slide 20.
e. *Hystricosporites* sp. D1940C, slide 20.
f. *Ancyrospora* sp. D1940A, slide 21.
g. *Auroraspora macromanifestus* (Hacquebard) Richardson. D1940C, slide 20.
h. Unidentified megaspore. D1940A, slide 21.

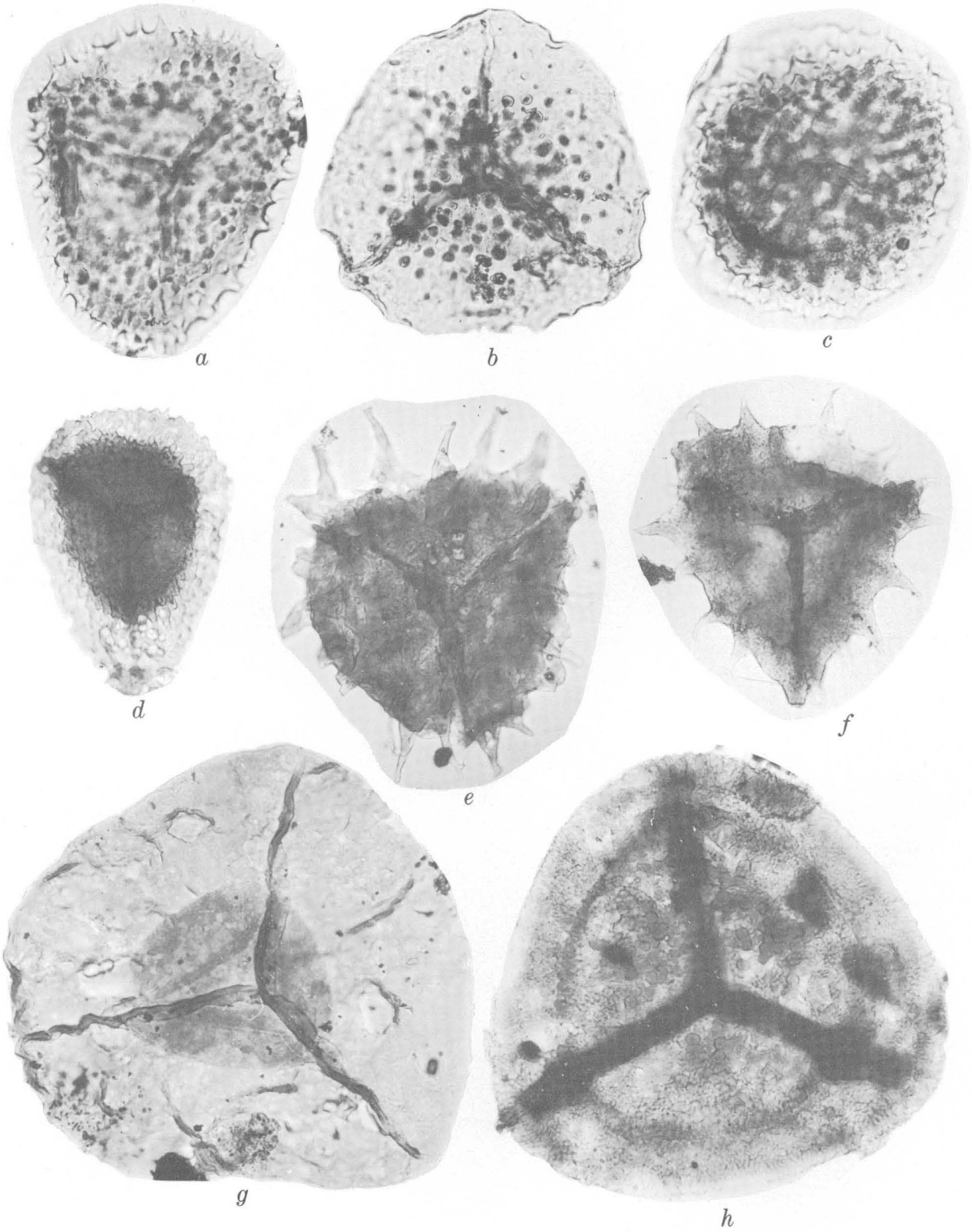

a

b

c

d

e

f

g

h

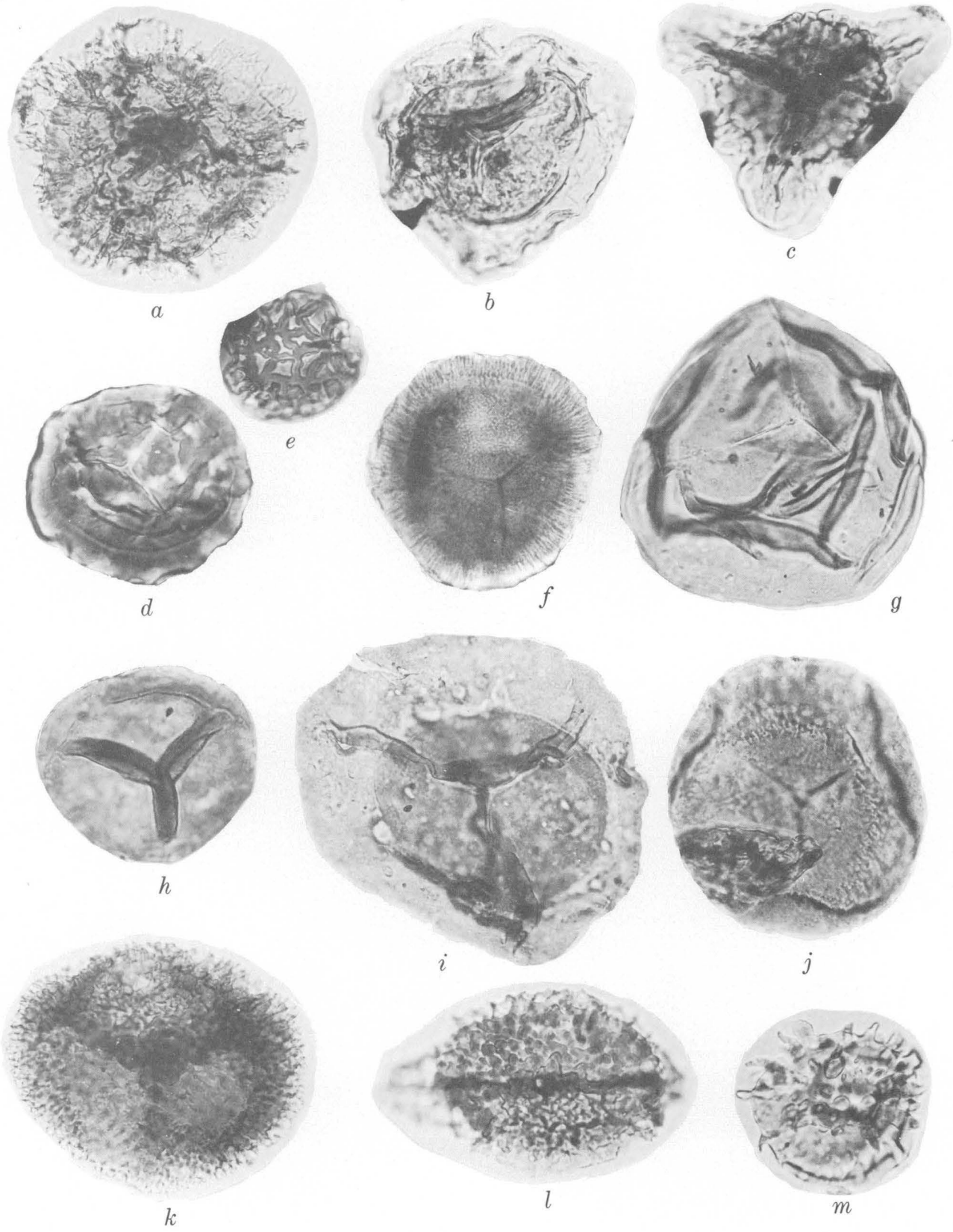
a
b
c
d
e
f
g
h
i
j
k
l
m

Middle Old Red Sandstone, has been identified tentatively by McGregor and Owens (1966) from the Lower and Middle Devonian of Canada. It is represented in the Nation River Formation by an undescribed species (fig. 3*k*).

Despite these and other similarities, the Nation River Formation apparently is not as old as Middle Devonian, because it contains genera not known to range below the Upper Devonian. Vigran (1964) points out that the genus *Foveosporites* Balmé has not been reported from beds definitely older than Late Devonian. *Diaphanospora* Balmé and Hassell, described from the Upper Devonian of Australia, and not known from below the Upper Devonian in Canada (McGregor and Owens, 1966), is present in the Nation River Formation (fig. 3*b*). Richardson (1965) reports that monolete spores, represented in the Nation River Formation (fig. 3*l*) and in the Upper Devonian of Canada (McGregor and Owens, 1966) by *Archaeoperisaccus*, have been found only once in the Middle Devonian (Russia) but are known from the Upper Devonian of Russia, North America, and Australia.

The original determination of David White (*in* Mertie, 1930) for the age of the Nation River Formation is borne out by this preliminary examination of plant spores from its upper beds. We attempted to obtain for palynological examination the specimens White studied, but they have been discarded (S. H. Mamay, oral commun., 1966). Because the Nation River plant microfossil assemblage from the type area of the formation is in striking contrast to well-known assemblages from the late Paleozoic, a Pennsylvanian or Permian age for the Nation River Formation is precluded.

FIGURE 3.—Spores from the Nation River Formation, east-central Alaska. All specimens × 500. Numbers are USGS paleobotany locality and slide numbers.

a. *Camptozonotriletes* sp. D1940A, slide 20.
b. *Diaphanospora* sp. D1940A, slide 21.
c. *Samarisporites triangulatus* Allen. D1940A, slide 21.
d. *Lophozonotriletes* sp. D1940C, slide 20.
e. cf. *Convolutispora mimerensis* (Vigran) Allen. D1940C, slide 20.
f. *Foveosporites pertusus* Vigran. D1940A, slide 20.
g. *Calamospora* sp. D1940C, slide 20.
h. *Leiotriletes* sp. D1940C, slide 20.
i. *Leiozonotriletes* sp. D1940C, slide 20.
j. *?Retusotriletes* sp. D1940A, slide 27.
k. *Corystisporites* sp. D1940C, slide 20.
l. *Archaeoperisaccus*, cf. *A. timanicus* Pashkevich. D1940A, slide 20.
m. *Raistrickia* sp. D1940A, slide 26.

REFERENCES

Allen, K. C., 1965, Lower and Middle Devonian spores of north and central Vestspitsbergen: Palaeontology, v. 8, p. 687–748.

Balmé, B. E., and Hassell, C. W., 1962, Upper Devonian spores from the Canning Basin, Western Australia: Micropaleontology, v. 8, p. 1–28.

Brabb, E. E., and Churkin, Michael, Jr., 1964, Preliminary geologic map of the Charley River quadrangle (1:250,000), east-central Alaska: U.S. Geol. Survey open-file report, 1 p.

Brooks, A. H., and Kindle, E. M., 1908, Paleozoic and associated rocks of the Upper Yukon, Alaska: Geol. Soc. America Bull., v. 19, p. 255–314.

Churkin, Michael, Jr., and Brabb, E. E., 1965, Ordovician, Silurian, and Devonian biostratigraphy of east-central Alaska: Am. Assoc. Petroleum Geologists Bull., v. 49, p. 172–185.

Laudon, L. R., Hartwig, A. E., Morgridge, D. L., and Omernik, J. B., 1966, Middle and Late Paleozoic stratigraphy, Alaska-Yukon border area between Yukon and Porcupine Rivers: Am. Assoc. Petroleum Geologists Bull., v. 50, p. 1868–1889.

McGregor, D. C., and Owens, B., 1966, Devonian spores of eastern and northern Canada: Canada Geol. Survey Paper 66–30, p. 1–66.

Mertie, J. B., 1930, Geology of the Eagle-Circle district, Alaska: U.S. Geol. Survey Bull. 816, p. 1–168.

Playford, Geoffrey, 1962, Lower Carboniferous microfloras of Spitsbergen: Palaeontology, v. 5, p. 619–678.

——— 1963, Miospores from the Mississippian Horton Group, eastern Canada: Canada Geol. Survey Bull. 107, p. 1–47.

Richardson, J. B., 1962, Spores with bifurcate processes from the Middle Old Red Sandstone of Scotland: Palaeontology, v. 5, p. 171–193.

——— 1965, Middle Old Red Sandstone spore assemblages from the Orcadian basin, north-east Scotland: Palaeontology, v. 7, p. 559–605.

Vigran, J. O., 1964, Spores from Devonian deposits, Mimerdalen, Spitsbergen: Norsk Polarinstitutt, Skr. no. 132, 32 p.

Winslow, M. R., 1962, Plant spores and other microfossils from Upper Devonian and Lower Mississippian rocks of Ohio: U.S. Geol. Survey Prof. Paper 364, 93 p.

TERTIARY STRATIGRAPHY AND GEOHYDROLOGY IN SOUTHWESTERN GEORGIA

By C. W. SEVER and S. M. HERRICK, Tifton, Ga., Atlanta, Ga.

Prepared in cooperation with the city of Cairo, Ga., and the Georgia Department of Mines, Mining, and Geology

Abstract.—The section of Oligocene rocks penetrated in the drilling of a test well at Cairo, Ga., is believed from foraminiferal evidence to include beds equivalent to the Marianna Limestone, a formation not known previously to occur in Georgia. Recognition of the Marianna necessitates assignment of some of the overlying beds, formerly considered to be part of the Ocala Limestone of late Eocene age, to the Byram Formation of Oligocene age. The Byram, not the Ocala, probably is the source of the inferior water previously thought to be contained by the Ocala in southwestern Georgia.

Sediments representing the middle and upper Oligocene section as known in the southeastern part of the Atlantic Coastal Plain were discovered in the drilling of a test well in southwestern Georgia. The test well (GGS 962) drilled by the U.S. Geological Survey at Cairo, Ga., (fig. 1) penetrated rocks of Oligocene age from a depth of 471 feet to 965 feet, where it bottomed in sediments belonging to the Marianna Limestone of middle Oligocene age. The Oligocene section penetrated by this well includes a thickness of 494 feet (fig. 2) which compares favorably with that previously described by Applin (1960, p. B208) from a well (GGS 509)[1] in Coffee County, Ga. In that well a thickness of approximately 635 feet was assigned to the late Oligocene, or post-Marianna part of the Oligocene section, as now recognized in Georgia.

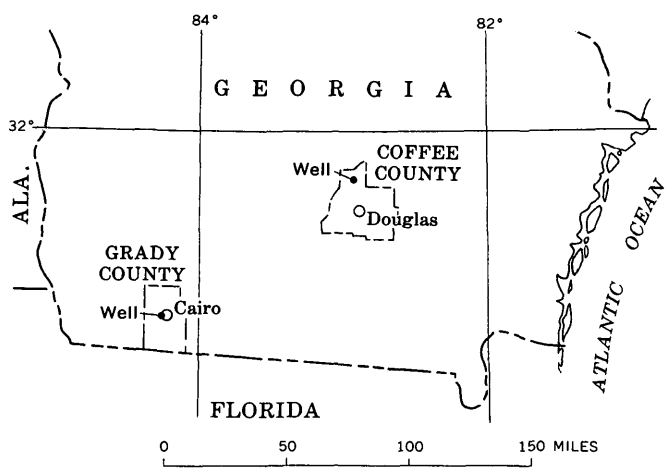

FIGURE 1.—Location of wells in Coffee and Grady Counties, Ga.

STRATIGRAPHY AND PALEONTOLOGY

In the Cairo test well the Suwannee Limestone of late Oligocene age occupies the 24-foot interval 471 – 495 feet. The sediments composing this part of the section are typically Suwannee, consisting of hard to soft yellowish-gray much calcitized crystalline fossiliferous limestone. Calcium carbonate makes up about 97 percent of the rock. The Foraminifera *Pararotalia mexicana* (Nuttall) var., *Asterigerina subacuta* Cushman, *A. alabamensis* Cushman and McGlamery, and *Quinqueloculina byramensis* Cushman are prominent in this interval and place this part of the section in the Suwannee.

The Byram Formation, of middle Oligocene age, occupies the interval 459 – 673 feet. These sediments consist predominantly of yellowish-brown dense clayey finely crystalline dolomite. They are similar to the Byram described by Puri and Vernon (1964, p. 102) where it crops out along State Highway 71 in Jackson County, Fla. Clay was not observed in untreated cuttings from the Byram at Cairo, but when the dolomite is dissolved in hydrochloric acid the residue is a green clay. The clay appears to occur within the rhombohedrons of dolomite instead of between them. Probably owing to their having been dolomitized, the strata assigned to the Byram in the Cairo test well yielded no identifiable fossils.

[1] Carpenter Oil Co., C. T. Thurman No. 2, Coffee County, Ga.

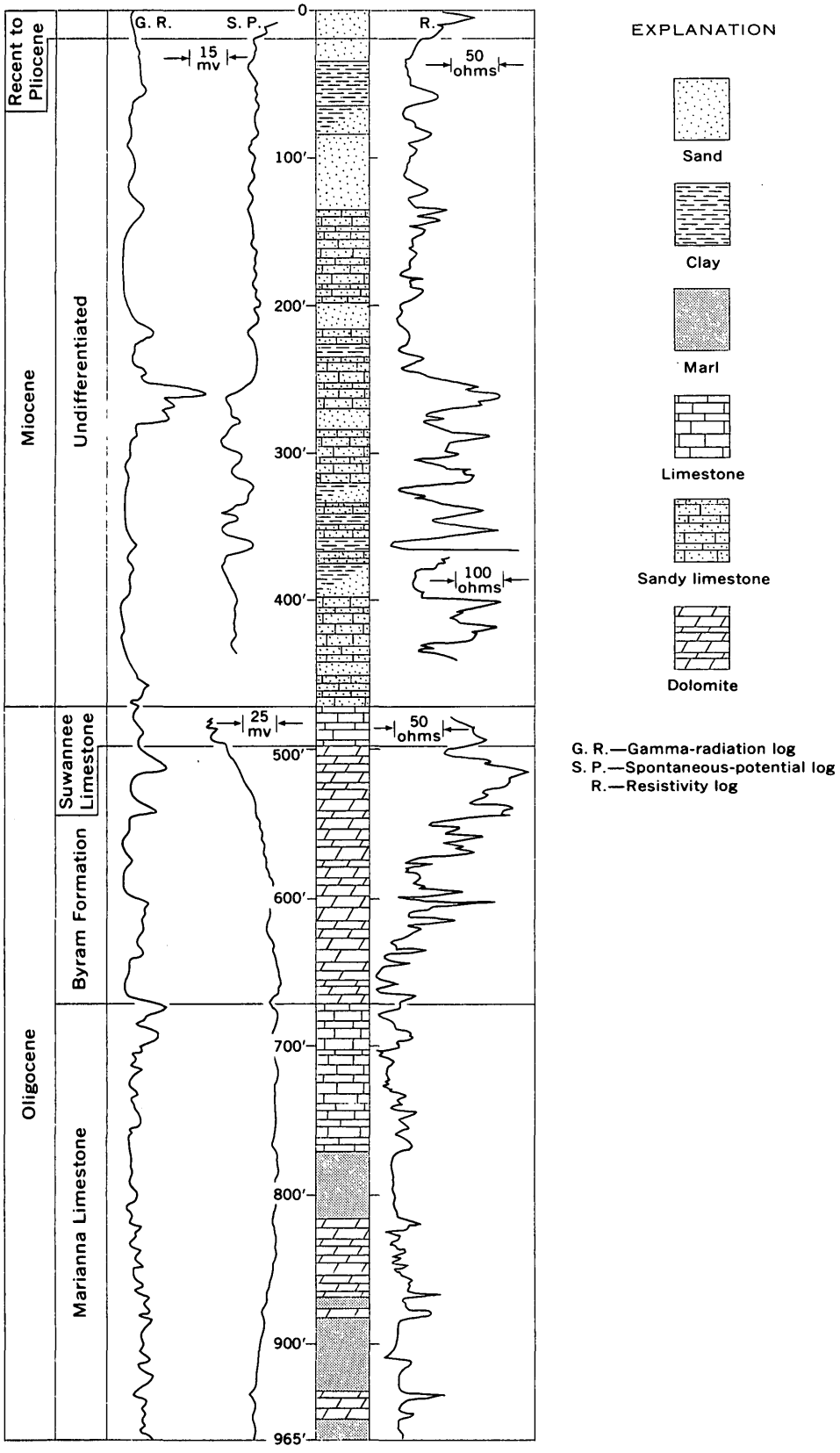

FIGURE 2.—Lithologic and electric log of U.S. Geological Survey test well GGS 962 at Cairo, Ga.

The interval 673–965 feet in the Cairo test well definitely belongs in the Marianna Limestone of middle Oligocene age. This part of the section consists of interbedded pale-orange to cream soft granular fossiliferous limestone, cream fossiliferous marl, and thin beds of pale-brown dolomite and dolomitic limestone. It is lithologically similar to exposures at the type locality near Marianna, Fla., as described by Puri and Vernon (1964, p. 98–102).

Foraminifera representative of the Marianna Limestone are listed below (according to order of first observed occurrence):

725–730 feet:
- *Robulus arcuato-striatus* (Hantken) var. *vicksburgensis* (Cushman)
- *Nonion affine* (Reuss)
- *Bolivina byramensis* Cushman
- *Ellipsonodosaria* cf. *E. jacksonensis* (Cushman and Applin)
- *Discorbis araucana* (D'Orbigny) *assulata* (Cushman)
- *Eponides advenus* (Cushman) *byramensis* (Cushman)
- *Siphonina advena* Cushman
- *Anomalina bilateralis* Cushman
- *Cibicidina mississippiensis* (Cushman)

730–735 feet:
- *Bulimina sculptilis* Cushman
- *Reussella byramensis* Cushman and Todd
- *Uvigerina vicksburgensis* Cushman and Ellisor
- *Cibicides choctawensis* Cushman and McGlamery
- *Cibicidina americana* (Cushman) var. *antiqua* (Cushman and Applin)

735–740 feet:
- *Marginulina* sp.

770–775 feet:
- *Globulina gibba* D'Orbigny

780–785 feet:
- *Robulus cf. R. alato-limbatus* (Gümbel)
- *Cibicides pippeni* Cushman and Garrett

850–855 feet:
- *Planulina cocoaensis* Cushman

925–930 feet:
- *Bolivina mississippiensis* Cushman var. *costifera* Cushman

930–935 feet:
- *Planulina mexicana* Cushman

940–945 feet:
- *Nodosaria latejugata* Gümbel *vertebralis* (Batsch)
- *Guttulina problema* (D'Orbigny)
- *Gyroidina vicksburgensis* (Cushman)
- *Cassidulina* cf. *C. laevigata* D'Orbigny

960–965 feet:
- *Bolivina choctawensis* Cushman and McGlamery

The fauna listed above contains the following species in common with those reported by Cole and Ponton (1930) from outcrops of the Marianna Limestone, Jackson County, Fla.: *Robulus arcuato-striatus*, *R. vicksburgensis*, *Nodosaria latejugata*, *N. vertebralis*, *Globulina gibba*, *Guttulina problema*, *Bulimina sculptilis*, *Bolivina byramensis*, *Reussella byramensis*, *Uvigerina vicksburgensis*, *Ellipsonodosaria* cf. *E. jacksonensis*, *Discorbis araucana*,[2] *Gyroidina vicksburgensis*, *Eponides byramensis*, *E. advenus*, *Nonion affine*,[3] *Siphonina advena*, *Anomalina bilateralis*, *Planulina mexicana*, *Cibicidina americana*, and *C. mississippiensis*. These Foraminifera constitute evidence for correlating the interval 673–965 feet in the Cairo test well with the Marianna Limestone of Florida.

Oligocene sediments in southwestern Georgia were deposited in a relatively shallow warm sea that apparently oscillated over the inner continental shelf. The limestones, dolomites, and marls composing the Oligocene in this part of Georgia are but a small part of the total volume of carbonates that were deposited in a warm shallow shelf sea that periodically covered the southeastern United States from Late Cretaceous to middle Miocene time. The marine invasions were oscillatory and interrupted by periods of subaerial erosion throughout much of the central Atlantic Coastal Plain as well as in southwestern Georgia, as suggested by Spangler and Peterson (1950, p. 97) and Applin (1960, p. B208). Applin further points out the spotty occurrences of known Oligocene deposits from North Carolina southward to and including Nassau and Duval Counties, Fla.

The Late Cretaceous to mid-Miocene sea in northeastern Florida was a relatively shallow and warm one, probably similar to present-day conditions off the west coast of Florida. This is suggested not only by the carbonate nature of the sediments but also by the foraminiferal species they contain, many of which have wide geographic distribution in the Gulf of Mexico and Caribbean areas. The smaller Foraminifera found in the Cairo test well, particularly the fauna belonging to the Marianna Limestone, show a preponderance of benthonic forms accompanied by a relative scarcity of planktonic species, such as those belonging to the *Globigerinidae* and the *Globorotaliidae*; this is additional evidence as to the shallow nature of this ancient sea.

Throughout much of southwestern Georgia the Oligocene sediments consist of an upper part, the Suwannee Limestone of late Oligocene age, and a lower part, the Byram Formation of middle Oligocene age. In the Cairo age, an additional unit, the Marianna Limestone also of middle Oligocene age, is present. Presumably the Marianna overlies the Ocala Limestone of late Eocene age in Grady County. How far this tripartite Oligocene section extends southwest-

[2] Reported by Cole and Ponton (1930, p. 40) as *Discorbis* sp.
[3] Identified by Cole and Ponton (1930, p. 37) as *Nonion umbilicatulum*.

ward as well as northeastward (toward Coffee County) from the Cairo area remains to be determined.

QUALITY-OF-WATER CONDITIONS

Ground-water studies have indicated that the Suwannee and Ocala Limestones together yield nearly all of the water pumped by the municipal and industrial wells that tap the principal artesian aquifer beneath southwestern Georgia. Some of the water, particularly that in the Cairo area, is known to be extremely hard and to contain concentrations of sulfate, iron, fluoride, and dissolved solids exceeding to a degree the recommended limits of the U.S. Public Health Service (1962).

Prior to the drilling of the Cairo test well the poor-quality ground water was thought to occur within the Ocala Limestone. However, geologic and water-quality studies in the Cairo test well plus reexamination of other wells in Grady and neighboring counties have shown that the inferior water actually is derived from the Byram Formation. The poor quality of water is attributed to the dolomitic character of the rocks in the Byram, a part of the geologic section that previously had been placed by Herrick (1961, p. 398) in the upper part of the Ocala. By stopping wells short of the deeper lying Byram Formation and limiting pumping to the Suwannee Limestone, or upper part of the Oligocene, the problem of inferior water could be avoided in the Cairo area. If more water is needed than can be obtained from the Suwannee and if additional water supplies are sought by drilling to the presumably much more deeply buried Ocala Limestone, the Byram Formation should be cased out in order to eliminate pumping inferior water from it.

REFERENCES

Applin, E. R., 1960, A tropical sea in central Georgia in late Oligocene time: U.S. Geol. Survey Prof. Paper 400-B, p. B207–B209, 2 figs.

Cole, W. S., and Ponton, G. M., 1930, The Foraminifera of the Marianna Limestone of Florida: Florida Geol. Survey Bull. 5, p. 19–69, pls. 5–11.

Herrick, S. M., 1961, Well logs of the Coastal Plain of Georgia: Georgia Geol. Survey Bull. 70, 461 p., 1 fig.

Puri, H. S., and Vernon, R. O., 1964, Summary of the geology of Florida and a guidebook to the classic exposures: Florida Geol. Survey Spec. Rept. 5 (revised), 292 p., 37 figs., 11 pls.

Spangler, W. B., and Peterson, J. J., 1950, Geology of Atlantic Coastal Plain in New Jersey, Delaware, Maryland, and Virginia: Am. Assoc. Petroleum Geologists Bull., v. 34, no. 1, p. 1–100.

U.S. Department of Health, Education, and Welfare, 1962, Public Health Service drinking water standards: Public Health Service Pub. 956, 61 p.

FUSTISPOLLENITES, A NEW LATE CRETACEOUS GENUS FROM KENTUCKY

By ROBERT H. TSCHUDY and HELEN M. PAKISER, Denver, Colo.

Work done in cooperation with the Kentucky Geological Survey

Abstract.—*Fustispollenites*, a new pollen genus from the Upper Cretaceous McNairy Formation of Kentucky, is described and may have biostratigraphic value. It has distinctive morphologic characteristics, including prominent apical and subequatorial clavae; comparisons are made with other genera sharing some of these characteristics.

During investigations of plant microfossils from the Mississippi embayment region, a rare, morphologically bizarre angiosperm pollen species was found. It was recovered from a sample of dark-gray clayey siltstone from the McNairy Formation of Late Cretaceous age. The sample is from an outcrop 1.35 miles northeast of Faxon School, Kentucky coordinates 1,289,050–135,150 (Carter coordinates 26–C–16), Hico quadrangle, Calloway County, Ky. The sample has been assigned USGS paleobotanical locality No. D3000.

The pollen is characterized by 5 colpi separated by 5 ridges, each ridge bearing two prominent subequatorial projections or clavae, and two polar clavae. This morphologically unusual pollen resembles in some aspects the genera *Senegalosporites* Jardiné and Magloire, 1963 (pl. IV, fig. 8; pl. V, fig. 1), *Elaterocolpites* Jardiné and Magloire 1963 (pl. IV, figs. 6, 7), and the species *Steevesipollenites binodosus* Stover 1964 (pl. 2, figs 7–9), all Upper Cretaceous forms from northwest Africa.

The spore genus *Senegalosporites* and the ephedroid pollen species *Steevesipollenites binodosus* both possess prominent polar nodes or clavae, but do not possess colpi. The pollen genus *Elaterocolpites*, perhaps closest morphologically to *Fustispollenites*, possesses colpi and 10 subequatorial projections or outgrowths of the exine, but no polar clavae.

Careful comparison reveals that resemblance to the above forms is only superficial and that this distinctive pollen merits description as a new genus and species. Samples from most of the Upper Cretaceous and lower Tertiary formations of the Mississippi embayment have been examined for fossil pollen content; the genus *Fustispollenites* has been observed only in the McNairy Formation. Although rare, its distinctive form makes it a potentially very useful marker fossil in the Late Cretaceous of the Mississippi embayment region.

SYSTEMATIC DESCRIPTIONS

All photographed specimens of the new genus and species described herein are on slides deposited in the U.S. National Museum, Washington, D.C. All illustrated specimens are within black-ink circles marked directly on the slides; they may also be located on the slides by the mechanical-stage coordinates given in the explanation of figure 1 of this paper. In order that others may convert their mechanical-stage readings to those recorded for our specimens, our coordinates for the center point of a 1 x 3-inch standard microscope slide are 108.0 and 12.3 mm. The method of accurately locating the center of a standard microscope slide is described by Tschudy (1966, p. D78).

Color photographs of the new genus and species described in this paper are available from the U.S. Geological Survey laboratory, Denver, Colo., on a limited loan basis.

EXPLANATION OF FIGURE 1

a–d Holotype (Slide T3), coordinates 86.3×14.2 mm. USNM 42633. *a–c*, taken at different focal planes to show details of colpi, clavae (cl), and surface ornamentation. *d*, taken with a Wratten-H filter to show detail of colpus (cp).

e–f Paratype (Slide T1), coord. 104.1×6.3 mm. USNM 42634.

g. (Slide T8) coord. 83.6×14.5 mm. USNM 42635. One clava has been broken out (upper right side of photograph).

h. (Slide T7) coord. 94.3×20.2 mm. USNM 42636. Note colpus, and vesicles at base of apical clava (acl.)

i–k. (Slide T12) coord. 86.6×3.9 mm. USNM 42637. Polar views, showing lobed outline and wall thickness. *k*, taken with a Wratten-H filter, shows the apical termination of a colpus (cp) and the granulate ornamantation of the outer wall.

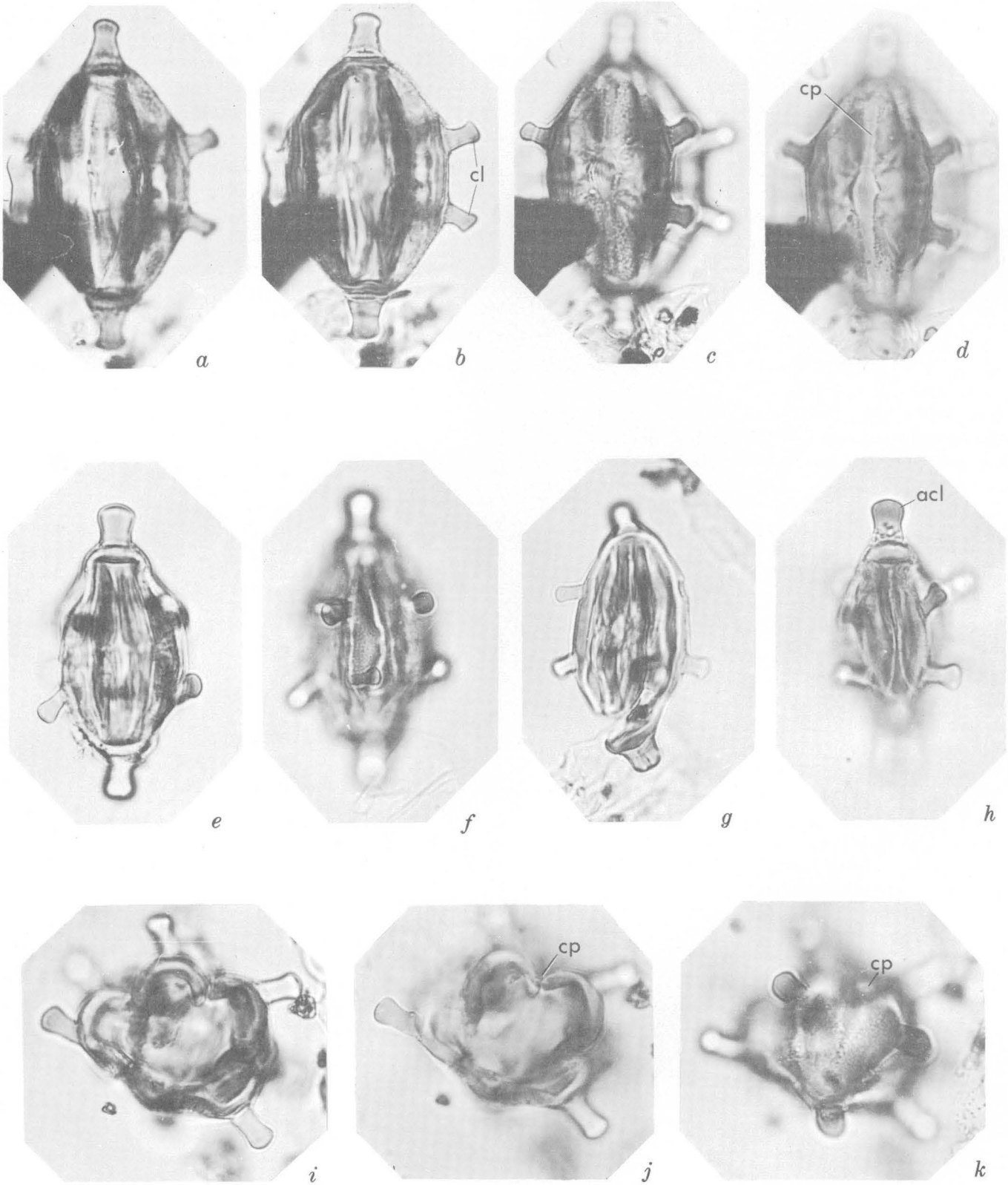

FIGURE 1.—*Fustispollenites conspicuus.* USGS paleobot. loc. D3000. × 1,000.

Genus *Fustispollenites* n. gen.

Type species.—*Fustispollenites conspicuus* n. sp.

Diagnosis.—Pentacolpate, ellipsoidal to fusiform pollen with 5 meridional ridges separating colpi. Exine two layered, the outer layer bearing 10 subequatorial clavae and two polar clavae. The distinctive ornamentation suggests the latin term "fustis", a knobbed stick or club.

Fustispollenites conspicuus n. sp.

Figure 1, *a–k*

Holotype: USNM 42633, slide D3000 (T3), coordinates 86.3 × 14.2, fig. 1, *a–d*. Size 43 microns × 28 microns exclusive of clavae.

Paratype: USNM 42634, slide D3000 (T1), coordinates 104.1 × 6.3, fig. 1, *e, f*. Size 38 microns × 24 microns exclusive of clavae.

Description (18 specimens).—These pentacolpate pollen grains are elongate, cylindrical to spindle shaped, and symmetrical around the longitudinal axis. In polar view the outline is five lobed, the colpi lying in the grooves between the lobes. The colpi extend about three-quarters of the distance to the poles. They are open, possess rounded ends, and are dilated at the equator, giving the appearance of a pore. The inner-wall layer (endexine) is uniformly slightly more than 2μ thick except at the colpi, where it is absent. The outer-wall layer (ektexine) is less than 1μ thick and possesses a finely granulate surface.

On each of the lobes of the outer wall, midway between the colpi, two clavae are inserted. The clavae are solid, smooth, and slightly enlarged at their ends. The subequatorial clavae range from 5 to 7μ in length, and average 3.1μ in diameter at their midpoints and 4.3μ in diameter at their ends. Two somewhat larger clavae are inserted on the two poles. They are 7 to 9μ in length and average 5μ in diameter at their midpoints and 6.4μ in diameter at their ends.

The size of this pollen grain, excluding the clavae, ranges from 37 to 43μ in length, and from 18 to 28μ in diameter.

Discussion.—The clavae are inserted into the outer layer of the wall, rather than being extensions of the wall. This is shown on figure 1, *g*, where one of the clavae has been clearly broken out. The granulate surface texture of the outer-wall layer is shown on *d* and *k*, taken with a Wratten-H filter.

Occurrence.—McNairy Formation of Kentucky.

Age.—Late Cretaceous, Maestrichtian.

Comparisons.—*Fustispollenites conspicuus* differs from other genera possessing prominent polar or lateral knobs or clavae as shown in table 1.

TABLE 1.—*Comparison of* Fustispollenites conspicuus *with other genera*

	Fustis-pollenites conspicuus	*Elatero-colpites*	*Senegalo-sporites*	*Steevesi-pollenites binodosus*
Polar knobs or clavae	+		+	+
10 subequatorial clavae or extensions of exine.	+	+		
Colpi	+	+		
Equatorial clavae as extensions of outer membrane.		+		

This distinctive, easily recognized angiospermous fossil pollen shows no direct affinity with any known palynomorph.

REFERENCES

Jardiné, Serge, and Magloire, L., 1963, Palynologie et Stratigraphie du Crétacé des Bassins du Sénégal, et de Cote d'Ivoire: Colloque International de Micropaleontologie, Dakar, 6–11 Mai, p. 187–245.

Stover, L. E., 1964, Cretaceous ephedroid pollen from West Africa: Micropaleontology, v. 10, no. 2, p. 145–156.

Tschudy, R. H., 1966, Associated megaspores and microspores of the Cretaceous genus *Ariadnaesporites* Potonié 1956, emend, *in* Geological Survey Research 1966: U.S. Geol. Survey Prof. Paper 550–D, p. D76–D82.

ORIENTATION OF CARBONATE CONCRETIONS IN THE UPPER DEVONIAN OF NEW YORK

By GEORGE W. COLTON, Beltsville, Md.

Abstract.—Argillaceous limestone concretions are abundant in the lower Upper Devonian marine sequence in New York. Typically they are elongate in plan view, and their long axes are preferentially oriented to the northeast. The alinement of the concretions is probably parallel to the primary depositional fabric of the enclosing rock. In turn, the fabric was probably controlled by, and oriented parallel to, marine currents.

The lower Upper Devonian rocks in the western half of New York consist of evenly interstratified black shale, gray shale and mudrock, siltstone, and sandstone. Regional stratigraphic studies (fig. 1) indicate that they accumulated in a marine basin whose axis and eastern shoreline trended approximately northeast-southwest. The Genesee, Sonyea, West Falls, Java, and Perrysburg Formations, which make up the lower Upper Devonian sequence, thicken to the east and southeast across most of the area. As the formations thicken, members composed largely of siltstone and sandstone increase in number and in thickness. Conversely, the percentage of gray shale and mudrock and of black shale in each formation decreases to the east and southeast.

Calcareous concretions occur in large numbers in all the formations. They are most abundant in members composed largely of shale and mudrock, and consequently occur in greatest abundance in the western part of the area, where shale and mudrock make up the bulk of the formations. The directional properties of concretions were studied at 27 localities in an area 105 miles wide, extending from Lake Erie eastward to Seneca Lake. Data were collected in the following counties: Chautauqua, Cattaraugus, Erie, Wyoming, Livingston, Ontario, Yates, Steuben, Schuyler, and Tompkins.

DESCRIPTIONS OF CONCRETIONS

"Concretion" is a general term used here to include three forms of accretionary structures: nodules, true concretions, and septaria or septarian nodules (Pettijohn, 1949, p. 149–154). All three forms are composed largely of clay, quartz, and calcium carbonate. Pyrite or marcasite, and barite are the most common accessory minerals. On the basis of field observations in New York, nodules in general are the smallest concretionary structures. They are commonly irregular in shape, have a warty or pustulose surface, and do not appear to be internally laminated. In many places, nodules occur in such great numbers along bedding planes that they locally coalesce to form lumpy lenses and lenticular beds of argillaceous limestone. True concretions are commonly larger, more symmetrical in shape, and have smoother surfaces than nodules, and, as a rule, contain an internal lamination that is parallel to that of the surrounding rocks. In most places, true concretions are widely spaced along the bedding plane in which they occur and coalesce less commonly than nodules. Septaria are characterized by fractures containing coarsely crystalline calcite and smaller amounts of pyrite, barite, siderite, and other minerals. The fractures have a tendency to radiate irregularly outward from near the center of the concretion and to become narrower or to terminate near its surface. Concentric banding, due largely to variations in the amounts of finely crystalline pyrite, calcite, and argillaceous material, is pronounced in many septaria. In size, shape, surface texture, and in their arrangement along bedding planes, septaria are similar to true concretions. The long axes of concretions range from a fraction of an inch to about 15 feet in length, and invariably lie along the bedding plane. With few exceptions, the short axis of the concretion is perpendicular to bedding. Small fragments of plants, pteropods, thin-shelled gastropods, and pelecypods occur in many true concretions and septaria and in some nodules. Most fossils in the concretions are undeformed by compac-

U.S. GEOL. SURVEY PROF. PAPER 575-B, PAGES B57-B59

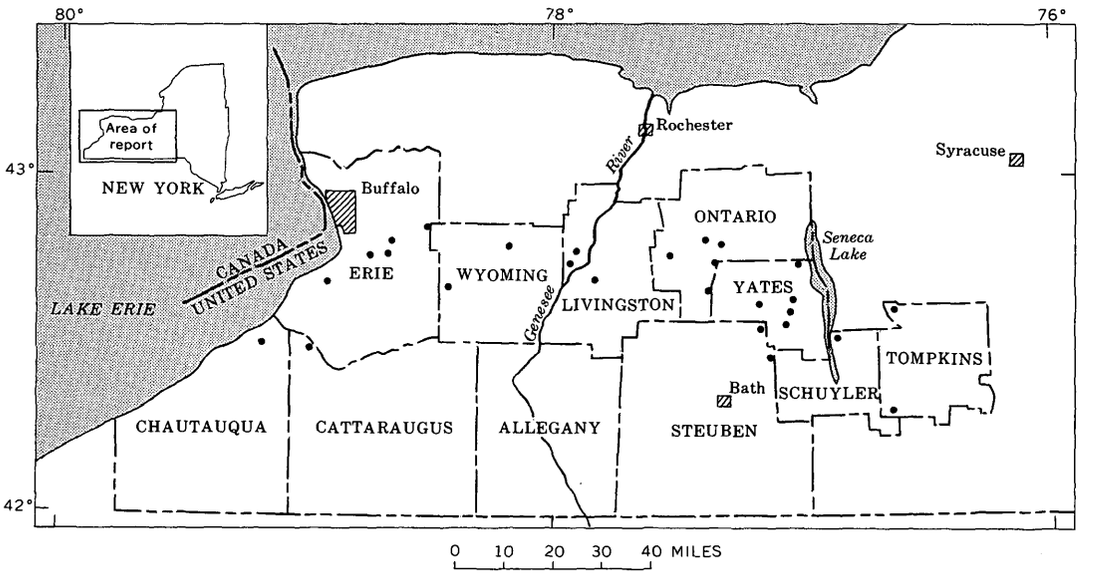

FIGURE 1.—Map of report area in western New York, showing localities (dots) where data were collected.

tion, whereas fossils in the surrounding shale or mudrock are highly compressed.

Of the concretions observed, approximately two-thirds are noticeably elongate in plan view, and the remainder are for the most part equant or highly irregular in plan view (fig. 2). The degree of elongation varies from slightly ellipsoidal in some specimens to rodlike or nearly cylindrical in others.

ORIENTATION OF CONCRETIONS

The orientations of the long axes of 647 concretions are compiled in figure 3. It is apparent that the long axes are preferentially grouped about a northeast axis and that the mean trend is N. 55° E. To determine if a relationship exists between the orientation of concretions and the environment of deposition of the enclosing rocks, the concretions were divided into two groups. One group includes concretions in the area west of the Genesee River, where the rock sequence is composed largely of shale and mudrock. These rocks accumulated in the marine basin far west of the shoreline. The other group includes concretions in the area east of the Genesee River, where siltstone and sandstone constitute an appreciable part of the sequence. The rocks in this area accumulated closer to the shoreline, presumably in shallower water under the influence of stronger currents.

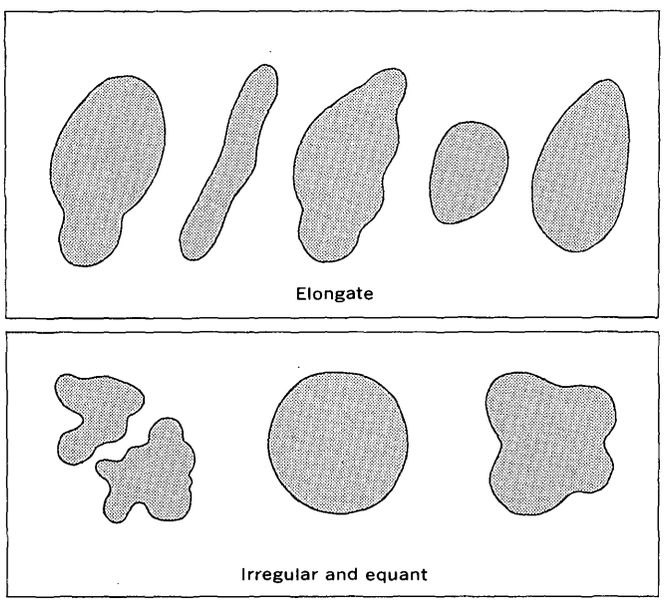

FIGURE 2.—Typical shapes of concretions.

The orientation of the long axes of the concretions in the two areas is compared in figure 3. The fact that the primary peaks of both groups coincide suggests that the principal orienting force or phenomena was constant in direction regardless of geographic location and environment. A secondary peak in the lower line (in the northwest quadrant) suggests another orienting force or the same force operating in a different direction or manner in the western area. This secondary maximum is absent among the elongate concretions measured in the east. Figure 3 also shows that the orientation of concretions in the west is less pronounced than that of concretions in the east.

An earlier investigation of other elongate sedimentary and organic structures in the same rock sequence (Colton, 1967) showed that specimens of *Fucoides graphica* Vanuxem and of plant fragments in shale

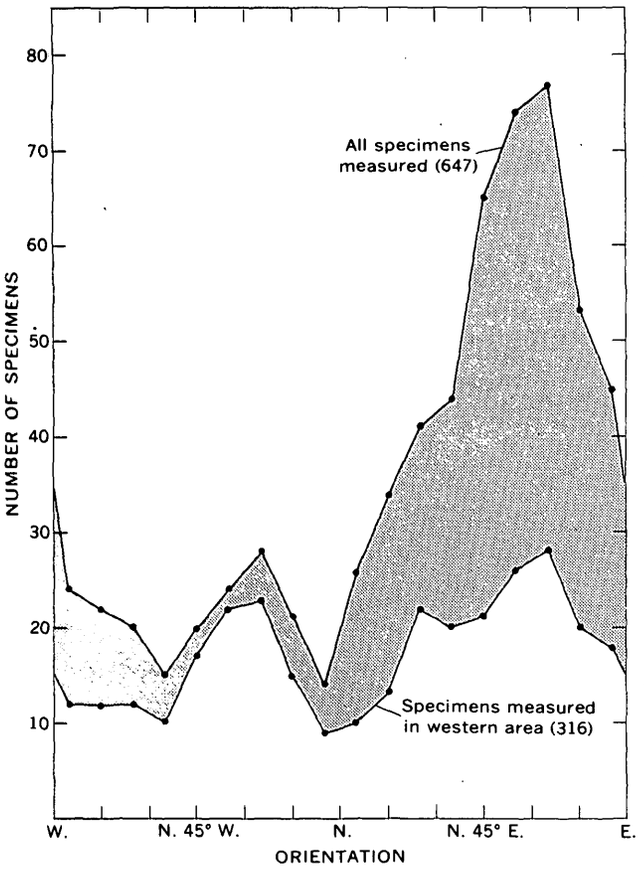

FIGURE 3.—Frequency diagram of long axes of elongate concretions. Shaded area is frequency polygon of concretions measured in eastern area.

and mudrock are oriented preferentially about a northeast axis. That investigation indicated that the orientation was caused by mud-depositing currents which flowed approximately parallel to the axis about which the fucoids and plant fragments are grouped. The frequency distribution of elongate concretions in beds of shale and mudrock agrees closely with the previously observed distribution of specimens of *Fucoides graphica* and plant fragments in the same beds or in closely associated beds. The vector mean trends for the long axes of concretions, fucoids, and plants are N. 55° E., N. 49° E., and N. 50° E., respectively. This parallelism strongly suggests that the orientation of concretions also is controlled by current action and that the long axes of the concretions tend to be parallel to the trend of the mud-depositing currents.

If we assume that marine currents are effective in orienting concretions, the frequency polygons in figure 3 suggest the following possibilities: (1) The less strongly developed preferential alinement in the western area may be attributed to marine currents that were weaker and less effective in orienting the specimens, or that the currents were less persistent in their direction of flow. (2) The secondary peak in the western area may indicate another direction of flow. A shoal area along the west edge of the area (Pepper and de Witt, 1951, fig. 8) may account for this secondary flow direction.

To date, no field criteria have been found to indicate whether the mud-depositing currents flowed from the northeast or the southwest, nor is it known how the currents controlled the elongation of the concretions. The presence of bedding-plane laminations in many concretions suggests that they accumulated contemporaneously with the enclosing sediment, and the presence of uncompressed thin-shelled invertebrate fossils in many concretions suggests that the concretions solidified before the surrounding sediments were compacted. Elongation may have been caused by preferential precipitation of calcium carbonate along a fabric pattern imparted to the sediment by the action of marine bottom currents. As suggested by J. F. Pepper (written commun., 1961), elongation may have been controlled by precipitation around elongate organic structures which were oriented by current action as they accumulated on the sea floor. However, except for a vaguely defined concentration of limonite in some specimens, which may represent a weathered iron sulfide mineral, there is no suggestion of foreign matter in the center of the great majority of concretions.

REFERENCES

Colton, G. W., 1967, Late Devonian current directions in western New York, with special reference to *Fucoides graphica*: Jour. Geology, v. 75, no. 1, p. 11–22.

Pepper, J. F., and de Witt, Wallace, Jr., 1951, Stratigraphy of the Late Devonian Perrysburg Formation in western and west-central New York: U.S. Geol. Survey, Oil and Gas Inv. Chart OC–45.

Pettijohn, F. J., 1949, Sedimentary rocks: New York, Harper and Brothers, 526 p.

241–334 O—67——5

A STATISTICAL MODEL OF SEDIMENT TRANSPORT

By W. J. CONOVER [1] and N. C. MATALAS, Manhattan, Kans., Washington, D.C.

Abstract.—A statistical model is constructed to simulate the behavior of sediment particles in flowing water in order to obtain a theoretical shape for the suspended-sediment concentration profile. The model yields the same shape or profile as does the classical deterministic model based on the linear-diffusion hypothesis.

Knowledge of the theoretical shapes of the velocity profile and sediment-concentration profile helps in determining the total suspended-sediment load being carried by a stream. The classical profile of suspended-sediment concentration given by Rouse (1950) has long been used for this purpose. This paper shows that for suspended particles of uniform fall velocity, the same theoretical shape of profile can be computed by a statistical model as by the differential equation model used in Rouse.

On the basis of a statistical model of turbulence, Matalas and Conover (1965) derived the vertical-velocity profile for two-dimensional uniform flow in open channels. The model itself was based on a probability law that governed the transfer of momentum of the fluid, taking into account momentum loss due to friction at the streambed and to fluid viscosity. Some simple modifications of this model alter its interpretation from that of the transfer of momentum to that of the transfer of mass. With these modifications, the model may be used in studies of sediment transport. In the following paragraphs, the main features of the mass-transfer model and the application of this model to derive the vertical sediment-concentration profile are presented.

Flow is assumed to be confined to a two-dimensional channel of depth D and unit width, with discharge restricted to the downstream direction. The channel of flow is considered to be subdivided into n different levels, B_i, ranging from B_1 just below the surface to B_n resting on the streambed. These levels resemble layers of unit width and depth $\Delta D=D/n$. As the model represents a situation which changes continuously in time, it will be convenient to denote "level i at time t" by $B_i(t)$. For the present, time will be considered in terms of discrete intervals of duration Δt. Later, a continuous model is evolved from the discrete model by allowing Δt and ΔD to approach zero.

The transfer of sediment mass from one level to another is assumed to be governed by the following probability law. The mass $M_i(t)$ associated with level $B_i(t)$ is transferred to level $B_{i-1}(t+\Delta t)$, $B_i(t+\Delta t)$, or $B_{i+1}(t+\Delta t)$ with probability p, q, or r, respectively, where $p+q+r=1$, for all values of i except $i=1$ and $i=n$. The stream surface and bed are assumed to act as reflecting barriers, so that any mass which attempts to penetrate these barriers is returned to the flow section in the following manner. The mass $M_1(t)$ associated with block $B_1(t)$ is transferred to level $B_1(t+\Delta t)$ or $B_2(t+\Delta t)$ with probability $(p+q)$ or r, respectively. And the mass $M_n(t)$ associated with level $B_n(t)$ is transferred to level $B_n(t+\Delta t)$ or $B_{n-1}(t+\Delta t)$ with probability $(r+q)$ or p, respectively. This probability law holds for the transfer of mass from any time t to time $t+\Delta t$ and, therefore, the total sediment mass at any time is a constant. The probabilities p, q, and r are referred to as 1-step transition probabilities.

If $P_{i,j}(k)$ denotes the k-step transition probability for the transfer of mass from $B_i(0)$ to $B_j(k\cdot\Delta t)$, where $t=0$ is an initial time reference point, then

$$\left.\begin{aligned} P_{i,j}(k)&=pP_{i,j+1}(k-1)+qP_{i,j}(k-1)\\ &\quad +rP_{i,j-1}(k-1); \qquad j=2,\ \ldots,\ n-1\\ P_{i,1}(k)&=(p+q)P_{i,1}(k-1)+pP_{i,2}(k-1);\\ &\qquad\qquad\qquad\qquad\qquad\qquad j=1\\ P_{i,n}(k)&=rP_{i,n-1}(k-1)+(q+r)P_{i,n}(k-1);\\ &\qquad\qquad\qquad\qquad\qquad\qquad j=n \end{aligned}\right\} \quad (1)$$

The expected value of the sediment mass transferred from $B_i(0)$ to $B_j(k\cdot\Delta t)$, denoted by $\overline{M}_{i,j}(k)$, is equal to $M_i(0)P_{i,j}(k)$, and the total expected value of mass contributed to $B_j(k\cdot\Delta t)$ from $B_i(0)$ for all values of i, denoted by $\overline{M}_j(k)$, is given by

$$\overline{M}_j(k)=\sum_{i=1}^{n}\overline{M}_{i,j}(k). \quad (2)$$

[1] Kansas State University.

To solve for $\overline{M}_j(k)$ in the limiting case where $n\to\infty$ and $k\to\infty$, the following properties of the probability model must be considered:

1. The transition probabilities have a long run distribution so that in the limit as $k\to\infty$, $P_{i,j}(k)\to\pi_j$, where π_j is some constant independent of i (Parzen, 1962).
2. For a fixed value of D, ΔD goes to zero as n goes to infinity and the ith level approaches the surface for a fixed value of i. Therefore, to consider the mass at a constant depth proportional to D as $n\to\infty$, let $1-i/n=m$, the proportionate height from the bed.
3. To obtain meaningful results as $\Delta D\to 0$, Δt must approach zero in such a way that $(\Delta D)^2/\Delta t$ approaches a constant (Feller, 1957).
4. Because the density of sediment exceeds that of water, $p<r$. Thus the expected level of a sediment particle starting at level i is $i+(r-p)$ after a time interval Δt, where $(r-p)$ is the expected fraction of ΔD that a sediment particle drops during the time interval Δt.
5. The total expected drop per unit time $(r-p)\Delta D/\Delta t$, which equals $(r-p)(\Delta D)^2 n/D\Delta t$, should approach a constant as ΔD and Δt go to zero for the model to be meaningful. Thus $n(r-p)$ approaches a constant. In particular let the constant $\beta=n(r-p)/r=n(1-p/r)$, so the above requirement is met. Then p/r is equal to $1-\beta/n$, which satisfies the condition that $p/r\to 1$ as $n\to\infty$ (Feller, 1957).

With these properties, the mass at level j as $k\to\infty$ is

$$\lim_{k\to\infty}\overline{M}_j(k)=\overline{M}_j=\sum_{i=1}^{n}M_i(0)\pi_j=n\overline{M}\pi_j, \tag{3}$$

where $\overline{M}$ denotes the mean value of the mass in the vertical. The values of π_j are obtained from the solution of the systems of equations 1 where π_j, π_{j+1}, π_{j-1}, π_1, π_1, π_2, π_n, π_{n-1}, and π_n are substituted for $P_{i,j}(k)$, $P_{i,j+1}(k-1)$, $P_{i,j-1}(k-1)$, $P_{i,1}(k)$, $P_{i,1}(k-1)$, $P_{i,2}(k-1)$, $P_{i,n}(k)$, $P_{i,n-1}(k-1)$, and $P_{i,n}(k-1)$, respectively. T his solution is given by

$$\pi_j=(p/r)^{n-j}[1-(p/r)]/[1-(p/r)^n]. \tag{4}$$

In the limit as $n\to\infty$,

$$\lim_{n\to\infty}n\pi_j=\beta e^{-\beta m}/(1-e^{-\beta}), \tag{5}$$

where $m=1-j/n$. Therefore, the sediment-concentration profile is given by

$$\lim n\overline{M}\pi_j=M_m=\overline{M}\beta e^{-\beta m}/(1-e^{-\beta}). \tag{6}$$

The parameter β is a function of the fall velocity of the sediment particles and of the intensity of turbulence. As $\beta\to 0$, the sediment-concentration profile approaches $\overline{M}$. That is, in the limit, the concentration of sediment is a constant, independent of depth. In general, the concentration is a minimum at the stream surface and increases exponentially to a maximum at the streambed. This description of the sediment-concentration profile is essentially the same as that obtained by the use of the differential equation of diffusion (Rouse, 1950). It is of some interest to note that equation 6 leads to

$$\frac{\partial M_m}{\partial mD}=-\frac{\beta}{D}M_m, \tag{7}$$

which has the same form as the differential equation in Rouse (1950). Therefore

$$\frac{\beta}{D}=\frac{W}{\epsilon},$$

where W is the fall velocity and ϵ is the turbulent mixing coefficient.

REFERENCES

Feller, William, 1957, An introduction to probability theory and its applications: New York, John Wiley and Sons, v. 1, 249 p.

Matalas, N. C., and Conover, W. J., 1965, Derivation of the velocity profile from a statistical model of turbulence: Water Resources Research, v. 1, no. 2, p. 235–261.

Parzen, Emanuel, 1962, Stochastic processes: San Francisco, Calif., Holden and Day, 325 p.

Rouse, Hunter, 1950, Engineering hydraulics: New York, John Wiley and Sons, p. 780–799.

NEW OBSERVATIONS ON THE SHEYENNE DELTA OF GLACIAL LAKE AGASSIZ

By CLAUD H. BAKER, JR., Salt Lake City, Utah

Work done in cooperation with the
North Dakota State Water Commission and the North Dakota Geological Survey

Abstract.—The Sheyenne delta is an extensive deposit of gravel, sand, and silt near the south end of the basin of glacial Lake Agassiz. The deposit has been called both a delta and a body of ice-contact stratified drift, but recent test drilling and field observations indicate that the deposit is a true delta and that the steep slope formerly described as an ice-contact face is probably a wave-cut "cliff." The delta is not so extensive as originally believed, and the boundaries have been redefined. The location of dunes on the delta surface with respect to possible sources of sand indicates that prevailing winds probably were from the southwest when the dunes were formed.

In late Pleistocene time, the valley now drained by the Red River of the North was the floor of a large proglacial lake. The existence of such a lake was recognized as early as 1823, and the lake was named Lake Agassiz by Warren Upham (1880, p. 85) in honor of Jean Louis Agassiz, an early advocate of the glacial theory. At its maximum, Lake Agassiz probably extended from northern South Dakota to central Manitoba.

At several points where large valleys enter the Lake Agassiz basin, the mouths of the valleys are marked by extensive bodies of gravel, sand, and silt, which are believed to be deltas deposited in the former lake by melt-water streams that emptied into it. One of the largest of these deposits is in southeastern North Dakota, near the southern end of glacial Lake Agassiz. Because it radiates from the point where the present Sheyenne River enters the Lake Agassiz plain, it has been called the Sheyenne delta (fig. 1).

Upham (1895) made the first comprehensive survey of the southern end of Lake Agassiz. Leverett (1913, 1932) generally agreed with Upham's views of the lake basin, but concluded that the deltas were ice-contact deposits of stratified drift. Although Elson (1957) agreed with Leverett on the origin of the deltas, Dennis and others (1949, 1950) found subsurface evidence to support Upham's views. Laird (1964) summarized the existing literature on Lake Agassiz.

This report is based on work done in 1963 and 1964 in connection with a study of the geology and groundwater resources of Richland County, N. Dak. The study was conducted under the cooperative program of the U.S. Geological Survey, the North Dakota State Water Commission, and the North Dakota Geological Survey.

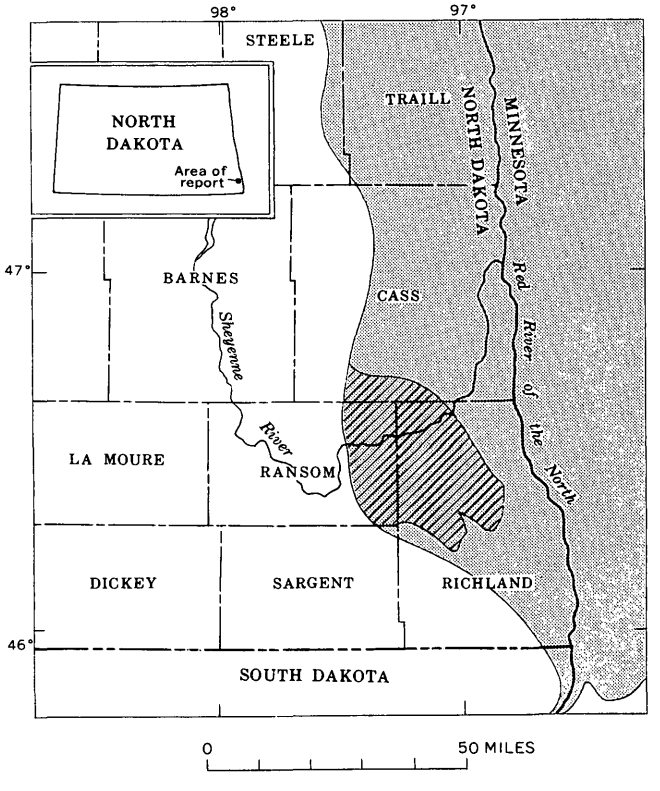

FIGURE 1.—Location of the Sheyenne delta (diagonal pattern) and the Lake Agassiz plain (stippled pattern).

Most of the information reported here about the delta has been obtained by test drilling. Thirty-four test holes were drilled during this study, and 53 test holes were drilled during earlier studies (Dennis and others, 1949, 1950, and unpublished data).

AREAL EXTENT AND TOPOGRAPHY

The Sheyenne delta has an area of about 750 square miles and is roughly deltoid in outline (fig. 1). It is bounded on the west and southwest by the drift prairie and on the northeast, east, and southeast by the Lake Agassiz plain. The northeastern edge is a well-defined steep slope, but the southeastern edge merges imperceptibly with the lake plain.

The area of the Sheyenne delta is somewhat less than was mapped originally by Upham (fig. 2). Upham's map included in the delta a portion of an ice-marginal channel called the Milnor channel (Baker, 1966) that is somewhat older than Lake Agassiz, an area of glacial till between the Milnor channel and the delta, a part of the lake floor, and a large sandy tract southeast of the delta. Presumably, Upham included the area of till in his map of the Sheyenne delta because he believed that the line of the Milnor channel represented the southwestern edge of the delta and the shoreline of Lake Agassiz. Recent studies by the writer indicate that the highest shoreline of Lake Agassiz is marked by the line of the Herman beach, and that the till southwest of the Herman beach does not appear to have ever been covered by water. The southern area of sand (Lake Agassiz beaches, fig. 2) is a beach complex of the same age as, or slightly younger than, the Sheyenne delta. Erosion of the delta may have furnished part of the sand to the southern beach complex, but the area is not a part of the delta proper. Part of the lake floor between the delta and the beach complex was apparently included in the delta by assuming that the eastern edges of the delta and the beach complex were continuous.

The Sheyenne River crosses the north end of the delta in a deeply incised meandering valley. The valley floor is as much as 100 feet below the adjacent delta surface.

A large part of the delta surface is covered by sand dunes. In places, the topography is highly undulating, with local relief as much as 75 feet. Most of the dunes are well stabilized by vegetation, but considerable sand movement still occurs whenever the vegetal cover is broken. The high dunes are bordered on the southwest by a wide band of nearly level sand on the delta; the average elevation of the sand plain is about 1,075 feet. The probable significance of the sand plain will be discussed in a later section of this report (p. B67).

THICKNESS, GRAIN SIZE, AND BEDDING OF SEDIMENTS

The bottom of the delta deposits cannot be distinguished in drill holes. An advancing delta is built out over its own bottomset beds, as well as over any preexisting lake-floor deposits, and it is nearly impossible to distinguish between delta bottomset beds and lake silts of similar composition. The thickness of the lake-floor deposits east of the delta averages about 60 feet. In this discussion the thickness of the Sheyenne delta will be taken as the total thickness of sand, silt, and clay—that is, the depth to the glacial till.

The greatest known thickness of the delta is 198 feet (fig. 3) and the average thickness of the eastern half is about 150 feet. West of the Richland-Ransom County boundary the surface of the till beneath the delta slopes sharply upward, and the delta is only a few feet thick near its western edge.

The average grain size of the delta sediments decreases from west to east (fig. 3). Near the western margin, where the deposits are only a few feet thick, they consist of very coarse sand and fine gravel; but near the eastern margin, where the deposits are more than 150 feet thick, they consist of very fine sand and silt. This gradation of average grain size is consistent with the increased distance of transport across the top of the growing delta.

The average grain size of the sediments also decreases from top to bottom. The decrease is not marked near the thin western margin of the delta but is quite apparent in the thicker central part. Near the eastern margin, material making up the entire thickness of the delta is fine grained, and vertical differences in grain size are difficult to determine. This too, is consistent with the concept of a delta that expanded eastward.

In figure 4, parts of the deposit have been distinguished as predominantly silt or predominantly sand. The silt is thickest near the eastern margin and wedges out to the west; the sand wedges out to the east. Again, these relationships would be expected in this particular deltaic environment.

Exposures of the bedding in the delta are very scarce. The best exposures found are in the bank of a short gully in the E½ sec. 15, T. 136 N., R. 51 W., near the northeastern edge of the delta (location 0–1, fig. 3). At this location, the sediment consists of very fine sand, silt, and clay. Here the sand and silt are well stratified, and ripple lamination is the most com-

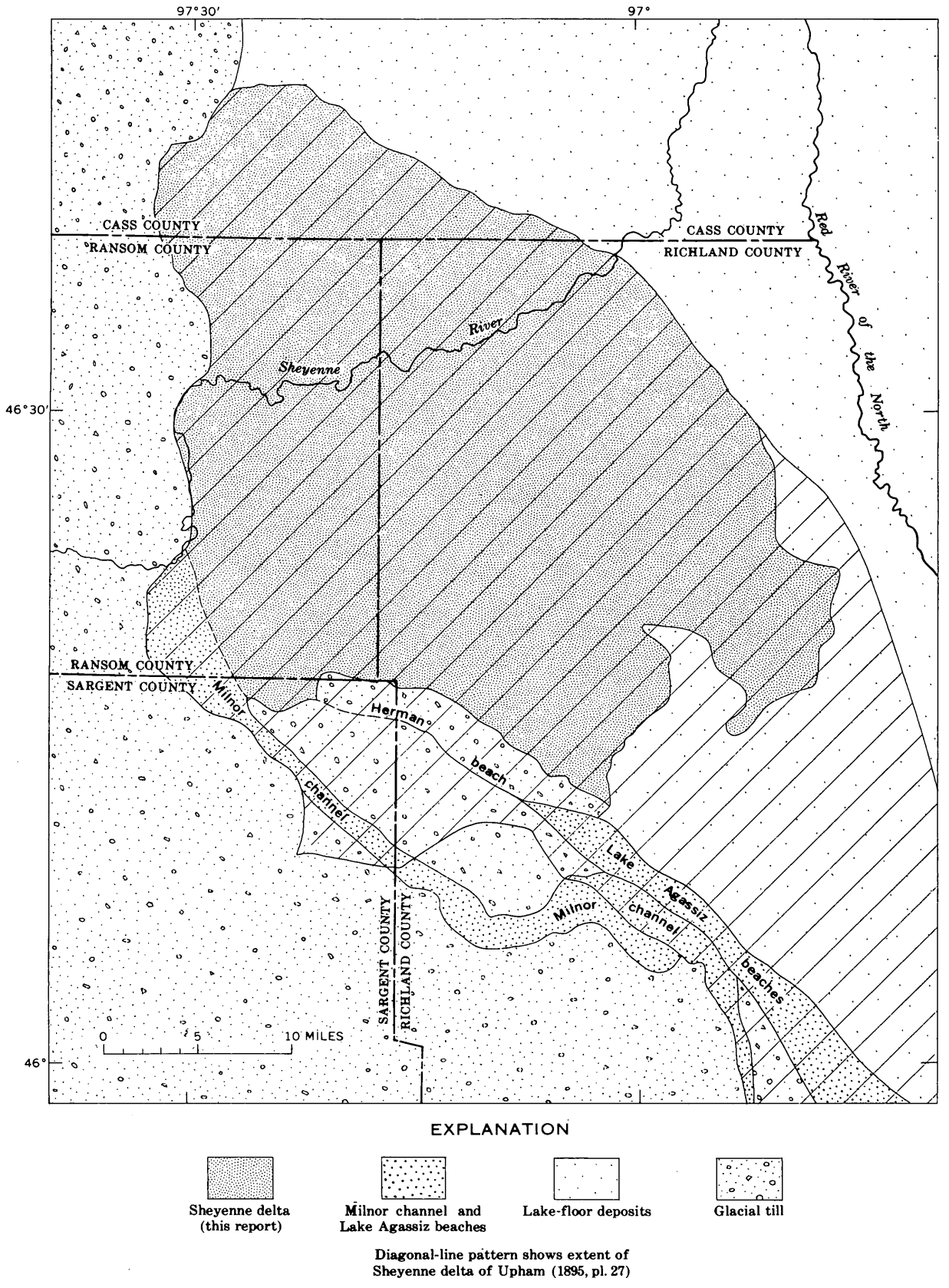

FIGURE 2.—Relationship of the Sheyenne delta as defined in this report, to the area included in the Sheyenne delta of Upham.

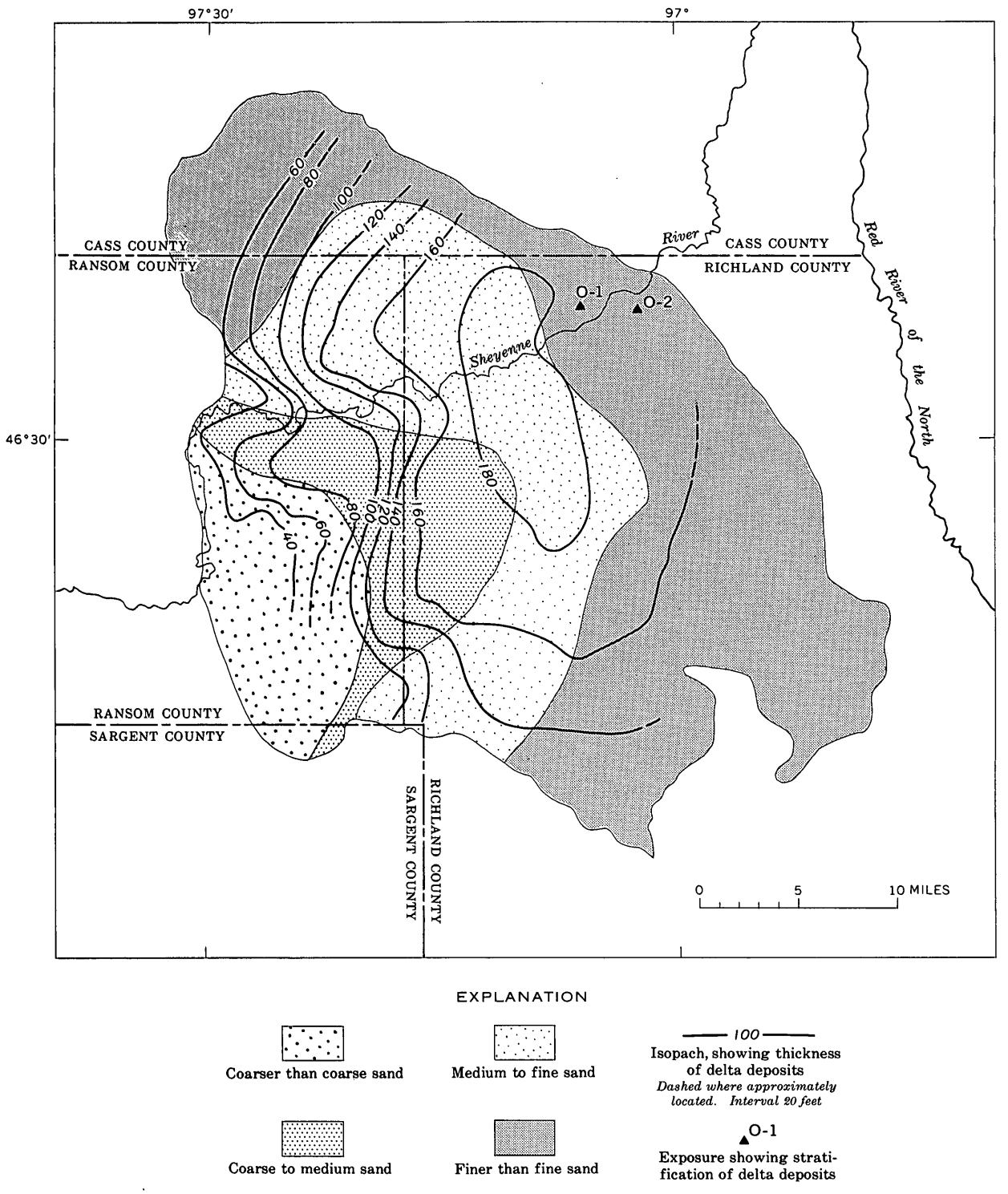

FIGURE 3.—Total thickness of delta deposits, in feet, and average grain size of the near-surface materials.

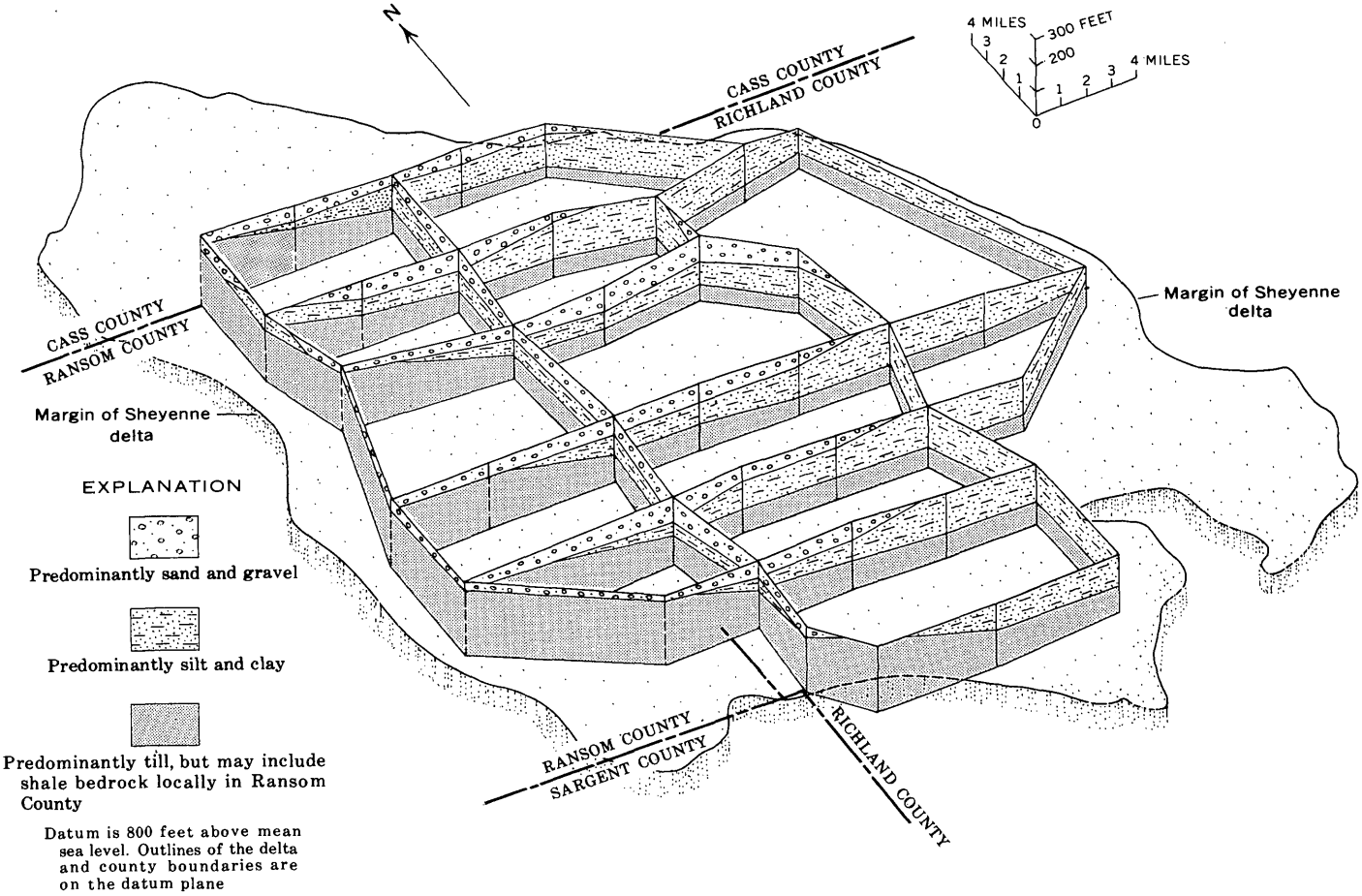

FIGURE 4.—Fence diagram of the Sheyenne delta.

mon form of stratification (fig. 5*A*). No stratification is apparent in the clay layers. Some of the sand and silt beds are strongly contorted on a small scale (fig. 5*B*), but the causes of this are not known. However, such contortions are common in deltaic and flood-plain deposits.

The delta bedding was exposed temporarily in a roadcut in the NE¼ sec. 13, T. 136 N., R. 51 W. (location 0-2, fig. 3). Here, the ripple-laminated sand contains thin films and pockets of carbonaceous material (fig. 5*C*). This exposure was destroyed later by road improvements.

PROBABLE PROCESS OF FORMATION

The Sheyenne delta probably was deposited rather rapidly, during the earliest and highest stages of Lake Agassiz. The Sheyenne River apparently was an ice-marginal stream just prior to the formation of Lake Agassiz (Baker, 1966) and probably was diverted into Lake Agassiz soon after the lake was formed. Because the river was fed primarily by glacial melt water, it must have carried abundant sediment, and deposition of the delta would have begun as soon as the stream began flowing into the lake.

Most of the surface of the delta is at or near the altitude of the highest (Herman) shoreline of Lake Agassiz. Two slightly lower shorelines (the Tintah and the Norcross) were mapped across the delta by Upham (1895), but this author was unable to distinguish them. The fourth, or Campbell, shoreline is probably represented by the steep slope at the northeastern edge of the delta.

The steep northeastern edge of the delta was the principal evidence cited by Leverett (1913, 1932) for his belief that the delta was a deposit of ice-contact stratified drift. Leverett (1932, p. 127) had very little subsurface data, and he thought that glacial till was only a few feet below the surface near the top of the slope. However, logs of test holes in the area show that the sand, silt, and silty clay are more than 150 feet thick near the northeastern edge of the delta. No other evidences of ice-contact deposition were found during the present study. The slope is at the level of the Campbell shoreline north and south of the delta, and this author concludes that the slope is a wave-cut

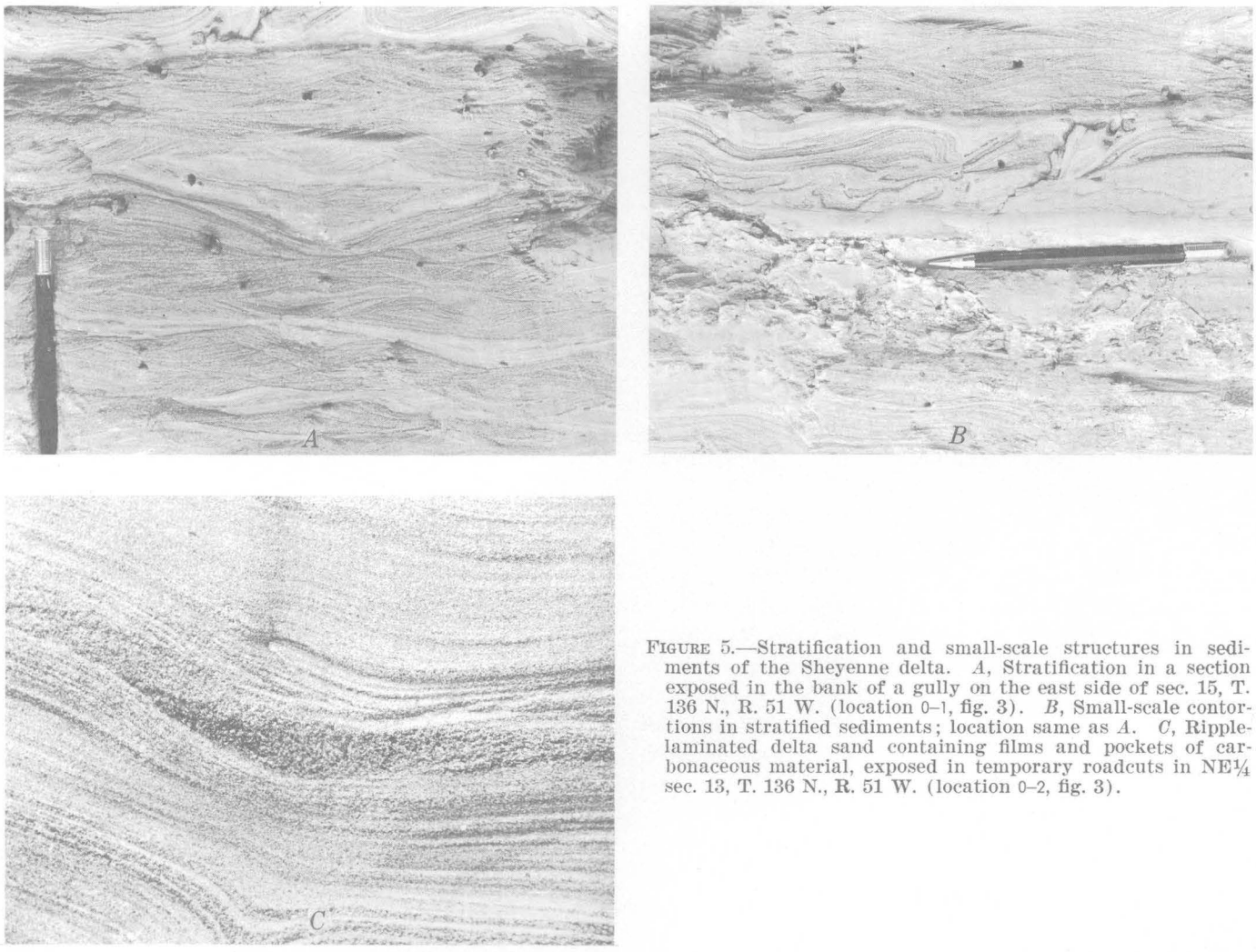

FIGURE 5.—Stratification and small-scale structures in sediments of the Sheyenne delta. *A*, Stratification in a section exposed in the bank of a gully on the east side of sec. 15, T. 136 N., R. 51 W. (location 0–1, fig. 3). *B*, Small-scale contortions in stratified sediments; location same as *A*. *C*, Ripple-laminated delta sand containing films and pockets of carbonaceous material, exposed in temporary roadcuts in NE¼ sec. 13, T. 136 N., R. 51 W. (location 0–2, fig. 3).

"cliff" representing the Campbell shoreline of Lake Agassiz.

When Lake Agassiz began to recede from its highest (Herman) level, the base level of the Sheyenne River was lowered, and the river entrenched itself into the recently formed delta. The position of the present valley was determined by the position that the river happened to occupy when the lake level was lowered.

SAND DUNES ON THE DELTA

The sand dunes that cover much of the surface of the delta probably began to form when Lake Agassiz was first lowered to the Campbell level. As the lake level declined, the emerging surface of the delta would have been highly susceptible to erosion by wind. The dunes are largest and most numerous near the northeastern margin of the delta and become smaller and less numerous southwestward. Thus, the broad sand plain on the part of the delta southwest of the high dunes may have been the source area of the dune sand, and, if this were so, the prevailing winds would have been from the southwest. Because the dune area consists of hummocky topography rather than of discrete well-formed dunes, the orientation of the dunes is of little help in determining wind directions. Furthermore, the stratification within the dunes is not exposed well enough to be used as a key to wind direction.

Clayton and others (1965, p. 655) have interpreted lineations on the Lake Agassiz plain to mean that prevailing winds were probably from the northwest or southeast in late Lake Agassiz time. However, the location of the dunes with respect to possible source areas of the sand does not support such a hypothesis. The sediments near the lakeward margin of the delta are predominantly silt size, whereas the material in the dunes is largely in the fine-sand range, and there is no nearby source of fine sand to the north, east, or southeast of the delta front. Although the evidence from the Sheyenne delta is hardly conclusive, the

presence of an extensive sand plain southwest of an area of dunes suggests that prevailing winds were from the southwest when the dunes were formed. Possibly the prevailing winds were from the southwest in Campbell time and shifted to northwest-southeast later.

If the sand plain was the source of the dune sand, the depth to which erosion by the wind lowered the surface of the sand plain would have been controlled by the water table in the delta sediments. Hence the 1,075-foot present elevation of the sand plain may have been the average elevation of the water table during Campbell time.

SUMMARY

In summary, recent studies of the Sheyenne delta lead to the following conclusions:

1. The form, lithology, and stratification all indicate that the Sheyenne delta is a true deltaic deposit, as suggested by Upham (1895), rather than a body of ice-contact stratified drift, as postulated by Leverett(1913, 1932). The steep northeastern slope is not an ice-contact face, but a wave-cut "cliff" marking a shoreline of Lake Agassiz.

2. Upham's map of the delta included parts of the Lake Agassiz beaches, a pre-Lake Agassiz outwash channel, and adjoining areas of ground moraine and lake floor that are not parts of the delta.

3. The location of dunes on the delta with respect to sources of sand indicates that prevailing winds probably were from the southwest when the dunes were formed, and that the average position of the water table at that time may have been at about the 1,075-foot elevation of the sand plain.

REFERENCES

Baker, C. H., Jr., 1966, The Milnor channel, an ice-marginal course of the Sheyenne River, *in* Geological Survey Research 1966: U.S. Geol. Survey Prof. Paper 550–B, p. B77–B79.

Clayton, Lee, Laird, W. M., Klassen, R. W., and Kupsch, W. O., 1965, Intersecting minor lineations on Lake Agassiz plain: Jour. Geology, v. 73, no. 4, p. 652–656.

Dennis, P. E., Akin, P. D., and Jones, S. L., 1949, Ground water in the Wyndmere area, Richland County, N. Dak.: North Dakota Ground-Water Studies 13, 55 p.

——— 1950, Ground water in the Kindred area, Cass and Richland Counties, N. Dak.: North Dakota Ground-Water Studies 14, 75 p.

Elson, J. A., 1957, Lake Agassiz and the Mankato-Valders problem: Science, v. 126, no. 3281, p. 999–1002.

Laird, W. M., 1964, The problem of Lake Agassiz: North Dakota Acad. Sci. Proc., v. 18, p. 114–134.

Leverett, Frank, 1913, Early stages and outlets of Lake Agassiz in relation to the waning ice sheet: North Dakota Agr. Coll. Survey, 6th Bienn. Rept., p. 18–28.

——— 1932, Quaternary geology of Minnesota and parts of adjacent states: U.S. Geol. Survey Prof. Paper 161, 149 p.

Upham, Warren, 1880, Preliminary report on the geology of central and western Minnesota: Geol. and Nat. History Survey of Minnesota, 8th Ann. Rept., p. 70–125.

——— 1895, The glacial Lake Agassiz: U.S. Geol. Survey Mon. 25, 658 p.

GROSS COMPOSITION OF PLEISTOCENE CLAYS IN SEATTLE, WASHINGTON

By DONAL R. MULLINEAUX, Denver, Colo.

Work done in cooperation with the Municipality of Metropolitan Seattle

Abstract.—Unweathered glaciolacustrine and glaciomarine deposits of relatively uniform composition are the principal clay formations in the Seattle area. Their major clay minerals, in order of decreasing abundance, are chlorite, illite, and montmorillonite, and their dominant exchangeable cations are calcium and magnesium. Nonglacial and weathered glacial clays are more variable in composition and are of smaller volume. Typically they contain more montmorillonite clay minerals and fewer exchangeable calcium cations. The differences in composition are useful for identification of clay units and for interpretation of their environments of deposition and history.

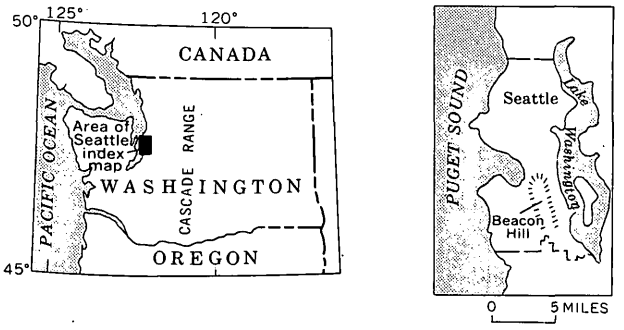

FIGURE 1.—Location of areas discussed in this report.

The bulk of Pleistocene clay formations in Seattle (fig. 1) are glacial deposits that are seemingly unweathered. These units are grossly uniform in composition; they show only minor variations in content from place to place within the same formation, or even from one formation to another. As expected, they consist largely of rock flour—even their predominant clay mineral probably was derived from the parent rocks by mechanical rather than chemical weathering. In contrast, nonglacial clay layers and weathered glacial clays are of relatively small volume and show wide variations in composition. Their clay-mineral content may be quite different from that of unweathered glacial deposits.

The clayey sediments in Seattle are being investigated to determine the composition of identifiable geologic units and the relation of composition to geologic origin, history, and engineering properties of those units. Clay-mineral and exchangeable-cation content especially can provide important clues to the identity and geologic record of sediments, and may strongly influence their engineering properties. This interim report describes the gross composition of some typical local clays as indicated by about 50 samples, and discusses briefly the origin of some of the clay minerals and the relation of composition to origin and history. The relation of composition to engineering properties and classification tests will be described in a later report.

For this investigation, constituent minerals were identified by T. C. Nichols, E. E. McGregor, P. D. Blackmon, and H. C. Starkey, of the U.S. Geological Survey, by X-ray diffraction techniques. The X-ray techniques are widely regarded as the most effective for identification of clay minerals (Weaver, 1958; Konta, 1963), but may be only roughly quantitative. Because of the quantitative limitations, only the relative abundance of clay minerals is presented in this report. The methods used for quantitative estimates on which the reported abundance is based are described by Schultz (1964). The exchangeable-cation data were determined by Starkey, and the other laboratory tests were performed by Nichols, McGregor, R. A. Speirer, and G. S. Erickson, all of the U.S. Geological Survey.

U.S. GEOL. SURVEY PROF. PAPER 575-B, PAGES B69-B76

Outcrop samples were collected by the writer. Drill-core samples, all from exploratory holes drilled for the Municipality of Metropolitan Seattle, were provided by E. R. McMaster and D. S. Tillson of the engineering firm serving the Municipality under contract.

TERMINOLOGY

Numerous terms used to describe clays may have one common meaning for surficial geologists, but another for engineers, planners, or even other geologists. Following are definitions, as used in this report, of several terms that have proved to be confusing. Most important are the terms "clay" and "silt," which are applied to either deposits or their constituents, and which may refer to plasticity, grain size, or nature of component minerals (see Grim, 1953, p. 1–2, or Mackenzie, 1963, for discussions). In this report the term "clay" is used in a general sense to describe a natural fine-grained sediment that exhibits readily detectable plasticity when mixed with a limited amount of water. The term "clay-size" refers to particles whose "size" or "diameter" is less than 2 microns, and the term "clay mineral" is used to describe certain hydrous aluminum silicate minerals that have special properties because of their sheetlike or layered structure and usual small size. Similarly, the term "silt" is used in a general sense to describe a fine-grained sediment that exhibits little or no plasticity. The term "silt-size" refers to particles whose diameters are between 2 and 64 microns. The term "nonclay" describes minerals that are more nearly equidimensional than sheetlike and do not have the special properties of clay minerals.

The names "chlorite," "illite," "montmorillonite," and "kaolinite" refer to clay-mineral groups, within which considerable chemical and some structural variation is possible (Grim, 1953, p. 27–38). The criteria for their identification in complex mixtures by X-ray diffraction are reviewed by Schultz (1964). Montmorillonite and mixed-layer minerals that consist mostly of montmorillonite are, for the present, reported simply as montmorillonite.

Although the terms "varved" and "varves" have sometimes been used to describe any distinctly laminated deposit of silt and clay, they are used here only to describe sediments that exhibit rhythmically alternating layers of silt and clay. Pairs of such layers are interpreted as varves, each pair consisting of one silt layer and an overlying clay layer that represent summer and winter layers, respectively, of an annual cycle of sedimentation (Mackin, 1937; Mackin and others, 1950). Restriction of the terms is useful in Seattle because, where present, the typical stratification helps to identify certain glaciolacustrine units.

The term "glacial" is used to describe deposits derived chiefly from southward-moving continental glaciers that occupied the Puget Sound lowland. The term "nonglacial" is used for deposits not genetically related to those glaciers. Some nonglacial sediments were deposited during warm climatic conditions, but others probably were deposited during colder times when alpine glaciers were extensive in the adjacent Cascade Range.

Most glacial deposits are described as unweathered, meaning that they show little or no evidence of leaching, oxidation, or clay-mineral transformation. The alteration of deposits described as weathered is evidenced by differences in color and structure as well as clay-mineral content (Mullineaux and others, 1964).

GLACIAL CLAYS

The largest, most extensively exposed glacial-clay units in Seattle are lacustrine in origin (table 1). They are thick units that probably were deposited in proglacial lakes formed by glaciers that blocked the normal northward drainage of the Puget Sound lowland. The deposits typically are well sorted and stratified, and are characterized by successions of thin laminations of markedly different grain size. No fossils have been found in them, but calcareous concretions are common. The glaciolacustrine sediments probably were deposited rapidly in relatively quiet water, with little postdepositional reworking by plants or animals, and with little disturbance except for minor subaqueous slumping.

TABLE 1.—*Categories of clay units discussed*

- Glacial clays
  - Glaciolacustrine
    - Unweathered
    - Weathered
  - Glaciomarine
- Nonglacial clays

Some glacial-clay units are regarded as at least partly marine in origin because locally they contain marine megafossils and microfossils and exchangeable sodium cations. For this report, even though the fossils and cations are sparse and are not distributed throughout these deposits, the entire units are described as glaciomarine. Lithologically, they are similar to glaciolacustrine deposits. Although the glaciomarine formations appear to contain more contorted strata and to be less well stratified, they presently cannot be differentiated where fossils and sodium cations are absent.

TABLE 2.—*Age and stratigraphic position of some principal deposits in Seattle*

Geologic-climate unit	Deposits	
Vashon Stade of Fraser Glaciation [1]	Vashon Drift	Till Esperance Sand Member Lawton Clay Member
Olympia Interglaciation	Nonglacial clay, silt, sand, gravel, and peat	
Pre-Vashon glaciations undifferentiated	Varved clay unit, underlain locally by till and gravel	
	Glaciomarine clay and "till"	

[1] The Vashon Glaciation of Willis (1898) and most later authors was the latest advance of the continental Puget glacier lobe over the Seattle-Tacoma area. Although the Vashon advance is only one event of several representing the last major (Fraser) glaciation of this region (Armstrong and others, 1965), it was the only advance of Fraser time during which the glacier reached the Seattle area.

The two most important glaciolacustrine units recognized presently (1966) are the Lawton Clay Member of Vashon Drift (Mullineaux and others, 1965; and table 2 of this paper), and a fine-grained member of an older, pre-Vashon drift that will be referred to as the "varved clay unit." The Lawton Member consists almost entirely of clay and silt, and its lower part is distinctly finer grained than its upper part. A few sand beds occur near the base and top of the member. In partly dry exposures, thin, light-gray silt layers typically contrast with dark-gray clay layers that generally are thicker (fig. 2). The Lawton Member is widespread and generally is about 80 feet thick. It probably underlies much of the northwestern and southwestern parts of Seattle between altitudes of about 70 and 150 feet. It is also known to underlie parts of the central business district and the northeastern section of the city, occurring between altitudes of about 100 and 180 feet. The Lawton is the youngest and best known clay unit of Seattle; it was laid down during the advance of the Puget glacier lobe of Vashon age shortly after 15,000 years ago (Mullineaux and others, 1965).

The varved clay unit in the pre-Vashon drift consists chiefly of thin, dark-gray clay layers and thicker, light-gray silt and sand layers (fig. 3) described as varves by Mackin (1937; 1948). Locally, however, it contains lenses of sand or gravel. In the lower part of the unit, the varves are both thicker and coarser grained than in the upper part. The maximum known thickness of the varved unit is about 140 feet, at the north end of Beacon Hill (fig. 1) just south of Seattle's main business district (Mackin, 1948), where it lies between altitudes of about 60 and 200 feet. Varved sediments thought to be part of the same unit crop out intermittently farther south for about a mile, but are thin and occur only between about 175 and 200 feet. Similar varved sediments lie between about 120 and 140 feet 2 miles north of Beacon Hill, but they have not been seen in the intervening area.

Pronounced weathering of glacial clay has been seen only in the upper part of the varved unit at one locality. The weathering profile is expressed by progressive upward changes in color, structure, and clay-mineral content (Mullineaux and others, 1964). The color change, from gray in the unweathered material to brownish green in the weathered zone, is accom-

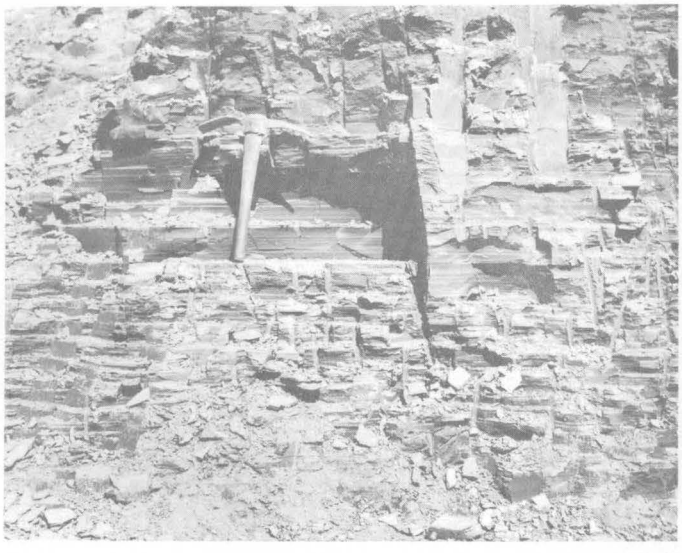

FIGURE 2.—Stratification in lower part of Lawton Clay Member of Vashon Drift. Light-gray silt layers generally are thinner than adjacent dark-gray clay layers.

FIGURE 3.—Stratification of the varved clay unit. Thin dark-gray clay layers alternate with thicker light-gray silt layers. Thickness of varves is variable; they typically are several inches thick in lower part of unit, and a few inches to less than 1 inch thick near the top.

panied by eradication of bedding and increase of deformation. In the upper, most-weathered material, varves are almost indistinguishable, and the clay is highly deformed and crossed by closely spaced, slickensided fractures.

The varved clay unit underlies nonglacial sediments of the Olympia Interglaciation, and probably was deposited during the next older glaciation. The weathering is believed to have occurred during the Olympia Interglaciation.

Scattered marine fossils have been discovered by H. H. Waldron (oral commun., 1963) in outcrops of pre-Vashon glacial deposits in Seattle, and by J. S. Fryberger and D. S. Tillson (oral commun., 1962) in subsurface samples taken east of Seattle during exploratory drilling for the Municipality of Metropolitan Seattle. The glaciomarine deposits that contain the fossils are thick and widespread units that consist chiefly of clay and silt, but contain more scattered stones and lenses of sand or gravel than do glaciolacustrine deposits. They also contain till-like masses of unstratified and unsorted stony silt and clay—in some places, the Beacon Till of Mackin and others (1950) is such a unit. Locally, stratification in the glaciomarine deposits is as well defined as that in glaciolacustrine sediments, but more commonly it is less distinct and may be obscure. Bedding that has been contorted by subaqueous slumping, however, is more common than in glaciolacustrine strata. In Seattle, the glaciomarine deposits have been recognized in outcrop only at Beacon Hill south of the varved clay localities, but exploratory drilling has shown that they are extensive under both the central business district and the northeastern section of the city. They are also extensive just east of Seattle along the east side of Lake Washington.

The fossils suggest deposition of these sediments in a marine environment, yet they are so sparse that this interpretation is not certain. It is conceivable, for example, that the few fossils were derived from a marine environment farther north and transported to Seattle by ice. Nevertheless, the fossils are presently regarded as recording a marine environment at Seattle, chiefly because some of the microfossil shells appear whole and unabraded and because they occur in clay containing exchangeable sodium cations, which have not been detected in any samples of unweathered clay deposited in a glaciolacustrine environment.

The ages of various glaciomarine units are not well known, but those in Seattle are all older than the Olympia Interglaciation, and glaciomarine clay may have been deposited during more than one glaciation.

Mineral composition

Glacial-clay formations in Seattle are composed chiefly of clay and nonclay minerals, but typically they include small amounts of rock fragments as well as noncrystalline material that is not identified by X-ray diffraction techniques. Organic material is very scarce.

Most of the clay and nonclay minerals are of clay and silt size, respectively, so that the proportion of clay minerals in a deposit increases as the overall grain size decreases. However, clay minerals also occur as silt-size particles, and make up as much as 40 percent of some fine-grained sediments in which only 10 percent of the particles are smaller than 2 microns. Similarly, nonclay minerals occur as clay-size particles, and make up as much as 30 percent of sediments in which only 20 percent of the particles are larger than 2 microns. In sediments in which half the particles are clay size, generally somewhat more than half are clay minerals.

The nonclay minerals are mostly quartz and feldspar. Feldspar generally is slightly less abundant than quartz, but it dominates some sediments that are rich in volcanic ash. Ferromagnesian minerals, mostly hornblende, are the only other nonclay minerals abundant enough to be identified by X-ray diffraction in all samples.

The principal clay minerals in unweathered glacial deposits are, in order of decreasing abundance, chlorite, illite, and montmorillonite (table 3). In unweathered glaciolacustrine clays, their proportions are especially consistent; the same order of abundance was found in all but one sample analyzed, even though sample sites are widely separated areally and stratigraphically. Chlorite not only is most abundant, but many samples contain as much or more chlorite as all other clay minerals combined. In only one glaciolacustrine sample (sample 2, table 3) did another clay mineral (illite) appear to be as plentiful as chlorite. The X-ray data suggest that the chlorite is well crystallized and iron rich, and the fraction reported as illite includes some material that is also well crystallized. Much of the montmorillonite includes some illite interlayers, and perhaps little or none of the montmorillonite is entirely pure. Kaolinite is present in most samples, but only in trace amounts.

Chlorite and illite are the most common clay minerals in the silt-size fraction, and montmorillonite occurs chiefly as clay-size particles. But even though most montmorillonite is of clay size, chlorite is the dominant clay mineral in clay-size as well as silt-size material in unweathered deposits.

The glaciomarine deposits contain the same clay

TABLE 3.—*Clay-mineral and exchangeable-cation content of clays studied in Seattle, Wash.*

Sample or group of samples	Geologic unit	General location	Number of samples	Source	Amount of sample (percent) with particle size <2 microns	Clay minerals [1]					Cation-exchange data (milliequivalents per 100 g)					
						Chlorite	Illite	Montmorillonite	Kaolinite	Vermiculite	Capacity	Sum	Calcium	Magnesium	Sodium	Hydrogen
Unweathered glaciolacustrine clay																
1	Lawton Clay Member.	Northwestern Seattle.	5	Natural outcrop.	10–85	A	B	C			9–27	19–32	15–23	4.1–10		
2	do	do	1	do	85	AB	AB	C			27	28	19	9.2		
3	do	Central Seattle	5	Artificial excavation.	39–67	A	B	C			12–21	17–24	12–17	4.7–7.6		
4	do	Northeastern Seattle.	4	Drill core	29–54	A	B	C			10–17	11–23	4.7–18	3.3–6.1		
5	Varved clay unit.	Southern Seattle.	3	Natural outcrop.	7–66	A	B	C			18–23	32–33	28–29	2.7–5.2		
6	do	Northern Seattle.	1	Artificial excavation.	65	A	B	C			28	32	24	8.0		
Weathered glaciolacustrine clay																
7	Varved clay unit.	Northern Seattle.	1	Artificial excavation.	49	AB	C	AB	D		35	33	22	11		
8	do	Central Seattle	1	do	33			A	B		[2]	[2]	[2]	[2]		
9	do	do	1	do	39	A	C	B			29	30	18	12		
10	do	Northern Seattle.	1	do	44	C		A	B		36	38	23	14	0.5	
Unweathered glaciomarine clay																
11	Unnamed	Northeastern Seattle.	7	Drill core	17–37	A	B	C			11–21	26–37	17–28	4.6–7.1	0.9–3.0	
12	do	do	4	do	21–78	A	BC	BC			14–26	25–36	21–26	2.1–7.8	2.2–3.2	
13	do	do	1	do	72	A	BC	BC	D		31	33	27	5.6		
14	do	do	1	do	90	A	C	B	D		32	34	26	7.6		
15	do	do	1	do	60	A	C	B			32	33	27	5.9		
16	do	Southern Seattle.	2	Artificial excavation.	29–38	A	B	C			15–17	37–46	26–33	9.2–11	1.6	
17	do	East of Seattle	5	Drill core	2–70	A	B	C			12–24	25–39	18–24	3.9–13	1.8–3.4	
18	do	do	1	Artificial excavation.	28	A	B	C			9.7	24	20	3.8		
Nonglacial clay																
19	Unnamed	Northeastern Seattle.	1	Artificial excavation.	13	AB	C	AB	D		8.9	14	4.5	8.1		1.6
20	do	do	1	do	32	A	BC	BC	D		13	11	5.2	6.0		
21	do	do	1	do	28	A					11	10	4.2	6.1		
22	do	do	1	Drill core	21	A	C	B	D	E	14	15	9.0	4.5		
23	do	do	1	do	38	A	B	C			16	18	8.5	6.2		3.5
24	do	do	1	do	15			A			5.2	7.3	2.9	1.5		2.9
25	do	do	1	do	33	A	C	B			16	16	8.6	3.3		4.3
26	do	Central Seattle.	1	Artificial excavation.	34	AB			C	AB	[2]	[2]	[2]	[2]		
27	do	Northwestern Seattle.	3	Natural outcrop.	18–27	B	C	A			19–23	21–22	12–15	6–10		
28	do	do	1	do	29	A	C	B			13	45	38	6.9		

[1] Alphabetical order of letters shows relative abundance of clay minerals that make up more than about 3 percent of the samples; doubled letters indicate approximately equal amounts.

[2] Not analyzed.

minerals as do those of glaciolacustrine origin, but their proportions appear to be slightly less consistent. The order of decreasing abundance of principal clay minerals was chlorite, illite, and montmorillonite in 15 of the 22 glaciomarine samples analyzed. Locally, the glaciomarine deposits contain somewhat less illite and more montmorillonite than do the glaciolacustrine sediments.

Weathered glacial clay varies widely in clay-mineral composition, and may be dominated by montmorillonite and kaolinite rather than by chlorite and illite. Montmorillonite and kaolinite are more abundant in even the lower part of a weathered zone in the varved unit than in the underlying, unweathered part of the unit, and make up almost the entire clay-mineral fraction in the upper part of the weathered zone.

Exchangeable cations

Exchangeable ions held by clay minerals are mostly cations, because the electrical charges of the clay particles are predominantly negative. Since the amount of exchangeable anions is small in the sediments studied, only the cation content has been determined for most samples. For some samples, the cation content exceeds the exchange capacity, which represents the number of positions around the clay particles available for occupation by exchangeable ions. Thus, not all

the cations around the clay particles are actually held in exchangeable positions.

Table 3 shows the cations identified and the measured exchange capacity of most samples for which mineralogy is reported. A cation content higher than the measured capacity is typical of glacial deposits. The dominant cations are calcium and magnesium. Sodium has not been detected in the glaciolacustrine varved clay unit or the Lawton Clay Member, but does occur in most samples of glaciomarine deposits. Even in the glaciomarine samples, however, sodium makes up only a minor proportion of exchangeable cations. Somewhat surprisingly, the cation content of each sample of weathered varved clay is similar to that of unweathered clay from the same unit. The excess of cations over capacity in glacial deposits indicates that neither the unweathered nor weathered parts have been substantially leached.

The dominance of calcium and magnesium is expectable, for these two cations are the most common and abundant in clays generally (Grim, 1953, p. 126), and are plentiful in rivers draining the adjacent Cascade Range (Griffin and others, 1962). Sodium is abundant in the same rivers, but calcium and magnesium are adsorbed preferentially over sodium under most conditions (see Grim, 1953, p. 144–146, and Mielenz and King, 1955, p. 210, for reviews).

The exchangeable sodium cations, like the marine fossils, probably record a marine or brackish-water environment at Seattle. The varved clay unit and the Lawton Member, in which exchangeable sodium was not detected, are interpreted from other evidence as fresh-water deposits. If they have not been significantly leached, their cation content represents that adsorbed during deposition in fresh water. The sodium adsorbed by clay increases, however, as its concentration in the surrounding water increases; thus the exchangeable sodium in some sediments implies their deposition in marine or brackish water. Yet sodium proportions in glaciomarine deposits in Seattle (table 3) are much lower than those in glaciomarine deposits in British Columbia (Ahmad, 1961). The lower proportion might record deposition in less salty water, or even initial deposition of the material in marine water north of Seattle and subsequent reworking by the glacier. If the latter is possible, the presence of exchangeable sodium is not certain proof of marine or brackish-water conditions at Seattle.

NONGLACIAL DEPOSITS

Nonglacial clays in Seattle are widespread, but their volume is small. In contrast to glacial clays, they occur in thin lenses that generally are interbedded with silt, sand, and gravel rather than in thick, relatively uniform deposits. Peat, wood, and diatoms are relatively abundant in these sediments, but concretions are rare. Bedding may be indistinct except where it is accentuated by concentrations of plant material. These features suggest that most nonglacial clays were laid down relatively slowly in shallow lakes and on flood plains where they were partly reworked by plants and animals during and after deposition.

The ratio of nonclay to clay minerals in most nonglacial sediments is about the same as in glacial deposits. Four of the five samples of nonglacial clays of Olympia age contained a slightly higher ratio of clay minerals to clay-size particles than glacial deposits. However, the few samples examined of nonglacial sediments older than Olympia age contained a lower ratio, probably because the older deposits sampled are rich in volcanic ash.

The principal clay minerals in nonglacial sediments include the three that are prevalent in glacial deposits, though in much less uniform proportions, plus kaolinite and vermiculite. Only one of the nonglacial clay samples analyzed (sample 23, table 3) showed the chlorite, illite, montmorillonite order of abundance that is common to unweathered glacial deposits. Montmorillonite, which was less abundant than chlorite and illite in most samples of glacial deposits, was predominant in nearly half the samples of nonglacial clay and less abundant than illite in only the one sample mentioned above. Kaolinite occurred in more than trace amounts in 4 of 12 samples. Vermiculite, which was unidentified in the glacial clays, was reported in two nonglacial samples; in one (sample 26, table 3), a mixed-layer mineral of vermiculite and chlorite was virtually the only clay mineral present. Thus the clay-mineral composition of the nonglacial deposits is highly varied. Even within single outcrops of sediments of Olympia age, there are differences from bed to bed that seemingly are not related to variations in grain size or to surficial weathering profiles. These differences might represent occasional variation in the detrital materials supplied during deposition, or differential alteration in place either before or after deposition of overlying beds.

In most nonglacial samples, the exchangeable-cation content approximately equaled rather than exceeded the exchange capacity. The prevalent cations are calcium and magnesium, but they are not as abundant as in glacial deposits. Sodium was not identified. Exchangeable hydrogen, which has not been identified in unweathered glacial deposits, was found in 4 of 12 samples of nonglacial clay; its irregular occurrence

probably reflects an acid environment produced by organic material in the nonglacial sediments.

ORIGIN OF CLAY MINERALS

A much-discussed point regarding the origin of clay minerals in sediments is whether they are detrital minerals that were formed elsewhere and transported into the depositional basin, or secondary minerals that were formed in place by weathering or diagenesis after the sediments were deposited. Most clay minerals in the sediments at Seattle probably are detrital. Chlorite and illite, for example, form the bulk of very uniform sediments such as the Lawton Clay Member that are seemingly unweathered. Perhaps these minerals might form uniformly throughout such sediments by diagenesis, but the proportion so formed is small even in marine sediments (Weaver, 1958, 1959; Keller, 1963; Biscaye, 1965), and little if any diagenesis is expected in fresh water (Grim, 1958). At Seattle, chlorite and illite are less predominant in glaciomarine clays than in glaciolacustrine, suggesting that diagenesis has not been significant even in the marine sediments. Since neither weathering nor diagenesis seems adequate to account for the chlorite and illite, they are regarded as detrital in both glacial and nonglacial sediments.

Montmorillonite, however, appears to be in part detrital and in part secondary. In unweathered glacial deposits, a detrital origin is suggested by uniform distribution of montmorillonite along with chlorite and illite throughout the Lawton Clay Member. Also, in nonglacial sediments, a largely detrital origin seems likely because of the abundance of montmorillonite in sediments of Olympia age. Its proportion in those sediments is much greater than in older glacial deposits; hence the montmorillonite was not formed by any overall alteration of unconsolidated deposits in place. Nor is it likely that it formed by surficial weathering shortly after deposition; possible layer-by-layer alteration cannot be completely discounted, but no montmorillonitic weathering profiles were evident in the sediments that were sampled. In contrast, the bulk of the montmorillonite and kaolinite in the weathered glacial clay evidently formed in place. Because the increase in those two minerals in the weathered zone is accompanied by a decrease in chlorite and illite, the montmorillonite and kaolinite probably formed chiefly from the chlorite and illite rather than from nonclay minerals.

The detrital clay minerals probably were derived from bedrock in source areas by both mechanical and chemical weathering. The chief source of sediments in the Seattle area is the Cascade Range of Washington (fig. 1). From the northern part of the range, detrital material is carried westward into the adjacent lowland by rivers; during glacial episodes, it is moved southward to the Seattle area by continental glaciers. From the central part of the range, detritus is carried directly into the area by rivers during both glacial and nonglacial episodes. Clay minerals, especially chlorite, fine-grained mica (illite), and kaolinite, have been reported as common in the bedrock of the Cascade crest by Smith and Calkins (1906) and most later authors. Thus, any of the clay minerals that are common in the lowland sediments probably could have been derived by mechanical weathering alone. The fact that well-crystallized, iron-rich chlorite generally is destroyed rather than formed by chemical weathering (Jackson and others, 1948; Jackson, 1963, p. 40–41) indicates that the chlorite is a product of mechanical weathering. The prevalence of chlorite in glacial deposits, in turn, indicates that mechanical weathering was predominant during glacial episodes. It seems likely that most clay minerals in glacial deposits at Seattle, like those in similar clays in New England (Allen and Johns, 1960), were ground from bedrock by glaciers, with little if any chemical change.

In contrast, clay minerals that form readily by chemical weathering, particularly montmorillonite, are plentiful in many nonglacial sediments (table 3). That such clay minerals are also largely detrital is indicated by the content, chiefly montmorillonite, of a sample of the clay being carried from the Cascade Range to Seattle by modern rivers. Conceivably, the plenitude of clay minerals other than chlorite and illite in nonglacial sediments might reflect only their greater abundance in bedrock of the central Cascades, the chief source of the nonglacial detritus. It seems more likely, however, that it results from generally more effective chemical weathering during nonglacial episodes. Comparison of clay mineral suites now being carried by rivers from northern and central parts, respectively, of the Cascade Range of Washington, should indicate whether or not different clay mineral suites are delivered from different parts of the range under similar weathering conditions. And comparison of the same suites with those from unweathered glacial deposits should indicate whether or not chemical weathering is more effective at present than during glacial episodes.

CONCLUSIONS

Clay-mineral and exchangeable-cation proportions seem adequate to distinguish between most glacial and nonglacial clays in the Seattle area, and exchangeable sodium cations distinguish some glaciomarine deposits.

241-334 O—67——6

However, the composition of at least some nonglacial clays is like that of unweathered glacial clays, the range of composition of weathered glacial clays matches that of nonglacial clays, and exchangeable sodium cations are not present in all samples of glaciomarine deposits.

Glaciolacustrine clays apparently have a very uniform composition. The only significant variation found in their composition was in weathered samples. The clay minerals in the glaciolacustrine deposits probably are largely detrital particles transported by streams into the Puget Sound lowland during glacial episodes, when glaciers were producing abundant rock flour in source areas. They evidently have been modified very little since deposition.

The clay-mineral composition of glaciomarine deposits is generally similar to that of glaciolacustrine sediments, but the former are distinguished by fossil and exchangeable-cation content. Their clay-mineral composition is somewhat more variable, but the cause of the variety is not presently known. The glaciomarine deposits probably record marine or brackish-water conditions at Seattle.

Nonglacial sediments vary widely in content of both clay minerals and exchangeable cations, but most are characterized by relatively abundant montmorillonite. Their composition may result from chemical weathering that was more effective during nonglacial times.

While recognition of the composition of clay deposits is important to geologic interpretations, it should also aid engineers in their efforts to understand, predict, and modify clay properties. In Seattle, knowledge of composition should afford better interpretation of test and exploratory data, and more effective extrapolation of experience from place to place in the metropolitan area.

REFERENCES

Ahmad, N., 1961, The stony marine clays of the upper Fraser Valley, British Columbia; 2. Chemical characteristics of the deposits: Soil Sci., v. 91, p. 328–331.

Allen, V. T., and Johns, W. D., 1960, Clays and clay minerals of New England and eastern Canada: Geol. Soc. America Bull., v. 71, p. 75–85.

Armstrong, J. E., Crandell, D. R., Easterbrook, D. J., and Noble, J. B., 1965, Late Pleistocene stratigraphy and chronology in southwestern British Columbia and northwestern Washington: Geol. Soc. America Bull., v. 76, p. 321–330.

Biscaye, P. E., 1965, Mineralogy and sedimentation of Recent deep-sea clay in the Atlantic Ocean and adjacent seas and oceans: Geol. Soc. America Bull., v. 76, p. 803–832.

Griffin, W. C., Sceva, J. E., Swenson, H. A., and Mundorff, M. J., 1962, Water resources of the Tacoma area, Washington: U.S. Geol. Survey Water-Supply Paper 1499–B, 101 p.

Grim, R. E., 1953, Clay mineralogy: New York, McGraw-Hill Book Co., 384 p.

Grim, R. E., 1958, Concept of diagenesis in argillaceous sediments: Am. Assoc. Petroleum Geologists Bull., v. 42, p. 246–253.

Jackson, M. L., 1963, Interlayering of expansible layer silicates in soils by chemical weathering, *in* Bradley, W. F., ed., Clays and clay minerals: Natl. Conf. Clays and Clay Minerals, 11th, Ottawa, Ontario, Aug., 1962, Proc., p. 29–46 (Issued as Earth Sci. Ser. Mon. 13 by Pergamon Press, New York).

Jackson, M. L., Tyler, S. A., Willis, A. L., Bourbeau, G. A., and Pennington, R. P., 1948, Weathering sequence of clay-size minerals in soils and sediments; I: Jour. Phys. and Colloid Chemistry, v. 52, no. 7, p. 1237–1260.

Keller, W. D., 1963, Diagenesis in clay minerals—a review, *in* Bradley, W. F., ed., Clays and clay minerals; Natl. Conf. Clays and Clay Minerals, 11th, Ottawa, Ontario, Aug., 1962, Proc., p. 136–157 (Issued as Earth Sci. Ser. Mon. 13 by Pergamon Press, New York).

Konta, J., 1963, Quantitative mineralogical analysis of "blue clay" from Vonšov, Bohemia; a comparative study by nine laboratories: Clay Minerals Bull., v. 5, p. 255–264.

Mackenzie, R. C., 1963, De Natura Lutorum: *in* Bradley, W. F., ed., Clays and clay minerals; Natl. Conf. Clays and Clay Minerals, 11th, Ottawa, Ontario, Aug., 1962, Proc., p. 11–28 (Issued as Earth Sci. Ser. Mon. 13 by Pergamon Press, New York).

Mackin, J. H., 1937, Varved clay section in the Puget Sound area [abs.]: Geol. Soc. America Proc. 1936, p. 318.

——— 1948, Possible sun-spot cycle in pre-Wisconsin varves in the Puget area, Washington [abs.]: Geol. Soc. America Bull., v. 59, p. 1376.

Mackin, J. H., Mullineaux, D. R., and Stark, W. J., 1950, Glacial geology of Seattle: Washington Univ. (Seattle), Trend in Engineering, v. 2, no. 4, p. 19–21.

Mielenz, R. C., and King, M. E., 1955, Physical-chemical properties and engineering performance of clays, *in* Pask, J. A., and Turner, M. D., eds., Clays and clay technology: California Div. Mines Bull. 169, p. 196–254.

Mullineaux, D. R., Nichols, T. C., and Speirer, R. A., 1964, A zone of montmorillonitic weathered clay in Pleistocene deposits at Seattle, Washington, *in* Geological Survey Research 1964: U.S. Geological Survey Prof. Paper 501–D, p. D99–D103.

Mullineaux, D. R., Waldron, H. H., and Rubin, Meyer, 1965, Stratigraphy and chronology of late interglacial and early Vashon glacial time in the Seattle area, Washington: U.S. Geol. Survey Bull. 1194–O, 10 p.

Schultz, L. G., 1964, Quantitative interpretation of mineralogical composition from X-ray and chemical data for the Pierre Shale: U.S. Geol. Survey Prof. Paper 391–C, 31 p.

Smith, G. O., and Calkins, F. C., 1906, Description of the Snoqualmie quadrangle [Washington]: U.S. Geol. Survey Geol. Atlas, Folio 139, 14 p.

Weaver, C. E., 1958, Geologic interpretation of argillaceous sediments, pt. 1, Origin and significance of clay minerals in sedimentary rocks: Am. Assoc. Petroleum Geologists Bull., v. 42, p. 254–271.

——— 1959, The clay petrology of sediments, *in* Swineford, Ada, ed., Clays and clay minerals; Natl. Conf. Clays and Clay Minerals, 6th, Berkeley, Calif., Aug. 1957, Proc., p. 154–187 (Issued as Earth Sci. Ser. Mon. 2 by Pergamon Press, New York).

Willis, Bailey, 1898, Drift phenomena of Puget Sound: Geol. Soc. America Bull., v. 9, p. 111–162.

SOME OBSERVATIONS ON A CHANNEL SCARP IN SOUTHEASTERN NEBRASKA

By J. C. MUNDORFF, Salt Lake City, Utah

Abstract.—Evidence suggests that manmade changes in a drainage system in southeastern Nebraska about 50 years ago may have caused the formation of a channel scarp that has moved about 3.5 miles upstream from about 1914 to 1963. Pronounced widening and deepening of the Muddy Creek channel have occurred as the scarp moved upstream. Rough estimates indicate that mainstem channel erosion resulting from scarp migration has contributed about 30,000 tons of sediment annually to the downstream reach of Muddy Creek and ultimately to the Little Nemaha River.

Manmade changes in mainstem stream channels and tributary channels can result in later natural changes in tributary channels. This report presents a history, partly inferred, of such a tributary channel from the time of a mainstem channel change in about 1914 to 1963.

In about 1914, a channel improvement project was undertaken on the Little Nemaha River in the vicinity of Syracuse, Nebr. (fig. 1). In some places, the existing channel was straightened; in other places, a new channel was excavated half a mile or more from the existing channel. About 8 miles southeast of Syracuse, in the area where Muddy Creek joined the Little Nemaha River, a straight channel was constructed about half a mile southwest of the natural channel of the Little Nemaha River. At about the same time, the junction of Muddy Creek and the Little Nemaha River was moved about 1 mile upstream by construction of a new channel for Muddy Creek. Information is not available on elevations of the Little Nemaha River and Muddy Creek channels at the new junction.

The drainage area of Muddy Creek is mantled mainly with loess and glacial till of Pleistocene age. For several miles upstream from the confluence with the Little Nemaha River, the valley is about half a mile wide, and the valley fill is unconsolidated alluvium. The scarp is being cut in a compact silty clay that is somewhat more resistant than the alluvium that forms the upper several feet of most of the valley.

DRAINAGE CHANGES

The position of former major channels of Muddy Creek and its principal tributaries, except where they coincide with the present channel of the main stream (or with new tributaries), are shown by dashed lines on figure 1. Prior to 1949 the main Muddy Creek channel was about ⅛ to ¼ of a mile south of its present course in sections 21, 22, and 23. Aerial photographs dated June 1949 indicate that a new main channel of Muddy Creek had developed in the N½ sec. 21, and a long reach upstream from sec. 21 had been straightened. Runoff from about 40 square miles, or about 85 percent of the drainage basin, had been diverted from the former main channel of Muddy Creek to enlarged manmade drainage ditches and a former tributary across the northern part of secs. 22 and 23.

As nearly as can be recontructed from reliable available data, the drainage changes in secs. 21, 22, and 23 occurred about as follows. The present nearly straight channel between State Highway 50 and the first tributary upstream from the highway may have developed from a small drainage ditch that originally was intended only to carry runoff from the northeast part of sec. 21. The drainage ditch, which probably was constructed before 1940, may have gradually eroded and deepened and, during one or more large floods on Muddy Creek, overbank flow may have caused major scour in the ditch. Then flow from this ditch was routed into the upstream end of a former tributary which headed in the northwest part of sec. 22 and flowed eastward. By 1949 all the flow of Muddy Creek upstream from Highway 50 was through the new straight reach and the former tributary, and together they had become the new main stream.

U.S. GEOL. SURVEY PROF. PAPER 575-B, PAGES B77-B79

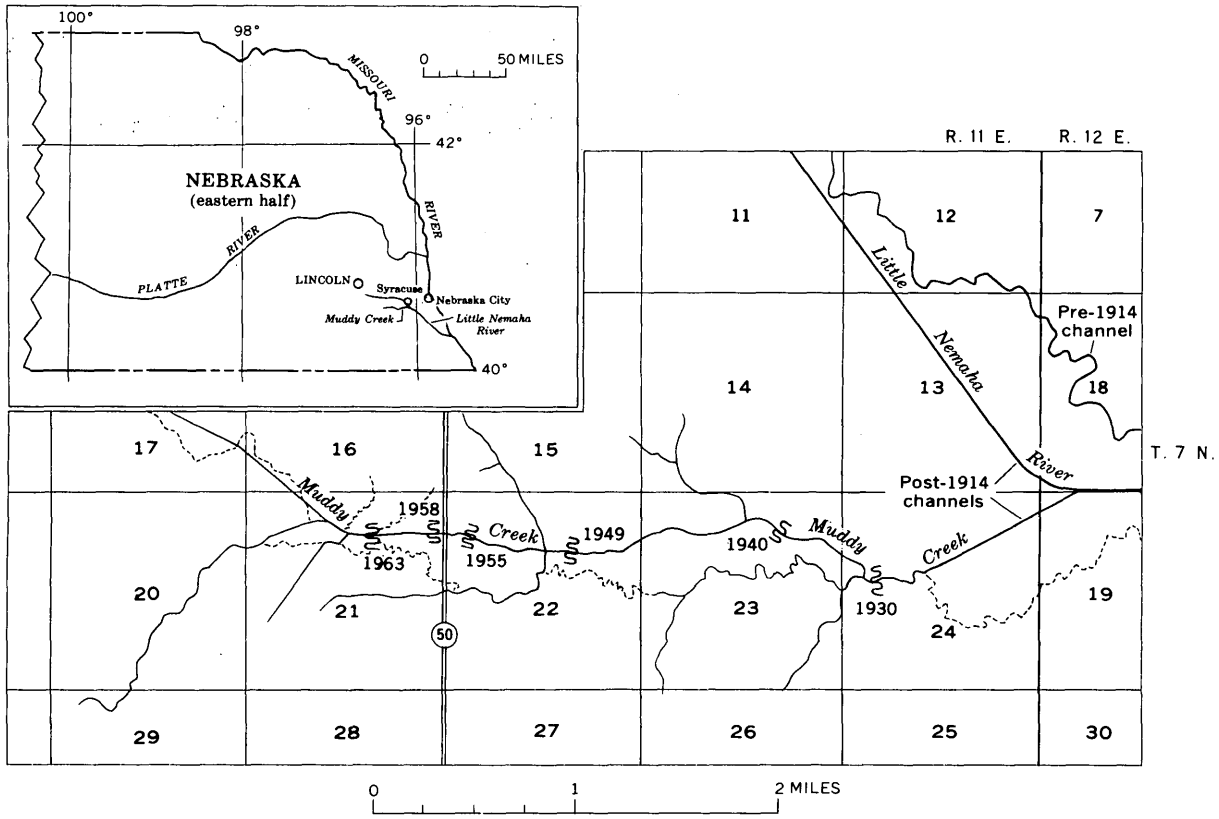

FIGURE 1.—Map showing location of Muddy Creek and location of channel scarp in 1930, 1940, 1949, 1955, 1958, and 1963. Former channels of Muddy Creek and its tributaries are shown by dashed lines.

Also by 1949 the old main channel downstream from Highway 50 was no longer continuous from the diversion in sec. 21 to the junction with the new Muddy Creek channel in sec. 24. It had become two tributaries to the new main stream, which by this time had settled in its present course—a former tributary—in secs. 22 and 23.

POSSIBLE CAUSES OF SCARP

In 1957 a channel scarp several feet high was observed on Muddy Creek immediately upstream from the bridge on State Highway 50 about 6 miles south of Syracuse and about 3.5 channel miles upstream from the present junction of Muddy Creek and the Little Nemaha River (fig. 1). In 1958 this scarp was about 280 feet upstream from the bridge. The scarp could have resulted from any of the following causes, which are listed in the order of estimated probability:

1. After construction, the channel of the Little Nemaha River may have deepened initially at a much faster rate than that of Muddy Creek. Perhaps a major flood shortly after construction resulted in significant deepening of the Little Nemaha River channel, and Muddy Creek may have been left as a hanging tributary with a scarp at the new point of junction of the two streams.

2. Muddy Creek may have been left as a hanging tributary purely as a result of channel construction.

3. During construction, a scarp may have been formed at the point where the constructed downstream reach of Muddy Creek was joined to the natural channel near the center of sec. 24, T. 7 N., R. 11 E.

4. The scarp may have existed before the Little Nemaha River and Muddy Creek channels were modified and may be the result of natural processes.

UPSTREAM RETREAT OF SCARP

A resident near the downstream end of Muddy Creek recalls that during the period 1920–30, the scarp moved slowly through the extreme south side of the northwest quarter of sec. 24. Aerial photographs taken in September 1940 do not show whether the scarp moved up the channel of Muddy Creek; the area where the scarp was most likely to have been in 1940 is obscured by a dense cover of overhanging trees. The photographs do indicate that a scarp was moving up the channel of a tributary—later to become the main channel of Muddy Creek—that was parallel to

and about a quarter of a mile north of the Muddy Creek channel. By 1940 the scarp in this tributary had moved about half a mile upstream from the junction with Muddy Creek (fig. 1).

Aerial photographs indicate that by 1949 the scarp had moved nearly halfway across sec. 22 or about 1 mile upstream from its location in 1940. Also by 1949 the former main channel had been abandoned in secs. 21, 22, and 23, and drainage from nearly the entire basin was carried by the former tributary channels in these sections.

Aerial photographs dated July 1955 show that the scarp was only about 500 feet downstream from the bridge at State Highway 50. Thus, the scarp moved about half a mile during the period 1949–55.

Between 1955 and 1958 the scarp moved to a point about 280 feet upstream from the bridge. During the winter of 1962–63 the scarp was about 1,850 feet upstream from the bridge and was about 690 feet downstream from the junction of Muddy Creek and a tributary (fig. 1). The average annual rate of movement of the scarp was about the same during 1949–55 as during 1956–63. The greatest rate of movement was during 1940–49, when a drainage ditch and the former tributary became the mainstem in secs. 21, 22, and 23.

Upstream from the scarp, the width of the channel bottom was commonly 18 to 25 feet; bank-to-bank width at bank lips averaged about 45 feet. Downstream from the scarp, the width of the channel bottom was 50 to 80 feet; bank-to-bank width was nearly 100 feet in places. Depth of the channel at any section depends somewhat on irregularities in bank elevation but probably averaged about 16 feet upstream from the scarp and about 26 feet downstream from the scarp. The distance from the lip of the scarp to the bottom of the scour pool was 9 to 10 feet when observed in 1963 (fig. 2).

In addition to the scarp in the main channel, other scarps probably occur in abandoned channels and in the tributaries in secs. 14, 15, and 23. The movement of the mainstem scarp past each tributary may have resulted in formation of a scarp in the tributary. In 1963 a 4-foot scarp and a series of steeply sloping steps were observed in a 150-foot reach of a tributary in sec. 22. The scarp and steps are believed to reflect the movement of the scarp up the main channel and past the mouth of the tributary during the period 1949–55.

FIGURE 2.—Channel scarp in Muddy Creek, February 1963.

EFFECTS OF SCARP RETREAT

Rough estimates based on observations during 1957–63 indicate that mainstem channel erosion resulting from the scarp migration has contributed about 30,000 tons of sediment annually to the downstream reach of Muddy Creek and ultimately to the Little Nemaha River. Tributary channel erosion resulting from the upstream migration of the mainstem scarp probably contributed additional large quantities of sediment to Muddy Creek. The channel changes have increased channel capacity and reduced bottom-land flooding in some areas; however, the long-term effects of these changes on the drainage system probably were not considered when the changes were made.

This scarp study site has been included in the Vigil Network of the U.S. Geological Survey, which consists of many sites throughout the United States at which observations of hydrologic and geomorphic processes will be repeated over a long period of time (Emmett, 1966; Leopold and Emmett, 1965).

REFERENCES

Emmett, W. W., 1966, The Vigil Network—Methods of measurement and a sampling of data collected: Internat. Assoc. Sci. Hydrology symposium, Budapest, 1965, pub. 66, p. 89–106.

Leopold, L. B., and Emmett, W. W., 1965, Vigil Network sites—A sample of data for permanent filing: Internat. Assoc. Sci. Hydrology Bull., v. 10, no. 3, p. 12–21.

EFFECT OF LANDSLIDES ON THE COURSE OF WHITETAIL CREEK, JEFFERSON COUNTY, MONTANA

By HAROLD J. PROSTKA, Denver, Colo.

Abstract.—Three or more landslides dammed the valley of Whitetail Creek causing channel migrations and development of unusual transverse valley profiles. The landslides very likely were caused by lateral stream corrasion, wet Pleistocene climate, springs, and earthquake shocks.

Whitetail Creek, a major tributary of the Jefferson River about 10–15 miles east of Butte, Mont., drains the southeast part of the South Boulder Mountains. In the north-central part of the Dry Mountain quadrangle the stream emerges from forested mountains at an altitude of 5,240 feet and flows southeastward for 3 miles across virtually barren semiarid rugged terrain to an altitude of 4,760 feet (fig. 1). In this 3-mile reach the stream follows a sinuous course through steep-walled narrow rocky canyons alternating with broad valleys eroded in unconsolidated landslide deposits. Profiles across canyon segments of the stream course have distinctive and unusual configurations as illustrated in figure 1. In each cross section there is a thick deposit of landslide material on one side of the valley separated from the gorge by a low ridge of bedrock. This profile is present in many places along the 3-mile stream segment, with the landslide deposits on one side or the other of the stream. The purpose of this paper is to discuss the unusual valley profiles and the manner in which they were formed.

LANDSLIDE DEPOSITS

The landslide deposits are porous and unstratified and are made up of poorly sorted angular fragments mainly of diorite porphyry and welded tuff in a matrix of weathered rock debris. Most of the fragments range in size from less than 1 inch to about 12 inches across, though a few are as much as 15 feet across. The landslide deposits are less than half a mile to more than a mile long, they slope toward the stream at about 6½°, and they probably are no more than 350 feet thick. Their surface has been modified by erosion which destroyed any preexisting hummocky topography. The shape of the deposits indicates that they had longitudinal ridges that bifurcated at their distal ends into lobate tongues. Their slope and configuration indicate movement at right angles to the valley. The deposits are of local origin, since the fragments are the same as the bedrock in the adjacent valley walls.

The deposits are interpreted as having formed by ancient landslides. Their slope is within the range observed for rockslide avalanches (Mudge, 1965, p. 1006), they are composed of a heterogeneous mixture of rock fragments, and they are generally lobate in form. Talus deposits are also porous but are much steeper, 26°–36° (Sharpe, 1938, p. 30). Mudflows and debris flows contain an abundant clayey matrix and generally are steeper than 6½° (Sharpe, 1938). The inferred direction of sliding is indicated by the lithologies of the fragments; those from the northeast are dominantly welded tuff, whereas the fragments from the southwest are mainly diorite porphyry. All three (or more) slides occurred at about the same time, as indicated by the similar degree of erosion each deposit has sustained and by the comparable dimensions of the associated bedrock canyons and rims. Although evidence is lacking for the age of the landslide deposits, they are very likely Pleistocene.

EFFECTS ON DRAINAGE

The landslides blocked the ancestral valley of Whitetail Creek and diverted the stream to a new course. The inferred process by which this was accomplished is shown in figure 2. Landslide debris partially filled and dammed the ancestral valley. The

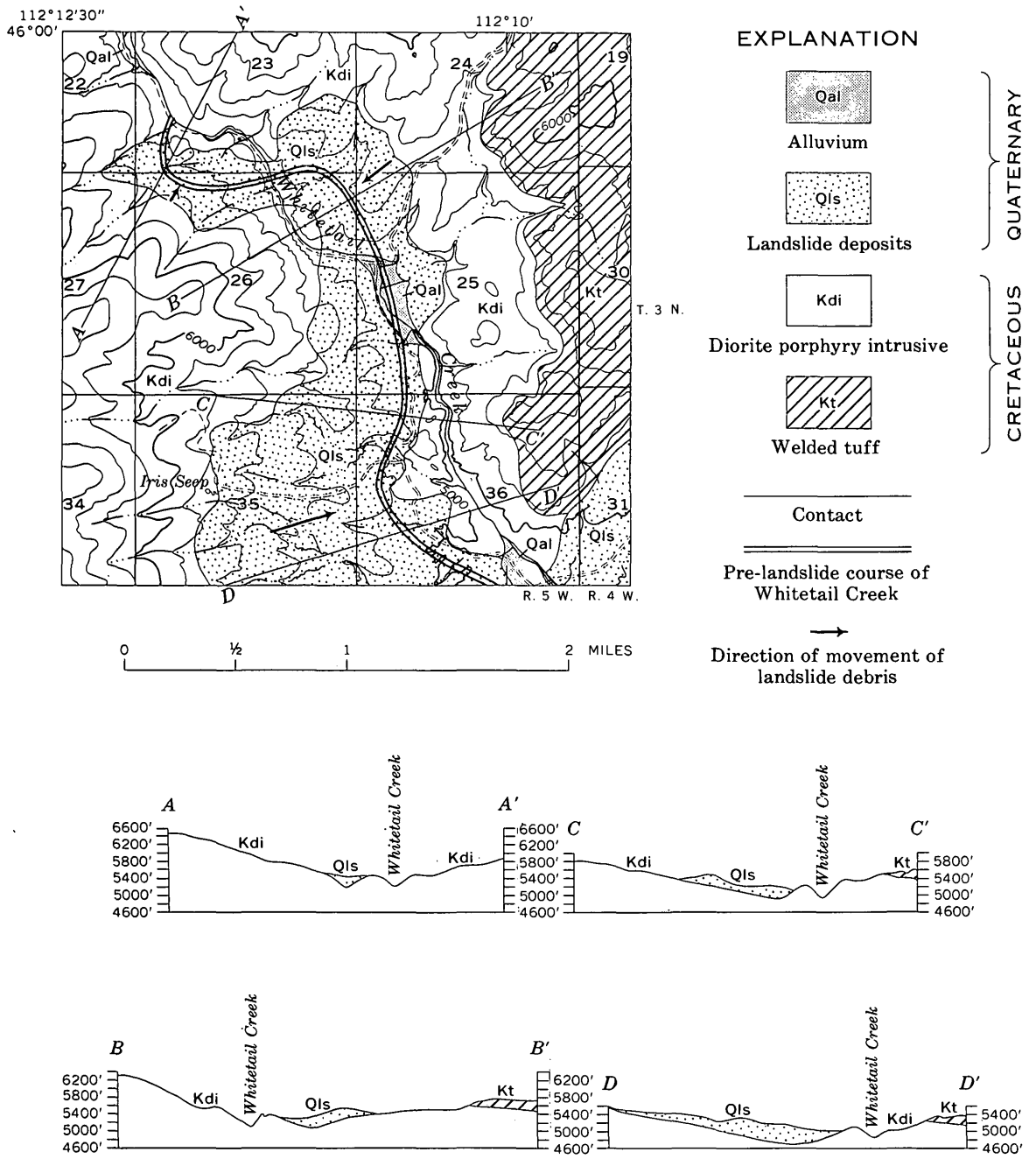

FIGURE 1.—Generalized geologic map and sections of a part of the Dry Mountain quadrangle, Montana. Base from U.S. Geological Survey Dry Mountain 7½-minute topographic quadrangle.

debris dam was at least 350 feet high and may have been as much as 600 feet high. The ponded waters eventually spilled over the debris and established the present channel alongside but above the floor of the ancestral channel. Erosion of the new channel in bedrock, and partial removal of slide material by rill wash and tributary streams produced a distinctive valley profile. The exhumed bedrock between the gorge and landslide deposit formed the characteristic "rimrock." The gorges are predominantly linear, northwest-trending features which probably were eroded along joints and fractures in the bedrock. The present stream channel is entirely in landslide debris where it crosses the landslide deposits, thus indicating that it is above the floor of the ancestral channel. From these and other map data the approximate location and depth of the ancestral channel can be inferred (fig. 1).

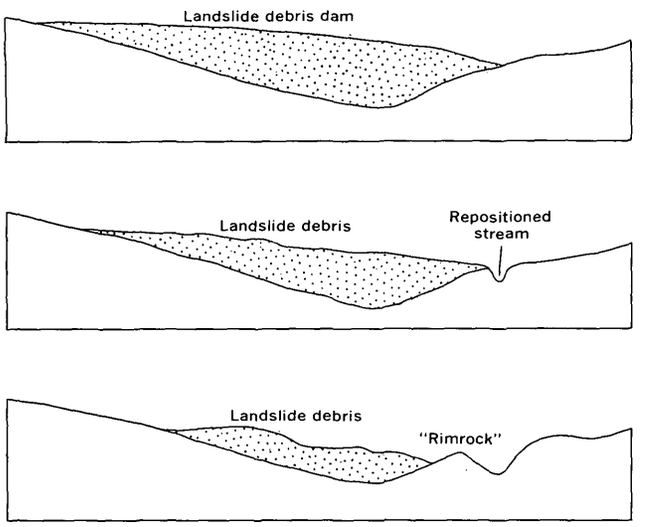

FIGURE 2.—Schematic sections showing development of valley profiles along Whitetail Creek.

CAUSES OF LANDSLIDING

The ancestral stream seems to have had a slightly meandering course, with the outer bend of each meander adjacent to the source of the slide debris. Here the steepening of valley walls by lateral stream corrasion may have been a contributing factor to landsliding.

Lateral corrasion alone, however, would not explain the slides. The bedrock, although extensively jointed, does maintain steep slopes such as those in the present stream gorges. Climatic changes account for some landslides—perhaps increased moisture due to a wetter Pleistocene climate was an important factor. Iris Seep, in the southwest part of the map area (fig. 1) is near the edge of a landslide deposit. Perhaps this and other now inactive springs may have supplied water which aided sliding.

Earthquakes also trigger landslides. Pardee (1926) described rockslides caused by the Montana earthquake of June 7, 1925. The Hebgen Lake slide in Montana occurred during an earthquake, and it has been suggested (Waldrop and Hyden, 1963, p. E13) that some of the large landslides in the Yellowstone area, Wyoming-Montana, were a result of earthquakes. Southwestern Montana has been seismically active throughout late Cenozoic time (Pardee, 1950; Ross and Nelson, 1964). Because all the landslides along Whitetail Creek apparently occurred at about the same time, it seems likely that they were triggered by an earthquake.

In summary, the landslides probably resulted from a combination of two or more of the following factors: lateral stream corrasion, wet Pleistocene climate, springs, and earthquake shocks. The landslides were responsible for channel migrations and development of unusual transverse valley profiles.

REFERENCES

Mudge, M. R., 1965, Rockfall-avalanche and rockslide-avalanche deposits at Sawtooth Ridge, Montana: Geol. Soc. America Bull., v. 76, p. 1003–1014.

Pardee, J. T., 1926, The Montana earthquake of June 27, 1925: U.S. Geol. Survey Prof. Paper 147–B, p. 7–23.

——— 1950, Late Cenozoic block faulting in western Montana: Geol. Soc. America Bull., v. 61, no. 4, p. 359–406.

Prostka, H. J., 1966, Igneous geology of the Dry Mountain quadrangle, Jefferson County, Montana: U.S. Geol. Survey Bull. 1221–F, p. F1–F21.

Ross, C. P., and Nelson, W. H., 1964, Regional seismicity and brief history of Montana earthquakes: U.S. Geol. Survey Prof. Paper 435, p. 25–30.

Sharpe, C. F. S., 1938, Landslides and related phenomena; a study of mass movements of soil and rock: New York, Columbia Univ. Press, 136 p.

Waldrop, H. A., and Hyden, H. J., 1963, Landslides near Gardiner, Montana: Art. 182 *in* U.S. Geol. Survey Prof. Paper 450–E, p. E11–E14.

VARVED LAKE BEDS IN NORTHERN IDAHO AND NORTHEASTERN WASHINGTON

By EUGENE H. WALKER, Boise, Idaho

Abstract.—Thick deposits of fine-grained sediment underlie the floors of the Purcell Trench, the Pend Oreille Valley and adjacent lowlands, and the Priest River valley in northern Idaho and northeastern Washington. The deposits formed in a late glacial lake while ice blocked the north-flowing stretch of the Pend Oreille River. Sheets of clay, distinctly varved in places, are interbedded with sheets of sand and silt. The sheets of sand and silt are interpreted as drainage varves that were deposited when the lake burst out past the ice dam at about 12- to 65-year intervals. The sheets of sand in the lowlands underlain by lake deposits provide small, but in most places adequate, water supplies for domestic and stock needs.

The principal lowlands of northern Idaho—the Pend Oreille Valley, the Purcell Trench, and the adjoining valleys (fig. 1)—are underlain by thick deposits of clay, silt, and fine-grained sand. The sediments accumulated in a lake that existed in late glacial time when ice dammed the stretch of the Pend Oreille Valley that extends northward into Canada.

GLACIAL LAKE IN WHICH VARVED BEDS WERE DEPOSITED

The lake had a maximum shoreline altitude of a little less than 2,500 feet above sea level, as shown by patches of lake deposits on the margins of the lowlands. The lake overflowed southward through a col south of Newport, Wash., and also, at times, southward past Athol, Idaho, to the Rathdrum Prairie.

This late glacial lake in the Purcell Trench and the Pend Oreille lowlands should not be confused with Lake Missoula, which was impounded in the Clark Fork drainage when ice several thousand feet thick occupied the Purcell Trench and extended at least to the southern end of Lake Pend Oreille. According to Alden (1953), Lake Missoula had a maximum water-level elevation of about 4,200 feet behind the ice dam in the gorge of Clark Fork and drained southward across the Rathdrum Prairie when the ice in the Purcell Trench thinned. The late glacial lake, which succeeded and was considerably smaller than Lake Missoula, disappeared when ice melted from the stretch of the Pend Oreille Valley that extends northward into Canada.

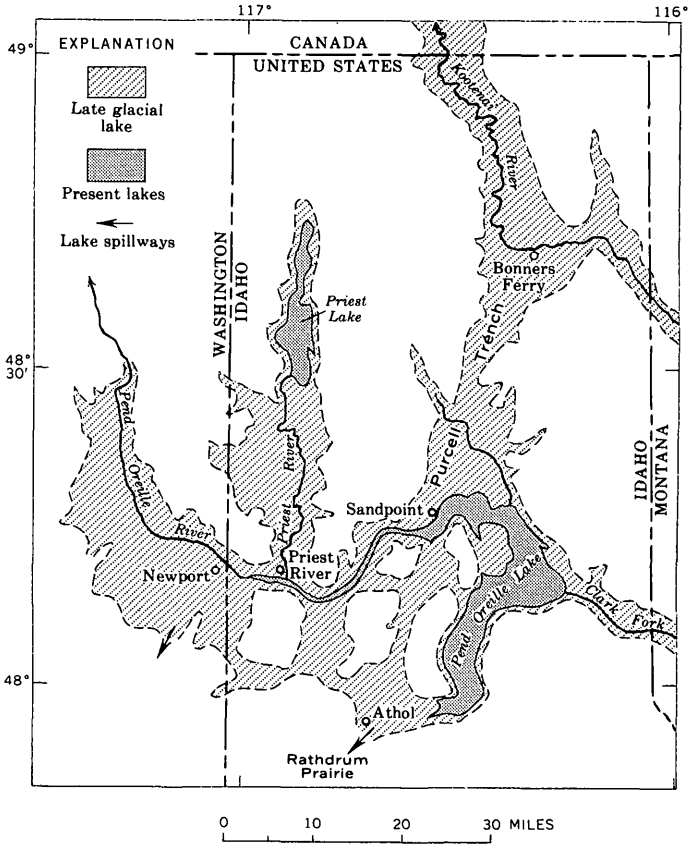

FIGURE 1.—Map showing extent of late glacial lake in the Pend Oreille and Priest River valleys and the Purcell Trench in northern Idaho and northeastern Washington.

U.S. GEOL. SURVEY PROF. PAPER 575-B, PAGES B83-B87

DESCRIPTION AND GEOLOGIC SIGNIFICANCE OF THE VARVED LAKE BEDS

Purcell Trench and Pend Oreille Valley

Thick lake deposits occupy the Purcell Trench and associated valleys. The trench was deepened by ice that was several thousand feet thick and covered all but the higher parts of the bordering mountains, which rise almost 5,000 feet above the present valley floors. Below part of Pend Oreille Lake the bedrock is at least 1,140 feet (the depth of the lake at its deepest known place) below the present lake level. This suggests that the sediment thickness in this part of the Purcell Trench may be about 1,000 feet. Wells drilled many years ago in unsuccessful attempts to obtain ground-water supplies at Sandpoint, Idaho, are reported to have penetrated lake deposits only to depths of nearly a thousand feet, and a recent unsuccessful water well, 11 miles north of Sandpoint, was finished in silt and clay at 330 feet (Walker, 1964). Although the lake deposits are thinner in the Pend Oreille Valley, a well near the town of Priest River penetrated 317 feet of silt, clay, and fine-grained sand before being completed in a thin bed of water-bearing gravel.

Exposures in most of the lowlands show that the lake deposits consist of alternating beds of yellow to blue clay, tan silt, and fine-grained sand. Bedding planes are indistinct, and material in the beds is poorly sorted. The beds of sand may be several feet thick and occur at intervals of from 10 to 20 feet. Beds of clay and sand tend to be silty, and beds of silt contain a good deal of clay.

Priest River valley

In the Priest River valley, however, the lake sediments consist of varved clay and beds of well-sorted silt and sand. Figure 2 shows a section of these beds along the highway about 3 miles north of the town of Priest River. A few minutes' work with a shovel exposes excellent glacial varves (fig. 3). Presumably, well-sorted deposits were formed at this location because the narrow arm of the lake in the Priest River valley was less disturbed by waves and currents than the wider parts of the lake in the Pend Oreille Valley and the Purcell Trench.

Description of a representative section.—The lake deposits of the Priest River valley are illustrated by a 28½-foot section (fig. 4) measured about 3 miles north of the town of Priest River.

Only 18 percent of this section is sand (table 1). That the rest is silt and clay shows that deposition occurred in relatively quiet water.

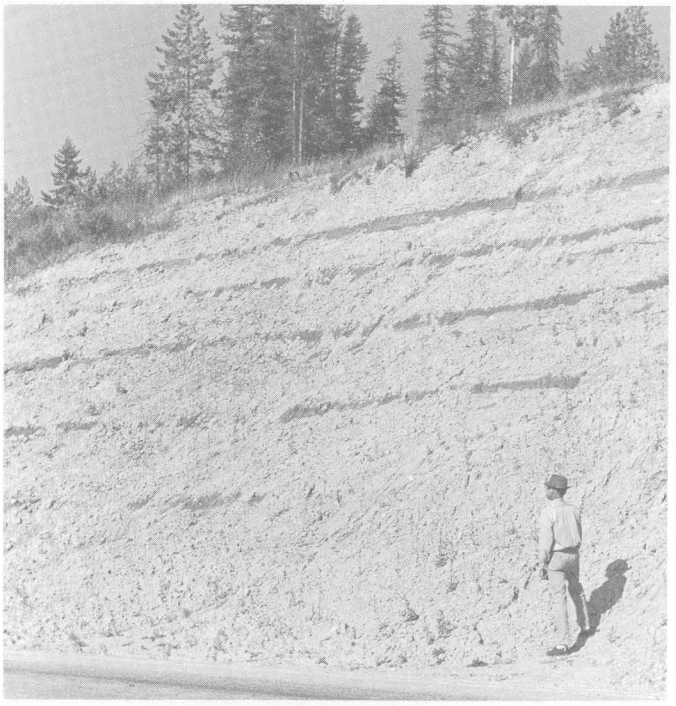

FIGURE 2.—Glacial-lake beds in the Priest River valley, 3 miles north of the town of Priest River, Idaho. The dark layers are wet beds of sand and the light layers are mainly varved clay coated with dry overwash.

FIGURE 3.—Typical varved clay in the southern part of the Priest River valley. About 14 years of deposits are represented in the photograph.

The varved clay indicates that the lake was ice covered in winter and open during part of the summer and was fed by melt water from an ice front. Also, the varved clay indicates a stable lake level, because currents produced by changing lake levels would interfere with the delicate sorting process necessary for the formation of varves.

At three places in the section, a foot or more of varves is so deformed by wrinkling that the varves cannot be counted or measured accurately. The deformation is more likely due to minor earth movements after the Priest River intrenched the deposits than to overriding by ice, for which there is no evidence. The varves are saturated with water and provide gliding planes for motion toward the center of the valley.

The varved clay accumulated at an average rate of a foot in about 16 years. The varves range in thickness from 0.3 to 3.1 inches and average about 0.8 inch, and they are slightly thinner toward the top of the section. Upward thinning of the varves can most logically be interpreted as indicating increasing distance to the local source of sediment—the ice front, which was shrinking northward in the Priest River valley.

The unvarved clay provides no clues as to the rate of deposition. Possibly it was deposited during periods when the ice cover was continuous from year to year and the only water entering the lake was from the base of the glacier. Such inflow would have carried in suspension the clay-sized products of glacial grinding. Many other glacial lakes contain some clay that lacks evidence of varving.

The beds of silt, generally less than a foot thick, are tan or light brown, and show thin laminations. They indicate currents strong enough to drift clay-sized particles elsewhere but too weak to move sand by traction.

The beds of sand range in thickness from 0.3 to 2 feet. The grains are mostly finer than 0.3 mm and are well sorted. Except for one thin bed that is cross-bedded, all the beds show thin horizontal laminae. The characteristics of the sand beds suggest sheetlike movement of water at velocities just strong enough to move small grains of sand.

Repetition of clay-sand-silt-clay sequence in the representative section.—A principal feature of the 28.5-foot section is the repetition, 4 times, of the following sequence: varved clay, a bed of sand, a bed of silt, then varved clay. The 4 distinct sand-silt couplets occupy about 7.5 feet of the 28.5-foot section.

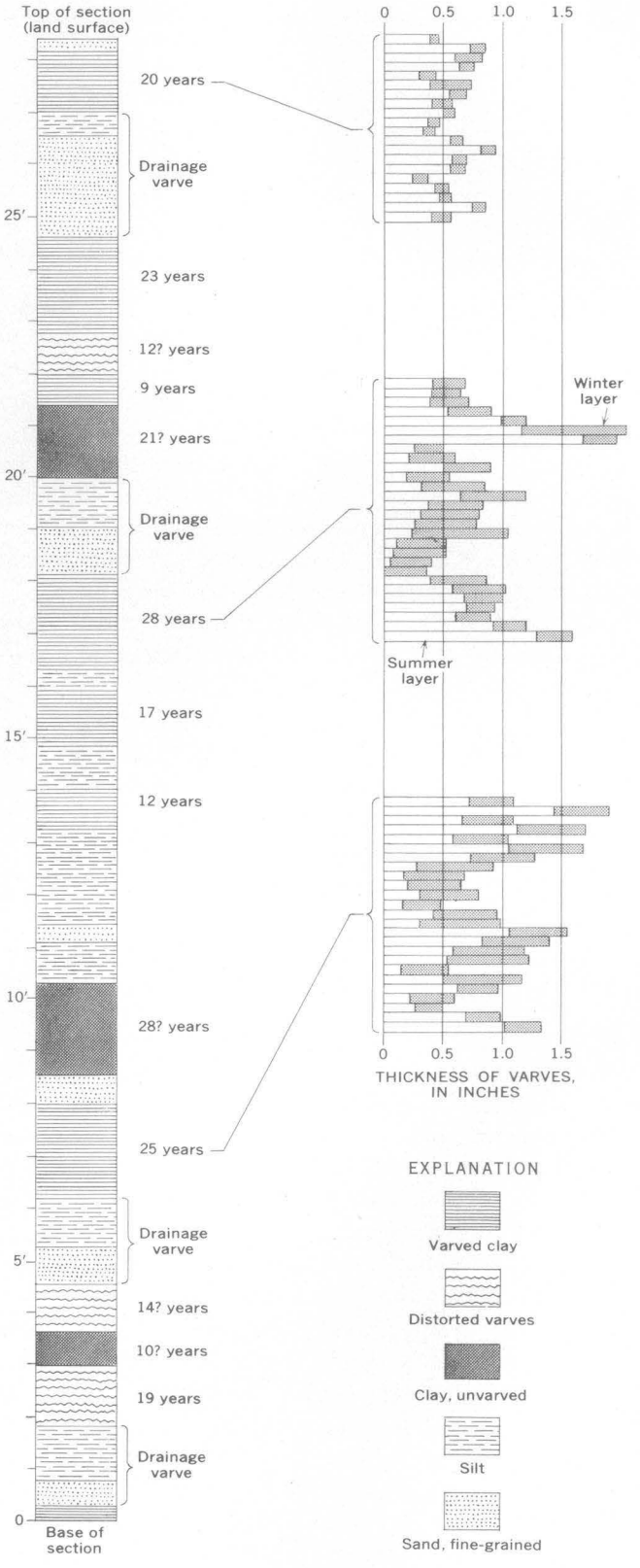

FIGURE 4.—Section of glacial-lake deposits measured in the Priest River valley, 3 miles north of the town of Priest River, Idaho.

TABLE 1.—*Summary of types of material found in representative section of lake deposits in the Priest River valley*

Type of material	Total thickness (feet)	Percentage of section
Clay, varved	12.4	43
Clay, unvarved	3.8	13
Silt	7.3	26
Sand, fine-grained	5.0	18
Total	28.5	100

The abrupt changes from varved clay to sand indicate the sudden development of currents strong enough to spread layers of sand where previously only silt and clay had been settling from still or very slowly moving water. The silt upon the sand shows a slackening of current. The varved clay upon the silt shows the reestablishment of still water in the lake. The most probable cause for such a sequence is that a gush of water suddenly escaped from the lake, thereby setting up currents throughout the lake, and that later, still water was reestablished. This train of events would have resulted from retreats and readvances of the ice that dammed the Pend Oreille Valley.

Probably the late glacial lake was dammed at this time by piedmont glaciers descending from the mountains on both sides of the stretch of the Pend Oreille Valley that runs northward into Canada, and not by a massive valley-filling lobe. Slight recession of whichever piedmont glacier dammed the lake would allow water to spill, and the ensuing flood would quickly widen the breach, as has happened, for example, during many historic outbreaks past ice dams in Iceland. The lake level then would stabilize against the next large mass of ice down the valley, and later it might rise to its original level if the upvalley tongue of ice advanced again.

The currents produced by release of large volumes of water would spread a sheet of sand over the floor of the lake. Then, after overflow ceased and currents died down the fine-grained material that had been stirred into suspension would settle out to form a bed of silt. Finally, varved clay would again accumulate.

According to this interpretation each sand-silt sequence constitutes a single varve. That outbursts of glacial lakes past ice dams and reestablishment of still water occur within single years is shown by historical records of outbursts of glacial lakes in the Alps, Himalayas, and Iceland. For example, the Mattmarksee in the Swiss Alps has broken out over its ice dam in 26 years since 1859 (Charlesworth, 1957, p. 453). In the Baltic area, unusually thick varves of coarse-textured materials have long been recognized as indicators of sudden drainage of glacial lakes. The thickness of the drainage varves in the Priest River valley, 1.5 to 2.4 feet (fig. 4), is not excessive; Pettijohn (1949, p. 468) states that megavarves may be several feet thick.

The section (fig. 4) also shows that at times the deposition of varved clay was interrupted and layers of silt a few inches to a foot thick were spread on the floor of the lake. Presumably such beds of silt indicate minor outbreaks that did not set up currents strong enough to spread a sheet of sand. If so, such beds of silt each represent a year.

The number of years between some of the outbursts can be determined by counting varves. The number of years between other outbursts may be estimated by assuming that varves which are too distorted to count accurately and unvarved clay accumulated at the same rate as the clay with countable varves. The results of such counting and estimates give the following chronology:

Drainage
  20 years
Drainage
  65? years, 44 years of varved clay, clay representing 21? years
Drainage
  28 years
Drainage, minor
  17 years
Drainage, minor
  12 years
Drainage
  28? years, clay
Drainage, minor
  25 years
Drainage
  43? years, 33 years of varved clay, clay representing 10? years
Drainage
  Varved clay, base of section

The intervals so determined and estimated between drainages range from 12 to about 65 years and average about 20 years. Presumably the drainages occurred in years of warmer-than-average weather, which caused glaciers to shrink.

Weather and climate as indicated by the varved beds

Some fluctuations in weather are recorded in the varves. In general, varves thicker than average indicate warmer years when the ice-free season lasted longer and the lake received more melt water and sediment than usual. Also, winter layers will be comparatively thin compared to summer layers in years when the ice cover persisted a relatively short time. Plots of three sections of undeformed varves (fig. 4) show that the thicknesses of varves increase and decrease through irregular intervals. Although the lower two sections show a slight tendency for the pro-

portions of summer-deposited sediment to increase toward the bounding drainage varves, the varves as a whole fail to show a distinct trend from warm to cool to warm again between years when drainage occurred. In other words, the varves do not consistently grow thinner above a drainage varve and then thicken upward toward the next overlying drainage varve, even though they seem to show some variations in yearly weather.

Rate of accumulation of the varved lake beds

Estimates indicate that the 28.5-foot section of lake deposits measured in the Priest River valley accumulated in about 250 years, or at an overall rate of about a foot in 9 years. Sediment must have accumulated much faster in the wider parts of the lake in the Purcell Trench and Pend Oreille Valley. At a rate of only a foot in 9 years it would have taken 10,000 years for the accumulation of the 1,000 feet or more of lake deposits in parts of the Purcell Trench, which is probably considerably longer than the life of this late glacial lake. Because the main part of the lake received sediment from extensive areas of glacial drainage to the Purcell Trench in Canada and also from the basin of Clark Fork where the soft and easily eroded deposits of former Lake Missoula provided large amounts of silt and clay, it seems likely that the rate of sediment accumulation throughout most of the lake would have been much greater than in the Priest River Valley.

Ground water in the varved lake beds

The sand beds in the lake deposits are the main source of ground water to domestic and stock wells in the area of the glacial lake. These beds also feed a number of small seep springs in the shallow valleys intrenched in the lake deposits of the valley floors. The yield of the beds of sand is very low, but groundwater supplies adequate for rural use are developed by boring wells about 3 feet in diameter and casing them with sections of culvert or similar pipe. Such wells store enough water to permit the pumping of several hundred gallons during a few daytime hours, and they fill again by seepage at rates of a gallon a minute or less during hours of no pumping.

REFERENCES

Alden, W. C., 1953, Physiography and glacial geology of western Montana and adjacent areas: U.S. Geol. Survey Prof. Paper 231, 200 p.

Charlesworth, J. K., 1957, The Quaternary Era: London, Edward Arnold, 2 vols., 1,700 p.

Pettijohn, F. J., 1949, Sedimentary rocks: New York, Harper and Brothers, 526 p.

Walker, E. H., 1964, Ground water in the Sandpoint region, Bonner County, Idaho: U.S. Geol. Survey Water-Supply Paper 1779–I, 29 p.

THE DALLES-UMATILLA SYNCLINE, OREGON AND WASHINGTON

By R. C. NEWCOMB, Portland, Oreg.

Abstract.—One of the associated east-west structures formed by the Cascadian orogeny in late(?) Pliocene to middle Pleistocene time is the 160-mile-long Dalles-Umatilla syncline in which the main exposed unit, the basalt of the Columbia River Group, is warped down 2,000 to 4,000 feet below the bordering uplifts. The western part is asymmetrically steeper in the shorter north limb; the eastern part is roughly symmetrical, but uplift of the southern limb is greater. The general tilt of the limbs is even and uniform, but local steepening and faulting occurs. The deformation imposed a consequent pattern on most of the drainage.

During studies of the effects of tectonic structure on the occurrence of ground water in northern Oregon and southern Washington, the structures of the basalt of the Columbia River Group were mapped in the 15-minute quadrangles between the Hood River Valley, Oreg., and Rufus, Oreg. Reconnaissance mapping of the geologic structure also was done in nearby areas not covered by previous reports. This paper summarized some of the genetic features of a large downwarp that was mapped in this study and that is of major importance to agriculture, transportation, and water resources of the Pacific Northwest.

The earth's crust has been warped down in one master syncline, herein called the Dalles-Umatilla syncline, which extends from Mill Creek, near the Dalles, eastward for 160 miles to a point on the Umatilla River about 15 miles upriver from Pendleton, Oreg. (fig. 1). The ends of the downwarp have previously been described separately: the Dalles syncline by Piper (1932), and the Umatilla syncline by Hogenson (1964, p. 29).

The width of the broad downwarp ranges from about 5 miles near the ends to about 50 miles in the middle. The warp lowers the top of the basalt bedrock to an altitude that ranges from 200 to 1,000 feet, which is generally 2,000 to 4,000 feet below the average altitudes of the basalt in the crests of the adjoining anticlines.

Rocks of Mesozoic and early Tertiary age are deformed in the Blue Mountains anticlinal uplift on the south (fig. 1), and, by inference, are also deformed at depth in the Dalles-Umatilla syncline. The exposed rocks within the syncline are of Tertiary and Quaternary age; the areas of older rock, except for a few small exposures near the Cascade Range, are shown on the map (fig. 1).

The basalt of the Columbia River Group (middle Miocene through early Pliocene) is the oldest exposed unit within most of the syncline. Except for some areas of sedimentary deposits and small areas of volcanic rocks overlying it, the basalt forms the land surface. The basalt is several thousand feet thick and consists of dark lava accordantly layered in flows averaging about 80 feet in thickness. The upward succession of the basalt, the Dalles Formation (early and middle(?) Pliocene) and possibly other Pliocene deposits, and the volcanic rocks of the High Cascades (Pliocene?, Pleistocene, and Recent) can be examined along the western part of the syncline.

The Dalles Formation consists of two facies, one of volcanic tuff, agglomerate, and associated volcanic-sedimentary rocks, and the other of sedimentary deposits (Newcomb, 1966). Along with its probable time equivalent, the Pliocene fanglomerate of Hogenson (1964), and possibly some undifferentiated Pliocene deposits, it overlies the basalt in a generally conformable manner but with a slight erosional disconformity. The thickness of the Dalles Formation decreases eastward from 2,000 feet in a former fan of volcanic debris at the edge of the Cascade Range to 250 feet in the sedimentary facies at the rim of the Deschutes River canyon and to 160 feet south of Rufus, Oreg. This eastern sedimentary part, with possibly small amounts of later Pliocene deposits and some local Quaternary deposits, underlies the plateaus along the Columbia and Umatilla Rivers eastward to the Pendleton, Oreg., area (Newcomb, 1966).

U.S. GEOL. SURVEY PROF. PAPER 575-B, PAGES B88-B93

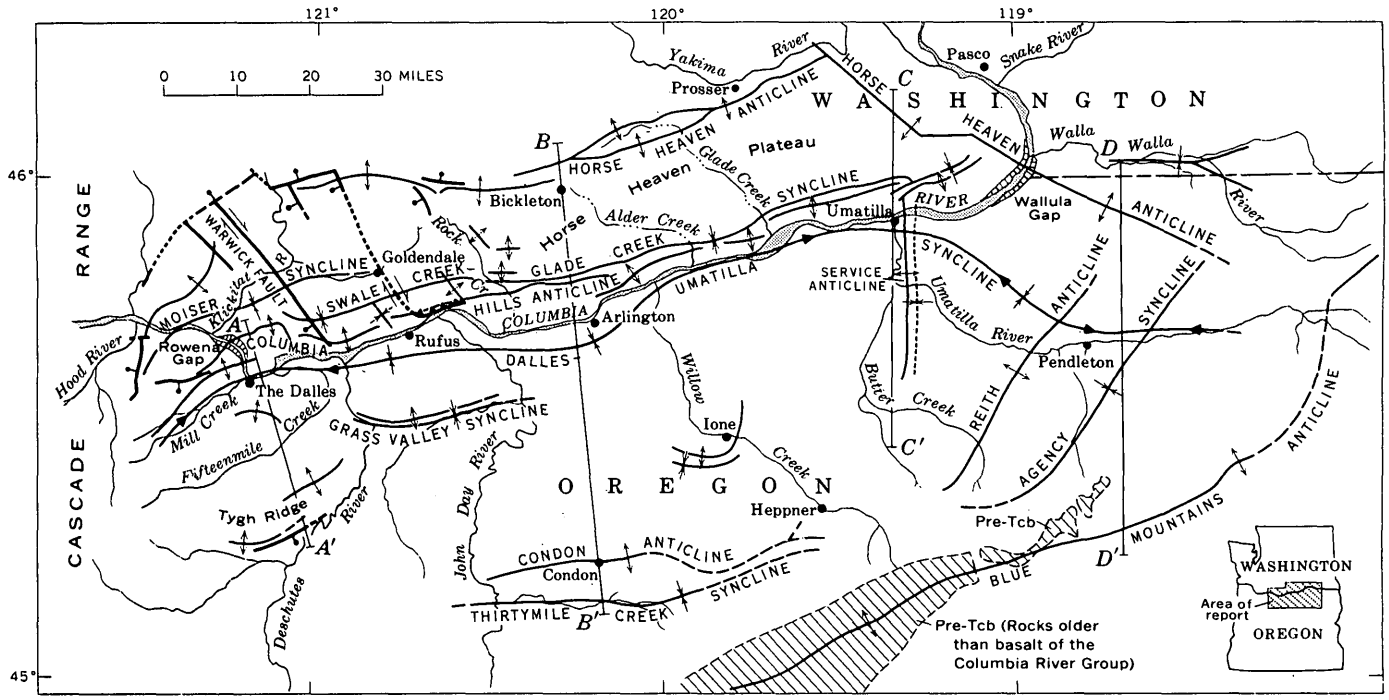

EXPLANATION

Approximate contact	Fault, showing relative movement	Thrust fault	Anticline	Syncline
	Bar and ball on downthrown side; dashed where approximately located, dotted where concealed	*Sawteeth on upper plate*	*Dashed where approximately located*	*Showing troughline and direction of plunge. Dashed where approximately located; dotted where concealed*

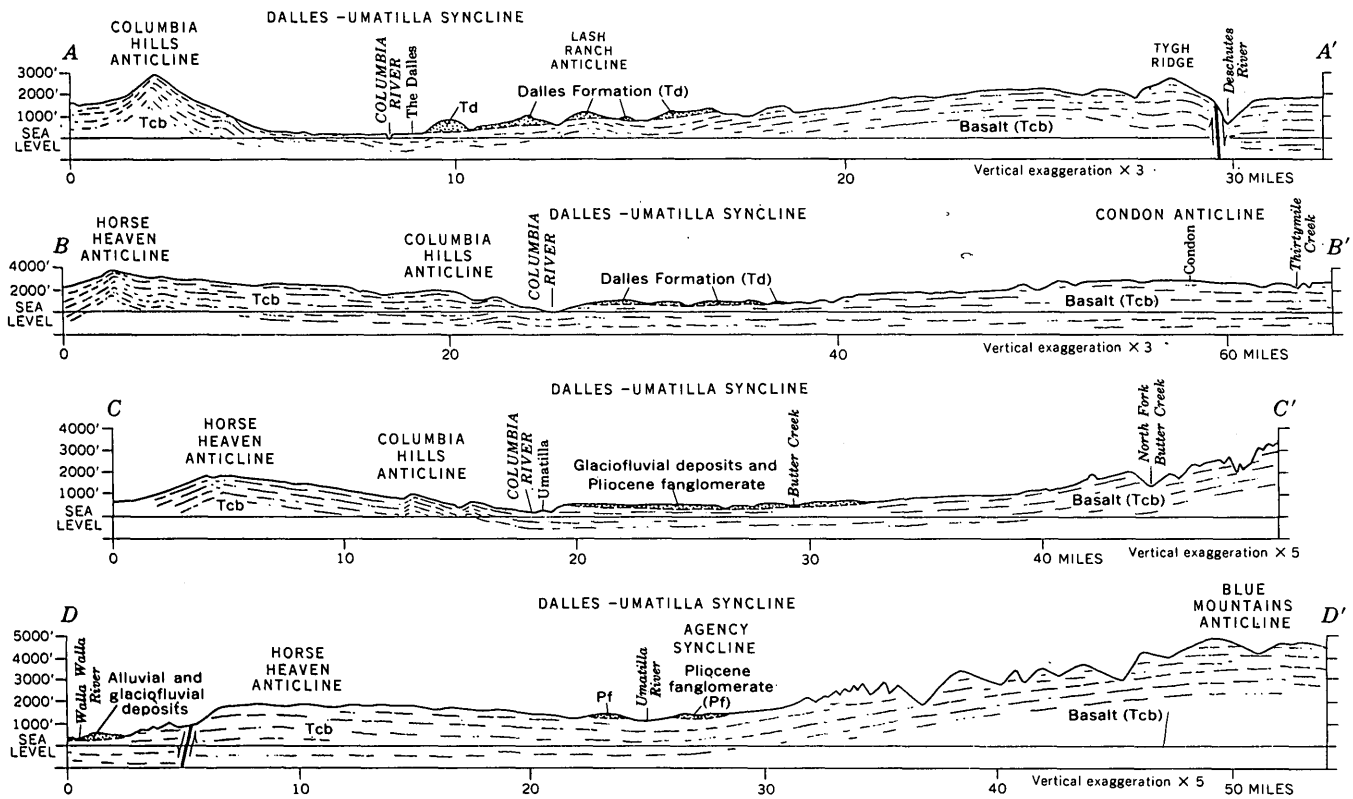

FIGURE 1.—The Dalles-Umatilla syncline and associated structures formed mainly in the Cascadian orogeny of late(?) Pliocene and Pleistocene time.

Younger volcanic rocks of the Cascade Range were grouped by Callaghan and Buddington (1938, map) under the name "volcanic rocks of High Cascades." The "Simcoe lavas" of the Horse Heaven anticline north of Goldendale, Wash., are generally mapped as being of similar age (Huntting and others, 1961). The early lavas of the "volcanic rocks of High Cascades" lie on erosion surfaces cut across deformed strata of the Dalles Formation.

STRUCTURE

Boundary anticlines

From near the east side of the Cascade Range 40 to 100 miles south of The Dalles, and south of the Dalles-Umatilla syncline, several wide uplifts trend northeast and east beneath the Columbia Plateaus. The southernmost is the broad structure which forms the west part of the Blue Mountains anticline (fig. 1). A low arch trends east-west through Condon, Oreg., and approaches the Blue Mountains uplift 100 miles east of the Cascade Range. In the western part, the rocks of the Dalles-Umatilla syncline slope upward mainly to the Condon anticline and to other arched warps along the north side of the Blue Mountains uplift. Eastward from the low end of the Condon anticline, near Heppner, Oreg., and on through the Umatilla River basin, the Blue Mountains anticline forms the south flank of the Dalles-Umatilla syncline. The Blue Mountains uplift trends north and east beyond the area shown on figure 1 and to the Craigmont uplift of Idaho (Lupher, 1945, p. 338), whence the deformation continues to the Rocky Mountains. East of Pendleton, Oreg., the trace of the axis of the Blue Mountains anticline can be located only generally in an upland where block faulting (Hogenson, 1964, pl. 1) continues north from the Grande Ronde Valley (Hampton and Brown, 1964, pls. 2 and 3).

From the east part of the Cascade Range, and north of the Dalles-Umatilla syncline, the complex linear Columbia Hills anticline (in part formerly called Ortley anticline) trends diagonally northeast and then curves more nearly east. East of Arlington, Oreg., the individual names for the low discontinuous anticlinal ridges of this same trend are commonly used, but in this paper the name "Columbia Hills anticline" is applied to all this general anticlinal trend. The Columbia Hills anticline is the southern and lower of two generally parallel linear uplifts that bound the Horse Heaven Plateau. The northern uplift is the Horse Heaven anticline, which trends east from the block-faulted upland of the Cascade Range near Mount Adams, joins a southeast trend near Prosser, Wash., and fades out at the flank of the Blue Mountains anticline 30 miles east of the mergence of the Columbia Hills anticline. The lowland along the Swale Creek–Glade Creek syncline connects, through sags and gaps in the Columbia Hills anticline, with the lowland of the broad Dalles-Umatilla syncline. Thus, in a broad sense, the northern limits of the Dalles-Umatilla syncline could be said to shift to the higher Horse Heaven anticline east of Arlington, Oreg.

Dalles-Umatilla syncline

Between the southwestern part of the Columbia Hills anticline and the long slope northward from Tygh Ridge, the Dalles syncline plunges northeast beneath Mill Creek valley to The Dalles (fig. 2). There, in a basinal low, the Dalles syncline swings east. Its floor ascends about 500 feet in the next 6 miles and, and as a 5- to 10-mile-wide band of horizontal rocks, it continues east to near Arlington, Oreg.; along this nonbasinal reach of the syncline the Columbia River is entrenched at the northern edge. East of Arlington, the Dalles syncline is continuous with the Umatilla syncline.

The Umatilla syncline begins, at its east end, in the complexly faulted area between the northeast-trending Blue Mountains anticline and the northwest-trending Horse Heaven anticline; in the plunge of the syncline to the lowest part of the valley of the Umatilla River the syncline is crossed by the Reith anticline. From the sag at Umatilla, Oreg., its axial trough ascends about 500 feet in a westward direction to Arlington, where it is continuous with the Dalles syncline.

The virtually horizontal rock of the broad axial zone of the Dalles-Umatilla syncline is flanked in its western part by rather unlike limbs. On the north, the syncline abuts against the steep upturn of the basalt along most of the length of the Columbia Hills anticline. The syncline is asymmetrical in cross section, the northern limb short and abrupt with 5° to 45° dips, and the southern limb long and gentle, commonly with dips of only 1° to 3°. In the eastern part, if the Columbia Hills anticline is ignored, the limbs are more nearly equal in width, although the Blue Mountains anticline is higher than the northern limb.

The Columbia River follows the axis of the syncline only within the Dalles and Umatilla basinal sags; elsewhere, its gorge is north of the synclinal axis, along the foot of the anticlinal slope. In the off-axis segment of its course, the river gorge is cut mostly in near-horizontal basalt; but at three places, opposite Arlington, Oreg., and the mouths of the Deschutes and John Day Rivers, the upper part of the north side of the gorge is cut into steeply tilted basalt.

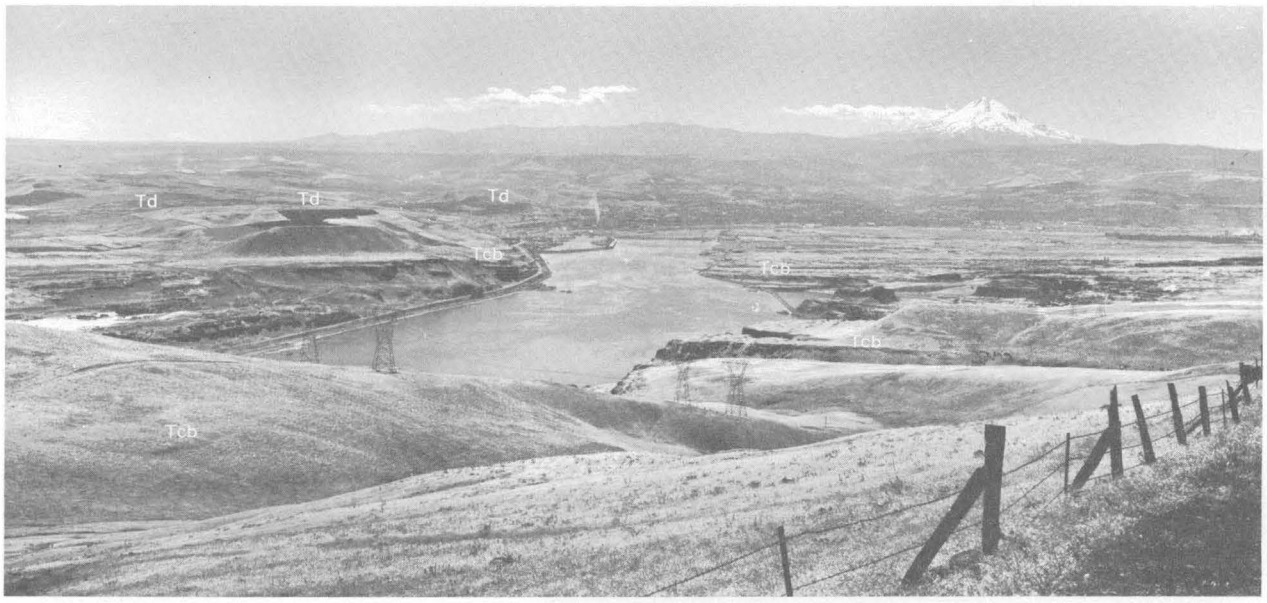

FIGURE 2.—View southwest down the general 2° to 5° dip of the basalt of the Columbia River Group (Tcb) to the basinal part of the Dalles-Umatilla syncline at The Dalles. The Dalles Formation (Td) underlies the rising slope south from The Dalles but is largely eroded from the basalt in the central part of the basin.

These intersections occur at exceptionally steep parts of the Columbia Hills anticline. Near the mouths of the Deschutes and John Day Rivers the basalt of the anticline is steeply folded and in places, is overturned, or thrust, to the south. The very steep folding occurs within blocks that are bounded on the west by strike-slip faults that have right-lateral movement.

Parts of the broad axial trough and the evenly dipping limbs of the syncline are interrupted by local bulges and sags of minor anticlines and synclines, the largest of which are shown on figure 1. Near the west end of the syncline, the basin at The Dalles is bordered by several subordinate warpings; the most important of these is a narrow curving anticline between the forks of Mill Creek. This anticline is the southern part of the Columbia Hills uplift, but farther north it diverges to the side of the main structure. It reaches east to the Columbia River in Wetle Butte at the northwest edge of The Dalles. The general uniform dip of the long slope into the syncline from the south is interrupted by subsidiary anticlines. Among the largest of these is a faulted anticline at Tygh Ridge. Others are Lash Ranch anticline (just south of The Dalles), Gordon Ridge anticline (just north of Grass Valley syncline), and Ione Butte anticline at Ione, Oreg. At the east end of the Dalles-Umatilla syncline, the subsidiary structures include the Service and Reith anticlines and Agency syncline, mapped by Hogenson (1964); the latter two structures parallel the trend of the Blue Mountains anticline and occupy flank positions equivalent to those of the Condon anticline and the Thirtymile Creek syncline (Collier, 1914, p. 17, cross section *B–B′*) farther west. A third sag along the axis of the Dalles-Umatilla syncline occurs where it crosses the Agency syncline east of Pendleton, Oreg.

The general cross-sectional shape and structure of the Dalles-Umatilla syncline is shown at four sections located on figure 1.

Fault displacements of the basalt are commonly associated with the steeper folds but occur also in places distant from any steeply folded rock. Fault displacements are lacking, however, in many exposures of the lesser deformed basalt. Only the larger fault displacements are shown on figure 1; most are near the Cascade Range and are associated with the block faulting from which the Horse Heaven anticline branches. The Warwick fault marks the west side of a block at the southern end of which the Columbia Hills anticline was folded steeply on the south side. In this steep fold the fault disappears, as do several that extend from the Cascade Range and the Horse Heaven anticline southeast to the Columbia Hills anticline.

This Warwick fault is in no way related to a "Warwick Fault" erroneously assumed by Hodge (1931, p. 958) to run east-west through a nearby part of the Columbia Hills.

241-334 O—67——7

Deformation

The Dalles-Umatilla syncline and the bordering anticlines were formed during movements of the earth's crust in the Cascadian orogeny. The manner in which the Columbia Hills anticline and the Dalles-Umatilla syncline continue from the Cascade Range indicates that their deformation was accompanied by tectonic movements in the Cascade Range.

The continuation of the Blue Mountains-Craigmont uplift to the Rocky Mountains, where the rocks were deformed mainly in an earlier orogeny, illustrates the extent and force of the crustal adjustments, of which this synclinal warp was a part. The length and convergence of the Columbia Hills and the Horse Heaven anticlines, along with the continuation of the Dalles-Umatilla syncline to the Blue Mountains uplift, also illustrate that these structures resulted from crustal forces acting beneath an extensive area. The structures contrast in length with others of their group (the Yakima Ridges farther north), some of the southernmost of which merge with the Horse Heaven anticline, and the remainder of which fade out north of Pasco, Wash., only halfway to the Rocky Mountains.

The deformation at the east end of the Dalles-Umatilla syncline (Hogenson, 1964) and the adjacent Walla Walla syncline (Newcomb, 1965) fails to show large tectonic displacements that might have occurred in the Miocene to Pliocene basalt as a result of movement at depth along a hypothetical Olympic-Wallowa lineament, although the same basalt is deformed in the Wallowa Mountains farther east.

The warping of the Dalles-Umatilla syncline involved two main stages. An erosional period that intervened between two epochs of deformation of the Dalles Formation was suggested by Piper (1932, p. 141) as possibly correlative in places with Buwalda's (1929) Ochoco surface. Early flows of the volcanic rocks of High Cascades covered parts of the erosion surface that bevels the Dalles Formation and basalt of the Columbia River Group in the uplands southwest of The Dalles. Much of the early part of these Pliocene(?) and Quaternary volcanics was deformed in the second, and main, epoch of folding. Similarly, two stages of uplift were found in the Blue Mountains at the east end of the syncline by Hogenson (1964, p. 34), in the Walla Walla Valley to the northeast by Newcomb (1965, p. 10), and in the upper Grande Ronde River basin to the southeast by Hampton and Brown (1964, p. 32).

Inasmuch as the Dalles Formation, which is wholly included in these deformations, is now considered to be of early Pliocene age and there may be a possibility that part of it could be middle Pliocene (Newcomb, 1966), the main warping of the Dalles-Umatilla syncline must have started in, or after, middle Pliocene.

The principal uplift of the Horse Heaven anticline, and depression of the Pasco Basin to the north, occurred about middle Pleistocene time, when the Columbia River was impounded in Lake Ringold of the Pasco Basin and was first diverted across the Horse Heaven anticline at Wallula Gap (Newcomb, 1958). Thus, the warping of the Dalles-Umatilla syncline occurred in two main stages during the interval from late middle, or late, Pliocene to middle Pleistocene. These two main uplifts may have postdated initial warpings of the basalt of the Columbia River Group in the Blue Mountains anticline.

EFFECTS OF TECTONIC STRUCTURE ON DRAINAGE

The middle Pleistocene diversion of the Columbia River into the Dalles-Umatilla syncline (Newcomb, 1958) has been followed by the carving of a nearly graded course through Wallula Gap (fig. 3), along a 100- to 1,000-foot deep gorge within the syncline, and through Rowena Gap, north of the syncline. The exit of the Columbia River from the syncline at Rowena Gap and the course within the syncline probably are partly inherited from the downvalley part of the ancestral Umatilla River. Rowena Gap, Willow Creek canyon through Ione Butte, and several other watercourses follow canyons established prior to a large part of the folding; but most stream courses, particularly those of the smaller streams, are consequent to the folded surface of the basalt.

REFERENCES

Buwalda, J. P., 1929, A Neocene erosion surface in central Oregon: Carnegie Inst. Washington Pub. 404, p. 1–10.

Callaghan, Eugene, and Buddington, A. F., 1938, Metalliferous mineral deposits of the Cascade Range in Oregon: U.S. Geol. Survey Bull. 893, 141 p., 22 pls., 7 figs.

Collier, A. J., 1914, The geology and mineral resources of the John Day region: Oregon Bur. Mines and Geology, v. 1, no. 3, 47 p., 11 illus., map.

Hampton, E. R., and Brown, S. G., 1964, Geology and groundwater resources of the upper Grande Ronde River basin, Union County, Oregon: U.S. Geol. Survey Water-Supply Paper 1597, 99 p., 6 pls., 16 figs.

Hodge, E. T., 1931, Columbia River fault scarp: Geol. Soc. America Bull., v. 42, p. 923–984.

FIGURE 3.—View northeast toward the Columbia River and up the gentle dip of the basalt in the southern part of the Wallula Gap through the Horse Heaven anticline.

Hogenson, G. M., 1964, Geology and ground water of the Umatilla River basin, Oregon: U.S. Geol. Survey Water-Supply Paper 1620, 162 p., 2 pls., 14 figs.

Huntting, M. T., and others, 1961 Geologic map of Washington: Washington Dept. Conservation, scale 1:500,000.

Lupher, R. L., 1945, Clarkston stage of the Northwest Pleistocene: Jour. Geology, v. 43, no. 5, p. 338.

Newcomb, R. C., 1958, Ringold Formation of Pleistocene age in type locality, The White Bluffs, Washington: Am. Jour. Sci., v. 256, p. 328–340.

Newcomb, R. C., 1965, Geology and ground-water resources of the Walla Walla River basin, Washington-Oregon: Washington Div. Water Resources Bull. 21, 151 p., 4 pls., 15 figs.

——— 1966, Lithology and eastward extension of the Dalles Formation, Oregon and Washington, *in* Geological Survey Research 1966: U.S. Geol. Survey, Prof. Paper 550–D, p. D59–D63.

Piper, A. M., 1932, Geology and ground-water resources of The Dalles region, Oregon: U.S. Geol. Survey Water-Supply Paper 659–B, p. 107–189, 9 pls., 3 figs.

ELECTRON MICROSCOPY OF LIMESTONES IN THE FRANCISCAN FORMATION OF CALIFORNIA

By ROBERT E. GARRISON and EDGAR H. BAILEY, Princeton, N.J.,[1] Menlo Park, Calif.

Abstract.—Electron microscopy reveals nannoplankton in peel replicas of limestones of Late Cretaceous age from the Franciscan Formation of western California. Red (Laytonville type) limestones from the northern Coast Ranges consist mostly of coccoliths. Gray (Calera type) limestones from the San Francisco peninsula contain fewer partly replaced coccoliths as well as problematical nannoplankton, but postdepositional changes may have obliterated many of their primary features. Both types of limestone generally occur closely associated with mafic volcanic rocks and are interpreted as pelagic deposits with little or no clastic detritus. The lack of detritus could have resulted from deposition on a seamount, above the general sea floor that received clastic sediments. Alternatively, these limestones might have formed by a very rapid proliferation of microorganisms resulting from volcanic extrusions warming the water and adding calcium and perhaps even carbonate to it.

Limestones aggregate less than 0.1 percent of the rocks in the Late Jurassic to Late Cretaceous Franciscan eugeosynclinal assemblage of the California Coast Ranges. They are, however, a particularly interesting component in that they furnish the closest approach to a "key bed," have provided many of the diagnostic fossils, and contribute evidence regarding the depositional environment of the sequence. They occur only in sporadic, small exposures, chiefly in a belt extending from the San Juan Bautista quadrangle on the south to the Scotia quadrangle in the north (fig. 1). Most of the other rocks of the Franciscan Formation are also sedimentary, with graywacke being much more abundant than shale or conglomerate. Mafic volcanic rocks that are believed to be largely submarine extrusives amount to about a tenth of the eugeosynclinal assemblage and are accompanied in many places by chert. Nearly all the limestones rest directly on, or are embedded in, volcanic piles. Bailey and others (1964, p. 77), although recognizing the organic origin of part of the limestone, believed that the bulk of the Franciscan limestones was a chemical precipitate directly related to the volcanism. Electron microscopy of selected Franciscan limestones, however, shows abundant nannoplankton (organisms smaller than 20 microns, Provasoli, 1963, p. 192), especially in red limestones most closely related to volcanic rocks, indicating that the organic component is far more abundant than formerly suspected. The abundance of these minute fossils in these limestones suggests that nannoplankton might also be abundant enough in some of the other more common rock types to provide a means for biostratigraphic dating within the generally unfossiliferous assemblage.

TYPES OF FRANCISCAN LIMESTONES

The limestones in the Franciscan Formation were differentiated by Bailey and others (1964, p. 68-77) into two general types, largely on the basis of occurrence and color, and were informally termed the Calera and Laytonville types of limestone. The Calera type of limestone is white weathering, light to dark gray where unweathered, and occurs in sequences of beds that are in some places a few hundred feet thick. The contrasting Laytonville type of limestone is pink to deep red and occurs in lenses a few feet to a few tens of feet thick. At a few places, the colored and white varieties are interlayered. Mostly, however, the limestones either contain enough iron oxide to give them an obvious deep-pink to red color or they lack iron oxides and are gray. The electron microscope also reveals the other differences between the two types of limestone in the Franciscan Formation that are described below.

Calera type of limestone

The Calera type of limestone is light colored, unusually hard, very fine grained, and locally contains numerous Foraminifera (fig. 2). On the San Fran-

[1] Present address: Department of Geology, University of British Columbia, Vancouver, Canada.

U.S. GEOL. SURVEY PROF. PAPER 575-B, PAGES B94-B100

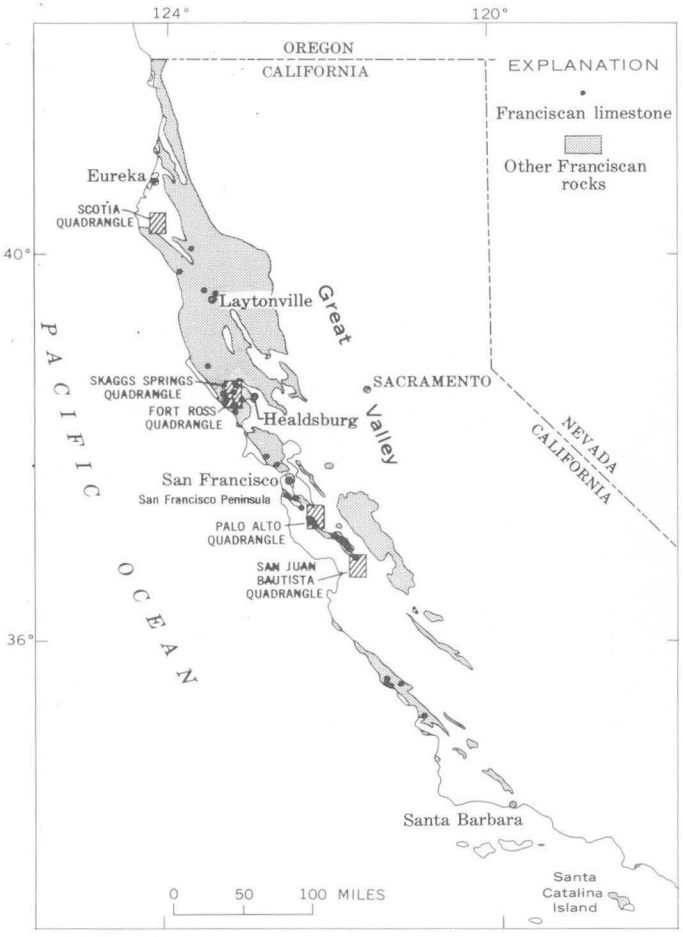

FIGURE 1.—Map of northern and central California, showing distribution of Franciscan rocks and location of areas referred to in text.

cisco peninsula, where it is most abundant, lenses of the Calera type of limestone are generally no more than a few tens of feet thick; in a few places they are much thicker and are quarried for use as aggregate or as raw material for cement. The lenses are closely associated with mafic volcanic rocks, some of which are pillow lavas, some aquagene tuffs, and some of indeterminate character. Locally, a small amount of graywacke occurs with what is dominantly a volcanic accumulation. In a few areas the light-colored limestone consists chiefly of oolites, pellets, or abraded fragments of various megafossils, suggesting either accumulation above wave base or redeposition of deposits initially formed above wave base.

The typical Calera type of limestone can be seen in thin section to consist of Foraminifera, mainly globotruncanids and globogerinids, in a matrix of micrite which makes up 70–80 percent of the rock (fig. 2). The term "micrite" is used for carbonate particles smaller than 30 microns (Leighton and Pendexter, 1962, p. 35). Wall structure of the foraminiferal tests is generally well preserved, and test interiors are filled with secondary sparry calcite, except for a few outer chambers that have been filled with micrite. Radiolaria that were completely replaced by calcite were found in one unusual specimen. The Foraminifera indicate that the limestones are of mid-Cretaceous (Albian to Cenomanian) age (Thalmann, 1942; Küpper, 1955; Loeblich and Tappen, 1961).

Laytonville type of limestone

The Laytonville type of limestone in the Franciscan Formation is pink to red and is everywhere associated with mafic volcanic rocks. Excellent exposures of red limestone are found in the Franciscan near Laytonville, where one exceptional lens is nearly 100 feet thick. In an area 15 miles west of Healdsburg, red limestone lenses are much thinner but more numerous. At many places, the red limestone occurs interbedded with red chert, some of which contains Radiolaria. Typically, the red limestone lies on mafic pillow lava, and locally it also occurs between pillows. Although neither megafossils nor fragments of megafossils have been found in the Laytonville type of limestone, it contains the same microfossil assemblage as does the Calera type of limestone.

The red limestones range from massive to thinly laminated rocks. Most of them consist of 70–90 percent micrite and 10–30 percent tests of pelagic Foraminifera and possibly some Radiolaria (fig. 3). Un-

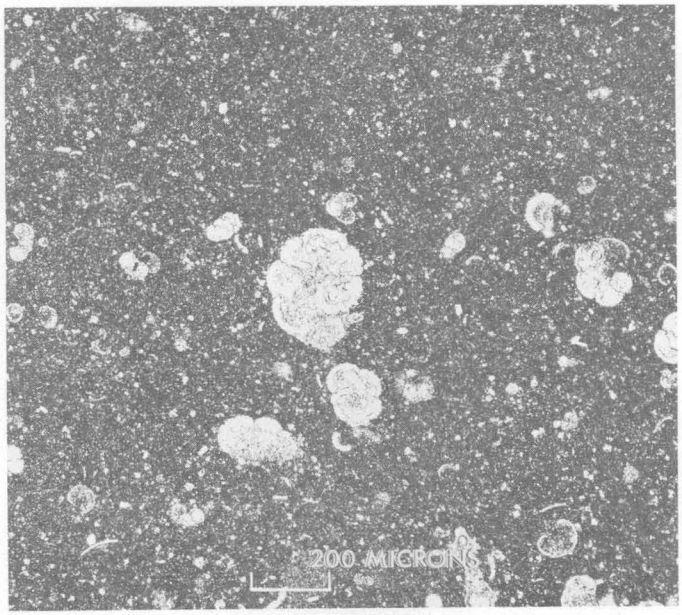

FIGURE 2.—Photomicrograph of the Calera type of limestone from Monte Bello ridge, Palo Alto quadrangle, showing planktonic Foraminifera in a micritic matrix. Scale indicates 200 microns. × 100. Plane-polarized light.

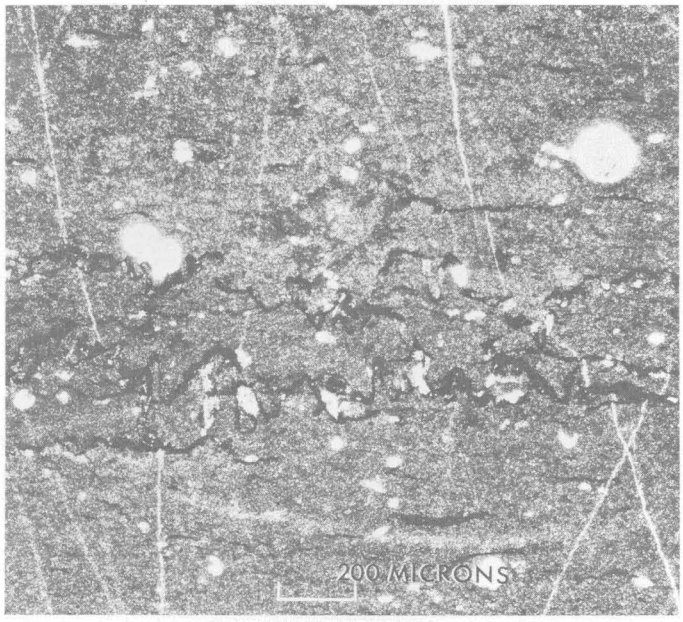

FIGURE 3.—Photomicrograph of a Laytonville type of limestone from Smith Ridge, Fort Ross quadrangle. Poorly preserved tests of microfossils (Radiolaria or Foraminifera?) are filled with clear sparry calcite; the majority of the rock is micrite. Thin, clear calcite veins are truncated by dark stylolites which are parallel to bedding. Scale indicates 200 microns. × 100. Plane-polarized light.

usual specimens, however, contain more than 50 percent Foraminifera tests (Bailey and others, 1964, photo 44, p. 74). The Foraminifera commonly are well preserved, though in some specimens they are coarsely recrystallized. Nearly all the red limestone contains closely spaced veins of calcite, which are readily apparent because they are iron free and therefore white. Minute stylolites locally are developed parallel to bedding. Despite the generally sheared and locally metamorphosed state of the Franciscan Formation, none of the Foraminifera seen in thin sections show distortion, although this would be readily apparent in the globular varieties.

The quantity of iron oxide, chiefly goethite, responsible for the red color is difficult to estimate, even in thin section, because of its extremely small grain size. Chemical analyses of deeply colored varieties, however, indicate less than 3.0 percent ferric oxide.

Nearly identical red limestones occur with mafic volcanic rocks in other eugeosynclinal areas and are perhaps a characteristic feature of this environment. Examples are provided by Eocene sequences on the Olympic Peninsula (Park, 1946) and the Late Cretaceous-Eocene sequences of Borneo (Reinhard and Wenk, 1951, p. 65–66).

ELECTRON MICROSCOPY

The electron microscope clearly reveals the composition of the micrite in these rocks, and shows that in some specimens the micrite contains a large amount of nannoplankton, especially coccoliths. None of the nannoplankton can be seen in thin section, although measurements show that some, if isolated, are clearly large enough to be seen with optical microscopes under high-power objectives. Even optical magnifications up to 1,100 times of ultrathin sections (thin sections 10 microns or less thick, Honjo and Fischer, 1965a, p. 242) of these limestones have shown only a mosaic of tiny, anhedral calcite grains in the micrite.

The techniques used to prepare peel replicas of limestones are described in detail by Honjo and Fischer (1965b) but are briefly described here for the benefit of those unfamiliar with them. Since even very thin slices of rocks are largely opaque to the electron beam, it is necessary to prepare a thin carbon replica of the rock surface. A small rock cube, about 5 mm on a side, is cut and mounted in an epoxide plug. One face of the cube, on which a surface of the rock is exposed, is ground flat and smooth through successive stages of grinding with finer and finer grinding compounds, ending with No. 3200 grit. The ground face is then polished using gamma alumina; care must be exercised in each stage of the grinding and polishing to avoid scratches. The polished rock surface is next delicately etched by immersing the plug in very weak hydrochloric acid (0.1 to 0.05*N*) for 60–80 seconds.

After the plug is gently rinsed in distilled water and allowed to dry, the etched limestone surface is replicated in two stages. First, a thin acetate peel is made. This is mounted on a glass slide, placed in a vacuum evaporator, and shadowed at an angle of about 30° with evaporated chromium. Next, a thin layer of evaporated carbon is applied to the peel at an angle of 90°. The carbon layer is transparent to the electron beam, and the chromium shadowing serves to heighten the contrast. Finally, the carbon-coated peel is cut into small pieces which are placed in acetone to dissolve the acetate film. The carbon replicas are scooped from the acetone with electron grids and are ready for observation with the electron microscope.

The Calera type of limestone was studied by peel replicas of four specimens from Cahil Ridge in San Mateo County (southern part of the San Francisco peninsula), and from Monte Bello Ridge and the Permanente Cement Co. quarry in Santa Clara County (southeast of the San Francisco peninsula). As shown in figures 4 and 5, these specimens have a

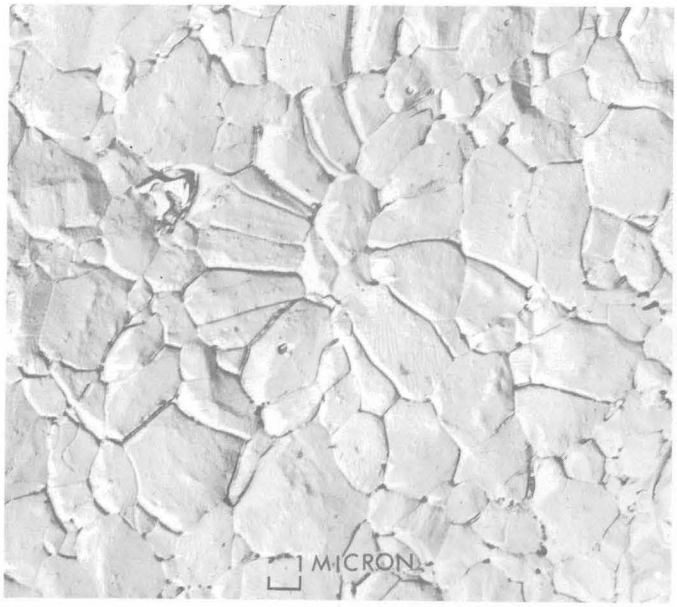

FIGURE 4.—Electron micrograph of the Calera type of limestone from Cahil Ridge, Montara Mountain quadrangle, on the San Francisco peninsula. Radially arranged calcite wedges in the center of the photograph are a probable nannoplanktonic form. × 5,000. Scale in this and the following electron micrographs indicates 1 micron.

micritic matrix consisting largely of anhedral calcite grains from half a micron to about 8 microns in maximum dimension. Scattered through this material are a few coccolith fragments and a probable nannoplanktonic fossil with a rosette structure (figs. 4 and 5). The latter form, which is very similar to forms found in Upper Jurassic (Tithonian) limestones of the Alps (Honjo and Fischer, 1964, fig. 3, p. 838), consists of 10–20 calcite wedges arranged radially around what appears to have been a central cavity that is now filled with calcite. Each of the calcite wedges is 2–3 microns long; the diameter of the rosette is 7–10 microns. This form resembles the problematic genus *Nannoconus* but differs from it mainly in the lack of a smooth external wall (Brönnimann, 1955, p. 28–30).

No complete coccoliths were observed in the Calera specimens. The few plates noted (fig. 5) have been partly replaced by adjacent anhedral grains—a process termed "grain growth" by Bathurst (1958, p. 24–31), and it is likely that other coccoliths have been completely destroyed by this process. The remaining rosettes and partial coccoliths compose from about 1 percent (Permanente quarry) to nearly 30 percent (Cahill and Monte Bello Ridges) of the micrite in the Calera type of limestone.

The Laytonville type of limestone was investigated by peel replicas from five samples from different localities in the Skaggs quadrangle, Sonoma County. As is shown in figures 6 and 7, the micrite of the red limestone consists almost entirely of coccoliths, both as fragments and whole specimens. The number of coccoliths observed in the electron micrographs suggests abundances on the order of 4 to 6 million coccoliths per cubic millimeter of rock. Some solution along edges of coccoliths is suggested by the abrupt truncation of the plate structure (fig. 6), but this may be due to overlapping of plates, which is difficult to detect on the plane surfaces replicated in the peels. It is equally possible that the coccoliths have been fragmented during sedimentation or compaction. The large coccolith in the center of figure 7 seems to have been broken along the calcite-filled fracture, and it also has been partly replaced by the calcite in this fracture. However, the resistant nature of coccoliths is indicated by the specimen seen protruding slightly into the secondary calcite at the upper right of the photograph (fig. 7).

ORIGIN OF FRANCISCAN LIMESTONES

The enigmatic nature of the micrite in the fine-grained Franciscan limestones, and the close association of these limestones with submarine volcanic rocks, has led to the suggestion that they were largely inorganic chemical precipitates due to submarine volcanism (Bailey and others, 1964, p. 76–77). A similar inorganic origin has also been proposed for the vir-

FIGURE 5.—Electron micrograph of the same specimen of the Calera type of limestone shown in figure 4. A partially replaced coccolith is at the upper left, and another nannoplanktonic form with rosette structure is toward the lower right. × 5,000.

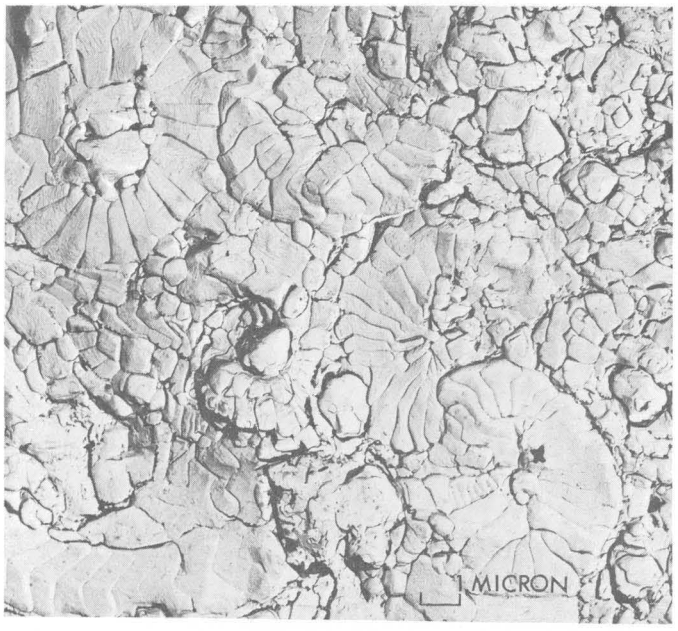

FIGURE 6.—Electron micrograph of the Laytonville type of limestone from Smith Ridge, Fort Ross quadrangle, showing abundant coccoliths. × 5,000.

tually identical red limestones of the Olympic Peninsula by Park (1946, p. 310–311), following the origin postulated by Kania (1929) for limestones associated with volcanic rocks in western Canada. The discovery of the organic nature of a large proportion of the micrite in the Franciscan limestones, however, shows that they are not chiefly primary chemical precipitates and requires a reassessment of the ideas regarding their origin. Although they bear similarities to pelagic oozes, normal, slow, deep-sea accumulation does not appear to adequately explain all their peculiarities.

In its organic content, the Laytonville type of limestone is much like indurated coccolith oozes accumulated through particle-by-particle settling of pelagic organic skeletons. Coccoliths are the individual skeletal plates from minute unicellular algae, most of which live today within the photic zone of the open oceans. These red limestones are comparable to *Globigerina* ooze described by Black (1956, p. 173) as having coccoliths as a major component. Similar, well-indurated coccolith limestones have been described from pelagic facies of Late Jurassic to early Tertiary age in the Alps and in Spain (Honjo and Fischer, 1964, p. 837; Garrison, 1964, p. 103–145). This type of sedimentation implies an absence of clastic deposition, or "starved basin" sedimentation, but it does not necessarily imply bathyl or abyssal depths.

The ubiquitous association of the red limestones with submarine volcanic rocks, generally pillow lavas, might be merely a physical one with the limestone collecting on volcanic seamounts. This would permit the isolation of a site of slow particle-by-particle deposition within a basin of rapid clastic accumulation, such as must have provided the environment for the deposition of tens of thousands of feet of Franciscan graywacke. The newly discovered organic character of the limestone seems to fit well with this speculation. Other factors, however, do not seem to fit this concept so well. For example, some of the lenses of red limestone a foot or more thick occur with masses of volcanic rock that also have apparent thicknesses of only a few feet to a few tens of feet. Although postdepositional tectonic movements might have distorted the relations, it seems unlikely that such a thin layer of volcanic material could have provided the required isolation for particle-by-particle deposition through the period of time required by normal rates of accumulation of pelagic ooze (roughly 1 cm per thousand years). Also, seamount isolation does not aid in explaining the abundance of red iron oxide or its remarkably uniform distribution through many feet of beds. It seems possible that there is more than a physical relation between the greenstone and limestone and that a more complex genetic relation exists between volcanism and limestone deposition. Perhaps the relationship results from the rate of multiplication of the coccolithophorids being greatly increased lo-

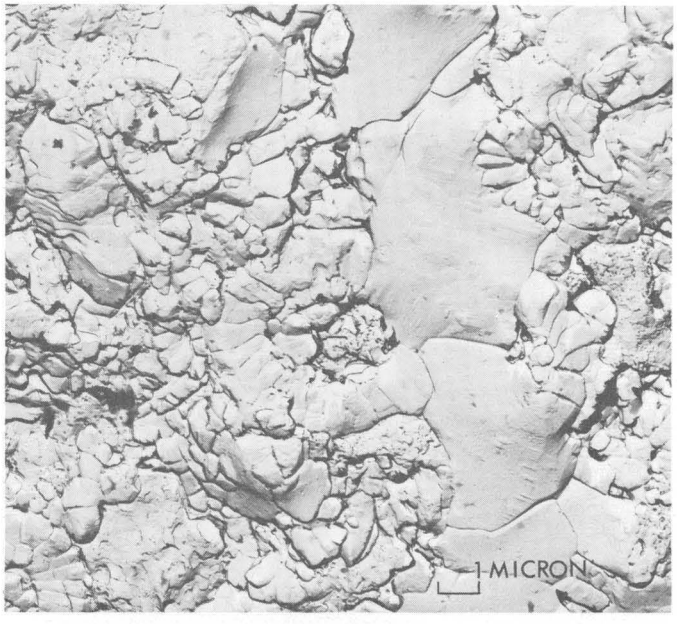

FIGURE 7.—Electron micrograph of the same limestone shown in figure 6. A calcite vein runs from top to bottom across the micrograph. See text for discussion. × 5,000.

cally by the action of lava extrusion through either (1) warming of the water and increasing the nutrient supply, or (2) the addition of calcium from the lava. As indicated by Bailey and others (1964, p. 77), chemical analyses of pillow lavas and aquagene tuffs in the Franciscan strongly suggest that large amounts of calcium were extracted from the volcanic material and added to the sea water.

The origin of the iron-free Calera type of limestone remains even more obscure. The preliminary electron-microscope studies showed only scattered nannoplankton and suggested greater recrystallization than in the Laytonville type. We cannot yet be sure if many more nannoplankton were present and have been destroyed, or if a larger proportion of the micrite may have been inorganic. Strictly diagenetic processes seem inadequate to explain the poor preservation of coccoliths in the Calera limestones we studied, inasmuch as calcite coccoliths have been shown to be very resistant to alteration (Robertson, 1964, p. 544). Thus, although the electron-microscope studies of the Calera type of limestone tend to justify considering it as different from the Laytonville type, more samples must be studied before conclusions regarding the content or origin of its micrite are warranted.

POSSIBILITIES FOR BIOSTRATIGRAPHIC DATING

Study of the nannoplankton offers a possibility for finer and more widespread biostratigraphic dating within the Franciscan. No attempt has been made to compare the forms observed in this study with known and described species, although the degree of coccolith preservation (figs. 8 and 9) indicates that for the Laytonville limestones this could be done. One might expect some difficulties because of the general lack of knowledge of these nannoplankton, their taxonomy, and their stratigraphic ranges, and because of the problems introduced by comparing electron micrographs of replicas with free specimens observed with the optical microscope (Honjo and Fischer, 1964, p. 839; Bramlette and Martini, 1964, p. 293–294). The nannoplankton, however, can be expected to occur also throughout the Franciscan in shales from which free specimens might be extracted and concentrated for study. In the latter case, an electron microscope, although helpful, is not a necessity as most biostratigraphic studies of the nannoplankton till now have been made with the optical microscope. If the nannoplankton can be recovered from these generally unfossiliferous rocks, they should provide a much-needed means of correlating or differentiating sequences within the Franciscan Formation.

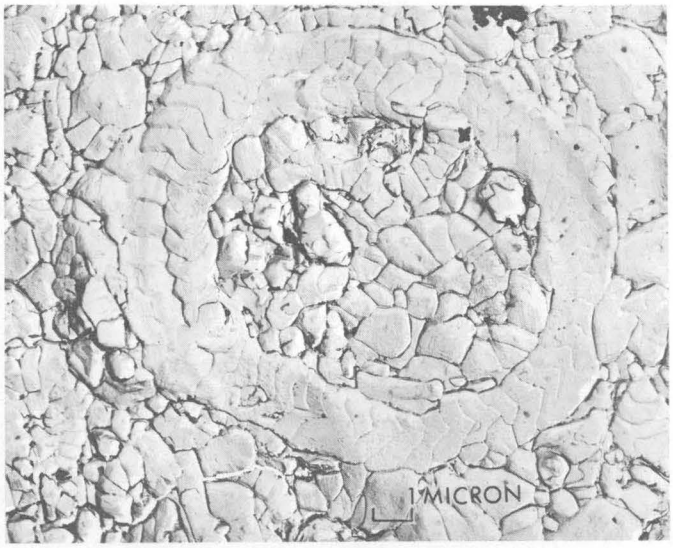

FIGURE 8.—Electron micrograph of the Laytonville type of limestone from Smith Ridge, Fort Ross quadrangle, showing a large coccolith surrounded by smaller coccoliths and containing fragments of coccoliths within a central cavity. × 5,000.

ACKNOWLEDGMENTS

The support of the Petroleum Research Fund of the American Chemical Society (contract PRF 1114–81–A2) made possible the laboratory investigation of the first author and is most gratefully acknowledged. Use of an electron microscope was kindly made available by Dr. L. I. Rebhun, Department of Biology, Princeton University. Dr. A. G. Fischer, of Princeton University, gave helpful advice during all stages of the investigation. The laboratory work was conducted while the first author was a postdoctoral fellow at Princeton University.

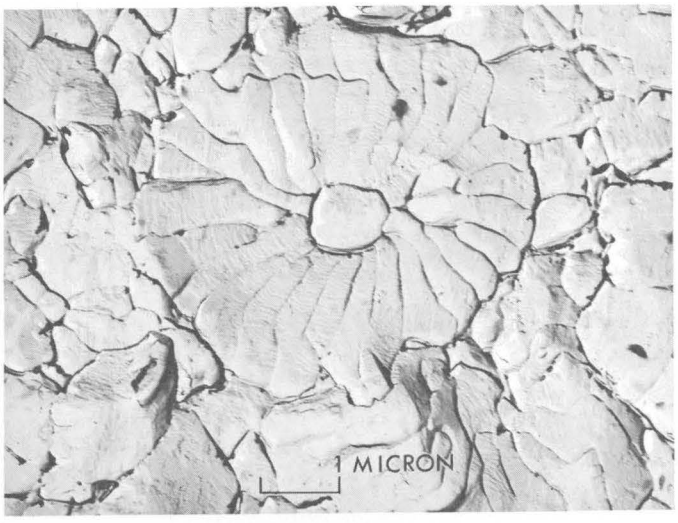

FIGURE 9.—Electron micrograph of same limestone as in figure 7, showing a very well preserved coccolith. × 10,000.

REFERENCES

Bailey, E. H., Irwin, W. P., and Jones, D. L., 1964, Franciscan and related rocks and their significance in the geology of western California: California Div. Mines and Geology Bull. 183, 177 p.

Bathurst, R. G. C., 1958, Diagenetic fabrics in some British Dinantian limestones: Liverpool and Manchester Geol. Jour., v. 2, p. 11–36.

Black, Maurice, 1956, The finer constituents of *Globigerina* ooze [abs.]: Internat. Geol. Cong. 20th, Mexico City 1956, Resumeres de los Trabajos Presentados, p. 173.

Bramlette, M. N., and Martini, E., 1964, The great change in calcareous nannoplankton fossils between the Maestrichtian and Danian: Micropaleontology, v. 10, p. 291–322.

Brönnimann, Paul, 1955, Microfossils incertae sedis from the Upper Jurassic and Lower Cretaceous of Cuba: Micropaleontology, v. 1, p. 28–51.

Garrison, R. E., 1964, Jurassic and early Cretaceous sedimentation in the Unken Valley area, Austria: Princeton Univ., Ph.D. thesis, 188 p.

Honjo, Susumu, and Fischer, A. G., 1964, Fossil coccoliths in limestone examined by electron microscopy: Science, v. 144, p. 837–839.

——— 1965a, Thin sections and peels for high magnification study and phase-contrast microscopy, *in* Kummel, Bernhard, and Raup, D. M., eds., Handbook of paleontological techniques: San Francisco, W. H. Freeman and Co., p. 241–247.

——— 1965b, Paleontological investigation of limestones by electron microscope, *in* Kummel, Bernhard, and Raup, D. M. eds., Handbook of paleontological techniques: San Francisco, W. H. Freeman and Co., p. 326–334.

Kania, J. E. A., 1929, Precipitation of limestone by submarine vents, fumaroles, and lava flows: Am. Jour. Sci., 5th ser., v. 18, p. 347–359.

Küpper, Klaus, 1955, Upper Cretaceous Foraminifera from the "Franciscan Series," New Almaden district, California: Cushman Found. Foram. Research Contr., v. 6, p. 112–118.

Leighton, M. W., and Pendexter, Charles, 1962, Carbonate rock types, *in* Ham, W. E., and Pray, L. C., eds., Classification of carbonate rocks: Am. Assoc. Petroleum Geologists Mem. 1, p. 33–61.

Loeblich, A. R., Jr., and Tappan, H. R., 1961, Cretaceous planktonic Foraminifera, pt. 1, Cenomanian: Micropaleontology, v. 7, no. 3, p. 257–304.

Park, C. F., Jr., 1946, The spilite and manganese problems of the Olympic Peninsula, Washington: Am. Jour. Sci., new ser., v. 244, p. 305–323.

Provasoli, Luigi, 1963, Organic regulation of phytoplankton fertility, *in* Hill, M. N., The sea, v. 2: New York, Interscience Publishers, p. 165–219.

Reinhard, Max, and Wenk, Eduard, 1961, Geology of the Colony of North Borneo: Borneo (British Terr.) Geol. Survey Dept. Bull. 1, 160 p.

Robertson, E. C., 1964, Experimental consolidation of carbonate mud [abs.]: Am. Assoc. Petroleum Geologists Bull., v. 48, p. 544.

Thalmann, H. E., 1942, *Globotruncana* in the Franciscan limestone, Santa Clara County, California [abs.]: Geol. Soc. America Bull., v. 3, no. 12, pt. 2, p. 1838.

X-RAY DETERMINATIVE CURVE FOR SOME ORTHOPYROXENES OF COMPOSITION Mg_{48-85} FROM THE STILLWATER COMPLEX, MONTANA

By GLEN R. HIMMELBERG and EVERETT D. JACKSON, Menlo Park, Calif.

Abstract.—An X-ray determinative curve for 12 chemically analyzed orthopyroxenes based on $\Delta 2\theta$ (131) orthopyroxene − (111) lithium fluoride gives the regression equation $\Delta 2\theta$ ($CuK\alpha_1$) $= 4.112 - 0.009132Mg$. Two sigma for the regression equation is $\pm 0.012°2\theta$, which corresponds to about ± 1.3 percent Mg.

An X-ray determinative method similar to that developed by Jackson (1960) for natural olivines was applied to 12 orthopyroxenes from the Precambrian Stillwater complex, Montana. These orthopyroxenes were separated by the method described by Schoen and Lee (1964). Purity of the separates was estimated from grain counts, and ranged between 98.9 and 99.7 percent. Two of the samples were split to make hidden duplicates which were then treated as separate samples. The 14 samples were chemically analyzed, and the Mg content of each sample was calculated as the ionic ratio of Mg to total octahedral cations. Splits of each of the 14 analyzed samples were divided into 3 separate parts for X-ray examination. These 42 separate parts were assigned random numbers to determine run order, mixed with about 10 percent lithium fluoride (reagent), and prepared as slurries on cover glasses ⅞ inch in diameter. The cover glasses containing the slurries were placed in a rotating sample holder, and sample heights were adjusted by placing prepared disks of the proper thickness under the samples. Each of the 42 subsamples was allowed to oscillate up and down twice between 34.5° and 40°2θ on a diffractometer using copper radiation and a focusing monochrometer. A 1° divergent slit, a 4° preslit, and a 1° receiving slit were used. The scan speed was ¼° per minute, and the chart scale was 2 inches per degree 2θ. The distances between the orthopyroxene (131) peak and the lithium fluoride (111) peak were measured directly in degrees from the charts and were compiled; means and standard deviations of $\Delta 2\theta$ were calculated from them. Mg content, calculated from the analyses, and X-ray data are summarized in table 1.

The information in table 1 forms the basis for the determinative curve in figure 1. The X-ray data are plotted directly as degrees $\Delta 2\theta$ ($CuK\alpha_1$) on the ordinate, the Mg value on the abscissa. A regression analysis was made considering the 14 measurement sets to represent individual samples, using the average X-ray parameter $\Delta 2\theta$ as the dependent variable, and taking the chemically derived value of Mg as the independent variable. The linear equation is:

$$\Delta 2\theta \ (CuK\alpha_1) \ (131) \text{ orthopyroxene} - (111) \text{ lithium fluoride} = 4.112 - 0.009132Mg.$$

Two sigma for the regression equation is $\pm 0.012°$ 2θ, which corresponds to about ± 1.3 percent Mg.

The determinative curve shown is based on orthopyroxenes from a single petrographic province and with similar minor-element contents. The aluminum content ranges from 0.038 to 0.119 ion per formula of 6

TABLE 1.—*Mg content and X-ray measurements of orthopyroxene samples*

Field No.	Mg[1]	Mean of 12 readings of $2\theta_{131}$ (orthopyroxene) $- 2\theta_{111}$ (LiF) (degrees)[2]	Standard deviation of 12 readings (degrees)
55BE-1	48.69	3.665	0.0139
53IN-2	52.47	3.635	.0156
53NB-11	54.27	3.621	.0108
55NB-1[3]	54.23	3.612	.0086
55BE-2	72.08	3.461	.0089
55BE-4	72.25	3.449	.0067
55BE-7	79.04	3.400	.0106
52BE-35	82.49	3.365	.0120
52BE-29	83.51	3.358	.0097
55MV-32	82.98	3.348	.0064
55MB-2[4]	83.02	3.352	.0072
55MV-29	82.91	3.349	.0073
55MV-26	84.08	3.343	.0108
61SC-B	83.93	3.339	.0130

[1] Ionic ratio of Mg to the sum of Mg, Fe^{+2}, Mn, Ni, Co, Cu, Al^{VI}, Fe^{+3}, Cr, V, Sc, Ti, Zr, Mo, and Sn × 100.
[2] $CuK\alpha_1$ radiation.
[3] Hidden duplicate of 53NB-11.
[4] Hidden duplicate of 55MV-32.

oxygens (0.86 to 2.87 weight percent Al_2O_3); the calcium content ranges from 0.045 to 0.112 ion per formula of 6 oxygens (1.10 to 2.98 weight percent CaO). Some of this calcium however, is present in clinopyroxene exsolution lamellae. Hess (1952), Kuno (1954), and Zwaan (1954) have shown that orthopyroxene X-ray parameters are affected by aluminum and calcium contents. The determinative curve should therefore be used with caution in estimating or comparing orthopyroxenes from different chemical, thermal, or barometric environments.

REFERENCES

Hess, H. H., 1952, Orthopyroxenes of the Bushveld type, ion substitutions and changes in unit cell dimensions: Am. Jour. Sci., Bowen volume, p. 173–187.

Jackson, E. D., 1960, X-ray determinative curve for natural olivine of composition Fo_{80-90}: Art. 197 *in* U.S. Geol. Survey Prof. Paper 400–B, p. B432–B434.

Kuno, Hisashi, 1954, Study of orthopyroxenes from volcanic rocks: Am. Mineralogist, v. 39, p. 30–46.

Schoen, Robert, and Lee, D. E., 1964, Successful separation of silt-size minerals in heavy liquids, *in* Geological Survey Research 1964: U.S. Geol. Survey Prof. Paper 501–B, p. B154–B157.

Zwaan, P. C., 1954, On the determination of pyroxenes by X-ray powder diagrams: Leidse Geol. Mededeel, v. 19, p. 167–276.

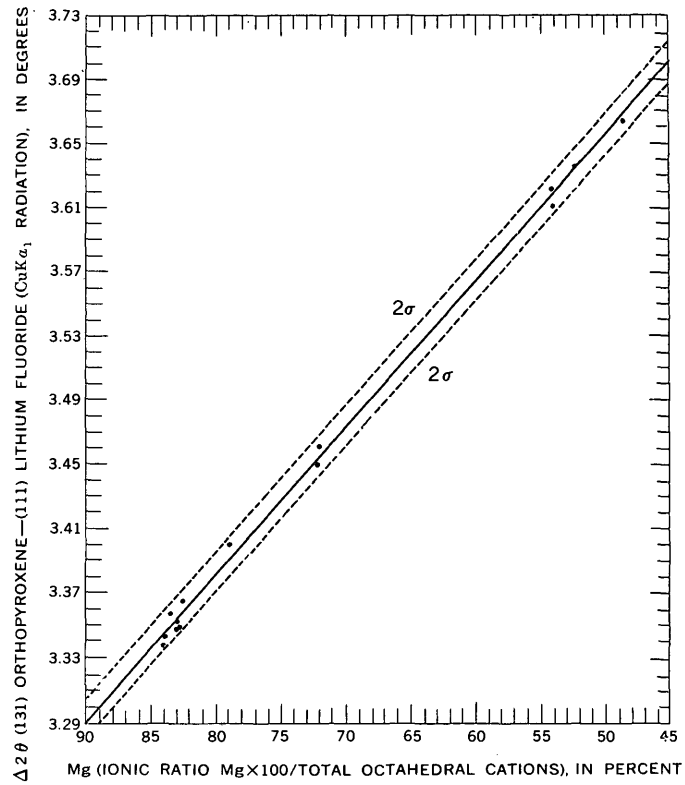

FIGURE 1.—X-ray determination curve for orthopyroxenes of composition Mg_{48-85}.

SERPENTINE-MINERAL ANALYSES AND PHYSICAL PROPERTIES

By NORMAN J. PAGE and ROBERT G. COLEMAN, Menlo Park, Calif.

Abstract.—Purified separates of serpentine minerals were prepared from seven serpentinite samples from California and New Zealand. Chemical and spectrographic analyses for the separates are presented, together with their optical, physical, and X-ray properties. A new serpentinite mineral assemblage consisting of clinochrysotile and corundum with or without magnetite was found in a vein cutting massive serpentinite at New Idria, Calif.

Chemical analyses of purified serpentine minerals, accompanied by X-ray identification and physical descriptions, are sparse in modern literature. The purpose of this paper is to present new data on analysed serpentine minerals that have been used as standards in a more comprehensive long-term study of the serpentines (Page, 1966; Hostetler and others, 1966) by the U.S. Geological Survey. Each sample was carefully purified before analysis to insure that the analyzed material consisted of a single phase. Standard heavy-liquid techniques were used to separate the serpentine minerals from the parent serpentinites, except for fibrous clinochrysotile. This mineral was disaggregated and heavy minerals intergrown with it were removed by repeated elutriation. The terminology and classification of the serpentine minerals used in this report are those of Faust and Fahey (1962) and Whittaker and Zussman (1956).

Acknowledgments.—The chrysotile sample from the Union Carbide Corp. plant was supplied by Dr. Fred Mumpton. Miss Terry Clark, U.S. Geological Survey, provided some of the mineralogical support on this study.

NEW CHEMICAL AND MINERALOGICAL DATA ON SERPENTINE MINERALS

Complete chemical analyses of the serpentine minerals studied are given in table 1 and are comparable with analyses by Faust and Fahey (1962). Spectrographic analyses and descriptions of the samples are also given in table 1.

Table 2 presents indexed d-spacings and intensities for six of the specimens. In sample 3, traces of clinochrysotile are present; in sample 5, traces of lizardite are present and in sample 6, peaks of corundum are present. The d-spacings are similar to those given by Whittaker and Zussman (1965) and completely characterize the serpentine species for each sample.

Optical measurements of the different serpentine minerals (table 3) were made in sodium light. Fibers of sample 4 were impossible to mount on a spindle stage, so only an index parallel to the fiber axis (α) could be measured, whereas in samples 5 and 6 of clinochrysotile, α and β appeared to be equal. Refined unit-cell parameters and observed and calculated specific gravities are also given in table 3.

The distribution of cations between octahedral and tetrahedral positions, on the basis of 18 anions per mineral for 6 samples, is shown in table 4. No calculations were made for sample 6 because of the abundance of Al_2O_3 that is present as corundum.

The chemical singularity of antigorite is clearly demonstrated both in tables 1 and 4. The antigorites have a ratio of FeO to Fe_2O_3 greater than one, and apparently all the alumina is present in octahedral coordination and none in tetrahedral coordination; in lizardite and clinochrysotile the reverse is true. The data also suggest that lizardites differ chemically from clinochrysotiles by having a large amount of total iron (Page, 1966).

ASSEMBLAGE CLINOCHRYSOTILE AND CORUNDUM

In sample 6, the assemblage clinochrysotile + corundum with or without magnetite is present. The corundum is irregularly distributed and occurs as colorless to pale-yellow euhedral and subhedral grains varying in size from submicroscopic to 0.1 mm in diameter. Some sections subparallel with (0001) exhibit a small $2V$ that is anomalous for an uniaxial mineral but that is common in corundum (Deer and others, 1962). The corundum was concentrated by dissolution of the clinochrysotile in a mixture of HCl, H_2SO_4, HNO_3, and HF.

TABLE 1.—*Chemical and spectrographic analyses of serpentine minerals from New Idria, Calif., and New Zealand*

[Gravimetric chemical analyses by L. B. Beatty, U.S. Geol. Survey; spectrographic analyses by R. E. Mays, U.S. Geol. Survey]

	Antigorite			Lizardite	Clinochrysotile			
	1	1a	2	3	4	5	[1] 6	7
CHEMICAL ANALYSES (WEIGHT PERCENT)								
SiO_2	44.2	44.8	43.1	41.1	42.2	41.4	32.1	41.0
Al_2O_3	.90	.5	1.3	.78	.66	.70	34.6	.7
Fe_2O_3	.27	.2	.80	2.4	1.2	1.4	.82	1.3
FeO	2.1	2.2	2.6	.21	.09	1.3	1.3	.95
MgO	40.1	39.9	39.8	41.5	41.7	41.4	20.9	40.7
CaO	.02	.02	.02	.02	.01	.04	.84	.13
Na_2O	----	.00	----	----	----	----	----	.04
K_2O	----	.00	----	----	----	----	----	.00
TiO_2	.01	.0	.002	.003	.002	.002	.18	<.01
Cr_2O_3	.22	.15	.06	.20	.02	.01	.009	.23
NiO	.13	.5	.11	.11	.04	.02	.002	.22
MnO	.02	.02	.03	.05	.06	.04	.04	.07
H_2O^+	11.9	11.8	11.9	13.3	13.3	13.0	7.6	12.8
H_2O^-	.15	.13	.07	.63	.95	.63	1.4	1.5
Total	100.02	99.9	99.79	100.30	100.23	99.94	99.78	99.6
SPECTROGRAPHIC ANALYSES (PARTS PER MILLION)								
Cu	7	13	5	8	2	18	70	9
Sn	----	----	----	----	20	<10	<10	----
Mn	110	100	220	360	420	320	280	460
Co	30	14	26	40	40	46	26	70
Ni	1,000	1,200	900	900	300	160	17	1,700
V	14	8	16	<10	<10	<10	30	<20
Zr	----	----	----	<10	<10	<10	440	----
Sc	<4	----	12	----	----	----	----	4
Sr	----	----	----	<4	<4	<4	60	----
Ba	----	----	----	8	<4	<4	65	9
B	20	----	----	60	60	<20	100	30
Cr	1,500	1,200	400	1,400	1,400	420	650	1,000

[1] Analysis of a mixture of corundum and clinochrysotile.

1. Field No. 38-NZ-62-5; lab. No. 63M-409. Massive greenish-black antigorite from a rock with the assemblage antigorite, talc, and magnetite. This same material produces a clear translucent gem-quality material referred to as bowenite (Reed, 1957). Veins in dunite mylonite, Milford Sound, South Island, New Zealand (Coleman, 1966).

1a. Lab. No. 65M-643. Same as sample 1, but a different separate.

2. Field No. 94-NZ-62; lab. No. 63M-410. Antigorite from a rock with an interlocking matte of antigorite laths (0.5–0.1 mm length) perpendicular to each other with the assemblage antigorite and magnesite with or without talc, magnetite, or olivine. This sample is from the same area as the antigorite discussed by Zussman (1954); geology and petrology described by Coleman (1966). Lens in biotite-garnet schists, Griffin Range, Westland, New Zealand.

3. Field No. 19-NI-63A; lab. No. 63M-826. Light-green lizardite from a vein with mesh structure cut by cross-fiber chrysotile veins with the assemblage lizardite and magnetite with or without heazlewoodite and clinochrysotile. Vein in serpentinite, Joe No. 5 Pit, Union Carbide Corp., New Idria, San Benito County, Calif. Taken from same outcrop as sample 4.

4. Field No. 19-NI-63B; lab. No. 63M-827. White to pale-green clinochrysotile slip fiber matte composed of fine "thread-like" material, consisting of serpentine encrusting massive serpentinite. Joe No. 5 Pit, Union Carbide Corp., New Idria, San Benito County, Calif. Taken from same outcrop as sample 3.

5. Field No. 14-NI-63A; lab. No. 63M-828. Green to black massive bladed clinochrysotile vein with traces of lizardite; in thin section, perpendicular to blades; pseudoisotropic. Vein in serpentinite, Butler Estate chrome mine, New Idria, San Benito County, Calif. Taken from same outcrop as sample 6.

6. Field No. 14-NI-63C; lab. No. 63M-829. A mixture of clinochrysotile and corundum from a ½- to 1½-inch vein of clinochrysotile and magnetite with or without corundum. Cross-fiber vein in serpentinite, Butler Estate chrome mine, New Idria, San Benito County, Calif. Taken from same outcrop as sample 5.

7. Union Carbide mill product; lab. No. 65M-1119. Clinochrysotile, representative mill product from Union Carbide Corp., King City, Calif., plant. From Joe No. 5 Pit, Union Carbide Corp., New Idria, San Benito County, Calif.

TABLE 2.—*Indexed d-spacing and intensity for serpentine minerals* [1] [2]

[Symbols: vs, very strong; s, strong; m, moderate; mw, moderately weak; w, weak; vw, very weak]

Antigorite					Lizardite			Clinochrysotile						
	1		2			3			4		5		6	
(*hkl*)	*d*(A)	*I*	*d*(A)	*I*	(*hkl*)	*d*(A)	*I*	(*hkl*)	*d*(A)	*I*	*d*(A)	*I*	*d*(A)	*I*
001	7. 30	vs	7. 29	vs	001	7. 37	vs	002	7. 15	-------	7. 31	vs	7. 34	------
			6. 43	w	020	4. 61	m	020	4. 53	-------	4. 57	m	4. 55	------
401	6. 23	w						$\bar{1}12$	4. 06	-------	4. 05	vw		
$\bar{6}10$			5. 82	w	022, 111	3. 88	w							
311			5. 15	w	002	3. 66	vs	004	3. 66	-------	3. 65	s	3. 66	------
$\bar{5}11$	4. 93	mw											[3] 3. 48	------
020			4. 64	mw				023	3. 36	-------			3. 34	------
$\bar{4}20$			4. 26	w	200	2. 669	w							
711	4. 20	w			130, 210	2. 603	vw							
021	4. 01	vw						201	2. 588	-------			[3] 2. 55	------
901			3. 99	vw	131	2. 504	s							
12. 0. 0, 002	3. 62	s	3. 61	s	003	2. 455	vs	[4] 003			2. 45	vw		
$\bar{1}1$. 4. 0	3. 44	w						202, 006	2. 435	-------			2. 453	------
$\bar{1}1$. 2. 1, $\bar{3}31$			2. 794	w				$\bar{2}03$					[3] 2. 382	------
$\bar{7}30$, $\bar{4}22$	2. 790	w						203			2. 270	w		
15. 0. 1, $\bar{6}22$			2. 667	vw				$\bar{2}04$, $\bar{1}16$			2. 205	w	2. 207	------
$\bar{1}2$. 0. 2, $\bar{7}31$,			2. 596	w	[5] 204	2. 095	w	204, 007, 043	2. 083	-------	2. 092	w	2. 084	------
$\bar{1}$. 4. 20								224, 205	1. 991	-------			2. 010	------
16. 0. 1	2. 530	vs	2. 525	vs				$\bar{2}40$					1. 913	------
$93\bar{1}$			2. 458	m	004	1. 825	vw	008, $\bar{2}05$	1. 823	-------	1. 827	w		
$\bar{1}7$. 0. 1, $\bar{2}03$	2. 423	w	2. 429	w				$\bar{1}35$						
$\bar{1}4$. 0. 2			2. 386	w	203	1. 797	vw							
141, $\bar{1}41$, $\bar{6}40$			2. 210	w	[5] 206	1. 745	vw	206, $\bar{2}40$	1. 744	-------	1. 744	w		
$83\bar{2}$, 901			2. 172	m	024, 114, 311	1. 700	vw							
21. 1. 1	1. 940	w						153	1. 635	-------			[3] 1. 601	------
18. 2. 2, 842			1. 833	w	060	1. 539	s	060			1. 535	m	1. 534	------
15. 1. 3, 151,	1. 814	w	1. 812	w				$\bar{1}38$	1. 524	-------				
20. 1. 2, 240					061	1. 505	w	[4] 061			1. 506	w		
$\bar{6}50$			1. 795	w	005	1. 459	m	0. 0. 10, 063	1. 466	-------	1. 463	w	1. 489	------
$\bar{3}14$	1. 780	w												
751, $\bar{2}0$. 2. 2	1. 741	w	1. 742	w	062	1. 417	w	[4] 062					[3] 1. 405	------
$\bar{2}3$. 2. 1			1. 709	vw	261	1. 311	w	2. 1. 10,	1. 310	-------	1. 313	w	1. 311	------
$\bar{9}51$	1. 702	m						262, 401						
22. 1. 2			1. 694	m	170	1. 279	m							
452			1. 627	w	402, 262	1. 252	vw	$\bar{4}05$					1. 238	------
22. 4. 0	1. 508	w						$\bar{4}24$, $\bar{2}65$			1. 222	-------		
$\bar{2}6$. 4. 2			1. 278	vw	006	1. 215	vw	[3] 006			1. 219	-------		
36. 0. 0, 13. 6. 3			1. 209	vw				354, 265, $\bar{3}55$					1. 189	------
$\bar{2}6$. 5. 2			1. 181	vw				$\bar{3}55$						

[1] See table 1 for sample descriptions.
[2] Indexing by computer program 9214, U.S. Geol. Survey, Menlo Park, Calif.
[3] Corundum *d*-spacing.
[4] Lizardite *d*-spacing.
[5] Clinochrysotile *d*-spacing.

TABLE 3.—*Optical and physical properties of serpentine minerals* [1]

	Antigorite			Lizardite	Clinochrysotile		
	1	1a	2	3	4	5	6
OPTICAL PROPERTIES							
α_{Na}	1.563±0.001	1.562±0.002	1.556–1.558	1.561±0.002		1.569±0.002	1.545±0.002
β_{Na}	1.565± .002	1.565± .002	1.565–1.567	1.565± .002			
γ_{Na}	1.570± .002	1.567± .002	1.572–1.569	1.567± .002	1.557±0.004	1.570± .002	
$2V_\alpha$	73±5°	78°	61±3°	Small			42°
Birefrigence	.007	.005	.016– .011	.006	∼.001	.001	∼.002
PHYSICAL PROPERTIES Unit-cell data [2]							
a A	43.445±0.007		43.53±0.01	5.339±0.003	5.3143±0.0002	5.3129±0.0009	5.325±0.001
b A	9.374± .002		9.259± .003	9.226± .002	9.2533± .0004	9.120 ± .003	9.173± .003
c A	7.294± .002		7.263± .007	7.315± .006	14.6307± .0003	14.637 ± .002	14.669± .008
β degrees	90°47.9′±0.7′		91°8.4′±1.6′	90°	92°52.4′±0.2′	93°9.8′±0.6′	93°20.6′±1.6′
Cell volume (obs) A^3	2,907.2± .8		2,927.2± 2.3	360.3± .3	718.56± .02	708.2± .3	715.3± .3
Cell volume (calc) A^3		2,925.4	2,886.0	363.5		731.2	
Specific gravity							
Observed		2.605–2.610	2.65	2.55±0.03		2.53±0.01	
Calculated [2]	2.56		2.61	2.57	2.56	2.61	

[1] See table 1 for sample descriptions.
[2] Computer program 9214, least-squares unit-cell refinement translated into Algol from original Fortran 4,U.S. Geol. Survey, Menlo Park, Calif.

TABLE 4.—*Structural formulas of the serpentine minerals, calculated by the hydrogen equivalent method based on 18 anions per formula* [1] [2]

		Antigorite			Lizardite	Clinochrysotile		
		1	1a	2	3	4	5	7
Tetrahedral	Si^{+4}	4. 146	4. 201	4. 067	3. 832	3. 923	3. 843	3. 897
	Al^{+3}				. 086	. 072	. 077	. 078
	Total	4. 146	4. 201	4. 067	3. 918	3. 996	3. 910	3. 975
Octahedral	Al^{+3}	4. 100	. 055	0. 145				
	Cr^{+3}	. 016	. 011	. 005	. 015	. 002	. 001	. 017
	Fe^{+3}	. 019	. 014	. 057	. 168	. 084	. 098	. 093
	Ti^{+4}	. 001						. 001
	Mg^{+2}	5. 606	5. 576	5. 597	5. 768	5. 778	5. 727	5. 766
	Ni^{+2}	. 010	. 038	. 008	. 008	. 003	. 002	. 017
	Fe^{+2}	. 165	. 173	. 205	. 016	. 007	. 101	. 076
	Mn^{+2}	. 002	. 002	. 002	. 004	. 005	. 003	. 006
	Total	5. 919	5. 869	6. 019	5. 979	5. 879	5. 932	5. 976
	OH^{-1}	7. 445	7. 380	7. 489	8. 272	8. 248	8. 438	8. 115
	O^{-2}	10. 555	10. 620	10. 511	9. 728	9. 752	9. 562	9. 885

[1] See table 1 for sample descriptions.
[2] Computer program Mineral Norms 9377, U.S. Geol. Survey, Menlo Park, Calif.

REFERENCES

Coleman, R. G., 1966, New Zealand serpentinites and associated metasomatic rocks: New Zealand Geol. Survey Bull. 76, 102 p.

Deer, W. A., Howie, R. A., and Zussman, J., 1962, Non-silicates, v. 5 *of* Rock-forming minerals: London, Longmans, Green, and Co., Ltd., 371 p.

Faust, G. T., and Fahey, J. J., 1962, The serpentine-group minerals: U.S. Geol. Survey Prof. Paper 384–A, p. A1–A92.

Hostetler, P. B., Coleman, R. G., Mumpton, F. A., and Evans, B. W., 1966, Brucite in Alpine serpentinites: Am. Mineralogist, v. 51, nos. 1–2, p. 75–98.

Page, N. J., 1966, Mineralogy and chemistry of the serpentine-group minerals and the serpentinization process: California Univ., Berkeley, Ph. D. thesis.

Reed, J. J., 1957, Use of the terms greenstone, nephrite, bowenite, and jade: Polynesian Soc. Jour., v. 66, no. 2, 2 p.

Whittaker, E. J. W., and Zussman, J., 1956, The characterization of serpentine minerals by X-ray diffraction: Mineralog. Mag. [London], v. 31, no. 233, p. 107–126.

Zussman, J., 1954, Investigation of the crystal structure of antigorite: Mineralog. Mag. [London], v. 30, no. 227, p. 498–512.

A NEW(?) YTTRIUM RARE-EARTH IRON ARSENATE MINERAL FROM HAMILTON, NEVADA

By ARTHUR S. RADTKE and CHARLES M. TAYLOR,[1]
Menlo Park, Calif., Palo Alto, Calif.

Abstract.—Magnetite grains in manganoan calcite or "black calcite" associated with silver ores at Treasure Hill, Hamilton, Nev., contain significant amounts of a new(?) yttrium rare-earth iron arsenate mineral. Chemical analyses made with the electron microprobe analyzer shows the approximate formula to be

$$3(Y,Ce,Nd,Dy,Gd,Er)_2O_3 \cdot Fe_2O_3 \cdot 2As_2O_5 \pm 14H_2O.$$

Small particle size and distribution of the rare-earth-rich mineral precluded obtaining X-ray powder data. Certain physical and optical data are given.

A sample of manganoan calcite, "black calcite," from Treasure Hill, Hamilton, Nev. (an abandoned mining town about 40 miles west of Ely, in east-central Nevada), collected by D. F. Hewett, of the U.S. Geological Survey, contains a rare-earth-rich mineral disseminated through grains of magnetite. The formula of the mineral is approximately

$$3(Y,Ce,Nd,Dy,Gd,Er)_2O_3 \cdot Fe_2O_3 \cdot 2As_2O_5 \pm 14H_2O.$$

The composition, as determined with the Materials Analysis Co. model-400 electron microprobe analyzer and calculated as oxides, is shown in table 1. Iron, vanadium, and manganese have been calculated arbitrarily as the highest valence oxides. Elemental weight percentages of arsenic and iron were determined to be 17.3 and 5.9, respectively. The molecular ratio of As_2O_5 to Fe_2O_3 is then approximately 2 to 1.

The only known yttrium arsenate mineral is retzian, which is distinctly different in composition. Palache and others (1951, p. 795) reported that retzian contains 19.2 percent CaO, 1.7 percent FeO, 10.3 percent rare earths, and 24.4 percent As_2O_5.

The grain size of the mineral is approximately 50 microns by less than 10 microns in magnetite host grains that are approximately 200 microns by 400 microns. The manner of distribution of these extremely small particles precludes obtaining X-ray powder diffraction patterns and other crystallographic data. The mineral hardness is 3 to 3½ on Mohs scale, on the basis of the relief as compared with that of magnetite; its surface is soft, granular, "earthy," and has a dull luster. The mineral is anisotropic and is a medium brownish gray in reflected light compared to the lighter cream gray of the host magnetite. Small euhedral grains of zircon containing 0.4 percent hafnium are also confined to and locked within magnetite.

The yttrium rare-earth iron arsenate is associated with manganoan calcite, pyrolusite, cerargyrite, argentian todorokite, magnetite, and zircon (fig. 1).

TABLE 1.—*Chemical analysis of a yttrium rare-earth iron arsenate mineral*

Oxides [1]	Element [2] weight percentage	Oxide weight percentage	Molecular proportions	
Y_2O_3	21.6	27.4	0.121	
Ce_2O_3	4.0	4.7	.014	
Nd_2O_3	3.0	3.5	.010	
Dy_2O_3	2.2	2.5	.007	
Gd_2O_3	2.0	2.3	.006	
Er_2O_3	2.0	2.3	.006	0.186
Sm_2O_3	.7	.8	.002	
La_2O_3	.7	.8	.003	
Yb_2O_3	.5	.6	.002	
Pr_2O_3	.4	.5	.002	
Ho_2O_3	.1	.1	.0003	
CaO	.5	.7	.013	
Fe_2O_3	5.9	8.4	.053	
TiO_2	.3	.5	.008	.066
V_2O_5	.4	.7	.003	
MnO_2	.1	.2	.002	
As_2O_5	17.3	26.5	.115	.117
P_2O_5	.1	.2	.002	
H_2O [3]		17.3	.960	.960

[1] Other elements detected include trace amounts of In, Sc, Si, Al, and Lu.
[2] Elemental data derived from electron microprobe analyzer.
[3] Calculated as the difference between total element weight percentage and 100 percent.

[1] Materials Analysis Co.

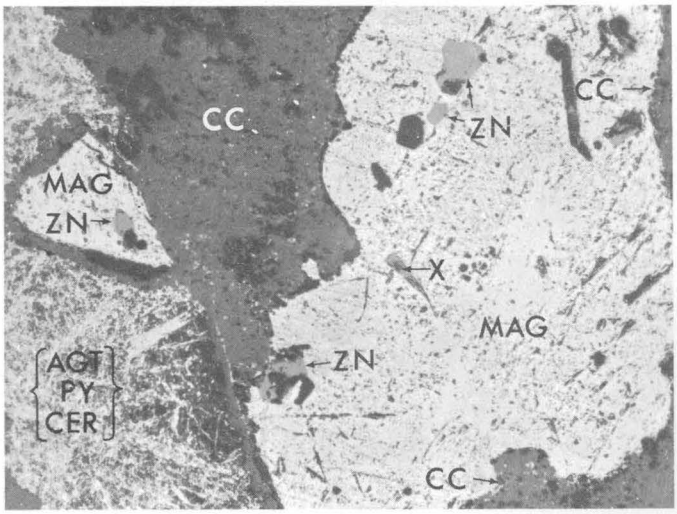

FIGURE 1.—Photomicrograph showing magnetite grain (MAG) containing rare-earth mineral (X) and zircon (ZN) within manganoan calcite (CC). Light-gray fine-grained bladed argentian todorokite (AGT) is intergrown with dark-gray pyrolusite (PY) and cerargyrite (CER) at left. Magnification × 205.

These minerals, together with other manganese oxides and quartz, compose zones of "black calcite" in the limestone which hosts the massive silver chloride ores of the Hamilton district.

The rare-earth mineral occurs as small euhedral wedge-shaped grains locked in magnetite (fig. 2). Straight regular contacts between the rare-earth mineral and magnetite preclude any conclusion on the paragenesis of the two minerals. The general rounding and corroded borders of the magnetite suggest that the magnetite, together with the rare-earth mineral and zircon, formed before the manganoan calcite, manganese oxides, and silver minerals (fig. 1).

Formation of both the rare-earth mineral and the magnetite host took place within a few hundred feet of the surface under oxidizing conditions during early hypogene mineralization. The combination of the rare earths with arsenic rather than phosphorus reflects the abundance of arsenic in low-temperature epithermal silver ores of this type.

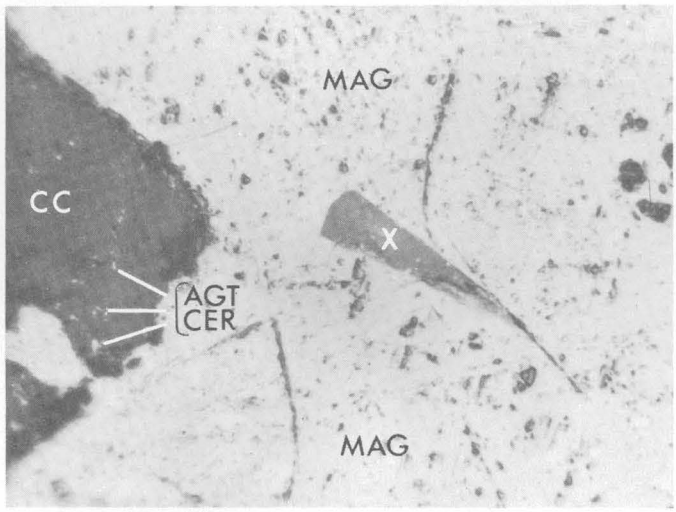

FIGURE 2.—Photomicrograph showing wedge-shaped rare-earth mineral (X) in magnetite host (MAG). Small dark spots on magnetite are micropits and scratches produced in final polishing. Dark-gray manganoan calcite (CC) contains small light-gray inclusions of argentian todorokite (AGT) and cerargyrite (CER). Magnification × 855.

REFERENCES

Palache, Charles, Berman, Harry, and Frondel, Clifford, 1951, The system of mineralogy of . . . Dana . . . , v. 2, Halides, nitrates, . . . etc., 7th ed., rev.: New York, John Wiley and Sons, 1,124 p.

HYDROTHERMAL ALTERATION OF BASALTIC ANDESITE AND OTHER ROCKS IN DRILL HOLE GS-6, STEAMBOAT SPRINGS, NEVADA

By ROBERT SCHOEN and DONALD E. WHITE, Menlo Park, Calif.

Abstract.—Geothermal waters produced two recognizable patterns of hydrothermal alteration in the rocks in drill hole GS–6. During an early period, the rocks were subjected to potassium metasomatism that formed K-feldspar and celadonite from unstable feldspars and ferromagnesian minerals, respectively. A later period of hydrogen metasomatism produced mixed-layer illite-montmorillonite, montmorillonite, and kaolinite, probably as a series directly related to the intensity of alteration. The clays formed during hydrogen metasomatism are irregularly distributed with depth and probably are related to reactions involving CO_2 and H_2S. This later period of argillization still may be in progress.

This paper presents the results of a mineralogic study of GS–6, one of eight holes drilled at Steamboat Springs, Nev., by the U.S. Geological Survey for geologic information. Steamboat Springs, located in the west-central part of Nevada, 10 miles south of Reno, is an area of active hot springs (fig. 1). Economic geologists have been interested in these springs for about 100 years because minerals of antimony and mercury, together with small amounts of gold and silver, precipitate from the hot waters.

The Steamboat Springs thermal area straddles the boundary between the Mount Rose and Virginia City quadrangles. The regional geology of these quadrangles has been described recently by Thompson and White (1964). White and others (1964) have presented the detailed geology of the thermal area, including an account of earlier studies and the logs of all drill holes, including GS–6.

The mineralogy of hydrothermally altered core from 4 of the U.S. Geological Survey drill holes has been described by Sigvaldason and White (1961, 1962), and Schoen and White (1965) similarly have described an additional 2 drill holes. In addition to presenting the detailed mineralogy of core from drill hole GS–6, the present paper compares the mineralogy of this drill hole with the others, and considers briefly the relationships between the compositions of waters and the observed alteration patterns.

The generalized geology of the thermal area is shown in figure 1. The basement rocks consist of a granodiorite pluton of late Mesozoic age intruded into metamorphosed sedimentary and volcanic rocks of probable early Mesozoic age. Tertiary and Quaternary volcanic and sedimentary rocks were deposited intermittently on the eroded surface of this basement, and andesite dikes intruded the granodiorite. Outcrops of the Tertiary volcanic and sedimentary rocks are too small to distinguish in figure 1, but core samples of these rocks, from drill hole GS–6, are shown in figure 2.

The oldest Cenozoic rocks found in the thermal area are soda trachyte flows, tuff breccias, and associated sediments of the Alta Formation of Oligocene(?) age. These were followed by andesite flows, tuff breccias, and andesite dikes of the Kate Peak Formation of Miocene or Pliocene age. The pre-Lousetown alluvium consists of silt, sand, and gravel. Local patches of orthoquartzite, pediment gravels, and chalcedonic hot-spring sinter are found associated with this alluvium. The Steamboat basaltic andesite of the Lousetown Formation was erupted in early Pleistocene time followed immediately by domes of pumiceous rhyolite of the Steamboat Hills Rhyolite. Pre-Lake Lahontan alluvium is approximately middle Pleistocene in age and consists of fragments of older rocks, many of which are cemented by hot-spring sinter. Post-Lousetown chalcedonic sinter consists of sinter older than deposits of Lake Lahontan and now mostly converted to chalcedony or cristobalite. Younger hot-spring sinter deposits, consisting largely of uncrystallized opal, range up to the present in age. Both Post-Lousetown chalcedonic sinter and the opaline hot-spring deposits are combined under "Sinter" in figure 1. Late Pleistocene alluvium that is contempo-

U.S. GEOL. SURVEY PROF. PAPER 575–B, PAGES B110–B119

FIGURE 1.—Generalized geologic map of Steamboat Springs thermal area, Washoe County, Nev. (Modified from detailed map, White and others, 1964.)

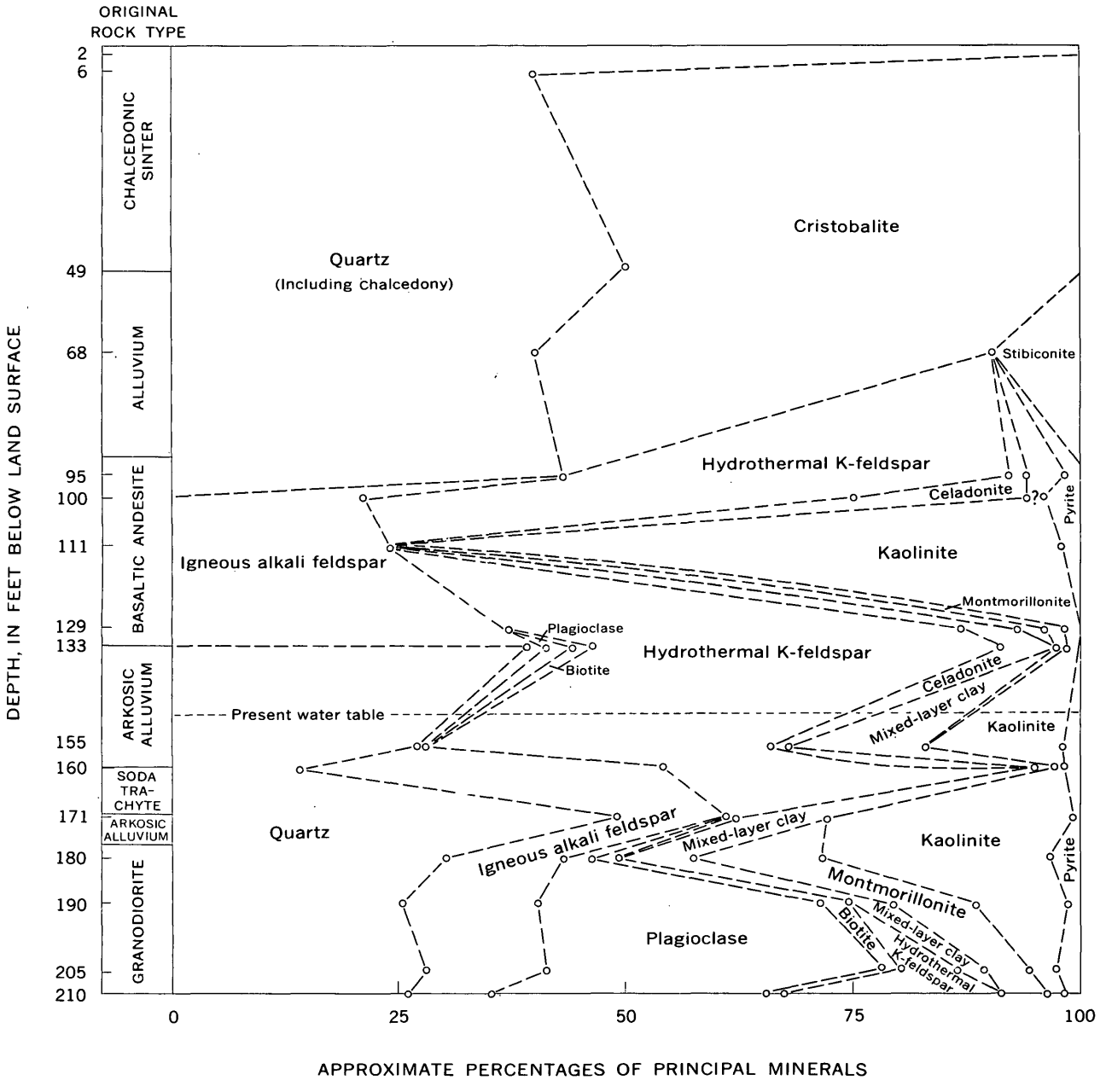

FIGURE 2.—Semiquantitative plot of mineralogy from drill hole GS–6. Dashed lines arbitrarily drawn straight between sample points.

raneous with Lake Lahontan, and very small patches of Recent alluvium in the stream valleys, complete the depositional history of the area. All three alluvial units, Pre-Lake Lahontan alluvium, alluvium contemporaneous with Lake Lahontan, and Recent alluvium, are combined under "Alluvium" in figure 1.

During this time of extensive deposition in the Cenozoic, the Steamboat Springs thermal area was also undergoing episodes of deformation and periods of erosion. An account of the Cenozoic geologic history of the area and a more detailed description of the stratigraphy can be found in the paper by White and others (1964).

Drill hole GS–6 is collared at an altitude of 4,838 feet in an extensive mass of relatively old silicious sinter known as Sinter Hill (fig. 1). The depth of the hole is 212 feet, and the depth to the water table is approximately 148 feet. Several months after drilling was completed, the water at the bottom of the drill hole had a temperature of 102.5°C, a pH of 6.7, a chloride content of only 12 parts per million, and a specific conductance of 372 micromhos. This ex-

tremely dilute water is very different from the fluids found in drill holes on the three thermally active terraces; typically, the temperature there is about 170°C, pH is about 6.2, chloride content is about 820 ppm, and specific conductance is about 3,000 micromhos. The dilute water of GS–6 is probably precipitation that fell on the area, percolated underground, and was heated moderately in the thermal environment.

Active construction of hot-spring sinter terraces is taking place today in the Steamboat Springs area at lower altitudes where hot chloride water containing 300 ppm or more of SiO_2 discharges at the surface (White and others, 1956). The sinter deposits of Sinter Hill prove that high-temperature, silica-bearing waters discharged in the past at altitudes at least 148 feet above the present water table. The different types and ages of the hot-spring sinters have been described in detail by White and others (1964).

Hydrothermal alteration of the rocks in the vicinity of GS–6 was a complex process, but two major stages of alteration can be recognized. An early period of potash metasomatism produced hydrothermal K-feldspar and celadonite as alteration products. This stage probably coincided with the construction of the silicious sinter deposit in which GS–6 is collared. During later hydrogen metasomatism, clay minerals and, locally, opal were produced. This last stage, dominated by argillization, still may be in progress today.

METHODS

X-ray diffraction was the principal tool used to study the mineralogy of whole-rock and clay fractions of all samples of drill core. Thin-section microscopy and chemical and spectrographic analyses of rocks and mineral concentrates provided essential additional information.

The mineralogy of the rocks cut by drill hole GS–6 is depicted in figure 2 as a semiquantitative plot of sample mineralogy versus sample depth. Details of the factors considered in the construction of such a diagram are given in an earlier paper (Schoen and White, 1965). In brief, modal analyses and X-ray diffractograms of unaltered rocks were used to evaluate the changes in mineralogy in hydrothermally affected rocks. The decrease in the height of an X-ray peak for a mineral from an altered rock is assumed to be linearly related to the decrease in abundance of the mineral in volume percent. Minerals produced by hydrothermal alteration are assumed to be equal in volume percent to the mineral or minerals they replaced. Application of these assumptions to the X-ray diffractograms, together with supporting evidence from thin sections and chemical analyses, provide mineral percentages for each sample of drill core.

Chemical analyses of altered rocks and fresh rock equivalents of the igneous rocks in GS–6 are presented in table 1. Additional chemical, normative, and modal analyses for other rocks from the Steamboat Springs area are presented by White and others (1964, tables 1 and 2).

Good quantitative mineralogic control exists for the granodiorite that underlies most of the Steamboat Springs thermal area, because of its relative homogeneity and the availability of chemically and petrographically analyzed fresh samples. Therefore, the granodiorite samples in drill hole GS–6 were evaluated for semiquantitative mineralogy in the same manner used for drill holes GS–3 and GS–4 (Schoen and White, 1965). The mineralogic compositions of the fresh soda trachyte and basaltic andesite are known with less certainty because of their fine-grained groundmasses. However, quantitative control is still reasonably good. The highly variable original composition of the arkosic sediments makes it difficult to determine semiquantitative mineralogy in the altered equivalents.

Because of these practical limitations, as well as the recognized theoretical limitations imposed by assuming a linear relationship between X-ray peak height and volume percent, the diagram of the mineralogy of drill hole GS–6 (fig. 2) is only a semiquantitative estimate. The reported percentage for each mineral present may be in error by as little as 5 percent for quartz, but the error is likely to be greater for most of the others, especially the clays. Nevertheless, the determination of the relative amount of each mineral in a sample has been found to be reproducible. This is the major requirement for a study of alteration where relative changes are important.

MINERALOGY

The mineralogy of the drill core is plotted semiquantitatively against depth in figure 2, and chemical analyses of selected samples are shown in table 1. The field designated "igneous alkali feldspar" in figure 2 represents anorthoclase and sanidine in the volcanic rocks, orthoclase in the granodiorite, and mixtures of all three in the alluvium.

Post-Lousetown chalcedonic sinter

The silicious sinter, that extends to a depth of 50 feet in GS–6 (fig. 2), was originally deposited as amorphous opal (White and others, 1964) but is now composed principally of about equal amounts of chalcedonic quartz and opal (β or high cristobalite by X-ray).

TABLE 1.—*Chemical analyses, by rapid methods, of rock from drill hole GS-6, Sinter Hill, Steamboat Springs, Nev., and of nearby unaltered equivalent rocks*

[Analysts (U.S. Geol. Survey): Leonard Shapiro (1-12); S. M. Berthold and E. A. Nygaard (3-5, 7, 9, 11, 12); H. F. Phillips (1, 2, 6, 8, 10); K. E. White (1, 2, 6, 8, 10); W. W. Brannock (13)]

	Altered rocks of GS-6										Unaltered nearby rocks		
Analysis number	1	2	3	4	5	6	7	8	9	10	11	12	13
Sample depth (feet)	2	6	68	100	111	129	160	190	205	210			
Description	Chalcedonic sinter	Chalcedonic sinter	Alluvium	Steamboat basaltic andesite of Lousetown Formation			Soda trachyte of Alta Formation	Granodiorite			Granodiorite	Soda trachyte of Alta Formation	Basaltic andesite of Lousetown Formation
SiO_2	97.9	96.4	91.3	58.3	60.9	61.3	67.7	68.9	72.2	74.0	65.6	65.0	54.38
Al_2O_3	.06	.30	.84	19.6	19.6	18.5	13.8	15.1	11.4	12.8	16.5	18.6	17.83
Fe_2O_3	.12	.08	.04	1.6	1.0	1.2	.5	.05	.3	.02	2.2	1.5	2.57
FeO	.0	.0	.17	.87	.23	.70	.30	.81	.60	.74	2.1	2.0	4.97
MgO	.00	.01	.10	.14	.26	.10	.15	.90	.40	.53	1.7	.74	4.12
CaO	.00	.14	.40	.50	1.1	1.8	1.2	1.0	1.2	1.1	3.2	3.1	6.58
Na_2O	.22	.20	.11	.78	1.6	2.5	1.6	1.8	1.8	2.1	3.6	5.0	4.03
K_2O	.10	.10	.10	10.9	2.8	8.8	8.7	4.4	4.7	4.8	2.9	3.2	2.50
H_2O	1.1	2.8	5.7	3.5	7.8	1.9	.0	4.2	2.9	1.9	.55	.25	.28
TiO_2	.00	.00	.58	1.4	1.5	1.5	.42	.34	.35	.28	.55	.46	1.89
P_2O_5	.00	.00	.01	.46	.45	.56	.10	.06	.11	.06	.15	.21	.57
MnO	.00	.00	.02	.05	.01	.01	.05	.02	.04	.02	.06	.14	.11
FeS_2	.02	.02	------	1.9	1.3	.62	4.5	1.9	3.7	2.1	------	------	.00
CO_2	<.05	<.05	<.05	<.05	<.05	<.05	<.05	<.05	<.05	<.05	.09	------	.01
SO_3	------	------	.12	<.2	.35	------	.62	------	------	------	.00	------	------
Total	100	100	100	100	99	100	100	100	100	100	99	100	100
Specific gravity (powder)	2.59	2.26	2.16	2.60	2.40	2.62	2.63	2.64	2.68	2.67	2.69	2.58	2.80
Specific gravity (lump)	2.36	1.80	1.95	2.41	2.04	2.50	2.58	2.20	2.41	2.54	2.62	2.52	2.59

The β cristobalite commonly is filled with inclusions, has an index of refraction ranging between 1.460 and 1.480, and is characterized by a strong 4.10A X-ray peak. Some α (low) cristobalite may be present at a depth of 49 feet where the mineral grains contain few inclusions, have indices of refraction above 1.480, and produce a strong 4.06A X-ray peak. Cristobalite is absent from the upper few feet of the core and from other zones (irregularly distributed throughout the sinter) that have been completely converted to chalcedony.

Pre-Lake Lahontan alluvium

Alluvial sediments occur from a depth of 50 feet to 91 feet. At 68 feet, where the alluvium has been extensively opalized, its present chemical and mineralogic composition is very similar to that of the overlying sinter (table 1, fig. 2). Stibiconite, a hydrous antimony oxide, is present at a depth of 68 feet in sufficient amount to color powdered samples of alluvium a pinkish yellow and produce four characteristic X-ray diffraction lines. Rounded fragments of basaltic andesite are common in the lower part of the alluvium, and they are generally rimmed by the green iron-rich mica, celadonite.

Steamboat basaltic andesite of Lousetown Formation

The Steamboat basaltic andesite lava flow was penetrated from a depth of 91 feet to 133 feet (fig. 2). Where unaltered this rock consists of phenocrysts of plagioclase and olivine in a cryptocrystalline groundmass composed largely of monoclinic alkali feldspar. The plagioclase phenocrysts are rimmed by overgrowths of anorthoclase that, in turn, may grade into sanidine in the groundmass; a change that probably occurred during the rapid cooling associated with eruption. Quartz is very rare in the fresh rock, and the large amount in the sample at 95 feet is caused by the downward settling of alluvium into the scoriaceous top of the flow.

K-metasomatism of the basaltic andesite produced nearly pure hydrothermal K-feldspar from all the primary plagioclase phenocrysts and exchanged K for Na in most of the original anorthoclase and sanidine. Small amounts of celadonite and pyrite formed, during K-metasomatism, from primary olivine, aluminum released in the breakdown of plagioclase, and sulfide ions in the thermal water. Few minerals susceptible to further alteration remained in the altered basaltic andesite, thus partially explaining the paucity of clay

minerals produced during a later period of H-metasomatism.

The sample from a depth of 111 feet requires special discussion because it does not fit the patterns described in the preceding paragraph. The original plagioclase phenocrysts are completely replaced by disordered kaolinite; hydrothermal K-feldspar and celadonite are absent. Because elsewhere plagioclase is easily kaolinized in an acid environment but K-feldspar is commonly metastable and is the last silicate mineral to be altered, it is concluded that the basaltic andesite from 111 feet in depth near the center of the flow was insulated from the early episode of K-metasomatism. Subsequently, during an episode of H-metasomatism, while the K-feldspathized basaltic andesite was metastable, all plagioclase at 111 feet was kaolinized. The massive impermeable nature of the flow, and fracturing caused by structural deformation that occurred between the two periods of alteration, probably explain the difference in access of the altering fluids.

The identification of the small amount of kaolinite in the sample at 100 feet is questionable. The mineral has a 7A periodicity, a d_{001} spacing of 7.15A, and is dioctahedral. Its index of refraction, however, is slightly above 1.57 and, therefore, the mineral may be dioctahedral septechlorite rather than kaolinite.

Pre-Lousetown alluvium

From a depth of 133 feet to 160 feet, arkosic alluvium contains abundant recognizable fragments of granodiorite and soda trachyte. Other fragments include andesite and metamorphic rocks.

The sample from a depth of 148 feet presents evidence that suggests a period of hydrothermal alteration predating the deposition of these sediments. A fragment of granodiorite contains chlorite that is pseudomorphic after primary biotite. The fragment is enclosed by a fine-grained matrix containing many bleached biotite flakes but none altering to chlorite. The pseudomorphic alteration of biotite to chlorite is common in drill holes GS–3 and GS–4 as an early product of H-metasomatism (Schoen and White, 1965). In GS–6, however, chlorite is very rare, apparently because K-metasomatism either bleached the biotite or converted it to celadonite. It is, therefore, possible that this granodiorite fragment was hydrothermally altered prior to its erosion and deposition. This supports White's conclusion that some hydrothermal activity predated the extrusion of the Steamboat basaltic andesite (White and others, 1964, p. B33).

Volcanic plagioclase and some plutonic plagioclase were converted to hydrothermal K-feldspar during K-metasomatism of the alluvium. Celadonite and pyrite formed as products of the thermal water and the breakdown of all primary ferromagnesian minerals except biotite, which in general simply was bleached. Later H-metasomatism of the alluvium produced clay minerals from the most susceptible minerals, especially remnant plutonic plagioclase.

Alta Formation

An altered soda-trachyte lava of the Alta Formation occurs between a depth of 160 feet and 170 feet. Fresh trachyte from nearby areas consists of plagioclase phenocrysts and numerous tiny oriented sodic plagioclase crystals in a very fine grained groundmass of anorthoclase and quartz. Hornblende and biotite are common but minor in amount. Quartz makes up about 15 percent of the rock.

K-metasomatism of the trachyte converted all plagioclase and some of the anorthoclase to hydrothermal K-feldspar. Subsequent H-metasomatism (argillization) was relatively ineffective in altering the K-feldspar and residual anorthoclase to clay minerals.

A thin bed of arkosic sediment extends from a depth of 170 feet to 177 feet. This rock was originally composed entirely of granodioritic debris. K-metasomatism converted some plagioclase to hydrothermal K-feldspar, but most of the plagioclase persisted until later when it was changed to clay minerals by H-metasomatism. It is possible, however, that some of the clay minerals, especially kaolinite, might have formed by weathering of plagioclase prior to hydrothermal alteration.

Granodiorite

Granodiorite extends from 177 feet to the bottom of the hole at 212 feet. Fresh granodiorite contains plagioclase, quartz, orthoclase, biotite, hornblende, and chlorite in order of decreasing abundance. K-metasomatism changed some of the plagioclase to hydrothermal K-feldspar in the samples from depths of 205 feet and 210 feet. But at 180 and 190 feet no hydrothermal K-feldspar was produced and, instead, most of the plagioclase was altered to clay minerals, probably during later argillization. As mentioned in the preceding paragraph, the kaolinite may have formed by weathering prior to hydrothermal alteration.

Clay mineralogy

The clay minerals in these rocks deserve special mention because they are apparently related to differences in the alteration process.

Kaolinite, montmorillonite, and mixed-layer illite-montmorillonite are the common clay minerals in GS–6. The kaolinite is well crystallized except in core samples from above a depth of 155 feet, where it is disordered. The montmorillonite gives a 12.4A basal X-ray spacing which probably indicates natural saturation of the clay with sodium and potassium ions. When exposed to ethylene glycol vapor the montmorillonite expands to 17A in a normal manner. The mixed-layer illite-montmorillonite in GS–6 is present as two varieties. A regular mixed-layer illite-montmorillonite is present only in the granodiorite, whereas a randomly interlayered illite-montmorillonite is restricted to other rock types.

In the regular mixed-layer clay, the illite and montmorillonite layers are inferred to be present in equal proportions, and the *d*-spacing and intensity data are similar to those of the mineral allevardite (Brindley, 1956). In particular, the large increase in intensity of the 003 and 004 peaks after saturation with ethylene glycol is similar to that reported for allevardite (fig. 3*A*, *B*, *C*). Unlike allevardite, however, odd-order reflections cannot be detected after heating for 1 hour at 550°C, probably because of the small amount of clay contained in the samples (fig. 2). The *d*-spacings obtained from air-dried, glycolated, and heat-treated samples of this clay from depths of 180, 190, and 205 feet are consistent with an interpretation of equal amounts of 10A illite and 12.4A montmorillonite regularly interleaved. With the limited data available, it is best to refer to this mineral by the general name, regular mixed-layer illite-montmorillonite, rather than using the special name "allevardite".

In GS–6, random mixed-layer illite-montmorillonite is commonly found in hydrothermally altered rocks other than granodiorite (fig. 3*D*, *E*, *F*). This mineral is similar to that reported from granodiorite in drill holes GS–3 and GS–4 (Schoen and White, 1965). Excellent agreement in the proportions of component layers is generally obtained by assuming a 10A illite and a 12.4A montmorillonite that expands to 17.0A on glycolation. This clay mineral is somewhat similar to a random illite-montmorillonite interstratification reported by MacEwan (1956), especially in having a reflection at about 30A without integral suborder reflections (fig. 3*E*). According to Weaver (1956, p. 217) and MacEwan (1956, p. 167), this is due to some statistical regularity within a long sequence of layers. At present, we can offer no explanation for restriction of the more ordered mixed-layer clay to the granodiorite in GS–6.

Other drill holes

Comparison of the mineralogy of drill hole GS–6 with the six other drill holes already described in detail (Sigvaldason and White, 1961, 1962; Schoen and White, 1965), indicates generally similar alteration patterns for the same rock types.

As might be expected, GS–2, located only 1,500 feet northeast of GS–6 on the High Terrace (fig. 1), bears close resemblance mineralogically to GS–6, especially in regard to abundant hydrothermal K-feldspar in the upper part of the hole. GS–2 is 398 feet deep with maximum temperatures and chloride concentrations of 154°C and 464 ppm, respectively, indicating greater present-day hydrothermal activity than in GS–6. GS–2 contains some unreplaced volcanic plagioclase in the upper 200 feet, implying that the intensity of K-metasomatism was somewhat less than in GS–6, where all volcanic plagioclase was replaced. The deeper parts of drill hole GS–2 contain corrensite and chlorite (Sigvaldason and White, 1961, p. D120) that are either absent or very rare in GS–6. In GS–2, hydrothermal K-feldspar decreased with depth below 200 feet, and mixed-layer illite-montmorillonite increased. GS–6 is too shallow to evaluate these possibilities.

The strong hypogene H-metasomatism associated with fractures in GS–3 and GS–4 (Schoen and White, 1965) that produces a rock composed entirely of illite, quartz, and pyrite, is not evident in GS–6. Apparently the K-metasomatism that affected the rocks in GS–6 was characterized by K^{+1}/H^{+1} ratios that exceeded the stability limit of illite (Hemley, 1959, p. 246). In addition, silicification is unimportant in GS–6 because the minerals produced by K-metasomatism contain as much or more silica than the minerals they replace.

The common occurrence of an easily alterable mineral like celadonite above the water table indicates that the rocks in GS–6 have not been subjected to the intense sulfuric acid leaching noted in GS–7 (Sigvaldason and White, 1962) as well as near the surface in GS–3 and GS–4 (Schoen and White, 1965). This kind of alteration is caused by hydrogen sulfide gas escaping upward from a subsurface body of thermal water, oxidizing near the ground surface, and dissolving in water from precipitation or from condensing steam. The acid then percolates back down to the water table, reacts with unstable minerals on its way, and produces opaline residues. This type of intense leaching is rare in GS–6, occuring only in the upper part of the Pre-Lake Lahontan alluvium.

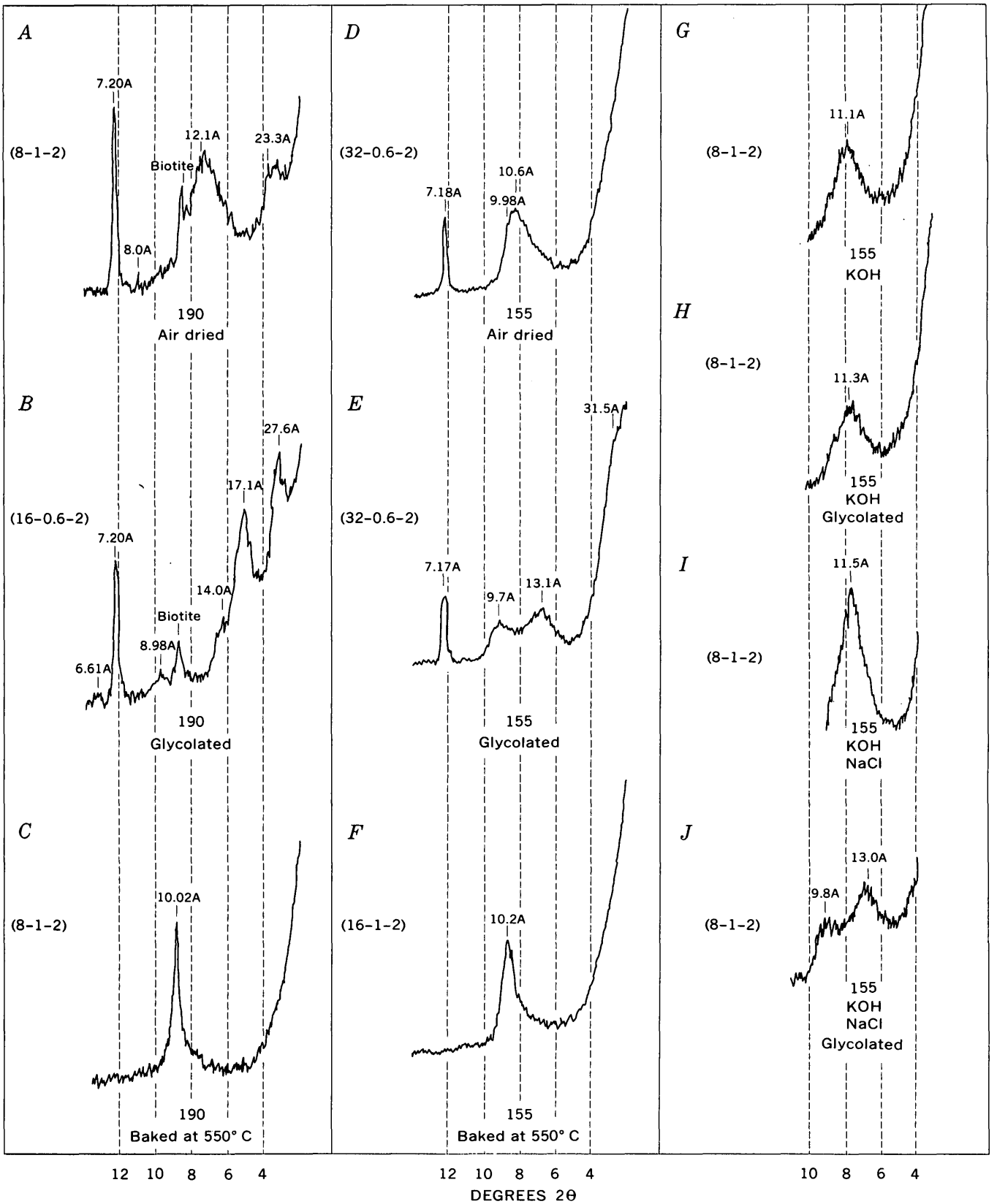

FIGURE 3.—X-ray diffractograms of representative clay-mineral fractions, drill hole GS–6. *A–C*, sample collected at 190 feet, *D–J*, sample collected at 155 feet. The nature of the treatment each sample was given prior to X-ray analysis is listed below each diffractogram. The numbers in parentheses show the scale factor, multiplier, and time constant, respectively, used during the recording of the X-ray diffractogram.

GEOCHEMISTRY

The general patterns of mineral distribution shown in figure 2 can be correlated with the kind and sequence of alteration reactions that occurred in the rocks.

K-metasomatism

The distribution of hydrothermal K-feldspar is primarily related to the original abundance of minerals most sensitive to K-metasomatism. Volcanic plagioclase is the feldspar most susceptible to replacement by K-feldspar during K-metasomatism, followed by plutonic calcic plagioclase, sodic plagioclase, volcanic alkali feldspars (anorthoclase and sanidine), and finally orthoclase, which is inert during K-metasomatism.

Olivine, hornblende, and pyroxene were destroyed during the early stages of the K-metasomatism, and the iron and magnesium liberated were used in forming celadonite. Therefore, the original distribution of celadonite and hydrothermal K-feldspar was somewhat similar. Later alteration has tended to argillize most of the celadonite, which may account for its apparent absence below a depth of 155 feet (fig. 2). Small amounts of celadonite, however, are recognizable in thin sections of most samples to the bottom of the hole. Celadonite is rare or absent in all other drill core from Steamboat Springs, and the abundance of celadonite in GS–6 is probably related to the high initial abundance of iron and magnesium in the rocks.

Biotite was converted to a bleached mineral pseudomorphic after the original biotite, during K-metasomatism, and exhibits a broadened and reduced 10A X-ray periodicity that does not expand with ethylene glycol. This bleached biotite is more resistant to H-metasomatism than some plutonic plagioclase, as evidenced by its presence in the highly argillized upper parts of the granodiorite.

H-metasomatism

The experimental work of Hemley (1959) indicates that the clay minerals K-mica (illite) and kaolinite precipitate from solution at moderate to low K^{+1}/H^{+1} ratios, respectively, and that K-feldspar precipitates at high K^{+1}/H^{+1} ratios. We conclude from this that the coexisting clay minerals and hydrothermal K-feldspar in GS–6 formed at different times and from different solutions. Because clay minerals form at the expense of feldspars in fluids with relatively low ratios of other cations to hydrogen ions (Hemley and Jones, 1964), the term H-metasomatism has been used in this report to describe this argillization.

Although K-feldspar can persist metastably in nonequilibrium environments, clay minerals are characterized by relatively rapid changes in response to changing environments. Environmental sensitivity of the random mixed-layer illite-montmorillonite of a sample from 155 feet in GS–6 is shown by X-ray diffractograms after soaking in 1*N* KOH at room temperature for 24 hours (fig. 3*G*); the same sample after glycolation (fig. 3*H*) showing the loss of expansibility compared to figure 3*E*; the same sample after soaking in 1*N* NaCl at room temperature for 43 hours (fig. 3*I*); and the same sample glycolated (fig. 3*J*) now apparently restored to the condition shown in figure 3*E*. If the clay minerals in GS–6 had formed prior to K-metasomatism, they should have been converted to K-mica or possibly even to K-feldspar. The fact that clays are now present in GS–6 indicates that they formed after K–metasomatism.

Kaolinite, however, may be an exception. Its constant iron- and magnesium-free composition and generally coarse grain size may make it less sensitive to alteration than other clay minerals. Thus, the abundant kaolinite that formed at the expense of plagioclase in the upper part of the granodiorite may be a result of ancient subaerial weathering. However, the presence of residual biotite in this zone seems inimical to this hypothesis. The origin of the unique mineral assemblage from a depth of 180 feet is still in doubt.

Genesis and distribution of clays

The three clay minerals in GS–6 (mixed-layer illite-montmorillonite, montmorillonite, and kaolinite) probably formed in response to decreasing K^{+1}/H^{+1} ratios and decreasing temperatures in the aqueous environment. Both variables favor the formation of montmorillonite from mixed-layer illite-montmorillonite and kaolinite from montmorillonite. This is in accord with Hemley's experimental work (Hemley and Jones, 1964) as well as the field observations of Altschuler and others (1963).

Several factors controlled the abundance and distribution of clay minerals in GS–6. Most important was the saturation of the rock with water of low cation/H^{+1} ratio. A low ratio of other cations to H^{+1} in the water is fundamental to the formation of clays (Hemley, 1959). Except for the sample from 111 feet, clay minerals are abundant only below a depth of about 150 feet, which is the level of the present-day water table (fig. 2). As an example, in the sample from 155 feet, which is below the water table, all plagioclase that was not previously altered to hydrothermal K-feldspar has been argillized. The sample from 133 feet and above the water table still contains unreplaced plagioclase and little clay.

A second factor is the relative abundance of easily alterable minerals at the time H-metasomatism began.

This is well illustrated by comparing the sample from 160 feet (trachyte) with the sample from 171 feet (arkose). The volcanic plagioclase in the sample from 160 feet was previously replaced completely by hydrothermal K-feldspar, which remained metastable during subsequent argillization, whereas much of the plutonic plagioclase in the sample from 171 feet resisted K-feldspathization and was then still available for later argillization.

The anomaly of abundant kaolinite in the sample from 111 feet is, in part, related to the proximity of a fault zone (White and others, 1964, p. B17) that served as a channel for H-metasomatizing fluids.

SYNTHESIS

The alteration of the rocks cut by drill hole GS–6 was a complex process that left fragmentary evidence. The conclusions based on this evidence are necessarily tentative, but we believe these conclusions have the fewest inconsistencies.

Hydrothermal alteration probably began in the vicinity of GS–6 after deposition of the Pre-Lake Lahontan alluvium. Hot silica-laden water rose and discharged onto the land surface, forming opaline sinter deposits. At the same time that sinter was forming at the surface, K-metasomatism was probably taking place at depth.

The high ratios of K^{+1}/H^{+1} necessary to produce K-metasomatism by the water were probably achieved by two mechanisms that were active at this time As the hot water rose from depth, the decrease in confining pressure allowed boiling to occur, and volatiles such as CO_2 and H_2S were rapidly lost to a vapor phase. The loss of CO_2 caused a decrease in the H^{+1} activity and a consequent increase in the K^{+1}/H^{+1} ratio. Such a mechanism is probably responsible for restricting K-metasomatism to the upper part of the spring system. A contributory factor in causing high K^{+1}/H^{+1} ratios during the very early stages of activity may have been the freshness of the rock adjacent to deep channels in the spring system. The reaction of thermal water with fresh rock should have consumed more of the available H^{+1} while also assuring enough K^{+1} to yield fluids with higher K^{+1}/H^{+1} ratios than are now found in the thermal waters.

Many factors contributed toward ending K-metasomatism in the vicinity of GS–6. Among the more important are: (1) insulation of the deep channels by altered rock, resulting in thermal waters near the surface having compositions high in H^{+1}; (2) lowering of the water table below the land surface, which greatly reduced the throughflow of mineralized thermal water and allowed evolved H_2S to form sulfuric acid above the water table that subsequently drained downward to be incorporated in part by the water circulating at depth; and (3) sealing of the deep channels by deposition of minerals resulting in further decreases in the supply of thermal water. Both decreasing K^{+1}/H^{+1} ratios and decreasing temperatures favored the formation of clay minerals from the readily alterable minerals remaining in the rocks. This argillization still may be going on in the vicinity of drill hole GS–6.

REFERENCES

Altschuler, Z. S., Dwornik, E. J., and Kramer, Henry, 1963, Transformation of montmorillonite to kaolinite during weathering: Science, v. 141, p. 148–152.

Brindley, G. W., 1956, Allevardite, a swelling double-layer mica mineral: Am. Mineralogist, v. 41, p. 91–103.

Hemley, J. J., 1959, Some mineralogical equilibria in the system K_2O—Al_2O_3—SiO_2—H_2O: Am. Jour. Sci., v. 257, p. 241–270.

Hemley, J. J., and Jones, W. R., 1964, Chemical aspects of hydrothermal alteration with emphasis on hydrogen metasomatism: Econ. Geology, v. 59, p. 538–569.

MacEwan, D. M. C., 1956, A study of an interstratified illite-montmorillonite clay from Worcestershire, England: Clays and Clay Minerals, Proc. 4th Natl. Conf., NAS–NRC pub. 456, p. 166–172.

Schoen, Robert, and White, D. E., 1965, Hydrothermal alteration in GS–3 and GS–4 drill holes, Main Terrace, Steamboat Springs, Nevada: Econ. Geology, v. 60, p. 1411–1421.

Sigvaldason, G. E., and White, D. E., 1961, Hydrothermal alteration of rocks in two drill holes at Steamboat Springs, Washoe County, Nevada: Art. 331 *in* U.S. Geol. Survey Prof. Paper 424–D, p. D116–D122.

——— 1962, Hydrothermal alteration in drill holes GS–5 and GS–7, Steamboat Springs, Nevada: Art. 153 *in* U.S. Geol. Survey Prof. Paper 450–D, p. D113–D117.

Thompson, G. A. and White, D. E., 1964, Regional geology of the Steamboat Springs Area, Washoe County, Nevada: U.S. Geol. Survey Prof. Paper 458–A, p. A1–A52.

Weaver, C. E., 1956, The distribution and identification of mixed-layer clay in sedimentary rocks: Am. Mineralogist, v. 41, p. 202–221.

White, D. E., Brannock, W. W., and Murata, K. J., 1956, Silica in hot-spring waters: Geochim. et Cosmochim. Acta, v. 10, p. 27–59.

White, D. E., Thompson, G. A., and Sandberg, C. H., 1964, Rocks, structure, and geologic history of the Steamboat Springs thermal area, Washoe County, Nevada: U.S. Geol. Survey Prof. Paper 458–B, p. B1–B63.

WATER AND DEUTERIUM IN PUMICE FROM THE 1959–60 ERUPTION OF KILAUEA VOLCANO, HAWAII

By IRVING FRIEDMAN, Denver, Colo.

Abstract.—Water was extracted from samples of pumice collected during the 1959–60 summit and flank eruptions of Kilauea Volcano, Hawaii, and the amount of H_2O and the relative deuterium content were determined. Water content of the samples from the summit eruption of Kilauea Iki ranged from 0.064 to 0.099 percent, by weight, and showed an inverse relation to relative deuterium content, which ranged from −5.5 to −7.9 percent relative to that of SMOW (standard mean ocean water). The samples collected from the Kapoho flank eruption contained 0.086 to 0.104 percent H_2O, and showed a wide range in deuterium content, from −5.7 to −9.1 percent relative to that of SMOW. These data are discussed in terms of the changing chemistry of the lavas.

The origin of water in rhyolitic glass has been investigated (Friedman and Smith, 1958) using the abundance of deuterium in water dissolved in the glass as a clue to the origin of such water. Rhyolitic glass was used because of its common occurrence and because it remains relatively unaltered for long periods of time. Recently, K. J. Murata, of the U.S. Geological Survey, made available for study a suite of basaltic pumice and lava samples from the 1959–60 eruption of Kilauea that permits a similar investigation to be made of the origin of water in basic rocks. Acknowledgement is made to Mr. Joseph Harris and to Miss Betsy Levin for their aid in some of the experimental work.

The 1959 summit eruption of Kilauea began on November 19, 1959, at Kilauea Iki (fig. 1) and persisted until November 21, when the level of the lava reached the level of the eruptive vent. During the next 4 weeks, 16 additional eruptive events occurred. The last eruptive phase ended on December 20, 1959.

The next outbreak of activity occurred on January 13, 1960, when fountaining began near sea level at Kapoho on the east rift zone of Kilauea. This activity continued until February 19, 1960, when the 1959–60 eruption ended.

ANALYTICAL METHODS

The samples analyzed were coarsely crushed in a diamond mortar, and about 3–5 grams of each sample was immediately weighed into a previously outgassed platinum crucible. The covered crucible was placed in a Vycor tube and connected to a vacuum system. The sample was heated in vacuum to 110°C for 2–12 hours to remove adsorbed water, which was pumped away. It was then slowly heated by means of an induction heater to 1,400°–1,600°C and allowed to remain at that temperature for at least 15 minutes. The evolved water was collected by freezing at liquid-nitrogen temperature. After a check was made for noncondensable gas, the ice was allowed to warm, and the water vapor was reacted with uranium metal at 700°C. The amount of hydrogen gas formed by this reaction was measured volumetrically and provided a quantitative measurement of the amount of water collected from the melted volcanic glass. This measurement is accurate to ±5 percent of the amount of water present. The hydrogen gas was then transferred to a specially constructed mass spectrometer, and the ratio of deuterium to hydrogen in the gas was compared to the ratio of deuterium to hydrogen in a standard sample. Differences in the ratios, between the sample and the standard, of as little as 0.1 percent of the ratio in the standard can be measured. All the deuterium results in this paper are given in relation to SMOW (standard mean ocean water), which has an isotopic composition close to that of average ocean water. Previous results (Friedman and Smith, 1958) were given in relation to a standard Lake Michigan water which has 4.2 percent less deuterium than does SMOW. The technique of water and deuterium determination is described in greater detail in Friedman and Smith (1958).

U.S. GEOL. SURVEY PROF. PAPER 575-B, PAGES B120-B127

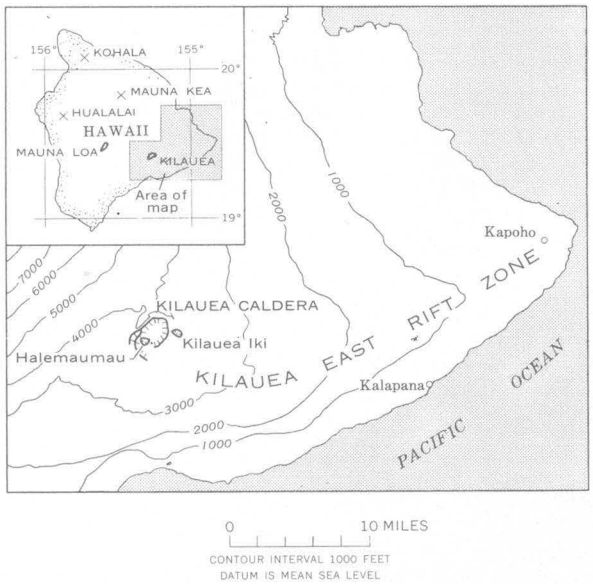

FIGURE 1.—Index map of eastern Hawaii, showing the summit region and east rift of Kilauea Volcano.

All samples were analyzed in duplicate. If satisfactory checks were not obtained on the duplicates, additional pairs were analyzed. Sample selection proved to be very critical. The first group of analyses was made on samples of finely vesicular pumice of density ≈ 0.3 grams/cubic centimeter that contain few crystals, as determined when the crushed material was immersed in oil and examined with the polarizing microscope. The discussion in this paper is limited to these samples. Samples of coarsely vesicular pumice and of crystallized lavas were also analyzed; however, the results obtained vary widely from one replicate analysis to another, and no correlations of any kind can be made on these samples. During the eruption of these materials, water was lost from the large open vesicles. In addition, various amounts of water also were lost during the partial or total crystallization of the lava as it cooled.

Water extracted from the finely vesicular glassy pumice probably represents water present in the magma just prior to eruption. During eruption, the pressure on the magma was suddenly lowered, and the water that was dissolved in the magma came out of solution in the form of fine bubbles. The large increase in volume of the magma due to this vesiculation undoubtedly aided the ejection of material from the vent. The pumice so ejected was rapidly chilled, freezing in the vesicular structure of largely unconnected bubbles. Water vapor caught in the bubbles rapidly diffused into the cooling lava and was thus trapped. Its cellular nature allowed pumice from the vents at Kapoho to float long distances in the sea, some of it eventually reaching the island of Kauai, about 350 miles away.

Errors due to the uptake of additional water after the samples were erupted were minimized by the (1) protection afforded by a skin of nonvesicular lava on the surface of the pumice lumps, (2) rapid collection of the material shortly after eruption, and (3) selection of large pieces of pumice for analysis. Again it must be emphasized that the relationships to be discussed hold only for these selected pumice samples. Figure 2 shows photographs of this finely vesicular pumice.

RESULTS

Content of water, deuterium, and selected constituents in the glass

Table 1 gives analyses for water and selected constituents from the glass, in weight percent, and the

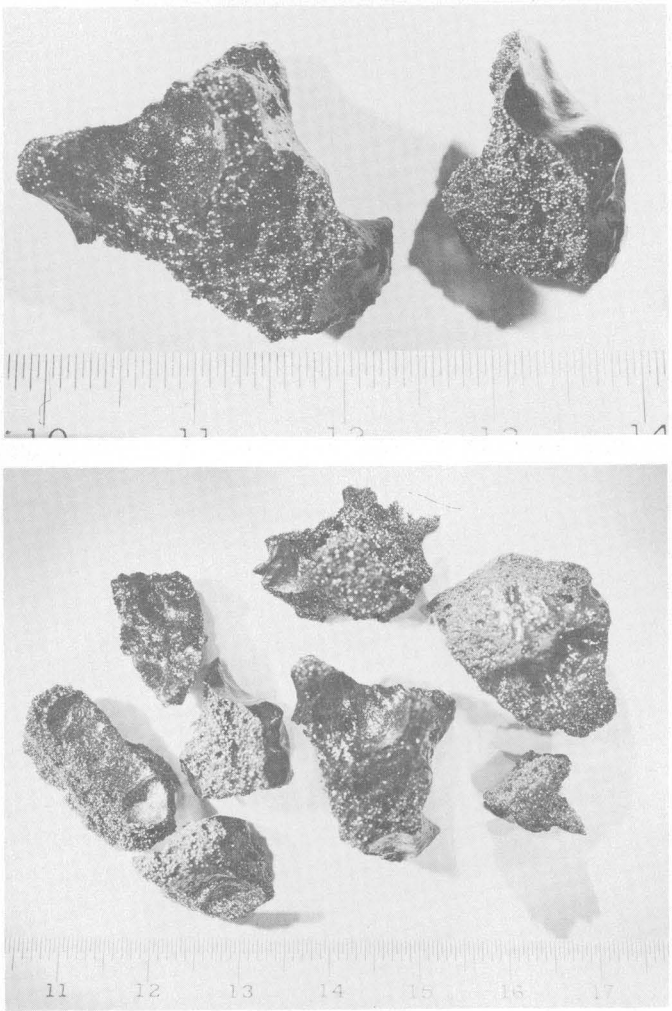

FIGURE 2.—Pumice fragments of the type used in the study described in this paper. Note finely vesicular nature of the pumice, and outer skin that acted as a shield to inhibit secondary exchange of water with the atmospbere. Scale is in centimeters.

TABLE 1.—*Content of selected constituents and water, and relative deuterium concentration in the water, in glass erupted from Kilauea Volcano*

Lab. No.	Field No.	Date and time of eruption	Selected constituents and water (weight percent)				D/H [2] (percent)
			SiO_2 [1]	MgO [1]	K_2O [1]	H_2O	
KILAUEA IKI (SUMMIT ERUPTION) 1954							
First phase							
S-4	3125-9	Nov. 17, 1500	49.0	11.5	0.47	0.099	−7.9
S-5	3125-3	Nov. 18, 1700	46.7	19.5	.35	.064	−6.6
IK-3	3125-10	Nov. 19, 0800	47.6	[3] 16.0	(.42)	.073	−7.0
S-7	3134-6	Nov. 20, 0700	48.2	13.7	.45	.084	−7.5
Later phases							
S-3	3125-12	Nov. 29, 2100	49.4	8.9	0.54	0.090	−7.5
S-19	3134-1	Dec. 11, 0600	47.3	16.6	.41	.075	−6.6
S-21	3134-2	Dec. 14, 1400	46.7	19.2	.41	.071	−7.2
S-24	3125-4	Dec. 19, 0615	47.0	18.2	.38	.068	−6.9
KAPOHO (FLANK ERUPTION) 1960							
P-2	3134-8	Jan. 15, 1730	50.6	[3] 6.5	[3] 0.65	0.098	−9.1
F-3	3125-5	Jan. 17, 1900	50.6	6.4	.65	.095	−8.3
F-7	3134-11	Jan. 26, 1900	50.4	7.0	.62	.086	−5.7
F-12	3134-13	Feb. 2, 0800	49.3	10.6	.54	.090	−7.6
F-13	3134-14	Feb. 4, 1130	48.9	12.1	.50	.090	−7.7
F-17	3125-6	Feb. 13, 1900	48.8	13.1	.49	.087	−6.0
F-18	3134-15	Feb. 16, 2030	49.3	11.1	.51	.104	−6.4
F-19	3125-7	Feb. 18, 1630	48.9	12.5	.48	.101	−7.5

[1] Analyses from Murata and Richter (1966).
[2] Relative deuterium concentration in the water extracted from the glass as compared with the concentration of deuterium in SMOW, in percent.
[3] Composition obtained by interpolation (on the basis of the SiO_2 percentage) on the variation diagram given by Murata and Richter (1966).

relative deuterium concentration in the water as compared with that in SMOW, in percent. The chemical analyses for the selected constituents were obtained on conventional finely ground samples of pumice, whereas the water determinations were made on coarsely crushed pieces of the same pumice. Owing to the porphyritic nature of many of the pumice samples, this difference in sample preparation introduces a slight uncertainty as to whether the analytical data for the selected constituents apply exactly for the portions used in determining water. However, the relatively large number of pieces taken (3 to 5 grams) probably minimized this error, as is indicated by the satisfactory agreement obtained on duplicate analyses.

In figure 3, K_2O, H_2O, and relative deuterium content of pumice from the Kilauea Iki summit eruption and from the flank eruption at Kapoho are plotted in separate columns. Magnesia is plotted as the reference constituent along the abscissa, following the practice of Murata and Richter (1966), so that the variations of water and relative deuterium content can be readily correlated with the variations of all other constituents.

Kilauea Iki samples consist principally of varied amounts of olivine phenocrysts set in a frothy matrix of basaltic glass. The samples represent the first stage of differentiation of the primitive magma, in which the separation and settling of olivine phenocrysts lead to greater concentrations of olivine in the lower part and lesser concentrations in the upper part of the magma body. The primitive magma contains about 10 percent MgO, so samples with less MgO represent olivine-depleted residual magmas, whereas those with more MgO represent olivine-enriched accumulate magmas.

Constituents that are not incorporated in olivine, such as K_2O, Na_2O, TiO_2, and P_2O_5, occur in the melt (glass). In terms of bulk composition these constituents are concentrated in residual magmas and diluted, by olivine, in accumulate magmas. In a quantitative test of these relations, Murata and Richter (1966) show that the preceding 4 constituents uniformly are 1.418 times more concentrated (within the range of 1.411–1.421) in a Kilauea Iki pumice containing 8.0 percent MgO than in one containing 19.0 percent MgO. The inverse relationship between K_2O and MgO is illustrated in figure 3*C*, and this particular type of straight-line variation, due solely to variation in amount of olivine, has been called the "olivine-control line" by Powers (1955). Because H_2O is not incorporated in olivine, it too might be expected to manifest a similar olivine-control line.

The variation of the percentage of H_2O with that of MgO is shown on figure 3*B*. The dashed line indicates the variation to be expected solely on the basis of olivine control (1.42 times higher concentration of water at 8.0 percent MgO than at 19.0 percent MgO). The solid line represents the trend of all the points more closely, and it suggests an enrichment of water in olivine-depleted magmas over and above that due to olivine control. A line drawn through the points for samples S–4, S–7, IK–3, and S–5, from the first phase of the summit eruption, would indicate the excessive enrichment of water even more strongly. The first eruptive phase was not complicated by repeated eruption and withdrawal of magma characteristic of the later phases; thus samples from the first phase might be expected to preserve the H_2O-MgO relationship most faithfully. In a column of differentiated summit magma, the upper part, therefore, contains relatively more H_2O than K_2O, Na_2O, and other constituents that concentrate in residual magmas. Such a relationship agrees with Kennedy's hypothesis (1955) regarding the vertical distribution of H_2O in a magma body, but does not support a similar distribution for the alkalies.

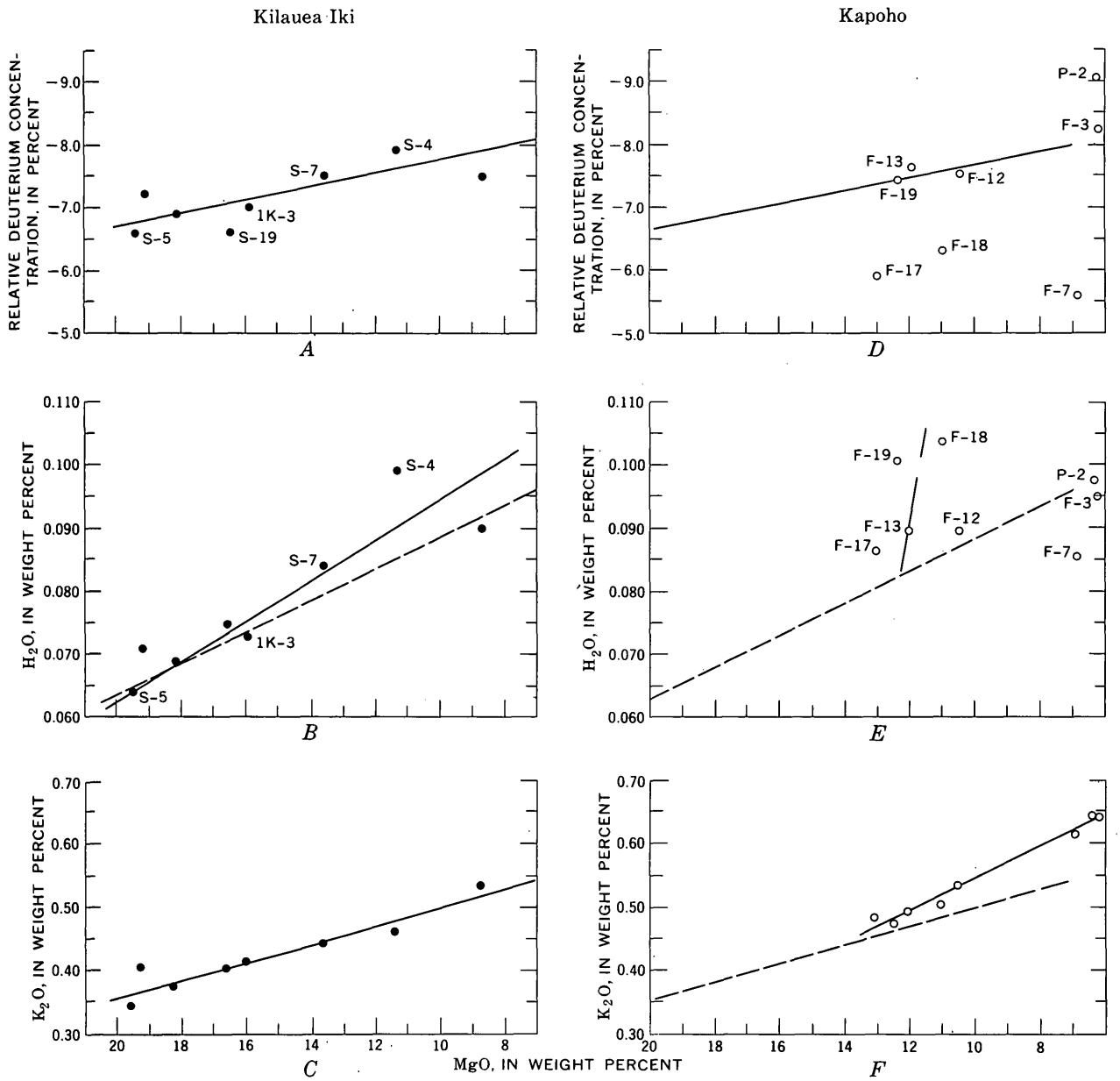

FIGURE 3.—Plots of K_2O, H_2O, and relative deuterium content versus MgO for pumice from the Kilauea Iki and Kapoho phases of the 1959–60 eruption of Kilauea. Numbers refer to samples listed in table 1.

Figure 3A shows the relationship between relative deuterium content of the H_2O and percentage of MgO. Except for the aberrancy of sample S–19, the results clearly indicate that the H_2O in low-lying accumulate magmas is richer in deuterium (has lower negative deuterium values) than that present in less-magnesian magmas of the upper part of the magma column. This relationship most likely depends somewhat on the previously mentioned nonuniform distribution of H_2O in the magma column, and, like the distribution of H_2O, is most strongly manifested by samples from the first eruptive phase.

The covariance of K_2O and MgO in samples from the flank eruption at Kapoho is shown on figure 3*F*, and is compared with the trend due to olivine control in Kilauea Iki samples. The Kapoho materials represent more advanced stages of basaltic differentiation than do those from Kilauea Iki, and their uniformly higher content of K_2O (relative to MgO) is due to the continued concentration of K_2O in residual magmas of the later differentiation stages.

The solid curve in figure 3*E* indicates the H_2O content to be expected in the 1960 Kapoho samples if H_2O were to concentrate in residual magmas at the same rate as K_2O. Only 3 samples (F–12, F–13, and F–17) out of the total of 8 have such a concentration of H_2O. Samples P–2, F–3, and F–7 represent old magma that was not expelled during the 1955 flank eruption; they are greatly deficient in H_2O, suggesting a loss of H_2O from the old magma during its storage within the volcano.

Samples F–12, F–13, and F–17 to F–19 are considered by Murata and Richter (1966) to represent newer magma that migrated, within a month or so prior to eruption, from the summit region to the eruption site at Kapoho. The high H_2O content of samples F–18 and F–19 shows that an excess enrichment (beyond the degree of enrichment of K_2O) occurred in the newer flank magma, just as it did in the summit magma of Kilauea Iki. But the excess enrichment in the Kapoho magma does not correlate with the MgO content. There is a suggestion that the later expelled portions of the magma (samples F–18 and F–19) were richer in H_2O than portions expelled earlier, but no reason for this can be advanced.

As shown on figure 3*D* samples of the old magma (P–2, F–3, and F–7) have a very wide range of deuterium content, entirely out of proportion to slight differences in chemical composition with respect to K_2O, MgO, and other less mobile constituents. Two factors might have promoted the development of the wide variation in deuterium in the old magma—its long period of storage within the volcano, and its substantial loss of H_2O (relative to K_2O).

The deuterium content of the newer Kapoho magma (samples F–12, F–13, and F–17 to F–19 of table 1) is not closely related to the H_2O content and, in general, is higher than would be expected. It is evident that the complicated deuterium and H_2O relationships in the old and new magmas of Kapoho cannot be explained satisfactorily at present. However, the independent migration of H_2O relative to the other constituents is clearly evident in the data on these magmas. The following discussion is limited to the relationships established for the primitive magma of Kilauea Iki, whose preeruption history was much shorter and simpler than that of derivative magmas erupted at Kapoho.

Figure 4 is a plot of the relative deuterium content versus H_2O content, in weight percent. It is obvious that, in general, the samples from the flank eruption at Kapoho have a higher H_2O content than do the samples from the summit eruption (Kilauea Iki) (table 1). Also, the samples from the flank eruption have a wider range of deuterium values than the Kilauea Iki summit samples. The summit samples, and to a small extent the flank samples, show an inverse relationship between H_2O content and deuterium content of the H_2O, and the samples with a higher H_2O content contain less deuterium (higher negative deuterium values). These basalt glasses are all enriched in deuterium as compared with rhyolitic glasses. The rhyolitic glasses range in relative deuterium concentration from −9.6 to −17 percent compared with −5.7 to −9.1 percent for the basalt glasses (table 1).

Although there is evidence that sea water was in contact with the molten magma at the beginning of the flank eruption, the H_2O from the glasses of the flank eruption (Kopoho) is no closer in hydrogen isotopic composition to sea water than are the glasses from the summit eruption of Kilauea Iki. If sea water is an

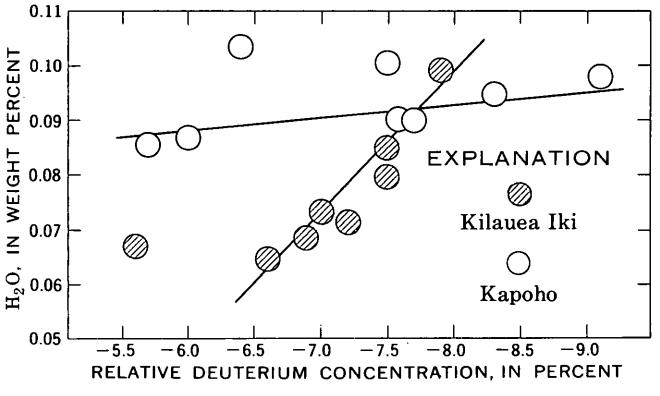

FIGURE 4.—Relative deuterium concentration versus H_2O content in pumice from the Kilauea Iki and Kapoho phases of the 1959–60 eruption of Kilauea.

important contaminant in these Hawaiian magmas, it must have been introduced at depth so that it has an equal influence on both the summit and flank magmas.

Kokubu and others (1961) analyzed two samples of Hawaiian lava and concluded that the H_2O in Hawaiian lava is not entirely a result of contamination, but is in part juvenile. The first sample, listed as an Hawaii volcanic bomb from the 1955 eruption of Kilauea, contained 0.09 percent H_2O having a D/H (relative deuterium concentration in H_2O as compared with that in SMOW) of −8.5 percent. The second, a "Hawaiian glassy spatter" from the 1954 Kilauea eruption, contained 0.09 percent H_2O with a D/H of −7.8 percent.

The data in their paper indicate a range in deuterium content of 3.5 percent, the most concentrated sample being 5.7 percent less concentrated than present-day sea water. Until the effects of fractionation processes on the isotopic composition of H_2O in magmas are better understood, conclusions, such as those made by Kokubu and others seem premature.

Reasons for variation in content of H_2O, selected constituents, and deuterium

The percentage of H_2O, SiO_2, and K_2O, the relative percentage of D/H, and the accumulated amount of lava extruded from Kilauea Iki are all plotted on figure 5 as a function of time for the summit eruption.

The changes in H_2O, SiO_2, and K_2O content of the lavas can be explained if olivine formed near the cooler top of a vertical magma chamber and settled part of the way down the column prior to eruption. However, the mechanism of sinking olivine cannot account for the change in the deuterium content of the H_2O in the lavas.

The variations in deuterium content, which in the samples from the summit correlate with the H_2O, SiO_2, and K_2O contents, may be explained in several ways:

1. Variation in deuterium content is an intrinsic property of the chemical composition or temperature of the magma. This assumes that the bonding of the H_2O to the silicate was a process in which there was an isotope effect, and that this isotopic fractionation of the hydrogen was dependent upon temperature and the structure of the melt. The structure of the melt in turn would depend upon the chemistry of the melt and therefore on its composition.

The foregoing could explain the relations found during the summit eruption, but it does not explain why the flank eruption does not give similar relationships between the deuterium and the K_2O and SiO_2.

2. Another explanation, closely related to the first, is that there is a fractionation of hydrogen isotopes when water is bound to the melt, but this fractionation

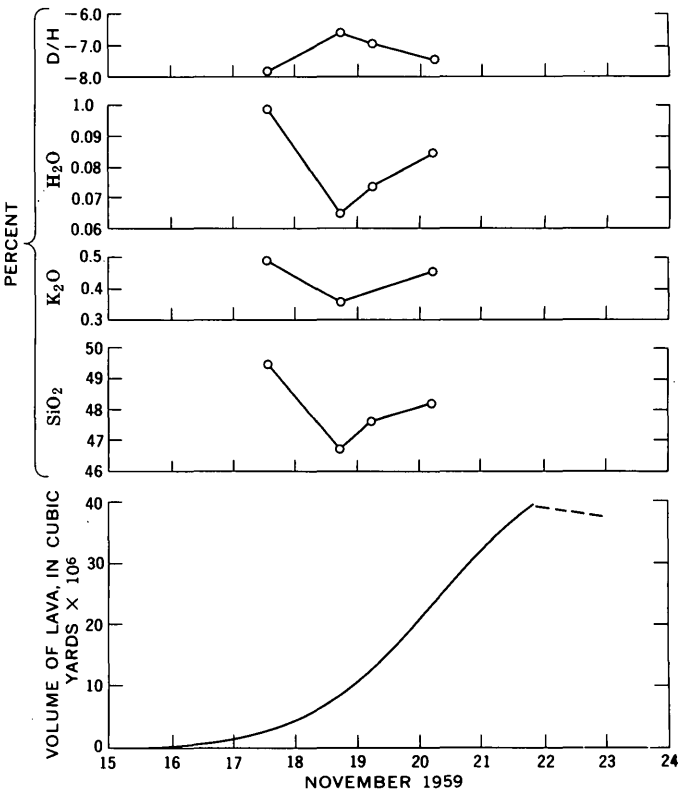

FIGURE 5.—Relative deuterium concentration (D/H); content of H_2O, K_2O, and SiO_2; and accumulated amount of lava extruded from Kilauea Iki, as a function of time for the summit eruption.

is relatively independent of the melt composition. If we then assume that the magma loses H_2O, and that it loses "light" H_2O (H_2O enriched in the light hydrogen isotope) preferentially, the H_2O-versus-deuterium relation can be satisfied. Again, this cannot explain the results of the flank eruption.

3. Explanations based on differential solubility of H_2O in melts of different composition will not explain the data from the flank eruption. In fact any explanation based solely on the intrinsic properties of the magma will fail to explain all the data. Clearly then, we must look to the mechanics of the eruption for at least part of the explanation.

Murata and Richter (1966) are of the opinion that the changes in the major chemistry of the lavas during the first phase of the summit eruption can be caused by (1) settling of olivine in a primary magma chamber, at a depth of perhaps 5 kilometers from the summit, and then (2) tapping of the top of the chamber. During the eruption there will be mixing of the settled magma with primitive magma rising from a depth of 20–30 km. The reversal in the trend of percentage of SiO_2 and

percentage of K_2O that occurred on November 18–19, 1959, might be due to uneven mixing or to the emptying of a reservoir of olivine-rich magma. The first phase of the summit eruption would consist of initially tapping the top of a magma chamber depleted in olivine by crystal settling, with or without primitive magma. This would be followed by tapping a mixture of primitive magma plus an olivine-rich magma containing the olivine that settled from above, with progressively more of the olivine-rich magma, until November 18–19. After that time, the amounts of admixed olivine-rich magma would decrease.

Probably a temperature gradient will be established in the primary magma chamber. The existence of this chamber is based on tilt data that indicate a swelling at about 5 km below the summit months before the summit eruption. If the rate of diffusion of H_2O in the magma is greater than convective mixing of the magma, a deuterium gradient might also be established, resulting in deuterium concentrating in the lower region, which will be the region of the high olivine content and therefore of low K_2O, SiO_2, and H_2O content.

Would storage of the magma, in a magma chamber of large vertical extent having a thermal gradient, concentrate the deuterium at the hotter, bottom end of the chamber? Two processes could possibly act to yield such an isotopic fractionation.

The first process is the fractionation that would occur upon diffusion of H_2O. During such diffusion, the lighter isotope would move more rapidly than the heavier. If H_2O had been diffusing from the hot part of the magma into the cooler, as suggested by Kennedy (1955), a concentration gradient of deuterium would result, the deuterium being more concentrated in the hotter residue and depleted in the H_2O-richer, cooler top.

The second process is thermal diffusion in a column in which separation of isotopes can take place. Unfortunately the process is very complicated, and even the direction of separation cannot be estimated.

The deuterium content obtained for samples from the flank eruption shows as wide a variation as for samples from the summit material (table 1). However, the deuterium content correlates poorly with H_2O, SiO_2, and K_2O content. The deuterium variations can be due to the cause suggested for the variations in the summit material—diffusion of H_2O. This would also explain the slight change of H_2O content with deuterium observed in the samples of the flank eruption.

The flank magma may have been emplaced as early as 1924. Some of this magma was erupted in 1955. The 1960 lava, then, can represent a sample of magma that has had a long time to differentiate. In addition, it has had to move laterally about 40 km from its probable feeder. The K_2O and H_2O contents of the most primitive 1960 flank material show it to be already highly differentiated compared with the summit lava. However, in contrast with the summit samples, we do not get a total sample of the crystals that have settled from this magma, owing to the fact that they have had time to settle out. Therefore, the K_2O, SiO_2, and H_2O contents are not as low in the flank samples as in the summit samples (see table 1).

The flank magma has a much more complicated history than the summit magma. The long storage time in the rift zone, the long lateral movement within the rift zone, the great size and probable complex shape of the rift-zone storage chamber, and the possible complexity of various exits from the rift-zone chamber tapping different parts of the magma chamber are all factors complicating understanding of the flank lavas. Therefore, it is not surprising that the points representing the flank data show more scatter than do the summit points (figs. 3 and 5).

Other volatiles

The fluorine content of the pumices given by Murata and Richter (1966) ranges from 0.02 to 0.04 percent, a variation not considered significant in view of the precision of these analyses. The average fluorine content is 0.03±0.01 percent.

The CO_2 values in the glass are small; therefore the variations between samples are not considered significant, not only because of the analytical errors, but also because varied amounts of magmatic CO_2 will be retained by the different types of pumice in the vesicles. The average content of CO_2 can be taken as 0.01±0.01 percent.

The chlorine content of 0.02+0.1 percent appears to be reasonably constant from sample to sample. The low chloride would mean either little incorporation of sea water into the magma, or incorporation of sea water and loss of HCl from the magma due to the low solubility of HCl in the melt (Murata, 1966). Although chlorides are observed in fumerolic deposits, the small amount observed would provide an argument against a major amount of sea water having been incorporated in the magma.

REFERENCES

Friedman, Irving, 1953, Deuterium content of natural water and other substances: Geochim. et Cosmochim. Acta, v. 4, p. 89–103.

Friedman, Irving, and Smith, R. L., 1958, The deuterium content of water in some volcanic glasses: Geochim. et Cosmochim. Acta, v. 15, p. 218–228.

Kennedy, G. C., 1955, Some aspects of the role of water in rock melts, *in* Poldervaart, Arie, Crust of the earth—a symposium: Geol. Soc. America Spec. Paper 62, p. 489–504.

Kokubu, Nobuhide, Mayeda, T., and Urey, H. C., 1961, Deuterium content of minerals, rocks and liquid inclusions from rocks: Geochim. et Cosmochim. Acta, v. 21, p. 247–256.

Murata, K. J., 1966, An acid fumerolic gas from Kilauea Iki: U.S. Geol. Survey Prof. Paper 537–C, p. C1–C6.

Murata, K. J., and Richter, D. H., 1966, Chemistry of the lavas of the 1959–60 eruption of Kilauea Volcano, Hawaii: U.S. Geol. Survey Prof. Paper 537–A, p. A1–A26.

Powers, H. A., 1955, Composition and origin of basaltic magma of the Hawaiian Islands: Geochem. et Cosmochim. Acta, v. 7, nos. 1–2, p. 77–107.

FORMATION OF CRYSTALLINE HYDROUS ALUMINOSILICATES IN AQUEOUS SOLUTIONS AT ROOM TEMPERATURE

By W. L. POLZER, J. D. HEM, and H. J. GABE, Menlo Park, Calif.

Abstract.—The reaction solutions containing partly polymerized aluminum hydroxide with an initial aluminum concentration of 0.310×10^{-3} moles Al/liter (8.6 ppm), an initial ratio of $(OH)_{bound}/Al$ of 2.9, an initial ionic strength of 10×10^{-3}, and with different concentrations of dissolved silica were observed at room temperature by solution chemistry, X-ray diffraction, and electron-microscopy techniques. Initial concentrations of 0.00 and 3.16×10^{-5} moles SiO_2/liter resulted in the formation of gibbsite. A significant amount of tubular or lathlike "kaolin" was formed with an initial concentration of 30.0×10^{-5} moles SiO_2/liter. In an initial solution of 1.63×10^{-3} moles SiO_2/liter, the results indicated a predominantly amorphous aluminosilicate with an Al/SiO_2 ratio of 1. A few unidentified crystalline particles of hexagonal shape also were observed.

Aluminosilicate minerals are known to form in natural environments at low temperature. Little is known, however, about the processes involved in their formation. In recent years, many investigators have tried to synthesize silicate minerals at low temperatures in the laboratory. Siffert (1962), Hénin and Caillére (1963), and Gastuche (1964) have reviewed the literature with respect to research in this field and the current status of knowledge of the processes involved. The synthetic aluminosilicates which have been obtained commonly are mixtures of amorphous gels and crystalline material, with the yield of crystalline material being very poor at low temperature. Better yields of crystalline material are obtained at low pH (<3) and high temperature (175°C) (Gastuche, 1964). Most work on aluminosilicate mineral synthesis has been done at temperatures of 40°C to 60°C or higher, and using dialyzed gels or dispersed aluminum hydroxide to initiate the reactions. Siffert (1962) did, however, obtain a "protokaolin" at room temperature by mixing solutions of an aluminum oxalate complex $[Al(C_2O_4)_3]^{-3}$ and silicic acid.

J. D. Hem and C. E. Roberson, of the U.S. Geological Survey, have shed new light on the form and stability of aluminum hydroxide complexes in dilute solutions, and on the chemical mechanisms which produce the complexes, in a report now in preparation. These investigators have demonstrated that octahedra of aluminum six-coordinated with hydroxide polymerize by sharing edges. Upon aging of solutions in which the number of bound hydroxide ions per aluminum ion ranged from about 2.0 to nearly 3.0, the polymerization proceeded slowly to produce macromolecules, and finally very small crystals of gibbsite, $Al(OH)_3$.

This paper presents some preliminary results obtained from study of solutions of polymerizing aluminum hydroxide and silicic acid.

ANALYTICAL TECHNIQUES

Four solutions were used; all contained 0.01 mole per liter of perchlorate ions, and a sufficient concentration of sodium ions to maintain an ionic balance in the presence of small concentrations ($\approx10^{-3}$ or 10^{-4}) of Al^{+3}, H^{+1}, or OH^{-1}. The perchlorate ion has not been shown to participate in complexing reactions of aluminum and silica (Sillén and Martell, 1964), but does provide a system having approximately constant ionic strength, and a concentration of solutes which is in the range common in natural weathering solutions.

The methods of preparing the aluminum-perchlorate solutions and initiating the polymerization process are described in detail in the forthcoming report by Hem and Roberson and will not be repeated here. For the work described below, solutions were prepared that contained 3.10×10^{-4} moles/liter of aluminum, with an average of 2.9 OH ions bound per aluminum ion, and a range in silicic acid concentration of 0.00 to 1.63×10^{-3} molal. Various amounts of sodium perchlorate were also added to these solutions to maintain a constant ionic strength (0.010 moles ClO_4^{-1}/liter).

The silicic acid solution was prepared by dissolving the appropriate weight of sodium silicate ($Na_2SiO_3\cdot9H_2O$) in distilled water. This solution was then passed

through hydrogen-saturated IR-120 cation-exchange resin. The solution was made up to the proper volume with the correct concentration of sodium perchlorate solution. The silica solution was prepared immediately before the mixing of the final solutions.

The silica and aluminum-perchlorate solutions were mixed by magnetic stirrers. The solutions were stored in a CO_2-free atmosphere at room temperature (22°C± 2°). Periodically, aliquots of these solutions were filtered through plastic-membrane filters having pores of 0.10μ. The filtrate was analyzed for aluminum and silica and the precipitate on the filter was examined by X-ray diffraction. pH measurements were made on aliquots of the original solution at the time of filtration. The aluminum and silica contents of the unfiltered solution also were determined.

An electron microscope was used to study the very small polymeric units more closely. Small aliquots of the unfiltered solutions were air dried on formvar film supported by grids. Carbon was evaporated onto these samples for a shadow effect.

A sufficient amount of precipitate was obtained only from solution 2D for direct analyses of aluminum and silica. Therefore, the composition of the precipitate from solutions 2B and 2C was estimated from the difference in concentrations of these substances in the solutions before and after filtration.

The ferron-orthophenanthroline method was used for determining aluminum and the molybdate blue method was used for determining silica (Rainwater and Thatcher, 1960), but both were modified to insure that the determination included polymerized or colloidal species. The solutions for the aluminum determination were digested on a steam bath for 6 hours with hydroxylamine at pH 1.5 before the other reagents were added. The solutions for silica determinations were heated on a steam bath with 2 ml of 0.5 percent NaOH, in platinum dishes, for 1 hour. They were then cooled, neutralized with hydrochloric acid, and the procedure completed in the regular manner.

The accuracy estimates for the determination of Al and SiO_2 are given in table 1.

TABLE 1.—*Accuracy of alumina and silica determinations*

Constituent	Accuracy of determination (in moles/liter)	Quantity analyses (in moles/liter)
Al	[1] 3.7×10^{-5}	30×10^{-5}
SiO_2	$\pm0.33\times10^{-5}$	3.3×10^{-5}
	$\pm3.4\times10^{-5}$	33×10^{-5}
	$\pm8.3\times10^{-5}$	[2] 170×10^{-5}

[1] 3.7×10^{-5} moles Al/liter equivalent to 1 ppm Al.
[2] 1.77×10^{-5} moles SiO_2/liter equivalent to 1 ppm SiO_2.

RESULTS

The results obtained from the four solutions, 2A, 2B, 2C, and 2D, are summarized in table 2. The pH of silica-free solution 2A decreased considerably with aging after 14 days. Smaller decreases occurred in the other silica-bearing solutions. Decreases in pH also accompanied the polymerization of aluminum hydroxide in the work described by Hem and Roberson.

Some decrease in the amount of aluminum or silica passing through the filters occurred with time. Most of the material, however, which could be removed by filtration had formed in less than 24 hours. The continuing change in pH suggests that some alteration or rearrangement of the precipitate was taking place throughout the 82 days of the experiment.

The apparent increase in dissolved aluminum, which occurred in filtered solution 2C between 1 day and 14 days is evidently related to a decrease in size of particles, as most of the aluminum could be separated from the solution by filtering through a filter with 0.01μ diameter pores (data for 82 days).

The difference between the concentration of aluminum is filtered and unfiltered aliquots, and the difference for similar data for silica, is the basis for calculating the mole ratio of aluminum for silica in precipitate. Both in solution 2C and in 2D these values show some scatter, but after 14 days all were near 1.0 with the exception of the one for 82-day aging. This represented a finer grained product which might have included some gibbsite.

Very little silica was lost from solution 2B by polymerization. Solutions 2C and 2D, however, lost substantial amounts. The best conditions in these experiments for the formation of aluminosilicates seem to be in solutions in which silica concentrations equal or exceed the aluminum concentrations.

The electron micrographs give definite indications of some crystalline products for all four solutions. In solutions 2A and 2B, however, the material has the hexagonal outline typical of gibbsite, whose presence also was indicated by X-ray diffraction. Figure 1 portrays material from solutions 2A and 2B, respectively. Silica was not significantly present in precipitates formed from either of these solutions.

X-ray diffraction patterns for the precipitate from solutions 2C and 2D after 14 days indicate the material was amorphous (table 2). These results, however, do not verify absence of crystalline material. The amount of material used for X-ray diffraction was small and the crystals may have been too small or too few in number to be detected. Electron micrographs give more information on the presence of crystalline material.

TABLE 2.—*Chemical, X-ray diffraction, and electron-microscopy data for the reaction of silica-aluminum hydroxide solutions at room temperature and low ionic strength*

Time (days)	pH				Aluminum (molality × 10^6)								Total SiO_2 (molality × 10^5)							
					Nonfiltered				Filtered [1]				Nonfiltered				Filtered [1]			
	2A	2B	2C	2D	2A	2B	2C	2D	2A	2B	2C	2D	2A	2B	2C	2D	2A	2B	2C	2d
0.02	5.49	5.43	5.12	4.94	31.0	31.0	31.0	31.0						3.16	33.1	163				
1	5.58	5.48	5.09	4.80	29.3	29.6	29.6	30.7	4.81	4.44	12.2	2.96		3.49	26.6	163		3.83	20.0	143
14	4.99	4.94	4.98	4.90	28.5	28.9	28.9	29.3	3.33	4.07	27.0	1.48		3.49	30.0	155		3.16	26.6	133
48																				
56																				
76	3.88	4.82	4.96	4.70	26.7	27.4	27.8	28.1	2.22	1.85	26.3	3.33		3.16	26.6	150			25.0	131
82			4.93				20.0				4.44				26.6				15.5	

Time (days)	Mole ratio Al/SiO_2 (in precipitate)								X-ray data				Electron-microscopy data			
	By difference				Wet chemical											
	2A	2B	2C	2D	2A	2B	2C	2D	2A	2B	2C	2D	2A	2B	2C	2D
0.02																
1			1.9	1.4					(2)	(2)	(2)	(2)				
14			1.2	1.0				1.1	(3)	(3)	(2)	(2)				
48													(3)			
56														(3)	(4)	(5)
76			1.0	0.9					(3)	(3)	(2)	(2)				
82			1.8								(2)					

[1] Filtration through 0.10μ filter, except for 82-day samples, which were filtered through 0.01μ filter.
[2] Amorphous.
[3] Gibbsite.
[4] Tubular kaolin and rounded crystals and gel.
[5] Gel and few crystals.

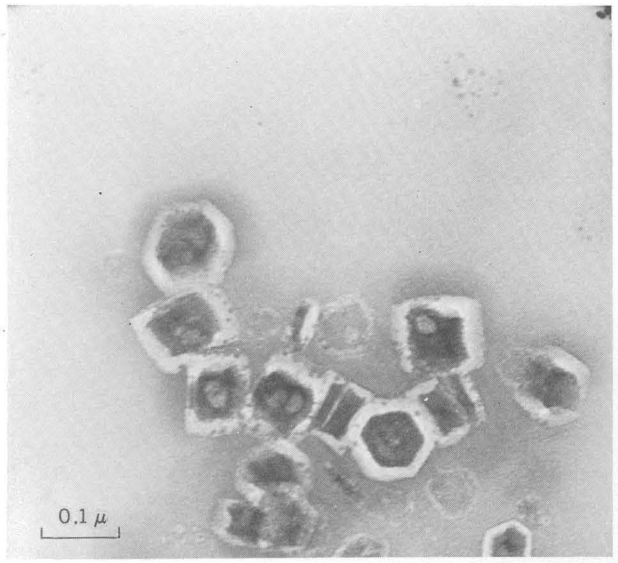

FIGURE 1.—Electron micrograph of evaporated solution 2A, gibbsite crystals. 1 cm=0.1μ.

Micrographs of solution 2C after 56 days are given in figure 2. These micrographs indicate relatively large amounts of tubular or possibly lathlike material having a crystalline appearance. Figure 2A indicates the presence of large particles which were always observed with a group of tabular or lathlike crystals. The relationship between the two morphologically distinct crystals, if any, is not known. It is also significant to note that for many of the smaller particles (fig. 2*B*, in particular), the pattern is one of a lighter colored material, surrounding a nucleus of darker material. This suggests that a crystalline material is formed initially and then, with time, an outward growth of material either of the same species or of another. Micrographs of solution 2D (fig. 3) show scattered particles having the appearance of hexagonal crystals. But, by and large, the material is of amorphous nature, possibly allophane.

Hénin and Caillére (1963) and Gastuche (1964) have concluded that one of the prerequisites for the formation of aluminosilicate minerals is the presence of a gibbsite or pre-gibbsite type structure. If this is true, one might interpret the dark nucleus as being gibbsite in nature and the lighter material being a growth of an aluminosilicate initiated by the gibbsite nucleus. Although not much significance can be placed in the mole ratio of Al/SiO_2 as calculated by difference (table 2), because of the large effect of analytical errors, the data do indicate a mole ratio of approximately unity for the tubular or lathlike material. The data for the 0.01μ or larger material suggest a higher ratio of Al/SiO_2. These relationships suggest that the small nucleus in the smaller particles may be gibbsite with the outer growth being an aluminosilicate, an assumption, however, that is not documented by the data now at hand.

The crystalline-appearing particles in solutions 2C and 2D have not been identified as yet by X-ray or electron diffraction. The tubular or lathlike material found in solution 2C has the morphological appearance of tubular "kaolin" as identified by Bates (1958). Tubular kaolin, however, cannot be identified as halloysite or kaolinite solely on the basis of its morphology (Hope and Kittrick, 1964).

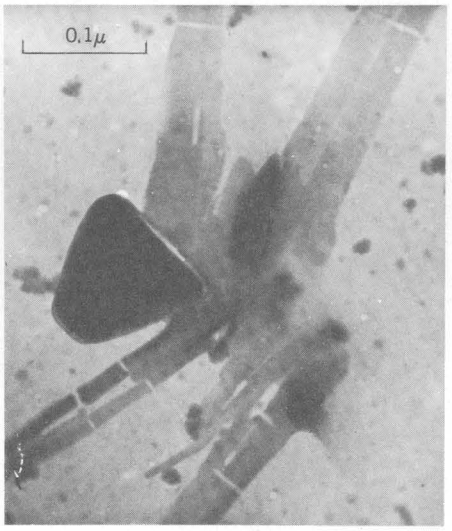

A

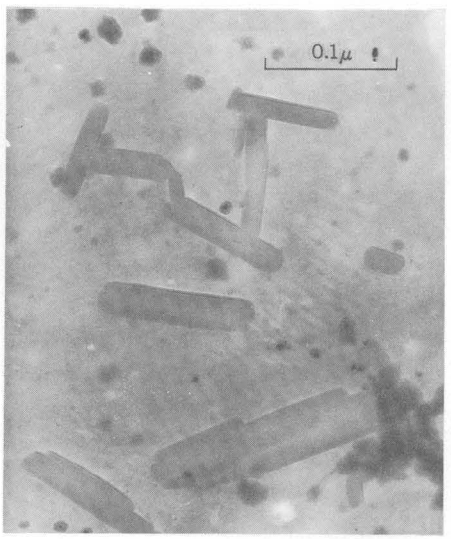

B

FIGURE 2.—Electron micrograph s of evaporated solution 2C. 1 cm=0.625μ. *A*, Tubular or lathlike "kaolin" and large nontubular crystal. *B*, Tubular or lathlike "kaolin" and smaller crystalline-type particles.

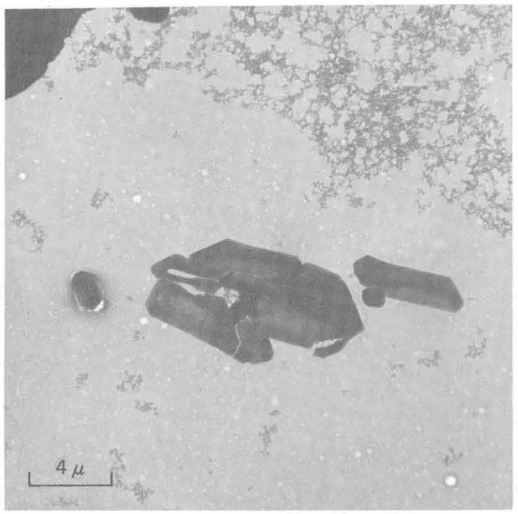

FIGURE 3.—Electron micrograph of evaporated solution 2D. Large hexagonal-type crystals and amorphous material. 1 cm=4μ.

CONCLUSIONS

The information obtained thus far suggests that a crystalline aluminosilicate resembling a kaolin-type mineral can be produced from dilute solutions of aluminum and silica at a temperature near 25°C. The molar ratio of aluminum to silica in this material is near 1 and remains so even when silica concentration in solution exceeds that of aluminum by factors of between 10 and 100.

REFERENCES

Bates, T. F., 1958, Selected electron micrographs of clays and other fine grained materials: Pennsylvania State Univ. Mineral Industries Expt. Sta. Circ. 51, 61 p.

Gastuche, M. C., 1964, The octahedral layer, *in* Clays and clay minerals, 12th Natl. Conf., Atlanta, Ga., 1963: Proc., New York, Macmillan Co., p. 471–493.

Hénin, S., and Caillére, S., 1963, Synthese des mineraux a basse temperature: essai de mise au point [Synthesis of minerals at low temperature: A review]: Clay Minerals Bull., v. 5, p. 265–271.

Hope, E. W., and Kittrick, J. H., 1964, Surface tension and the morphology of halloysite: Am. Mineralogist, v. 49, p. 859–966.

Rainwater, F. H., and Thatcher, L. L., 1960, Methods for collection and analysis of water samples: U.S. Geol. Survey Water-Supply Paper 1454, 301 p.

Siffert, Bernard, 1962, Quelques reactions de la silice en solution: La formation des argiles [Some reactions of silica in solution: The formation of argillites]: Memoires du Service de al carte Geologique d'Alsace et de Lorraine, no. 21, 86 p.

Sillén, L. G., and Martell, A. E., 1964, Stability constants of metal-ion complexes: London, The Chemical Society, Burlington House.

REFERENCE SAMPLE FOR DETERMINING THE ISOTOPIC COMPOSITION OF THORIUM IN CRUSTAL ROCKS

By J. N. ROSHOLT, JR., Z. E. PETERMAN, and A. J. BARTEL, Denver, Colo.

Abstract.—A natural-occurring reference sample has been obtained that is believed to be in radioactive equilibrium and to have a U/Th ratio similar to that of most crustal rocks. The reference sample is used to compare the Th^{230}/Th^{232} activity ratios determined in crustal rocks and to establish the condition of radioactive equilibrium of Th^{230} to U^{238} or Th^{230} to U^{234} in these rocks, on the basis of their Th^{230}/Th^{232} and U^{238}/Th^{232} content. The natural reference sample is a portion of a drill core from a depth of 7,300 feet, about 80 feet below the top of the Precambrian basement complex, in southwestern Saskatchewan, Canada. The rock, a porphyritic biotite granite, contains 24.1±0.2 ppm of uranium and 82.8±0.9 ppm of thorium.

In the study of geochemical processes involved in the migration of uranium and its isotopes (U^{234}, U^{235}, U^{238}) in the hydrologic cycle, the natural daughter-product tracers (Th^{230} as a tracer of U^{234} and Pa^{231} as a tracer of U^{235}) have proved quite useful. The amount of radioactive tracer in a rock sample as compared with the amount of radioactive parent isotope present can be determined most accurately by using direct measurements of isotopic ratios of individual elements. However, for each element, a reference sample known to be in radioactive equilibrium is required to relate the isotopic ratios of one element to another in a radioactive decay series.

A National Bureau of Standards reference sample, Republic of Congo pitchblende ore (BCP reference), has been used for several years (Rosholt and others, 1963) to determine the isotopic composition of uranium. Although the BCP reference is in radioactive equilibrium, it does not contain a sufficient amount of Th^{232} to permit its use as a suitable reference for determining the isotopic composition of thorium in crustal rocks. The desirable reference should have a thorium-to-uranium ratio of about 3 or 4; in addition, the U^{238}-U^{234}-Th^{230} and the U^{235}-Pa^{231} decay sequences should be in radioactive equilibrium.

After comparison of analyses of about 100 granite and volcanic rock samples, most of which do not meet the criteria of radioactive equilibrium, a porphyritic biotite granite (No. 3633) with a relatively high concentration of uranium and thorium was selected for the reference. The U^{238}-U^{234}-Th^{230} decay sequence is in equilibrium in the granite, and the Pa^{231} is presumed to be in equilibrium with U^{235}. The rock is one of the very few specimens available that meets the criteria for a good reference for thorium isotopes; thus, the significance and need for such a reference warrants a detailed description of the mineralogy and occurrence of the rock and the method of analysis used to determine its condition of equilibrium.

SAMPLE DESCRIPTION

The sample of biotite granite was obtained from a 3½-inch-diameter core of Precambrian basement from the Mobil Oil Woodley Sinclair Cantuar X–2–21 well in southwestern Saskatchewan, Canada. Precambrian basement was struck at 7,218 feet, and the sample was obtained from the 7,285–7,305-foot interval. The well was drilled on an ancient basement high, called the Swift Current nose, which was a positive feature in Middle Cambrian time (Sawatzky and others, 1960).

Composition

Chemical and modal analyses, and normative minerals in the sample are given in table 1. In hand specimen the rock is medium gray, porphyritic, and is characterized by milky-blue phenocrysts of quartz. Textually, the rock has a hypidiomorphic groundmass with a grain size averaging about 0.6 mm. The coarse constituents are euhedral to subhedral phenocrysts of feldspar, up to 15 mm in length, and anhedral ovoidal phenocrysts of quartz up to 10 mm in length; they make up about 35 percent of the rock. In thin section the blue quartz phenocrysts show marked undulatory extinction with some fracturing. Microcline is unaltered, locally poikilitic, and contains both vein and

TABLE 1.—*Composition of the granite reference sample (No. 3633)*

[Sample location: Legal subdivision 2, sec. 21, T. 16 N., R. 71 W. 3, Saskatchewan]

Chemical analysis [1] (weight percent)		Modal analysis (volume percent)		Mesonorm [2] (mole percent)	
SiO_2	71.96	Quartz	41	Q	29.98
Al_2O_3	12.73	Microcline	31	Or	29.48
Fe_2O_3	.53	Albite (An_7)	20	Ab	25.75
FeO	3.17	Biotite	7.7	An	5.15
MgO	.44	Epidote	.8	C	.14
CaO	1.37	Allanite	.6	Bi	7.87
Na_2O	2.80	Hornblende	.3	Ti	.84
K_2O	5.67	Magnetite	.3	Mt	.55
H_2O^+	.41	Zircon	Tr.	Ap	.13
H_2O^-	.02	Apatite	Tr.		
TiO_2	.40	Fluorite	Tr.		
P_2O_5	.07	Chlorite	Tr.		
MnO	.06	Sericite	Tr.		
CO_2	.01	Carbonate	Tr.		
Cl	.05				
F	.30				
Subtotal	99.99				
Less O	.14				
Total	99.85				

[1] Analyst: George O. Riddle, U.S. Geological Survey.
[2] Mesonorm calculations according to Barth (1959, 1962).

patch-type perthitic intergrowths. Plagioclase (An_7) is moderately altered to sericite. The mafic minerals —biotite, magnetite, epidote, allanite, and hornblende —commonly are clustered together. Some of the allanite has well-developed coronas of euhedral epidote.

Mineralogically the rock is a granite or quartz monzonite, depending on the classification used. The lack of agreement between the modal analysis and the normative minerals (table 1) is in part due to the porphyritic texture of the rock and the difficulty in obtaining a representative thin section. Probably for the essential minerals the norm is a more realistic estimate than the mode. The chemical composition of the rock is similar to the composition of Nockolds' (1954) average biotite granite, but the rock contains more FeO and slightly less SiO_2.

Regional geology

The Precambrian basement from which the sample was cored is part of the subsurface continuation of the Churchill geologic province of the Canadian Shield (Burwash and others, 1962), which was strongly affected by the Hudsonian orogeny 1.65 to 1.85 billion years ago. Microcline from the biotite granite was dated at 1.66±0.08 b.y. by the Rb-Sr method (Peterman and Hedge, 1964). An indication of a subsequent event is suggested by a K-Ar age of 1.20 b.y. on biotite from the same sample (Burwash and others, 1962). Similar discordant ages were obtained on a porphyritic rhyolite from an adjacent well. Hornblende from the rhyolite was dated at 1.49 b.y. (Burwash and others, 1962), whereas the total rock was dated by the Rb-Sr method at 1.71±0.19 b.y. The area has probably not been affected by thermal events since Precambrian time.

PROCEDURES

Uranium and thorium concentration

A microsplitter was used to obtain separate samples for determining the uranium and thorium concentration; the technique of isotope dilution was used for these analyses (Rosholt and others, 1966). A U^{235} spike and a Th^{230} spike were added from a combined spike solution to a 0.5-gram sample in HNO_3 in a Teflon dish. The sample was decomposed with HF, HNO_3, and $HClO_4$, and evaporated to dryness in nitrate form. The sample in 6*N* HNO_3 solution was loaded on an anion exchange column (NO_3^- form), washed with 6*N* HNO_3, and thorium and uranium were eluted with 0.5*N* HCl. The eluate was repurified by anion exchange in a similar manner on a smaller column. The sample was evaporated to dryness with one drop of $HClO_4$ and HNO_3 mixture to destroy any organic matter, and then was loaded on the multiple filament for mass-spectrometry measurement of uranium and thorium isotopes.

Isolation of uranium and thorium

A 2-g sample was decomposed by HNO_3, HF, and $HClO_4$ in a 400-milliliter Teflon dish. A 20-g sample was also used to test the isolation of uranium and thorium from a larger sample than actually required for analysis. The insoluble residue remaining after acid decomposition was removed by centrifugation or filtration from a 6*N* HCl solution. The solution was loaded on an anion exchange column (Cl^{-1} form), washed with 6*N* HCl, and uranium was eluted with 0.5*N* HCl. The eluant and chloride washings were retained for isolation of thorium. The eluate was converted to nitrate form, approximately 50 ml of saturated $Al(NO_3)_3$ solution was added for a salting-out agent, and uranium was extracted into hexone. Uranium was back-extracted from hexone with H_2O and reextracted with hexone, using NH_4NO_3 for a salting-out agent. The purified sample was loaded on multiple filaments for mass-spectrometric measurements.

Isolation of thorium

The eluant from the chloride anion exchange column was converted to nitrate by successive evaporation with 6*N* HNO_3. The solution was loaded on an anion exchange column (NO_3^{-1} form), washed with 6*N* HNO_3 and eluted with 0.5*N* HCl. A second anion exchange separation was made using a smaller column. To completely remove uranium from thorium, the eluant was

converted to chloride form, passed through a small column (Cl^{-1} form), and washed with 6*N* HCl. The purified solution, in which thorium isotopes were included together with the wash solution, was evaporated to dryness with one drop of $HClO_4$ in a 10-ml Teflon beaker. A thin source of thorium for alpha spectrometry measurement was prepared by electroplating from a 2*N* NH_4Cl solution (pH 6) at 6 volts and 0.4 ampere for 1½ hours.

Isotopic measurements

The mass spectrometric and alpha spectrometric measurements used were the same as those described by Rosholt and others (1966). For a minimum statistical variation, a large number of counts were obtained on the alpha spectrometer measurements. Approximately 70,000 counts of Th^{232} were obtained for each of 4 different sample splits for Th^{230}/Th^{232} ratios, and approximately 60,000 counts of U^{238} were obtained for each measurement of the U^{234}/U^{238} ratios.

RESULTS

The results of these analyses are shown in table 2; uranium content is 24.1±0.2 parts per million, and thorium content is 82.8±0.9 ppm. The U/Th ratio has less analytical variation than the actual concentrations of these elements because, using a combined spike, any variation in the weight of the spike produces the same variation for each element. Variation of the U/Th ratio in any individual analysis did not exceed 0.4 percent of the average value.

The isotopic ratios U^{238}/U^{235}, U^{235}/U^{234}, U^{238}/U^{234}, and Th^{230}/Th^{232} are shown in table 3. No analytically significant variation of the U^{238}/U^{235} ratio was measured, and the U^{235}/U^{234} ratio indicates that U^{234} is less than 0.5 percent deficient compared to U^{238} or U^{235}.

TABLE 2.—*Uranium and thorium concentration, in parts per million, determined by isotope dilution, and* U/Th *weight ratio, of the granite reference sample (No. 3633)*

Sample split	U	Th	$\frac{U}{Th}$	$\frac{U^{238}}{Th^{232}}$
5	23. 91	81. 99	0. 2916	0. 2894
6	24. 45	84. 28	. 2901	. 2880
7	23. 98	82. 20	. 2917	. 2896
Average	24. 1	82. 8	. 2911	. 2890
Standard deviation	±0. 2	±0. 9		±0. 0008

The equation for the calculation of the unity reference ratio of thorium isotopes is given in table 3; unity reference is the ratio of the activity of Th^{230}, in equilibrium with 1 ppm of U^{238}, to the activity of 1 ppm of Th^{232}. This reference ratio is used for comparison with the measured Th^{230}/Th^{232} activity ratio determined on rock samples for which the Th^{230}/U^{238} relation is sought. Division of the Th^{230}/Th^{232} activity ratio of a sample by the unity reference ratio is made so that a direct comparison can be made with the U^{238}/Th^{232} concentration ratio in the sample. Thus,

$$\frac{Th^{230}/Th^{232}\ \text{(sample)}}{Th^{230}/Th^{232}\ \text{(unity ref.)}} = \frac{\text{equivalent } Th^{230}\ \text{(ppm)}}{Th^{232}\ \text{(ppm)}}\ \text{(sample)}.$$

The right-hand term of the equation is an equivalent weight-to-weight ratio which can also be defined as the amount of U^{238}, in parts per million, that would be required to support, in radioactive equilibrium, the measured amount of Th^{230} for each part per million of thorium in the sample. Thus, any activity ratio will yield an equivalent weight ratio after comparison with the reference. In the comparison of the Th^{230} (equiv.)/Th^{232} weight ratio with the U^{238}/Th^{232} weight ratio,

TABLE 3.—*Isotopic composition of uranium and thorium, and* Th^{230}/Th^{232} *reference value of the granite reference sample (No. 3633)*

Sample split	Mass spectrometric determination		Alpha spectrometric determination	
	$\frac{U^{235}/U^{235}\ \text{(BCP ref.)}}{U^{235}/U^{235}\ \text{(granite)}}$	$\frac{U^{235}/U^{234}\ \text{(BCP ref.)}}{U^{235}/U^{234}\ \text{(granite)}}$	$\frac{U^{235}/U^{234}\ \text{(BCP ref.)}}{U^{238}/U^{234}\ \text{(granite)}}$	Th^{230}/Th^{232} (granite) (activity ratio)
1	1. 001	0. 995		0. 8872
2	1. 001	. 999	0. 995	. 8719
3	. 998	. 998	. 999	. 8561
4				. 8649

$\frac{Th^{230}}{Th^{232}}$ (activity ratio) = 0.870±0.008; $\frac{U^{238}}{Th^{232}}$ (weight ratio) = 0.2890±0.0008.

$\frac{Th^{230}}{Th^{232}}$ (unity reference)[1] = $\frac{Th^{230}/Th^{232}\ \text{(activity ratio)}}{U^{238}/Th^{232}\ \text{(weight ratio)}} = \frac{0.870}{0.289} = 3.01 \pm 0.03$.

[1] Ratio of the alpha radioactivity of Th^{230}, in equilibrium with 1 ppm of U^{238}, to the alpha radioactivity of 1 ppm of Th^{232}. Unity reference is used for the following comparison:

$$\frac{Th^{230}/Th^{232}\ \text{(sample)}}{Th^{230}/Th^{232}\ \text{(unity ref.)}} = \frac{\text{equivalent } Th^{230}\ \text{(ppm)}}{Th^{232}\ \text{(ppm)}}\ \text{(sample)},$$

and for rock sample:

$$\frac{Th^{230}}{U^{238}}\ \text{(activity ratio)} = \frac{\text{equiv. } Th^{230}\ \text{(ppm)}/Th^{232}\ \text{(ppm)}}{U^{238}\ \text{(ppm)}/Th^{232}\ \text{(ppm)}}.$$

values of the former ratio that are greater than the U^{238}/Th^{232} ratio indicate an excess of Th^{230} compared with U^{238}.

An additional check of equilibrium conditions of the granite reference can be made by comparing the unity reference ratio with the value that would be obtained from the decay constants of U^{238} and Th^{232}. Using 4.51×10^9 years for the half life of U^{238} (Fleming and others, 1952) and the adopted "best" value (Hyde and others, 1964, p. 489) of 1.39×10^{10} years for the half life of Th^{232} (Kovarik and Adams, 1938; Picciotto and Wilgain, 1956), a unity reference ratio is calculated by the following equation:

$$\frac{\lambda^{238}N^{238}}{\lambda^{232}N^{232}}=3.01,$$

where λ is the decay constant and N is the number of atoms. This number is nearly identical with the value in table 3 measured for the reference sample (No. 3633).

REFERENCES

Barth, T. F. W., 1959, Principles of classification and norm calculations of metamorphic rocks: Jour. Geology, v. 67, no. 2, p. 135–152.

——— 1962, A final proposal for calculating the mesonorm of metamorphic rocks: Jour. Geology, v. 70, no. 4, p. 497–498.

Burwash, R. A., Baadsgaard, H., and Peterman, Z. E., 1962, Precambrian K-Ar dates from the western Canada sedimentary basin: Jour. Geophys. Research, v. 67, no. 4, p. 1617–1625.

Fleming, E. H., Jr., Ghiorso, A., and Cunningham, B. B., 1952, The specific alpha-activities and half-lives of U^{234}, U^{235}, and U^{238}: Phys. Rev., v. 88, p. 642.

Hyde, E. K., Perlman, I., and Seaborg, G. T., 1964, The nuclear properties of the heavy elements, v. 2, Detailed radioactivity properties: Englewood Cliffs, N.J., Prentice-Hall, Inc., p. 409–1107.

Kovarik, A. F., and Adams, N. I., Jr., 1938, The disintegration constant of thorium and the branching ratio of thorium-C: Phys. Rev., v. 54, p. 413.

Nockolds, S. R., 1954, Average chemical compositions of some igneous rocks: Geol. Soc. America Bull., v. 65, p. 1007–1032.

Peterman, Z. E., and Hedge, C. E., 1964, Age of basement rocks from the Williston basin of North Dakota and adjacent areas: Art. 141 *in* U.S. Geol. Survey Prof. Paper 475–D, p. D100–D104.

Picciotto, E., and Wilgain, S., 1956, Confirmation de la periode du Thorium–232: Nuoro Cimento, ser. 10, v. 4, p. 1525–1528.

Rosholt, J. N., Jr., Doe, B. R., and Tatsumoto, M., 1966, Evolution of the isotopic composition of uranium and thorium in soil profiles: Geol. Soc. America Bull., v. 77, p. 987–1004.

Rosholt, J. N., Jr., Shields, W. R., and Garner, E. L., 1963, Isotopic fractionation of uranium in sandstone: Science, v. 59, p. 224–226.

Sawatzky, H. B., Agarwal, R. G., and Wilson, W., 1960, Helium prospects in southwest Saskatchewan: Saskatchewan Dept. Mineral Resources Rept. 49, 26 p.

GEOCHEMISTRY OF DEEP-SEA SEDIMENT ALONG THE 160° W. MERIDIAN IN THE NORTH PACIFIC OCEAN

By VERNON E. SWANSON, JAMES G. PALACAS, and ALONZA H. LOVE, Denver, Colo.

Work done in cooperation with the U.S. Coast and Geodetic Survey

Abstract.—The lithology and chemical composition of the upper 25 cm of light-brown clay are remarkably uniform along the 2,000-mile traverse from southern Alaska to the Hawaiian Islands, except for the olive-gray color and relatively higher organic matter content of the Aleutian Trench sample. Six of seven shallow cores contained ice-rafted pebbles, most of which have a thin ferromanganese coating. Analyses of sediment show little variation from the average content of 0.21 percent organic carbon, 0.05 percent nitrogen, 85 ppm of soluble humic fraction, and 45 ppm of soluble bitumen fraction. The exception is the Aleutian Trench sediment, which contains about 0.5 percent organic carbon, and 590 ppm of soluble humic fraction. The average pH of the upper 2–3 cm of sediment of all the cores of the traverse is 7.2, compared to 7.9 for the immediately overlying water; the average Eh of the sediment is +259 mv, compared to +182 mv for the water.

This report is based on core samples obtained by the U.S. Coast and Geodetic Survey oceanographic ship *Surveyor* during its cruise from Alaska to Hawaii in September 1964. The seven coring stations are located along the 160° W. meridian from about 150 miles south of the Shumagin Islands at the eastern end of the Aleutian chain, southward to a few hundred miles north of the Hawaiian Islands (fig. 1, table 1). Four of the cores were obtained with a steel box corer (8 × 8 × 15 inches) which was constructed aboard ship. This large but shallow-penetration corer provided sufficiently large volumes of sediment to conduct a variety of chemical analyses, particularly those required to characterize the organic matter in the sediments. Three cores were obtained with a Phleger corer, but sediment samples from cores C3 and C5 (table 1) were not made available for chemical analysis. In this report the cores are labeled as follows: BC, box core (collected on the *Surveyor* 1964 cruise); C, Phleger or modified-piston core (collected on the *Surveyor* 1964 cruise); P, *Pioneer* (1963) core. Individual samples of certain cores are labeled in lowercase letters (as for example, BC2a, 2b, and so forth).

This study of the uppermost, most recently deposited, deep-sea sediment from the North Pacific is aimed at determining sediment composition, particularly the contained organic material, and at adding to our knowledge about the geochemical processes active near the sediment-water interface. The results are related to similar studies on older and deeper parts of other North Pacific cores (Palacas and others, 1966), and to studies in progress on Atlantic continental-shelf sediments and bay sediments from the Atlantic and Gulf of Mexico coasts.

The senior author, who was aboard ship, acknowledges with gratitude the advice and assistance of the crew of the *Surveyor* in obtaining the cores, especially Capt. Don A. Jones, Comdr. J. D. Boyer, Comdr. R. G. Metcalf, Lt. Comdr. S. M. Levine, Chief Surveyor Tech. Dudley Doe, and Chief Engineer Tech. Peterson. The cooperation of T. V. Ryan, N. P. Laird, and W. A. Anikouchine, of the U.S. Coast and Geodetic Survey, and of Thomas A. Hendricks and George W. Moore, of the U.S. Geological Survey, also is greatly appreciated.

PROCEDURES

Immediately after the cores were hoisted aboard the *Surveyor*, pH, Eh, and temperature measurements were made, and the core material was divided into sample intervals. The pH and Eh determinations (table 1) were made with a portable pH meter on small samples of the water trapped in the corer just above the sediment and of the uppermost 2–3 centimeters of the sediment itself. Most of these samples were obtained from a Phleger corer, which was used

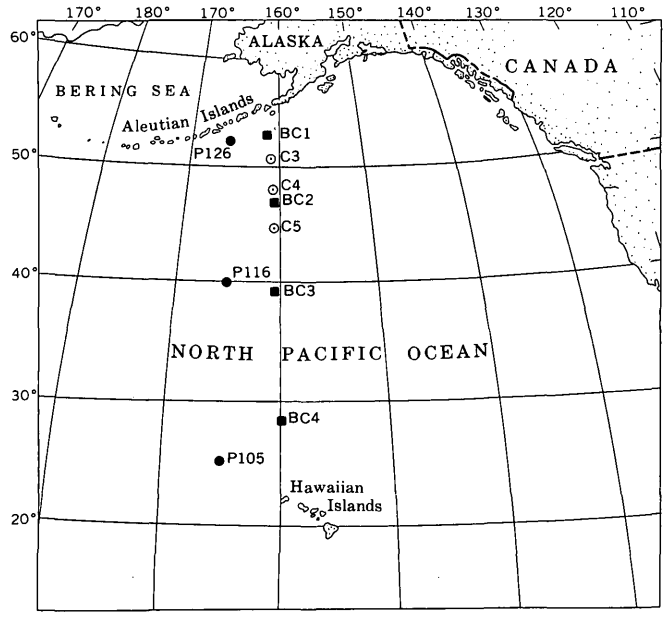

FIGURE 1.—Map showing position of core stations in North Pacific Ocean. *BC*, box core, and *C*, Phleger or modified-piston core, *Surveyor* (1964). P, *Pioneer* (1963) core (Palacas and others, 1966).

as the tripping weight for the box corer or a large piston corer, so that the sediment in the larger corers was not disturbed.

The pH meter was standardized and checked with appropriate buffer solutions, both before and after measurement of a sample. A reading was recorded immediately on inserting the instrument probes into the sample, and another reading was recorded after 30 seconds, both corrected for temperature. The pH and Eh readings given in table 1 are those taken after 30 seconds, at which time equilibrium conditions were generally attained, as indicated by negligible needle-drift on the instrument. The precision of these values is probably ± 0.1 pH unit and $\pm$ 10 millivolts Eh.

No stratification was observed in any of the short cores (7.5–34.5 cm) described in this report, so sample intervals of generally 3 or 6 cm were arbitrarily chosen. The core samples were frozen in the ship's food locker, and kept frozen to minimize bacterial decay and oxidation until they were analyzed. General description of the sediment in the cores was made at time of collection, and small representative fractions of the samples were later examined for grain size, texture, color, mineralogy, and fossil content.

All sample preparation and analytical methods employed in the laboratory are the same as those described by Palacas and others (1966, p. C103) for the *Pioneer* (1963) cores, with the following exceptions:

The soluble humic fraction was extracted with 0.1*N* NaOH in two steps by ultrasonic agitation for 5–10 minutes; the step of shaking on a mechanical shaker for 8–10 hours was omitted as unnecessary. Organic-nitrogen analysis of the sediment was substituted for amino-acid analysis with the intent of providing a somewhat broader and more easily obtained organic geochemical parameter. Percentage of nitrogen was determined in duplicate by micro-Kjeldahl analysis slightly modified after McKenzie and Wallace (1954).

pH, Eh, AND TEMPERATURE OF BOTTOM WATER AND SEDIMENT

All the deep bottom waters and bottom sediments described are slightly alkaline and oxidizing, which is typical of most oceans. From a geochemical viewpoint, significant differences in pH and Eh exist between the water and the sediment (table 1). The pH of the uppermost sediment is invariably lower than that of the overlying water at each station; the Eh is, with one exception (C4, table 1), higher in the sediment than in the overlying water. The pH and Eh measurements do not, however, indicate major chemical differences between environments of sedimentation, such as one might suspect between the Aleutian Trench (BC1) and the North Pacific abyssal plains to the south (BC2–4).

TABLE 1.—*Geographic position of cores and measurements taken at each sample station*

[BC, box core; C, Phleger or modified-piston core]

Core designation	*SURVEYOR* station and sample Nos.	Coordinates	Depth of water		Bottom-water measurements		Upper-sediment measurements	
			(m)	(ft)	pH	Eh (mv)	pH	Eh (mv)
BC1	S–18–64	53°11.4′ N., 161°54.0′ W.	6,670	21,883	8.24	+175	7.02	+272
C3	S–19–64	50°51.3′ N., 161°08.1′ W.	5,020	16,470	7.78	+194	7.30	+257
C4	S–20–64	48°18.1′ N., 160°47.9′ W.	5,060	16,602	7.73	+203	7.52	+179
BC2	S–21–64	47°19.0′ N., 160°45.0′ W.	5,090	16,699	7.91	+160	7.18	+247
C5	S–22–64	45°02.0′ N., 160°39.0′ W.	5,300	17,388	7.52	+179	7.27	+295
BC3		39°25.5′ N., 160°24.8′ W.	5,273	17,300	7.75	+185	7.10	+311
BC4	S–23–64	28°32.8′ N., 159°59.0′ W.	6,050	19,849	8.15	+181	7.27	+255

The average pH of the upper 2 cm of sediment is 7.2, but the average pH of the sea water a few centimeters above the sediment is 7.9. These data are very similar to those reported by Emery and Rittenberg (1952, p. 769) on 21 deep-sea cores from the central east Pacific; the topmost sediment of these cores had an average pH of 7.40 as compared with 7.85 for the overlying water. The difference in pH between the sediment and the overlying water has been explained by Siever and others (1965, p. 65) as being a result of bacterial oxidation of organic matter in the sediment, which causes buildup of CO_2 and lowers the pH. Actually, as Moore and others (1962) determined, the CO_2 content of North Pacific deep-sea sediment is indeed several times greater than that of the overlying water, which they attributed to decay of organic material within the sediment.

The average Eh of the water is +182 mv, and that of the sediment is +259 mv, suggesting that the bottom sediment is slightly more oxidizing than the overlying water. This relation is just the opposite of that observed in the marine basins off southern California (Emery and Rittenberg, 1952, figs. 6-17), where the sediments contain generally 10 times more organic matter than the North Pacific cores.

All the pH and Eh data, including the information recorded by Moore and others (1962, tables 33.1, 33.2), suggest continuous circulation of bottom water in most of the North Pacific Ocean. Furthermore, the amounts of organic matter in the sediment, as described later in this report, are apparently too small to produce the acidic and reducing conditions characteristic of the bottom water and sediment in some marine environments.

The temperature of all water and sediment samples, as measured immediately after collection, was about 1°C, which is common throughout the world at the depths these samples were collected.

DESCRIPTION OF SEDIMENT

Most of the sediment in the cores is typical oceanic abyssal clay—more descriptively, a tan to light-brown lutite. The detailed descriptions of the sediment in the samples that have been chemically analyzed are given in table 2, and the relative amounts of different minerals in these samples, as determined by X-ray diffraction analysis, are listed in table 3.

Ferromanganese nodules and grains are common in many bottom-sediment samples from the Pacific Ocean (Menard, 1964, fig. 8.3), but none of the *Surveyor* (1964) cores reported here contained more than a few isolated grains or thin ferromanganese crusts on pebbles.

TABLE 2.—*Description of sediment from North Pacific cores*

[BC, box core; C, Phleger or modified-piston core]

Core	Description
BC1 (7.5 cm)	Clay, olive gray (5*Y*4/1) when wet, light olive gray (5*Y*6/1) when dry; gummy and very cohesive when wet; about 5 percent biogenic material, diatoms abundant, few globular Radiolaria, few spines, and some brownish claylike fecal pellets; <5 percent fine sand, includes rock fragments of basaltic ash, reddish and yellowish chert, angular quartz, and few glass shards; heavy minerals not common; no visible stratification.
C4a (6.0 cm)	Silty clay, grayish brown (5*YR*3/2) when wet, moderate yellowish brown when dry; somewhat spongy; abundant diatoms of variable size, some globular Radiolaria, few Foraminifera, and few spines and spicules; about 5 percent angular rock fragments as much as 1 cm across, and very fine sand consisting of about 25 percent dark minerals; sharp contact with unit below.
C4b (7.0 cm)	Silty clay, light olive gray (5*Y*5/2) when wet, yellowish gray (5*Y*7/2) when dry; fossils as above, with few fishbone fragments; about 10 percent sand of variable grain size, angular to subrounded grains and fragments of quartz, basalt, chert, mica, and serpentine(?); magnetic minerals uncommon; about 5 percent angular to subrounded rock fragments as much as 1.3 cm across.
BC2 (34.5 cm, total)	Silty clay, dark yellowish brown (10*YR*4/2) when wet, pale yellowish brown (10*YR*6/2) with slight greenish hue when dry; no apparent stratification; silt, sand, and gravel of highly variable composition scattered throughout; pebbles, as much as 2.7 cm in diameter, make up as much as 10 percent, and sand and silt make up from a few to 5 percent; coarse fraction decreases in size and abundance downward; 10 to 40 percent biogenic material, with abundant diatoms, fairly abundant Radiolaria, spines common, very few Foraminifera, and some miscellaneous fossil types.
BC2a (3.0 cm, top sample)	As above, poorly sorted, about 10 percent sand and gravel; fairly abundant pebbles, 2.7-cm maximum dimension, angular to subrounded, partly crusted with ferromanganese, largely rock fragments including sandstone, quartzite, chert, basalt, and diorite; sand includes rock fragments and grains of olivine, epidote, pyroxene or hornblende, feldspar, muscovite, quartz, and some magnetite and ilmenite; about 20 percent siliceous skeletal material, small diatoms (60 percent), Radiolaria (25 percent), spines (5 percent), and a few Foraminifera, tubes, and unidentified material.

241-334 O—67——10

TABLE 2.—*Description of sediment from North Pacific cores*—Con

[BC, box core; C, Phleger or modified-piston core]

Core	Description
BC2b (3.0 cm)	Very similar to sample 2a except slightly less coarse material; pebbles slightly smaller, maximum of 1.6 cm across, with one flat siltstone chip 1.2 cm across, and small mollusk shell fragment.
BC2c (3.0 cm)	Very similar to sample 2a, but only 5–7 percent sand and gravel; magnetite slightly more abundant; some larger diameter diatoms.
BC2d (3.0 cm)	Similar to samples 2a–c, but overall grain size smaller, and sand fraction better sorted; angular quartz and feldspar more abundant; maximum pebble diameter 0.4 cm; diatoms relatively more abundant; chitinous shell of *Orbiculoidea*-type brachiopod, 2.7 mm diameter.
BC2e (3.0 cm)	Similar to samples 2a–d, with somewhat less coarse material; very few small pebbles; about 40 percent of sediment is diatoms, mainly larger diameter type.
BC2f (3.0 cm)	Similar to sample 2d; coarse fraction less than 5 percent, mostly quartz and feldspar grains and includes very few small pebbles, maximum diameter 0.2 cm; diatoms abundant.
BC2g (16.5 cm, bottom sample)	Similar to sample 2f; glass shards fairly abundant; diatoms abundant.
BC3 (20 cm)	Clay, moderate yellowish brown (10*YR*5/4) when wet, grayish orange (10*YR*7/4) when dry; slightly plastic; about 5 percent biogenic material, mainly Radiolaria, spines common, few diatoms, and a few unidentified fragments; scattered rock granules, subrounded to angular, 0.1–0.4 cm in diameter, mainly basalt, but also diorite quartzite, partly coated and stained by a very thin ferromanganese crust; about 3 percent very fine sand, mainly quartz, some magnetic grains, and a few glass shards; no visible stratification.
BC4 (22.5 cm, total)	Clay, dark yellowish brown (10*YR*4/2) when wet, pale yellowish brown (10*YR*6/2) when dry; upper 6 cm very sticky and gummy when wet, somewhat crumbly below 6-cm depth; stratification below 6-cm depth caused by several brownish-black laminae containing disseminated fine- and medium-size grains of basaltic ash; few Radiolaria, some siliceous spines, scattered small fishteeth, and bone fragments; a few ferromanganese and phosphatic(?) grains.
BC4a (6.0 cm, top sample)	As above, nonclay material <2 percent; fishteeth 0.1–.25 mm long common; few globular Radiolaria, needle-shaped, branching, and tetrapod spines, few minute bone fragments; few ferromanganese grains, reniform and botryoidal surfaces, 0.1–1.0 mm in diameter; yellowish phosphatic(?) grains, semitranslucent, 0.1–0.5 mm in diameter.

TABLE 2.—*Description of sediment from North Pacific cores*—Con.

[BC, box core, C, Phleger or modified-piston core]

Core	Description
BC4b (6.0 cm)	Similar to 4a, except grains or fragments of basaltic ash more common but <5 percent of sample; grains are dark gray, subrounded, 0.1–0.5 mm in diameter, and have spongy structure; biogenic material similar to 4a except broken spines and teeth common.
BC4c (10.5 cm, bottom sample)	Similar throughout to sample 4b.

The most notable characteristic of the bottom sediment is the inclusion of pebbles, granules, and sand in the clay of all except the southernmost core (BC4). Although gravel can be transported to the deep sea by many mechanisms (Emery, 1963), the variable size, shape, and mixture of rock types support the interpretation that the coarse material was ice rafted from the north, to at least as far south as 39°25.5′ N., about the latitude of Denver, Colo. The coarse material, which rarely made up more than 5 percent of the total sediment, was excluded from the samples chemically analyzed.

The gravel was present to a depth of at least 34.5 cm (BC2), but became less abundant with depth. All pebbles were at least partly coated with a thin ferromanganese crust; some pebbles apparently had been partly buried in the clay, and only their upper exposed parts were coated by precipitating ferromanganese.

Thin sections of 6 pebbles from the upper 9 cm of BC2 were studied under a polarizing microscope. The 6 angular to subrounded pebbles ranged from 1.4 to 4.4 cm in maximum diameter and were identified as follows: gabbro, porphyritic basalt, metamorphosed quartz diorite, poorly sorted quartzite, feldspathic mudstone, and dolomitic limestone.

No unusual biogenic material was observed in the cores. Lacy, siliceous, skeletal remains of diatoms and Radiolaria, and transparent siliceous spines are common in all samples. The few Foraminifera were found only in BC2 and 4 (table 2; fig 1). Minute conical fishteeth, many of them broken, were relatively abundant in BC4, and a few bone fragments were observed in all cores.

CHEMICAL COMPOSITION OF SEDIMENT

In general, the chemical composition of all samples is remarkably uniform, as shown by the narrow ranges of element contents in table 4. With the exception of minor differences in amounts of magnesium, calcium, and potassium, none of which show geographic or stratigraphic trends, there are no notable differences in major-element composition.

TABLE 3.—*Mineralogy of North Pacific bottom sediment, as determined by X-ray diffraction analysis*

[Percentages of minerals are approximate only; Tr., trace, indicates mineral identified, but amount is few percent or less. Paul D. Blackmon, analyst. BC, box core]

Sample No.	Amorphous silica	Montmorillonite	Chlorite	Mica	Quartz	Feldspar	Amphibole	Pyroxene	Phillipsite(?)	Manganese oxide	Other
BC1	10–15	Tr.	20–25	10–15	10–15	5–10	5–10	----	----	Tr.	[1] 5–10
BC2a	40	Tr.	Tr.	10	5–10	5–10	Tr.	5–10	Tr.	Tr.	[2] 5–10
BC3	20	Tr.	10–15	20–25	10–15	5–10	Tr.	----	Tr.	----	5–10
BC4a	10–15	[3] Tr.	20	20–25	10–15	5–10	Tr.	----	----	Tr.	5–10

[1] Includes trace of pyrite.
[2] Includes trace of calcite.
[3] Includes trace of mixed-layered mica-montmorillonite.

TABLE 4.—*Chemical composition of sediment in North Pacific box cores, based on 12 samples, and comparison with composition of USC&GS* Pioneer *cores and average composition of deep-sea clay*

[Analyses, in percent, by emission spectrographic methods. Where more than one sample, average of analyses given. Laboratory numbers of box-core samples are D120168–D120170 and D120815–D120822. Analysts: Harriet Neiman and A. L. Sutton, Jr. BC, box core; P, *Pioneer* (1963) core]

Element	BC1 (1 sample)	BC2 (7 samples)	BC3 (1 sample)	BC4 (3 samples)	P105, 116, 126 (Palacas and others, 1966) (3 cores, 3 samples)	Average deep-sea clay (Turekian and Wedepohl, 1961, table 2)
Si	>10	>10	>10	>10	>10	25
Al	>10	>10	>10	>10	>10	8.4
Fe	5	5	5	5	5	6.5
Mg	3	1.5	1.5	3	3	2.1
Ca	1.5	1.5	.5	1	1	2.9
Na	3	3	3	3	2	4
K	2	2	3	5	3	2.5
Ti	.3	.3	.3	.7	.5	.46
Mn	.3	.15	.1	.7	.5	.67
B	.005	.007	.01	.02	.01	.023
Ba	.1	.3	.2	.1	.5	.23
Co	.002	.005	.005	.015	.003	.0074
Cr	.015	.007	.01	.015	.01	.009
Cu	.007	.01	.015	.05	.015	.025
Ga	.002	.003	.005	.005	.003	.002
La	<.002	<.002	<.002	.007	.007	.0115
Mo	.0005	<.0005	.0005	.005	.0005	.0027
Nb	<.001	<.001	<.001	.0015	.002	.0014
Nd	<.01	<.01	<.01	.015	.01	.014
Ni	.005	.005	.007	.05	.007	.0225
Pb	<.001	.0015	.001	.005	.005	.008
Sc	.0015	.002	.002	.003	.005	.0019
Sr	.03	.03	.02	.02	.05	.018
V	.02	.02	.02	.02	.02	.012
Y	.0015	.003	.003	.007	.007	.009
Yb	.0002	.0003	.0003	.0005	.0007	.0015
Zr	.005	.01	.01	.015	.015	.015

Analyses reported in percent to the nearest number in a six-step series, for example 0.1, 0.15, 0.2, 0.3, 0.5, 0.7, 1, which represent approximate midpoints of group data on a geometric scale. Thirty-five elements, in addition to those reported, were looked for but were below the limit of detection.

The spectrographic analyses of the three samples in BC4 show that the percentages of seven elements increase with depth in this core (table 5). In the same samples the percentages of boron (0.2–0.015), barium (0.15–0.07), and gallium (0.005–0.003) decrease with depth.

The analyses of the seven 3-cm samples in BC2 (table 4) indicate a slight increase, with depth, of chromium, gallium, molybdenum, nickel, and zirconium, and a slight decrease of barium, manganese, and titanium. The major change in percentages of these elements occurs about 6 cm below the sediment surface.

With the exception of a few questionable grains, no nodules or spherules of ferromanganese were seen in any of the samples, though most of the pebbles in BC2, 3, and 4 were covered in part by very thin ferromanganese crusts. The iron and manganese analyses in table 6 indicate minor variations in content, but the limited data indicate no significant area or depth-of-sediment differences, nor differences between the coarser and finer fractions (BC2a, one sample <115 mesh and one sample >115 mesh). The range in percentage of manganese content is 0.16–0.45 and that of iron 3.5–5.2; the average content is 0.31 and 4.8

TABLE 5.—*Percentages of seven elements that increase with depth in BC4*

[Analyses, in percent, by emission spectrographic method. Laboratory numbers are D120168–D120170. Analyst: A. L. Sutton, Jr. BC, box core]

Sample interval (cm)	Elements						
	Co	Cu	La	Mo	Ni	Pb	Y
0–6	0.01	0.03	0.005	0.0015	0.03	0.003	0.003
6–12	.015	.05	.007	.005	.05	.005	.007
12–22.5	.02	.07	.01	.007	.05	.007	.01

percent, respectively, for the 4 cores. The presence of these metals in their oxidized state, MnO_2 and Fe_2O_3, is supported by observations of the sediment under the microscope (table 2), and by the positive Eh (table 1) of the sediment when collected.

Because copper is commonly closely associated with organic matter in carbonaceous sediment, the copper content of the samples was determined (table 6). The limited analytical data on copper in the sediment show no systematic increase of copper with increase of organic-matter content. The increase of copper content with depth in BC4, as indicated by the spectrographic analyses (table 5), actually suggests an inverse correlation between copper content and organic matter (see organic-matter analyses, table 7). The average copper content of the sediment is 0.014 percent, and the range is 0.0078–0.021 percent. The data do show a slight increase in copper content from north to south for the 4 box-core samples (BC1, 2, 3, 4), 78, 96, 190, and 210 parts per million, respectively, but this relation must be supported by much more data before it can be considered valid.

ORGANIC MATTER IN SEDIMENT

In the geochemical sense used here, organic matter in sediment includes the tissue of protoplasmic substances of plants and animals, and their decay products, that are composed predominantly of carbon, hydrogen, and oxygen, with small amounts of nitrogen, sulfur, and phosphorus; excluded are the silica, carbonate, and phosphatic material in shells or skeletons. The nonskeletal organic matter is not visible in the North Pacific sediment and must be determined chemically.

TABLE 6.—*Manganese, iron, and copper content of uppermost sediment in North Pacific cores*

[Analyses, in percent, by atomic-absorption method. J. D. Mensik, analyst. BC, box core]

Sample No.	Laboratory No.	Thickness of sample interval (cm)	Mn	Fe	Cu
BC1	D121117	7.5	0.37	5.2	0.0078
BC2a [1]	18	3.0	.24	4.6	.011
BC2a [2]	19	3.0	.29	3.5	.0092
BC2e	20	3.0	.16	3.9	.0092
BC3	21	20.0	.20	4.9	.019
BC4	22	6.0	.45	5.0	.021

[1] <115-mesh fraction.
[2] >115-mesh fraction.

The sediment in the *Surveyor* cores has been analyzed by several methods to characterize the organic matter. The four basic determinations are: percentage organic carbon, percentage nitrogen, percentage soluble humic fraction, and percentage soluble bitumen fraction. The organic-carbon determination is the best measure of the total organic matter in the sediment. The nitrogen content, as determined by the micro-Kjeldahl method, is in part a measure of the amount of proteinaceous substances in the organic matter. The amount of alkali-soluble humic material, may be indicative of the original biologic material, particularly of woody plant material and some types of algae. The organic matter soluble in benzene is the bitumen fraction and, although this fraction includes variable amounts of waxes, resins, fats, and oils, it may be considered a measure of the amounts of saturated and aromatic hydrocarbons and the asphaltic substances in the sediment. Bordovskiy (1965, p. 33-114) has presented an excellent summary of the ranges in content and the significance of these chemical components of organic matter in Recent marine sediments.

The general range of organic-matter content in North Pacific deep-sea sediment, based on analysis of the *Surveyor* cores, is 0.07 to 0.9 percent, but most commonly the sediment contains 0.2–0.5 percent organic matter. Based on 16 samples from 8 cores, 5 *Surveyor* cores (table 7) and 3 *Pioneer* (1963) cores (fig. 1; Palacas and others, 1966), the deep-sea sediment in the North Pacific contains an average of 0.4 percent organic matter.

The analytical data on the sequence of samples from BC4 (table 7) suggest a slight decrease in amount of organic matter with depth of sample. This relation is not supported, however, by the more detailed data of BC2. Certainly, many more samples must be analyzed to establish any regionally significant organic-matter–depth relation.

The combined humic and bitumen fractions range from 0.4 to 7 percent and average about 3 percent of the total organic matter. The humic fraction is generally about twice as large as the bitumen fraction, though, as might be expected in marine sediment nearer land areas, the humic fraction in the Aleutian Trench sample is nearly 10 times greater than the bitumen fraction (BC1, table 7).

TABLE 7.—*Organic-matter analyses of 13 samples from 5 North Pacific cores*

[All sulfur analyses, and carbon analyses on samples 2B, 2C, 2F, 2G, and 4C by I. C. Frost; other carbon analyses by Huffman Laboratories, Inc., Wheatridge, Colo. All analyses reported on dry-weight basis, except moisture content on wet-weight basis. BC, box core; C, Phleger or modified-piston core]

Sample No.	Thickness of sample interval (cm)	Moisture content (percent)	Total carbon (percent)	Carbonate carbon (percent)	Organic carbon (percent)	Nitrogen (percent)	Carbon/nitrogen ratio	Sulfur (percent)	Total organic matter (percentage organic carbon × 1.7)	Soluble humic fraction (ppm)	Bitumen fraction (ppm)
BC1	7. 5	46	0. 54	0. 002	0. 54	0. 062	8. 7	0. 07	0. 92	590	60
BC2a	3	59	. 32	. 025	. 30	. 047	6. 4	. 09	. 51	45	15
2b	3	56	. 30	. 023	. 28	. 033	8. 5	. 07	. 48	1	25
2c	3	49	. 28	. 02	. 27	. 038	7. 1	. 08	. 46	5	20
2d	3	47	. 35	. 02	. 33	. 045	7. 3	. 05	. 56	15	25
2e	3	55	. 25	. 029	. 22	. 039	5. 6	. 05	. 37	160	40
2f	3	53	. 33	. 03	. 30	-------	-------	. 05	. 51	90	20
2g	16. 5	50	. 34	. 03	. 31	. 035	8. 9	. 02	. 53	140	20
BC3	20	52	. 20	. 013	. 19	. 063	3. 0	. 02	. 32	120	40
BC4a	6	54	. 22	. 044	. 18	. 062	3. 0	. 05	. 31	135	95
4b	6	45	. 14	. 025	. 12	-------	-------	. 03	. 21	30	60
4c	10. 5	64	. 17	. 060	. 11	. 034	3. 2	. 03	. 19	35	50
C4a	6	-------	. 05	. 008	. 04	-------	-------	-------	. 07	-------	-------

The analyses of the sequence of samples in BC2 (table 7) show a distinct change in the amount of humic fraction with depth of sediment. The humic fraction is less than 0.5 percent of the organic matter in the upper 12 cm of sediment, whereas it is about 3 percent of the organic matter in the underlying sediment. If the average humic content of the upper 12 cm of sediment is compared to that of the lower 22.5 cm, the lower unit contains more than 7 times more soluble humic material than the upper unit. This increase in the humic fraction may be attributed to the alteration of the older organic material to soluble humic matter, but this explanation is not supported by data on other samples and must be considered highly speculative.

The bitumen fraction in the sediment is about 0.7 percent of the total organic matter, except in BC4, where the bitumen fraction is consistently 3 percent of the total organic matter from top to bottom of the core (22.5 cm).

The nitrogen content is generally 0.03 to 0.06 percent, and the carbon/nitrogen ratio ranges from 3.0 to 8.9. The carbon/nitrogen values are in general lower than those reported for marine organic matter in other deep-sea sediments (Bordovskiy, 1965, p. 48-49); for example, Degens and others (1961, p. 416) state that the carbon/nitrogen ratio of "surface sediments" is about 8, and is about 12 at depth (several feet). Interestingly, the carbon/nitrogen ratio is 8.7 for the Aleutian Trench sample (BC1), 7.3 for BC2 samples, and 3.0 for BC3 and 4 samples. If the nitrogen is solely a component of the organic matter, this change in ratio may suggest a proportional increase of proteinaceous substances with increasing distance southward from Alaska.

The set of carbonate, or mineral, carbon determinations is included in table 7 as this analysis is a part of the procedure to determine organic carbon. The carbonate carbon is a measure of the amount of calcite, dolomite, siderite, and other minerals whose composition includes the CO_3 radical. In North Pacific sediment, the carbonate-carbon content is extremely low, generally less than 0.05 percent, and the slight differences in the carbonate-carbon content cannot be related to geographic area or depth of sediment. The sulfur content is also low, less than 0.1 percent; a decrease of sulfur content with depth of sediment is noted, however, in the series of samples from BC2 and 4.

In general, the data on organic matter in the *Surveyor* cores are similar to those reported by Romankevich (1961) for sediment of the Western Pacific Ocean. For example, the average organic-carbon content of red abyssal clays of the Western Pacific is 0.22 percent; the soluble humic fraction is less than 2 percent of the organic-carbon content; and the soluble bitumen fraction is 1–4 percent of the organic-carbon content. The values for the same components, based on BC2, 3, and 4, are 0.21, 4, and 2.5 percent, respectively. The average values for other analyses of these cores are 0.05 percent nitrogen, 85 ppm of soluble humic fraction, and 45 ppm of soluble bitumen fraction.

The organic-carbon content of the Aleutian Trench sample (BC1) is almost exactly the same as that of the uppermost sediment of two cores farther west in the Aleutian Trench reported by Romankevich (1957, fig. 1); the humic fraction of the *Surveyor* sample was somewhat less, however, though the bitumen fraction was about the same.

The organic-matter analyses on three samples from the North Pacific (Palacas and others, 1966; also see fig. 1, this report), which were from intervals about 40–55 cm below the sediment surface, also are similar to those reported here. The only significant difference is in the amounts of soluble humic material extracted from the Aleutian Trench samples, 590 ppm from BC1 of this report, and 1,145 ppm from sample P126 (Palacas and others, 1966, table 2). However, both amounts are very large compared with the soluble humic material in other North Pacific sediment. Both the large amounts and the variation in amounts of this type of organic matter in Aleutian Trench samples are probably a result of their proximity to southern Alaska, which is presumably a major source area for the soluble humic organic matter.

REFERENCES

Bordovskiy, O. K., 1965, Accumulation and transformation of organic substances in marine sediments: Marine Geology, v. 3, no. 1/2, 3–114.

Degens, E. T., Prashnowsky, A., Emery, K. O., and Pimenta, J., 1961, Organic materials in recent and ancient sediments; pt. 2, Amino acids in marine sediments of Santa Barbara Basin, California: Neues Jahrb. Geologie u. Paläontologie, Monatsh., no. 8, p. 413–426.

Emery, K. O., 1963, Organic transportation of marine sediments, *in* M. N. Hill, ed., The sea: New York, Interscience Publishers, v. 3, p. 776–793.

Emery, K. O., and Rittenberg, S. C., 1952, Early diagenesis of California basin sediments in relation to origin of oil: Am. Assoc. Petroleum Geologists Bull., v. 36, no. 5, p. 735–806.

Goldberg, E. D., and Arrhenius, G. O. S., 1958, Chemistry of Pacific pelagic sediments: Geochim. et Cosmochim. Acta v. 13, p. 153–212.

McKenzie, H. A., and Wallace, H. S., 1954, The Kjeldahl determination of nitrogen; a critical study of digestion conditions—temperature, catalyst, and oxidizing agent: Australian Jour. Chemistry, v. 7, no. 1, p. 55–70.

Menard, H. W., 1964, Marine geology of the Pacific: New York, McGraw-Hill Book Co., 271 p.

Moore, G. W., Roberson, C. E., and Nygren, H. D., 1962, Electrode determination of the carbon dioxide content of sea water and deep-sea sediment: Art. 33 *in* U.S. Geol. Survey Prof. Paper 450–B, p. B83–B86.

Palacas, J. G., Swanson, V. E., and Moore, G. W., 1966, Organic geochemistry of three North Pacific deep-sea sediment samples, *in* Geological Survey Research 1966: U.S. Geol. Survey Prof. Paper 550–C, p. C102–C107.

Romankevich, E. A., 1957, The organic matter in core samples of bottom sediments in the northwestern part of the Pacific Ocean (east of Kamchatka): Doklady Akad. Nauk SSSR, v. 116, no. 3, p. 447–450 (translation by Assoc. Tech. Services, Inc., 5 p.).

——— 1961, Organic substance in the surface layer of bottom sediments in the Western Pacific Ocean [abs.]: Pacific Sci. Cong., 10th, Abstracts, Honolulu, Hawaii, p. 384–385.

Siever, Raymond, Beck, K. C., and Berner, R. A., 1965, Composition of interstitial waters of modern sediments: Jour. Geology, v. 73, no. 1, p. 39–73.

Turekian, K. K., and Wedepohl, K. H., 1961, Distribution of the elements in some major units of the Earth's crust: Geol. Soc. America Bull., v. 72, no. 2, p. 175–192.

RESULTS OF SOME GEOPHYSICAL INVESTIGATIONS IN THE WOOD HILLS AREA OF NORTHEASTERN NEVADA

By C. J. ZABLOCKI, Denver, Colo.

Abstract.—Near-surface magnetic anomalies have been discovered over an alluvial pediment along the southern flank of the Wood Hills and are probably due to fine-grained quartz latite, as suggested by auger samples. Electromagnetic and resistivity measurements over and near this magnetic anomaly have outlined a broad horizontal zone about 3,500 feet long and 1,500 feet wide having a conductivity of about 50 millimhos per meter at a depth of 70–100 feet. In places this zone is also characterized by a relatively large induced-polarization response (250 milliseconds). The configuration of the broad conductive zone suggests a water-saturated rock layer, rich in minerals (clays) with high ion-exchange capacity. A shallower, narrower, and more conductive zone also borders the flank of this magnetic anomaly.

An earlier geochemical reconnaissance of the Pequop Mountains, 10 miles east of the Wood Hills, and the Wood Hills, Elko County, Nev. (fig. 1), indicated areas which contained some anomalously high concentrations of metals (chiefly zinc, lead, and mercury). These metals occur in oxidized iron-rich fracture fillings and in small gossan pods in silicified dolomite and limestone, primarily in the Guilmette Formation and Simonson Dolomite of Devonian age (Erickson and others, 1966). Some of these anomalous areas are along the southeastern flank of the Wood Hills, where extensions of these zones may extend beneath the alluvial gravel cover.

This report summarizes some later geophysical investigations made in the Wood Hills area. Initially, a general reconnaissance was made with a truck-mounted magnetometer along most of the accessible roads that flank the Wood Hills and northern part of the Pequop Mountains, in order to find evidence of possible buried igneous masses. Four magnetic anomalies were found, one of which, along U.S. Highway 40 near the east side of the Pequop Mountains, is associated with volcanic rocks of Tertiary age (Thorman, 1962). Another magnetic anomaly of small extent is near the summit of a road that cuts through the Pequop Mountains about 16 miles south of Highway 40. Some small igneous dikes of intermediate to siliceous composition in this area may be the cause of this magnetic anomaly.

The other two anomalies, described in this paper, were detected in a gravel-covered pediment along the southern flank of the Wood Hills (fig. 1) and subsequently were surveyed by close-interval magnetometer traverses (fig. 2). Later, electromagnetic, resistivity, and induced-polarization studies were made of the northwesternmost of these two anomalies and showed that the terrane also includes anomalous electrically conductive rocks.

The geology of the Wood Hills, a small northward-trending elongate dome covering about 75 square miles, as mapped and described by C. H. Thorman (1962), is generalized on figure 1. The Wood Hills are underlain chiefly by marble, quartzite, and schist of Middle Cambrian through Middle Ordovician age. These metamorphic rocks are overthrust by unmetamorphosed Ordovician through Permian rocks that are preserved on the northeast, northwest, and south flanks of the dome. In the immediate vicinity of the area of investigation, the exposed units include the Ordovician Ely Springs Dolomite, the Silurian Laketown Dolomite, and the Devonian Simonson Dolomite.

Tertiary sedimentary and volcanic rocks lie unconformably on the metamorphic rocks in the northern part of the dome. Numerous small unmapped pegmatite dikes have been reported by Thorman (1962) as being present in the area.

EQUIPMENT, TECHNIQUES, AND RESULTS

Mobile magnetometer surveys

Total magnetic-field intensity was recorded continuously with a truck-mounted fluxgate-type magnetometer (ASQ–3) formerly used by the U.S. Geological

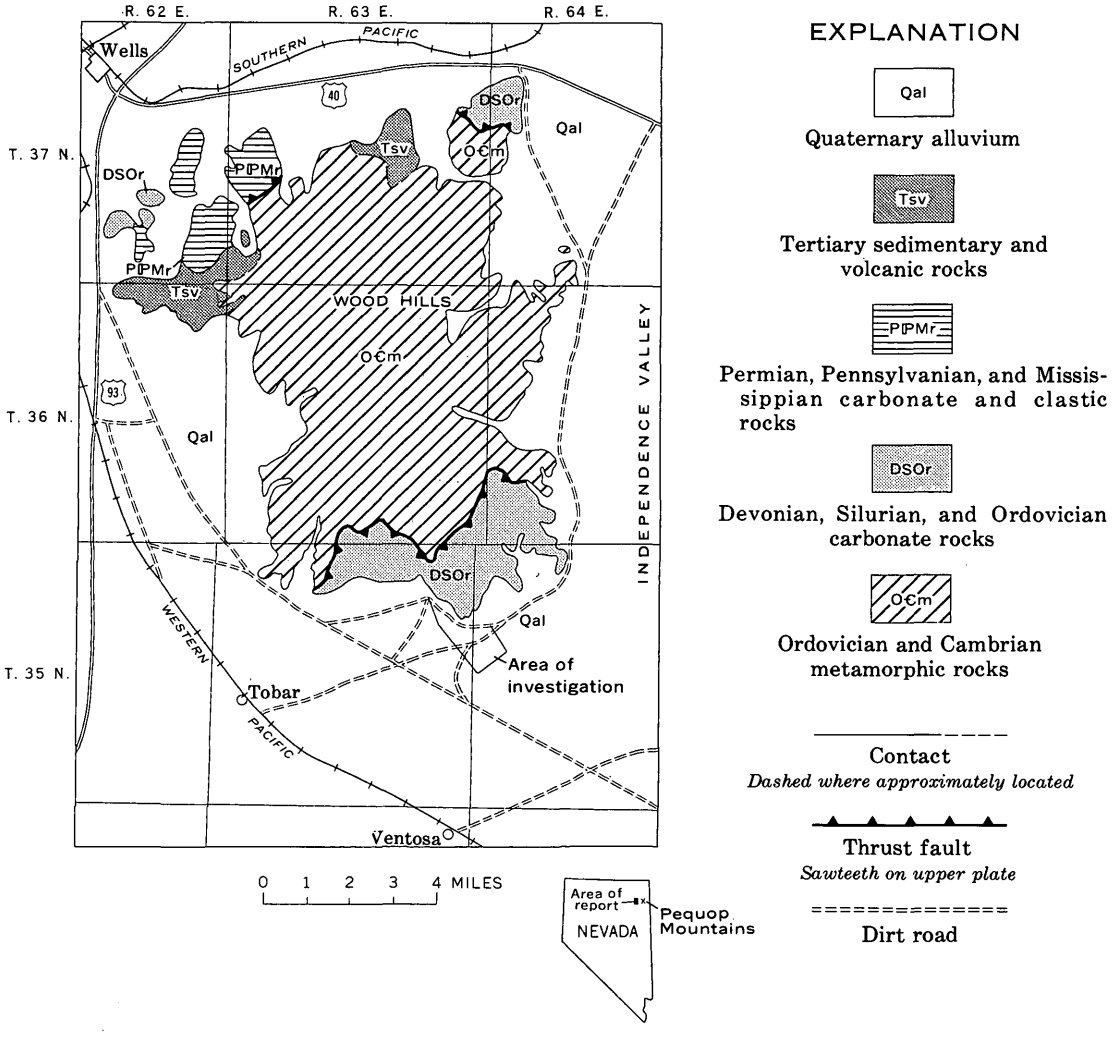

FIGURE 1.—Index map showing area of investigation and generalized geology of Wood Hills, Elko County, Nev. Geology adapted and simplified from Thorman (1962).

Survey in airborne operations. The sensing unit was attached to the end of an aluminum A-frame structure connected to the rear of a ¾-ton Carryall-type vehicle and extended 10 feet above the ground surface and 18 feet from the vehicle. Compensation for heading effects due to changes in the orientation of the vehicle with respect to the direction of the earth's magnetic field was accomplished by selectively placing strips of permalloy about the sensing head; this reduced the heading error from 140 gammas to about 22 gammas in changing from north to south orientation. The overall equivalent noise level of the system, including electronic and mechanical noise, was about 35 gammas. The magnetic-field intensity was plotted on a strip-chart recorder whose drive mechanism was geared by a synchro system with the vehicle's odometer. A chart-drive gearing of 1 inch per 0.1 mile was used for most of these studies with a recording sensitivity of 150 gammas per inch of deflection. The speed of measurements was limited to the normal driving speeds ordinarily used for given conditions, that is, 45 miles per hour on paved roads, 10–15 mph on dirt roads, and 3–5 mph over fairly flat terrain with small amounts of vegetation. Where possible, successive traverses were tied in with a base line to eliminate the instrumental drift inherent in the system.

The total-magnetic-field-intensity contour map resulting from the data obtained by the mobile magnetometer survey is shown on figures 2 and 3. An auger hole put down in the vicinity of the center of electrical sounding S (fig. 3) struck bedrock at 10 to 15 feet and obtained chips of quartz latite(?) that contain 1 to 1.5 percent magnetite. The magnetic susceptibility determined from these chips is 1.42×10^{-3} cgs units. A near-surface mass of quartz latite is therefore believed to cause the magnetic anomaly in this region.

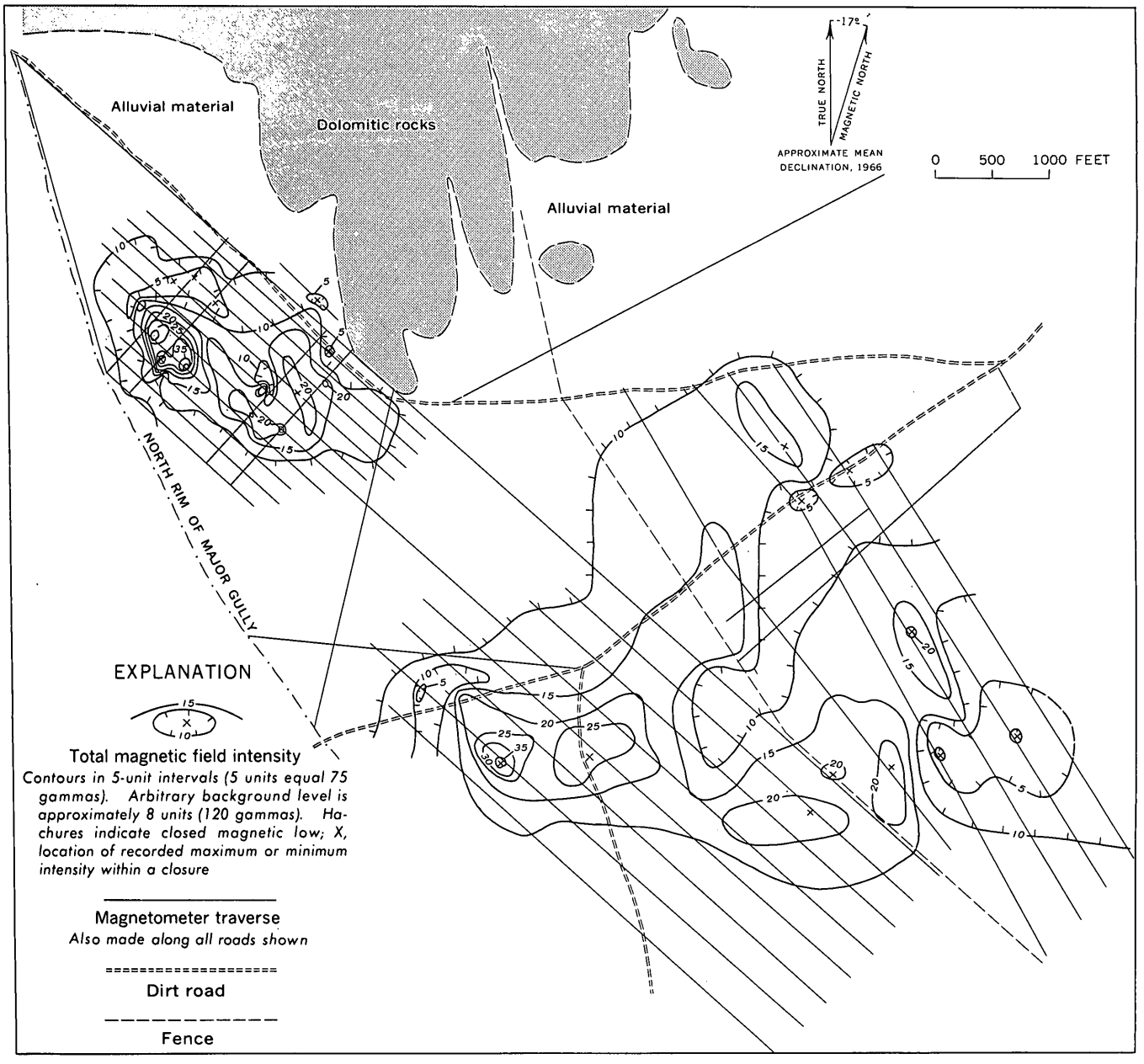

FIGURE 2.—Total-magnetic-field-intensity contour map of area covered in this study. (See fig. 1 for location of area.)

Electrical surveys

Electromagnetic.—The slingram method (Frischkencht, 1959) was used in making electromagnetic traverses across the general area of some of the magnetic anomalies. The equipment consisted of a battery-powered transmitter, transmitting and receiving coils, and a ratiometer. The system measured the mutual coupling between the transmitting and receiving coils at a frequency of 1,760 cycles per second and a fixed spacing of 200 feet. Both coils were oriented in the horizontal co-planar direction. The ratiometer compares the signal received from the transmitting coil with a reference signal transmitted directly by a connected cable. The amplitude and phase of the signal vary with the electrical conductivity of the earth between the transmitter and receiver. The amplitude and phase are measured in their Cartesian-coordinate equivalents of percentage amplitudes, that is, over a nonconductive earth (or at least one that is highly resistive) the signal is the free-space response, which is 100 percent in-phase and 0 percent out-of-phase. The presence of conductive rocks is indicated by a change in the in- and out-of-phase values. Stations were occupied at 50- or 100-foot intervals along the traverses.

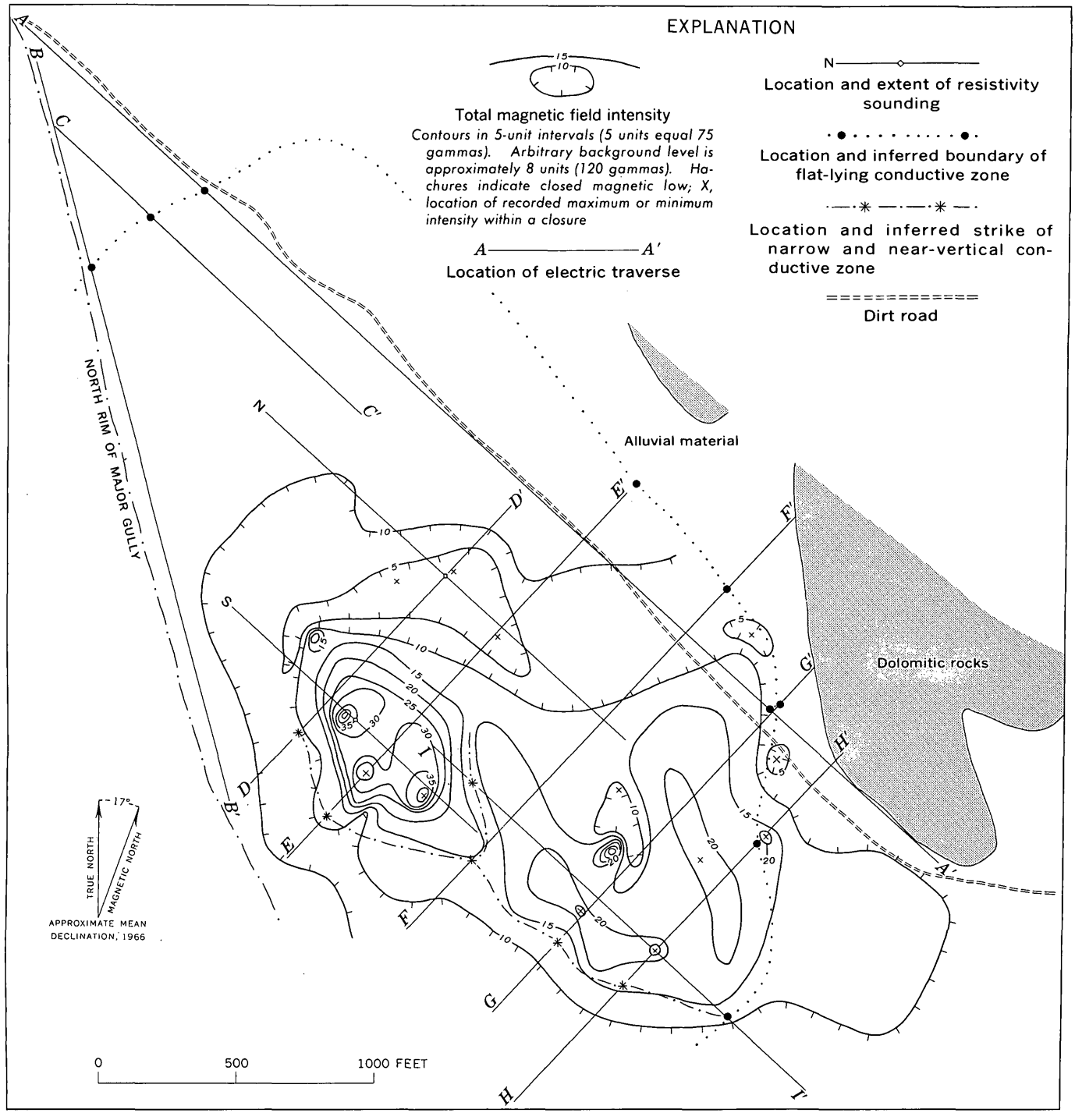

FIGURE 3.—Detailed total-magnetic-field-intensity contour map of the northwestern anomaly shown on figure 2, and location of electric soundings and traverses made.

The slingram profiles of traverses *A–A′* and *B–B′*, on the edges of the northwestern anomaly, are shown on figure 4. Five slingram profiles made across the general strike of the magnetic source (traverses *D–D′*, *E–E′*, *F–F′*, *G–G′*, and *H–H′*) and one parallel to the strike (*I–I′*) are shown on figure 5.

Resistivity and induced polarization.—The resistivity and induced-polarization profiles were made using a fixed Schlumberger electrode configuration (see, for example, Keller and Frischknecht, 1966) with a half-current electrode separation of 200 feet and a potential electrode separation of 20 feet. An all-solid-state power unit provided alternate positive and negative square wave current pulses of 3 seconds duration separated by a 3-second interval of no current flow. The receiving unit consisted of a high-input-impedance, high-gain, amplifier-integrator connected to two meters. It alternately indicated the peak voltage of the received signal during the current-on cycle and the integrated transient voltage signal during the current-off cycle. The resistivity was computed from the peak voltage and current values, and the induced-polarization response from the ratio of the integrated transient voltage to the peak voltage. Measurements were taken at 100-foot intervals along the traverses. Resistivity (determined in terms of conductivity) and induced-polarization-response profiles made along traverses *A–A′* and *C–C′* are shown on figure 4.

In addition to the resistivity profiles, two resistivity soundings, N and S (fig. 6), were made using the Schlumberger configuration. Sounding N was made in the approximate center of the anomalous area and parallel to the rocks that crop out to the northeast, and sounding S was made over the shallowest region of the magnetic source (fig. 3).

DISCUSSION OF RESULTS

The significance of the above geophysical data cannot be fully evaluated until supplemental data are acquired. However, on the basis of the measurements obtained so far some of the possible geological conditions compatible with these data are here presented.

Magnetic data

The relative differences in the azimuth of the magnetic polarization (horizontal direction between an anomaly high and low) between the northwestern and southeastern anomalies (fig. 2) suggest that the underlying magnetic rocks in these two areas may be geologically unrelated. Some of the anomalies in the southeastern part of the area appear to be polarized about 60° to 90° east of magnetic north, whereas the northwestern anomaly is polarized about 5° west of magnetic north. The deviation of the horizontal polarization from the earth's field direction for the southeastern anomalies appears to be too large to be attributable to body shape or orientation and, therefore, probably indicates the influence of remanent magnetization. Books (1962) observed that the direction of horizontal polarization was consistently different over intrusive and extrusive igneous masses (Eocene in age) in north-central Montana. In Montana, the extrusive masses are polarized in directions about 100° and 130° east of magnetic north, whereas the intrusive masses are polarized in a direction about 26° west of magnetic north.

The general strike of the magnetic anomalies tends to parallel the strike of the exposed dolomite rocks and probably represents the trend of the magnetic rocks beneath the gravel-covered pediments. The depth to the magnetic bedrock is only about 10 to 15 feet in the northwestern area, as indicated by drilling, and about 80 feet elsewhere.

In detail, the near-surface anomaly in the northwestern area is characterized by relatively large variations in magnetic-field intensity over short distances. This could be caused by: (1) large lateral variations in percentage of magnetite in the igneous rocks; (2) an irregular distribution of magnetic rocks, such as magnetic dikes intruded into near-surface basement rocks; (3) variations in the magnetite distribution, owing to oxidation or alteration of magnetite in local zones or along vertical fractures; or (4) variations in the direction and intensity of remanent magnetization of these rocks.

To determine the possible shape and extent of the magnetic source in the northwestern area, some model curves were computed using a program developed by G. I. Evenden (U.S. Geol. Survey, written commun., 1966) for comparison with the magnetic profile (*E–E′*) run across the approximate center of the anomaly. The comparison was made with a two-dimensional model which is adequate here where the ratio of half-length of the anomaly to an assumed depth is about 10 to 1. The initial model used was a rectangular-shaped mass that is 25 feet below the magnetometer (magnetometer 10 feet above land surface and source about 15 feet below surface in area of drill hole), 525 feet wide, and 1,000 feet in vertical extent, and that strikes 65° west of magnetic north. A uniform magnetic susceptibility of 1.4×10^{-3} cgs units was used where the total field intensity is 5.5×10^4 gammas inclined at 65° from the horizontal. The computed profile is shown in figure 7, together with the field curve. This model fits the field curve fairly well except

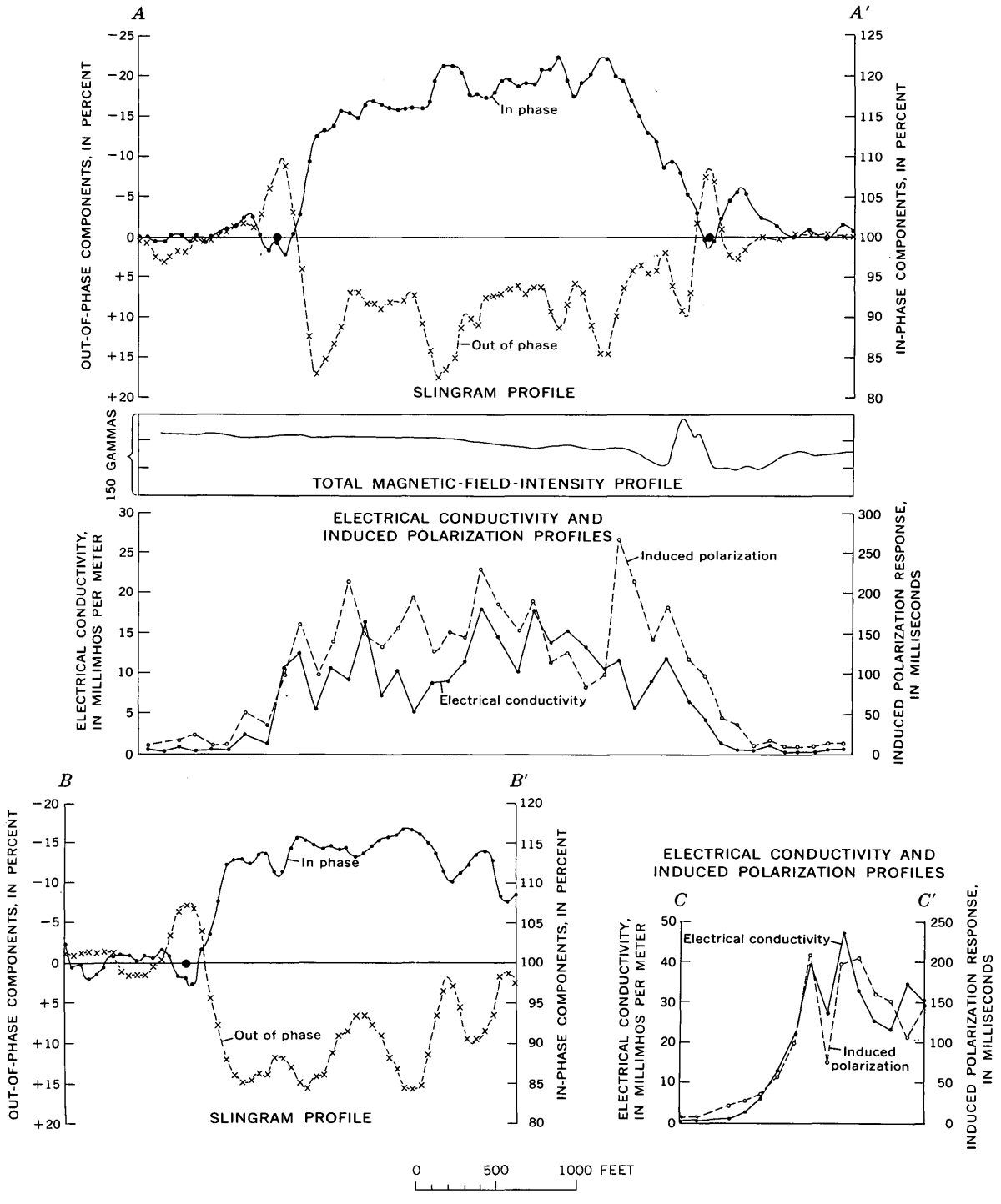

FIGURE 4.—Slingram profiles (*A*–*A*′ and *B*–*B*′) and profiles showing total magnetic field intensity (*A*–*A*′), and resistivity (plotted in terms of conductivity) and induced polarization (*A*–*A*′ and *C*–*C*′). The large dots on Slingram profiles indicate location of edge of flat-lying conductive zone. Location of profiles shown on figure 3.

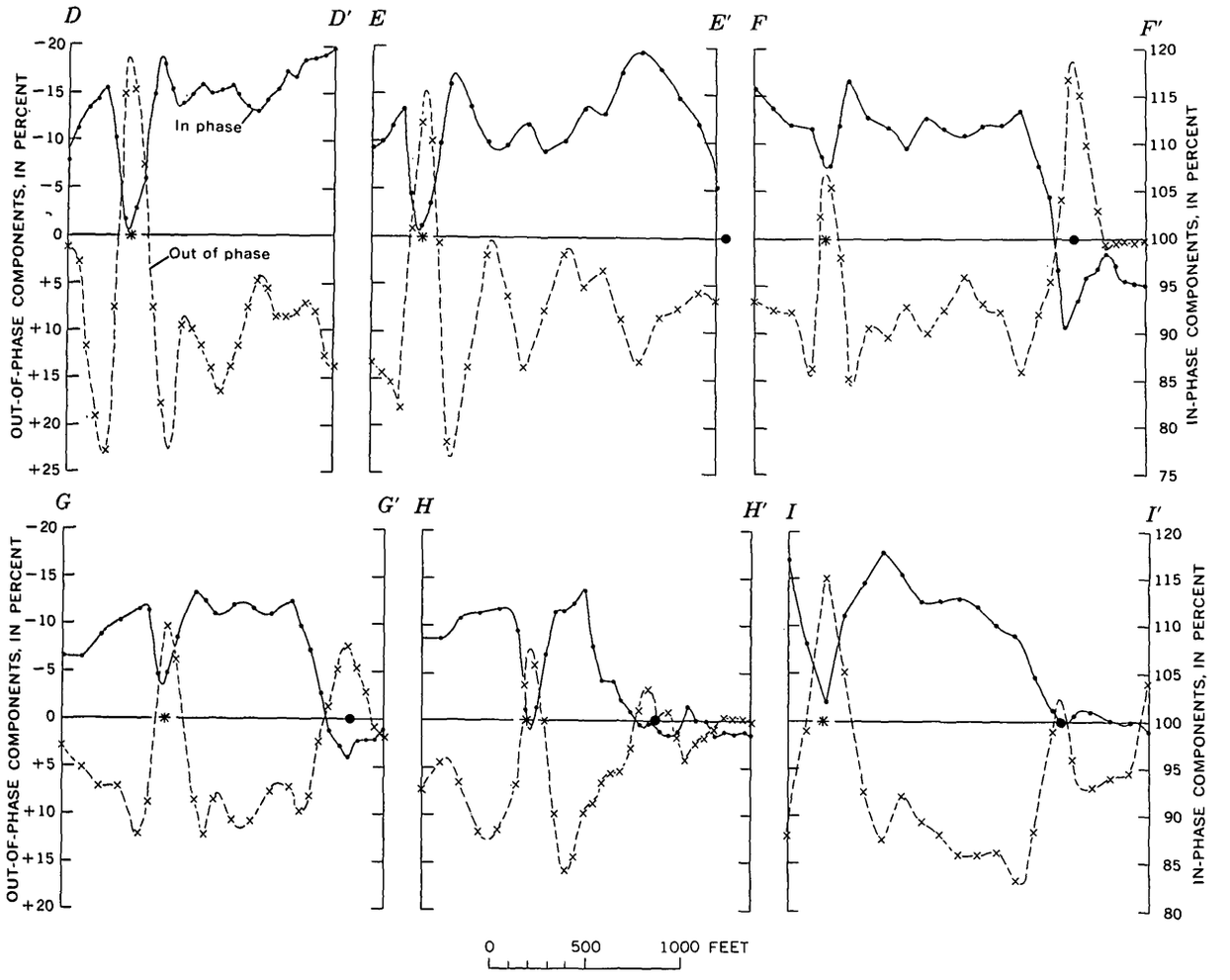

FIGURE 5.—Five slingram profiles made across the general strike of the magnetic source of the northwestern anomaly (traverses *D–D'*, *E–E'*, *F–F'*, *G–G'*, and *H–H'*) and one parallel to the strike (traverse *I–I'*). Asterisk (*), location of narrow and near-vertical conductive zone; large dot, location of flat-lying conductive zone. Location of profiles shown on figure 3.

at the edges. A model curve for a similar rectangular-shaped mass but only 300 feet in vertical extent shown in this figure fits the southwest edge of the field curve better, but the amplitude over the middle of the feature is too low. A model curve of a wedge-shaped mass, 525 feet wide at the top, with the southwest side tapering at 26° to the northeast, and the northeast side vertical and extending to 1,000 feet in depth, fits the leading edge and middle of the field curve better (fig. 7) but, like the other two model curves, does not fit the northeast edge too well.

A possible shape of the general mass in this area, assuming constant polarization, is that of a wedge, the northeast side of which may be some tens of feet deeper than the southwest side. A 1,000-foot or greater depth extent of the mass would suggest that it is intrusive in origin rather than an extrusive flow mass. If the magnetic susceptibility of the rocks increases with depth, the vertical extent of the mass could be shallower.

Electromagnetic data

As a guide to interpreting the slingram profiles, the results were compared with model curves, such as shown in figure 8, and with theoretically derived curves obtained from F. C. Frischknecht (U.S. Geological Survey, oral commun., 1965). Models A and B (fig. 8) represent vertical and inclined narrow-width conductors, respectively. The peak value of the in-phase component is less than 100 percent, and the out-of-phase component is always negative. For the inclined conductor, the shape of the response curves for both components is asymmetrical at the edges of the conductor as noted in figure 8, *B*. For a wide, flat-lying conductor (fig. 8, *C*) the in-phase component is greater than 100 percent and the out-of-phase component is

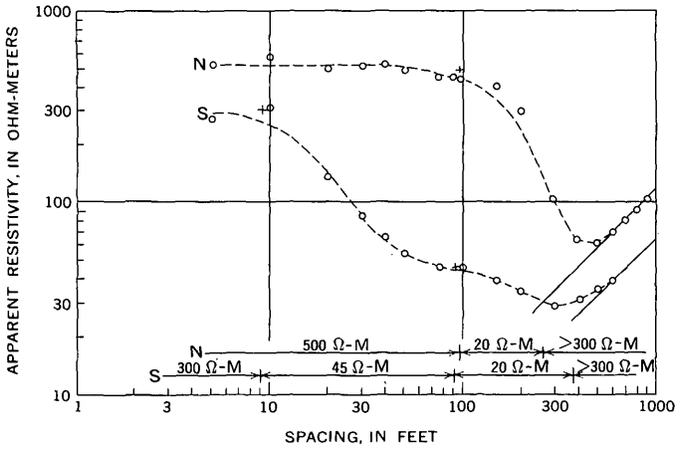

FIGURE 6.—Two resistivity sounding curves, N and S, obtained in the area of the northwestern anomaly, together with a possible interpretation of the electrical layers at these locations (see fig. 3, and text in the section "Discussion of Results"). Ω-M, ohm-meters.

positive over the conductor when the depth of burial is generally greater than about 0.35 times the coil separation. At the edge of the conductor, the responses are opposite in sense (fig. 8).

The edges of the conductive zones indicated on the slingram profiles were matched with these types of model curves; their locations and inferred continuity are shown on figure 3.

For many situations, a quantitative determination of the conductance (product of electrical conductivity and thickness of conductor) and depth of burial may readily be made. Because of the heterogeneous electrical properties of the rocks traversed by these studies, the electromagnetic data do not lend themselves to an accurate interpretation. Measurements at different frequencies and coil separations would lead to a better understanding of the electric section in this area. However, when the resistivity-sounding results are used as a guide, the slingram profiles, particularly in the area to the northeast of the magnetic anomaly, fit a general model of a flat-lying conductive zone greater than 50 feet thick, having a resistivity ranging from about 30 to 15 ohm-meters at a depth of 70 to 100 feet, and overlain by a relatively high-resistivity overburden.

The boundaries of this broad flat-lying conductive zone are fairly well defined along both ends of traverse *A–A′*, along the northwest end of traverse *B–B′*, and along the northeast ends of traverses *E–E′*, *F–F′*, *G–G′*, and *H–H′* (figs. 3 and 5), where both the in-phase and out-of-phase components diminish virtually to their free-space values. This indicates that the conductive zone terminates near the flanks of the outcrop belt of dolomite. The conductive zone is within the general area of the magnetic anomaly and is approximately 3,500 feet long and at least 1,500 feet wide. The southwest ends of traverses *D–D′*, *E–E′*, *F–F′*, *G–G′*, and *H–H′* do not indicate that the conductive zone ends, as both the in-phase and out-of-phase components, over most of these traverses, are still above their free-space value. Near the southwest ends of these traverses, however, there is an anomaly that may indicate a narrow, near-vertical, and shallow conductive zone superimposed on the broader, deeper, and flat-lying conductive zone. This conductor is probably less than 50 feet wide and may have a resistivity of less than 5 ohm-meters. On the basis of the asymmetry of the response curves over this narrow conductive zone, the zone may be inclined to the northeast as the southwest flank of the magnetic body may be inclined.

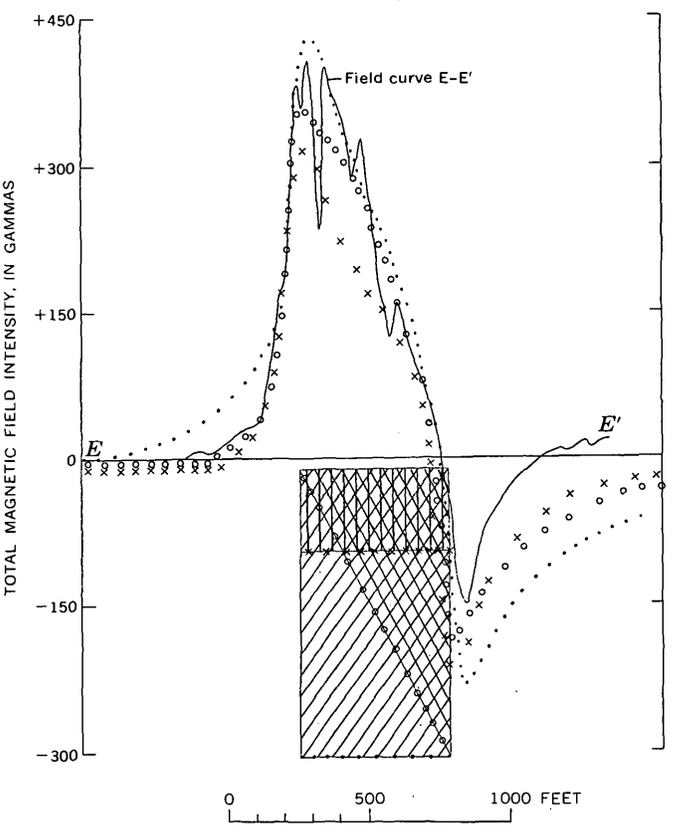

FIGURE 7.—Comparison of the magnetic profile (above) obtained across traverse *E–E′* with model curves (below) computed for three differently shaped two-dimensional bodies. Dots, 1000-foot-vertical-extent rectangular-model curve (outlined by right-slant lines on model); x symbols, 300-foot-vertical-extent rectangular-model curve (outlined by vertical lines on model); open circles, wedge-shaped model curve (outlined by left-slant lines on model). All models 525 feet wide and 25 feet below line of observation. Magnetic susceptibility, 1.4×10^{-3} cgs units; total field, 5.5×10^{4} gammas; inclination, 65°. Strike of model is 65° west of magnetic north.

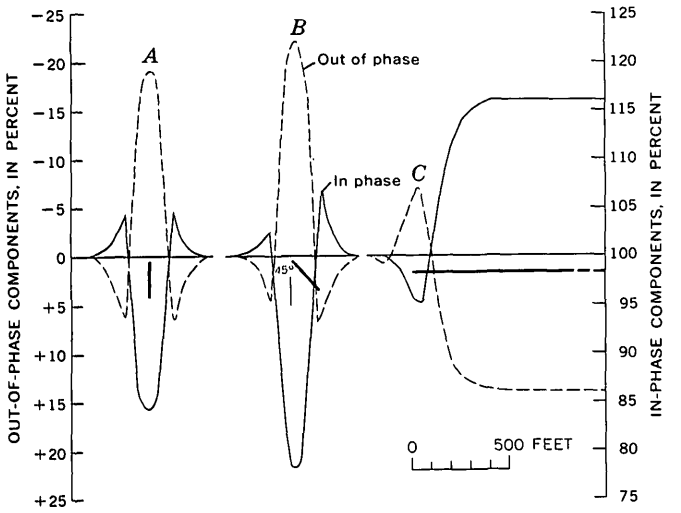

FIGURE 8.—Typical two-dimensional slingram model curves for thin conductive sheets with various orientations (after Frischknecht and Mangan, 1960). Depth to top of conductive sheet for *A* and *B*, 20 feet; for *C*, 80 feet. Length of *A* and *B*, 200 feet. Equivalent conductance for *A* and *B*, 5.4×10^3 mhos; for *C*, 1.52×10^3 mhos. Equivalent coil spacing, 200 feet. Position of conductive sheets indicated by heavy lines.

A definite spatial relationship between this narrow conductive zone and the magnetic body exists which can be seen on figure 3. In detail, the position of this zone is not coincident with the side of the magnetic body, but is offset to the southwest approximately 100 feet.

Along traverse *I–I′* (figs. 3 and 5), two anomalies are noted. The one to the northwest has a phase response similar to those of the electromagnetic anomalies along the southwest side of the magnetic anomaly discussed earlier. This narrow conductive zone is located in a saddle of the magnetic anomaly (fig. 3). This and the other narrow zones apparently are more conductive and shallower than a deeper and less conductive zone which bounds the magnetized rocks. These narrow zones could be the result of a highly porous and altered rock zone, rich in minerals having high ion-exchange capacities and being, therefore, fairly conductive.

The anomaly toward the southeast end of traverse *I–I′* indicates the southeastern extent of the flat-lying conductive zone.

Resistivity and induced-polarization data

The resistivity profiles made along *A–A′* and *C–C′* (fig. 3) show the variability in depth and (or) conductivity of the broad conductive zone (fig. 4). The mean apparent conductivity of the zone along traverse *A–A′* is about 14 millimhos per meter, whereas along *C–C′* the average is approximately 28 millimhos per meter. This would indicate that the conductive zone is much thicker or more conductive southwest of traverse *A–A′*.

The interpretation of the resistivity soundings, N and S (fig. 6), was based on models with horizontal and infinitely wide electrical layers. These assumptions may not be fully warranted, but they do permit a qualitative interpretation of these data.

One possible interpretation for sounding N (figs. 3 and 6) is that it indicates a fairly uniform surface layer that (1) has a resistivity of 500 ohm-meters and a thickness of 95 feet, and (2) overlies a layer with a resistivity of only 20 ohm-meters and a thickness of 165 feet, which in turn overlies a basement of very high resistivity.

Sounding S, in the vicinity of the magnetic feature, indicates a surface layer with a resistivity of about 300 ohm-meters and a thickness of 9 feet, overlying a layer with a resistivity of about 45 ohm-meters and a thickness of 80 feet. From 90 feet to 375 feet a more conductive layer with a resistivity of 20 ohm-meters lies on a basement with a very high resistivity.

A layer with a resistivity of 45 ohm-meters inferred, from sounding S, between 9 and 90 feet from the surface would presumably be in the magnetic rock. This resistivity value is too low for the rock chips recovered from the drill hole, because their interstitial porosity is less than 1 percent and the fracture porosity, which may be quite large, could not render the rock this conductive. Probably, local conductive zones of alteration or weathering near the top of the igneous rocks and adjacent to this sounding are causing lateral effects that make the apparent resistivity appear much less than the true value for the igneous rocks.

The transition between the 20-ohm-meter-resistivity layer and the one above it is too great, at least on sounding N, for one to assume that it reflects the top of the water table. The 45-ohm-meter-resistivity value from sounding S would imply that the water table is much shallower.

Induced-polarization responses obtained along traverses *A–A′* and *C–C′* exceed 200 milliseconds (or millivolt-seconds per volt) in places, the maximum value recorded being 270 milliseconds. Because no additional measurements were made in this or other areas to obtain some measure of the background level, it is not possible to evaluate the significance of these apparently high responses. In general, large responses may result from disseminated sulfides (electrometallic polarization) or from clay-type minerals (membrane polarization) (Marshall and Madden, 1959).

SUMMARY AND CONCLUSIONS

Two areas containing prominent magnetic anomalies were discovered over the alluvial pediment along the southern flank of the Wood Hills in northeastern Nevada. The anomalies in both areas tend to parallel the strike of the exposed dolomite, indicating a possible relationship between the magnetic rocks causing the anomalies and the structure of the underlying Paleozoic carbonate rocks. Some of the anomalies in the southeastern area are polarized in an easterly direction, indicating strong remanent magnetization, whereas the anomalies in the northwestern area are normally polarized. The variance in the magnetic polarization may mean that the source rocks in these two areas are geologically unrelated. An auger hole over the near-surface anomaly in the northwestern area at one place struck quartz latite(?) at a depth of 10 to 15 feet. Chips of this rock contain about 1 to 1.5 percent magnetite, and the magnetic susceptibility of these chips is of the right order of magnitude to account for the magnetic anomaly.

Electric studies made primarily over and near the magnetic anomaly in the northwestern area indicate a broad, low-resistivity zone of about 20 ohm-meters at an approximate depth of 70 to 100 feet from the surface. This zone bounds the magnetic anomaly and is approximately 3,500 feet long and at least 1,500 feet wide. A shallower, narrower, and perhaps more electrically conductive zone borders the southwest flank of the magnetic anomaly. A generalized cross section (E–E') as inferred from these studies is shown in figure 9.

Because of the rather large areal extent and relatively uniform electrical conductance of the flat-lying zone, a possible source for this conductive anomaly is a water-saturated alteration zone containing clay with a high ion-exchange capacity; the rock chips of quartz latite contain altered plagioclase, indicating that alteration zones in the latite may be responsible for the conductive zone. Similarly, the induced-polarization responses over this area, although relatively large, may be caused by membrane polarization which commonly occurs in altered rocks.

Geochemical studies of the soils and caliche in this immediate area did not detect any significant amounts of base metals. It is therefore unlikely that the magnetic and electrical anomalies are associated with a mineral deposit.

REFERENCES

Books, K. G., 1962, Remanent magnetism as a contributor to some aeromagnetic anomalies: Geophysics, v. 27, no. 3, p. 359–375.

Erickson, R. L., and others, 1966, Geochemical reconnaissance in the Pequop Mountains and Wood Hills, Elko County, Nevada: U.S. Geol. Survey Bull. 1198–E.

Frischknecht, F. C., 1959, Scandinavian electromagnetic prospecting: Am. Inst. Mining Metall. Engineers Trans., v. 214, p. 932–937.

Frischknecht, F. C., and Mangan, G. B., 1960, Preliminary report on electromagnetic model studies: U.S. Geol. Survey open-file rept., 12 p.

Keller, G. V., and Frischknecht, F. C., 1966, Electrical methods in geophysical prospecting: New York, Pergamon Press, 517 p.

Marshall, D. J., and Madden, T. R., 1959, Induced polarization, a study of its causes: Geophysics, v. 24, p. 790–816.

Thorman, C. H., 1962, Structure and stratigraphy of the Wood Hills and a portion of the northern Pequop Mountains, Elko County, Nevada: Univ. Washington Ph. D. thesis, 278 p.

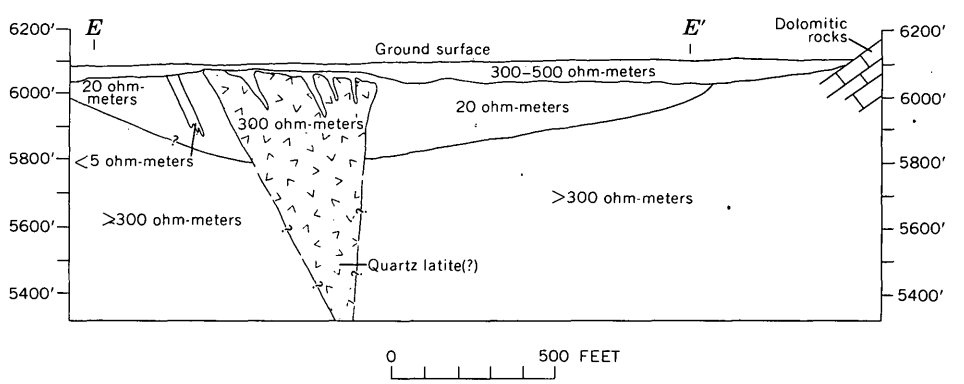

FIGURE 9.—Generalized cross section along traverse E–E' of figure 3, showing the assumed shape of the quartz latite(?) mass, the attitude of the dolomitic rocks, and the electrical-resistivity values of the various zones defined by the electrical surveys.

TIME, SHADOWS, TERRAIN, AND PHOTOINTERPRETATION

By ROBERT J. HACKMAN, Washington, D.C.

Abstract.—To illustrate the effect of sun angle in the photointerpretation of aerial photographs, a plaster terrain model was photographed at 10° increments of illumination, ranging from 70° to horizontal. The resulting photographs show that as the angle of illumination is decreased, tone differences become less apparent. In contrast, the enhancement by shadow effect of the topography, especially the microrelief (texture), becomes more apparent. This study suggests that photographs of the terrain at both high and low sun altitude provide the greatest amount of terrain intelligence for the photointerpreter. If only one picture can be taken, one with the sun angle at approximately 30° is the most satisfactory.

Are we taking aerial photographs at the right time of day to make the best use of shadows in photointerpretation of terrain? According to the "Manual of Photographic Interpretation" (American Society of Photogrammetry, 1960, p. 102–103), shadows may help the interpreter by providing him with profile representation of objects of interest. Shadows are particularly helpful if objects are very small or lack tonal contrast with their surroundings. Under these conditions the contrasting dark tone of shadows may enable the interpreter to identify objects that are otherwise beneath the "threshold" of recognition. Although photographs taken at low angles of illumination have been used in some military, agricultural, and archaeological studies, virtually all photography used in the interpretation of earth terrain (mainly geological and geomorphological studies) is taken with the sun at a high angle.

Most work that has been published concerning the effects of angle of illumination has been with regard to recognizing features on the lunar surface (Baldwin, 1949; Kuiper, 1959; Hackman, 1961; and others). In fact, many of the geologic studies of the lunar surface are made from photographs taken at times of very low sun angle. In comparing the full-moon and half-moon photographs (fig. 1), it is very apparent that more topographic forms are visible near the terminator (sunset zone) on the half-moon photographs than in the same area on the full-moon photograph. In contrast, however, it should be pointed out that differences in tone values, visible on the full-moon photograph, become less apparent as the angle of illumination is decreased, and many are indiscernible near the terminator (Hackman, 1961).

To further illustrate the desirability of using photographs taken with the sun at various angular altitudes, the author undertook a controlled experiment, utilizing a terrain model that could be viewed and photographed at various angles of illumination.

EXPERIMENT DESIGN AND PROCEDURE

The model (fig. 2) used in this study is a plaster cast of part of the U.S. Army Map Service plastic relief map of the Harrisburg, Pa., quadrangle (NK 18-10) (vertical scale exaggerated x 3). This cast was modified by adding some minor topographic and textural details (fig. 2). A tilting platform (fig. 3) was constructed that enabled the model to be photographed at different angles of illumination. To provide near-parallel light (hence, sharply defined shadows), sunlight passing through a small window into an otherwise darkened room was used as a source of illumination.

The model was photographed at angular increments of 10° from the horizontal to 70° with light coming first from the right and then the left. Because the shadow of the camera partly obscured the model at high angles of illumination, photographs were not taken at angles greater than 70°. A press camera and panchromatic film were used to take the model photographs. Prints were made on high-contrast paper.

U.S. GEOL. SURVEY PROF. PAPER 575-B, PAGES B155–B160

241-334 O—67——11

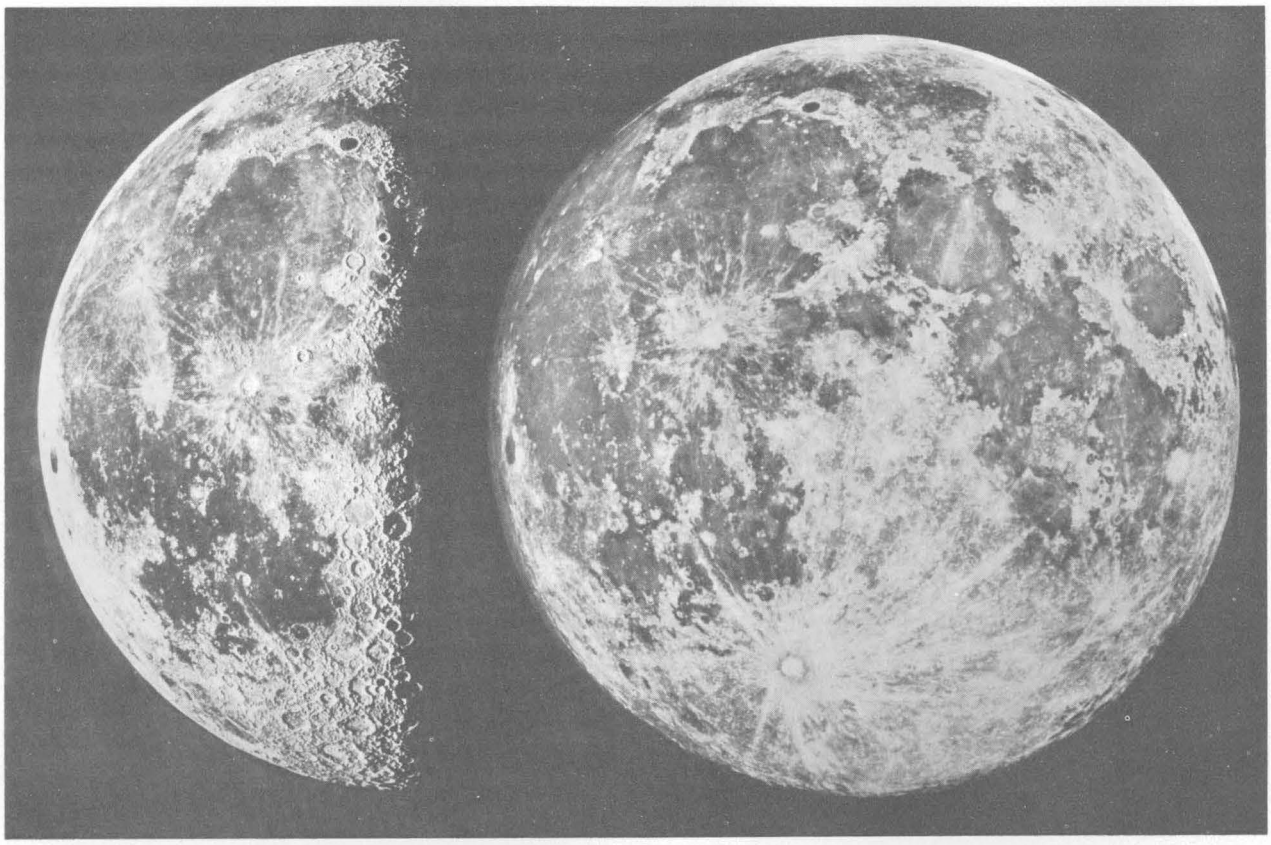

FIGURE 1.—Photographs of the full moon and half moon (3d-quarter phase). On the full-moon photograph the ray patterns are distinct, whereas topographic detail is obscure. On the half-moon photograph, topographic detail is conspicuous, especially along the terminator (sunset zone), whereas many of the ray patterns are not readily distinguishable.

ENHANCEMENT AND TONE CONTRAST

Figures 2, 4, and 5 are 3 of the 16 photographs taken of the model. They are all illuminated by light coming from the same direction but at different angles of illumination. It is readily apparent that, except where obscured by shadow, the photograph taken with an illumination angle of 10° from the horizontal (fig. 4) shows the greatest detail of relief, especially detail of microrelief (texture). Figure 5 is a photograph taken at the highest angle of illumination (70°). In comparing figures 4 and 5, note that most of the fine structure has been enhanced by the shadows and that the edges of the shadows exaggerate the profile shape of features, thus providing data on their ruggedness. The angular sharpness of the surface of the crushed-glass material is certainly apparent from the shadow effect.

The orientation of features, however, strongly affects their appearance on photographs taken at low angles of illumination. For example, the raised ridge, *C*, near the right side of figure 2 is so oriented that it casts no shadow and is, therefore, less apparent than the three similar ridges, also labeled *C*, to the left of it which are oriented obliquely to the direction of illumination and cast strong shadows.

Although only photographs illuminated by light coming from the same direction are shown in the illustrations, photographs of the model under opposite lighting, as would be expected, show similar enhancement.

The crushed-glass material is darker in tone than the surrounding white plaster material on photographs taken with relatively high angles of illumination, that is, 70° (fig. 5) and 30° (fig. 2). But with low angles of illumination, namely 10° (fig. 4), no difference is detectable. This loss of tone contrast at low angles of illumination is in agreement with similar effects observed on lunar photographs.

Terrestrial aerial photographs taken at different times of day are not readily available. However, some were produced in conjunction with recent infrared studies of Kilauea Volcano, Hawaii (Fischer and

FIGURE 2.—Plaster-cast model of part of the U.S. Army Map Service plastic relief map of the Harrisburg, Pa., quadrangle, NK 18-10 (vertical exaggeration × 3). It is shown here at a 30° angle of illumination. Letters *A* through *F* indicate some sculptural and textural detail added to the plaster cast: *A*, circular depressions; *B*, crosshatched and linear grooves; *C*, small ridges; *D*, smooth flat area; *E*, coarse fragments of plaster; and *F*, patch of dark crushed-glass beads. The fine-lined lineations from right to left are brush marks.

others, 1964). These photographs, taken at a scale of 1:10,000 (figs. 6 and 7), are of an area adjacent to the rim of Kilauea crater on the island of Hawaii. Figure 6 was taken at 8:00 a.m., solar altitude 21°, and figure 7 at 11:59 a.m, solar altitude 53°. These two photographs demonstrate the value of photographs taken at times of low sun angle. In figure 6 the minor relief and textural patterns are more easily discernible than in figure 7. Tone differences, however, are more noticeable in figure 7 than in figure 6.

By viewing these protographs stereoscopically the difference in the information content in them can be easily seen. Stereoscopic viewing of photographs taken at different sun angles has been very helpful in lunar studies (Hackman, 1961).

A comparison of figure 6 with a topographic map of the area shows that much of the microrelief is not defined by the 20-foot topographic contours. For example, relief difference of the rugged-appearing lava flow seen at *A* in figure 6 must be as little as a fraction of a foot to a few feet but less than 20 feet, whereas the topographic map with 20-foot contours shows this as a relatively smooth surface.

Figure 8 shows two Gemini V photographs taken over southern Iran. These photographs, although taken as part of a synoptic terrain photographic study (Lowman, 1966), fortuitously demonstrate shadow enhancement resulting from different angles of illumination. Figure 8*A* was taken at approximately 6:00 a.m. (local time in Iran), August 26, 1965, solar altitude 15½°, whereas figure 8*B* was taken at approximately 8:30 a.m., August 22, 1965, solar altitude 30°. It is readily apparent that the lower sun altitude of figure 8*A* results in greater shadow enhancement in delineating the complexly folded structure of the Cenozoic sedimentary rocks in the area.

SUMMARY AND CONCLUSIONS

Investigations using models photographed at different angles of illumination indicate that:

1. Photographs taken of areas with the sun 10° or less above the horizon will show subtle differences in relief and textural pattern that would otherwise be unrecognizable. These photographic subtleties are helpful in many photointerpretation studies. The use of such photography would, of course, be controlled in most cases by the amount of large-scale relief. This photography is commonly more useful in areas of low relief than in areas of high relief because shadows of large topographic elements would obscure too much of the area.

2. As a result of loss of tone values accompanying increased shadow enhancement of microrelief on low sun-angle photographs, the interpreter should use two photographs of the same area—one taken at a high angle of illumination and one at a low angle. These photographs are especially helpful if combinations of high-angle and low-angle photographs are studied stereoscopically.

3. If only one set of photographs can be taken, those taken with a sun angle of 20° to 30° are the most satisfactory.

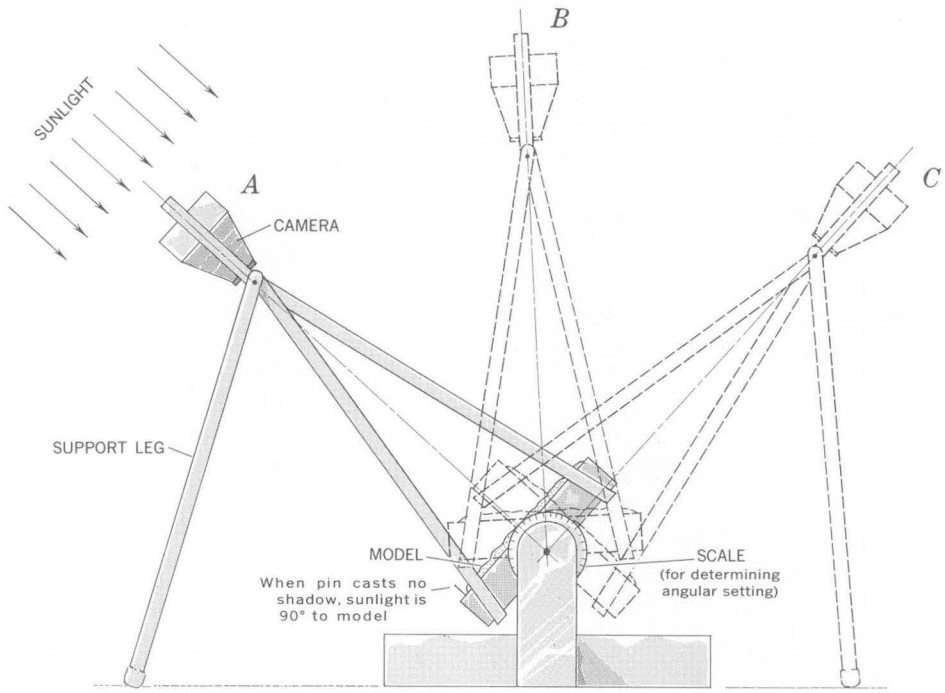

FIGURE 3.—Camera- and model-holding frame. The model can be tilted and photographed under different angles of illumination: *A*, sunlight normal (90°) to plane of model; *B*, sunlight 45° to plane of model; and *C*, sunlight parallel (0°) to plane of model.

FIGURE 4.—Photograph of the model under a 10° angle of illumination.

FIGURE 5.—Photograph of the model under a 70° angle of illumination.

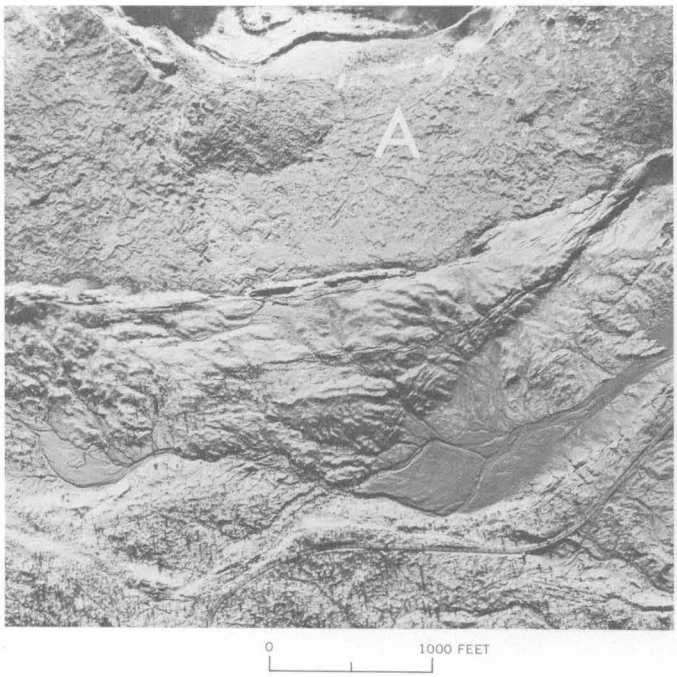

FIGURE 6.—Area adjacent to rim of Kilauea crater, island of Hawaii, photographed with a sun angle of 21° from the horizon. *A*, area of 1921 lava flow.

FIGURE 7.—The same area as figure 6, but with a sun angle of 53° from the horizon.

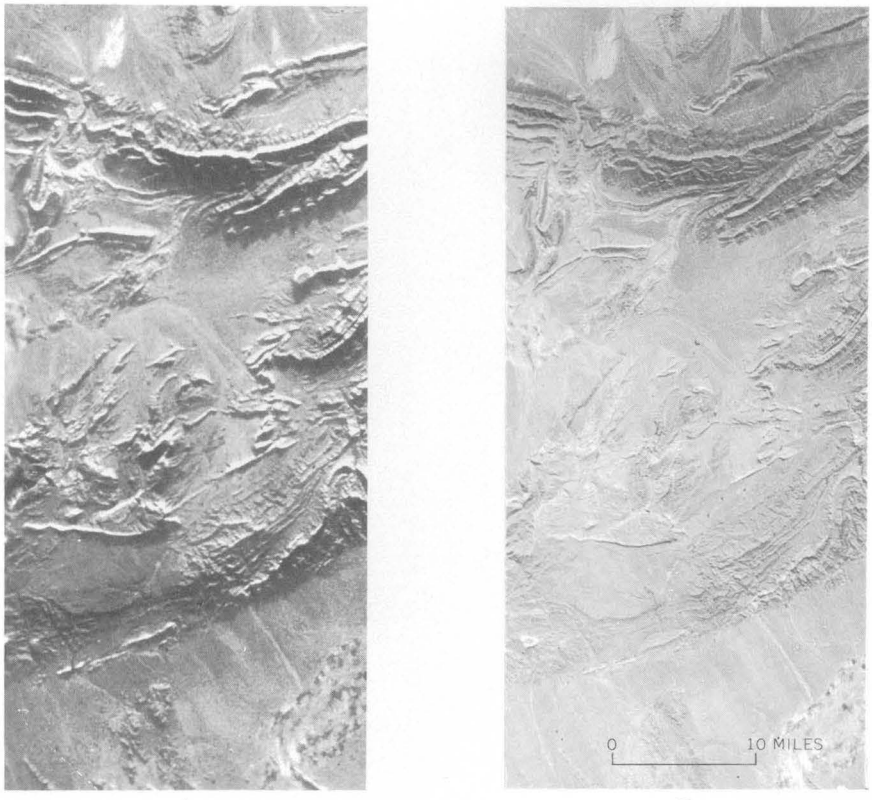

A *B*

FIGURE 8.—Area of Iran covered by two Gemini V photographs, each taken under different angles of illumination. *A*, taken August 26, 1965, solar altitude 15½°. *B*, taken August 22, 1965, solar altitude 30°. (Photography courtesy of the U.S. National Aeronautics and Space Administration, photograph Nos. S–65–45345 and 45480.)

REFERENCES

American Society of Photogrammetry, 1960, Manual of photographic interpretation: Washington, D.C., 868 p.

Baldwin, R. B., 1949, The face of the moon: University of Chicago Press, 239 pages.

Fischer, W. A., Moxham, R. M., Polcyn, R., and Landis, G. H., 1964, Infrared survey of Hawaiian volcanoes: Science, v. 146, no. 3645, Nov. 6, p. 733–742.

Hackman, R. J., 1961, Photointerpretation of the lunar surface: Photogramm. Eng., v. XXVII. p. 377–386.

Kuiper, G. P., 1959, The exploration of the Moon, *in* Vistas in astronautics, v. 2: New York, Pergamon Press, p. 273–312.

Lowman, P. O., 1966, Experiment S–5, Synoptic terrain photography, *in* Manned space-flight experiments, interim report, Gemini V mission: Natl. Aeronautics and Space Adm., Goddard Space Flight Center, Greenbelt, Md., p. 9–17.

THE PHOTOELECTRIC DETERMINATION OF LITHIUM

By SOL BERMAN, Washington, D.C.

Abstract.—The strong reversal of the Li 6707.84A line with increasing lithium concentration in spectrochemical analyses is reflected in a calibration curve with intensity first increasing with concentration, passing through a maximum, and finally decreasing. This problem is avoided by widening the exit slit of the spectrograph and "reading" the entire broadened line, as shown in studies on synthetic biotite. Lithium can then be determined in the range from 0.0001 to 0.02 percent with excellent precision by a direct-reading d-c arc spectrochemical method using a gas-jet controlled atmosphere of oxygen and argon.

In low concentrations (0.0001–0.02 percent), lithium is determined spectrochemically in powdered solid samples with the 6707.84A line. As the concentration of lithium is increased to a few hundredths of a percent, the analytical line exhibits self-reversal and at 1 percent this line is extremely broad. When determined photographically, these phenomena are readily recognized. To circumvent these difficulties, either another line such as lithium 3232.61A is substituted at the higher concentrations, or a line-width measurement is made in place of an optical-transmission or density measurement. If a receiving slit of a width within the same order of magnitude as the entrance slit is used for direct-reading observations, erroneous results may be obtained with the 6707.84A line. As the lithium content of the sample increases, the observed intensity increases to a maximum and then decreases. Thus, two very different concentrations of lithium produce the same observed result.

Previous standard methods for determining lithium in rocks and minerals have utilized flame-photometric and spectrographic techniques (Ahrens and Taylor, 1961; Bastron and others, 1960; American Society for Testing Materials, 1964; Dean, 1960; and Vinogradov and Ryabchikov, 1962). In a survey of photoelectric methods by Krondrasheva and others (1955), a method was given in which lithium was determined photoelectrically at 4972.0A in the visible (green) portion of the spectrum.

The purpose of this investigation was to determine lithium over a large analytical range, using only one line. Because the determination of lithium is greatly affected by the matrix, a synthetic biotite was prepared to test the method.

APPARATUS AND REAGENTS

Apparatus

Electrode assembly:
- Upper electrode: Cathode, UC–1964.
- Lower electrode: Anode, UC–1590.
- Analytical gap: 4 mm.
- Atmosphere: 80 percent argon, 20 percent oxygen.
- 6.6 l/m (argon gage).
- Gas jet (Helz, 1964).

Excitation source: Direct-current arc; 5 amps and 15 amps; open-circuit voltage, 220.

Spectrograph: 3.4-meter, Ebert convertible spectrograph with direct-reading head. For external optics a cylindrical lens (f=450 mm), axis horizontal, is used to focus the source on the collimator.
- Slit height: 10 mm.
- Entrance-slit width: 50 microns.
- Exit-slit widths: 100 microns for the sodium line and 1 mm for the lithium line.
- Filters: Corning filter No. 3387, color spec. 3–72, visible transmitting, in front of the lithium receiving tube. Corning filter No. 9863, color spec. 7–54, ultraviolet transmitting, in front of the sodium receiving tube.

Phototube multipliers: (2) RCA–1P28, spectral response S–5.

Exposure timing:
- Prearc: None.
- Exposure: 10 sec at 5 amps plus 110 sec at 15 amps.

Analytical line: Lithium (I) 6707.84A.

Internal standard line: Sodium (I) 3302.323A.

Reagents

1. National Bureau of Standards, standard sample 183 lithium ore (lepidolite).
2. Synthetic biotite matrix made from purified crystal quartz, Specpure oxides of aluminum, iron, magnesium, titanium, and manganese, and Specpure carbonates of calcium, sodium, and potassium.

U.S. GEOL. SURVEY PROF. PAPER 575–B, PAGES B161–B163

The composition of the "biotite" matrix is given below.

Compound	Percentage	Compound	Percentage
SiO_2	36.10	Na_2O	0.20
Al_2O_3	15.30	K_2O	9.10
Fe_2O_3	30.20	TiO_2	2.70
MgO	5.70	MnO	.50
CaO	.20		

PROCEDURE

1. Weigh out the pure compounds for the matrix into an agate mortar and thoroughly mix and grind into a homogeneous powder.

2. Dilute the NBS–183 standard containing 1.92 percent lithium with the matrix to 1 percent lithium and from this prepare a series down to 0.0001 percent lithium using the reciprocal of the cube root of 10 (0.4642) as the dilution factor.

3. Mix and grind thoroughly all standards with sodium carbonate in a boron carbide mortar in a 1:1.5 ratio.

4. Arc 25-milligram portions of the standards (0.0001–0.02 percent Li) and the matrix in duplicate in a gas jet with a controlled atmosphere consisting of 20 percent oxygen and 80 percent argon. Samples for analyses are mixed, ground, and arced in the same manner as the standards.

5. To obtain the analytical curve, read the intensities of lithium and sodium from the standards and matrix. Calculate the lithium sodium ratios and correct for the matrix blank. Plot the log intensity ratio versus log concentration.

6. To determine the lithium concentration obtain the intensities of lithium and sodium from the samples photoelectrically and calculate the lithium sodium ratio. Lithium concentrations can then be read directly from the analytical curve.

RESULTS

1. *Lithium intensity as a function of concentration.*—A plot of the lithium intensity as a function of concentration is given in figure 1. Data were obtained with a 1-mm receiving slit. (Usually the width of the exit slit is twice or half that of the entrance slit.) The line is fairly linear from 0.0001 to 0.01 percent lithium, still shows some effects of self-reversal in the approximate range of 0.01 to 0.5 percent, and at the latter point again becomes linear up to 2 percent. Thus, lithium can be determined throughout the entire range without the possibility of errors associated with self-reversal. In practice the samples whose lithium contents occur in the higher ranges are diluted with the matrix so that the lithium response then falls on the linear part of the curve.

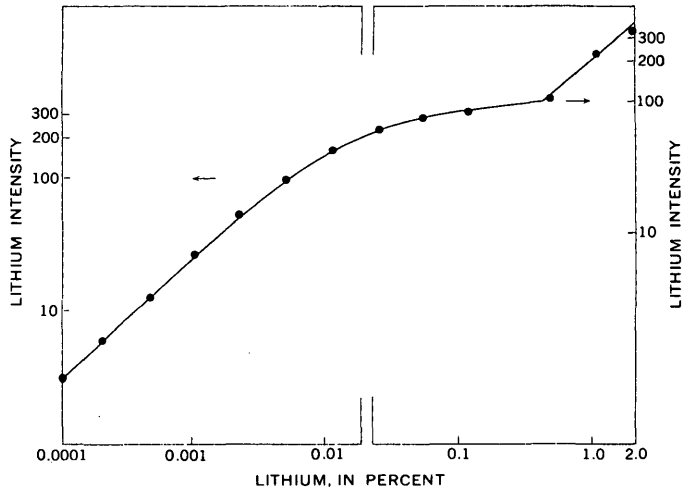

FIGURE 1.—Variation of lithium intensity with varying lithium concentration.

2. *Detector.*—Because of the difficulty of installing special red-sensitive tubes and the unavailability of these tubes in the more common 11-pin base mounting, a 1P28 (RCA) multiplier phototube was used; it proved successful even though the lithium line is near the limit of the spectral sensitivity of this tube.

3. *Precision and accuracy.*—To determine precision, duplicate determinations were made on nine standards. Estimates for the coefficient of variation for lithium and sodium intensities and the Li:Na ratios are listed in table 1.

TABLE 1.—*Precision of line intensities*

Element	Pairs of determinations	Coefficient of variation (percent)
Na	9	1.7
Li	9	1.8

Results by direct reading are compared with those obtained by flame photometry in table 2. The average difference between the methods is approximately 4 percent.

TABLE 2.—*Comparison of results by independent methods*

Biotite	Flame photometer Li (percent)	Direct-reading Li (percent)
1	0.013	0.012
2	.0060	.0059
3	.040	.041
4	.021	.022

REFERENCES

Ahrens, L. H. and Taylor, S. R., 1961, Spectrochemical analysis, 2d. ed.: Reading, Mass., Addison Wesley Pub. Co., Inc., 454 p.

American Society for Testing Materials, 1964, Methods for emission spectrochemical analysis, 4th ed.: Philadelphia, Pa., 862 p.

Bastron, Harry, Barnett, P. R., and Murata, K. J., 1960, Method for the quantitative spectrochemical analysis of rocks, minerals, ores and other materials by a powder d-c arc technique: U.S. Geol. Survey Bull. 1084–G, p. 165–182.

Dean, V. A., 1960, Flame photometry; New York, McGraw Hill Book Co., 354 p.

Helz, A. W., 1964, A gas jet for d-c arc spectroscopy: Art. 159 *in* U.S. Geol. Survey Prof. Paper 475–D, p. D176–D178.

Krondrasheva, L. D., Podmoshensku, I. V., and Prokof'ev, V. K., 1955, Fotoelektricheskiye metody emissionnogo spektral'-nogo analiza [Photoelectric methods of emission spectrum analysis]: Zavodskaya Lab., v. 21, p. 1446–1455.

Vinogradov, A. P. and Ryabchikov, D. I., 1962, Metody opredelniya i analiza redkikh elementov [Detection and analysis of rare elements]: Akademiya Nauk SSSR. Institut Geokhimii 1 Analiticheskoi Khimii im., V. I Vernadskogo (Translation published for the Natl. Sci. Foundation, Washington, D.C., and the U.S. Dept. Commerce, by the Israel Program for Scientific Translations, Jerusalem, 1962).

A COMPARISON OF POTASSIUM ANALYSES BY GAMMA-RAY SPECTROMETRY AND OTHER TECHNIQUES

By C. M. BUNKER and C. A. BUSH, Denver, Colo.

Abstract.—A combination of mathematical and graphical interpretation techniques, applied to gamma-ray spectra obtained from whole-rock samples, minimizes interfering effects of other radioisotopes and differences in sample size, weight, and density. With the present detection system, a minimum potassium concentration of about 0.10 percent is required to provide an adequate spectrum for quantitative interpretation. The coefficient of variation of 1-percent increments in a range of 0.10 to 3.4 percent K is 7.5 to 1.1 percent; the coefficient of variation for all samples is 2.68 percent.

Potassium analysis was included in a series of investigations on radioelement analyses by gamma-ray spectrometry to improve previously reported techniques and to determine the sensitivity and reliability of systems and methods used by the authors. Such radioelement analyses have important geological applications because they may (1) aid age determinations, (2) be used as an exploration method for locating hydrothermally altered host rock containing nonradioactive ore minerals (Moxham and others, 1965), and (3) provide radioelement data required for studies of heat flow.

Potassium is the only light element amenable to analysis by gamma-ray-spectrometer measurements of natural radioactivity. The presence of potassium in a sample is determined by measuring the 1.46-million electron volt (Mev) gamma ray emitted by K^{40} as it decays to Ar^{40}. The K^{40} constituent of natural potassium is virtually constant at about 0.0118 percent; therefore, the potassium element content can be determined by measuring the radioisotope content from the radiation intensity (peak amplitude) of the K^{40} energy.

Gamma-ray-spectrometer measurements provide an independent and nondestructive analytical technique which has several advantages over other types of measurements. Sample preparation is limited to crushing and weighing, and no chemistry is involved. The use of samples weighing a few hundred grams permits analysis of a more easily obtained representative sample than the smaller amounts that are used for other types of analytical methods. The method has been used for several years; techniques for radioelement analyses have been described by Hofstader and McIntyre (1950), Kahn and Lyon (1953), Hurley (1956), Adams and others (1958), Mero (1960), and Moxham and others (1965). The technique described here is similar to that used by previous investigators inasmuch as the 1.46-Mev gamma-ray energy from K^{40} is used for the analysis, but the technique differs in the method of interpretation. The present interpretation method minimizes interfering effects of other gamma-ray energies on the 1.46-Mev energy peak and the effects of different sample volumes, weights, and densities.

Acknowledgments.—The aid of H. A. Tourtelot, who furnished 105 samples of Upper Cretaceous Pierre Shale or its stratigraphic equivalents and made available the chemical analyses for potassium of these samples, is gratefully acknowledged.

INSTRUMENTATION AND OPERATIONAL PROCEDURES

The spectrometer system consists of two 5-inch-diameter by 4-inch-thickness NaI crystal detectors, each viewed by a 5-inch-diameter photomultiplier tube; a a 400-channel pulse-height analyzer, a recorder that plots counts against an energy scale; and a paper-tape punch and tape reader to record background data. A characteristic trace of the gamma-ray spectrum thus obtained is shown in figure 1. Each photomultiplier-tube-crystal unit is connected to separate halves of the pulse-height analyzer to permit simultaneous analyses of two samples. Each detector is centered in a lead box 4 inches thick and having internal dimensions of 20 inches on a side and 26 inches high.

The data accumulation time varies according to the radiation intensity of each sample; for operational

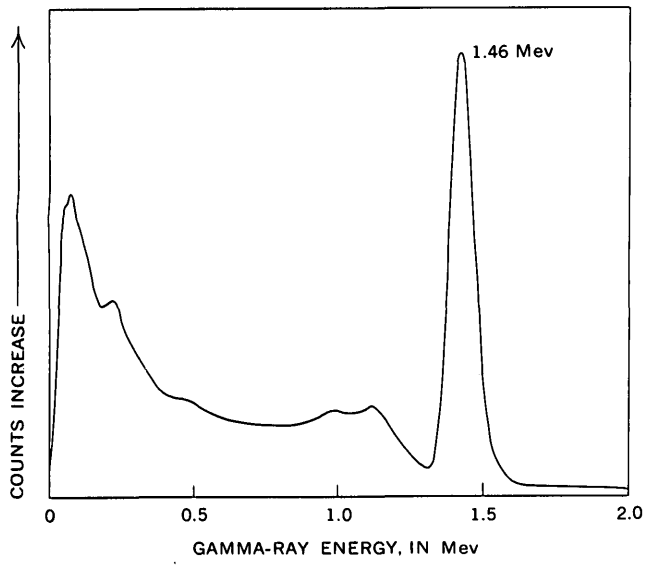

FIGURE 1.—Gamma-ray spectrum of K^{40} in 400-g sample of K_2CO_3, 56.58 percent potassium.

convenience, time is recorded in steps of 100, 400, or 1,000 minutes. The 1,000-minute analyses are required for samples containing less than 0.5 percent K and are run overnight for expediency. Samples that require counting for more than 1,000 minutes can be analyzed more efficiently by other techniques.

The spectrometer system is adjusted to accept gamma-ray energies from 0 to 2.0 Mev. This range includes the gamma rays from K^{40}, most of those from U and Th daughters, and most fission products in fallout. Although only K analyses are discussed here, other radioisotopes are measured from the same spectra. A background spectrum based on a sample of quartz flour or barium sulfate, of virtually the same size and weight as the unknown sample, is subtracted from the measured spectrum. This spectrum is accumulated in 200 channels of the analyzer. At the end of sample measurement, the net spectrum is recorded in counts versus energy (Mev) and is punched on the tape. The gamma-ray-energy peak amplitudes are measured on the trace of counts versus energy.

Samples are crushed to less than about 8 mesh, weighed, enclosed in thin-walled plastic containers with lids, and sealed with tape to prevent radon (Rn^{222}) and thoron (Rn^{220}) loss. Sample sizes differ depending on the amount of material available. Nominal 200-gram samples are put in containers 3 inches in diameter and 1 inch in depth. Larger samples are put in containers 6 inches in diameter and about 1.5 inches in depth.

CALIBRATION AND INTERPRETATION METHODS

The gamma-ray-spectrometer system is calibrated by relating, quantitatively, the peak amplitude to known quantities of potassium. Factors, in addition to the potassium content in samples, that affect the peak amplitude include: internal characteristics of the system; dimensions, weight, and density of the sample; and the distance between the sample and the detector. The effects of these parameters are determined empirically from samples of different sizes, weights, densities, and potassium content. The effect of distance between sample and detector is eliminated by placing all samples on the detector.

Artificial standards are prepared for calibrating the spectrometer system by mixing potassium compounds (KCl, K_2CO_3, $K_2Cr_2O_7$) with borax, sand, or dunite to obtain different potassium concentrations and densities. These are split into several weight increments and placed in standard-size sample containers. Several rock samples, containing also uranium and thorium, that had been analyzed by other techniques, were used to verify and supplement the results obtained from the artificial standards.

A portion of the spectrum from 1.0 to 2.0 Mev that includes the K^{40} energy peak is shown in figure 2. A consistent method for determining the amplitude of this peak is necessary for quantitative interpretation. Spectra from samples containing only potassium can be interpreted adequately by measuring the peak amplitude from the x axis, which represents zero counts, and relating the amplitude to potassium content with a cali-

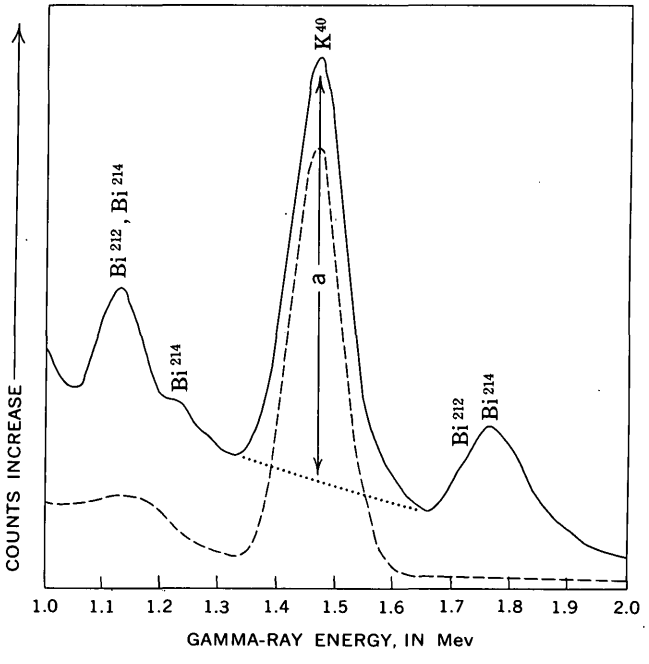

FIGURE 2.—Partial gamma-ray spectrum of K (dashed line) and mixture of same quantity of K in multienergy U and Th daughter radioisotopes (solid line). Peak amplitude (a) is measured between adjusted baseline (dotted) and top of peak.

bration curve; this is the method used by previous investigators. Spectra from samples containing other radioisotopes which emit energies greater than 1.46 Mev cannot be interpreted as accurately in the same way because these energies cause an apparent increase in the K^{40} peak as a result of Compton scattering and additional beta radiation. As an example, spectra of uranium and thorium daughter products Bi^{212} and Bi^{214} were added to the K^{40} spectrum to simulate the spectrum from a rock sample (fig. 2). The gamma-ray spectrum of a sample containing several radioisotopes is characterized by a series of peaks and valleys (minima) which represent the presence and absence, respectively, of individual gamma-ray energies. Most of the minima lie on a line which curves upward toward the zero energy end of the spectrum; some do not depress to the line because the energy resolution of the system does not permit complete separation of energies in close proximity. In the present interpretation method, a line is drawn through the minima near the K^{40} peak (fig. 2) to establish an adjusted baseline from which the peak amplitude is measured. The controlling minima are not necessarily adjacent to the 1.46-Mev peak. The peak amplitudes above this adjusted baseline are not affected by beta activity or by any gamma-ray scattering that does not create a spurious energy peak; therefore, this adjusted baseline minimizes these potentially interfering effects.

The relation between counting rate and potassium content in samples of virtually the same weight and density is a straight line with a slope of one (fig. 3). This relation permits the periodic use of a few standards to determine whether changes in instrument response have occurred and to adjust the analyses accordingly. Standardization checks are made intermittently during a series of sample analyses.

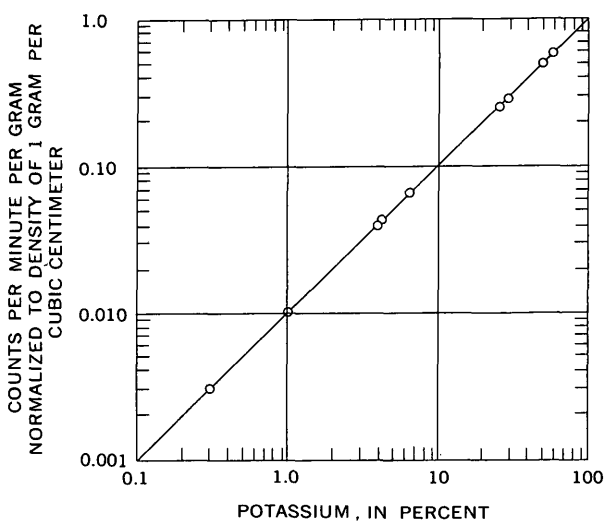

FIGURE 3.—Relation between counting rate and potassium content in samples of same weight and density.

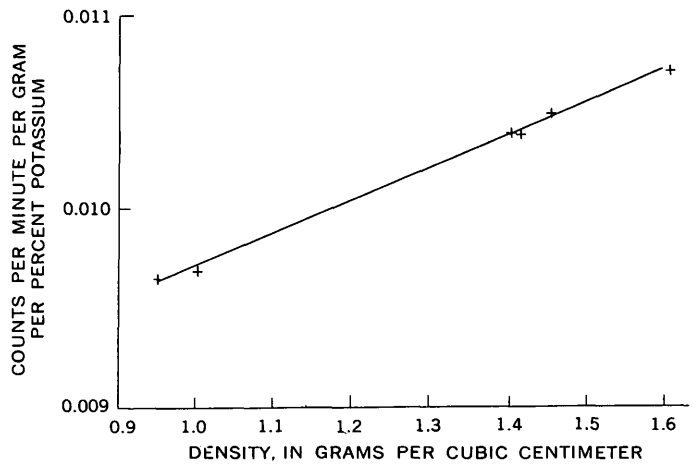

FIGURE 4.—Effect of density of sample on counting rate obtained with 400-g samples.

The relation between the density of the sample and counting rate was determined empirically with a group of 400-g samples (fig. 4). Increasing the density of the sample causes in increase in counting rate.

A calibration chart consisting of a series of calibration curves obtained from the standard samples (fig. 5) is used for interpreting potassium content of samples containing unknown quantities of the radioelement.

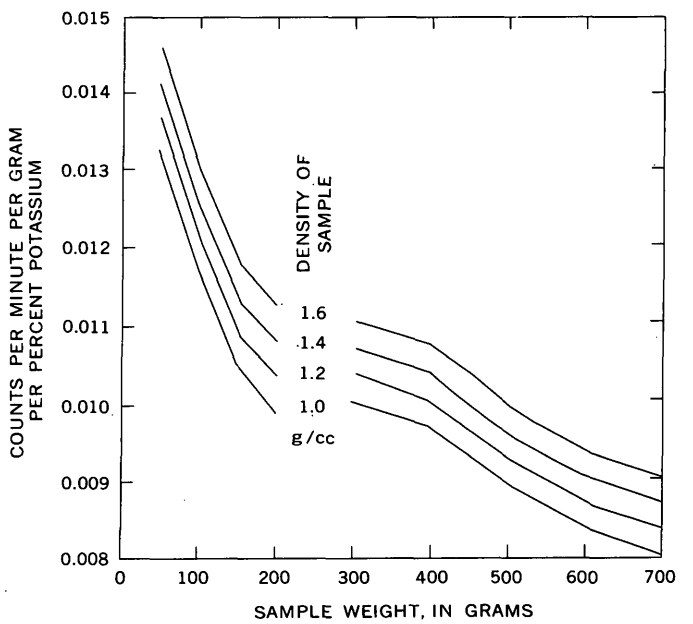

FIGURE 5.—Calibration chart relating counting rate, sample weight, and density of sample. Samples weighing 50–200 g are in containers of 3-inch diameter and 1-inch depth; 300–700-g samples are in containers of 6-inch diameter and 1.5-inch depth.

The sample weight is measured, the density is estimated from the volume occupied in the sample container, and the peak amplitude (in counts) is measured from the gamma-ray spectrum. The potassium concentration in the sample is determined using the equation

$$\text{K (percent)} = \frac{\text{Net counts/minute/gram (sample)}}{\text{Counts per minute/gram/percent K (standard)}}$$

in which the denominator is obtained from the calibration chart (fig. 5).

RESULTS

Samples of Pierre Shale, or its stratigraphic equivalents, were analyzed by gamma-ray spectrometry to verify the validity of the interpretation method and to determine detection limits, accuracy, and sensitivity. Splits of these samples had been analyzed previously for K_2O content by rapid rock or standard rock techniques; these are reported by 2-digit and 3-digit numbers, respectively. For this study, the chemical analyses were treated as unequivocally correct. A comparison of the results from the two types of analyses is shown in table 1. Two 200-g samples contained less than 0.10 percent K and were eliminated from statistical evaluations because the peak amplitudes in the spectra were too small to be interpreted; one sample was eliminated because the difference in K concentrations was too large to be related to the analytical technique.

The relation between the potassium values determined by gamma-ray spectrometry and by chemical techniques ($K_{\gamma\ spec.}/K_{chem.}$) in table 1 indicates the ratio between the two potassium values. A ratio of 1.03 indicates a 3 percent higher value determined from the spectrometer data than was determined by chemical analysis. The 2-digit numbers provided by the rapid rock analyses in the range of potassium concentrations in the Pierre Shale samples preclude calculating realistic differences less than about 4 percent and, in low concentrations, exclude some calculated differences less than 9 percent, as for example, 1.1/1.2. This may explain the nonnormal distribution of differences shown in figure 6. A cumulative curve shows the differences (regardless of sign) between the two sets of data (fig. 7). Ninety-five percent of the sample analyses (the 95-percent confidence level) obtained by gamma-ray spectrometry agree within 8 percent of the analyses by other techniques. Standard deviations and coefficients of variation for these sets of data are:

K concentration (percent)	Standard deviation	Coefficient of variation (percent)
0. 10–3. 4	0. 0538	2. 68
0. 10–0. 99	. 0190	7. 5
1. 00–1. 99	. 0378	2. 25
2. 00–2. 99	. 0620	2. 76
3. 00–3. 4	. 0351	1. 10

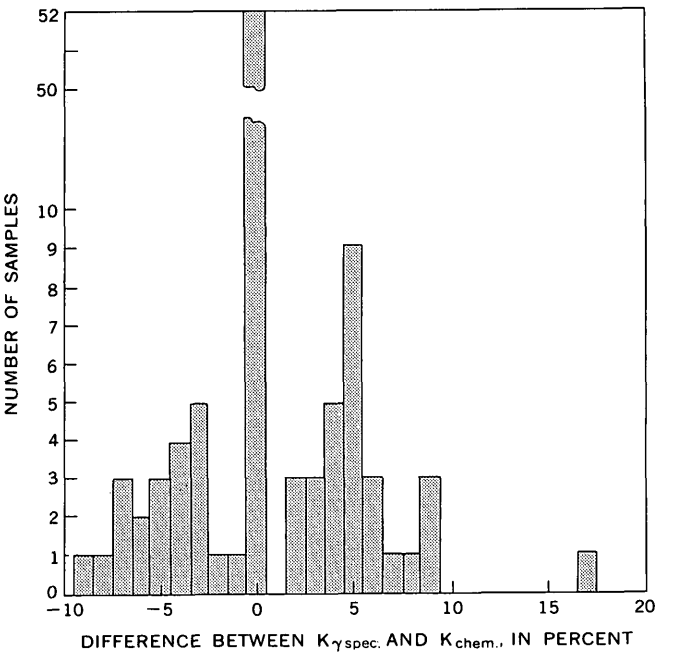

FIGURE 6.—Distribution of difference between potassium analyses by gamma-ray spectrometry and by other analytical chemical techniques. Negative values along abscissa indicate that gamma-ray spectroscopic analysis for K was lower than that obtained by other analytical chemical techniques; positive values indicate the K analyses were higher by gamma-ray spectrometry.

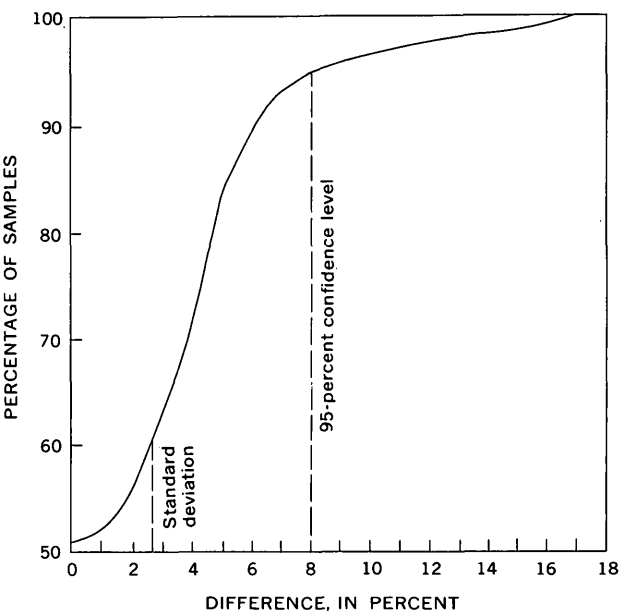

FIGURE 7.—Cumulative relationship of percentage of samples and absolute difference between potassium content determined by gamma-ray spectrometry and by other analytical chemical methods for 102 samples.

TABLE 1.—*Comparison of potassium content of samples of Pierre Shale or its stratigraphic equivalents, by chemical analyses and by gamma-ray spectrometry*

Sample No.	Weight (g)	K analyses (percent)		$K_{\gamma\ spec.}/K_{chem.}$
		Chem.	γ spec.	
WYOMING				
Salt Creek				
D516	415.5	2.4	2.41	1.00
D517	409.5	2.1	2.10	1.00
D518	430.6	2.1	2.10	1.00
D519	393.5	1.6	1.67	1.06
D520	473.2	1.5	1.53	1.00
D521	450.9	2.0	2.01	1.00
D522	131.1	1.2	1.32	1.08
D523	494.7	1.9	1.91	1.00
D524	401.1	1.6	1.61	1.00
D525	504.7	2.0	2.04	1.00
D526	433.1	2.31	2.23	.97
D527	460.1	2.0	1.94	.95
D528	400.0	.13	.13	1.00
D529	512.7	2.1	2.22	1.05
D530	457.3	1.5	1.54	1.00
D531	497.0	2.2	2.21	1.00
MONTANA				
Hardin area				
D534	430.3	2.3	2.25	1.00
D535	400.8	.15	.141	.93
D536	388.1	1.5	1.47	1.00
D537	463.8	2.31	2.40	1.04
D538	359.6	1.2	1.18	1.00
D539	471.1	2.2	2.26	1.05
D540	485.5	2.2	2.31	1.05
D541	360.2	1.8	1.77	1.00
D542	419.2	1.9	1.98	1.05
D543	446.2	1.7	1.71	1.00
Porcupine dome				
D546	396.3	2.6	2.54	0.96
D547	530.4	2.2	2.22	1.00
D548	442.6	2.6	2.53	.96
D549	585.6	.36	.33	.92
D550	467.3	2.0	2.14	1.05
D551	459.2	1.9	1.93	1.00
D552	484.8	2.11	2.12	1.00
D553	438.1	2.0	2.01	1.00
D554	477.2	2.2	2.19	1.00
D555	500.0	2.2	2.20	1.00
D556	523.6	2.2	2.41	1.09

Sample No.	Weight (g)	K analyses (percent)		$K_{\gamma\ spec.}/K_{chem.}$
		Chem.	γ spec.	
MONTANA (CON.)				
Woman's Pocket				
D600	510.0	2.6	2.59	1.00
D601	521.1	1.7	1.74	1.00
D602	400.8	.32	.328	1.03
D603	538.1	2.2	2.41	1.09
D604	568.9	2.8	2.81	1.00
D605	602.1	2.0	2.05	1.00
D606	528.7	2.0	2.07	1.05
D607	582.6	1.9	1.92	1.00
D608	480.1	1.7	1.57	.94
D609	411.6	1.9	1.93	1.00
D610	602.9	1.84	1.78	.97
Livingstone				
D638	400.0	2.1	2.19	1.05
D639	400.3	2.5	2.58	1.04
D640	461.6	2.2	2.26	1.05
D641	400.0	1.8	1.78	1.00
D642	400.0	1.9	1.98	1.05
D643	486.6	1.44	1.48	1.03
D644	609.5	3.4	3.37	1.00
D645	570.4	2.2	2.16	1.00
D646	500.0	2.0	2.02	1.00
Dearborn River				
D649	373.1	2.5	2.40	0.96
D650	578.7	2.7	2.72	1.00
D651	500.0	3.2	3.21	1.00
D652	350.0	2.1	2.10	1.00
D653	479.4	1.7	1.73	1.00
D564	401.8	3.2	3.18	1.00
D655	398.9	2.3	2.34	1.00
D656	500.3	3.04	2.93	.96
D657	566.6	2.6	2.66	1.04
D658	538.5	2.2	2.17	1.00
SOUTH DAKOTA				
Missouri River (Oahe Dam)				
259538	200.0	1.3	1.34	1.00
259540	373.0	1.7	1.68	1.00
259543	200.0	2.32	2.31	1.00
259545	409.9	2.2	2.26	1.04

Sample No.	Weight (g)	K analyses (percent)		$K_{\gamma\ spec.}/K_{chem.}$
		Chem.	γ spec.	
SOUTH DAKOTA (CON.)				
Missouri River (Chamberlain)				
259547	371.5	2.70	2.50	0.93
548	200.0	.30	.35	1.17
549	289.1	1.89	1.90	1.00
550	183.9	1.7	1.73	1.00
551	352.2	1.4	1.42	1.00
552	366.8	1.8	1.83	1.00
553	144.0	1.42	1.52	1.07
555	366.0	1.8	1.94	1.06
Missouri River (Wheeler Bridge)				
259556	200.3	2.03	1.98	0.97
558	401.4	2.18	1.98	.91
559	386.7	2.12	2.08	.98
560	397.4	1.7	1.64	.94
561	350.0	2.7	3.09	1.15
562	450.0	2.2	2.15	1.00
563	100.7	2.80	2.90	1.03
Black Hills (Hot Springs and Red Bird)				
259569	357.6	2.2	2.42	1.09
570	353.2	2.0	2.02	1.00
571	200.0	2.2	2.20	1.00
573	200.0	2.2	2.14	.95
574	200.0	2.5	2.60	1.04
575	200.0	2.23	2.16	.97
576	200.0	3.15	3.20	1.02
577	200.0	2.50	2.43	.97
578	400.0	1.95	1.93	.99
579	215.1	2.07	1.92	.93
580	359.5	2.11	2.16	1.02
581	388.9	2.31	2.19	.95
582	150.0	1.90	1.94	1.02
Black Hills (Owl Creek)				
259589	361.9	1.8	1.86	1.06
590	365.0	2.0	2.04	1.00
591	396.4	1.6	1.56	1.00
594	449.3	2.3	2.28	1.00

The average potassium concentrations in all samples determined chemically and by gamma-ray spectrometry are 2.01 and 2.02 percent, respectively. These measures of precision are smaller than those for X-ray spectrometry for K-Ar age determinations (Wanless and others, 1965). Therefore this method provides data adequate for K-Ar age determinations when samples of sufficient size are available; the results are probably adequate for most other applications of K-analyses.

The lower limit of detection is related directly to the interdependent factors of radiation intensity of the K^{40} energy (because an energy peak of sufficient amplitude to work with must be obtained) and data-accumulation time. Another limiting factor is the presence of a peak which obscures the K^{40} energy peak. Because geologic studies require analyses of natural radioisotopes with a wide range of ratios, establishing detection limits with only one radioisotope present in a sample results in a meaningless value. Based on the suite of Pierre Shale samples, a practical detection limit for potassium is about 0.10 percent when potassium is present in a mixture of other radioisotopes and when sample sizes range from 200 to 600 g.

Repetitive 40-minute measurements during a 1-day period were made on a sample of K_2CO_3 to determine the repeatability of the detection system and the interpretation method. The peak amplitudes accumulated were sufficient to reduce the standard deviation of counting statistics to less than 1.1 percent; therefore, all other differences causing a greater error in interpreted results are caused by the detection system or by interpretation. The results in table 2 show that neither instrumentation nor interpretation causes an appreciable difference between the calculated and observed errors.

Sensitivity, the ability to measure small changes, was estimated from the results of the repeated measurements on the same sample and from the data obtained from the test suite of samples. Differences of about 5 percent of any determined value can commonly be measured.

As a result of this investigation, some modifications have been made in the detection system in an effort to lower the detection limit. Sample containers have been designed to surround each crystal, except for the end on which the photomultiplier tube is mounted.

TABLE 2.—*Ten repeated measurements of the counting rate on a 400-g sample of granular K_2CO_3, with 40-minute accumulation time per analysis*

Analysis No.	*Net counts*	*Counts per minute*
1	8,760	219.00
2	8,680	217.00
3	8,610	215.25
4	8,810	220.25
5	8,640	216.00
6	8,860	221.50
7	8,740	218.50
8	8,760	219.00
9	8,700	217.50
10	8,680	217.00
Average	8,724	218.1
Maximum variance from average:		
Counts	−114, +136	−2.9, +3.4
Percentage	−1.31, +1.56	−1.33, +1.56

Preliminary measurements with this configuration indicate that the detection limit will be improved by at least one order of magnitude.

REFERENCES

Adams, J. A. S., Richardson, J. E., and Templeton, C. C., 1958, Determinations of thorium and uranium in sedimentary rocks by two independent methods: Geochim. et Cosmochim. Acta, v. 13, p. 270–279.

Hurley, P. M., 1956, Direct radiometric measurement by gamma-ray scintillation spectrometer. Pt. I and II: Geol. Soc. America, Bull., v. 67, p. 395–412.

Hofstader, Robert, and McIntyre, J. A., 1950, Gamma-ray spectrometry with crystals of NaI(Tl): Nucleonics, v. 7, no. 3, p. 32–37.

Kahn, B., and Lyon, W. S., 1953, Scintillation spectrometer in radio-chemical analysis: Nucleonics, v. 11, no. 11, p. 61–63.

Mero, J. L., 1960, Uses of the gamma-ray spectrometer in mineral exploration: Geophysics, v. 25, no. 5, p. 1054–1076.

Moxham, R. M., Foote, R. S., and Bunker, C. M., 1965, Gamma-ray spectrometer studies of hydrothermally altered rock: Econ. Geology, v. 60, no. 4, p. 653–671.

Wanless, R. K., Stevens, R. D., Lachance, G. R., and Rimsaite, R. Y. H., 1965, Age determinations and geologic studies, Pt. I. Isotope ages, report 5: Geol. Survey of Canada, Paper 64–17.

ISOTOPE-DILUTION DETERMINATION OF FIVE ELEMENTS IN G–2 (GRANITE), WITH A DISCUSSION OF THE ANALYSIS OF LEAD

By BRUCE R. DOE, MITSUNOBU TATSUMOTO, M. H. DELEVAUX, and ZELL E. PETERMAN, Denver, Colo.

Abstract.—Concentrations of selected elements in the reference sample G–2 (granite) were determined by isotope dilution to be: lead, 30.8 ppm; rubidium, 174 ppm; strontium, 481 ppm; thorium, 24.3 ppm; and uranium, 1.9 ppm. A statistical study of the analytical uncertainties involved in lead-isotope analysis shows the uncertainties to be systematic and to closely approach those expected from fractionation of lead isotopes within the mass spectrometer. The ranges in Pb^{206}/Pb^{204} and Pb^{208}/Pb^{204} on samples approach four times those expected from the tests of the mass spectrometer, because of a sample-loading effect. The precision can be increased, approximately to a level expected only from the mass spectrometer effects, by loading an amount of NH_4NO_3 solution proportional to the amount of lead loaded.

The determination of selected elements in reference samples prepared by the U.S. Geological Survey has been undertaken as part of a program of interlaboratory standardization. The first reference sample to be studied is the granite G-2 (split 66, position 20). To keep this paper within reasonable length, the detailed discussion of analysis will be limited to lead. The discussion includes details of the determination of lead by isotope dilution and problems met in the isotopic analysis of lead.

RESULTS

Concentrations of the selected elements are given in table 1, and the isotopic compositions of lead and strontium are given in table 2. In table 2, raw strontium isotope ratios represent ratios directly read from the mass spectrometer, whereas Sr^{87}/Sr^{86} nor. is a normalized value of Sr^{87}/Sr^{86} by half the percentage needed to make the observed Sr^{86}/Sr^{88} equal 0.1194. The CIT shelf refers to the California Institute of Technology shelf lead sample. Recommended values for the G–1 reference sample by Fleischer (1965), which came from the same general region as G–2 but from a different quarry, are: Pb, 50 parts per million, Rb, 220 ppm; Sr, 250–280 ppm; Th, 52 ppm; and U, 3.7 ppm. The values of Pb, Th, and U in G–2 are roughly half those in G–1; the value of Sr is roughly twice that in G–1; and the value of Rb is about 0.8

TABLE 1.—*Concentration of selected elements in reference sample G–2*

Sample	Dissolution method	Analyst	Sample size (grams)	Concentration (ppm)				
				Pb	Rb	Sr	Th	U
1	$HF-HClO_4$	(1)	1	30.9			24.0	1.73
2	Borax fusion	(1)	.5				25.0	2.00
3	$HF-HClO_4$	(2)	1.5				24.2	1.90
4	do	(1)	1.0	30.7				
5	X-ray fluorescence	(3)	.75	≈30				
6	$HF-HClO_4$	(4)	1				24.2	2.14
7	do	(5)	1		173	478		
8	do	(5)	1		174	480		
9	do	(5)	1		175	486		
Mean values				30.8	174	481	24.3	1.94
Range about mean values (percent)				<1	1.4	1.7	4.1	21

[1] B. R. Doe.
[2] Ardith Bartel.
[3] Willis Doering.
[4] Richard Price.
[5] Zell E. Peterman and William Henderson.

TABLE 2.—*Isotopic composition of lead and strontium in G–2 and shelf solutions*

Sample		Sr-isotope ratios			Pb-isotope ratios				
No.	Description	Sr^{86}/Sr^{88}raw	Sr^{87}/Sr^{86}raw	Sr^{87}/Sr^{86}nor.	Pb^{206}/Pb^{204}	Pb^{207}/Pb^{204}	Pb^{208}/Pb^{204}	Pb^{206}/Pb^{207}	Pb^{206}/Pb^{208}
1	G–2 [1,2] (Re–4)	0. 1201	0. 7079	0. 7099	18. 526	15. 74	39. 67	1. 1771	0. 4706
2	G–2 [1,3] (Re–4)	. 1198	. 7089	. 7102	18. 509	15. 77	39. 34	1. 1734	. 4705
3	G–2 (mean)				18. 518	15. 76	39. 50	1. 1754	. 4706
4	Mean ocean water			. 7093					
5	USGS shelf Sr (13 analyses).			. 7106					
6	CIT shelf [3,4,5] (8 analyses) (Re–4).				16. 754	15. 66	36. 88	1. 0700	. 4543
7	CIT shelf [3,5] (6 analyses) (Re–3) (Doe and others, 1965).				16. 752	15. 65	36. 89	1. 0701	. 4541
8	GS/4 [4] (6 analyses) (Re–4).				16. 331	15. 66	36. 61	1. 0432	. 4461
9	GS/4 [6,7] (12 analyses) (Re–3).				16. 297	15. 61	36. 42	1. 0437	. 4475
Reproducibility (in standard deviation as percent of a ratio)					0. 29	0. 37	0. 47	0. 16	0. 29

Strontium analyses by: [1] Zell E. Peterman.
[2] Robert Zartman.
Lead analyses by: [3] B. R. Doe.
[4] M. H. Delevaux.
[5] M. Tatsumoto.
[6] J. S. Stacey.
[7] A. G. McNish.

that in G–1. Some key ratios of elements are similar in the two reference samples; for example, Th/U is 14 in G–1 and 12.5 in G–2, Pb/U is 13.5 in G–1 and 15.9 in G–2. The Rb/Sr ratios are significantly different—0.8 in G–1 and 0.36 in G–2.

The observed value of U^{238}/Pb^{204} is about 3.3 and of Th^{232}/U^{238}, about 13. The value of U^{238}/Pb^{204} is the lowest known for silicic rocks, and the value of Th^{232}/U^{238} is unusually high. Comparison of the lead-isotope ratios with the observed U^{238}/Pb^{204} and Th^{232}/U^{238} ratios indicates that the unusual concentration ratios are long lived and not simply induced in the sample preparation. A Pb^{206}/Pb^{207} ratio of 1.17 suggests a U^{238}/Pb^{204} ratio in the rock of less than 9, and a Pb^{208}/Pb^{204} ratio greater than 38.5–39 suggests a value of Th^{232}/Pb^{204} greater than 36 (the measured value is 43).

TECHNIQUES OF LEAD ANALYSIS

Reagents

The reagents used in the purification and extraction of lead from silicate rocks are:

Water: First distilled in a conductance still, then passed through a mixed-bed resin column, then through two stills with optical quartz reflux condensers. Last still has a Vycor boiler.

Hydrofluoric acid (concentrated): Same as that used by Tilton and others (1955) except that vessel containing water is a 5-liter Teflon bottle.

Perchloric acid: Commercial, vacuum distilled in Vycor, shipped in Vycor reagent.

Nitric acid (concentrated): Same as that used by Tilton and others (1955).

Chloroform: Commercial reagent, double distilled.

Ammonium hydroxide: Commercial NH_3 gas passed through a polyethylene "strike back" valve into distilled water to make 15-percent NH_4OH in ice-cooled polyethylene bottles.

Hydrochloric acid: 35-percent HCl made by passing commercial HCl gas through a polyethlene "strike back" valve into distilled water in polyethylene bottle.

Ammonium citrate: Commercial reagent dissolved in water to make 30-percent solution. NH_3 gas bubbled in to bring the pH to 9. Solution extracted twice with dithizone in chloroform, and entrapped dithizone removed by chloroform rinses.

Potassium cyanide: Commercial reagent dissolved in distilled water to make a 10-percent solution and extracted twice with dithizone in chloroform.

Dithizone: May be purified for lowest contamination, but contamination in an analysis with raw dithizone, purified KCN, and purified ammonium citrate is only 0.05 microgram.

Ammonium nitrate (2 percent): Made from concentrated pure reagents.

Hydrochloric acid (1.4*N*): Concentrated HCl diluted with distilled water to a specific gravity of 1.025.

Nitric acid (dilute): Two milliliters of concentrated HNO_3 diluted with distilled water to make 100 ml.

Analytical techniques

To a 1-gram sample of powder in a 100-ml Teflon dish add (1) 10 ml of $HClO_4$, (2) 12.94 micrograms of Pb^{203} "spike" using a 100λ (0.1 ml) micropipet, and (3) 15 ml of HF. Cover the dish with a Teflon watch glass and allow to stand for 1 hour in the hood; then stir with a Teflon stirring rod. Leave stirring rod in dish in such a position as to keep back of cover raised. Place dish on a hot plate at 250 watts for 1 hour, then turn up power to 300 watts until perchlorate fumes develop.

241–334 O—67——12

To minimize condensation, shine a hot lamp on the cover. Once perchlorate fumes have developed, increase power to 400 watts and evaporate solution to dryness. Remove dish from hot plate; add 10 ml of HF and 2 ml of $HClO_4$. Repeat heating procedure. After evaporating solution to dryness rinse down the sides of dish and cover with about 10 ml of quadruply distilled water. Add 2 or 3 ml of $HClO_4$ and repeat heating procedure.

Dissolve residue completely in 50 ml of HNO_3 by heating below the boiling point. Separate the lead using a $Ba(NO_3)_2$ coprecipitation (Tatsumoto, in press). Dissolve the $Ba(NO_3)_2$ precipitate in 20 ml of purified water, and extract the lead with dithizone in solution in chloroform using ammonium citrate and potassium cyanide as complexing agents as described in Doe and others (1965). Testing of the contamination met in this procedure gives values of 0.12–0.14 micrograms of lead.

Although the sample appeared to go completely into solution using an HF–$HClO_4$ decomposition step, this appearance was checked by a borax fusion step for uranium and thorium on a 0.5-g sample. Lead-rich minerals that may not be taken into solution as a result of an HF–$HClO_4$ decomposition are also rich in uranium and thorium; such minerals are, for example, zircon and monazite. The agreement of the Th and U values in the fusion procedure with the HF–$HClO_4$ procedure also indicates complete reaction (table 1).

Take the final 2-percent HNO_3 solution containing the lead from the dithizone extraction to dryness in a 10-ml Teflon beaker. Take the lead back into solution in about 2 ml of 2-percent NH_4NO_3 at pH 4. Heat the solution in the Teflon beaker to just below the boiling point, and transfer the solution to a 2-ml Pyrex centrifuge tube. Add a few bubbles of H_2S through a drawn-out Pyrex glass tube to form PbS. Centrifuge the solution for about 1 minute, remove, and tap the tube to release PbS adhering to the walls. The walls of the centrifuge tube are scraped with a Pyrex glass rod or the drawn-out tubing only in lead samples of less than 20 μg. Such scraping increases the Na signal in the mass spectrometer, and may ruin the stability of the lead signal. Load about 20–40 μg of the sample onto a rhenium filament (0.001×0.030 inch in cross section) with a split drop of the NH_4NO_3 solution. Pass a current starting at 1 ampere and increasing to 1.5 amperes through the filament until dryness.

Isotopic spikes

The spike used in the lead analyses was obtained from Oak Ridge National Laboratory (ORNL); the lead has the following isotopic composition (in atom percent):

	204	206	207	208
ORNL	<0.02	99.85	0.15	<0.02
USGS (Ta lot 1) (1–31–63)	<.006	99.802	.142	.049
USGS (Re lot 6) (1–26–66)	<.008	99.84	.13	.02

The spike was in the form of $Pb(NO_3)_2$ and was dissolved in 100 ml of a 10-percent HNO_3 solution, February 1963. One milliliter of the concentrated lead solution in a 1-percent HNO_3 solution was weighed into a second 100-ml volumetric flask. Assuming that the $Pb(NO_3)_2$ was stoichiometric, the concentration of lead in the dilute solution was calculated to be 11.89 μg Pb/gram of solution. A shelf standard was prepared from a lead pellet taken from the spectrographically pure lead bar of reference sample GS/4. A known amount of Pb^{206} spike solution was mixed with a known amount of GS/4 lead standard. The results of this test indicated the dilute Pb^{206} spike solution contained 11.96 μg Pb/gram of solution, within 1 percent of the chemical value.

A three-way comparison (Pb^{206} spike–GS/4, Pb^{208} spike–GS/4, and Pb^{206} spike–Pb^{208} spike) was made between the dilute Pb^{208} spike, dilute Pb^{206} spike, and the GS/4 shelf standard. The dilute Pb^{208} spike contained 14.50 μg of Pb/gram of solution via GS/4 and 14.58 μg Pb/gram of solution via the dilute Pb^{206} spike, again giving agreement within 1 percent. The Pb^{208} spike was found to have the following isotopic lead composition (in atom percent):

	204	206	207	208
ORNL	0.07	1.15	0.82	97.98
USGS (Ta–1( )2–5–63)	.08	1.17	.83	97.93

In January 1964, a second spike was prepared from the concentrated Pb^{206} solution and a new shelf solution from GS/4 lead metal with 12.97 μg Pb/100λ solution. In February 1965, the dilute Pb^{206} solution checked well at 12.94 μg Pb/100λ solution. A new Pb^{208} dilute solution was prepared in March 1965. It was found to contain 32.03 μg Pb/gram of solution via the new GS/4 solution and 32.26 μg Pb/gram of solution via the new dilute Pb^{206} spike. Once again agreement was within 1 percent.

MASS SPECTROMETRY

Description and operation of equipment

The mass spectrometer used for Pb, U, and Th is a Nier-type instrument as modified by Mark Inghram and W. R. Shields. The magnet has a 60° sector and 12-in. radius of curvature. The tube has a 68° sector of curvature. Lead is volatilized and ionized by a single rhenium filament heated to approximately 950°C, and Pb^{+1} ions are collected in a Faraday cup. No electron multiplier is used. Filament voltage is regulated electronically. The magnet is operated at about 6,000 gauss, and the ions are accelerated in a potential drop

of 10,000 volts. Ion intensities are measured with Carey vibrating reeds equipped with a 10^{11}-ohm resistor. Intensities are recorded on a strip chart equipped with an "expanded scale" similar to that supplied by Leeds and Northrup Corp. Shunt corrections of the system are less than 0.1 percent as determined by Ernest Wilson and Marcel Dube (oral commun., 1966). Vacuum is attained with an 80-liter mercury diffusion pump on the source. The tube is evacuated with a 100-liter Vacion pump.

The Rb and Sr concentrations are determined on a 6-in., 60° mass spectrometer using a triple-filament mode of ionization.

Nature of analytical uncertainties

Previously the analytical uncertainties of solid-source lead analyses have been shown not to be random but to depend upon the filament materials used (Doe and others, 1965) as well as on an effect of a fractionation type for repeated analyses of individual samples (Doe and others, 1966). The systematics of the analytical uncertainties for GS/4 lead shelf solution have been studied statistically. Figure 1 shows Pb^{206}/Pb^{204} versus Pb^{206}/Pb^{208}, and figure 2 shows Pb^{206}/Pb^{204} versus Pb^{206}/Pb^{207} for all GS/4 data included in the study by Delevaux and others (1966). The PbI_2 data are treated as one set, the PbS data as another set, and the least-squares lines are drawn through each set. In addition, subsets of lead data for samples on tantalum and on rhenium filament materials have been considered separately, but least-squares lines checked through each subset have not been found to be different from the whole set of mixed-filament materials.

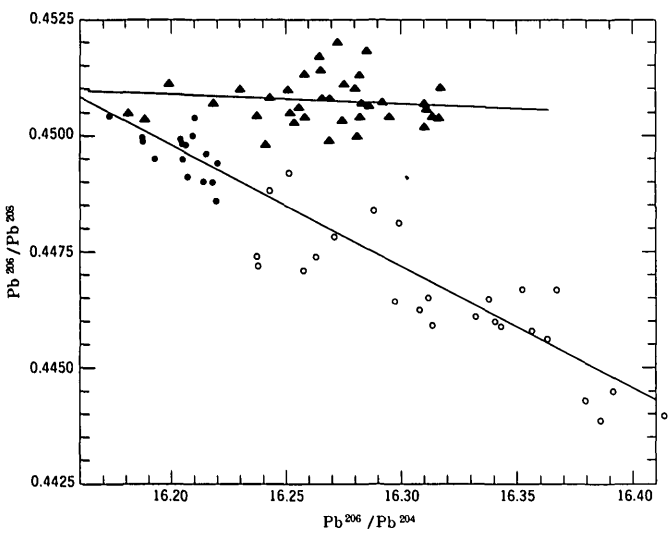

FIGURE 1.—Analytical uncertainties on GS/4 for Pb^{206}/Pb^{204} versus Pb^{206}/Pb^{208}. The solid lines represent the least-squares line through the PbI_2 results and through the combined Re- and Ta-filament thermal-emission work. Triangles, PbI_2; solid circles, PbS/Ta; open circles, Re.

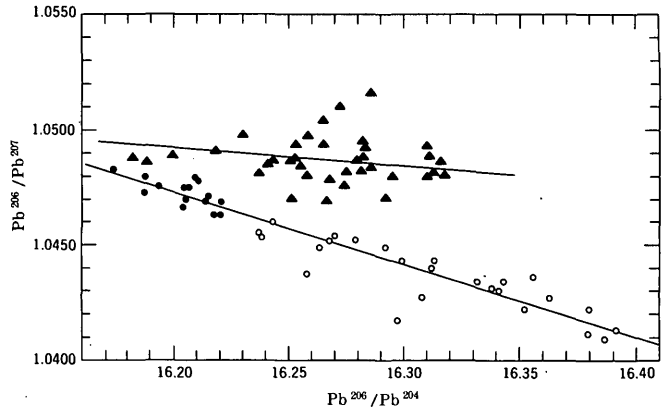

FIGURE 2.—Analytical uncertainties on GS/4 for Pb^{206}/Pb^{204} versus Pb^{206}/Pb^{207}. The solid lines represent the least-squares line through the PbI_2 results and through the combined Re- and Ta-filament thermal-emission work. Triangles, PbI_2; solid circles, PbS/Ta; open circles, Re.

Pb^{204}, which is the least abundant isotope, enters only into the abscissa of figures 1 and 2. If uncertainties in measurement of Pb^{204} are the prime source of error, the least-squares lines should have zero slope. This is seen to be approximately the case in the PbI_2 set, but not for the PbS set of results.

The PbS set of data has slopes approximately fitting what we will call the fractionation index:

$$\left[\left(\frac{\Delta(Pb^{206}/Pb^{208})}{\Delta(Pb^{206}/Pb^{204})}\right)\right]\times\frac{\overline{Pb^{208}}}{\overline{Pb^{204}}}=1 \qquad (1)$$

$$\left[\left(\frac{\Delta(Pb^{206}/Pb^{207})}{\Delta(Pb^{206}/Pb^{204})}\right)\right]\times\frac{\overline{Pb^{207}}}{\overline{Pb^{204}}}=1/2, \qquad (2)$$

where $\overline{Pb^{208}}/Pb^{204}$ and $\overline{Pb^{207}}/Pb^{204}$ are the mean values for these lead-isotope ratios. The observed fractionation index for the PbS set is 0.945 for figure 1, to which expression 1 applies, and 0.493 for figure 2, to which expression 2 applies. Equations 1 and 2 are approximations for mass-dependent effects or fractionation of isotopes of an element. This is the type of fractionation most generally assumed in thermal-emission analyses. It is used, for example, in obtaining high precision Sr^{87}/Sr^{86} values in almost all strontium isotope work. The statistical study of Pb indicates that the assumption is a good one. The equivalent fractionation indices for PbI_2 are 0.074 (expression 1) and 0.128 (expression 2), values close to the error for pure Pb^{204}.

As the analytical uncertainties are not completely random, standard deviations cannot be interpreted in the normal sense. In the thermal-emission work, for example, the uncertainty in Pb^{206}/Pb^{204} will commonly have the same sign as Pb^{207}/Pb^{204} and Pb^{208}/Pb^{204}. With this relationship in mind, it is still useful to compare data in terms of standard deviations, as in

table 2, to give some idea of just how well the data between two samples can be compared. There is no sample size control involved in the statistics quoted in table 2.

Causes of analytical uncertainties

Several tests have been carried out to determine the causes of the fractionation type of effects remaining even when samples are analyzed on a common-filament material. First the precision obtained by multiple analysis of individual sample loads is established. Next, the possible effects of extended analyses, degree of vacuum, other cations, and rapidity of analysis are examined to establish limits that the mass spectrometer may impose on the precision of the ratio measurements. Finally, the sample-loading effect is established and discussed.

Individual sample loads.—In order to determine the analytical uncertainties due solely to mass spectrometry, three samples were tested. They were loaded, analyzed, and then removed from the mass spectrometer. They were then reanalyzed a number of times over a period of a year in 1 of 2 mass spectrometers (table 3). Sample 1 of table 3 was not of normal intensity, and data were usually recorded on a decreasing ion signal. The other two samples had normal intensity, and data were recorded on growing signals. Data are recorded as ratios of Pb^{206}/Pb^{204}, Pb^{206}/Pb^{207}, and Pb^{206}/Pb^{208}, and much of the discussion that follows will involve only these three ratios. The ranges observed in each ratio for samples 1, 2, and 3, as percentage of each ratio, are given in table 3. When there are no chemical effects present, ratios then can be measured with ranges of 0.3 percent for Pb^{206}/Pb^{204}, and 0.15 percent for Pb^{206}/Pb^{207}, and 0.25 percent for Pb^{206}/Pb^{208} averaged and rounded to the nearest 0.05 percent. The data for Pb^{206}/Pb^{207} are probably better than for the other two ratios because the two isotopes are only of one mass unit difference and are of about equal abundance. These factors minimize effects of electronic fluctuations of the instrument as well as any fractionation of lead isotopes that might occur in the mass spectrometer.

Some investigators have suggested that one possible uncertainty in the measurement of lead-isotope ratios by solid-source mass spectrometry is lack of reproducible positioning of the sample filament on the optic plane. To test this possibility, the filament was bent from its original position in the x-y plane (the plane of the tube) and realined for some runs (table 3). The resulting data on samples 1 and 3 are well within the range of the other data so that sample positioning does not seem to have an effect. There is also no effect resulting from analyzing the samples on different mass spectrometers of the same design, such as mass spectrometers 1 and 2 (table 3).

Extended analyses.—Examples of results of individual analyses over a long period of time are shown in

TABLE 3.—*Comparative analyses of single lead-isotope sample loads given by (1) two different mass spectrometers, (2) different positions of filament, and (3) redeterminations at different times throughout one year*

Sample	Lab. No.	Mass spectrometer	Date	Pb-isotope ratios				
				206/204	207/204	208/204	206/207	206/208
1	4T282 [1]	2	3–19–65	18. 162	15. 80	38. 92	1. 1493	0. 4667
		1	3–27–65	18. 149	15. 79	38. 90	1. 1495	. 4666
		2	5–19–65 [2]	18. 146	15. 78	38. 94	1. 1496	. 4660
		1	9–13–65 [3]	18. 172	15. 80	38. 90	1. 1500	. 4660
		1	11–26–65 [3]	18. 195	15. 84	39. 08	1. 1488	. 4656
		1	3–21–66 [3]	18. 172	15. 82	39. 02	1. 1486	. 4657
Ranges in ratio as percentage of mean value.				. 28	. 38	. 46	. 10	. 25
2	2T275b	2	3–18–65	17. 090	15. 61	38. 51	1. 0948	. 4438
		1	3–27–65	17. 108	15. 62	38. 56	1. 0950	. 4437
		2	5–19–65	17. 095	15. 62	38. 54	1. 0942	. 4436
		1	9– 2–65 [3]	17. 119	15. 65	38. 63	1. 0937	. 4432
		1	11–26–65 [3]	17. 118	15. 65	38. 66	1. 0936	. 4427
		1	3–17–66 [3]	17. 139	15. 68	38. 72	1. 0931	. 4427
Ranges in ratio as percentage of mean value.				. 29	. 44	. 55	. 17	. 25
3	2T275a	2	3–18–65	17. 276	15. 64	38. 55	1. 1048	. 4482
		1	3–27–65 [2]	17. 290	15. 63	38. 55	1. 1059	. 4485
		2	5–19–65	17. 299	15. 65	38. 58	1. 1056	. 4484
		1	9– 9–65 [3]	17. 300	15. 66	38. 61	1. 1050	. 4480
		1	11–26–65 [3]	17. 302	15. 66	38. 64	1. 1047	. 4478
		1	3–18–66 [3]	17. 313	15. 67	38. 67	1. 1046	. 4477
Ranges in ratio as percentage of mean value.				. 27	. 26	. 31	. 12	. 18

[1] Sample 4T282 on mass spectrometer 1 was preceded by three runs spiked with pure Pb^{206} and Pb^{208}

[2] Filament bent out of the way and then realined.

[3] Second analyst.

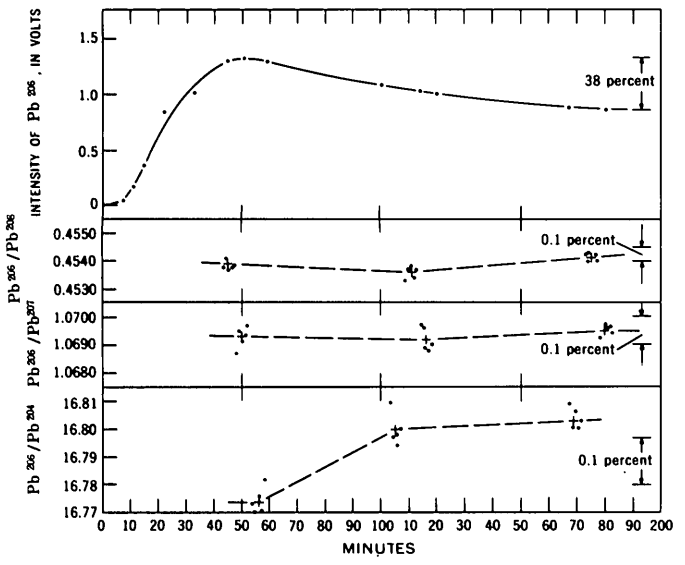

FIGURE 3.—Extended mass-spectrometer analysis of CIT shelf lead reference sample. Crosses represent means for dots in each cluster. The intensity of Pb^{206} decreased 38 percent from the maximum intensity observed during the test. Ranges of 0.1 percent of each ratio are shown at the right-hand side of the graph for each isotope ratio to give a scale against which to compare observed variations in each isotope ratio.

figures 3 and 4. No systemic change in ratios with time is observed. The intensity of the Pb^{206} signal, expressed as volts, is shown at the top of figures 3 and 4. Figure 3 is an extended analysis of a sample of lead extracted from K-feldspar, and ranges in the means of the ratios are about 0.1 percent. Figure 4 is an extended analysis of a spectrographically pure lead-isotope mixture (often referred to as the Tilton 20:1 gravimetric mixture) with ranges in the means similar to the K-feldspar sample. Refocusing the magnet during the test had no effect on the analytical results. This lack of a fractionation effect with time is contrary to observations on lighter elements. For one example, Shields and others (1961) noted a 0.2-percent change in Ag^{107}/Ag^{109} over a 20-minute span of time.

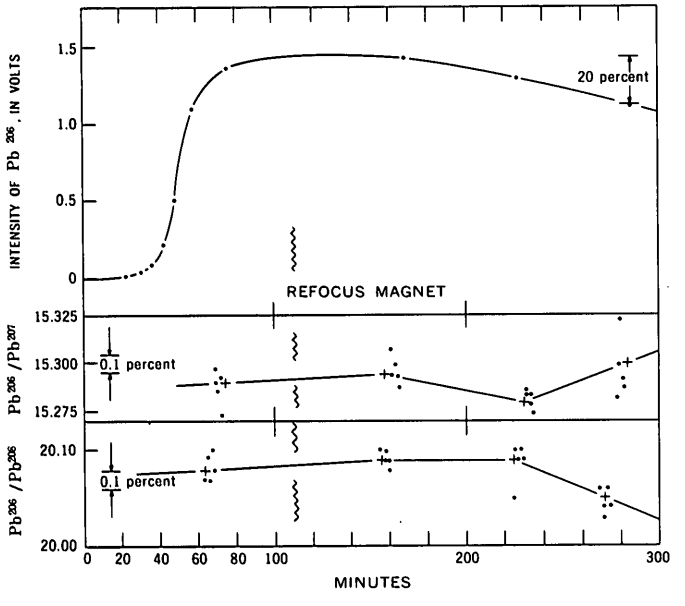

FIGURE 4.—Measurements at different times during the extended mass-spectrometer analysis of the Tilton 20:1 gravimetric lead mixture. The intensity of Pb^{206} decreased 20 percent from the maximum intensity observed during the test. Ranges of 0.1 percent of each ratio are shown at the left-hand side of the graph for each isotope ratio to give a scale against which to compare observed variations of each ratio.

Vacuum.—The possible effect of degrees of vacuum between 3 and 13×10^{-8} mm Hg on resulting data was tested by loosening the flange on the source area of the mass spectrometer and then gradually tightening it. The degree of vacuum was monitored at the mass spectrometer tube. Again possible effects are less than 0.1 percent. Data are usually taken between 6 to 10×10^{-8} mm Hg in the tube.

Effect of other cations.—Lead-isotope ratios were measured as a function of Na signal, expressed as volts, during runs on two different samples. Effects of other cations on the analytical results are less than 0.1 percent of a ratio. At normal running temperatures, sodium and potassium are the only common cations formed. The sodium probably comes from the borosilicate glassware used in the precipitation step and has a measured intensity 10 to 100 times the lead signal. Potassium is not abundant in analyses, even though KCN is used in the chemical purification of lead.

Rapidity of analysis.—Table 4 shows the results of tests with different mass spectrometers and different techniques of analyzing samples. On May 13, 1965, two filaments were loaded by operator B within minutes of precipitating some shelf-lead solution. The samples were inserted simultaneously in the two mass spectrometers. Operator A gradually raised the filament temperature of one mass spectrometer, and a lead signal was observed in about 20 minutes. Operator B rapidly raised the filament temperature on the other mass spectrometer, and a lead signal was observed in about 1 minute. Data were accumulated starting about 12 minutes after the mass spectrometer was turned on. Operator A then prepared two filaments with lead from the same shelf solution a week later in the same manner, and the analyzing procedure was repeated. For each individual date, the data are in excellent agreement, indicating no operator effect on the mass spectrometer, but the differences between dates are 2–3 times those expected if no sample loading is involved. There appears to be, therefore, some effect in the sample-precipitation and filament-loading steps, as these were the only two steps involved.

TABLE 4.—*Effect of rapid versus slow rates of analysis on results for CIT shelf lead (Re-4 filament)*

Sample	Mass spectrometer operator	Mass spectrometer	Date	Speed of run	Pb-isotope ratios		
					206/204	207/204	208/204
Precipitated and loaded by operator B							
1	A	1	5/13/65	Slow	16.754	15.66	36.85
2	B	2	5/13/65	Fast	16.720	15.63	36.76
Precipitated and loaded by operator A							
3	A	1	5/20/65	Slow	16.849	15.78	37.25
4	B	2	5/20/65	Fast	16.838	15.77	37.24
Differences (percent) between dates for average values of each ratio					0.64	0.90	1.62

Sample-loading effects are further illustrated in table 5, which shows results of "aging" for a sample loaded and analyzed on April 13, 1965, and reanalyzed nearly a month later from the same precipitate loaded on another filament.

TABLE 5.—*"Aging" effect of lead from Niland, Calif., brine (Ta-1 filament, one precipitate)*

[Determinations made by operator B on spectrometer 1]

Sample	Date	Pb-isotope ratio		
		206/204	207/204	208/204
1	4/13/63	19. 288	15. 85	39. 66
2	5/10/63	19. 147	15. 69	39. 12
Difference (percent) between dates for each isotope ratio		0. 75	1. 02	1. 35

Sample-loading effect.—Sample-loading effect could have several causes, and we attempted to isolate them by two experiments. The first experiment was to determine if the amount of lead precipitated in a constant volume of NH_4NO_3 solution has any effect (fig. 5). In this procedure, 20, 40, and 80 μg of Pb were each precipitated in 2 ml of NH_4NO_3 solution, and the total Pb sample with a proportional volume of NH_4OH solution was loaded on filaments within a few minutes of precipitation. Most analyses of samples are made in the range 20–40 μg of lead. Certainly there is no large effect on the measured ratios, even though different mass spectrometers and operators were used. Thus the precipitation step is not critical, at least on spectrographically pure shelf solutions of lead.

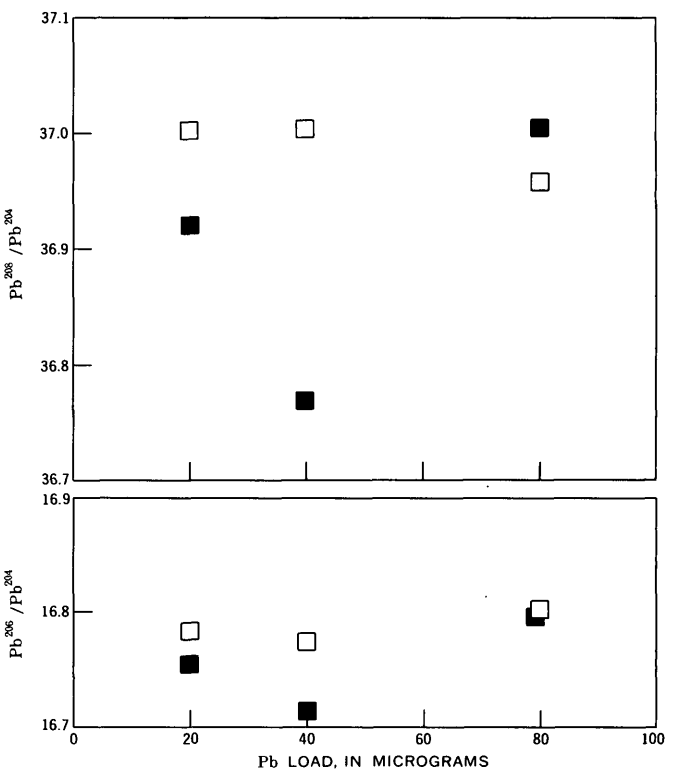

FIGURE 5.—Lead-isotope ratios measured for CIT shelf lead 1 when the size of the lead load is proportional to the volume of NH_4NO_3 loaded on the filament. Open squares, determined by operator A; solid squares, determined by operator C.

In the second test, the volume of solution loaded on a filament was held roughly constant, but the lead loaded was varied between 20 and 80 μg (fig. 6). A definite effect is observed with greater lead-isotope ratios

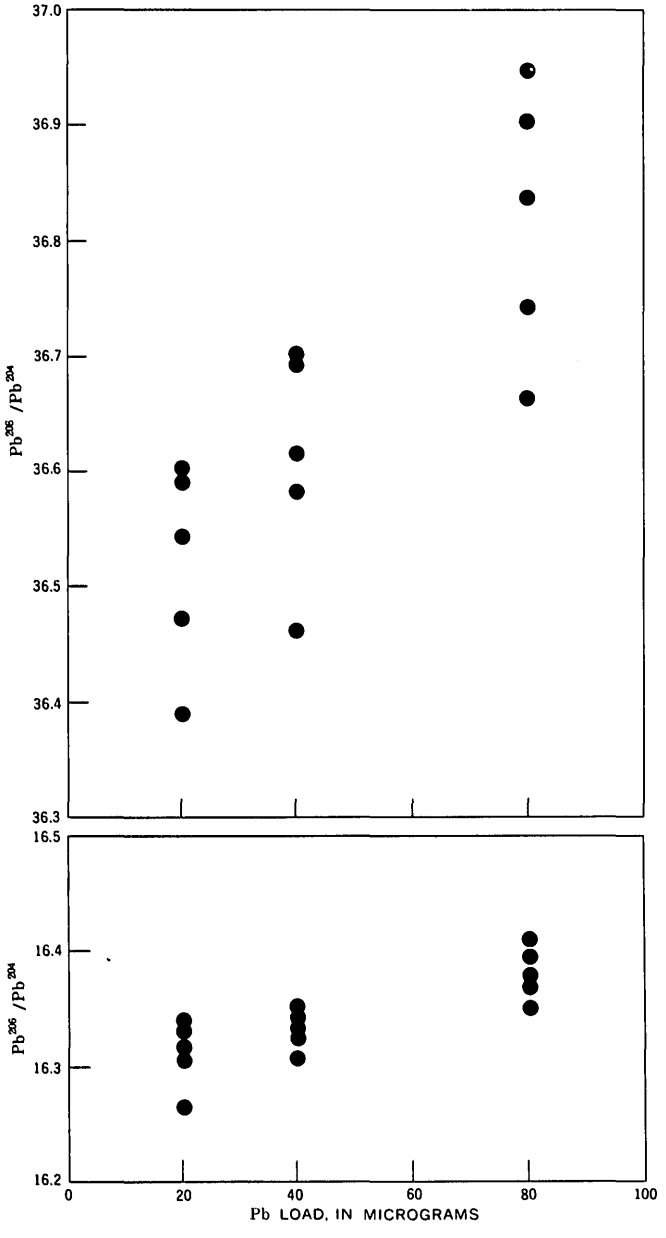

FIGURE 6.—Measured lead-isotope ratios for GS/4 shelf lead when the size of the lead load is varied, but the volume of NH_4NO_3 solution loaded on the filament is held approximately constant.

accompanying larger lead loads. There is no overlap of the data for Pb^{208}/Pb^{204} from 20-μg loads with data from 80-μg loads. The difference in the means of the extreme loads is 0.9 percent for Pb^{208}/Pb^{204}. The data on the smaller lead loads is somewhat better than for the larger lead loads—about 0.6 percent range for Pb^{208}/Pb^{204} of 20-μg loads and 0.8 percent for 80-μg lead loads. This sort of effect could well account for the common observation that values of Pb^{207}/Pb^{204} are greater in ores than in rocks with similar ratios of Pb^{206}/Pb^{204}. In analyzing ores, one probably loads more lead when it is available, but the volume of solution loaded is usually about constant. The theoretical reasons for the sample loading effect are not known.

REFERENCES

Delevaux, M. H., Pierce, A. P., and Antweiler, J. C., 1966, New isotopic measurements of Colorado ore leads, *in* Geological Survey Research 1966: U.S. Geol. Survey Prof. Paper 550–C, p. C178–C186.

Doe, B. R., Hedge, C. E., White, D. E., 1966, Preliminary investigation of the source of lead and strontium in deep geothermal brines underlying the Salton Sea geothermal basin: Econ. Geology, v. 61, p. 462–483.

Doe, B. R., Tilton, G. R., and Hopson, C. A., 1965, Lead isotopes in feldspars from selected granitic rocks associated with regional metamorphism: Jour. Geophys. Research, v. 70, p. 1947–1968.

Fleischer, Michael, 1965, Summary of new data on rock samples G–1 and W–1, 1962–1965: Geochim. et Cosmochim. Acta, v. 29, p. 1263–1284.

Shields, W. R., Garner, E. L., and Dibler, V. H., 1961, Absolute isotopic abundance of terrestrial silver: Jour. Research, Natl. Bur. Standards, v. 66A, p. 1–3.

Tatsumoto, M., 1966, Isotopic composition of lead in volcanic rocks from Hawaii, Iwo Jima and Japan: Jour. Geophys. Research, v. 71, p. 1721–1733.

Tilton, G. R., Patterson, C. C., Brown, H., Inghram, M., Haydon, R., Hess, D., and Larsen, E., Jr., 1955, Isotopic composition and distribution of lead, uranium, and thorium in a Precambrian granite: Geol. Soc. America Bull., v. 66, p. 1131–1148.

A METHOD FOR THE ANALYSIS OF FLUID INCLUSIONS BY OPTICAL EMISSION SPECTROGRAPHY

By JOSEPH HAFFTY and DARRELL M. PINCKNEY, Denver, Colo.

Abstract.—A spectrographic method is described for the determination of calcium, magnesium, and sodium in fluid inclusions whereby 200 microliters of solution is evaporated onto a pair of flat-top graphite electrodes. Uni-arc conditions are then used to excite the residue, thereby providing good sensitivity.

A primary fluid inclusion is usually a very small amount of fluid trapped in a cavity of a growing crystal. The cavity therefore contains a sample of the fluid from which the crystal has formed (fig. 1). Consequently, analysis of fluid inclusions aids in understanding the chemical environment during crystallization of minerals and ores.

The recovery and preparation of the fluid for analysis follow the procedure described by Roedder and others (1963). The recovered sample of fluid generally has a volume of 10 to 20 milliliters and has been diluted from its original state of concentration by a factor of 2,000 to 7,000. A suitable method for analysis of the fluid must be one that works on small samples and one that is capable of determining the kind and amount of many elements that may be present in the sample. The method described here meets these requirements.

The method of optical emission spectrography described in the present paper is designed to determine calcium, magnesium, and sodium in the spectral region 2400–4800A, where many of the elements present in fluid inclusions are sought. Other elements can be included in the list of elements determined when the present procedure for obtaining the fluid from the inclusion is modified. Potassium is not included in the list of elements determined because a separate exposure is required to measure the 7664.91A line. It is considered more convenient and practical to analyze for this one element by atomic-absorption spectroscopy.

Previously a "copper spark" procedure for the analysis of calcium, magnesium, and strontium in liquids was reported (Alexander and others, 1954). However, copper concentrations in fluid inclusions are of interest and therefore copper electrodes can not be used. In addition to this, copper electrodes involve a handling problem whereby they have to be machined on a lathe and are not very satisfactory for use with acid solutions. The graphite electrodes come preformed and ready for use.

APPARATUS AND OPERATING CONDITIONS

Excitation source.—Manufacturer's designation: spark-ignited full-wave uni-arc (see text), with 280-volt power supply.

Radio frequency current, amp	1.9
The parameters of the initiating circuit are as follows:	
Capacitance, μf	0.0025
Inductance, μh	Residual
Primary resistance, dial setting	5
Secondary resistance, ohm	Residual
Discharge voltage, v	15,000
Number of discharges per half cycle	7
Current, amp, rf	5.5

Spectrograph.—Folded, 3-meter, Rowland circle-mounted grating with 21,000 lines per inch giving a reciprocal linear dispersion of 4A per mm in the first order.

Wavelength region, angstroms	2400–4800, first order
Slit width, microns	40
Illumination	Arc image focused on grating
Analytical gap, mm	3
Transmission, percent	100
Exposure, seconds	20
Electrodes	ASTM type C–3

ANALYTICAL PROCEDURE

Standards containing the cations calcium, magnesium, potassium, and sodium are made in a 1-volume-percent hydrochloric acid solution. The concentrations of these elements are based on analyses of fluid inclusions reported in the literature (Hall and Friedman, 1963). The stock solution which was used to pre-

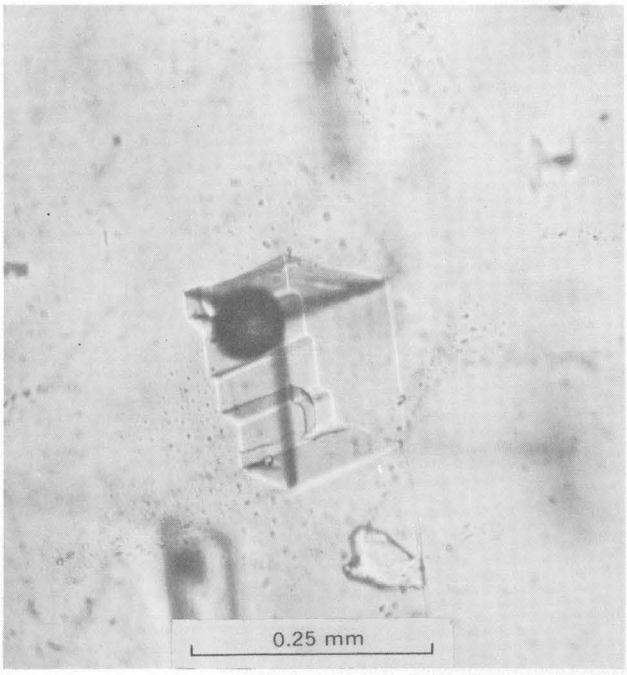

FIGURE 1.—Fluid inclusions in fluorite crystal. The cuboid body is a cavity containing liquid and a spherical gas bubble. Other fluid inclusions appear as tiny specks or larger bodies which are out of focus.

pare a series of standard solutions covering the ranges of concentrations indicated in table 1 contained 464 parts per million of sodium, 100 ppm of calcium, 46.4 ppm of magnesium, and 46.4 ppm of potassium. The standards, including potassium, are analogous to the average naturally occurring material described by Hall and Friedman (1963). The inclusion of potassium makes possible the use of the same standards for its determination by atomic absorption.

To minimize the effect of the wide range of element concentration found in fluid inclusions, it is necessary to incorporate a buffer-internal-standard system in the analysis. Four parts by volume of unknown sample are mixed with one part of a buffer-internal-standard solution containing lithium as buffer and molybdenum as internal standard. The lithium in the final mixture is equivalent to 50 ppm and the molybdenum to 0.1 ppm.

Two flat-top graphite electrodes are first waterproofed with two drops each of a petroleum-ether solution of Apiezon "N" grease (5 g/liter). One hundred microliters of the unknown sample or the standard, both containing the buffer–internal standard, are added to each electrode in 50 μl increments and evaporated by means of a heat lamp. The electrodes are kept under the heat lamp until placed in the arc-spark stand. Each exposure consists of exciting the residue of 200 μl of solution on the 2 electrodes.

The type of excitation source used (spark-ignited full-wave uni-arc) is an intermittent d-c arc. The primary power source is a full-wave rectified 280-volt power supply. The primary power source is initiated by a high-voltage condensed spark synchronized to initiate each half cycle. The arc is carried on both halves of the cycle, thereby exciting the residue on the two electrodes.

Spectra are recorded on SA–1 plates and calibrated by means of an iron bead arced at 5 amps d-c and exposed for 15 seconds at a transmission of 4.8 percent. The iron bead is formed prior to use by successively arcing portions of iron powder at 5 amps in a large (about ¼-inch inner diameter) cupped electrode until the bead extends up above the sides of the cup (Haffty, 1960). The iron lines used for calibration were selected from a list of homologous lines (Crosswhite, 1950; Bastron and others, 1960).

The analytical and the internal-standard lines used in constructing the analytical curves are listed in table 1 along with their concentration ranges. The concentrations read from the analytical curves, an example of which is shown in figure 2, are multiplied by the factor

TABLE 1.—*Analytical line pairs used in analysis of fluid inclusions*

Element	Analytical line (angstroms)	Internal-standard line (angstroms)	Concentration range (ppm)
Calcium	Ca 4302. 53	Mo 3170. 35	0.20 to 8.0
	Ca 4318. 65	Mo 3170. 35	2.0 to 37
Magnesium	Mg 2779. 83	Mo 3170. 35	.05 to 4.0
Sodium	Na 3302. 32	Mo 3170. 35	.80 to 17
	Na 3302. 99	Mo 3170. 35	.80 to 37

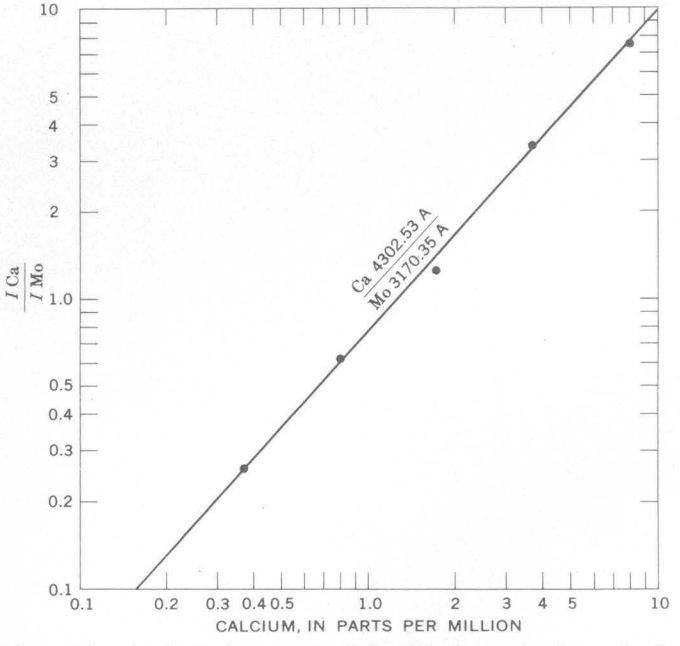

FIGURE 2.—Analytical curve used for the determination of calcium, in fluid inclusions, from the ratio of the intensity (I) of calcium to that of molybdenum, the internal standard.

TABLE 2.—*Comparison of spectrographic and atomic-absorption analyses of composite leaches of fluid inclusions*

[In parts per million]

Sample No.	Magnesium			Sodium			Calcium		
	Spectrographic		Atomic absorption	Spectrographic		Atomic absorption	Spectrographic		Atomic absorption
	Run 1	Run 2		Run 1	Run 2		Run 1	Run 2	
23	0.06	0.05	0.062	6.2	6.0	5.9	1.9	1.8	1.7
30	.17	.16	.15	9.0	8.9	11	17	18	18
36	.13	.13	.098	1.1	1.3	1.0	.75	.68	.60
29							320	360	330

1.25, owing to the addition of the buffer–internal-standard solution. When the concentrations of the elements are high the samples are diluted to bring them in range of the analytical curves. Good comparative data were obtained for calcium on sample 29 (table 2), which was diluted 1:99 for the spectrographic result and 1:199 for the atomic-absorption result.

A measure of the accuracy is obtained by comparing the spectrographic results with those obtained by atomic-absorption spectroscopy (table 2). In order to have sufficient sample for the accuracy tests made, composite samples (table 2) were submitted. These samples represent composites of water and acid leaches of fluid inclusions and are not intended for any geologic interpretation.

REFERENCES

Alexander, G. V., Nusbaum, R. E., and MacDonald, N. S., 1954, Strontium and calcium in municipal water supplies: Am. Water Works Assoc. Jour., v. 46, p. 643–654.

Bastron, Harry, Barnett, P. R., and Murata, K. J., 1960, Method for the quantitative spectrochemical analysis of rocks, minerals, ores, and other materials by a powder d-c arc technique: U.S. Geol. Survey Bull. 1084–G, p. 165–182.

Crosswhite, H. M., 1950, Photoelectric intensity measurements in the iron arc: Spectrochim. Acta, v. 4, p. 122–151.

Haffty, Joseph, 1960, Residue method for common minor elements: U.S. Geol. Survey Water-Supply Paper 1540–A.

Hall, W. E., and Friedman, Irving, 1963, Composition of fluid inclusions, Cave-in-Rock fluorite di strict, Illinois, and Upper Mississippi Valley zinc-lead district: Econ. Geology, v. 58, p. 886–911.

Roedder, Edwin, Ingram, Blanche, and Hall, W. E., 1963, Studies of fluid inclusions III—extraction and quantitative analysis of inclusions in the milligram range: Econ. Geology, v. 58, p. 353–374.

DATA ON THE ROCK GSP–1 (GRANODIORITE) AND THE ISOTOPE-DILUTION METHOD OF ANALYSIS FOR Rb AND Sr

By ZELL E. PETERMAN, BRUCE R. DOE, and ARDITH BARTEL, Denver, Colo.

Abstract.—Concentrations of selected elements in the U.S. Geological Survey standard granodiorite, GSP–1, as determined by isotope dilution are 268 ppm of Rb, 240 ppm of Sr, 58.7 ppm of 2.4 ppm of U, and 106 ppm of Th. Duplicate analyses of Rb, Sr, and Pb agree to within 1 percent. Replicate analyses of U and Th show larger variations. The range in U values is ±20 percent of the mean and in Th value, ±8 percent of the mean. The isotopic compositions of Pb and Sr are given, and the analytical techniques for the determination of Rb and Sr are discussed. The Sr^{87}/Sr^{86} ratio after normalization is 0.7687±0.0011. The isotopic composition of lead is given by the following ratios: Pb^{206}/Pb^{204}, 18.077; Pb^{207}/Pb^{204}, 15.67; and Pb^{208}/Pb^{204}, 47.33.

This paper is one in a series reporting isotope-dilution analyses of selected elements in a group of standard rock samples prepared by the U.S. Geological Survey. Doe and others (1967) have dealt with the standard granite G–2 and have discussed the determination of lead by isotope dilution and the isotopic analysis of lead. In the present report, isotopic data for the standard granodiodite GSP-1 (split 1, position 23) are presented, and the analytical techniques used in the isotope-dilution analyses for Rb and Sr and in the isotopic analyses of Sr are discussed.

The standard rock sample GSP-1 is a granodiorite collected from the Precambrian Silver Plume Granite near Georgetown, Colo., in the Colorado Front Range.

RESULTS

Concentrations of the selected elements Rb, Sr, Pb, Th, and U are given in table 1. Of these, U shows the greatest spread in the replicate analyses, for which the total range can be expressed as ±20 percent of the mean value. The range in the Th concentrations is±8 percent of the mean. The duplicate analyses for Rb, Sr, and Pb agree to within 1 percent. The large ranges in U and Th analyses are clearly outside of normal analytical uncertainty as indicatd by replicate analyses of volcanic glasses (B. R. Doe, unpub. data). These may be the result of mineral inhomogeneities in the powdered material which results in difficulty in obtaining a representative aliquot of a material in which the minor elements may be strongly concentrated in accessory minerals. The U and Th contents of the two aliquots, which were split with a microsplitter (table 1), are in closer agreement than those that were poured from the sample bottle. The means of these samples are used as the preferred values.

Isotopic analyses of Pb and Sr are given in table 2. The precision of Pb isotopic analyses has been discussed by Doe and others (1967) (p. B173, this chapter). Because of the variations in Pb isotopic ratios, that are due in part to the filament material used (Doe and others, 1965), both the observed ratios (on Re, lot 6) and the converted values (Ta, lot 1) are shown in table 2. The conversion is accomplished by adjusting the observed values by amounts determined through replicate analyses of standard samples on the various filament materials. A detailed discussion of the Sr isotopic analyses is given in following sections of this paper.

TABLE 1.—*Concentrations of selected elements in the standard granodiorite GSP–1*

Sample	Analyst	Dissolution method	Type of sample aliquot	Concentration (ppm)				
				Rb	Sr	Pb	U	Th
1	(1)	$HF-H_2SO_4$	Spatula	269	241			
2	(1)	do	do	267	239			
3	(2)	$HF-HClO_4$	Poured				2. 2	109
4	(3)	do	do				3. 3	117
5	(3)	do	Split				2. 2	105
6	(4)	do	Poured			58. 7	3. 2	120
7	(4)	Borax fusion	Split			58. 6	2. 5	108
Mean values				268	240	58. 7	2. 7	112
Preferred values				268	240	58. 7	2. 4	106

[1] Z. E. Peterman and W. T. Henderson.
[2] R. K. Price.
[3] Ardith Bartel and M. H. Delavaux.
[4] B. R. Doe, Ardith Bartel, and M. H. Delavaux.

TABLE 2.—*Isotopic composition of* Pb *and* Sr *in the standard granodiorite GSP–1*

Sample	Analyst	Filaments	Dissolution method	Sr-isotope ratios			Pb-isotope ratios				
				Sr^{86}/Sr^{88}	Sr^{87}/Sr^{86}	$(Sr^{87}/Sr^{86})_n$ [1]	Pb^{206}/Pb^{204}	Pb^{207}/Pb^{204}	Pb^{208}/Pb^{204}	Pb^{206}/Pb^{207}	Pb^{206}/Pb^{208}
1	(2)	Re	$HF-H_2SO_4$	0.11974	0. 7676	0. 7687					
2	(2)	Re	do	.11973	. 7675	. 7686					
3	(3)	Re, lot 6	$HF-HClO_4$				18. 169	15. 79	47. 76	1. 1506	0. 3804
4	(3)	Ta, lot-1 conversion	do				18. 071	15. 66	47. 24	1. 1537	. 3825
5	(4)	Re, lot 6	do				18. 183	15. 80	47. 93	1. 1511	. 3794
6	(4)	Ta, lot-1 conversion	do				18. 084	15. 67	47. 41	1. 1543	. 3814

[1] Sr^{87}/Sr^{86} normalized to a Sr^{86}/Sr^{88} ratio of 0.1194.
[2] Z. E. Peterman and W. T. Henderson.
[3] B. R. Doe.
[4] B. R. Doe and M. H. Delavaux.

Some unusual ratios of elements in granodiorite GSP–x are of special geochemical interest. The ratio μ (U^{238}/Pb^{204}) is 2.95 and is the lowest value observed for intermediate to silicic igneous rocks. The Th/U ratio is 44.3 and is abnormally high, because most crustal rocks have Th/U ratios less than 10 and more commonly between 2 and 6.

The unusually high Th/Pb ratio and a Rb/Sr ratio of 1.12 allow calculation of the Th/Pb and Rb/Sr total-rock ages. Assuming an initial Sr^{87}/Sr^{86} ratio of 0.703 the Rb/Sr age is 1.36±0.05 billion years (using the 47–b.y. half life for Rb^{87}). This is in agreement with a total-rock isochron age of 1.37 b.y. obtained on the Longs Peak Granite of Fuller (1924), which is typical of Silver Plume Granite (Z. E. Peterman, C. E. Hedge, and W. A. Braddock, unpub. data).

Similarly, the Th^{232}/Pb^{208} age can be calculated by assuming an initial Pb^{208}/Pb^{204} ratio. If an initial ratio such as that observed for feldspar leads from the St. Kevin Granite of the Sawatch Range is assumed (Doe, 1967), the calculated age is 1.55 b.y. If a more precise Th/Pb age is to be obtained, it would be necessary to determine the initial Pb^{208}/Pb^{204} ratio; however, within the limits of uncertainty the Th/Pb and Rb/Sr ages are in agreement.

ANALYTICAL METHODS FOR Rb AND Sr

Most of our work dealing with Rb and Sr is an application of the $Rb^{87}-Sr^{87}$ decay scheme to the measurement of geologic time and to Sr isotopic tracer studies. The following discussion is therefore limited to the methods used in determining Rb and Sr in silicate samples.

An extremely important part of the procedure for dating rocks and minerals is sampling and sample preparation. For the analyses of total-rock samples, 1 kilogram or more of sample is collected, depending on grain size and uniformity of the rock. The samples are crushed to −40 mesh and carefully split to produce a minimum size sample of 15 grams. These splits are pulverized to about −200 mesh and thoroughly mixed. The final splits for analyses are made either with a microsplitter or by carefully mixing the sample by rolling it on paper and taking random portions with a spatula.

Reagents

The following reagents are used in the chemical preparation of silicate samples for Rb and Sr analyses:

Water: triple distilled, using a Barnstead still coupled with a 400 ml/hr Engelhard double-stage quartz still.

Hydrochloric acid: 6.2*N* HCl prepared by bubbling commercial HCl gas through triple-distilled water in a polyethylene bottle. 2.5*N* HCl prepared by diluting 6.2*N* HCl with triple-distilled water.

Hydrofluoric acid: 48 to 51 percent, commercial analytical grade.

Sulfuric acid: concentrated, commercial analytical grade.

Spikes

The Rb and Sr spikes were obtained from the Oak Ridge National Laboratory and are enriched in Rb^{87} and Sr^{86}, respectively. These were dissolved in triple-distilled water to obtain the primary spike solutions. Aliquots of the primary solutions are diluted volumetrically by a factor of 50 to obtain the working spike solutions. Concentrations, in micrograms per milliliter in the working spikes at the time the present analyses were made are given below:

Rb^{85}	0.0364	Sr^{86}	8.327
Rb^{87}	4.368	Sr^{87}	.0577
		Sr^{88}	.1505

Concentrations of the spike solutions are checked at least every 6 months against standard solutions of normal Rb and Sr. These standards are prepared from 99.95 percent pure $Sr(NO_3)_2$ obtained from Johnson, Mathey and Co., Ltd., and from 99.8 percent pure Rb_2SO_4 obtained from United Mineral and Chemical Corp. Standard solutions of about 2,000 μg/ml of Rb and Sr are prepared and calibrated gravimetrically. These are also checked at least every 6 months.

Blanks

During the last year (1965) a number of determinations indicated that the blanks have been about 0.02 μg Rb and 0.04 μg Sr for an analysis. Because these are well below the precision of the method no corrections are made.

Sample dissolution

Depending on the Rb and Sr concentrations in the rock or mineral as estimated from preliminary X-ray fluorescence analyses, between 0.3 and 0.6 gram of sample is weighed in a 40-ml Pt dish. Accurately measured volumes (by calibrated pipets) of Rb and Sr spike solutions are added to the sample along with 0.5-ml concentrated sulfuric acid. The spike solutions are evaporated down to the sulfuric acid on a hotplate at 250°–275°C. About 25 ml of hydrofluoric acid is added, and the sample is digested at 250°–275°C on a hotplate. Hydrofluoric acid is added again as needed. When the sample has been completely digested it is taken to dryness and the heat is raised to 350°–375°C until the sulfuric acid is fumed off. This rids the sample of all hydrofluoric acid and converts the remaining cations to sulfates. The dish is removed from the hotplate, 6 ml of 2.5*N* HCl is added, and the residue is allowed to leach for about an hour. About half the liquid is centrifuged, transferred to a 5-ml beaker, and taken to dryness. This aliquot is used without further purification for the Rb analysis.

The remaining solution is also centrifuged and passed through an ion-exchange column containing Dowex 50 WX-8 (200–400 mesh) resin to obtain a purified Sr sample. When the proper amount of 2.5*N* HCl eluant has passed through the column the last 30 ml are collected in a Vycor beaker and taken down to 2 or 3 ml on a hot plate. This is transferred to a 5-ml beaker and taken to dryness. The Sr sample is now ready for analysis.

Unspiked samples for Sr isotopic analyses are prepared using the same procedure as outlined above except that the Rb and Sr spiking are omitted.

Sample loading

The Rb sample is leached with a small amount of triple-distilled water. About 1 to 3 drops of the supernatant liquid is loaded onto the Re sample filaments and taken to dryness at 1.5 amperes.

Approximately 5 drops of 2.5*N* HCl is added to the Sr sample (spiked or unspiked). About half of this is loaded onto the Re sample filaments and taken to dryness at 1.8 amps. Upon dryness, the filaments are heated to a very slight dull-red glow for 2 minutes (2.0 to 2.2 amps).

Mass spectrometer

Nearly all the analyses for Rb and Sr concentration are determined on a 6-inch, 60° mass spectrometer of the Nier type as modified by W. R. Shields, National Bureau of Standards. A triple-filament mode of ionization is utilized. The source, collector, and electronics are similar to those of the 12-inch spectrometer described previously by Doe and others (1967) (p. B172, this chapter). Rb and Sr are volatilized from two Re sample filaments and ionized by a Re center filament. The ions are accelerated in a potential drop of 5,000 volts.

Isotopic analyses

Because of the long half life of Rb^{87}, which is 47×10^9 years according to Flynn and Glendenin (1959) or 50×10^9 years according to Aldrich and others (1956), it is necessary to determine Rb and Sr concentrations, and Sr isotopic composition to the highest possible degree of precision in order to reduce to a minimum the analytical uncertainties of the measured ages.

In the concentration work, the greater part of the analytical uncertainty lies in the chemical preparation of the the samples (sample splitting, weighing, spiking, spike calibrations, and so forth), and not in the isotopic analyses.

Rb *analyses*.—Natural Rb consists of two isotopes, with masses of 85 and 87. The isotopic composition most commonly assumed is that determined by Nier (1950), who reported a Rb^{85}/Rb^{87} ratio of 2.591. More recently Shields and others (1963) report a mean Rb^{85}/Rb^{87} ratio of 2.5995 ± 0.0015 (95-percent confidence level) for 27 natural silicate samples. A highly significant contribution of their work is that they found no variations in the isotopic composition of Rb outside of experimental error, and therefore it can be safely assumed that the Rb^{85}/Rb^{87} ratio is constant in nature. Because of this invariant ratio we do not routinely analyze unspiked Rb samples. However, on our mass spectrometers we do obtain a Rb^{85}/Rb^{87} ratio for normal Rb identical with that reported by Shields and others (1963). In order to be consistent with other laboratories and the Rb^{87} half life determined by Flynn and Glendenin (1959) our observed Rb^{85}/Rb^{87} ratios are normalized to the 2.591 value obtained by Nier (1950).

Sr *analyses*.—Natural Sr consists of 4 stable isotopes of masses 84, 86, 87, and 88 of which all but Sr^{87} are assumed to be constant in nature. The abundance of Sr^{87} has changed with time because of the radioactive decay of Rb^{87}, which is the basis for the Rb-Sr method of age determination. The commonly accepted values for isotopic composition for nonradiogenic Sr are those determined by Nier (1938), which are $Sr^{84}/Sr^{88}=0.0068$ and $Sr^{86}/Sr^{88}=0.1194$.

For many samples of the type presently being dated (those with a small enrichment of radiogenic Sr^{87}) it is necessary to determine the Sr concentrations and Sr isotopic compositions on separate splits. For samples which are considerably enriched in radiogenic Sr^{87} as a result of a large Rb/Sr ratio and (or) an old age, it is often sufficient to calculate the amount of radiogenic Sr^{87} from the spike Sr analysis.

One of the major problems that arises during the isotopic analyses is the fractionation of Sr during the analysis. Fractionation is considerably reduced by using the triple-filament mode of ionization (see Hedge and Walthall, 1963, fig. 1, p. 1214). Other parameters which may be controlled during the analyses to reduce fractionation are discussed by Shields and others (1963, p. 2331) with regard to Rb, but they are also applicable to Sr. In order to correct for fractionation effects it is common practice to normalize the observed Sr^{86}/Sr^{88} values to a value of 0.1194, and to adjust the observed Sr^{87}/Sr^{86} values half this amount. The normalization procedure assumes that there are no natural variations in the nonradiogenic Sr isotopes.

The precision of the Sr isotopic measurements is determined by replicate analyses of a standard Sr solution containing 500 μg of Sr per milliliter (strontium nitrate, United Mineral and Chemical Corp., lot B 857), which will be referred to as the USGS

standard Sr. Precision data for the standard Sr are shown in table 3. In November 1965, an improved technique for analyzing Sr was developed which involves sample loading and operation of the filaments at considerably lower temperatures than had previously been done. In the following discussion the new method will be referred to as the "low-temperature method" in contrast to the previously used "high-temperature method." The operating conditions for the filaments (Re ribbon, 1×30 mils, 0.5 inch in length) are as follows: (1) The center filament is turned to 4.8 amps (approximately 1,600°C) to burn off any Rb present, and the side filaments to 0.10 amp. Normally 1 to 3 minutes under these conditions reduces the Rb signal sufficiently. (2) The center filament is turned down to 3.8 amps (approximately 1,450°C), and the Sr signal is increased by turning up the side filaments by increments of about 0.10 amp until a suitable signal is obtained (normally 150 to 300 millivolts signal for Sr^{86} with a 2.5×10^{11} ohm resistor in the preamplifier circuit of the Carey vibrating-reed electrometer). Generally, a growing or stable signal is obtained 10 to 20 minutes after the run is started.

TABLE 3.—*Precision of* Sr *isotopic measurements for USGS standard* Sr, *and for routine rock analyses*

	Sr^{86}/Sr^{88}	Sr^{87}/Sr^{86}	$Sr^{87}/Sr^{86}{}_n$
USGS STANDARD Sr			
High-temperature method [1]			
Mean	0.1200	0.7087	0.7106
Range	.1196–.1206	.7074–.7097	.7100–.7115
σ	.00035	.00085	.00055
σ (percent)	.290	.120	.077
Low-temperature method [2]			
Mean	0.1198	0.7091	0.7104
Range	.1197–.1200	.7085–.7099	.7100–.7108
σ	.00010	.00048	.00037
σ (percent)	.083	.068	.052
ROUTINE ROCK ANALYSES (IGNEOUS, METAMORPHIC, AND SEDIMENTARY ROCKS)			
High-temperature method [3]			
Mean	0.1200	----------	----------
Range	.1194–.1207	----------	----------
σ	.00033	----------	----------
σ (percent)	.275	----------	----------
Low-temperature method [4]			
Mean	0.1198	----------	----------
Range	.1193–.1203	----------	----------
σ	.00019	----------	----------
σ (percent)	.150	----------	----------

[1] 11 analyses, Mar. 1965 to Sept. 1965.
[2] 6 analyses, Nov. 1965 to Apr. 1966.
[3] 71 analyses, Mar. 1965 to Oct. 1965.
[4] 73 analyses, Nov. 1965 to Mar. 1966.

A comparison of data obtained on the standard Sr by the low- and high-temperature methods is given in table 3. The improvement in precision for the Sr^{86}/Sr^{88} data with the low-temperature method is significant and indicates a decrease in fractionation effects. At the 95-percent confidence level, using Student's t factor for a limited statistical sample, the precision of the Sr^{86}/Sr^{88} ratio for a single analysis has been reduced from ±0.65 percent to ±0.21 percent. This decrease of fractionation is also shown by comparing the Sr^{87}/Sr^{86} data. For the high-temperature method the precision in Sr^{87}/Sr^{86} ratios is improved by a factor of 1.6 by the normalization procedure, whereas the Sr^{87}/Sr^{86} ratios by the low-temperature method are little improved by normalization (table 3).

Perhaps more applicable to routine analyses of rocks and minerals are the data shown in table 3 for 71 silicate samples determined by the high-temperature method and 73 silicate samples determined by the low-temperature method. The analytical precision of the data is increased by nearly a factor of 2, using the low-temperature method. At the present time it appears that the precision in the Sr^{86}/Sr^{88} ratios using the low-temperature method is ±0.30 percent at the 95-percent confidence level.

These data also indicate more precisely than previous results that there is no significant fractionation of Sr in nature. From the 73 analyses by the low-temperature method it can be stated that at the 95-percent confidence level the isotopic fractionation of Sr in natural environments is less than ±0.30 percent of the Sr^{86}/Sr^{88} ratio.

For intralaboratory comparison of Sr isotopic data, the standard Sr is analyzed on the various mass spectrometers. For comparison with data obtained by other laboratories it is sufficient to report here that on the USGS 6-inch spectrometer, on which the present data were obtained, we have determined Sr^{87}/Sr^{86} values of 0.7085 on the MIT (Massachusetts Institute of Technology) shelf Sr and 0.7093 for modern sea water.

REFERENCES

Aldrich, L. T., Wetherill, G. W., Tilton, G. R., and Davis, G. L., 1956, Half-life of Rb^{87}: Phys. Rev., v. 103, p. 1045–1047.

Doe, B. R., 1967, The bearing of lead isotopes on the source of granitic magma: Jour. Petrology, v. 8, p. 1–33.

Doe, B. R., Tilton, G. R., Hopson, C. A., 1965, Lead isotopes in feldspars from selected granitic rocks associated with regional metamorphism: Jour. Geophys. Research, v. 70, p. 1947–1968.

Doe, B. R., Tatsumoto, M., Delevaux, M., and Peterman, Z. E., 1967, Isotope-dilution determination of five elements in G–2 (granite), with a discussion of the analysis of lead, *in* Geological Survey Research 1967: U.S. Geol. Survey Prof. Paper 575–B, p. B170–B177.

Flynn, K. F., and Glendenin, L. E., 1959, Half-life and beta spectrum of Rb^{87}: Phys. Rev., v. 116, p. 744–748.

Fuller, M. B., 1924, General features of pre-Cambrian structure along the Big Thompson River in Colorado: Jour. Geology, v. 32, no. 1, p. 49–63.

Hedge, C. E., and Walthall, F. G., 1963, Radiogenic strontium-87 as an index of geological processes: Science, v. 140, no. 3572, p. 1214–1217.

Nier, A. O., 1938, Isotopic constitution of Sr, Bi, Tl and Hg: Phys. Rev., v. 54, p. 275–278.

——— 1950, A redetermination of the relative abundances of the isotopes of neon, krypton, rubidium, xenon, and mercury: Phys. Rev., v. 79, p. 450–454.

Shields, W. R., Garner, E. L., Hedge, C. E., and Goldich, S. S., 1963, Survey of Rb^{85}/Rb^{87} ratios in minerals: Jour. Geophys. Research, v. 68, no. 8, p. 2331–2334.

RAPID ANALYSIS OF ROCKS AND MINERALS BY A SINGLE-SOLUTION METHOD

By LEONARD SHAPIRO, Washington, D.C.

Abstract.—Previously reported procedures for the rapid analysis of rocks by spectrophotometric methods now have been supplemented by atomic-absorption spectrophotometric methods for determination of CaO, MgO, Na_2O, K_2O, and MnO. A single solution prepared after fusion of the sample with lithium metaborate replaces the two solutions previously used in the rapid-analysis method. As a result of these modifications the time required for the complete analysis of a rock has been halved.

Methods described for the rapid analysis of rocks by spectrophotometric methods (Shapiro and Brannock, 1962) have been supplemented now by atomic-absorption spectrophotometric methods for the analysis of CaO, MgO, Na_2O, K_2O, and MnO. Atomic-absorption methods have been described by a number of authors (for example, Trent and Slavin, 1964; Billings and Adams, 1964), and the accuracy of such methods has been discussed by Billings (1965).The use of atomic-absorption methods has made possible the substitution of a single solution for the two solutions formerly used in determining the major rock-forming elements. As a consequence, gains in accuracy (especially for MgO) and speed have resulted. For example, with the methods described by Shapiro and Brannock (1962) a third of the time required for an analysis is consumed in preparing the solutions. Now the time required for solution preparation is reduced by 90 percent because of the single-solution procedure described in this paper.

The single-solution method depends on initial fusion of the sample with lithium metaborate. This method originated with Ingamells (1964), who later suggested its use with atomic-absorption spectrophotometry (Suhr and Ingamells, 1966) and described spectrophotometric procedures (Ingamells, 1966) as applied to the rapid analysis of silicates.

In preparing a single solution suitable for determining SiO_2, Al_2O_3, CaO, MgO, Na_2O, K_2O, Fe_2O_3, MnO, TiO_2, and P_2O_5, concentration is a vital factor that must be considered. If the solution is to be stable, the SiO_2 concentration cannot exceed approximately 150 parts per million; otherwise the SiO_2 will start to polymerize and precipitate. On the other hand, if the solution is too dilute, low levels of the other constituents cannot be determined accurately by the methods described by Shapiro and Brannock (1962). A solution, prepared from a rock powder, that is sufficiently dilute for stability of SiO_2 is sufficiently concentrated for determining the other constituents, if atomic absorption spectrophotometry is used.

The solution concentration found to be best is 100 milligrams of sample per liter. This provides a solution that without further dilution allows SiO_2, Al_2O_3, Fe_2O_3, TiO_2, and P_2O_5 to be determined by simple spectrophotometric procedures, and CaO, MgO, Na_2O, K_2O, and MnO to be determined by atomic-absorption spectrophotometry. The spectrophotometric procedure for P_2O_5 is based on a molybdenum-blue color which is about 100 times more sensitive than the molybdivanadate previously used for silicates, but the other spectrophotometric procedures remain virtually unchanged from those described by Shapiro and Brannock (1962). With carbonate and phosphate rocks the unusually high content of CaO and P_2O_5 may be determined with somewhat better accuracy by simple rapid-analysis methods described for this purpose by Shapiro and Brannock (1962). Ferrous iron, H_2O, and CO_2 must, of course, still be determined on separate portions of sample as also described for the rapid-analysis methods. The equipment for the general scheme of analysis from a single solution is illustrated in figure 1.

PREPARATION OF SAMPLE

Weigh 0.10000 ± 0.0001 gram of the sample powder (previously ground to 100 mesh or finer) and transfer to a new graphite crucible. Place approximately 0.6 g of lithium metaborate on top of the sample. In addition to the rock samples prepare a blank and 1 or

U.S. GEOL. SURVEY PROF. PAPER 575-B, PAGES B187-B191

241-334 O—67——13

2 standards of known silica, alumina, titania, and iron oxide content within the ranges 50–75 percent SiO_2, 12–20 percent Al_2O_3, 1–2 percent TiO_2 and 10–15 percent Fe_2O_3. The granite, G–1, and diabase, W–1, are used as standards in the writer's laboratory. Place the crucibles onto a silica tray and insert into a muffle furnace at 1,000° C after preheating in front of the open furnace for several minutes. Fuse for 1 hour. Remove the resulting fused beads from the furnace and cool to room temperature.

To a series of 1-liter plastic beakers add 1 liter of water. Place the beakers on magnetic stirrers, add Teflon-coated stirring bars, and stir rapidly. Transfer the cooled beads from the crucibles to the beakers. They will come out of the crucible without difficulty if new crucibles are used. Add 15 milliliters of concentrated HCl. The time required for complete solution of the beads will range from 1½ to 3 hours, depending on the stirring rate, the shape of the vessel, and other factors. When the pellets have completely dissolved, the solutions are ready to be used.

SPECTROPHOTOMETRIC DETERMINATION

The spectrophotometric determinations, except the one for P_2O_5, follow closely the procedures described by Shapiro and Brannock (1962), except for minor changes noted below.

SiO_2

The procedure for the analysis of SiO_2 is based on the development of a molybdenum-blue color. A pipet to deliver about 4.5 ml is used to take aliquots from the sample solutions; the pipet is best in the form of a stopcock device. Reagents to develop the color are best added by a pipetting machine, but an alternative procedure also can be used. The blank, standards, and sample solutions are run at the same time. (See Shapiro and Brannock, 1962, p. A5–A17, A20, and A24 for details of above changes.)

Al_2O_3

Al_2O_3 is determined from measurements of the absorbance of the color of a calcium aluminum alizarin red-S complex. A pipet to deliver 7–8 ml is used, and either the procedure for machine pipetting or an alternative procedure is followed (Shapiro and Brannock, 1962, p. A20 and A25–A27).

TiO_2

The procedure for analysis of TiO_2 utilizes the yellow color produced with Tiron (disodium-1,2-dihydroxybenzene-3,5-disulfonate). This procedure is the one described by Shapiro and Brannock (1962, p. A29), except that 50 ml of the sample solution is used in step 1; step 2 is deleted; and in step 4, 20 ml of the buffer is added. The W–1 used as the titanium standard contains 1.1 percent TiO_2.

Fe_2O_3 (total Fe as Fe_2O_3)

Iron is determined from the orange color produced with orthophenanthroline. The procedure is that described by Shapiro and Brannock (1962, p. A28) except that 50 ml of the sample solution is transferred to 100–150-ml beakers instead of volumetric flasks, and in step 3, 10 ml of orthophenanthroline is added. No dilution is required after the addition of citrate. The W–1 may be used as the standard and contains 11.0 percent Fe_2O_3. Alternatively, iron may be determined by atomic absorption spectrophotometry.

P_2O_5 in silicates

For concentrations of P_2O_5 up to 1.0 percent, a molybdenum-blue method as described below is used. Above 1.0 percent P_2O_5 content, the method described by Shapiro and Brannock (1962) for phosphate rocks should be used.

Preparation of reagents

Ammonium molybdate solution.—Dissolve 12.5 g of $(NH_4)_6Mo_7O_{24}4H\cdot_2O$ in 340 ml of H_2O; then add 160 ml of 1+1 H_2SO_4.

Stannous chloride solution.—Crush a few crystals of $SnCl_2\cdot 2H_2O$ in a mortar and weigh out approximately 150 mg. Transfer to a small beaker and dissolve in 25 ml of concentrated HCl. Add 25 ml of water. This solution should be prepared at the time it is to be used.

Standard P_2O_5 *solution.*—Using National Bureau of Standards standard sample 56b (phosphate rock), prepare a sample solution as with any other sample after a fusion with $LiBO_2$. This provides a 31.7 percent P_2O_5 standard. Transfer 31.5 ml of this solution to a 1-liter volumetric flask and add 10 ml of conc. HCl and about 500 ml of water. Then add and dissolve approximately 0.6 g of $LiBO_2$ and make to volume. This is the 1-percent P_2O_5 working solution.

Procedure

1. Transfer 50-ml portions of the blank, the 1 percent standard, and the sample solutions to a series of 150-ml beakers, using a graduate.
2. Add 2 ml of the ammonium molybdate solution to the first 10 beakers, then add 1 ml of the stannous chloride solution.
3. Four to five minutes after adding the stannous chloride to the first solution, proceed to measure.

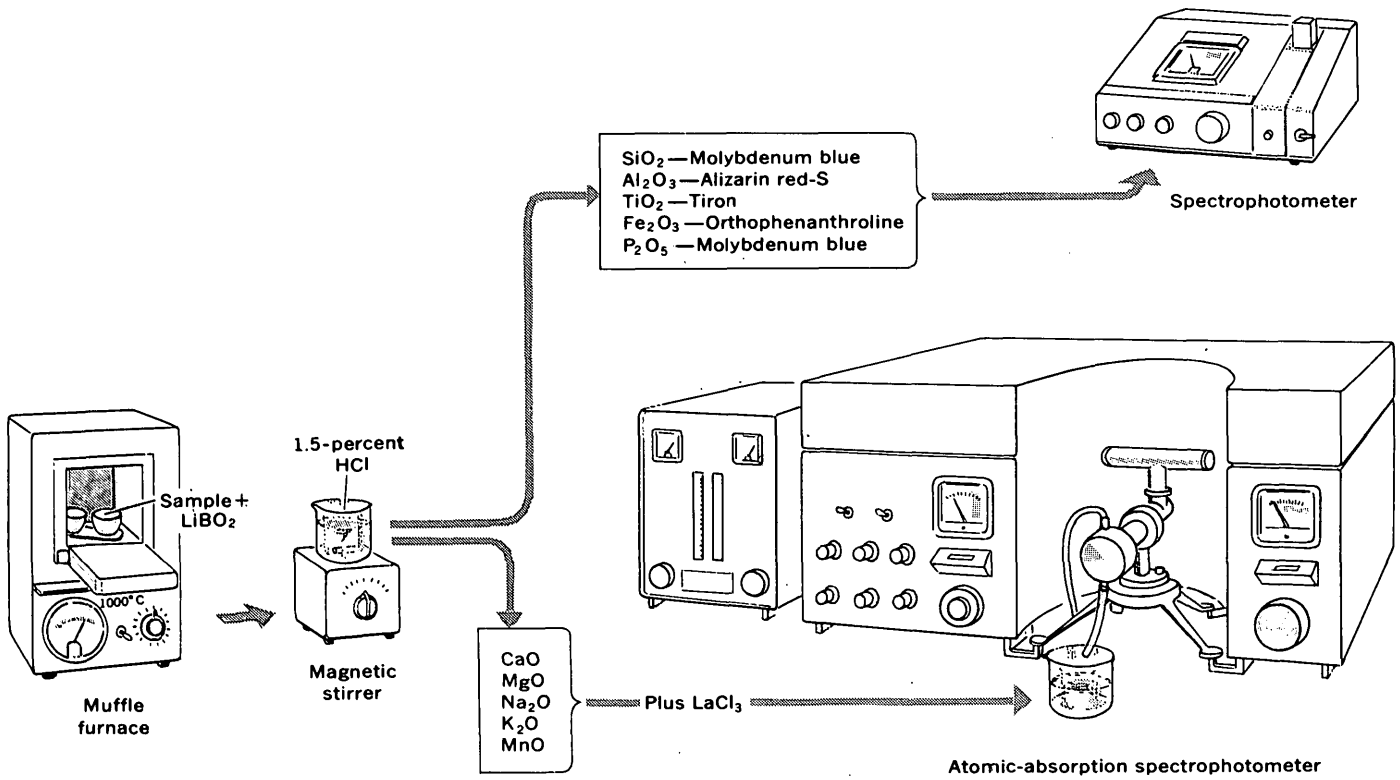

FIGURE 1.—Schematic diagram of the equipment used in the analysis of rocks from a single solution.

on the spectrophotometer, the percent transmission at 640 mμ, using the blank as reference. The blue color developed reaches a peak in 4 minutes and is stable for the next 10 minutes, after which it begins to decrease. Ten solutions can easily be measured in this time span.

4. Repeat steps 2 and 3 with the remainder of the solutions, 10 at a time.

Calculations

1. Convert the reading for percent transmission to absorbance.
2. Compute the factor:

$$\text{Factor}=\frac{1.00}{\text{Absorbance of standard}}$$

3. Factor × absorbance of sample = percentage of P_2O_5 in sample.

P_2O_5 in phosphate rocks

In the analysis of phosphatic rocks, resulting in solutions with concentrations of P_2O_5 over 1.0 percent, the method described by Shapiro and Brannock (1962, p. A32) is used. The standard solution is the one described for the silicate level P_2O_5, that is, the solution of NBS sample 56b which is equivalent to 31.7 percent P_2O_5. For the development of the vanadomolybdate color the procedure described by Shapiro and Brannock (1962, p. A32) is modified slightly. Steps 1 and 2 are omitted, as the sample solutions are sufficiently dilute. In step 3, 50 ml of sample solution is used instead of the indicated 15 ml. In the 4th step, 15, 25, and 50 ml of the standard solution are used. Otherwise, the procedure is unchanged. This procedure can lead to results within 0.1 percent P_2O_5, which is adequate accuracy for percentages above 1 percent but not for those below this level.

CaO in carbonate and phosphate rocks

CaO may be readily determined with 1–2 percent relative accuracy by atomic absorption. This is adequate in most cases for the levels found in silicates but not for carbonates and phosphates where CaO can often be 40–50 percent of the rock. Accuracies to within 0.5 percent of the amount of CaO + MgO present can readily be obtained by using visual titration (Shapiro and Brannock, 1962, p. A38–A40). After the determination of MgO by atomic absorption, the CaO + MgO value can be used to calculate the CaO value. As MgO is generally relatively a minor constituent, the calculated CaO retains the accuracy inherent in the precise visual titration.

ATOMIC-ABSORPTION SPECTROPHOTOMETRIC PROCEDURES

The instrument used in the writer's laboratory for atomic-absorption spectrophotometric determinations is the Perkin-Elmar Model 303 with a digital readout attachment, but other instruments can be used with comparable results. The fuel used is acetylene-air. The directions provided with any of the instruments are detailed and need not be discussed here, but a brief description of our technique, which differs slightly from manufacturer's suggestion will be given.

Standard solutions

A set of standard solutions is prepared containing the equivalent of 0, 0.15, 3.00, 6.00, 9.00, 12.00, and 15.00 percent Na_2O, K_2O, CaO, and MgO and also, 0.015, 0.3, 0.6, 0.9, 1.2, and 1.5 percent MnO. To make these, first prepare a "1,500-percent" solution of these constituents by transferring into a 500-ml volumetric flask 1.1872 g of KCl, 1.4145 g of NaCl, 1.3386 g of $CaCO_3$, 0.4568 g of Mg ribbon (such ribbon is generally close to 99 percent pure and the given weight allows for this) and 5.6 ml of a commercially available solution of 10,000 ppm of Mn. Add about 250 ml of water, 10 ml of conc. HCl, and boil for several minutes to dissolve all the constituents. Cool to room temperature and make to volume.

In a series of seven 1-liter volumetric flasks marked "blank," "0.15," "3," "6," "9," "12," and "15," dissolve 0.6 g of $LiBO_2$, 500 ml of H_2O and 10 ml of conc. HCl. To the flasks marked "3," "6," "9," "12," and "15" add 2, 4, 6, 8, and 10 ml of the "1,500-percent" standard. Make these and the blank to the mark and mix. Transfer 10 ml of the solution from the flask marked "15" to the 0.15 flask, make it to the mark, and mix. Each flask has its indicated percentage of all the constituents except MnO, which has 1/10 the amount.

Lanthanum solution

Transfer 140 g of lanthanum oxide (99.997 percent pure) into a 2-liter beaker. Slowly add 300 ml of conc. HCl, allowing time for the reaction to be completed after each addition of acid. The large beaker reduces difficulties from spatter. After all the acid is added, the oxide should all be dissolved as the chloride. Add 200 ml of H_2O. Four ml of the solution thus contains approximately 1 g of La.

To prepare the solutions for atomic-absorption spectrophotometry, transfer 50 ml of the sample and standard solutions (measured approximately with a plastic graduate) to 100- or 150-ml beakers and add 2 ml of the lanthanum solution to each. No other solutions or dilutions are required. The lanthanum is used as a releasing agent (Dinnin, 1960) for CaO and MgO determinations that otherwise would be affected by aluminum, phosphate, silica, and other constituents.

Operation of the instrument

The sensitivity range of the instrument and the concentration range as normally found in rocks vary for the required elements. Calcium and manganese are at concentrations which require the optimum setting of the instrument, and so these are adjusted exactly in accordance with the instructions provided with the instrument. Sodium, calcium, and magnesium are more concentrated than is suitable for an accurate determination, especially at levels above a few percent. Rather than dilute the solutions to bring them into the range of the instrument, it is simpler to position the percent-absorption counter to about 50 percent by loosening the set screws which retain the burner and then to rotate and reposition the flame while aspirating the highest standard, until the needle indicates a balance at the center line. In this way, the light from the hollow cathode passes through a smaller fraction of the flame, and sensitivity is reduced.

Absorption here, as in spectrophotometry, is a logarithmic function of element concentration. After 50-percent absorption is exceeded the sensitivity falls off rapidly. With the procedure described, results can be reproduced within the limits of the standard to the nearest 0.1 percent. If desired, the determination of low-level constituents can be improved easily by resetting the flame position to optimum response while aspirating the 3-percent standard.

It is important to bracket the sample readings between standards, as the responses are not quite linear, but otherwise there are no inter-element or other effects in rock constituents to affect results adversely.

DISCUSSION

The accuracy obtained by the procedures described is within the guidelines given for rapid rock analysis (Shapiro and Brannock, 1962). It is quite feasible for one analyst to process 30 samples through the 10 determinations in about 2 days. If only a few samples are required in as short a time as possible, it is feasible to do these determinations within a few hours, assuming that reagent and standard solutions are already available.

The time required to prepare sample solutions from a few samples can be reduced appreciably by grinding the sample with $LiBO_2$ in a boron carbide mortar and pestle, fusing for 10 minutes and then crushing the melt in a Plattner mortar. The resultant small crystals dissolve within 20–30 minutes in the 1½-percent HCl.

Much smaller sample sizes can be handled if desired. The analysis has been conducted with 20 mg of sample plus 0.12 g of $LiBO_2$ dissolved in 200 ml of H_2O plus 3 ml of HCl with stirring, and the results were indistinguishable from those obtained with 100 mg of sample. In samples of rock, too small a sample size can lead to large sampling error, but with minerals this problem does not exist, and any size of sample that can be weighed accurately can be used by maintaining a 1:6:10 ratio (in milligrams) between sample, flux, and water.

REFERENCES

Billings, K. G., 1965, Analysis of geological material by atomic absorption, pt. II. Accuracy tests: Perkins-Elmer Atomic Absorption Newsletter, no. 7.

Billings, K. G., and Adams, J. A. S., 1964, Analysis of geological material by atomic absorption: Perkins-Elmer Atomic Absorption Newsletter, no. 23.

Dinnin, J. I., 1960, Releasing effects in flame photometry: Anal. Chemistry, v. 32, p. 1475.

Ingamells, C. O., 1964, Rapid chemical analysis of silicate rocks: Talanta, v. 11, p. 665–666.

——— 1966, Absorptiometric methods in silicate analysis: Anal. Chemistry, v. 38, p. 1228–1234.

Shapiro, Leonard, and Brannock, W. W., 1962, Rapid analysis of silicate, carbonate, and phosphate rocks: U.S. Geol. Survey Bulletin 1144–A, 56 p.

Suhr, N. H., and Ingamells, C. O., 1966, Solution technique for analysis of silicates: Anal. Chemistry, v. 38, p. 730–734.

Trent, Dorothy, and Slavin, Walter, 1964, Determination of the major elements in granitic and diabasic rocks by atomic absorption spectroscopy: Perkins-Elmer Atomic Absorption Newsletter, no. 19.

HYDROLOGY OF GLACIATED VALLEYS IN THE JAMESTOWN AREA OF SOUTHWESTERN NEW YORK

By LESLIE J. CRAIN, Albany, N.Y.

Work done in cooperation with the city of Jamestown, N.Y.

Abstract.—The glaciated valleys of southwestern New York contain relatively thin deposits of Pleistocene outwash sand and gravel interbedded in a thick sequence of lacustrine silt and clay. These sand and gravel layers are the principal source of ground water and are recharged through deltas built along the sides of the main valleys by tributary streams. The maximum dependable yield of the major aquifer at the Jamestown well field is about 10 million gallons per day. The results of the study in the Jamestown area may be applicable to other glaciated valleys in the southwestern and south-central parts of New York, and possibly to other glaciated areas.

A recent ground-water study in the Jamestown area in southwestern New York provides considerable insight into the hydrology of the valley-fill deposits in the glaciated valleys of the region. The information gained on the origin, character, and hydrology of the valley fill may be applicable to other valleys in the southwestern and south-central parts of New York and possibly in certain other glaciated areas.

The Jamestown area is characterized by three broad, flat-bottomed valleys, one containing a lake, lying between rounded uplands rising to as much as 1,000 feet above the valley bottoms (fig. 1). The valley walls and uplands generally consist of thin glacial till on Upper Devonian shales and siltstones. The valley-fill deposits are predominantly Pleistocene in age and range from about 400 feet in maximum thickness in the Chautauqua Lake valley to more than 1,000 feet in the Conewango Creek valley. The deposits in all the valleys are similar in origin and character. Detailed discussions of the bedrock stratigraphy and Pleistocene geology are available in reports by Tesmer (1963) and Muller (1963).

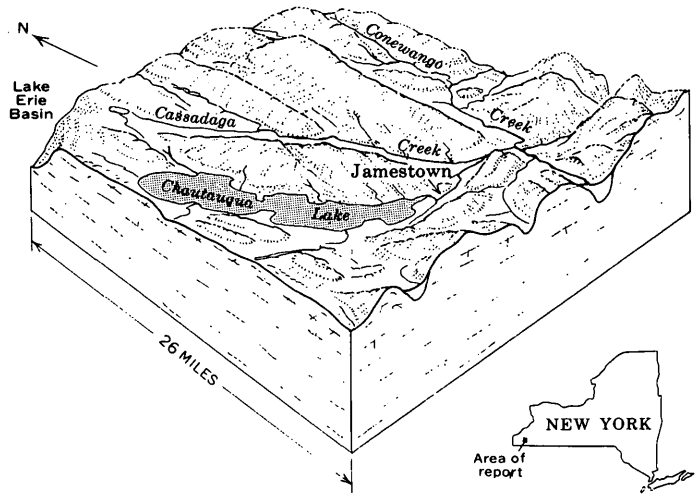

FIGURE 1.—Block diagram of the Jamestown area, New York.

GEOHYDROLOGY OF THE JAMESTOWN AQUIFER AREA

The surficial deposits in the valleys (fig. 2) consist of fluvial sand and gravel and of lacustrine silt and clay. Most of the deposits of sand and gravel underlie fan-shaped areas where tributary streams enter the main valleys. These deposits are the uppermost beds of deltas built by the streams as they entered the lakes that occupied the valleys after the melting of the last Pleistocene ice sheet The general character and extent of the unconsolidated deposits underlying the Cassadaga Creek valley are shown in an idealized block diagram in figure 3. The deposits in the other valleys of the area are similar. Most of the deposits consist of silt and clay, but the delta deposits along the sides of the valley and the relatively thin, extensive layer of sand and gravel embedded in the silt and clay are

U.S. GEOL. SURVEY PROF. PAPER 575-B, PAGES B192-B198

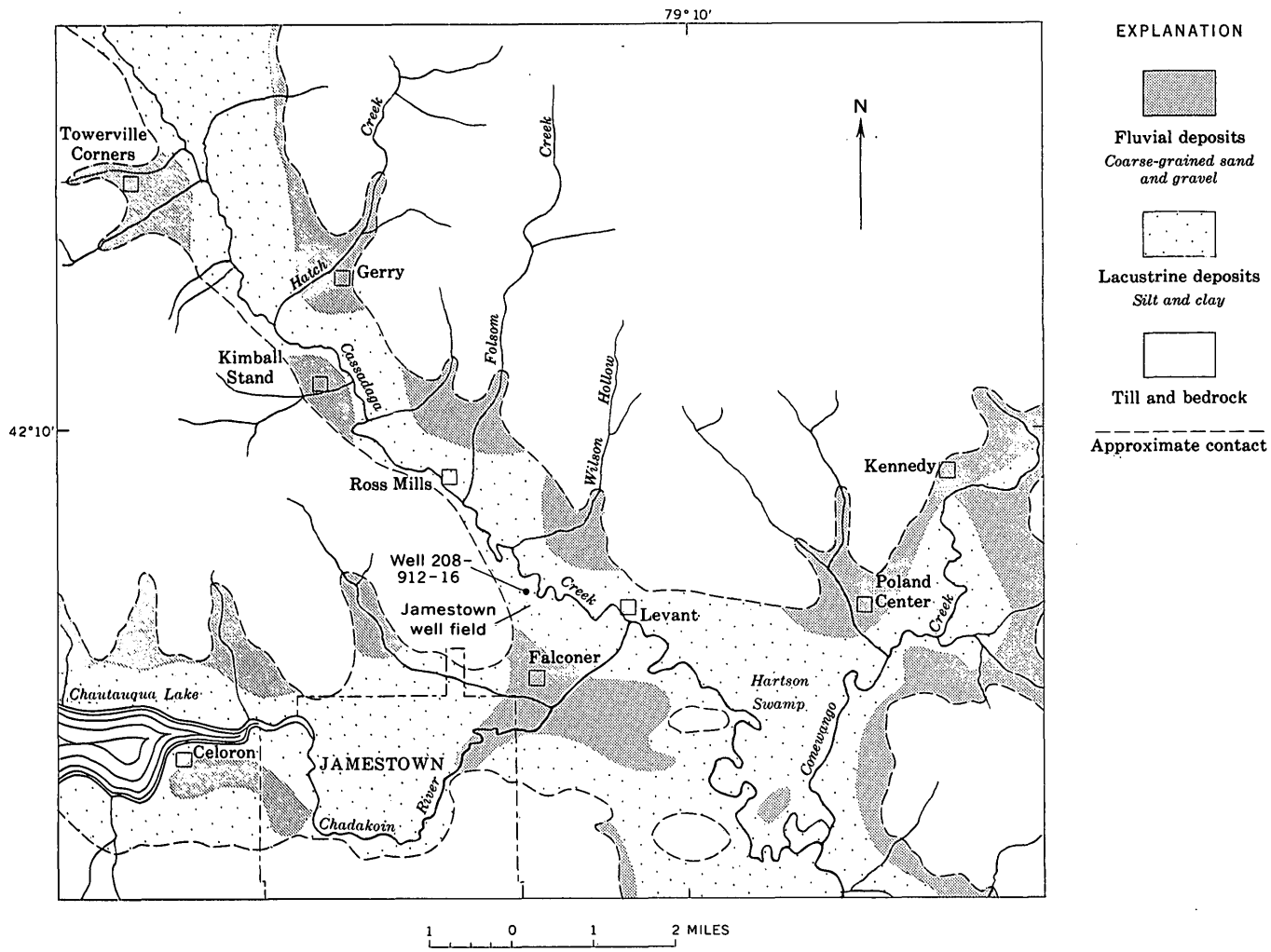

FIGURE 2.—Surficial deposits in part of the Chautauqua Lake and Cassadaga and Conewango Creek valleys near Jamestown, N.Y.

coarse grained. The extensive layer of sand and gravel, which is referred to in this report as the Jamestown aquifer, is believed to have been deposited as outwash by the last ice sheet to occupy the valley. Although other layers of sand and gravel are known to exist below the Jamestown aquifer, relatively few data are available on them. However, it is known that none of these other layers are as extensive or permeable as the Jamestown aquifer. Therefore, they have been omitted from the illustrations and the discussion of the valley hydrology in this paper.

The geologic history of the area is important in understanding the hydrologic relationships of the different deposits. Significant relationships are the interconnection of the deltaic deposits with the outwash (the Jamestown aquifer) and the interfingering of the deltaic deposits with the lacustrine silt and clay. The interconnection of the deltas and outwash indicate that deposition of the deltas began as soon as the ice had melted from the valleys, and the interfingering of the deltas and the lake deposits suggests relatively stable lake levels over a long period of time. It is believed that the lakes were destroyed by sedimentation rather than by erosion of their outlets, which would have left the deltas stranded at higher altitudes along the valley walls.

The Jamestown aquifer is discussed in the remainder of this paper because it has been more thoroughly investigated than similar outwash deposits in the other valleys. The Jamestown aquifer ranges from 10 to 30 feet in thickness, is overlain by 40 to 140 feet of silt and clay, and is underlain by an undetermined thickness of similar fine-grained materials. At the Jamestown well field (fig. 2) the aquifer averages 20 feet in thickness and is overlain by 120 feet of silt and clay. The known extent and the altitude of the top

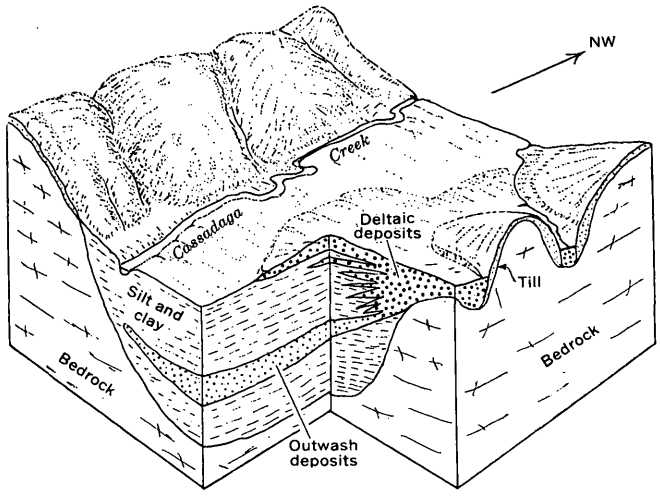

FIGURE 3.—Idealized block diagram of part of the Cassadaga Creek valley, showing general character of unconsolidated deposits that are typical of the Jamestown area.

of the aquifer are shown in figure 4. From its highest point in the Conewango Creek valley, the top of the aquifer slopes northwestward rather steeply in the area east of Falconer and then more gradually northward in the Cassadaga Creek valley.

The Jamestown aquifer has been used as a source of supply by the city of Jamestown since at least 1888, first from wells near Levant and, since 1923, from the present well field. The withdrawal of water has increased over the years to the present rate of about 6 million gallons per day. The increase in the rate of withdrawal has been accompanied by a decline in water level at the well field. In the long-range planning for the city, therefore, the hydrology of the aquifer has been thoroughly investigated. Particular attention has been given to the location of recharge areas, the amount of available recharge, and the capacity of the aquifer to transmit water.

Geologic studies, including the construction of test wells, indicated that recharge may occur through the delta deposits. In order to confirm this, and to determine how much recharge was available, a series of low-flow measurements was made on all of the tributary streams in the Cassadaga Creek valley during the spring and early summer of 1962. Streams crossing the deltas between the well field (Wilson Hollow) and Gerry (including Hatch Creek) were found to be losing water to the deltas.

In order to determine the relationship between streamflow and water levels in the deltas and in the Jamestown aquifer, two test wells were drilled in the delta of Folsom Creek near Ross Mills (fig. 2) and equipped with water-level recorders. One of these wells was located near the head of the delta and one near the periphery. During the spring, water levels in the two wells fluctuate with changes in the stage of Folsom Creek. However, by early summer, the quantity of steamflow from the uplands becomes very small and the water levels in both wells begin to decline. By late summer, the water level in the well near the head of the delta declines to an altitude lower than the water level in the well near the periphery, indicating that the hydraulic connection between the delta and the aquifer is near the valley wall. During the first period of high discharge of Folsom Creek in the fall of 1962, the water level in the well near the head of the delta responded immediately, rising nearly 20 feet in 3 days. However, the water level in the well near the periphery did not begin to rise until a month later, indicating that a large amount of storage had to be replaced in the delta.

PUMPING AND GROUND-WATER LEVELS

The principal discharge from the Jamestown aquifer is through the Jamestown well field. The drawdown effects of pumping at the well field are detectable as far north as Gerry and as far east as the vicinity of Hartson Swamp (fig. 2). Figure 5 shows the contours of the piezometric surface on June 7, 1963, when the rate of pumping at the Jamestown well field was approximately 6.5 mgd. Water levels were relatively stable at that time, and an analysis of flow lines and gradients indicated that the average permeability of the aquifer in the area surrounding the well field was about 8,500 gallons per day per square foot. Flow-net analyses using these and other measurements indicate that nearly 90 percent of the water at the well field is being supplied from that part of the Cassadaga Creek valley north of the field and that the remaining water is derived from the valley south of the well field and from the Conewango Creek valley.

The Jamestown aquifer may be compared to a pipeline or conduit transporting water from a series of reservoirs (the deltas) that are releasing water from storage each summer and being refilled by runoff from the uplands during the winter and spring. Figure 6 shows a hydrologic model of the relationship between the Jamestown aquifer and the deltas.

The maximum perennial yield of the Jamestown aquifer at the well field depends principally on three factors: (1) the maximum gradient that may be established with the available drawdown, (2) the amount of recharge to the deltas, and (3) the storage in the deltas that is available to the aquifer.

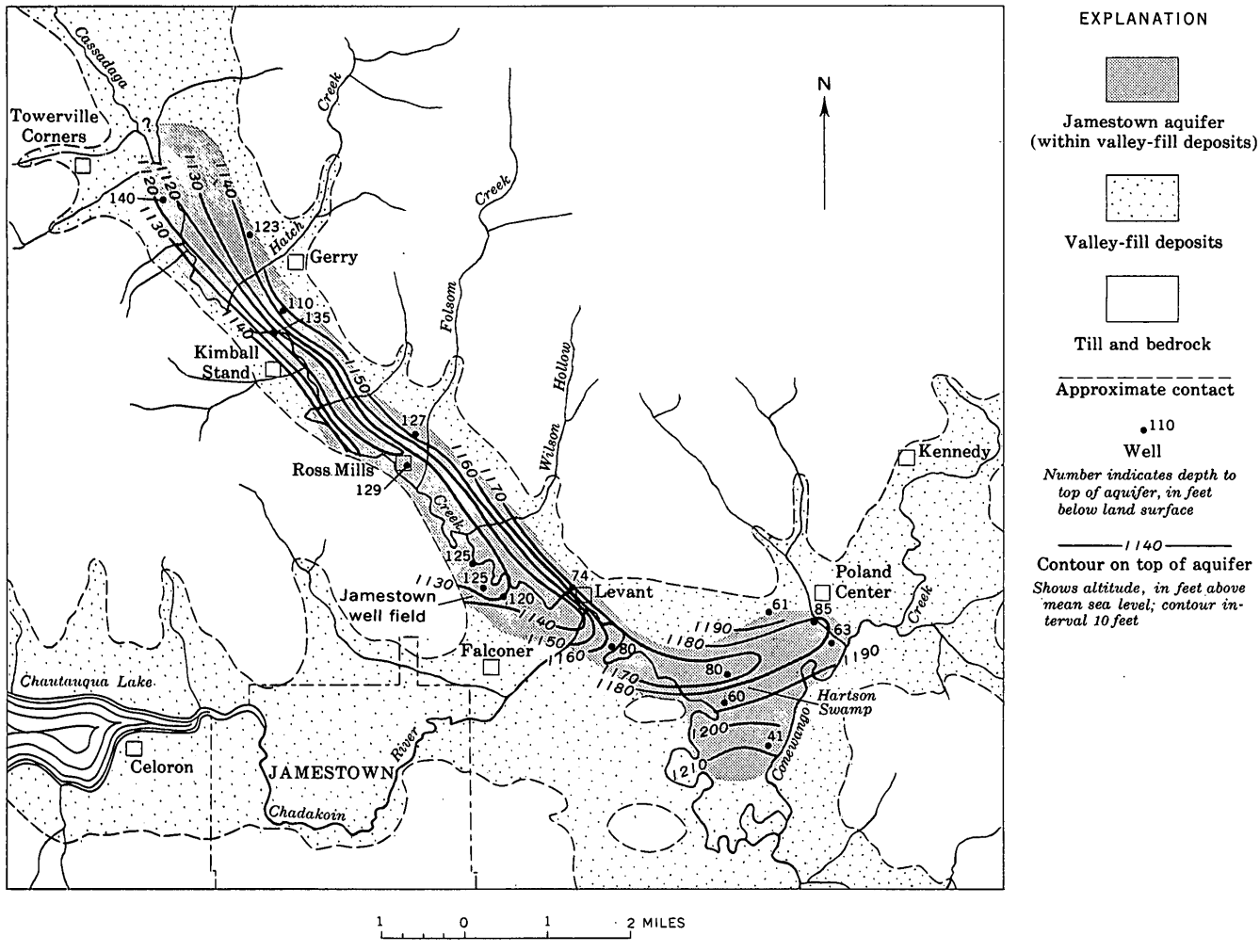

FIGURE 4.—Areal extent and altitude of the top of the Jamestown aquifer.

The maximum gradient that would be established in the aquifer with the maximum available drawdown at the well field can be determined only hypothetically. The top of the Jamestown aquifer is about 120 feet below land surface at the well field, and this value has been selected as the maximum desirable drawdown because it would not result in dewatering of the aquifer. By using this value and the actual gradients in the aquifer under different rates of pumping at the well field, it is possible to construct probable future gradients.

Figure 7 shows two profiles of gradients in the Jamestown aquifer from the well field northward in the Cassadaga Creek valley. The uppermost profile was actually measured in the aquifer on June 7, 1963, while pumping at the well field was at a rate of 6.5 mgd. The largest proportion of this pumpage, as shown by the steepness of the profile, was being obtained from the Cassadaga Creek valley between Ross Mills and the well field.

The lower profile in figure 7 was computed by using a maximum drawdown of 120 feet at the well field and by assuming that the same relative proportions of water would be derived from the several deltas and transported through the aquifer, as under the actual pumping conditions that are indicated on the upper profile. The assumed profile shows that about 10 mgd could be transported from the Cassadaga Creek valley to the well field. The amount of water that would be moving through each segment of the aquifer was computed by using the projected gradient and the minimum width of the aquifer in each section. Again, it should be noticed that the largest amount of water is derived from those deltas closest to the well field. The computations have ignored the area south of the well field, from which it seems reasonable that at least 1 to 2 mgd could be derived.

Therefore, analysis of the possible maximum gradient in the aquifer indicates that the field can produce a perennial yield of from 10 to 12 mgd. However, the

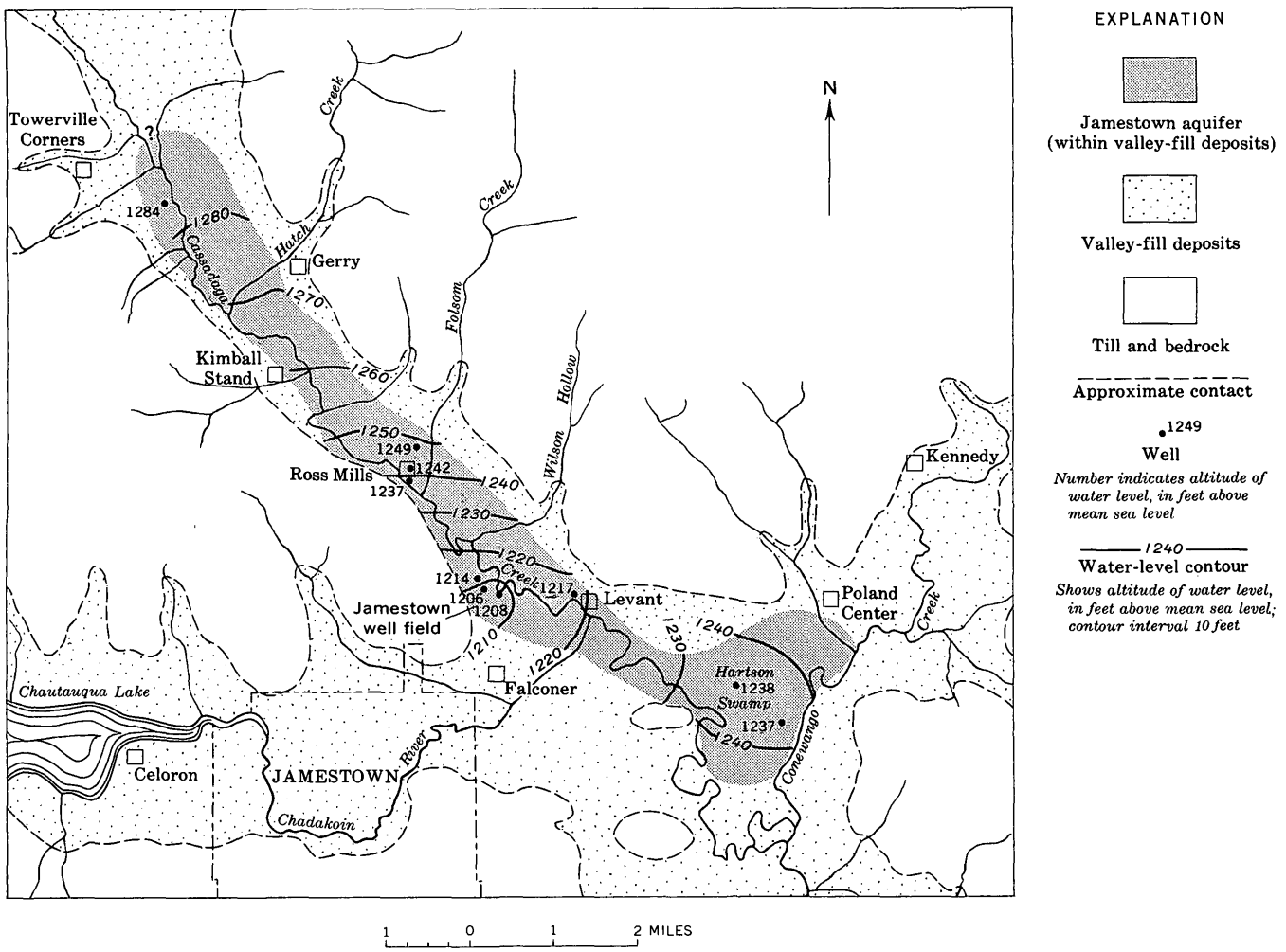

FIGURE 5.—The altitude and configuration of the piezometric surface of the Jamestown aquifer on June 7, 1963.

amount of recharge to the deltas and the quantity of water stored in them must be evaluated to determine whether sufficient water is available.

The recharge available to the deltas is influent seepage from streams draining the uplands. On the basis of records for two long-term gaging stations in the area, the natural stream runoff for the region averages 1.1 mgd per square mile of drainage area. This discharge, multiplied by the drainage areas of the streams above the 5 deltas north of the well field (fig. 2), gives an average yield of 31 mgd to the deltas. However, there are wide seasonal variations in runoff, especially from the streams draining the till and bedrock uplands. Most of the runoff occurs during brief periods in the late fall and spring in amounts greater than are needed to replace delta storage, and the excess runs off through the major streams draining the valleys. In the summer and early fall, streamflow is inadequate to replace the water that drains from the deltas in response to pumping and natural discharge. Therefore, water pumped at the Jamestown well field during the summer and early fall must be supplied largely from storage in the deltas, which is replenished during periods of high runoff in the late fall and spring.

The water available to the Jamestown well field from the delta deposits is that which would be dewatered under conditions of maximum drawdown at the well field. By assuming that the gradient in figure 7 is a reasonable projection of the future gradient under these conditions, it was determined that the maximum possible dewatering of the deltas would range from 10 feet at Towerville Corners to 100 feet in the Wilson Hollow delta opposite the well field. By assuming further that the deltas are shaped roughly like inverted cones (fig. 3) and have a specific yield of 0.2, the amount of projected dewatering was com-

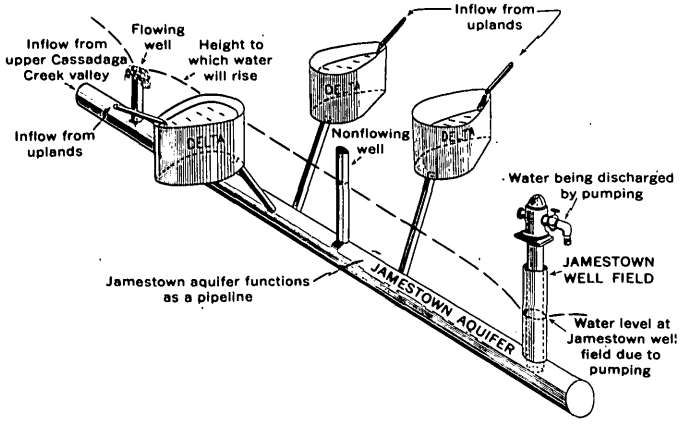

FIGURE 6.—Hydrologic model of the Jamestown aquifer and delta deposits.

puted. These storage computations indicate that the dewatering of the 5 deltas would yield about 1.7 billion gallons of water, or 6 mgd for 280 days or 10 mgd during the 170 days from early May to the end of September.

Past records of water levels at the Jamestown well field provide a better means of estimating the maximum perennial yield of the well field. At present, pumping is constant, except for a few hours each week, and 6 to 8 wells are in use all the time. Although it is impossible to observe static water-level conditions at the field, the U.S. Geological Survey has maintained a water-level recorder on an observation well in the well field since 1952 in order to determine seasonal and long-term water-level trends. The water level in the observation well represents an integration of the drawdown effects of those factors determining the yield of all wells that are pumped.

Hydrographs from the recorder and pumpage records from the city have been compared and evaluated for the period 1953–64. Graph *A* in figure 8 shows hydrographs for well 208–912–16, which is in the center of the Jamestown well field about 200 feet from the nearest well that is pumped, and for well 203–929–1, which is about 10 miles west of Jamestown and is in the same climatic environment as Jamestown, but not influenced by pumping. Although the water level in both wells rises and declines seasonally, only the water level in well 208–912–16 shows a progressive long-term decline due to pumping. A trend line of the annual lowest water levels in well 208–912–16 has been drawn on graph *A*. In drawing this line, the years 1956 and 1958 were ignored because the summers of both years were marked by unusually heavy rainfall and abundant recharge to the deltas. Graph *B*, showing the annual average daily pumpage at the Jamestown well field for the same period, indicates a gradual increase for the 12-year period.

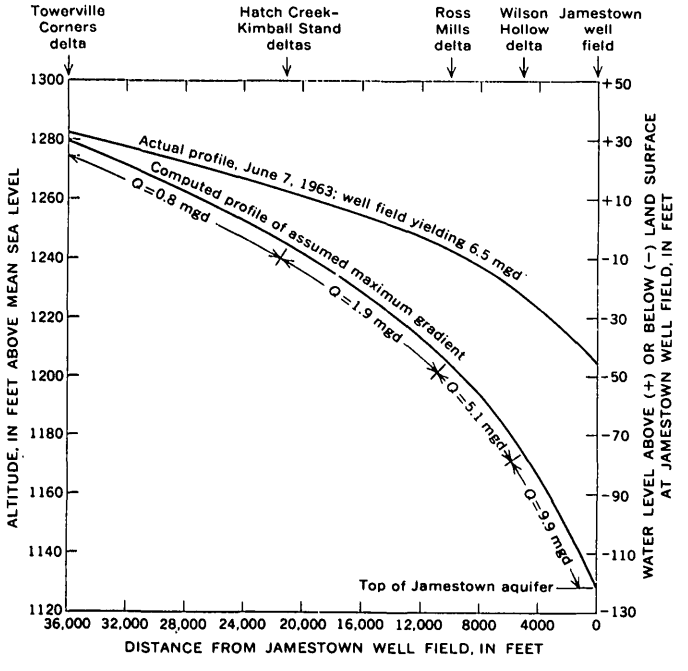

FIGURE 7.—Two profiles of gradients in the Jamestown aquifer.

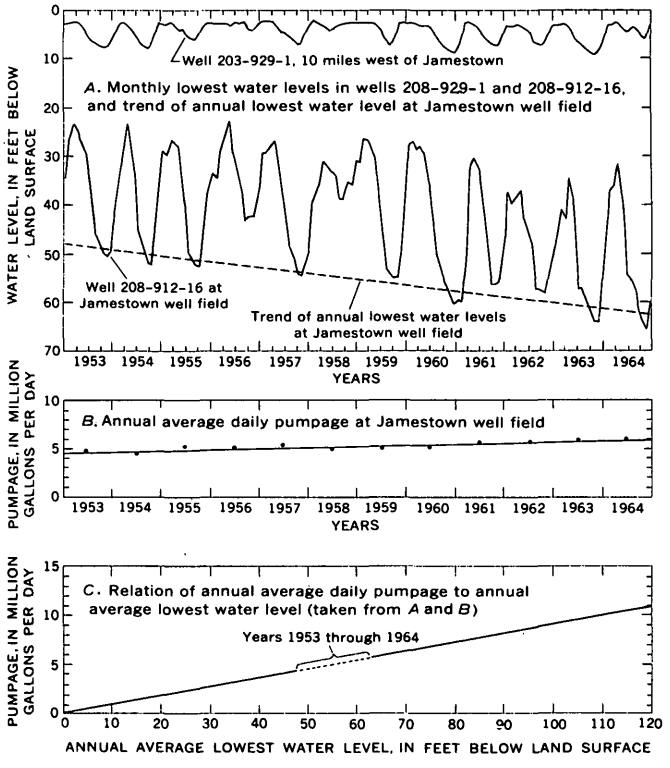

FIGURE 8.—Graphs showing monthly lowest water levels in two wells (*A*), pumpage at the Jamestown well field (*B*), and the relation of pumpage to water level (*C*).

Graph *C* in figure 8 compares annual lowest water levels with average daily pumpage. The line intersects the 120-foot line at slightly more than 11 mgd, indicating that an average daily pumpage of about 11 mgd would cause an annual low-water level of 120 feet below land surface in well 208–912–16. However, well 208–912–16 is an unpumped observation well that is 200 feet from the nearest pumping well, and the water level in the pumping well is 10 feet lower than that in the observation well. This difference is due mainly to a head loss caused by the gradient necessary for water to pass from the aquifer through the well screen into the well. Also, the trend line of annual lowest water levels is actually a few feet above the lowest recorded levels. Therefore, because the actual pumping levels may be as much as 15 feet below the levels indicated by the trend line on graph *A*, the maximum dependable yield of the well field is probably not more than about 10 mgd.

CONCLUSIONS

The evaluation of the maximum perennial yield of the Jamestown aquifer is based on the assumption that the relationship of pumpage to water levels will, at higher pumping rates, continue to be the same as in the past. At the higher pumping rates, however, additional hydraulic or hydrologic boundaries may be reached. Should this occur, the slope of the trend line would change and the actual maximum perennial yield would probably be lower than predicted.

Although this evaluation has dealt with the hydrology of a specific valley, the methods may be applicable in similar evaluations of other valleys.

REFERENCES

Muller, E. H., 1963, Geology of Chautaugua County, pt. 2, Pleistocene geology: New York State Mus. Bull. 392, 60 p.

Tesmer, I. H., 1963, Geology of Chautaugua County, pt. 1, Stratigraphy and paleontology (Upper Devonian): New York State Mus. Bull. 391, 65 p.

DEVELOPMENT OF A GROUND-WATER SUPPLY AT CAPE LISBURNE, ALASKA, BY MODIFICATION OF THE THERMAL REGIME OF PERMAFROST

By ALVIN J. FEULNER and JOHN R. WILLIAMS, Anchorage, Alaska, Boston, Mass.

Work done in cooperation with the U.S. Air Force, Alaskan Air Command

Abstract.—A water supply has been developed in formerly frozen alluvium beneath a small intermittent stream by modification of the thermal regime of permafrost. The modification, largely a byproduct of road and reservoir construction, was effected by: (1) removal of tundra vegetation and the upper few feet of alluvium, which allows warming of gravel and water in the summer; (2) construction of a reservoir upvalley, from which water recharges the alluvium during the summer; and (3) installation of galleries downvalley from the reservoir to collect the water. Similar methods may make it possible to obtain water supplies elsewhere in arctic regions where stream alluvium extends below the depth of winter freezing.

In the arctic region of Alaska, between the Brooks Range and the Arctic Ocean, permafrost occurs nearly everywhere (Ferrians, 1965) and extends to depths as great as 1,330 feet (Brewer, 1958; Black, 1957; Hopkins and others, 1955). Because of the presence and great thickness of the permafrost, and because ground water in bedrock below the permafrost is commonly brackish or saline, year-round supplies of potable water are difficult to discover and maintain. Unfrozen zones between the lower limit of seasonal frost and the top of permafrost occur normally only beneath large rivers which flow throughout the winter and beneath lakes deeper than 8 feet and wider than 2,000 feet (Hopkins and others, 1955, p. 119). The presence of unfrozen zones is due to the geothermal effects of bodies of water in these areas (Lachenbruch and others, 1962). Beneath small intermittent streams the seasonal frost commonly extends to permafrost and ground water is available only in summer.

The distribution and thickness of permafrost are controlled by the thermal regime of the ground, which in turn is chiefly controlled, under natural conditions, by several geographic and climatological factors (Muller, 1947, p. 14). These factors include: geographic position, topographic relief, air temperature, cloudiness, precipitation, and the direction of prevailing wind. Other factors, which may be controlled to some extent by man, include: snow cover, vegetation, moisture content of the ground, and surface evaporation. Cederstrom (1952, p. 36) proposed that by modifying the thermal regime the upper part of the permafrost at Kotzebue, Alaska, could be thawed. He further proposed that the depth to which the winter frost penetrated could be reduced through installation of snow fences in the area.

As part of a program to provide technical assistance to the Alaskan Air Command, U.S. Air Force, various methods of providing water supplies have been tested in localities underlain by permafrost. At Cape Lisburne, the locality described in this report, development of a water supply by modification of the thermal regime was largely a byproduct of road and reservoir construction. However, the procedures and their effects were virtually the same as those suggested by Cederstrom.

GEOGRAPHIC AND GEOLOGIC SETTING

Cape Lisburne, Alaska, is the northwestern extremity of the Lisburne Hills, facing the Chukchi Sea (fig. 1). The area described in this report is adjacent to Selin Creek, which flows northward across a narrow coastal lowland, from the Lisburne Hills to the ocean, about 2½ miles east of Cape Lisburne. The lower part of the stream valley is entrenched 15 to 20 feet into the tundra surface of the coastal lowland.

The regime of Selin Creek is controlled by the arctic climate, which is characterized by long cold winters and short cool summers. The average annual precipi-

U.S. GEOL. SURVEY PROF. PAPER 575-B, PAGES B199-B202

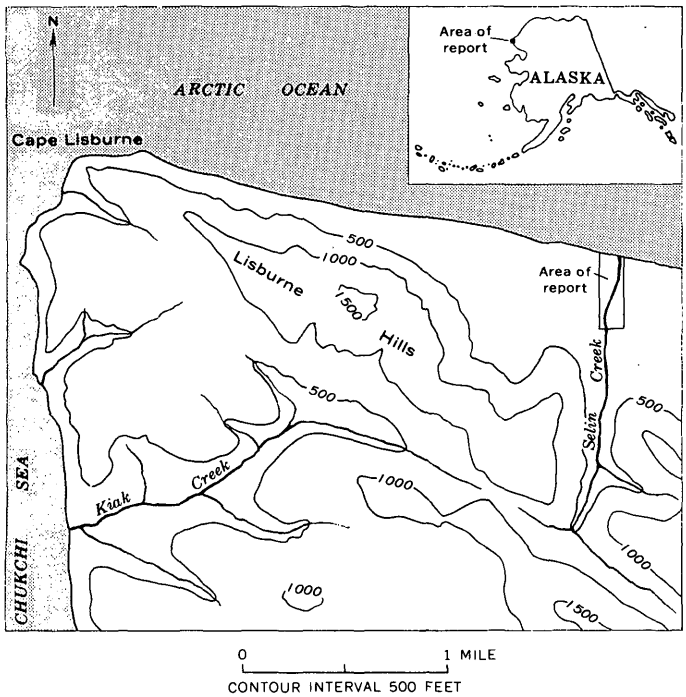

FIGURE 1.—Index map of the Cape Lisburne area, northwestern Alaska, showing area described in this report.

tation at Cape Lisburne for the years of record, about 15 inches, is considerably higher than that for most arctic areas. The average annual temperature, 16.8°F, is well below that at which permafrost forms under natural conditions. The depth of summer thawing in undisturbed ground is about 1 to 4 feet; during each winter, seasonal frost penetrates to the top of the permafrost. The total thickness of permafrost at Cape Lisburne is not known, but a thickness of about 1,200 feet was recorded in a similar coastal plain at Cape Thompson, about 50 miles south of Cape Lisburne (Lachenbruch and others, 1960).

At Cape Lisburne the coastal lowland is composed of Quaternary deposits that overlie frozen siltstone and shale. The Quaternary deposits thicken rapidly seaward. They consist of intermixed and stratified silt or clay, fine to coarse gravel, and bouldery talus of limestone and chert. Near the sea the deposits contain a lens of clay interbedded locally with boulders and beach deposits. This lens, which parallels the shoreline, is considered to be material laid down in a stream-fed coastal lagoon. The thickness of the lens and the thickness and lithology of the underlying deposits are unknown.

EARLY WATER SUPPLY

The first water-supply installation at Cape Lisburne, constructed in the summer of 1951, consisted of a lateral gallery 80 feet long excavated into the naturally thawed gravels that underlie Selin Creek (fig. 2). The gallery was chosen in preference to other types of supply systems because at that time the gravelly alluvium in the creek valley was frozen beneath a point about 6 feet below ground surface, and wells were not believed to be practical.

The gallery produced water for only a few weeks after the stream ceased to flow during the fall of 1951, and for a similar period during the early winter of 1952. In 1953 a reservoir (off the map in figure 2) was constructed approximately 500 feet upstream from the gallery to provide a winter source of water. Leakage through the highly permeable alluvium underlying the reservoir, however, made the attempt unsuccessful in spite of attempts to seal the bottom.

It then became necessary to build storage tanks and to melt snow to supplement the winter water supply at Cape Lisburne. However, further study of alternate

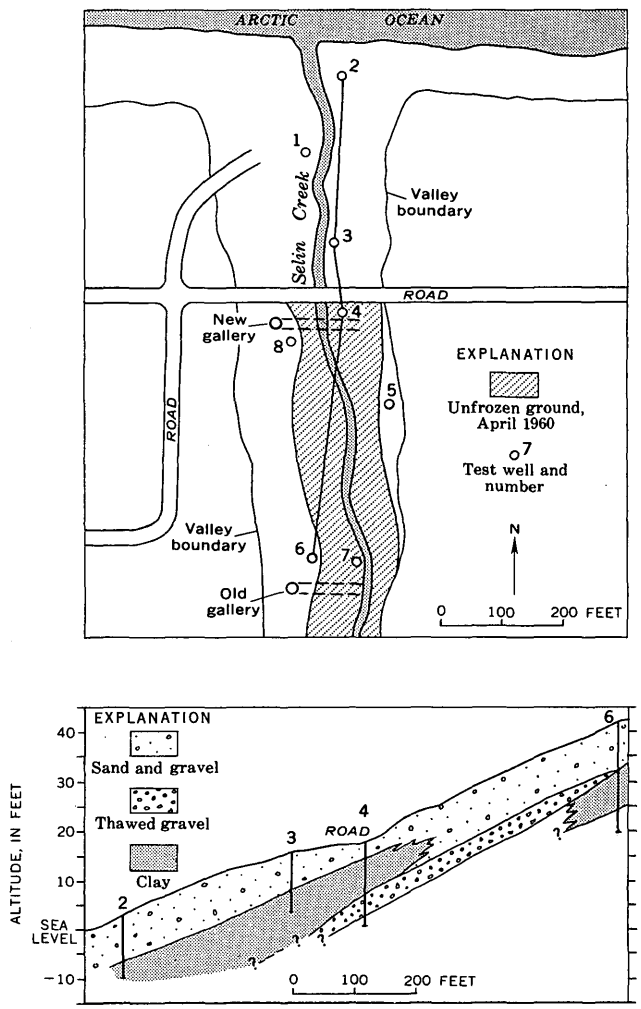

FIGURE 2.—Sketch map showing location of test wells, and geologic section showing extent of unfrozen ground and subsurface conditions along Selin Creek.

water sources became warranted when the tanks proved to be too small to store an annual supply of water and when the melting of snow was found to be a tedious and unsatisfactory method of water supply.

LATER WATER SUPPLY AFTER MODIFICATION OF THERMAL REGIME OF PERMAFROST

A study of alternative sources of water suggested that changes in the thermal regime of the alluvium of Selin Creek were taking place after the tundra cover had been stripped from the flood plain to uncover road-building material between 1951–1955, and after construction of the reservoir in 1953. In order to verify these inferences eight test holes were drilled in the stripped portion of the flood plain along Selin Creek (fig. 2) in 1960.

Test holes 1, 2, and 3, drilled between the beach and the road across Selin Creek, penetrated only frozen materials. Test holes 4–8 were drilled in the flood plain between the road and the old gallery upvalley. In test hole 4, water-bearing gravel was reached at a depth of 13.5 feet and frozen gravel (permafrost) was reached at a depth of 16 feet. Holes 5, 6, and 8, drilled along the edge of the flood plain, penetrated only frozen materials. Hole 7, drilled to a depth of 23 feet near the old gallery in the center of the stream channels, penetrated frozen silt and gravel to a depth of 7 feet, dry gravel between 7 and 9.5 feet, and frozen silt and boulders (permafrost) between 9.5 and 23 feet.

Because unfrozen ground was found upstream and only frozen ground was found downstream from the road, it is inferred that the winter frost penetrated the alluvium under the relatively snow-free road (fig. 2) and formed a ground-water dam which prevented or retarded the seaward movement of water in the creekbed alluvium. It is also thought that the presence of the lens of clay shown on figure 2 may have aided in retarding the seaward movement of water during the summer months. Without the retarding effect of either the lens of clay or the ground-water dam, the fresh water in the lower portion of the thawed zone would move seaward and allow the gallery to become dry by midwinter.

On the basis of the presence of unfrozen ground a new lateral gallery 90 feet long at right angles to the streambed of Selin Creek was installed near well 4 (fig. 3). The gallery pipe, perforated throughout its length to permit entry of water, slopes slightly toward a vertical sump, the bottom of which is about 20 feet below the streambed. Two steam lines, 2 inches in diameter, were installed along the gallery pipe to prevent inward freezing along the gallery during late winter and thus to provide access for water both during the winter from snowmelt and when the first spring thaw takes place.

The gallery and related structures were completed by the end of April 1961 and were placed in operation in August 1961. Since that time, sufficient water has been obtained for the Air Force installation each year by combined use of the gallery and of tank storage, and the melting of snow has not been necessary. In some years the gallery is not pumped during the period February–May because stored water obtained by pumping through January has been sufficient. However, the gallery still contains water during this critical period of the year, as was demonstrated in 1963 and in 1965; in each of these years about 400,000 gallons of water was pumped during the period February–May.

Continued production from the gallery can be assured by (1) pumping during the early winter, to

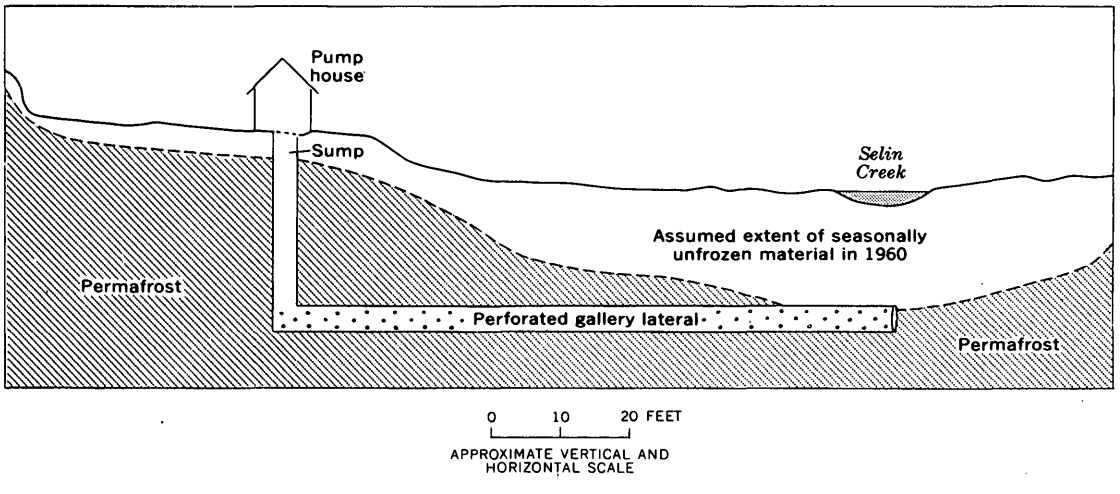

FIGURE 3.—Sketch of new gallery installation.

obtain the shallow ground water and to dewater the upper part of the unfrozen zone; (2) continuing pumping but at a lower rate during the later winter months, partly to induce movement of water toward the gallery and partly to prevent freezing; and (3) retaining the reservoir to provide a point where surface water, warmed slightly by retention in the surface reservoir, can enter the aquifer and thaw the frozen ground. Continuing seepage from the reservoir during midsummer and late summer will promote percolation from the reservoir site downward to the permafrost and laterally downgradient. The percolating water will carry enough heat from the surface to increase the depth of thawing. Erection and maintenance of snow fences upstream from the new gallery location and downstream from the reservoir site will not only provide an insulating snow cover that will reduce the depth of seasonal frost penetration but also will provide a source of early spring recharge.

The ground water created by changing the thermal regime of the alluvium beneath Selin Creek is the most economical and convenient source of water at Cape Lisburne. Disturbance of the thermal regime permitted deeper penetration of solar heat and thus caused the permafrost table to decline from a depth of from 4 to 6 feet below ground surface in 1950 to nearly 16 feet below ground surface in 1960. Addition of snow fences between the new and old gallery locations across the flood plain of Selin Creek increased the depth of snow cover and reduced the depth of seasonal frost penetration. These steps created a body of unfrozen alluvium from which water can be pumped during the winter. The gallery has eliminated the problems involved in melting snow and, when used in conjunction with tank storage, provides water throughout the year.

REFERENCES

Black, R. F., 1957, Some problems in engineering geology caused by permafrost in the Arctic coastal plain, northern Alaska: Arctic, v. 10, no. 7, p. 230–240.

Brewer, M. C., 1958, The thermal regime of an arctic lake: Am. Geophys. Union Trans., v. 39, no. 2, p. 278–284.

Cederstrom, D. J., 1952, Summary of ground-water development in Alaska, 1950: U.S. Geol. Survey Circ. 169, 37 p.

Ferrians, O. J., Jr., 1965, Permafrost map of Alaska: U.S. Geol. Survey Misc. Inv. Map I–445.

Hopkins, D. M., Karlstrom, T. N. V., and others, 1955, Permafrost and ground water in Alaska: U.S. Geol. Survey Prof. Paper 264–F, p. 113–146.

Lackenbruch, A. H., Green, G. W., and Marshall, B. V., 1960, Preliminary results of geothermal studies at Ogotoruk Creek, AEC Project Chariot test site, northwestern Alaska: Alaskan Sci. Conf., 11th, Anchorage, 1960, Proc., p. 167.

Lackenbruch, A. H., and others, 1962, Temperatures in permafrost: Temperature—Its Measurement and Control in Science and Industry, v. 3, pt. 1, p. 791–803.

Muller, S. W., 1947, Permafrost or permanently-frozen ground and related engineering problems: Ann Arbor, Mich., J. W. Edwards, Inc., 1947, 231 p.

THE PERMEABILITY OF FRACTURED CRYSTALLINE ROCK AT THE SAVANNAH RIVER PLANT NEAR AIKEN, SOUTH CAROLINA

By I. WENDELL MARINE, Aiken, S.C.

Work done in cooperation with the U.S. Atomic Energy Commission

Abstract.—The apparent permeability of finely fractured crystalline rock beneath the coastal-plain sediments at the Savannah River Plant is estimated from swabbing tests to be less than 0.004 gallon per day per square foot and to average about 0.0003 gallon per day per square foot. Laboratory analyses give similar values for this type of rock. The apparent permeability of zones of more open fractures is estimated from pumping tests to average about 1 gallon per day per square foot even though some fractured sections within these zones locally exceed this value.

An exploratory drilling and testing program, part of an investigation of the feasibility of storing radioactive waste in artificially excavated chambers in crystalline rock, was completed in June 1963 at the U.S. Atomic Energy Commission's Savannah River Plant near Aiken, S. C. (Christl, 1964; Siple, 1964; Proctor and Marine, 1965). The Savannah River Plant is located on the Atlantic Coastal Plain about 20 miles southeast of the Fall Line, which is the boundary between the coastal plain and the Piedmont province where the crystalline rocks crop out (fig. 1). The crystalline rocks at the proposed storage site are buried beneath approximately 930 feet of unconsolidated to semiconsolidated sediments consisting predominantly of sand and clay. To the depths explored by drilling (about 2,000 feet below the land surface and 1,000 feet below the lowermost sedimentary deposit), the crystalline rock is composed predominantly of schist and gneiss with lesser amounts of quartzite; the schistosity or foliation strikes generally northeast and has an average dip of about 55° SE. Immediately overlying the crystalline rock is a layer of clay called saprolite, which is the residual product of subaerial weathering of the crystalline rock before the deposition of the overlying sediments. The saprolite averages 50 feet in thickness and effectively separates the water in the fractured crystalline rock from that in the overlying sediments.

As part of the investigation, the hydrologic and hydraulic characteristics of the crystalline rock were studied. An earlier paper by the author (Marine, 1966) presents evidence for two types of water-transmitting fractures in the upper 1,000 feet of the buried crystalline rock. One type pervades the entire rock mass but consists of fractures so minute that water movement through them is exceedingly slow. The other type is restricted to definite zones and consists of larger openings that transmit water at a faster rate. The earlier paper also presents a possible areal correlation of the second type of fracture based on hydraulic information. In this paper the methods used to estimate the coefficients of transmissibility, permeability, and storage for both types of fractures are described, and the ranges and average values are given.

TRANSMISSIBILITY AND PERMEABILITY

The ability of crystalline rock to transmit water is governed by the size and abundance of open fractures in it. If all the fractures are minute, the rate at which water is transmitted is low. Conversely, if some of the fractures are more open, the rate at which water is transmitted is greater. The upper 1,000 feet of crystalline rock contains sufficient minute fractures that, if enough time is allowed, the entire rock mass acts as a hydraulic unit. As a result of these minute fractures, drill holes for which there is no evidence of definite zones of fluid inflow slowly fill with water to the static water level in that section of rock. This water level responds to changes in pressure due to withdrawal or injection at other places within the

U.S. GEOL. SURVEY PROF. PAPER 575-B, PAGES B203-B211

241-334 O—67——14

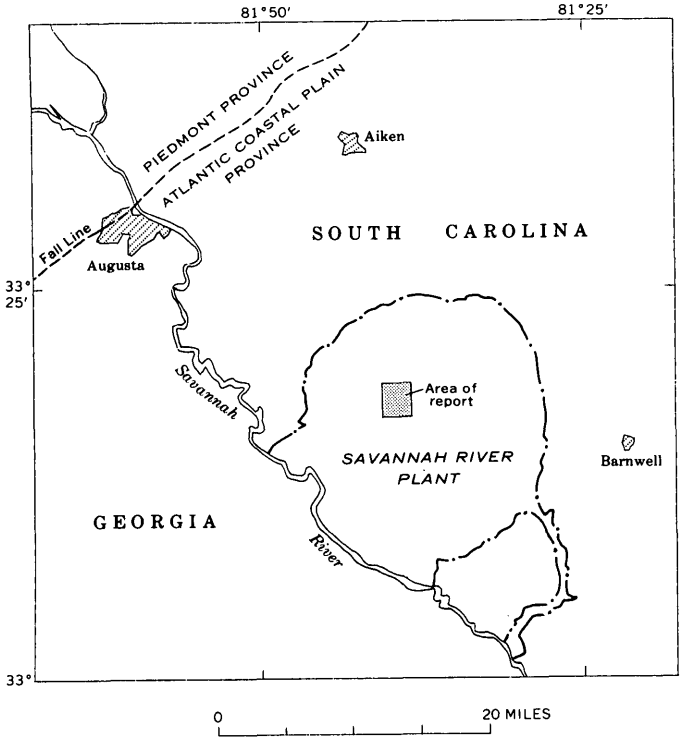

FIGURE 1.—Location of the Savannah River Plant and area of report.

rock, but the response is both delayed and protracted compared to that in a hole that is open to one or more zones of larger fractures. In this report rock that includes only these minute fractures is termed virtually impermeable. In the explored region of crystalline rock there are at least two zones in which fractures are more open and along which more rapid hydraulic responses take place. Any well that yields more than 1 gallon per minute from the crystalline rock has penetrated at least one of the zones of more open fractures.

The equations used in most field methods of determining permeability are based on an assumption that the rock is homogeneous and isotropic. These assumptions are not strictly applicable to aquifers that consist of fractured crystalline rocks. However, in view of the lack of equations derived specifically for this type of aquifer, the available equations are useful provided their limitations are recognized. The values computed for the hydraulic constants should be regarded as apparent, rather than actual. They may be thought of as characteristic of a homogeneous and isotropic aquifer in which the water-level response to the withdrawal of water is equivalent to the water-level response in the tested section of rock. The degree to which the fractured crystalline rock actually conforms to the assumptions of the analysis probably varies from section to section. In some sections the fractures are probably sufficiently numerous that the rock is broken into blocks, thus making it analogous to a very coarse grained granular medium, and the apparent hydraulic constants are not greatly different from the actual. In other sections the water transmission may be along one, or at most only a few, discrete fractures, and the apparent hydraulic constants may depart from the actual.

METHODS OF STUDY

Several different methods were used to determine the ability of the crystalline rock to transmit water. Laboratory tests were made on sections of unbroken core from drill holes. Intervals of drill holes were isolated by means of packers, and one or more of the following done: (1) water was injected under pressure to determine the rate of acceptance; (2) water was extracted by swabbing to determine the rate of inflow where the yield exceeded the swabbing rate; (3) water was swabbed from the packed-off interval and observations were made of the rate of water-level recovery after swabbing stopped where continuous swabbing could not be maintained; (4) a column of water (slug) was released instantaneously into the packed-off interval and observations were made of the rate of water-level recovery. Of these, only methods 3 and 4 could be used quantitatively to determine the coefficients of transmissibility and permeability. Lastly, several pumping tests were made; water was pumped from one of the drill holes and measurements of the water-level drawdown and subsequent recovery were made in other drill holes.

The laboratory analyses were of value only on virtually impermeable rock because open fractures could never be included in the specimens tested. The swabbing and recovery tests were primarily of value on virtually impermeable rock because of difficulty in both collecting and analyzing data where the recovery was fast and the time taken for swabbing was significant compared to the time for recovery. The "slug" tests were primarily of value in determining the local transmissibility of zones of relatively open fractures. Pumping tests were used to obtain average values for areally extensive zones that contained relatively open fractures.

Laboratory tests

Permeability was measured on 29 samples of unbroken rock core in the South Atlantic Division Laboratory of the U.S. Army Corps of Engineers in

Marietta, Ga. About two-thirds of the measurements were less than 0.8×10^{-6} gallons per day per square foot, which was the lowest value measurable by the testing equipment and procedure (1,000 pounds per square inch differential pressure for 30 days). However, the other one-third of the samples had measurable permeabilities that ranged up to a maximum of 0.002 gpd/sq ft and averaged 0.0005 gpd/sq ft. In each sample that had measurable permeability the water leakage occurred at some inhomogeneity such as a minute fracture, a healed fracture, a chlorite seam, or the contact between schist and gneiss. Probably in the mass of crystalline rock these inhomogeneities are so common that they render large sections of apparently sound rock nearly homogeneous with respect to permeability. Because rock cores tend to expand when removed from the hole owing to the removal of the rock pressure that is due to the weight of the overburden, the values obtained for the coefficient of permeability may be somewhat higher than they would have been if the rock could have been tested in place.

Packer tests

Injection tests

In order to test individual sections of the rock for their water-transmitting properties in place, packers were set in the well at the top and bottom of the section to be tested, and water was either injected into or removed from that section. In the injection tests attempts were made to pump water into the packed-off interval at pressures of 20, 40, and 60 psi measured at land surface. However, the flow into most sections was so low as to be unmeasurable. Although the tests provided a qualitative evaluation of the water-transmitting properties of the rock, it was not possible to use the test data to estimate the apparent permeability, and about halfway through the investigation the injection tests were abandoned in favor of swabbing tests.

Swabbing tests

These tests consisted of swabbing water out of the drill pipe that connected the packed-off interval to the surface, and also consisted of measuring the water-level recovery. In these tests the swab and its overlying column of water were first lifted from about 200, 400, 600, and 900 feet below land surface; then all succeeding swabs were lifted from about 900 feet. If inflow into the packed off interval was so small that 3 successive swabbing lifts from a depth of 900 feet produced no water, water-level recovery measurements were begun. These were continued for at least 2 hours and sometimes for as long as 60 hours. If inflow into the packed off interval from successive swabbing lifts from a depth of 900 feet was sufficient to produce water, swabbing was continued at least until a volume of water equal to that of the pipe and the packed-off section of the well had been removed. Water level recovery measurements were then begun.

The results of both the injection tests and the swabbing tests (table 1) should be considered only in a qualitative manner. Figure 2 shows the location of the exploration wells.

TABLE 1.—*Results of injection and swabbing tests*

U: Unmeasurable small rate of acceptance under an injection pressure of 60 pounds per square inch measured at land surface, where no swabbing test was made.
A: Rate of acceptance under injection pressure of 60 pounds per square inch measured at land surface, where no swabbing test was made.
I: Average rate of inflow that entered packed-off interval between 60 and 120 minutes from the midpoint of the swabbing time.
Y: Average yield to continuous swabbing.

[Static water levels were measured on January 13, 1964, and are depths below land surface]

Packed-off interval (feet below land surface)	Depth to water 60 minutes after midpoint of swabbing time (feet below land surface)	Acceptance or inflow	
		Type of flow	Rate of flow (gpm)
DRB 1. Approximate static waterlevel, 68.5 feet			
903– 943	----------	U	----------
943– 963	----------	A	6.5
963– 983	----------	U	----------
1,024–1,044	----------	A	1.4
1,063–1,103	----------	U	----------
1,103–1,123	----------	A	1.3
1,265–1,285	----------	U	----------
1,287–1,307	----------	A	2.3
1,307–1,367	----------	U	----------
1,367–1,387	----------	A	3.0
1,387–1,407	----------	A	1.7
1,407–1,870	----------	U	----------
1,870–1,904	----------	A	3.0
DRB 2.[1] Approximate static water level, 92.1 feet			
982–1,041	802	I	0.01
1,041–1,144	----------	U	----------
1,144–1,247	----------	U	----------
1,248–1,351	1,003	I	.01
1,350–1,453	----------	U	----------
1,453–1,556	355	I	.32
1,556–1,659	588	I	.01
1,658–1,761	729	I	.04
1,762–1,865	----------	U	----------
1,865–1,968	650	I	.05
983–1,968	390	I	.27
DRB 3. Approximate static water level, 95.3 feet			
951–1,047	----------	Y	12.0
1,029–1,132	----------	U	----------
1,132–1,235	----------	U	----------
1,226–1,329	836	I	.02
1,332–1,435	----------	U	----------
1,427–1,530	740	I	.04
1,521–1,624	----------	U	----------
1,617–1,720	555	I	.57
1,721–1,824	----------	U	----------
1,818–1,921	705	I	.02
1,918–1,942	717	I	.02

See footnote at end of table.

TABLE 1.—*Results of injection and swabbing tests*—Continued

U: Unmeasurable small rate of acceptance under an injection pressure of 60 pounds per square inch measured at land surface, where no swabbing test was made.
A: Rate of acceptance under injection pressure of 60 pounds per square inch measured at land surface, where no swabbing test was made.
I: Average rate of inflow that entered packed-off interval between 60 and 120 minutes from the midpoint of the swabbing time.
Y: Average yield to continuous swabbing.

[Static water levels were measured on January 13, 1964, and are depths below land surface]

Packed-off interval (feet below land surface)	Depth to water 60 minutes after midpoint of swabbing time (feet below land surface)	Acceptance or inflow	
		Type of flow	Rate of flow (gpm)
DRB 4. Approximate static water level, 56.6 feet			
960–1, 076	----------	A	18. 0
1, 085–1, 208	----------	U	----------
1, 236–1, 359	----------	U	----------
1, 337–1, 460	----------	U	----------
1, 457–1, 580	----------	U	----------
1, 579–1, 702	----------	U	----------
1, 668–1, 693	1, 463	I	. 21
1, 677–1, 800	----------	U	----------
1, 729–1, 754	1, 060	I	. 7
1, 817–1, 841	----------	Y	. 8
1, 837–1, 861	----------	Y	. 9
1, 857–1, 881	----------	Y	. 6
1, 443–1, 740	739	I	. 04
1, 448–1, 938	250	I	. 57
DRB 5. Approximate static water level, 94.5 feet			
1, 130–1, 417	----------	Y	17. 2
1, 419–1, 522	----------	Y	6. 5
1, 518–1, 621	----------	Y	3. 6
1, 619–1, 722	----------	Y	1. 5
1, 700–1, 838	----------	Y	2. 8
1, 399–1, 838	----------	Y	13. 0
DRB 6. Approximate static water level, 81.3 feet			
1, 100–1, 200	744	I	0. 06
1, 195–1, 305	737	I	. 002
1, 300–1, 410	736	I	. 1
1, 405–1, 515	739	I	. 06
1, 514–1, 624	717	I	. 09
1, 615–1, 725	694	I	. 02
1, 650–1, 760	762	I	. 05
1, 760–1, 830	----------	Y	17. 8
1, 799–1, 913	----------	Y	8. 0
1, 870–1, 913	----------	Y	10. 5
DRB 7. Approximate static water level, 89.6 feet			
1, 115–1, 371	934	I	0. 006
1, 370–1, 480	722	I	. 03
1, 477–1, 587	870	I	. 04
1, 571–1, 681	945	I	. 003
1, 677–1, 787	893	I	. 05
1, 788–1, 898	690	I	. 01
1, 115–1, 969	607	I	. 02

[1] Packers were expanded inside the casing in DRB 2 to test the leakage of the packer mechanism. Water was swabbed out in a manner similar to the other tests. At 60 minutes from the midpoint of the swabbing time the water level was 567 feet below the surface. Between 60 and 120 minutes, an average of 0.006 gpm entered the packed off interval.

The analysis for the coefficient of transmissibility originally used for the swabbing tests (Christl, 1964; Proctor and Marine, 1965) was a modification of the slug-test method described by Ferris and others (1962, p. 104). However, in January 1966, H. H. Cooper, Jr., brought to the attention of the writer that this method of analysis assumes that release (or removal) of the volume of water to (or from) the well approximates an instantaneous line source (or sink) in an infinite region and that this assumption is rarely justified for a well of finite diameter. H. H. Cooper, Jr., J. D. Bredehoeft, and I. S. Papadopulos (U.S. Geol. Survey, written commun., Jan. 1966) devised a method for determining the coefficient of transmissibility by analyzing the rate of recovery of water level in a well after an instantaneous injection (or removal) of water. Their method, which does not assume that the well has an infinitesimal diameter, uses a graphic solution in which the ratio of the residual head (H) to the initial head (H_0), (H/H_0), is plotted on the arithmetic scale of semilogarithmic paper, and time (t) is plotted on the logarithmic scale. The graph is then matched to a type curve obtained by plotting H/H_0 on the arithmetic scale and Tt/r_c^2 on the logarithmic scale. (T is the coefficient of transmissibility, t is time since recovery began, and r_c is the radius of the well casing or packer tubing in which the water-level change is taking place.) From the match and knowledge of the well or tube radius, the coefficient of transmissibility can be determined.

If the assumption is made that the fractures are uniformly distributed throughout the packed-off interval, the apparent permeability may be obtained by dividing the transmissibility by the length of the packed-off interval.

Some of the water that enters the boring through the wall of the packed-off interval may come from rock above the upper packer and below the lower packer, thus making the flow three dimensional in the vicinity of the packers. Because of this, both the actual transmissibility and apparent permeability may be slightly less than the computed values. This error is thought to be negligible, however, because the low permeability of the rock and the length of the packed-off sections (commonly about 100 feet) make the percentage of water so contributed very small.

Figure 3 shows the analysis of data from a swabbing test on virtually impermeable rock by the method developed by Cooper, Bredehoeft, and Papadopulos. It shows a graph of the ratio of the residual head to the initial head (H/H_0) plotted against time (t) since recovery began. The type curve given by Cooper, which the data seemed to fit best, together with the match point used for calculation are shown also. The axis showing H/H_0 is the same for both graphs. The t scale for the plot of the data is at the bottom of the graph, whereas the Tt/r_c^2 scale for the type curve is at the top

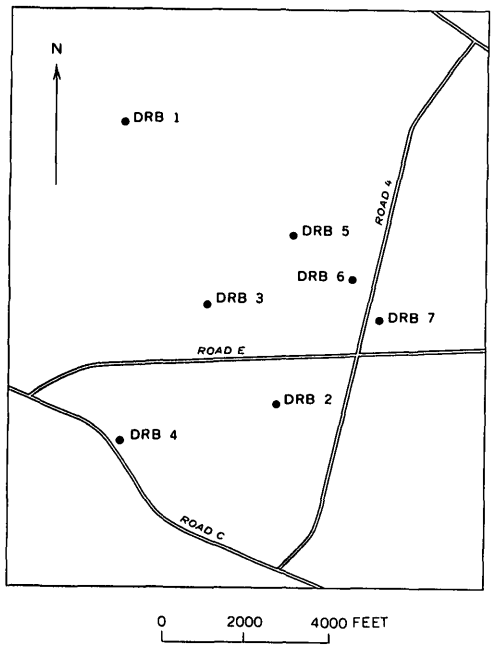

FIGURE 2.—Location of exploration wells cored into crystalline rock at the Savannah River Plant.

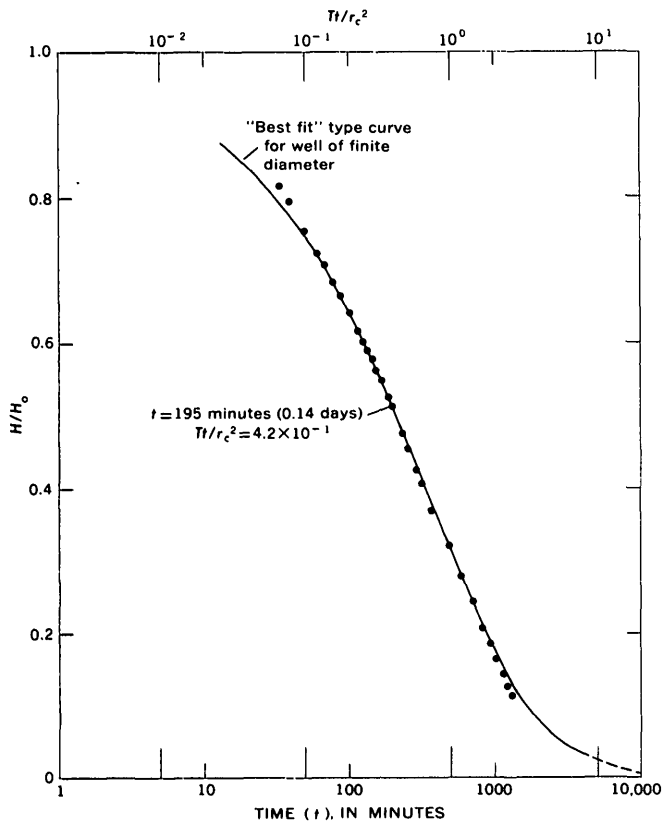

FIGURE 3.—Ratio of residual head (H) to the initial head (H_o) versus time (t) since water-level recovery began (swabbing test on virtually impermeable rock). Well DRB 2, zone 1,453 to 1,556 feet.

of the graph. For this particular test the radius of the pipe in which the water-level changes took place (internal diameter of packer pipe is 2.313 inches) is constant and known, and a value for time is given by the match point. Therefore, the transmissibility may be calculated from the relationship

$$T=\left(\frac{Tt}{r_c^2}\right)\frac{r_c^2}{t}$$

where T is the coefficient of transmissibility,
t is time since recovery began, and
r_c is the radius of the pipe in which the recovery is taking place.

Substituting the values for the particular example shown in figure 3:

$$T=\frac{4.2\times10^{-1}\times9.3\times10^{-3}\ \text{sq ft}}{1.4\times10^{-1}\ \text{day}}$$

$$=28\times10^{-3}\ \text{cu ft/day/ft}$$

$$=0.2\ \text{gpd/ft}$$

Division of this value by the length of the packed-off zone (103 ft) gives 0.002 gpd/sq ft for the apparent coefficient of permeability.

The results of analyzing 25 swabbing tests of individual packed-off sections of virtually impermeable rock by the method of Cooper, Bredehoeft, and Papadopulos are given in table 2. In the original analysis of the swabbing-test data (Christl, 1964; Proctor and Marine, 1965), 0.002 gpd/sq ft was used as a maximum apparent coefficient of permeability for virtually impermeable rock.

TABLE 2.—*Results of swabbing virtually impermeable rock*

Well	Packed-off interval (feet below land surface)	Coefficient of transmissibility (gpd/ft)	Coefficient of apparent permeability gpd/sq ft)
DRB 2	1, 453–1, 556	0. 2	0. 002
DRB 3	1, 617–1, 720	. 4	. 004
All other tests (DRB 2, 3, 6, 7):			
Max		. 09	. 0008
Avg		. 03	. 0003
Min		. 002	. 00002

Instantaneous injection tests (slug tests)

Although the swabbing tests provided qualitative information on the yield of the fractured zones that transmitted the larger quantities of water (table 1), they could not be analyzed for coefficients of transmissibility because the duration of swabbing was signifi-

cant compared to the duration of recovery. Thus, the swabbing period could not be considered as instantaneous.

Subsequent to the tests in which water was removed by swabbing, tests were made by instantaneously releasing a column of water to a selected zone of rock. After the selected zone of rock had been packed-off, the packer pipe, which was sealed with a plug at the bottom, was filled with water. Then a weight on a wire line was used to knock out the plug, thus releasing the water in the pipe to the packed-off zone. Because the time of release was instantaneous, this method was amenable to analysis even though in some tests the water level returned to its static position quickly.

The data from these tests were analyzed by the same methods as used in the previous swabbing tests. Because the water-level recovery in some of the tests generally was rapid, the plotted data commonly produced a recovery curve that was far more complete than was the curve obtained from the swabbing tests on virtually impermeable rock.

Figure 4 shows the analysis of data from a test where a column of water was instantaneously released to a packed-off interval. As in figure 3, H/H_0 is plotted on the ordinate and the time (t) since recovery began on the abscissa. The "best fit" type curve is also shown with the abscissa scale for Tt/r_c^2 at the top. The internal diameter of the packer pipe for these additional tests was 4.00 inches and the value used for time is given by the match point shown on figure 4. These values are substitued in the same formula as previously used:

$$T=\left(\frac{Tt}{r_c^2}\right)\frac{r_c^2}{t}$$

$$=\frac{1.0\times 2.8\times 10^{-2}}{1.8\times 10^{-3}}\frac{\text{sq ft}}{\text{day}}$$

$$=16 \text{ cu ft/day ft}$$

$$=120 \text{ gpd/ft}$$

Because the section transmitting the water is very likely only a small part of the packed-off interval (15 ft), it would be meaningless to divide the coefficient of transmissibility by the thickness of the packed-off interval to obtain a value for the apparent coefficient of permeability.

By making several slug-injection tests, a clearer concept of the nature of the fracturing in the water-transmitting fracture zones was obtained. The results of such tests in two wells are shown on figure 5. It is known from other work (Marine, 1966) that the water-transmitting sections shown in the two wells

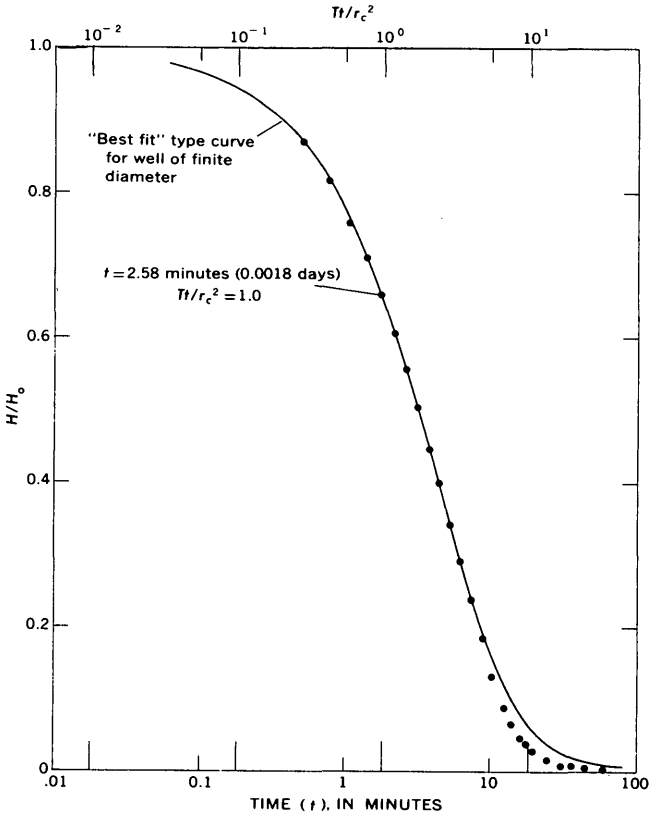

FIGURE 4.—Ratio of residual head (H) to the initial head (H_0) versus time (t) since water-level recovery began (slug test on a water-transmitting section in crystalline rock). Well DRB 5, zone 1,468 to 1,483 feet.

are connected. In the correlated zone shown on figure 5, the sum of the individual transmissibilities in well DRB 5 is 158 gpd/ft, and in well DRB 6 it is 165 gpd/ft. These sums correlate very well with the coefficients of transmissibility determined by pumping tests.

Pumping tests

Field tests for the average coefficient of transmissibility of the major fracture zones over relatively large areas were made by means of pumping tests in which one well was pumped at a constant discharge while the water levels in other wells were measured. Figure 6 shows the water levels in observation wells during and after one such test. A cement plug was set from 1,557 and 1,734 feet in well DRB 4 around a 1-inch piezometer pipe so that water levels in the shallow fracture zone and the deeper fracture zone could be measured separately in this boring. The water level of the deeper fracture zone is designated DRB 4(p) and that of the shallow fracture zone DRB 4(c) on figure 6. In the other observation wells no packers were used during the pumping test, thus the water levels measured were composite for the entire hole.

However, as shown by the results of the swabbing tests, the virtually impermeable rock transmits so little water that, for practical purposes, it can be assumed that the pumped water was derived entirely from the major fracture zones; therefore, the values obtained from the tests are applicable to the fractured zones as though they constituted discrete aquifers bounded both above and below by aquicludes.

During most of the pumping period the water level in the pumped well (not shown on fig. 6) ranged, after the first day, between elevations of +10 and −37 feet from mean sea level. The slight rise in water level in well DRB 5 just prior to starting the test was caused by injection of a tracer into that well. The tracer never appeared in detectible concentration at the pumped well.

A typical analysis of the recovery data from one of the observation wells is shown on figure 7. This observation well (DRB 5) is 1,765 feet from well DRB 6, which was pumped at a nearly constant rate of 20.5 gpm for 31 days. The logarithm of the water-level recovery in the well was plotted against the logarithm of time since pumping stopped. Using the method of Theis (1935) the curve defined by these points was superposed on and fitted to a type curve plotted from data given by Wenzel (1942). In figure 7 the scales for the data from the test are given on the left and bottom whereas the scale for the type curve is given at the right and top. The values obtained from the match point can be substituted in the formula

$$T=\frac{114.6QW(u)}{s}$$

where T=coefficient of transmissibility, in gallons per day per foot,

Q=discharge, in gallons per minute,

$W(u)$=well function of u, where $u=\frac{1.87r^2S}{Tt}$

where r=distance, in feet, from the pumped well to the observation well,

S=coefficient of storage,

t=time, in days, since pumping started (or stopped),

s=drawdown (or recovery), in feet.

Then,

$$T=\frac{114.6\times20.5\times2.4}{30.55}=185 \text{ gpd/ft}$$

Table 3 gives the results of similar analyses for the coefficient of transmissibility at the other observation wells. The rate of water-level drawdown and recovery in well DRB 1 indicates that perhaps a boundary condition appeared after about 8 days. Only the data prior to that time were used in computing the coefficient of transmissibility given in table 3. Meaningful analysis of the data from wells DRB 2 and DRB 7 could not be made because these wells are entirely in virtually impermeable rock. Furthermore, analysis could not be made of the drawdown data from the pumping well (DRB 6) because head loss was excessive owing to turbulence around the well and because small changes in the pumping rate resulted in relatively large variations in the water level.

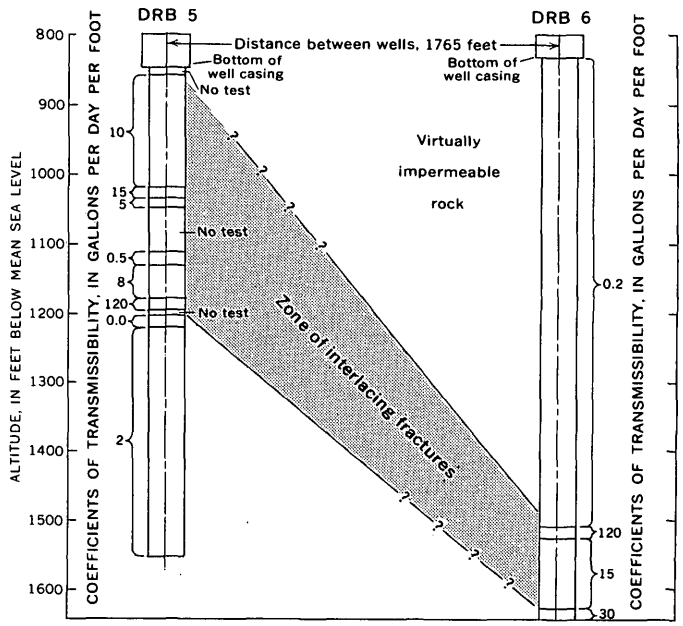

FIGURE 5.—Results of slug tests in wells DRB 5 and DRB 6.

Two water-transmitting zones—the one at the top of the crystalline rock and the inclined zone shown on figure 5 (this report)—were discussed by Marine (1966). The fracture zone at the top of the rock includes the sections given in table 3 for wells DRB 1, DRB 3, and DRB 4(c); the inclined fracture zone includes wells DRB 4(p), DRB 5, and DRB 6. The two zones intersect, probably along a line between DRB 3 and DRB 5 and thus they are treated as one aquifer in the analysis of the pumping test. Additional water-transmitting zones in DRB 1 and DRB 5 are not correlated with the two zones involved in the test (Marine, 1966). Because of these zones, the drawdowns in DRB 1 and DRB 5 during the test may have been less than they would have been had the wells penetrated only the zones that were being tested. The effect of such lessened drawdown would be to make the computed coefficient of transmissibility greater than the actual. However, the error thus introduced is thought to be small and the computed values are

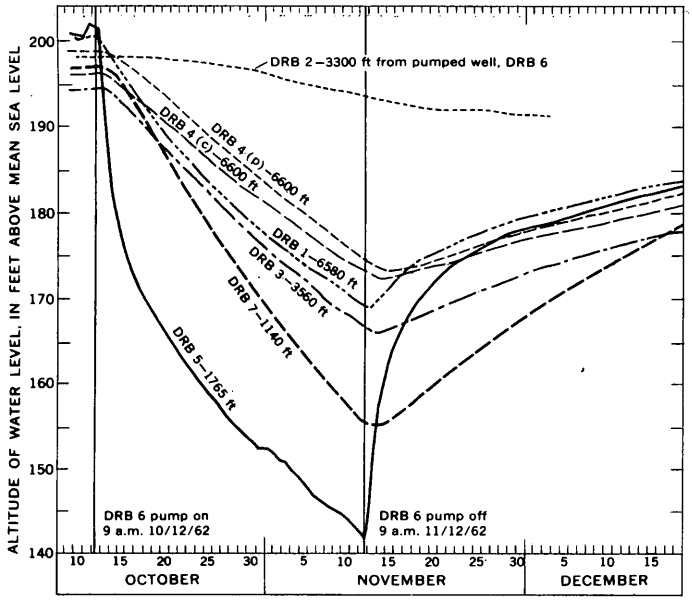

FIGURE 6.—Graphs of the water levels in observation wells during and following pumping from well DRB 6 at a nearly constant rate of 20.5 gpm for 31 days.

used in calculating the average coefficient of transmissibility.

The average apparent coefficient of permeability of 0.77 gpd/sq ft may be obtained by dividing the average coefficient of transmissibility by the average thickness of the water-transmitting zone. The zones given on table 3 are the ones affected most directly by the pumping test, but their thickness is estimated from previous and subsequent packer tests. The thicknesses are thus only approximate and depend in part on the lengths of the packed-off intervals. In view of this, the apparent permeability is rounded off to about 1 gpd/sq ft. Even this value has meaning only to the extent that the water-transmitting zone of rock consists of interlacing fractures that render it somewhat uniform in relation to water transmission.

Once the coefficient of transmissibility has been determined, the coefficient of storage can be computed from

$$S=\frac{T\left(\frac{t}{r^2}\right)}{1.87(1/u)},$$

where S=coefficient of storage,

T=coefficient of transmissibility, in gallons per day per foot,

t=time, in days, given by the match point,

r=the distance, in feet from the pumped well to the observation well, and

$$u=\frac{1.87r^2S}{Tt}.$$

Substituting the values of t and $1/u$ from the match point in figure 7,

$$S=\frac{185\times\frac{6}{(1765)^2}}{1.87\times20}=9.5\times10^{-6}.$$

The coefficients of storage determined from the data for both drawdown and recovery are shown in table 3.

CONCLUSIONS

The computation of hydraulic constants for fractured crystalline rock by the methods just described is based on the assumption that fractures are so uniformly distributed that the idealized conditions of homogeneity and isotropy are reasonably well satisfied. The computed constants are affected differently by departures from these idealized conditions. In the extreme situation, where all of the water transmitted by a given section of crystalline rock flows through a single fracture within that section, the coefficient of transmissibility is probably little affected. As flow through porous media can be simulated by a viscous fluid flowing between two parallel plates (Todd, 1954), flow between two parallel plates (a fracture) can be simulated by flow through a porous medium. The mathematical analysis developed for porous media should, therefore, still be applicable. On the other hand, the apparent coefficient of permeability for the same situation would be unrealistic because the thickness of the water-transmitting section would be much less than that used for the computation. However, as nearly as can be determined, the actual fractures

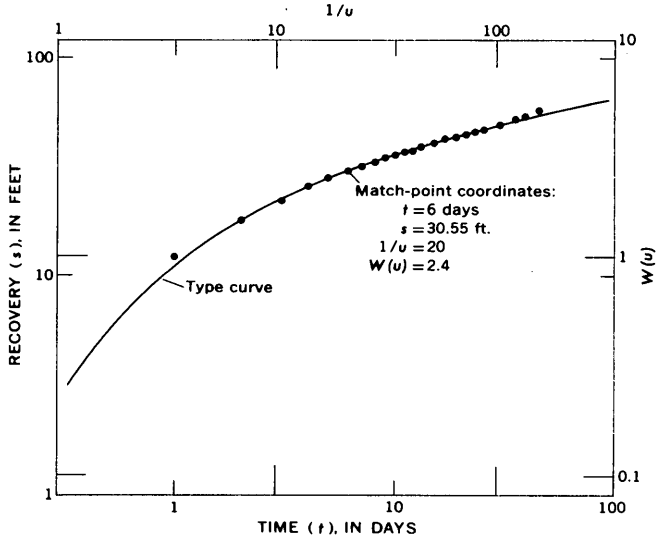

FIGURE 7.—Graph of the logarithm of water-level recovery in observation well DRB 5 versus the logarithm of time since pumping stopped in well DRB 6 and the trace of the type curve in the region of the data.

TABLE 3.—*Results of a pumping test in the crystalline rock*

Well	Distance from pumped well (DRB 6) (ft)	Zone of water-transmitting rock probably affected by pumping test, determined from packer tests		Coefficient of transmissibility		Coefficient of Storage	
		Depth (ft)	Thickness (ft)	Drawdown (gpd/ft)	Recovery (gpd/ft)	Drawdown ($\times 10^{6}$)	Recovery ($\times 10^{6}$)
DRB 1	6, 580	890–1, 307	417	257	304	4. 9	5. 5
2	3, 300						
3	3, 560	951–1, 047	96	95	104	28	35
4(p)	6, 600	1, 740–1, 881	141	117	98	9. 4	14
4(c)	6, 600	960–1, 076	116	168	125	10	14
5	1, 765	1, 130–1, 492	362	184	185	8. 6	9. 5
6		1, 775–1, 913	138		152		
7	1, 140						
Average			211	162		14	

are not single, smooth-walled, planar openings of large separation on an areal basis, even though locally some sections of rock may have a much greater permeability than other sections of the same fractured zone.

The coefficient of storage is, of course, affected by any error in the coefficient of transmissibility. It is also affected by the fact that the distance between two wells at the surface may not correspond to the path distance of the fractures that connect the two wells hydraulically.

In addition to inhomogeneities in the rock, other factors complicate attempts at exact analysis. Among the factors are changes in the specific gravity of the water as it is pumped or swabbed. These changes are caused by the removal of previously introduced fresh water used in drilling or in setting the packers and its replacement by more saline natural water. When the head on a well is depressed, gas dissolved in the native water of the rock may be released and tend to "airlift" the water column, thereby giving progressively less apparent drawdown than would have been measured if the gas had not evolved.

In summary, most of the crystalline rock that has been investigated consists of virtually impermeable rock whose average apparent permeability is about 0.0003 gpd/sq ft. However, a few zones of interlacing fractures occur within the rock that have an overall coefficient of transmissibility of about 160 gpd/ft. The average apparent permeability of these zones is about 1 gpd/sq ft. Within the zones of interlacing fractures a few section have transmissibilities as high as 120 gpd/ft. It is not possible with present knowledge to convert the transmissibilities into values of apparent permeability because the separation and wall conditions of the fractures are not known. However, even the relatively high apparent permeability that is indicated for some sections of rock is probably meaningless on a regional basis because these sections are limited areally within a more extensive zone of interlacing fractures.

In applying computed hydraulic constants to problems of fluid transmission, it must be realized that their computation is tenuous. However, the constants probably are of a correct order of magnitude because on an areal basis the idealized assumptions may be approximately fulfilled. The entire analysis should be regarded as preliminary and subject to some modification when more data are available.

REFERENCES

Christl, R. J., 1964, Storage of radioactive waste in basement rock beneath the Savannah River Plant: E. I. du Pont de Nemours & Co., Savannah River Laboratory, DP–844, 106 p.

Ferris, J. G., Knowles, D. B., Brown, R. H., and Stallman, R. W., 1962, Theory of aquifer tests: U.S. Geol. Survey Water-Supply Paper 1536–E, p. 69–174.

Marine, I. W., 1966, Hydraulic correlation of fracture zones in buried crystalline rock at the Savannah River Plant near Aiken, S.C.: U.S. Geol. Survey Prof. Paper 550–D, p. D223–D227.

Proctor, J. F., and Marine, I. W., 1965, Geologic, hydrologic, and safety considerations in the storage of radioactive wastes in a vault excavated in crystalline rock: Nuclear Sci. and Eng., v. 22, p. 350–365.

Siple, G. E., 1964, Geohydrology of storage of radioactive waste in crystalline rocks at the AEC Savannah River Plant, South Carolina: U.S. Geol. Survey Prof. Paper 501–C, p. C180–C184.

Theis, C. V., 1935, Relation between the lowering of the piezometric surface and the rate and duration of discharge of a well using ground-water storage: Am. Geophys. Union Trans., pt. 2, p. 519–524.

Todd, D. K., 1954, Unsteady flow in porous media by means of a Hele-Shaw viscous fluid model: Am. Geophys. Union Trans., v. 35, no. 6, p. 905–916.

Wenzel, L. K., 1942, Methods for determining permeability of water-bearing materials with special reference to discharging-well methods, *with a section on* Direct laboratory methods and bibliography on permeability and laminar flow, by V. C. Fishel: U.S. Geol. Survey Water-Supply Paper 887, 192 p.

EFFECT OF URBAN DEVELOPMENT ON QUALITY OF GROUND WATER, RALEIGH, NORTH CAROLINA

By JOSEPH C. CHEMERYS, Raleigh, N.C.

Work done in cooperation with the North Carolina Department of Water Resources

Abstract.—In the Raleigh area samples taken from wells 25 to 200 feet deep have not yielded appreciable amounts of ABS detergent (alkylbenzenesulfonate)—a major component of hard synthetic detergents. The potential movement of ABS detergents in water with time was checked by analyses of water from selected wells in 1962 and again in 1965. Determinations were also made on related constituents that might be useful precursors of pollution. The area is underlain chiefly by granites, schists, and gneisses, which are blanketed in most places by residual soils and a cover of vegetation. Soil in which septic tanks lie is effective in removing or retarding the movement of most contaminants in the ground. Shallow wells draw water from the soil mantle, but deep wells draw water directly from fractures in the rock.

Since the time when hard synthetic detergents virtually replaced soap shortly after World War II, there has been concern about contamination of water wells by the newer detergents. Alkylbenzenesulfonate (ABS), a major component of hard detergents, is resistant to biodegradation and is concentrated in circulating ground waters. The hard detergent has acted as a tracer of septic-tank effluent and has pointed to potential pollution problems for many well users (Perlmutter and others, 1964).

A survey in housing subdivisions that have been developed recently in the Raleigh, N.C., area (fig. 1) was conducted to determine the extent of ABS contamination in ground waters. Growth of the city has been so rapid that it has exceeded the ability of the city government to provide for equally rapid expansion of public utilities and services. Thus, Raleigh is typical of many cities where the older incorporated area is served by a central municipal water and sewer system, but where the newer fringe area is served by private wells and septic tanks. Some wells and septic tanks in the Raleigh area have been in use for more than 20 years, whereas others have been installed more recently.

PHYSICAL AND GEOLOGIC FEATURES

The Raleigh area is a part of the Piedmont physiographic province and is underlain by granites, schists, and gneisses. Rolling hills that have been moderately dissected by perennial streams represent the major land forms. A heavy layer of residual soil covers the bedrock in most places.

The ground-water reservoir in the Piedmont province consists of sandy clay soil and weathered material, which underlie the surface to depths generally ranging from several feet to several tens of feet, and the underlying bedrock. In the soil and weathered material, the water occurs interstitially, but in the underlying bedrock it occurs only in fractures. The water table commonly lies from 15 to 50 feet beneath the land surface, generally within the soil or weathered materials. More than 40 inches of annual precipitation, which is rather evenly distributed throughout the year, tends to keep the water table at a fairly high level. Thus, the water table is considered to be a subdued replica of the surface topography. Natural ground-water flow is from the upland interstream areas to the stream valleys.

Some wells are dug into the weathered material and are commonly less than 30 feet deep. Most wells, however, are drilled into the hard rock and are 100 to 200 feet deep. Homes from which well samples were taken typically are on lots of half an acre or more in size, although some are on lots of approximately a quarter of an acre. Generally, each septic tank is in

U.S. GEOL. SURVEY PROF. PAPER 575-B, PAGES B212-B216

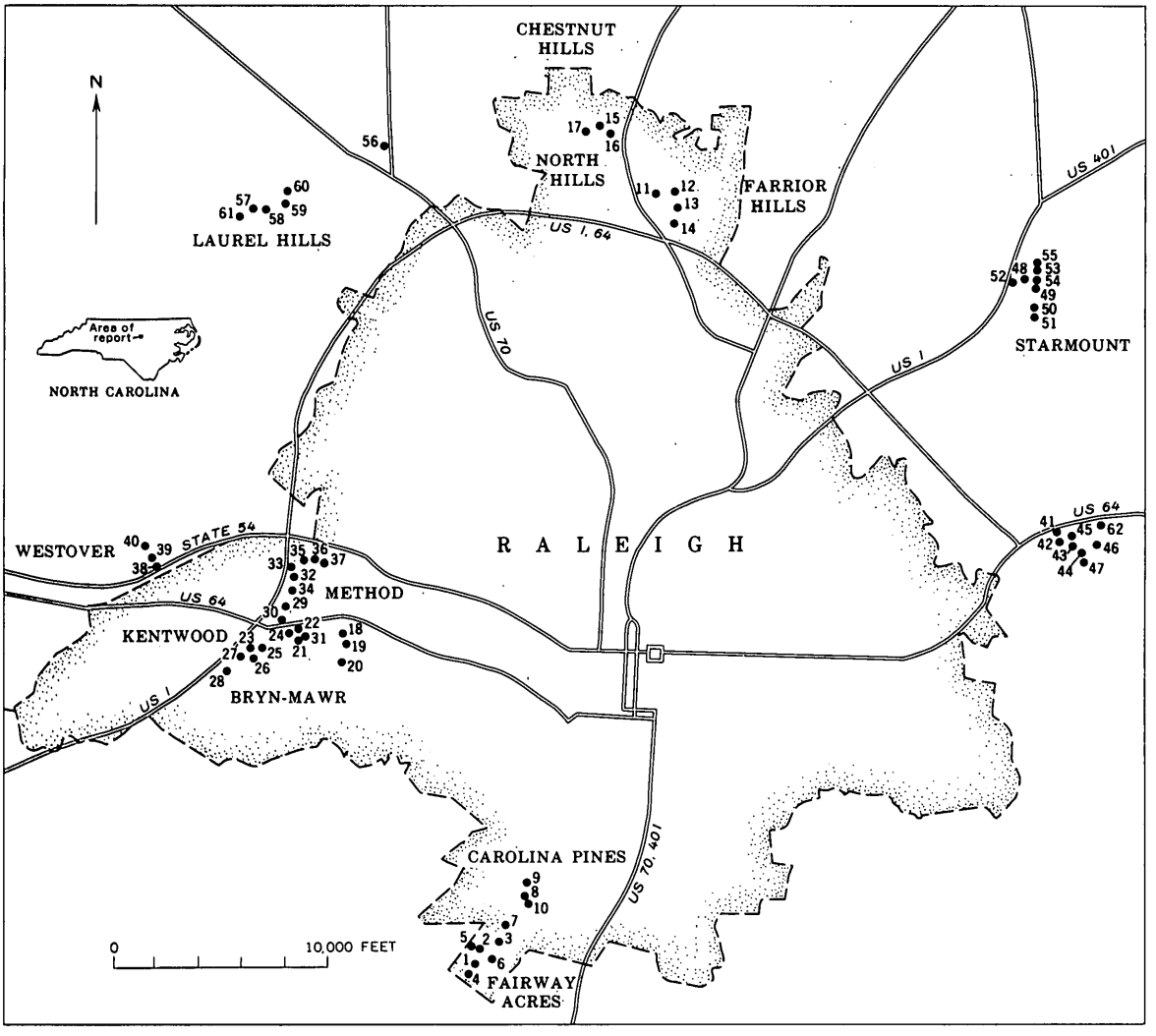

FIGURE 1.—Map of the Raleigh, N.C., area, showing newer residential areas, and wells (dots) referred to in text and in table 1.

the lower part of each lot, whereas the wells tend to be at slightly higher elevations.

RESULTS AND EVALUATION

Sixty two wells were examined during 1962–63 in 12 housing subdivisions in the Raleigh area, both in and outside the city limits (fig. 1). All the samples were collected from areas that had been using well water for at least 2 years; only 4 wells were known to have been used less than 4 years. Preference in sampling was given to the older areas where wells and septic tanks were in use longest, because the longer time has provided more chance for detergent buildup in the ground-water system. The wells sampled ranged in period of use from 2 to 30 years.

The amount of detergent found in the samples was low (see table 1). Fifty-two wells (84 percent of the wells) yielded 0.0 part per million of ABS, and 9 yielded 0.1 ppm of ABS. One well that yielded 0.2 ppm of ABS had been in operation 6 years. The U.S. Public Health Service (1962) recommends that water used for domestic purposes contain no more than 0.5 ppm of ABS.

Analyses for other constituents in the water showed relatively high concentrations of nitrate and chloride in 10 of the samples. Nitrates in amounts of more than 9 ppm do not occur naturally in the Raleigh area, and chlorides of more than 10 ppm are not common. The high nitrate and chloride concentrations suggested movement of water from septic tanks or other sources of contamination and may be precursors of coliform bacteria or detergents. Robeck and others (1962) studied the movement of salts and coliform bacteria from wastes disposed into ground waters and

TABLE 1.—*Data for wells sampled in the Raleigh, N.C., area*

Well No.	Date of sample collection	Depth (ft)	Rock type	Approximate distance of septic tank from well (ft)	Length of time well has been used (years)	Chemical constituents (ppm)						Specific conductance (micromhos at 25°C)	Coliform bacteria (no./100 ml)
						Sodium (Na)	Potassium (K)	Chloride (Cl)	Nitrate (NO_3)	Phosphate (PO_4)	Detergent (ABS)		
1	7-31-62	85	Mica gneiss	75	2	5.8	1.5	0.2	9.1	0.1	0.1	75	
	1- 6-65							.5	10		.0	78	0
2	7-31-62	125	do	120	5½	7.3	1.5	5.7	14	.0	.1	95	
3	7-31-62	80	do	90	4	5.0	1.4	5.5	2.9	.2	.0	66	
4	7-31-62		do	75	6½	7.5	2.8	7.5	24	.0	.1	110	
	1- 6-65							8.0	24		.1	130	0
5	7-31-62		do		6½	5.6	1.4	4.0	6.8	.2	.0	68	
6	7-31-62	150	do	90	4	6.7	1.1	2.0	12	.1	.1	73	
	1- 7-65							1.5	13		.0	91	0
7	7-31-62	200	Hornblende gneiss	45	1½	7.8	3.3	12	6.8	.0	.0	162	
8	7-31-62	80	do	75	12½	5.6	.8	3.0	2.	.1	.0	60	
9	7-31-62	100	do	60	11	5.0	1.1	3.0	.7	.1	.0	61	
10	7-31-62	100	do	45	10	5.3	1.1	2.5	1.8	.2	.0	70	
11	7-31-62		Mica gneiss	50	5	4.2	1.3	1.0	1.5	.0	.0	48	
12	7-31-62	75	do	60	5	3.6	1.3	.5	2.5	.0	.0	38	
13	7-31-62	85	do	90	4½	4.4	1.1	.5	1.7	.0	.0	56	
14	7-31-62	99	do	75	4	4.6	1.4	1.0	1.4	.1	.0	64	
15	7-31-62	60	do	40	8	4.6	1.4	4.0	.3	.0	.0	39	
	1- 6-65							6.5	.0		.0	38	0
16	7-31-62	75	do	75	8	4.2	1.8	4.0	.2	.0	.0	38	
17	7-31-62	75	do	50	8	3.1	1.1	.5	2.4	.0	.0	33	
18	8- 7-62	100	do	75	6	5.0	1.9	3.0	.1	.0	.0	69	
19	8- 7-62	99	do			6.4	2.8	4.0	.4	.0	.0	68	
20	8- 7-62	100	do	90	4	7.7	2.8	5.0	1.0	.1	.0	91	
21	8- 7-62	180	do	80	13	6.8	1.4	4.0	.4	.1	.0	99	
22	8- 7-62	36	do	45	22	4.0	1.2	6.5	.3	.2	.0	108	
23	8- 7-62	40	do	60	6	4.5	.3	3.5	1.4	3.2	.0	45	
24	8- 7-62	100	do	120	15	6.0	.8	5.5	.2	.1	.0	56	
25	8- 7-62	180	do	120	12	12	1.8	3.5	.7	.5	.0	110	
26	8- 7-62	78	do	60		3.8	.9	5.5	.1	.0	.0	128	
27	8- 7-62	100	do	60		4.7	1.6	5.5	.0	.1	.0	64	
28	8- 7-62	60	do	45		2.2	.6	1.0	.1	.0	.0	23	
29	8- 7-62	115	do	45	10	4.8	1.1	3.5	.1	.2	.0	60	
30	8- 7-62	125	do	75	11	8.7	1.3	.5	.0	.1	.0	73	
31	8- 7-62	25	do	90		2.6	3.3	4.0	1.1	.0	.0	37	
32	8- 7-62	100	do			24	.9	34	3.5	.0	.0	210	
33	8- 7-62	45	do	60	30	59	.9	67	21	.0	.1	328	
	1- 7-65							9.5	1.7		.0	128	0
34	8- 7-62	160	do	30		6.6	1.7	4.0	4.9	.1	.0	70	
35	8- 7-62	25	do	45		19	.5	28	4.9	.1	.1	118	
36	8- 7-62		do	75		22	.2	27	17	.0	.1	188	
	1- 7-65							21	16		.0	300	0
37	8- 7-62	40	do	75		19	.2	17	20	.0	.1	106	
	1- 6-65							14	18		.0	95	0
38	8- 7-62	40	do	70		6.0	.9	5.5	13	.0	.0	54	
39	8- 7-62		do	75		9.9	1.2	4.0	1.5	1.1	.0	64	
40	8- 7-62	63	do	30	15	8.8	1.6	5.0	.6	.3	.0	91	
41	4-10-63	172	Granite	60	5	7.8	.8	.0		.1	.0	67	
42	4-10-63	165	do	60	4	4.8	.4	1.0	3.6	.0	.0	54	
43	4-10-63		do	100	12	5.2	.8	2.0	13	.0	.0	74	
	1- 7-65							4.5	17		.0	86	6
44	4-10-63		do		5	5.4	.7	.0	5.5	.0	.0	74	
45	4-10-63	102	do	100	2½	8.1	1.1	1.0	8.3	.2	.0	70	
46	4-10-63		do		4½	8.1	.8	3.0	5.5	.1	.0	79	
47	4-10-63		do	100		7.2	.8	6.0	4.1	.0	.0	52	
48	4-10-63	115	do	100	7	7.0	1.6	4.0	2.9	.3	.0	61	
49	4-10-63		do	100		7.5	1.1	4.0	1.7	.3	.0	73	
50	4-10-63		do	100		6.7	1.3	1.0	4.1	.3	.0	55	
51	4-10-63	75	do	100		102	.4	3.1	.0	.0	.1	470	
52	4-10-63	75	Mica gneiss	100		5.5	1.9	.0	1.9	.3	.0	52	
53	4-10-63	100	Granite	100		6.2	1.3	2.0	3.0	.4	.0	58	
54	4-10-63		do		4½	7.7	1.0	5.0	1.3	.2	.0	83	
55	4-10-63		do		5½	7.3	1.4	.0	5.2	.4	.0	58	
56	4-10-63		Mica gneiss	100	6	8.4	1.5	1.0	.1	.0	.0	188	
57	4-10-63	75	do	75	2	5.4	1.0	.0	.0	.1	.0	44	
58	4-10-63	90	do	50	9	6.0	1.1	.6	.0	.0	.0	48	
59	4-10-63		do		6	4.1	1.4	2.0	.0	.1	.0	38	
60	4-10-63	80	do	50		7.0	1.5	.4	.0	.1	.0	59	
61	4-10-63					8.9	.9	.0	.1	.2	.0	60	
62	4-10-63		Granite		6	8.6	1.1	1.0	13	.0	.2	84	
Min		25		30	1.5	2.6	.2	0.2	0.0	0.0	0.0	23	
Max		200		120	30	102	3.3	67	24	3.2	.2	328	
Avg (calc)		85		73	7.8	9.5	1.3	5.5	4.3	.2	.02	86	

found that chloride and nitrate are apt to move faster than detergents through soils and that detergents move ahead of coliform organisms. Their conclusion applied to sandy soils, and may not hold true for the clayey soils found in the Raleigh area. The data in table 1 do not indicate any apparent correlation between the high nitrate and chloride concentrations and the amount of ABS found.

In January 1965, about 2 years after the preliminary investigation, waters from selected wells were analyzed again to determine whether there was any increase in ABS or change in concentration of other chemical constituents, notably chloride and nitrate. The wells selected for resampling (wells 1, 2, 4, 6, 15, 33, 35–38, 43, 51 and 62 of table 1) included all those that had previously yielded some ABS or had a higher

nitrate or chloride content than similar wells in the same area; also a few wells were resampled that had no ABS and were also low in nitrate and chloride content in 1962. Only 8 of the wells selected for further study could be resampled, and only 1 sample showed any ABS; this sample (well 4) contained only 0.1 ppm of ABS. All but one of the samples had about the same nitrate and chloride concentrations as previously found. The continued lack of correlation between the higher chloride and nitrate concentrations and ABS concentrations in the respective samples suggests (LeGrande, 1965, p. 88) that the zones of ground water contaminated with ABS around septic tanks are relatively small and may have stabilized in size so that the ABS may never reach the wells.

At the time the wells were resampled, water was also collected for examination for coliform bacteria. Coliform bacteria were found only in well 43, which had a low count of 6 coliform bacteria per 100 milliliters of water. No ABS was found either time the well was sampled. Chloride concentration was normally low both times, but nitrate concentration was higher both times than was normal for other wells in the area. The presence of coliform bacteria and the amount of nitrate with no ABS or additional chloride suggests that the pollution may be from some source other than septic-tank effluent.

In the 1965 sampling, a numerical environmental rating system developed by LeGrand (1964) was used to rate the possibility of contaminated water reaching the wells. The system is based on the following five factors showing the favorable or unfavorable tendencies of well sites to provide pollution-free wells:

1. Depth of water table—a deep water table is more favorable than a shallow one.
2. Permeability of soil—moderately permeable soil is favorable, because it is permeable enough to allow infiltration of contaminants but sufficiently impermeable to retard movement.
3. Presence of clay in soil—soil with some clay is favorable, because contaminants that reach it may be chemically or physically sorbed to earth materials.
4. Water-table gradient—a steep gradient from a waste site to a well is unfavorable.
5. Distance between well and waste site—a short distance is unfavorable.

Only very general conclusions were made from the rating system. Most of the wells without appreciable nitrate and chloride concentrations in the water had high ratings in the class of "improbable contamination"; wells with water containing appreciable nitrate and chloride were in the "probable or possible contamination" category.

During January 1965, samples were taken from 3 wells and a spring in general alinement on a 15° slope. The homes supplied by the wells had individual septic tanks that had been in use about 12 years, and each home was on a half-acre lot. At the bottom of the slope, the spring discharged into a small creek. All samples were free of ABS and had low nitrate concentrations. No coliform bacteria were found in the water from the wells; however, the spring had such an abundance of coliform bacteria that an accurate count could not be made. Contamination of the spring may have occurred after the ground water was discharged from the spring.

CONCLUSIONS

No appreciable amount of detergent was found in ground waters of the Raleigh area, and between 1962 and 1965 there was no evidence of an increase in ABS in waters sampled. This contrasts with some other areas of the country, where high ABS contamination has been found (Flynn and others, 1958; Walton, 1960).

Water in 10 of the 62 wells sampled in 1962 had high nitrate and chloride concentrations or a high nitrate concentration with very little or no ABS, suggesting the onset of pollution. After a 2-year period, water in these wells still lacked a significant amount (over 0.1 ppm) of detergent. One sample did have a low coliform bacteria count (6 per 100 ml) but no sign of hard-detergent contamination. The lack of correlation between the high concentrations of nitrate, chloride, and detergent suggests that the zones of ABS contamination in ground water do not extend as far as those of chloride and nitrate and may stabilize in size without extending to wells in the area.

Ground water in the Raleigh area appears to be relatively free of pollution in general. It is possible that the thick sandy clay soil in the Raleigh area is the most significant factor in keeping Raleigh wells free of ABS and other contaminants. With the advent of new biodegradable detergents on the market it is unlikely that many Raleigh ground-water users will have detergent problems in the future.

REFERENCES

Flynn, J. M., Andreoli, Aldo, and Guerrera, A. A., 1958, Study of synthetic detergents in ground water: Am. Water Works Assn. Jour., v. 50, no. 12, p. 1551.

LeGrand, H. E., 1964, System for evaluation of contamination potential of some waste disposal sites: Am. Water Works Assn. Jour., v. 56, no. 8, p. 959–974.

——— 1965, Pattern of contaminated zones of water in the ground: Water Resources Research Jour. v. 1, no. 1, p. 83–95.

Perlmutter, N. M., Lieber, Maxim, and Frauenthal, H. L., 1964, Contamination of ground water by detergents in a suburban environment—South Farmingdale area, Long Island, N.Y., *in* Geological Survey Research 1964: U.S. Geol. Survey Prof. Paper 501–C, p. C170–C175.

Robeck, G. S., Bryant, A. R., and Woodward, R. L., 1962, Influence of ABS on coliform movement through water-saturated sandy soils: Am. Water Works Assn. Jour., v. 54, no. 1, p. 75–82.

U.S. Public Health Service, 1962, Drinking water standards: U.S. Public Health Service Pub. 956, p. 22–25.

Walton, Graham, 1960, Effects of pollutants in water supplies—ABS contamination: Am. Water Works Assn. Jour., v. 52, no. 11, p. 1354.

RATE AND EXTENT OF MIGRATION OF A "ONE-SHOT" CONTAMINANT IN AN ALLUVIAL AQUIFER IN KEIZER, OREGON

By DON PRICE, Portland, Oreg.

Work done in cooperation with the Oregon State Engineer

Abstract.—Late in 1946, ground water in a shallow aquifer tapped by numerous domestic wells in Keizer, Oreg., was contaminated by industrial waste dumped into a borrow pit at an experimental aluminum-reduction plant. The concentration of sulfate (the principal constituent of the contaminant) at one time exceeded 1,000 parts per million locally. Samples of water from selected wells in the contaminated area were collected periodically and were analyzed for hardness, which was used as the principal indicator of contamination. At times the samples were analyzed for other constituents also. The contaminant, while becoming naturally diluted in the immediate vicinity of the borrow pit, spread into the aquifer downgradient for a distance of a little more than a mile during the period 1947–64.

Chemical contamination of ground water by industrial waste occurred in Keizer, an unincorporated community north of Salem, Oreg., in late 1946 and extended to an increasingly larger area as the contaminant spread downgradient. Keizer is the principal industrial area near Salem. The contaminant was introduced into a shallow water-table aquifer as a result of the dumping of a load of incompletely processed aluminum ore into a borrow pit. Later, the contaminant was partially removed by pumping of the ground water, and its distribution was monitored by periodic water sampling and analysis. An investigation of the cause and extent of the contamination was made in 1947 by F. D. Trauger, U.S. Geological Survey, in cooperation with the Oregon State Engineer. Some of their unpublished data have been used in this article.

GEOGRAPHIC AND GEOHYDROLOGIC SETTING

Salem, Oreg., is in the Willamette Valley about 45 miles south of Portland (fig. 1), and is midway between the Cascade and Coast Ranges of Oregon. The annual precipitation recorded at the Salem airport during the period 1893–1964 ranged from 24.56 to 63.50 inches and averaged about 40 inches. Most of the precipitation falls during the winter and early spring; summers usually are dry and warm.

The area of contamination is underlain to depths of about 50 feet by moderately to highly permeable alluvial deposits of Recent age from which many families draw their domestic water supply. Unconfined ground water in these deposits percolates generally northwestward to points of natural discharge along the Willamette River and its flood plain (Price, 1961). The average rate of lateral percolation is estimated to be about 4.5 feet per day.

The water table is shallow; in most parts of the area, it fluctuates from about 10 feet below the land surface during the winter to about 20 feet below during the summer. Locally the water table is less than 5 feet below the floor of topographic depressions or may even intersect the side slopes of such depressions. Contaminants may be introduced readily to the ground-water body where the water table is near the land surface.

BACKGROUND OF THE CONTAMINATION

Contamination of the ground water occurred during the period August 1945 to July 1946, when incompletely processed aluminum ore and milltailings, which had been treated with sulfuric acid and ammonium hydroxide, were sluiced into a borrow pit in the NW¼SE¼ sec. 11, T. 7 S., R. 3 W. (fig. 1). When this waste came into direct contact with the water in the pit, aluminum, sulfate, and other ions were dissolved and carried in solution into the adjacent saturated alluvium. The contamination was recognized first in late 1946 when local residents, who were pumping ground water for domestic use, complained of the

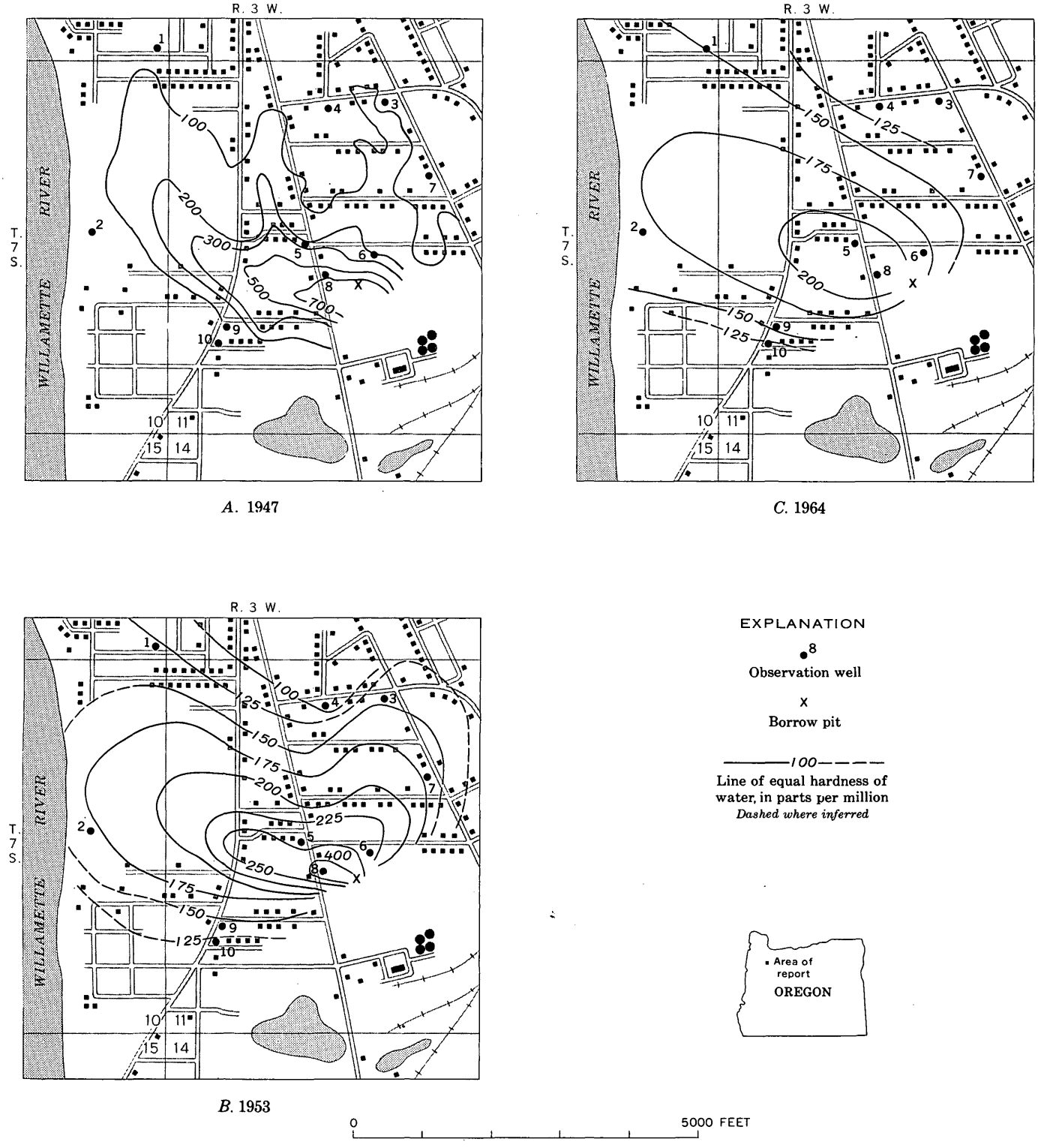

FIGURE 1.—Extent of area of contaminated ground water in Keizer, Oreg., in the autumns of 1947, 1953, and 1964, as indicated by water hardness. May *A* includes data prepared by F. D. Trauger for 136 wells.

deterioration of their supply. An early analysis showed that the total dissolved-solids concentration in the water from one well exceeded 1,000 parts per million.

In order to alleviate the problem and prevent further contamination, the waste was removed from the borrow pit in the spring of 1948. Then in July 1948 two large-yield wells (not shown on map) were drilled near the pit and were pumped intensively for several months to remove as much of the contaminated water from the aquifer as possible. Both wells reportedly had a capacity of more than 700 gallons per minute. The water was conveyed to the Willamette River through a large pipeline.

QUALITY-OF-WATER CONDITIONS AND MONITORING PROGRAM

Normally, the chemical quality of the water from the Recent alluvium is good to excellent for most uses. An analysis of water from a well that taps these deposits near the contaminated area was made in 1928 (prior to the contamination) and showed that the water contained 129 ppm of total dissolved solids and had a hardness of 81 ppm (Piper, 1942).

Beginning in 1947, after the contamination had been recognized, water samples from 10 wells in or near the vicinity of the borrow pit were analyzed so that natural dispersion of the contaminant could be monitored. The locations of the wells are shown on figure 1.

During the period 1947–54, a set of samples was collected 3 or 4 times each year and analyzed by field methods for hardness. After 1954, a set of samples was collected about every second or third year and analyzed in the laboratory for hardness and 1 or 2 constituents, such as chloride and sulfate. Selected data are given in table 1; the other data are available for reference in the office of the U.S. Geological Survey, Water Resources Division, Portland, Oreg.

Hardness of the water in excess of 125 ppm was used as an indication of the contamination because determinations for hardness are comparatively inexpensive and it was known that calcium and magnesium (which contribute to hardness of water) accompanied sulfate in the water as a waste product.

Figure 2 is a graph showing the relationship between hardness and concentration of sulfate in samples collected June 5, 1962, and November 27, 1964. As that figure shows, the samples having the higher values for hardness also have the higher concentrations of sulfate, so that the presence of excessive hardness is a reliable indicator of sulfate, the principal constituent of the contaminant.

TABLE 1.—*Selected data for observation wells in and near area of contaminated ground water*

Well No.	Depth of well (feet)	Date sampled	Temperature of water (°F)	Sulfate (SO_4) (ppm)	Chloride (Cl) (ppm)	Hardness as $CaCO_3$ (ppm)	Specific conductance (micromhos at 25°C)
1	42	11–11–47	----	------	------	95	------
		10– 7–53	----	------	------	128	------
		6– 5–62	58	34	10	149	347
		11–27–64	53	32	10	150	346
2	49	11– 7–47	----	------	------	80	------
		10– 7–53	----	------	------	172	------
		6– 5–62	54	74	7.8	175	403
		11–27–64	----	69	7.5	------	403
3	42	11–14–47	----	------	------	75	------
		10– 7–53	----	------	------	148	------
		6– 5–62	55	18	10	121	290
		11–27–64	48	14	10	121	282
4	25	11–14–47	----	------	------	80	------
		10– 7–53	----	------	------	96	------
		6– 5–62	55	19	6.0	84	212
		11–27–64	49	26	8.5	111	273
5	41	10–29–47	----	------	------	255	------
		12–21–53	----	------	------	236	------
		6– 5–62	----	99	6.0	227	501
		11–27–64	54	93	7.0	214	481
6	44	10–29–47	----	------	------	280	------
		10– 7–53	----	------	------	240	------
		6– 5–62	----	66	8.5	193	448
		11–27–64	53	58	7.5	181	412
7	----	11–12–47	----	------	------	95	------
		10– 7–53	----	------	------	172	------
		6– 5–62	----	15	9.8	122	282
		11–27–64	55	14	8.5	115	278
8	33	10–29–47	----	------	------	730	------
		12–21–53	----	------	------	456	------
		6– 5–62	----	140	6.8	246	564
		11–27–64	----	128	6.5	------	574
9	----	11– 4–47	----	------	------	60	------
		12–21–53	----	------	------	142	------
		6– 5–62	----	30	6.2	138	314
		11–27–64	57	46	5.8	154	348
10	42	11– 4–47	----	------	------	65	------
		10– 7–53	----	------	------	108	------
		6– 5–62	----	9.8	6.5	108	247
		11–27–64	56	23	6.0	129	293

AREA AFFECTED AND SPREAD OF CONTAMINANT

Maps *A*, *B*, and *C* in figure 1 show the extent of contamination (as indicated by lines of equal hardness) in the autumns of 1947, 1953, and 1964, respectively. As shown by the maps, the gradual spread of the contaminant in a northwestward direction—which is the general direction of ground-water movement—was accompanied by a decrease in concentration of the contaminant in the immediate vicinity of the borrow pit.

Map *A* shows that in 1947, shortly after the contamination was first noticed, the hardness of the ground water in the immediate vicinity of the borrow pit exceeded 700 ppm. The area in which the hardness of the ground water exceeded 125 ppm covered about 0.3 square mile, but there was no indication that the contaminant had spread a sufficient distance to affect the

241-334 O—67——15

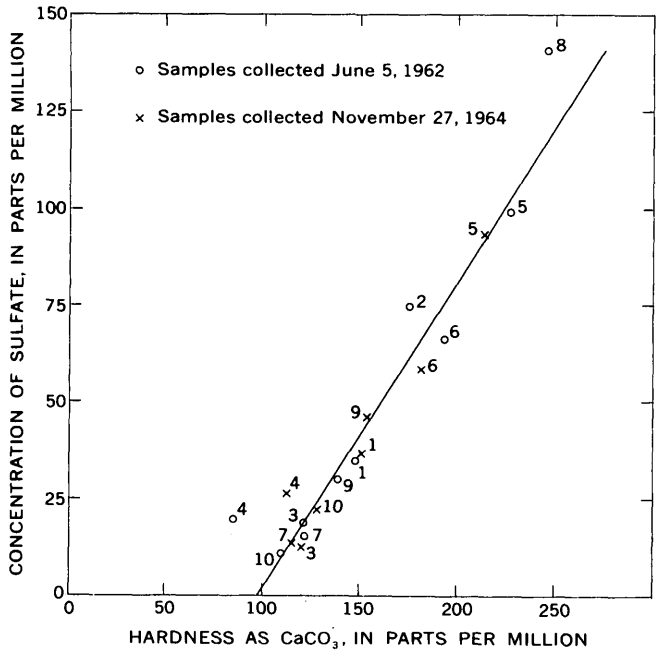

FIGURE 2.—Graph showing the relationship between concentration of sulfate and hardness of waters collected from selected wells in Keizer, Oreg. Numbers refer to wells shown on figure 1.

quality of the water pumped from wells 1, 2, 3, 4, 7, 9, and 10.

By the autumn of 1953, the hardness of the water in the immediate vicinity of the borrow pit had declined to less than 500 ppm, but the area enclosed by the 125-ppm line of equal hardness had increased to about 0.75 square mile (fig. 1, map *B*). Also, the hardness of water from all except one (well 4) of the observation wells exceed 100 ppm, indicating a continued spread of the contaminant downgradient.

By autumn of 1964, the hardness of the ground water in the immediate vicinity of the borrow pit had apparently declined to less than 300 ppm.[1] By then the area enclosed by the 125-ppm line of equal hardness had increased to nearly 1 square mile, and the hardness of the water from all the observation wells exceed 100 ppm, indicating a further spread of the contaminant.

[1] Although the hardness of the water in observation wells 2 and 8 was not determined in the autumn of 1964, it is considered likely that nowhere in the area of contamination at that time was the hardness greater than 300 ppm. (See fig. 1, map *C*.) The water from well 8, which is nearest the borrow pit and previously had the hardest water, probably had a hardness of about 260 ppm in 1964. This estimate is based on the relationship between hardness and concentration of sulfate, as shown in figure 2.

CONCLUSIONS

Chemical analyses of water from wells in and near the contaminated area during the period 1947–64 indicate that much of the sulfate and other constituents of the contaminant were removed from the aquifer during intensive pumping of two large wells tapping the aquifer near the borrow pit.

It is estimated that the ground water in the contaminated area percolates downgradient at a rate of about 4.5 feet per day, or about 1,700 feet per year. At this rate, one would expect the contaminated ground water to have been completely displaced by fresh, uncontaminated recharge water within a few years of the contamination because the natural points of discharge (along the Willamette River) are as near as 3,500 feet downgradient from the borrow pit. Ground water was not completely displaced, however, probably owing to the influence of one or more of the following factors and (or) other related factors: (a) some of the incompletely processed ore, which was in the form of a slime, may have seeped into the gravel beneath the borrow pit and was not removed by the pumping; (b) the rate of ground-water movement in the deeper part of the aquifer may be much slower than the estimated rate of 4.5 feet per day for the upper part; (c) some of the contaminant may have precipitated in the aquifer—perhaps as the water table declined each summer—and may have redissolved as the water table rose each winter, thus slowing the replacement of contaminated water.

Because of the slow rate of dispersion, it seems likely that some of the contaminant may remain in the aquifer for many years. However, the latest (1964) determinations of sulfate in samples from the 10 observation wells indicate that the concentration of that constituent has fallen well below the 250-ppm maximum limit that was established by the U.S. Public Health Service for drinking water used on interstate carriers and that was adopted by the American Water Works Association for public water supplies.

REFERENCES

Piper, A. M., 1942, Ground-water resources of the Willamette Valley, Oregon: U.S. Geol. Survey Water-Supply Paper 890, 194 p., 10 pls., 3 figs.

Price, Don, 1961, Records of wells, water levels, and chemical quality of ground water in the French Prairie–Mission Bottom area, northern Willamette Valley, Oregon; Oregon State Engineer Ground-Water Rept. 1, 314 p., 10 figs.

RELATION OF WATER QUALITY TO FISH KILL AT TRINITY RIVER FISH HATCHERY, LEWISTON, CALIFORNIA

By WILLIAM D. SILVEY, Sacramento, Calif.

Work done in cooperation with the California Department of Fish and Game, Inland Fisheries

Abstract.—High carbon dioxide content and related low pH of water caused a high mortality rate of salmon and steelhead eggs and fry at the Trinity River Fish Hatchery near Lewiston, Calif. Six days of continuous record show that low pH and high concentrations of carbon dioxide occurred during the early morning hours and on cloudy days. At these times, the eggs and fry died. To lower the concentration of carbon dioxide, limestone chips were placed in the intake works of the hatchery. The limestone reacted with excess carbon dioxide in the water and served to maintain pH in the range from 7.5 to 8.0. Since the treatment was started in September 1964, the hatchery has had no significant losses.

The Water Resources Division of the U.S. Geological Survey, in cooperation with the State of California, Department of Fish and Game, Inland Fisheries, made a study of the chemical quality of Trinity River, at the Trinity River Fish Hatchery (fig. 1), to determine if an inorganic constituent in the water at or upstream from the hatchery was interfering with the hatchery operations. Data on water chemistry near the hatchery for the years 1959–63 were reviewed. During the period June 1–4, 1964, water samples were obtained from various parts of the hatchery and from Lewiston Reservoir (fig. 1). On the same dates, in-place measurements of specific conductance, dissolved oxygen, pH, and alkalinity were made at the hatchery.

Analytical techniques utilized during this study include those standard in the Geological Survey (Rainwater and Thatcher, 1960) and some taken from the American Public Health Association and others (1960). Dissolved-oxygen content was determined with a galvanic cell and a 0- to 10-millivolt recorder. Carbon dioxide was calculated from the pH and bicarbonate values from in-place measurements.

WATER QUALITY

Although in its natural condition the water quality of the Trinity River is excellent for domestic and industrial uses, the water is too pure and soft for healthy fish cultivation. Most authorities agree that a hard, calcium bicarbonate type water is best suited for fish growth and development. Although the water in the Trinity River is of the calcium-magnesium bicarbonate type, its low dissolved-solids content (table 1) makes it weakly buffered and thus susceptible to pronounced pH changes. Shifts in pH, in turn, indicate changes in carbon dioxide concentration. On the basis of the information gained from this study, it is considered likely that the fish kills in the Trinity River Fish Hatchery were caused by such carbon dioxide changes.

Characteristics other than carbon dioxide content and pH

The dissolved-oxygen concentration of the Trinity River water is excellent for hatchery operations. According to Ellis (1937) 5 parts per million of dissolved oxygen is the minimum requirement for the maintenance of healthy fish. For the 5-year period 1959–64 the dissolved-oxygen content of the Trinity River near the hatchery was near saturation throughout each year. When 24-hour recordings of dissolved oxygen were made at the hatchery during the first week of June 1964, the dissolved-oxygen concentration was near saturation at all times. For a 24-hour period on June 3–4, the minimum dissolved-oxygen concentration observed was 9.4 ppm (81 percent saturation), at 11:23 a.m.

Analyses for 17 minor elements in and near the hatchery show that none of these is responsible for the loss of egg and fry at the Trinity River Fish Hatchery.

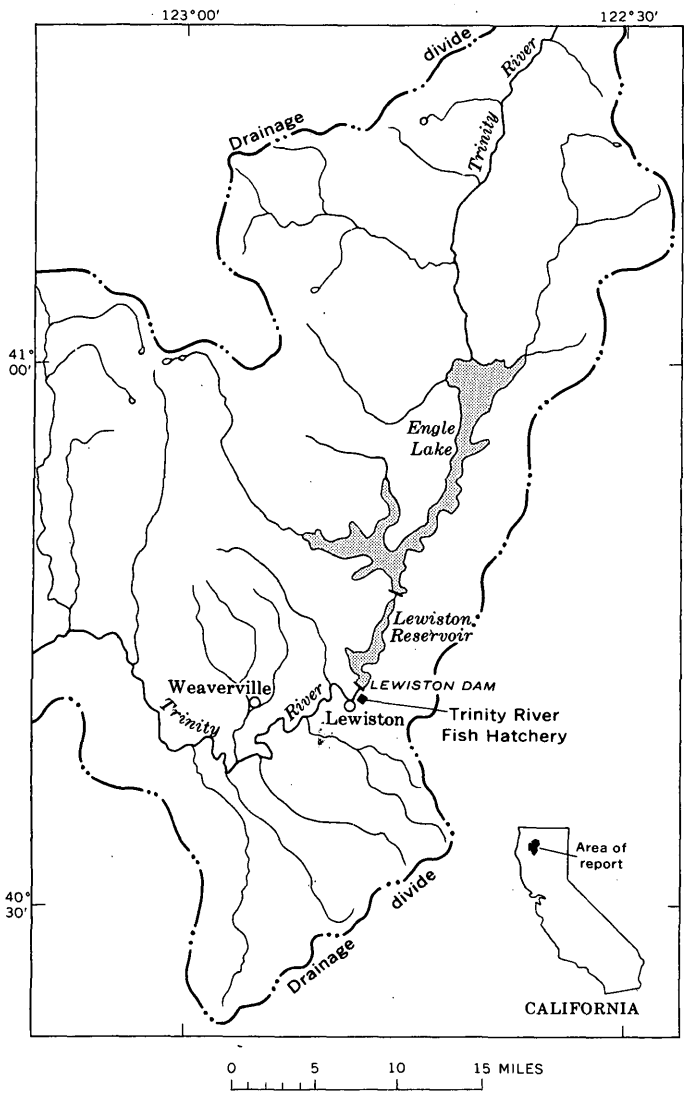

FIGURE 1.—Location of the Trinity River Fish Hatchery, near Lewiston, Calif.

The amount of suspended matter in the Trinity River is low and does not cause difficulty in fish cultivation. Turbidity of 3 samples, 2 collected within the hatchery and 1 sample from Lewiston Reservoir, was only 2, 4, and 2 ppm, respectively.

Temperature, another important factor in fish incubation and growth, also seems favorable in Trinity River water used in the hatchery. Davis (1953, p. 40) said that temperatures between 45°F and 50°F are best for rainbow- and brown-trout incubation, although growth will take place at temperatures as low as 40°F. He also cites data from Embody, who found that rainbow trout eggs will hatch in 30 days at a temperature of 50°F. In June 1964, steelhead eggs took between 70 and 80 days to hatch. However, the temperature in the tray incubators was generally 50°F; and on June 3 and 4, 1964, during water-quality measurements, it was never observed to be lower than 45°F. Therefore, the temperature probably was not below 40°F while the steelhead eggs were hatching. Thus, the delay in the steelhead hatching was probably caused by some factor other than water temperature.

Carbon dioxide content and pH

Study of the pH data from the river showed that shifting pH values probably are related to adverse effects on the fish life. Klein (1962, p. 264) citing Louis Ellis, indicates that a pH range from 6.7 to 8.6 is optimum for the maintenance of fish life. Data collected at the Lewiston gaging station from 1959 to 1964 indicate the pH measurements were made well within Ellis' range. It is significant, however, that the measurements were made on samples collected during daylight hours. If low pH values were occurring they would most likely occur during hours of darkness or during cloudy days, owing to a lack of photosynthesis at these times. To test this assumption, pH measurements were begun before dawn on June 3, 1964, and were continued until the evening of June 4th (table 2). These data indicate that during the 2-day period the pH was below the optimum range during early morning hours and during much of a cloudy day (June 4th). Discovery of the low pH values was an important beginning step in solving the fish-cultivation problem at the hatchery.

TABLE 1.—*Chemical analyses of water samples collected at Trinity River Fish Hatchery, June 4, 1964*

	U.S. Geological Survey Lab. No.		
	46606 [1]	46607 [2]	46608 [3]
Constituents (ppm):			
Silica (SiO_2)	12	12	12
Calcium (Ca)	5.8	5.8	6.0
Magnesium (Mg)	7.2	6.9	6.7
Sodium (Na)	2.6	2.4	2.0
Potassium (K)	.8	.8	.7
Bicarbonate (HCO_3)	51	52	52
Sulfate (SO_4)	.0	.0	.0
Chloride (Cl)	1.2	1.8	1.2
Fluoride (F)	.1	.0	.0
Nitrate (NO_3)	1.0	.6	1.0
Phosphate (PO_4)	.05	.05	.05
Boron (B)	.0	.0	.0
Dissolved solids (sum)	58	56	56
Hardness as $CaCO_3$	44	43	42
Noncarbonate hardness as $CaCO_3$	2	0	0
Alkalinity as $CaCO_3$	42	43	43
Specific conductance (micromhos at 25°C)	90	91	89
pH (laboratory)	7.2	7.1	7.6
Turbidity	2	4	2
Percent sodium	11	10	9

[1] Lewiston Reservoir, at inflow to hatchery.
[2] Incubator, trough outflow to Trinity River.
[3] Raceway outflow to Trinity River.

TABLE 2.—pH-HCO_3-CO_2 *measurements taken at Trinity River Fish Hatchery, June 3–4, 1964*

Time	pH	HCO_3 (ppm)	CO_2 (ppm)[1]
June 3, 1964 (clear, sunny)			
4:42 a.m.	6. 2	54	54
4:47	6. 1	54	70
5:22	6. 2	54	54
5:30	6. 1	54	70
6:14	6. 4	54	34
6:47	6. 5	54	27
7:45	6. 6	54	22
8:53	6. 3	55	44
9:28	6. 3	55	44
10:27	6. 7	55	17
10:52	6. 8	55	13
1:51 p.m.	7. 4	55	3. 2
3:21	7. 8	58	1. 2
4:53	7. 5	58	2. 9
5:34	6. 8	54	14
June 4, 1964 (cloudy, rainy)			
3:58 a.m.	6. 5	52	26
4:30	6. 5	52	26
5:00	6. 3	52	42
5:14	6. 3	52	42
5:37	6. 2	52	52
6:10	6. 3	52	42
9:10	6. 3	52	42
11:51	6. 6	52	21
2:34 p.m.	6. 9	52	10
3:28	6. 4	52	33
4:06	6. 3	52	42

[1] Calculated.

The relation between carbon dioxide (CO_2), alkalinity (HCO_3–CO_3), and pH is defined by Reid (1961, p. 156–162). Welch (1952, p. 189–198) discusses rather thoroughly how carbon dioxide affects organisms in the hydrologic environment. A brief, general explanation of the relation between pH, carbon dioxide, and alkalinity is as follows: Generally the alkalinity (HCO_3) of a stream varies but little over a period of 24 hours and, with no change in dissolved carbon dioxide, the pH will vary little. But if the carbon dioxide concentration varies widely during the 24-hour period, the pH will also vary. Presumably, changes in rates of photosynthesis and the respiration of carbon dioxide by algae are the principal controlling factors in the carbon dioxide, alkalinity, and pH relationship.

High concentration of carbon dioxide in hatchery water appears to be particularly detrimental to eggs and fry. Klein (1962, p. 264), citing Doudoroff and Katz, indicates that a carbon dioxide concentration of from 100 to 200 ppm in the water causes rapid death in sensitive fish even in the presence of a high content of dissolved oxygen. He further states that 50 to 100 ppm of carbon dioxide can cause fatalities upon prolonged exposure. The detrimental effect of high carbon dioxide content in hatchery water is shown by Reid (1961, p. 214), who indicates that of chum salmon eggs subjected to 200 ppm carbon dioxide for 9 days, only 2 percent or less hatched.

A review of the most recent chemical data collected just below the hatchery at Lewiston shows that carbon dioxide as measured during the daytime, was below the toxic limits (6–22 ppm of CO_2) cited in the literature. During the early morning hours, however, the carbon dioxide concentration was high (table 2). On June 3 the carbon dioxide concentration decreased during the day, reaching a minimum of 1.2 ppm at 3:21 p.m., and then began to rise again. There was no cloud cover on June 3 until 7:00 p.m., after which a complete cloud cover existed with intermittent showers, persisting throughout June 4 (table 2). The data in table 2 show that the hatchery water contained large amounts of carbon dioxide on June 4, when the cloud cover was present; the concentration dropped to a minimum of 10 ppm at 2:34 p.m., but then rose again to 42 ppm by 4:06 p.m., after which measurements were discontinued.

In addition to measurements obtained in the hatchery incubators and incubation troughs, measurements were made in other parts of the hatchery on June 4 before 7:00 a.m. Water entering the hatchery from Lewiston Reservoir contained 33 ppm of carbon dioxide, outflow of the raceways into the Trinity River contained 68 ppm, and water from a closed tap on one trough in the hatchery contained 82 ppm of carbon dioxide. These data indicate that high carbon dioxide concentration probably was killing the fish. A review of the literature (Klein, 1962; Welch, 1952) supports this conclusion; high concentration of carbon dioxide is noted repeatedly as having adverse effects on development of fish, particularly the egg and fry stages.

Why does a carbon dioxide problem exist at the Trinity River Fish Hatchery? First, and most important, the Trinity River was changed from a natural through-flowing stream to a reservoir system when the Lewistown diversion dam was constructed. This probably permitted a large buildup of algae and other organisms which did not flourish in the natural river system but which resulted in production of carbon dioxide on dark or cloudy days and at night. Second, the Lewiston Reservoir is in a narrow and rather steep-walled valley, and the walls of the valley support a heavy cover of vegetation that, during nights and dark days, expires carbon dioxide which concentrates in the valley floor; this increases the supply of carbon dioxide to the water and to the organisms in the hatchery beyond the amount that the fish life can readily tolerate.

SOLUTION OF THE FISH-KILL PROBLEM

To eliminate the carbon dioxide problem at the hatchery, either the source of carbon dioxide could be treated or the water could be treated chemically to reduce the amount of carbon dioxide. To treat the water chemically seemed more practical and economical. It required maintaining a pH of about 7.6 and a carbon dioxide content of about 2.0 ppm as well as using methods that would not cause the chemistry of the water to be detrimental to eggs, fry, or fingerlings. Common compounds that can be added to water to control the pH are soda ash, caustic soda, lime, and limestone. Soda ash and caustic soda are not desirable because if a large amount accidentally gets in the water, excessively high pH will result, and also because the essential calcium might be precipitated. Lime is not desirable because it might raise the pH excessively. Limestone is satisfactory and desirable because it will react only when carbon dioxide is present. Also, limestone requires no control, and is economical to use.

In September 1964, limestone treatment of the hatchery water was started, and since then there have been no significant losses of eggs or fry. Instead, through June 1965, 24 million fish have been produced at the facility, hereby returning the Trinity River Fish Hatchery to beneficial use.

REFERENCES

American Public Health Association, American Water Works Association, and Water Pollution Control Federation, 1960, Standard methods for the examination of water and waste water, including bottom sediments and sludges: New York, Am. Public Health Assoc., Inc., 626 p.

Davis, H. S., 1953, Culture and diseases of game fishes: Berkeley and Los Angeles, California Univ. Press, 122 p.

Ellis, M. M., 1937, Detection and measurement of stream pollution: U.S. Bur. Fisheries Bull. 22.

Klein, Louis, 1962, River pollution; 2, Causes and effects: London, Butterworth's, 456 p.

Rainwater, F. H., and Thatcher, L. L., 1960, Methods for collection and analysis of water samples: U.S. Geol. Survey Water-Supply Paper 1454, 301 p.

Reid, R. K., 1961, Ecology of inland waters and estuaries: New York, Reinhold Publishing Corp., 375 p.

Welch, P. S., 1952, Limnology: New York, McGraw-Hill Book Co., Inc., 536 p.

DISTINCTIVE BRINES IN GREAT SALT LAKE, UTAH

By A. H. HANDY, Salt Lake City, Utah

Work done in cooperation with, and publication authorized by, the Utah Geological and Mineralogical Survey

Abstract.—Data collected from Great Salt Lake, Utah, indicate the presence of at least four distinct brines in the lake. Each brine has a characteristic relationship between lithium or potassium concentration and brine density. The areas north of the causeway and just south of the causeway from 20 to 25 feet deep have higher concentrations of lithium and potassium than the rest of the lake and are of economic importance because of the higher concentrations. The areas occupied by the different brines are outlined.

The chemical composition of dissolved solids in the brine of Great Salt Lake has been determined from time to time since about 1850. These determinations indicate that the brine has contained from about 14 percent to about 29 percent (by weight) of dissolved solids (Handy and Hahl, 1966, p. 140) and that sodium and chloride have made up about 90 percent of the dissolved solids (Hahl and Langford, 1964, p. 26). The dissolved-solids concentration of the brine changes with lake stage and volume, but the composition of the dissolved solids does not change appreciably.

The construction of a causeway across Great Salt Lake in 1957 divided the lake into two nearly separate parts. (See fig. 1.) Most surface-water inflow enters the southern parts of the lake between the north end of Antelope Island and Promontory Point; there is no major inflow to the lake north of the causeway. The causeway is porous, however, and two small culverts pierce it; as a result there is some interchange and mixing of brine between the two parts of the lake.

Prior to construction of the causeway, the Great Salt Lake was believed to be a well-mixed body of water because of its shallow depth (less than 35 feet) and the action of the wind and currents. Since construction of the causeway, however, areal differences in mineralization of the brine have been observed. In October 1965, as part of a cooperative program with the Utah Geological and Mineralogical Survey, samples were collected from 26 sites distributed areally as shown in figure 1. The samples were taken at the surface and at depth intervals of about 5 feet, to within 1 foot of the lake bottom. As a result of this sampling program, Handy and Hahl (1966) reported that the brine north of the causeway was more highly mineralized than that south of the causeway. They also found that the brine north of the causeway is more uniform in composition than the brine south of the causeway and that the southern brine may be divided into at least three different types.

The different types of brine were determined by plotting density against concentrations of potassium and lithium. Density was determined by finding the weight of a given volume of sample at 20°C (Rainwater and Thatcher, 1960, p. 161), and potassium and lithium concentrations were determined by flame-photometric methods using a spectrophotometer with flame attachments.

Figure 2 shows the relationships between density and concentration of potassium and lithium. The brine north of the causeway, as indicated by samples taken from depths of 0–24 feet at sites 1–11 (fig. 1), generally has a density of about 1.22 grams per milliliter, with potassium concentrations that exceed 6,700 parts per million and lithium concentrations that exceed 60 ppm (upper triangle in each part of fig. 2). The brine south of the causeway, as indicated by samples taken from depths of 0–16 feet at sites 12–25, generally has a density of about 1.17 g/ml, with potassium concentrations less than 5,000 ppm and lithium concentrations of 41 ppm or less (lower triangle in each part of fig. 2). The brine south of the causeway is less dense than the brine north of the causeway because of the greater inflow of surface water to the southern part of the lake.

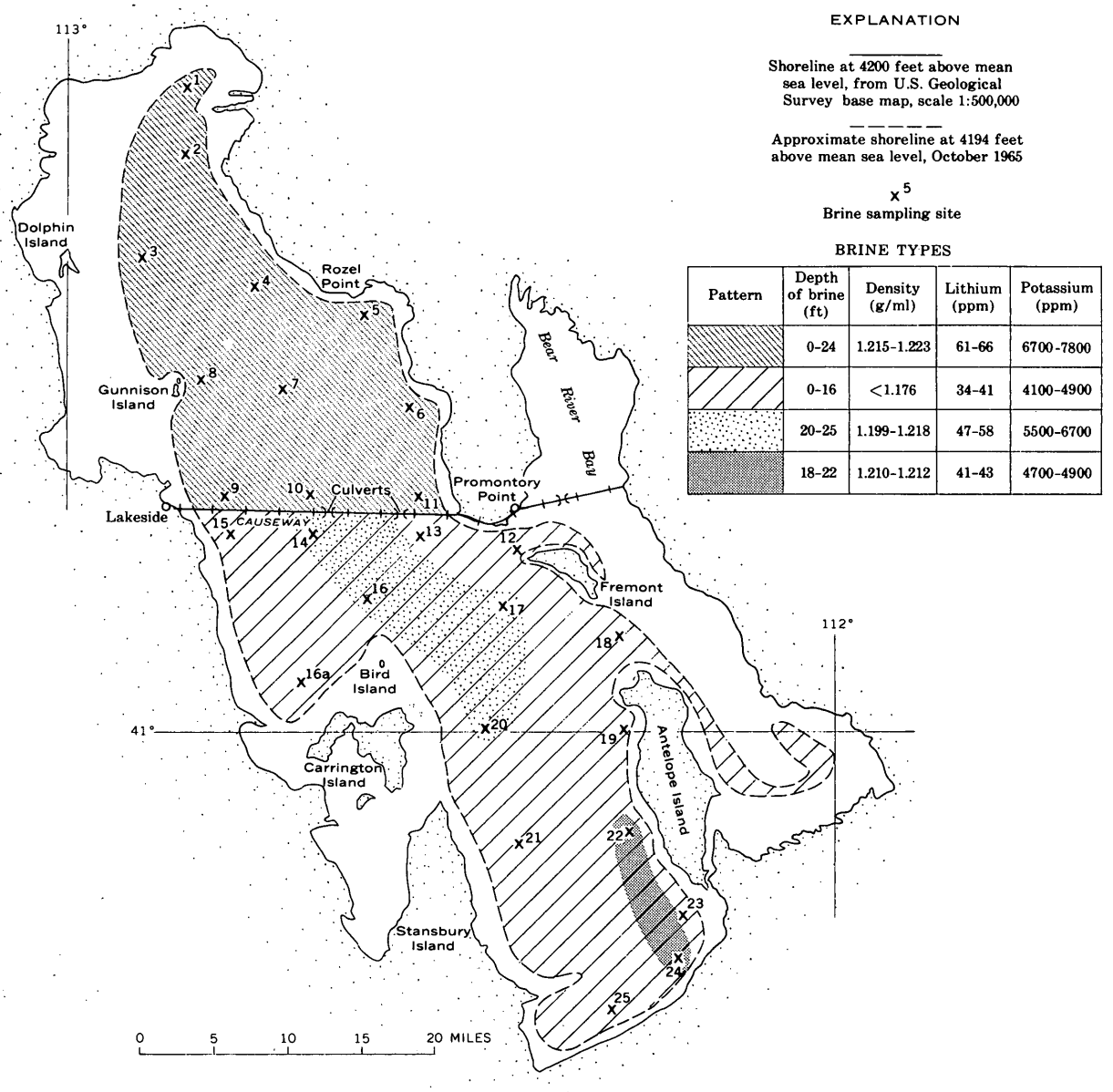

FIGURE 1.—Map of Great Salt Lake, showing brine types and sampling sites, October 1965.

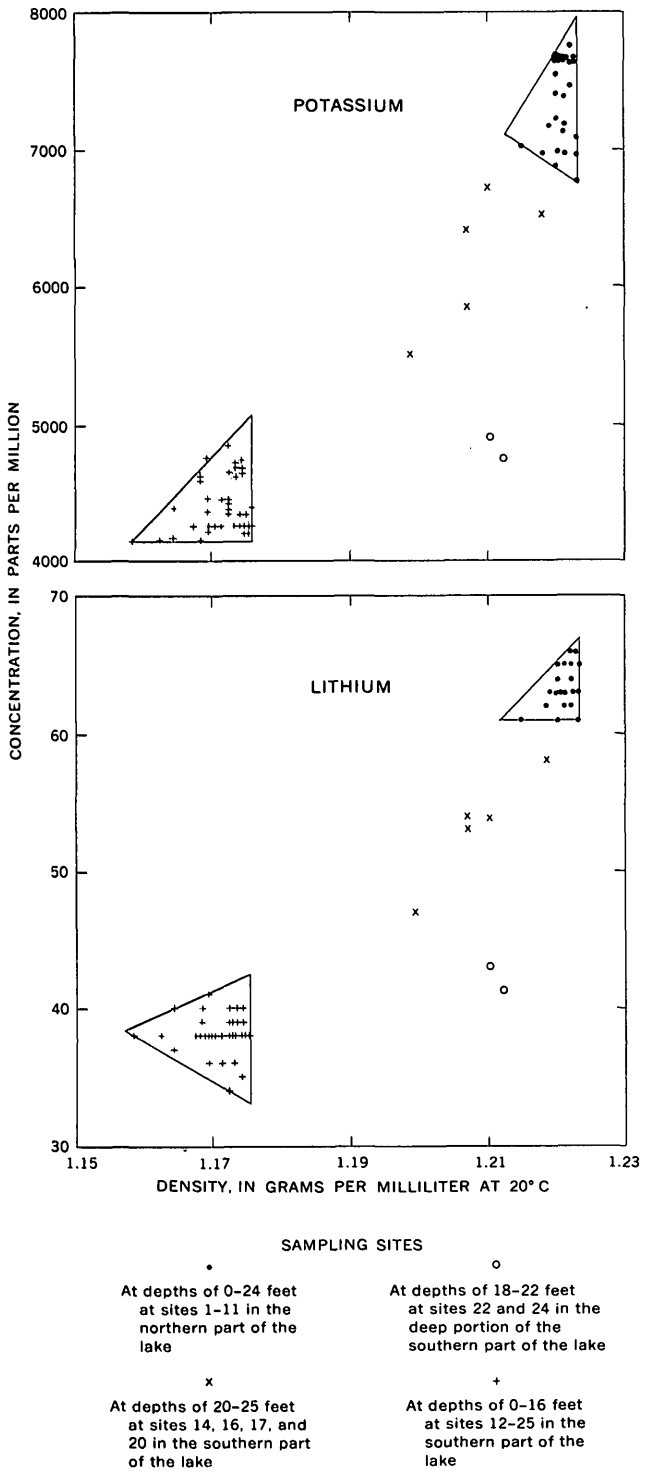

FIGURE 2.—Relationships of potassium and lithium concentrations to brine density in Great Salt Lake, October 1965.

At least two areas in the southern part of the lake contain brines that are considerably denser than most of the brine in the southern part. Samples taken from depths of 20–25 feet at sites 14 (two samples), 16, 17, and 20 (fig. 1) had densities ranging from about 1.20 to 1.22 g/ml, with potassium concentrations that exceed 5,000 ppm and lithium concentrations ranging 47–58 ppm (x's in fig. 2). Samples taken from depths of 18–22 feet at sites 22 and 24 had densities of about 1.21 g/ml with potassium concentrations less than 5,000 ppm and lithium concentrations af about 41 ppm (circles in fig. 2).

The areas south of the causeway that contain the denser brine are outlined in figure 1. These denser brines are in the deeper parts of the lake where the chemical quality of the water apparently is least affected by surface inflow to the lake. The deep brine in the area just south of the causeway also contains a higher concentration of potassium and lithium than does the shallow brine in the southern part of the lake. This indicates that brine from the northern part of the lake flows through the causeway and moves along the bottom of the southern part, but it does not mix thoroughly with the southern brines, despite the shallowness of the lake and the mixing action of winds and currents.

Plotting lithium or potassium concentration against brine density demonstrates the presence of at least four distinct brines in the Great Salt Lake. The approximate areal distribution of these brines has been outlined on the basis of available data. Elements such as lithium and potassium are found in commercially valuable quantities in Great Salt Lake; thus, these findings may be significant to those interested in mining the elements from the lake.

REFERENCES

Hahl, D. C., and Langford, R. H., 1964, Dissolved-mineral inflow to Great Salt Lake and chemical characteristics of the Salt Lake brine, pt. II, Technical report: Utah Geol. and Mineralog. Survey Water Resources Bull. 3., p. 12–14.

Handy, A. H., and Hahl, D. C., 1966, Great Salt Lake—chemistry of the water, *in* The Great Salt Lake: Utah Geol. Soc. guidebook to the geology of Utah, no. 20, p. 135–151.

Rainwater, F. H., and Thatcher, L. L., 1960, Methods for collection and analysis of water samples: U.S. Geol. Survey Water-Supply Paper 1454, 301 p.

COMPUTATION OF TRANSIENT FLOWS IN RIVERS AND ESTUARIES BY THE MULTIPLE-REACH IMPLICIT METHOD

By CHINTU LAI, Washington, D.C.

Abstract.—The technique and the computer programs developed for the solution of transient flows in a single reach of river by the implicit method have been extended to include transient flows in a river of relatively complex geometry and of considerably greater length composed of several subreaches. Based on theoretical analysis, computer programs have been written to solve m pairs of partial differential equations implicitly for unknown stages and discharges at points on the advanced time line, t_{k+1}, from known values at points on the present time line, t_k, and the two given boundary values. The graphical displays of computer outputs from two sample computations indicate the feasibility of the technique.

The determination of discharge and collection of other basic information on streams and rivers have long been among the important activities of the Water Resources Division of the U.S. Geological Survey. In many rivers, discharge can be accurately and economically determined when the flow is relatively steady or when a section control is acting. Difficulty arises in estuaries and in such portions of rivers where unsteady flows occur because of tides, ocean waves, regulation by dams and reservoirs, or because of heavy rains and floods. In order to devise accurate, economical, and more reliable methods for the determination of the discharge and other parameters of transient flow, research in this field was initiated in the Geological Survey by R. A. Baltzer and was later extended by the author. Three basic methods for solving unsteady flows of homogeneous density by use of a digital computer have been worked out, and the results have been released in three open-file reports (Baltzer and Shen, 1961; Lai, 1965a, 1965b).

However, in all three of these reports, the applications to actual rivers were made only to single river reaches of relatively short length, because accurate field data covering long reach are difficult to obtain and because the previous computer programs were written to handle only relatively simple and reasonably uniform river geometry. The slower speeds and lower capacities of earlier digital computers used by the Geological Survey researchers also deferred the practical study of multiple reaches until the present time (1966). In order to cover the case of more complex river geometry found in a much longer reach, the computer programs for solving unsteady flows by the implicit method (Lai, 1965b) have been revised, modified, and extended to solve transient flows along a long reach of a river that has variable cross sections, a variable flow-resistance coefficient, and variable lateral inflow. The theoretical description of the method and the steps for the computer solution are given in the following paragraphs.

The set of partial differential equations that describes one-dimensional transient open-channel flows of homogeneous density was derived in a previous report (Lai, 1965b). They are the equation of continuity,

$$B\frac{\partial Z}{\partial t}+\frac{\partial Q}{\partial x}-q=0, \qquad (1)$$

and the equation of motion,

$$\frac{\partial Q}{\partial t}+u\frac{\partial Q}{\partial x}+Q\frac{\partial u}{\partial x}+gA\frac{\partial Z}{\partial x}+\frac{gk}{AR^{4/3}}Q|Q|=0, \qquad (2)$$

in which x is a distance measured along the longitudinal axis (x axis), t is time, Z is the elevation of water surface measured from a horizontal datum plane (simply the "stage"), Q and u are the discharge and mean velocity of the flow passing a cross section of area A and surface width B, and q, g, and R stand for lateral inflow per unit length, gravitational acceleration, and hydraulic radius, respectively. The parameter k is a function of the flow resistance coefficient, η (similar to Manning's n), and is expressed as $k=\left(\frac{\eta}{1.49}\right)^2$ if the English system of units is used.

The governing partial differential equations 1 and 2 can be transformed into a set of corresponding partial difference equations

$$Q_D-Q_C+\frac{B_D+B_C}{2}\left(\frac{\Delta x}{\Delta t}\right)\left[\frac{Z_C+Z_D}{2}-\frac{Z_A+Z_B}{2}\right]-q_{M_2}\Delta x=0 \tag{3}$$

and

$$\left(\frac{\Delta x}{\Delta t}\right)\left[\frac{Q_C+Q_D}{2}-\frac{Q_A+Q_B}{2}\right]+\frac{u_C+u_D}{2}(Q_D-Q_C)$$
$$+\frac{Q_C+Q_D}{2}(u_D-u_C)+g\left(\frac{A_C+A_D}{2}\right)(Z_D-Z_C)$$
$$+gk\left(\frac{2}{R_C+R_D}\right)^{4/3}\left(\frac{u_C+u_D}{2}\right)\left|\frac{Q_C+Q_D}{2}\right|\Delta x=0, \tag{4}$$

in which the subscript indicates the point to which the variable is referenced. (See fig. 1.)

From the known quantities at the $t=t_k$ line, the unknowns at $t=t_{k+1}$ are to be found by the use of equations 3 and 4. However, these two equations have four unknowns, Z_C, Z_D, Q_C, and Q_D, and hence, the solution is indeterminate. If two of these unknowns are given as boundary values, the other two unknowns can be found by solving the equations simultaneously. This was done in the previous report by supplying two gage readings in the time sequence obtained from automatic digital stage recorders installed at each end of a reach. Continuous Q_C and Q_D values were then computed from equations 3 and 4 and from the given boundary values.

For a longer reach covering two segments of Δx, $\bar{x}_{j-1}\bar{x}_j$ and $\bar{x}_j\bar{x}_{j+1}$, 4 equations can be set up comprising 6 unknowns on 2 adjacent grid rectangles, for example, rectangles *ABDC* and *BGHD* in figure 1. They are Q_C, Q_D, Q_H, Z_C, Z_D, and Z_H. Again, if 2 of the 6 unknowns are given, the set reduces to 4 equations with 4 unknowns, thus enabling one to solve them simultaneously.

Similarly, for a very long reach covering m segments of Δx, $2m$ equations can be set up for m grid rectangles (two for each rectangle) with $2(m+1)$ unknowns on the advanced t line, that is, at $t=t_{k+1}$. If two unknowns are given at the boundaries, the rest of $2m$ unknowns can be found by solving the $2m$ equations simultaneously.

According to the above-described principles, computer programs have been written to solve transient flows for m segments along an open channel depicted by m grid rectangles in the x direction. It is supposed that all the elevations and discharges on the grid points along the channel at the current time line, $t=t_k$, are known (either as given initial conditions or as the results of a previous computation), and that the successive elevations at both ends of the channel will be given at every time step. (See fig. 2.)

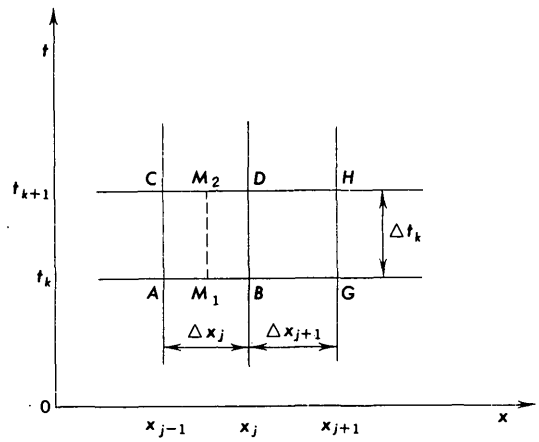

FIGURE 1.—Two adjacent rectangles.

As the first step of the computation, new elevations are assumed at all grid points on the advanced time line, $t=t_{k+1}$, say, by quadratic extrapolation from the previous elevations. By using these $m-1$ assumed values of elevations together with the two given elevations at the channel ends, and by repeatedly using the method of solution employed for a single reach in every rectangle, $2m$ values of discharge can be computed on the $t=t_{k+1}$ line. To illustrate, consider, for example, the jth grid rectangle in the x direction, that is, rectangle *ABDC*, at which two discharges Q_C and Q_D can be obtained, while for the $(j+1)$th grid rectangle, *BGHD*, Q_D and Q_H can be obtained; and so forth for all the rectangles throughout the entire channel between $t=t_k$ and $t=t_{k+1}$. For convenience, let the Q value at point D computed from rectangle *ABDC* be designated as Q_D and that from *BGHD* as Q'_D.

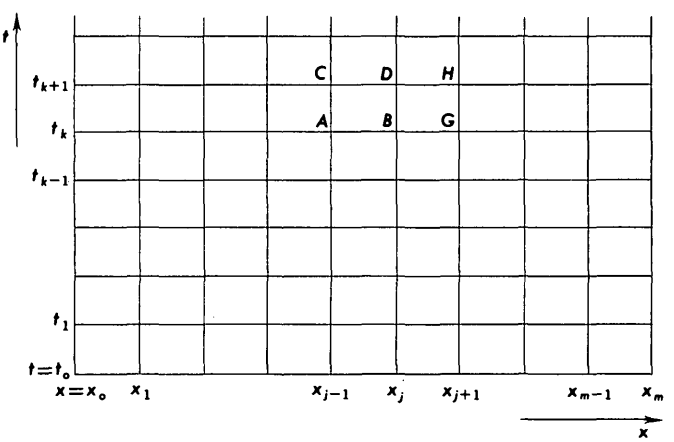

FIGURE 2.—Space-time (x, t) plane.

After all the $2m$ values of Q are computed, the difference of the two Q values at a grid point computed from the two adjacent rectangles, for example, $\Delta Q_D = Q'_D - Q_D$ at point D, is tested for every grid point from (x_1, t_{k+1}) to (x_{m-1}, t_{k+1}). The Z value at the grid point that has the largest difference of Q values is adjusted first until the difference reduces to a magnitude less than some preassigned tolerable error, ϵ. After the first adjustment is finished, the computer scans all the differences of Q's again, that is,

$$|\Delta Q_1|, |\Delta Q_2|, \ldots |\Delta Q_j|, \ldots |\Delta Q_{m-1}|, \text{ at } t=t_{k+1},$$

and locates the new grid point that has the new largest difference of Q's, that is, max $|\Delta Q|$. The Z value at that point is again adjusted as done before. The same procedure is repeated until all the differences are reduced to magnitudes less than ϵ; that is,

$$|\Delta Q_1| < \epsilon, |\Delta Q_2| < \epsilon, \ldots, |\Delta Q_j| < \epsilon, \ldots, |\Delta Q_{m-1}| < \epsilon.$$

The computation for $m+1$ values of Q and $m-1$ values of Z at the $t=t_{k+1}$ line is thus accomplished and the computer is ready to advance one time step, Δt, by using the newly obtained Z and Q values as knowns.

The computer program has been tested by using several sets of transient open-channel flow data, and the results appear promising. Two examples are shown below to demonstrate outputs obtainable from the computer program. The first example (fig. 3) is a tidal flow in the reach between Torresdale and Delair, Pa., on the Delaware River, which was solved as a single reach by the method of characteristics and by the implicit method in two previous reports by the author (Lai, 1965a, 1965b). In this example, the same reach is cut into four short subreaches having different flow-resistance coefficients and variable cross-sectional area. The water stages at both ends of the reach, that is, at Torresdale and Delair, were provided as boundary values, and the field-measured discharge determined at Tacony-Palmyra Bridge, near Philadelphia, Pa., is compared with the computed discharge at that point. The agreement appears very satisfactory.

The second example (fig. 4, p. B232) is a tidal flow in a hypothetical channel that has a uniform rectangular cross section but a reach length of about 24 miles. Two sinusoidal waves of the same amplitude (4 feet) and of the same period (12.4 hours) were applied to the boundaries; one at one end of the channel, and the other with a phase lag of about $\pi/4$ at the other end of the channel. The tidal computation was carried for five tidal cycles. A portion of the computer output is shown in figure 4. In the figure, three curves of stage versus time at three different points along the channel are plotted simultaneously from a line printer. Two of the three curves are numerically listed also.

The first of these two sample computations treats an actual field reach of relatively short length with actual field data; the second one treats a hypothetical channel with simulated tidal waves but of considerably long-reach length. The simulated tidal waves in the latter example have sinusoidal shapes with the period of an actual tidal cycle (12.4 hours). From these two examples and in view of the fact that tidal motions can be decomposed to many sinusoidal curves, the written computer program is believed to be applicable to many field reaches of considerable length.

REFERENCES

Baltzer, R. A., and Shen, J., 1961, Flows of homogeneous density in tidal reaches: U.S. Geol. Survey open-file report. 107 p.

Lai, Chintu, 1965a, Flows of homogeneous density in tidal reaches, solution by the method of characteristics: U.S. Geol. Survey open-file report. 58 p.

——— 1965b. Flows of homogeneous density in tidal reaches, solution by the implicit method: U.S. Geol. Survey open-file report. 43 p.

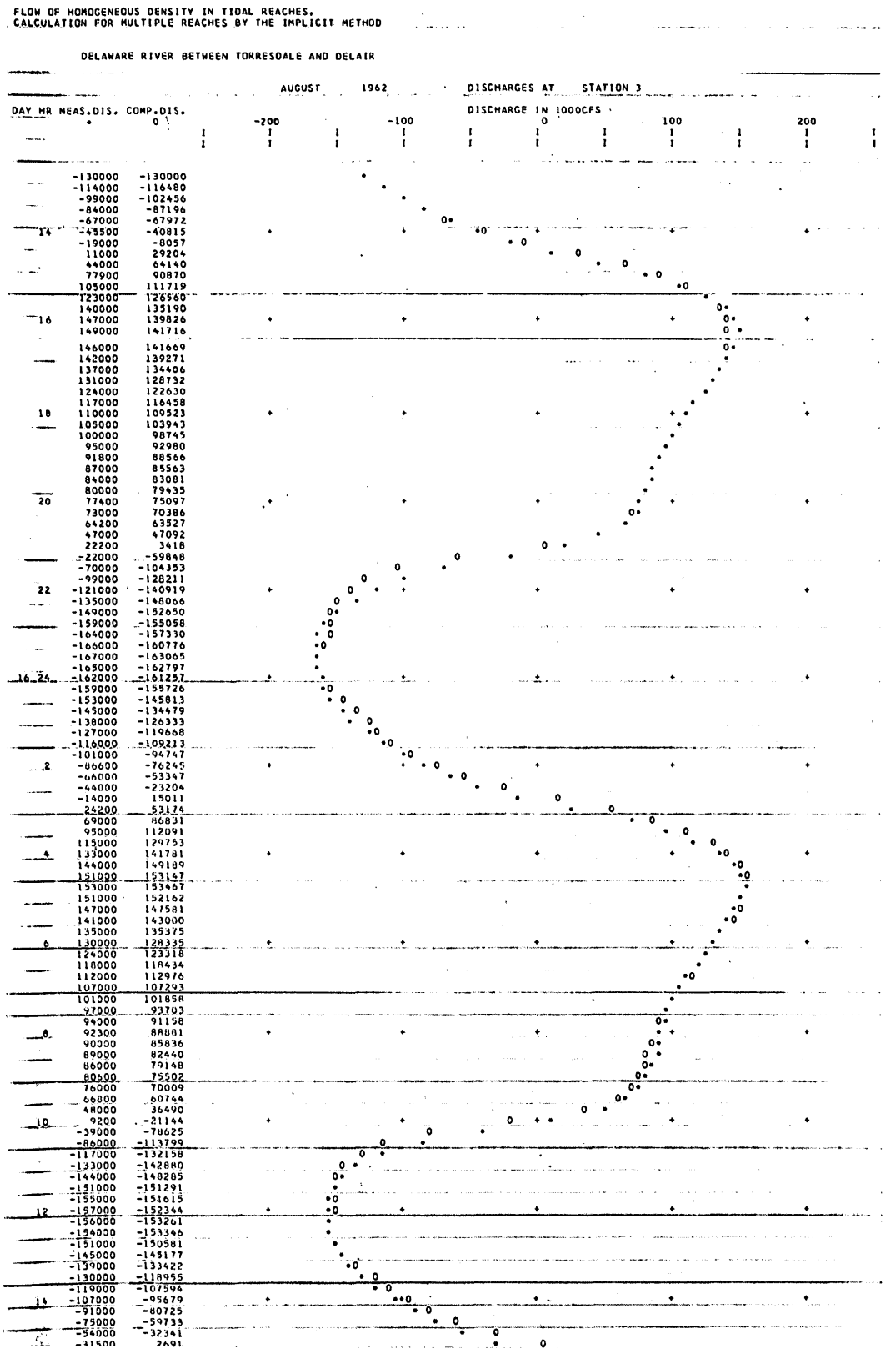

FIGURE 3.—Computed (o) and measured (*) discharges, Delaware River at the Tacony-Palmyra Bridge (between Torresdale and Delair), near Philadelphia, Pa., reproduced directly from computer print-out page.

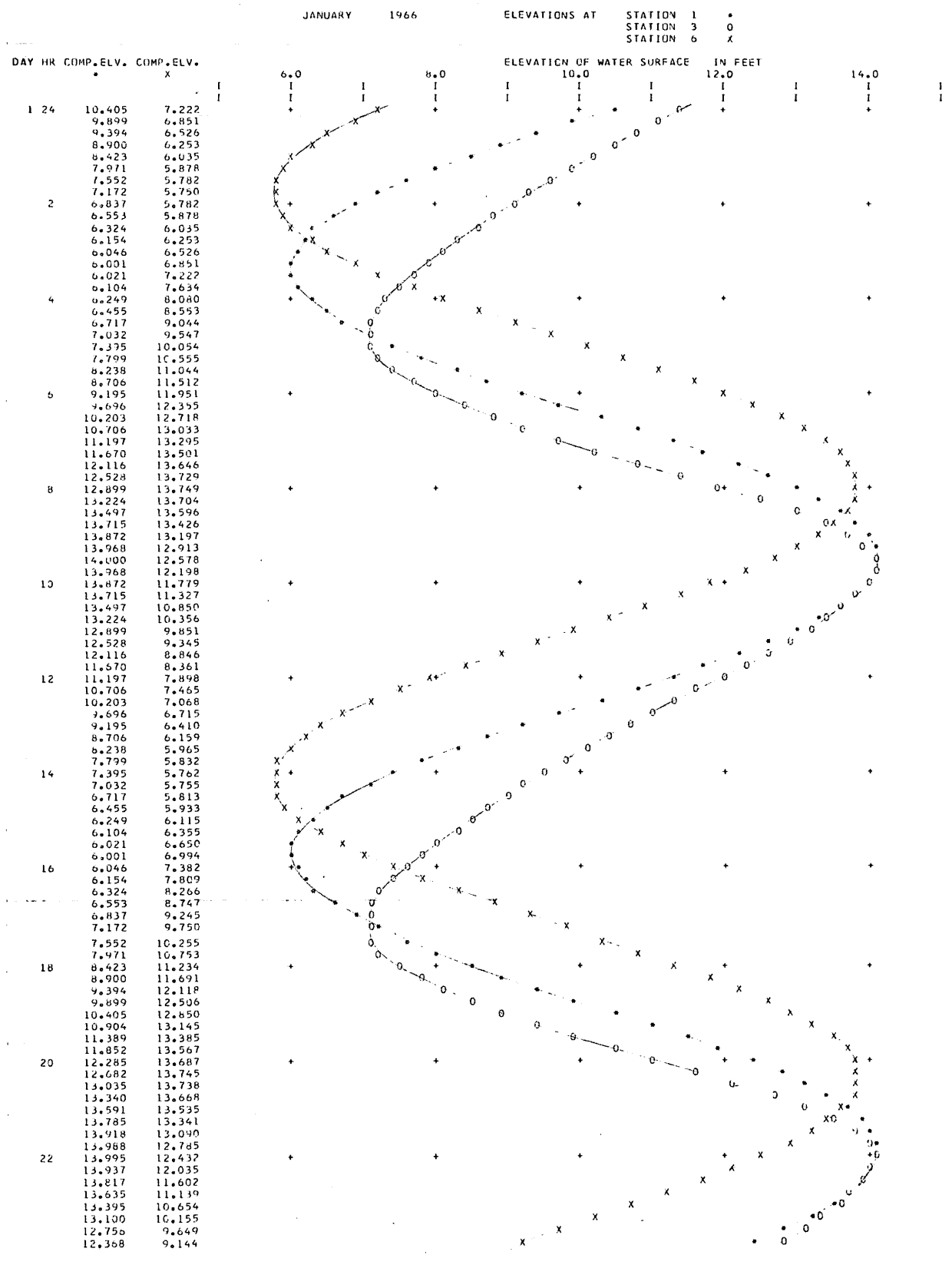

FIGURE 4.—Computed stage versus time curves along points on a long rectangular channel, reproduced directly from computer print-out page. Numerical listings are given on the left for stations 1 and 6 but not for station 3.

DIURNAL TEMPERATURE FLUCTUATIONS OF THREE NEBRASKA STREAMS

By KENNETH A. MacKICHAN, Lincoln, Nebr.

Abstract.—Average diurnal variations in water temperatures at 1 site on each of 3 streams followed similar cyclic patterns during May, July, and November. The times of the daily minimum and maximum temperature for 2 of the streams were nearly the same but were about 1 hour later for the third.

Some streams in the midcontinent area have large diurnal fluctuations of temperature during part of the year; for example, a fluctuation of as much as 25°F was observed on the Niobrara River near Verdel, Nebr., on a day in May. The average fluctuations in summer are much greater than those in winter, and no fluctuations occur when the streams are covered with ice.

Thermograph records for varying periods are available for three streams in northern Nebraska—the Snake River above Merritt Reservoir, the Niobrara River near Verdel, and the Middle Loup River at Dunning. The fluctuations during May, July, and November were investigated. July was selected because fluctuations during this month are large, and November because the fluctuations are small and the stream is not likely to have an ice cover. Although May was thought to represent an intermediate condition, it proved to be more nearly like July than November.

AMPLITUDE OF THE FLUCTUATION

The maximum fluctuation observed was on the Niobrara River near Verdel during May and is only 1° more than the maximum for July at the same site. There was no fluctuation during at least 1 day during November on the Snake River above Merritt Reservoir and on the Middle Loup River at Dunning. Table 1 shows the maximum, minimum, and average amplitudes of diurnal fluctuation in temperature at each of the three sites. As records were not collected concurrently at the three sites, the tabulated values are not necessarily for the same years.

TABLE 1.—*Amplitude of diurnal temperature fluctuations, in degrees Fahrenheit*

	May	July	November
Niobrara River near Verdel			
Months of record	2	4	2
Temperature:			
Maximum	25	24	10
Minimum	2	6	1
Mean	11.8	15.8	4.6
Middle Loup River at Dunning			
Months of record	3	3	2
Temperature:			
Maximum	21	22	14
Minimum	3	6	0
Mean	12.4	14.0	6.9
Snake River above Merritt Reservoir			
Months of record	1	1	1
Temperature:			
Maximum	20	16	7
Minimum	4	5	0
Mean	12.5	11.0	3.2

Temperature fluctuations in each of the three streams investigated appear to follow a similar pattern on most days in both winter and summer. Generally, the temperature reaches a minimum between 7 a.m. and 10 a.m., and a maximum between 4 p.m. and 6 p.m. The temperature does not follow this pattern on a few days each year, but the fluctuations are almost always small on these days.

Diurnal fluctuations may be reduced to nondimensional terms by comparing temperatures for particular times during a day with the mean temperature for that day and expressing the differences as percentage of the total fluctuation for the day. (See fig. 1.) Temperatures less than the mean are expressed as negative departures and those greater than the mean as positive departures. Obviously, the departure for the minimum temperature of the day is a negative

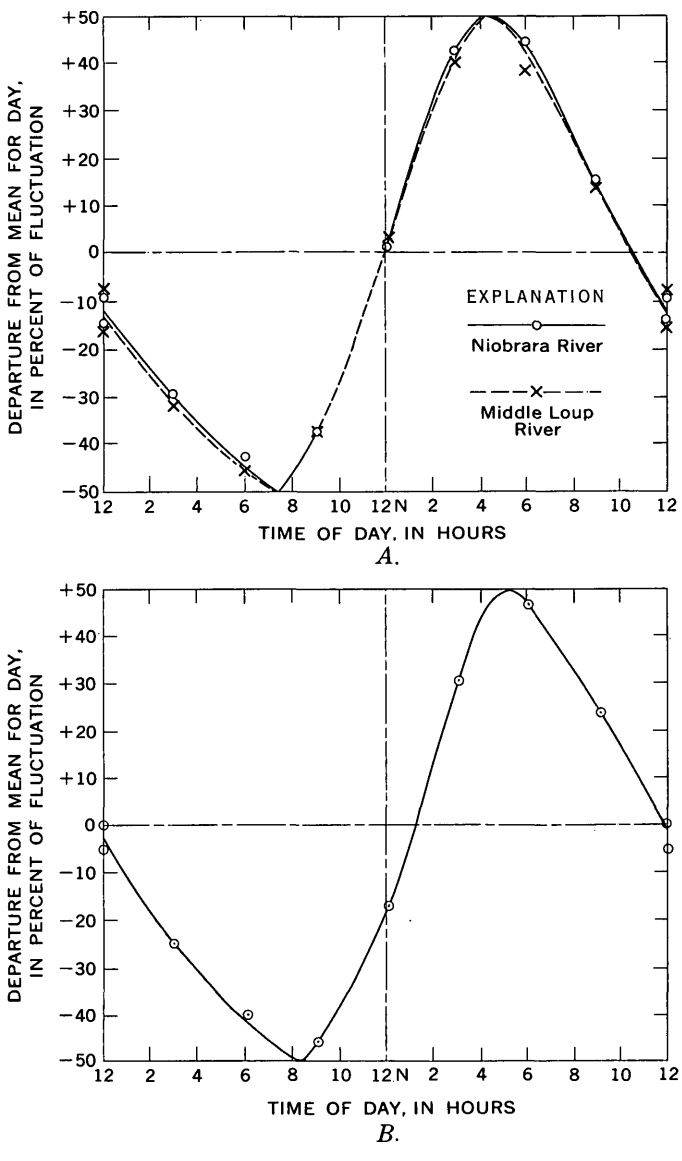

FIGURE 1.—Average diurnal departures from the mean daily water temperature of three rivers in Nebraska. *A*, Niobrara River near Verdel and Middle Loup River at Dunning; *B*, Snake River above Merritt Reservoir.

50 percent and for the maximum a positive 50 percent.

The data for the 3 months appear to define a single relationship at each location. One might expect that the average minimum would occur a little later in the morning during winter than during summer because the sun rises later. There was no discernible trend of this kind in the data for the 3 months selected for study. Data for other months, for other streams, or for longer periods of record might reveal such a trend.

The temperature fluctuations of the Niobrara River near Verdel and the Middle Loup River at Dunning are nearly identical. The maximum and minimum temperatures of the Snake River above Merritt Reservoir occurred about 1 hour later than those of the Niobrara and Middle Loup Rivers (fig. 1). The reasons for the difference in time of the maximum and minimum temperature at the Snake River station and at Dunning and Verdel are not known. Some possible causes are differences in depth of the stream, in vegetation along the streambanks, and in depth of the valley.

CONCLUSIONS

The following conclusions can be drawn concerning temperature variations in the three streams investigated:

1. The temperature of the water at any hour during a day can be estimated if the maximum and minimum water temperatures for the day are known.

2. Water temperatures observed once a day may not provide a valid average value, particularly if they are consistently read in early morning or late afternoon.

3. The change from minimum to maximum water temperature occurs during an interval of about 8 hours, whereas the change from maximum to minimum occurs during an interval of about 16 hours.

WATER-QUALITY CHANGES IN A DESTRATIFIED WATER COLUMN ENCLOSED BY POLYETHYLENE SHEET

By KEITH V. SLACK and GARRY G. EHRLICH, Menlo Park, Calif.

Abstract.—A 21-meter vertical column of water in a reservoir, enclosed in a polyethylene cylinder 1 square meter in cross section, was destratified with compressed air. Nearly complete thermal and chemical destratification rapidly followed air injection. Thermal stratification rapidly reformed when air flow ceased, but nearly complete chemical homogeneity persisted. Dissolved-oxygen concentration increased during 4 days of intermittent air injection. Phytoplankton concentrations and photosynthesis decreased inside the cylinder relative to the outside water. Apparently the environment following air injection was unfavorable for existing phytoplankton species.

Induced circulation of stagnant lakes and reservoirs has been widely used for water-quality control (Reddick, 1957; Heath, 1961; Patriarche, 1961; Woods, 1961; Ford, 1963; and Koberg and Ford, 1965). Although the benefits of artificial circulation are sometimes striking, destratification may produce other problems such as accelerated phytoplankton growth caused by transferring nutrients from bottom waters into the photosynthetic zone. Because of the many factors involved it usually is not possible to predict the effects of destratification of a particular environment on the biota.

An empirical approach to this problem, using a vertical polyethylene cylinder similar to the one described by Goldman (1962), open at the top and closed at the bottom, has been tested in Lake Cachuma, Santa Barbara County, Calif. Strickland and Terhune (1961) described a large submerged sphere in which the water was stirred during studies of photosynthesis in a marine bay. Goldman and Carter (1965) used an elongate polyethylene test cell with closed ends to study primary productivity and phytoplankton standing crop in Lake Tahoe, Calif. Induced circulation of isolated water columns is an obvious extension of the technique which appears useful for fundamental studies of stratification-related phenomena.

This report describes initial tests of an enclosed in-situ colunm of water used as a model reservoir ecosystem. In brief, a column of water in stratified Lake Cachuma was enclosed by a hollow cylinder made of thin plastic sheet. The cylinder was open to the atmosphere above and open to the reservoir bed below, but the enclosed water was physically separated from the surrounding water. The column was destratified, and simultaneous measurements were made inside and outside the cylinder to study the effects of induced circulation on water and plankton in the cylinder.

The main objective of the first test was to evaluate the feasibility of the method as a field technique. A second objective was to determine the effects of induced circulation on isolated columns of Lake Cachuma water.

METHODS

Cylinder construction

A hollow cylinder 21 meters long and 1 square meter in cross section was constructed by taping 0.25-mm (0.01-in.) translucent polyethylene sheet into a tube and attaching one end to a circular bottom-anchor ring of iron weighing about 18 kilograms (40 pounds). The tube was shaped into a circular form on a sheet metal and plywood drum 1.5 m high and slightly smaller in diameter than the tube. Aluminum-wire reinforcing hoops were taped to the tube at 1-m intervals. The tube was lowered into the water from the drum through an opening in the deck of a specially constructed raft by means of three lines attached to the anchor ring. When the anchor ring was embedded in the bottom, the cylinder length was adjusted to keep the upper tube end above the water surface, and the lowering lines were pulled taut and attached to a surface float.

The raft, anchored on the north side of the cylinder to minimize interference with underwater light, carried instruments and an air compressor. Compressed

U.S. GEOL. SURVEY PROF. PAPER 575-B, PAGES B235-B239

241-334 O—67——16

air, passed through rubber tubing outside the cylinder, was discharged into the cylinder from a riser pipe about 1 m above the bottom. At the completion of the study the plastic cylinder was recovered intact on the forming drum.

Data collection

Depth profiles of temperature, dissolved oxygen, and specific conductance were made by sensing elements attached to a multiconductor cable marked at 1-m intervals and lowered directly into the water. A guideline down the center of the cylinder facilitated lowering of the equipment into the cylinder.

Temperatures at 4 fixed depths inside the cylinder and at 2 fixed depths outside were recorded sequentially on an Esterline-Angus recording milliammeter using thermistors and a 6-channel automatic sequencer developed by the U.S. Geological Survey.

Water samples for chemical and plankton analysis were collected with a free-flushing plastic sampler closed by rubber ball valves. Samples for later processing in the Menlo Park, Calif., laboratory were treated with suitable preservatives. Chemical determinations followed the procedures of Rainwater and Thatcher (1960). Plankton samples were filtered through 0.45-micron filters in the field.

The transparency of water inside and outside the cylinder was estimated from the depth at which a standard Secchi disk just disappeared from view.

RESULTS

The initial tests in Lake Cachuma were conducted in 21 m of water. The site was selected because it was deep enough to include a part of the hypolimnion, it was largely protected from wind, and it was in the shallow upper part of the lake where many nuisance algal growths first appear.

Temperature

The cylinder was lowered into the water on June 6, 1966, and allowed to equilibrate for 24 hours. Temperature profiles taken inside and outside the cylinder on June 7 were nearly identical. A series of intermittent air-pumping cycles were performed during the next 3 days, and on June 11 a nominal air flow of 14 liters (0.5 cubic foot) per minute was injected for about 9 hours Figure 1 shows temperatures at four depths inside the cylinder during this test series. Water temperatures at depths of 1 and 9 m inside the cylinder dropped rapidly with the onset of air pumping. The temperature at 11 m increased slightly and at 20 m was relatively unaffected, showing that the mixed zone in the cylinder extended from the top of the air riser pipe, 1 m above the bottom, to the surface

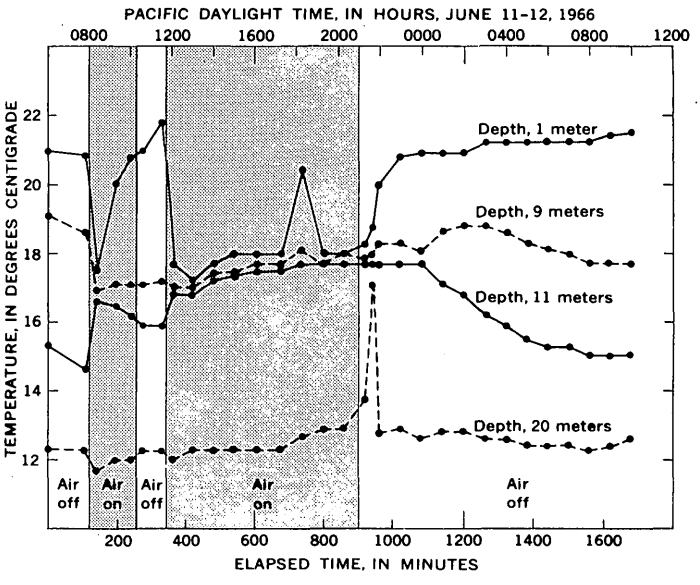

FIGURE 1.—Effects of air injection on water temperature at four depths in an enclosed column of water. The column was 21 meters long with a cross sectional area of 1 square meter. Air was introduced at a depth of 20 meters.

with a relatively undisturbed pool of water lying below. Only a slight temperature gradient existed in the cylinder during the extended test period. Temperatures of the surrounding water during the test are represented fairly accurately by the initial temperature profile inside the cylinder shown at zero time on figure 1.

One of the most unexpected results of the study was the rapid increase of water temperature at 1 meter depth when air injection ceased. The rapid fall in water temperature at 1 meter with the onset of pumping and rapid rise when the air flow was stopped were shown through all cycles of pumping. Several hours after termination of pumping, temperature equilibrium was virtually restored between the water in the cylinder and the surrounding water. Examination of figure 1 suggests that the heat relationships between the uninsulated confined column and the surrounding water are complex. Detailed analysis was not attempted.

Dissolved oxygen

Dissolved-oxygen profiles inside and outside the cylinder prior to air injection were virtually the same. During the pumping tests dissolved oxygen steadily increased in the water of the cylinder as shown by dissolved-oxygen profiles taken prior to the daily pumping tests (fig. 2). A sharp break in dissolved oxygen at 16 m occurred on the fourth and fifth days. It is not known whether this break is the result of diffusional processes or of biological activity in the

lower depths. A dissolved-oxygen profile taken during the pumping test of June 11 is shown in figure 3, together with the corresponding profile taken before the start of the pumping test. The pool of unmixed water near the bottom is clearly indicated. In general the water was supersaturated with oxygen as a result of air injection.

Specific conductance

No change in specific conductance resulted from the destratification experiments.

Inorganic nutrients

Samples for determination of key inorganic nutrients were taken at several depths inside and outside the cylinder (table 1). Water samples were taken before air pumping on June 9, about 18 hours after the previous pumping test had terminated. Nitrate, phosphate, and silica values were virtually the same at 5 and 15 m, suggesting that chemical homogeneity persisted after thermal stratification was reestablished. Nitrate and phosphate concentrations were significantly higher at 5 m inside the cylinder than at 5 m outside the cylinder. At 15 m, nitrate and phosphate concentrations were about the same inside and outside the cylinder. Silica concentration was uniform with depth both inside and outside the cylinder.

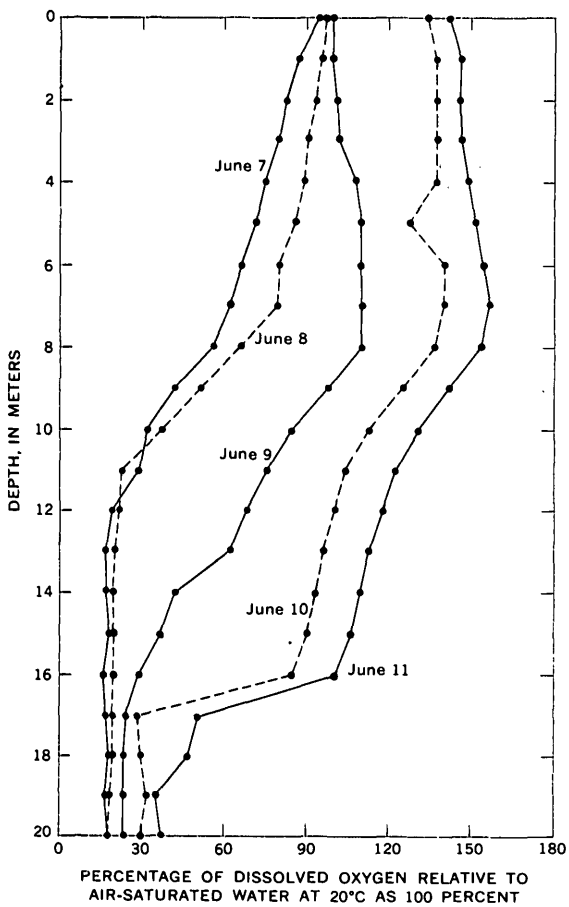

FIGURE 2.—Progressive increase of dissolved oxygen in an enclosed column of water subjected to periodic air injection.

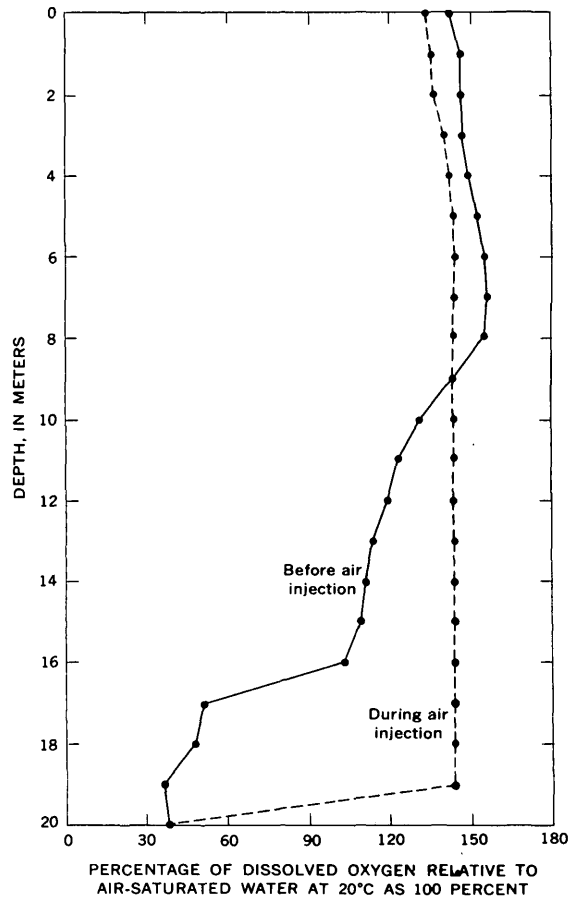

FIGURE 3.—Dissolved-oxygen profiles in an enclosed column of water before and during air injection, June 11, 1966.

On June 11, during air pumping, concentrations of nitrate, phosphate, and silica were again uniform with depth inside the cylinder, and were at approximately the same levels as on June 9. The 1-m sample taken outside the cylinder on June 11 showed significantly lower concentrations of nitrate and phosphate than the samples taken from the cylinder on that date (table 1).

Alkalinity and pH

Alkalinity and pH were measured on freshly collected water samples from several depths inside and outside the cylinder before air pumping commenced on June 9 and 10. Values of bicarbonate concentration were computed on the basis of total alkalinity represented as bicarbonate ions. Figure 4 shows that the water in the cylinder was homogeneous with respect to pH, bicarbonate, and carbon dioxide, thus

TABLE 1.—*Concentration of key nutrients at various depths inside and outside an enclosed column of water*

Date (1966)	Depth (meters)	Concentration (ppm)					
		NO_3		PO_4		SiO_2	
		Inside	Outside	Inside	Outside	Inside	Outside
June 9	5	0.97	0.13	0.33	0.19	9.9	10.2
	15	.98	.96	.35	.36	10.9	11.0
June 11 [1]	1	------	.15	------	.22	------	11.0
	5	1.06	------	.36	------	10.6	------
	15	.85	------	.37	------	10.8	------
	20	.92	------	.36	------	10.9	------

[1] Samples taken during air injection.

supporting the earlier conclusion of the persistence of chemical destratification in the presence of thermal stratification. Appearance of high pH and low CO_2 concentration outside the cylinder indicates that active photosynthesis was taking place in the upper 5 to 10 m of the lake. Absence of these effects in the cylinder suggests that less active photosynthesis was taking place either due to a smaller phytoplankton population or to other effects inhibitory to photosynthesis.

Two samples were taken in the cylinder during air pumping on June 11 (table 2). Similarity of these values with those in figure 4 indicates that air pumping did not appreciably effect pH, bicarbonate, and free CO_2.

Clarity of water

The only indication of the relative clarity of water inside and outside the cylinder is from Secchi disk measurements. On June 10 the disk depth was 1.4 m outside and 1.2 m inside. At least part of the difference in water clarity between the lake and the cylinder is attributed to innumerable small gas bubbles in the cylinder.

Phytoplankton

Counting of plankton from cylinder samples was difficult because many organisms appeared dead or were undergoing lysis. However, table 3 shows that phytoplankton concentrations at various depths were lower inside than outside the cylinder. The samples of June 9 and 10 were taken before air injection and after the cylinder had been thermally stratified for about 18 hours. Lower phytoplankton concentration near the surface in the cylinder is attributed to decreased turbulence, which permitted the organisms to settle. The samples taken on June 11 during air injection show uniform phytoplankton concentration with depth in the destratified cylinder.

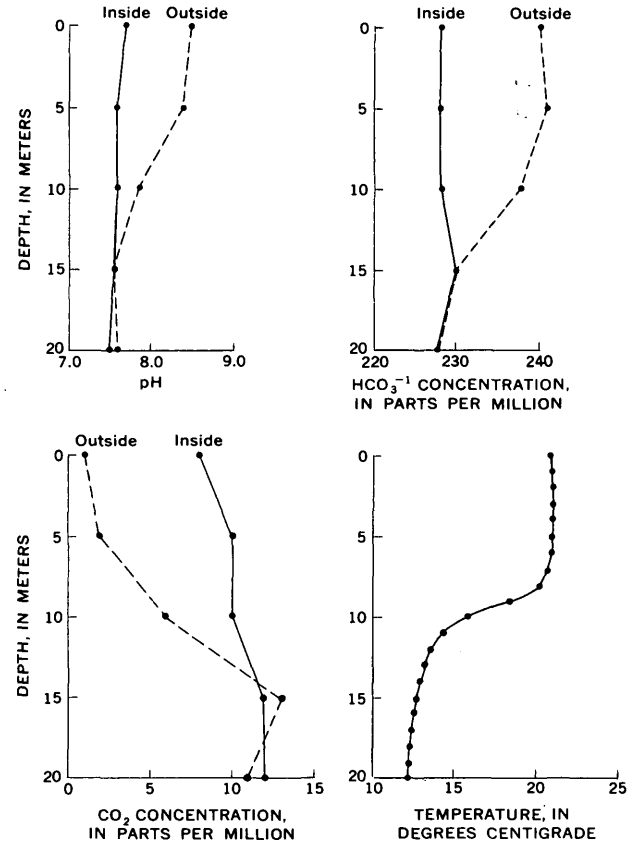

FIGURE 4.—Comparison of pH, temperature, bicarbonate ion, and carbon dioxide concentrations inside and outside an enclosed column of water. Water temperatures were identical inside and outside. The column had been thermally stratified for about 18 hours.

CONCLUSIONS

Evidence of inhibited biological activity inside the test cylinder relative to that outside the cylinder was shown by (1) the lower phytoplankton concentration at various depths inside the cylinder, (2) an active phtosynthetic zone outside but not inside (high pH and low free CO_2), and (3) higher nutrient concentrations near the surface inside.

Destratification changed the physical and chemical properties of the water. Apparently the changed environment was unfavorable for the existing phytoplankton species, which began to die off. The population decline is seen in the plankton data and possibly in differences in nutrient concentrations inside and outside the cylinder. The test did not continue long enough for a new group of organisms, adapted to the changed conditions, to appear. However, succession of species is to be expected in longer studies and in destratification projects involving entire reservoirs.

TABLE 2.—*Temperature, pH, and bicarbonate and CO_2 concentrations in an enclosed column of water during air injection, June 11, 1966*

Depth (meters)	Temperature (degrees C)	pH	HCO_3 (ppm)	CO_2 (ppm)
5	18. 3	7. 65	227	10
15	16. 8	7. 66	230	10

Enclosure of parts of aquatic environments by thin plastic sheet is a promising technique for fundamental and applied studies in hydrology. These in-situ enclosures are a practical compromise between the use of an entire hydrologic unit and a laboratory scale model. They are adaptable to many experimental treatments and are relatively undisturbed, they may be of large size, and they are exposed to the natural ranges of temperature and illumination of the water body.

A few of the potential uses of plastic enclosures are in studies of: phytoplankton productivity and population dynamics, effects of altered water composition on aquatic organisms, mechanisms of thermal and chemical stratification and destratification, processes at the air-water and sediment-water interfaces, effectiveness of control methods for nuisance organisms, fate of pesticides and monomolecular films in aquatic environments, and effects of sewage or other wastes on water quality.

TABLE 3.—*Number of phytoplankton organisms per milliliter inside and outside an enclosed column of water*

Depth (meters)	June 9		June 10		June 11
	Outside	Inside	Outside	Inside	Inside [1]
1	----	----	6, 550	470	----
5	4, 960	650	4, 100	1, 600	800
10	----	----	3, 550	1, 670	----
15	1, 100	2, 000	1, 300	1, 200	900

[1] During air injection.

REFERENCES

Ford, M. E., Jr., 1963, Air injection for control of reservoir limnology: Am. Water Works Assoc. Jour., v. 55, no. 3, p. 267–274.

Goldman, C. R., 1962, A method of studying nutrient limiting factors in situ in water columns isolated by polyethylene film: Limnology and Oceanography, v. 7, no. 1, p. 99–101.

Goldman, C. R., and Carter, R. C., 1965, An investigation by rapid carbon-14 bioassay of factors affecting the cultural eutrophication of Lake Tahoe, California-Nevada: Water Pollution Control Federation, v. 37, p. 1044–1059.

Heath, W. A., 1961, Compressed air revives polluted Swedish lakes: Water and Sewage Works, v. 108, no. 5, p. 200.

Koberg, G. E., and Ford, M. E., Jr., 1965, Elimination of thermal stratification in reservoirs and the resulting benefits: U.S. Geol. Survey Water-Supply Paper 1809–M, p. 1–28.

Patriarche, M. H., 1961, Air-induced circulation of two shallow Michigan lakes: Jour. Wildlife Management, v. 25, no. 3, p. 282–289.

Rainwater, F. H., and Thatcher, L. L., 1960, Methods for collection and analysis of water samples: U.S. Geol. Survey Water-Supply Paper 1454, 301 p.

Reddick, R. M., 1957, Forced circulation of reservoir waters yields multiple benefits at Ossining, N.Y.: Water and Sewage Works, v. 104, no. 6, p. 231–237.

Strickland, J. D. H., and Terhune, L. D. B., 1961, The study of in-situ marine photosynthesis using a large plastic bag: Limnology and Oceanography, v. 6, no. 1, p. 93–96.

Woods, D. E., 1961, The effect of compressed air on winter oxygen levels in a fertile southern Minnesota lake: Minnesota Fish and Game Inv., Fish Ser., no. 3, p. 51–60.

HYDRAULIC SAND-MODEL STUDY OF THE CYCLIC FLOW OF SALT WATER IN A COASTAL AQUIFER

By J. M. CAHILL, Phoenix, Ariz.

Work done in cooperation with the
U.S. Atomic Energy Commission, Division of Isotope Development

Abstract.—Model studies demonstrate visually that "cyclic flow" takes place in the denser fluid when fresh water flows seaward over intruding ocean water. When tidal fluctuations are simulated in the model by alternately raising and lowering the level of the free body of salt water, additional mixing of the two miscible fluids occurs and additional salt water is transported into the fresh-water region. The fluid movement was observed by following colored tracers that were injected into both fluids. These studies indicate that the degree of salt-water intrusion is controlled primarily by the flow of the fresh water rather than by tidal effects.

Early theories relating to the balance between fresh water and sea water in a coastal aquifer commonly were based on two assumptions: first, that the interface between the two miscible fluids is sharp; and second, that the salt water in the aquifer is static. Field observations of the Biscayne aquifer in Miami, Fla., have shown that the saline wedge is dynamically stable even though salt water is circulating through the wedge. As indicated by Cooper (1959), Cooper and others (1964), and Kohout (1960), salt water flows inland from the ocean and becomes diluted with fresh water, thereby creating a "zone of diffusion." This diluted sea water is then carried seaward through an upper flow region, which is defined simply as that region where flow is toward the sea. As the diluted sea water in the zone of diffusion is carried seaward it must be continually resupplied by an inland movement of more sea water through the underlying seawater wedge, thus causing "cyclic flow" of salt water in an aquifer. The intent of this paper is to illustrate —with hydraulic experiments on a sand model and time-lapse photography—how several factors may influence that flow.

The cyclic flow of salt water that occurs in a coastal aquifer was demonstrated visually by the models described in this article. The complexities of the problem of hydrodynamic equilibrium of salt-water encroachment have been described and partially summarized in the literature. For example, Henry (1959) described equations for the location of the interface and for boundary velocities for several boundary conditions assuming immiscible fluids, and Rumer and Harleman (1963) constructed laboratory models as a means for investigating intrusion and dispersion of sea water in confined coastal aquifers.

Acknowledgments.—The writer is indebted to H. E. Skibitzke and Akio Ogata for the fundamental concepts used in designing the model, to H. T. Chapman, who helped build the model, and to T. W. Anderson, who assisted in collecting the experimental data.

HYDRAULIC SAND MODEL

The sand model used in the tests was constructed of commercially bagged silica sand loosely packed in a watertight open-topped rectangular container. The model was designed to simulate a vertical section of a coastal aquifer, oriented perpendicular to the coastline and parallel to the seaward direction of fluid flow. The model as shown in figure 1 was 23 feet long, 18 inches high, and 2½ inches thick. The transparent front of the model was made of ½-inch plate glass. A regulated quantity of fresh water (light color in the photographs) was introduced from a tank (*A*) at the left, while salt water (dark color) was simultaneously introduced from a small tank (*C*) suspended from a stand at the right end of the model.

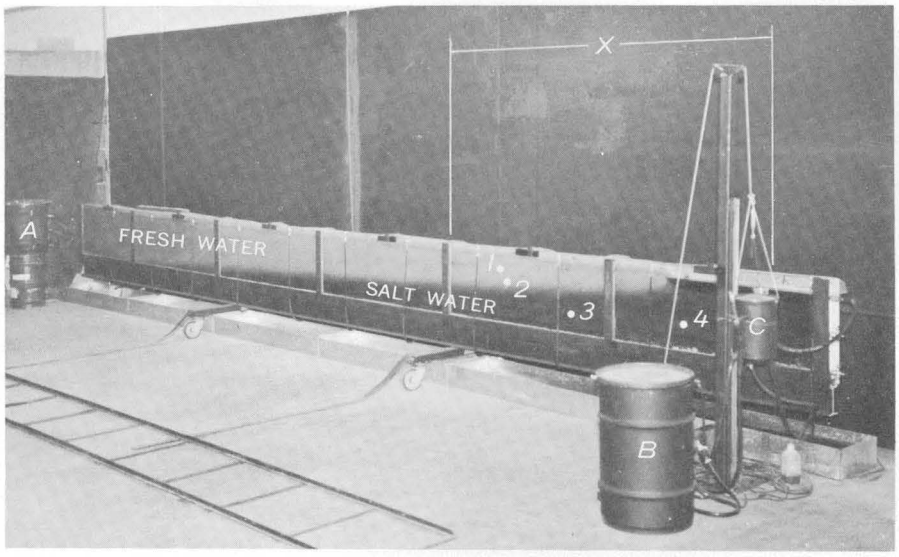

EXPLANATION

A, Fresh-water constant-head tank
B, Salt-water reservoir tank
C, Head tank to generate tides in salt-water zone
X, Area under study for cyclic flow in the fresh-water zone
1 and *2*, Position of tracer injection tubes in the fresh-water zone
3 and *4*, Position of tracer injection tubes in the salt-water zone

FIGURE 1.—Photograph of hydraulic sand model. The simulated shoreline is above tube 4. Fluid movement in a landward direction is to the left and in a seaward direction is to the right.

Simulated tidal effects were introduced into the model by moving the salt-water tank up and down so as to alternately increase and decrease the head of salt water. The flow conditions in the model compare closely with the conditions that exist in an unconfined aquifer discharging fresh water into the sea.

The direction of the fluid movement in the model was determined by watching the movement of red tracer fluid injected through four 1/16-inch-diameter brass tubes that penetrated vertically into the model. Two red tracer fluids were prepared, one with a density approximately identical to that of the fresh water in the model and the other with a density approximately identical to that of the salt water. These were injected into their respective environments in quantities small enough to cause a minimum of disturbance in the regional flow pattern. Two tubes were positioned in the fresh-water zone (see *1* and *2*, fig. 1), one ending just above the interface with the dark salt water and the other penetrating about half the depth of the fresh-water zone. Tube 4 was positioned in the salt-water zone just below the simulated "shoreline," and tube 3 was positioned farther "inland" in the same zone (fig. 1).

The salt water in the model was a solution of sodium chloride dissolved in tap water, and the fresh-water was tap water. The salt water was tinted with green organic dye in a glycerine base, so that a noticeable visual contrast existed between the salt- and fresh-water regions. Specific gravity of the salt-water source was maintained at 1.025. To prevent progressive change in density of the salt water, the mixed salt-water effluent from the upper flow region was collected at the "shoreline" and removed from the model.

OBSERVATION OF FLUID MOVEMENT IN MODEL

Nonoscillatory motion

In the steady-state tests, the fresh- and salt-water heads were maintained constant until the interface between the clear and the green water became static. A tracer solution of red organic dye in a glycerine base diluted in tap water was then injected into the fresh- and salt-water zones. The quantity injected was about one four-hundredth of the fresh-water input.

The red tracer fluid injected (from tubes *3* and *4*) in the salt-water zone moved landward (left) as shown by the photographs in figure 2. Figure 2*A* shows the position of the tracer about 30 hours after it was first injected in the model. Figure 2*B* shows the location of the tracer fluid after about 52 hours. A comparison of the photographs shows that some of the tracer in the salt-water zone moved horizontally away from the sea and downward while some of the tracer moved

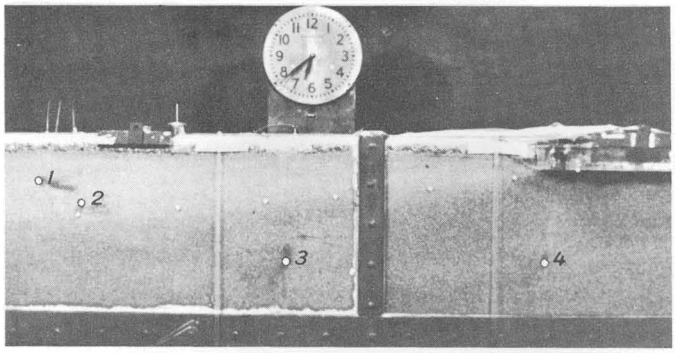

A

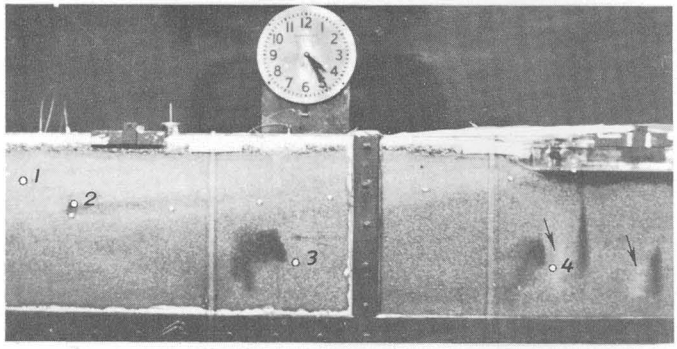

B

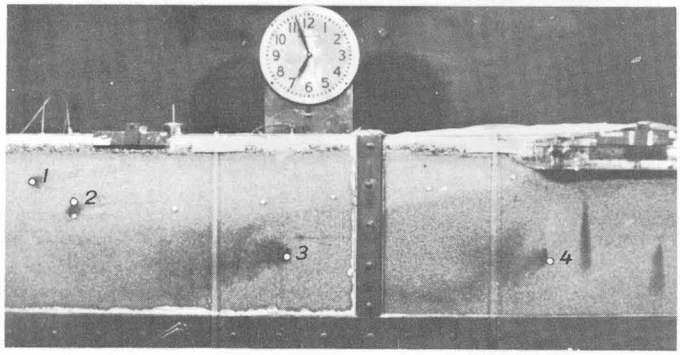

C

FIGURE 2.—Photographs of tracer movement through salt-water zone without tidal influence. Position of tracer in: *A*, 30 hours; *B*, 52 hours; and *C*, 150 hours after tracer injection began. Fliud movement in a landward direction is to the left and in a seaward direction is to the right.

horizontally landward and upward toward the interface between the green-dyed (salty) and clear (fresh) water. The two dark areas beneath the "sea" are residues from small crystals of potassium permanganate, which were inserted in the porous medium to act as an auxilliary tracer. Movement of this tracer is revealed by the bleached appearance of the water (see arrows, fig. 2*B*) and is obviously horizontally landward in the salt-water zone.

Figure 2*C* shows the tracer position about 150 hours after injection began. It can be seen in this photograph that some of the tracer fluid injected in the salt-water region has moved landward (left) into the interface region of fresh and salt water and then has curved back toward the sea. Only a faint outline of the red-dye tracer can be seen at the interface because of its rapid dilution in the seaward-flow region after it has passed upward across the interface.

The tracer fluid injection was stopped after 162 hours. The rate at which the injected tracer fluid moved horizontally landward (left) in the salt-water zone was observed by measuring the trailing edge of the tracer fluid after injection was stopped. The tracer injected at tube 4 (beneath the shoreline) was displaced landward 9 inches in a 36-hour period, whereas the tracer injected at tube 3 (2 feet inland from the shoreline) moved 6 inches in the same period. In comparison, movement of the tracer in the upper flow region was 4 inches per hour seaward (right).

Oscillatory motion

Effects of simulated tidal action.—In the oscillatory-motion phase of the model test, the level of the salt-water body was raised and lowered to simulate tidal action. The period of oscillation was 19 minutes, with a change in salt-water head of 0.7 inch from high to low. This tidal period was arbitrarily chosen to provide enough time for adjustment to the change in head to occur throughout the region of interest in the model.

Figure 3 shows the movement of the red-dye tracer when tidal fluctuation is simulated in the salt-water body. Figure 3*A* shows the tracer position 24 hours after injection began. As compared to the movement without tidal influence, the tracer movement in the saline wedge is more rapid with tidal influence. The tracer moved inland (left) and upward toward the salt-water–fresh-water interface, entered the zone of mixed saline and fresh water, and was carried seaward (right) by the regional flow in the upper zone.

As the test progressed, additional red tracer fluid was injected at a higher head into the salt-water zone (fig. 3*B*) to force some of the tracer low enough to depict fluid movement near the base of the model. The photograph in figure 3*B* shows the position of the injected tracer at about 114 hours after injection began. It can be seen in this photograph that the left edge of the body of tracer-tagged fluid is curved, the lower portion suggesting a dominant horizontal movement and the upper portion a large vertical component of movement. Thus, the upper portion of the tracer body reaches the salt-water–fresh-water interface within a short span of time and is carried back to the sea by movement in the upper flow region. The flow path for

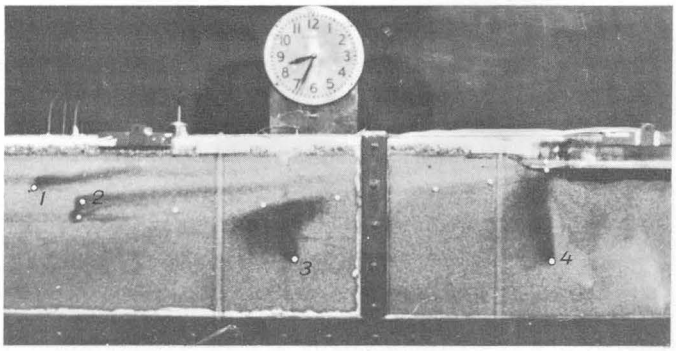

A

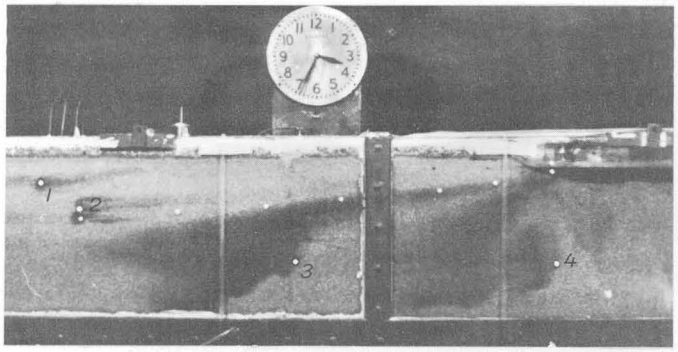

B

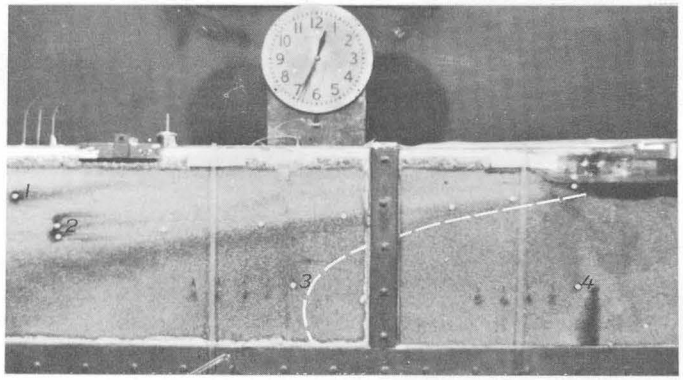

C

FIGURE 3.—Photographs of tracer movement through salt-water zone with tidal influence. Position of tracer in *A*, 24 hours; and *B*, 114 hours after tracer injection began. *C*, about 69 hours after tracer injection had ceased. Dashed line, trailing end of tracer from tube 4. Fliud movement in a landward direction is to the left and in a seaward direction is to the right.

the lower portion of the tracer body is longer and requires more time.

The tracer movement in the salt-water zone was observed for 4 days after injection was stopped with the tidal oscillation maintained. By 69 hours after injection ceased the tracer fluid from the inland injection point (tube 3) had moved landward (left) along the model base about 12 inches. (See fig. 3*C*). However, most of the injected tracer fluid from this area had already moved toward the salt-water–fresh-water interface, where it was carried back to the sea (right) through the upper flow region. The tracer fluid moved landward (left) about 18 inches from the injection point beneath the shoreline (tube 4). During the time that the tracer fluid from this injection point was moving landward, the trailing end of the dye tracer curved upward and then was carried seaward by the upper flow region. This curvature can be seen as a faint trace near the support post of the model and is depicted by the dashed line.

Effects of increased seaward flow of fresh water and of increased tide.—A 50 percent increase in the seaward flow of fresh water combined with a 50-percent increase in tidal amplitude resulted in a marked increase in the transport of salt water into the upper flow region. The increase in fresh-water flow pushed the saline wedge seaward (not shown), while the increase in tidal amplitude showed evidence of additional salt- and fresh-water mixing over the previously modeled conditions. The photograph in figure 4 shows the position of the red-tracer fluid, injected through only tube 3 (fig. 1), 40 hours after injection began. As compared to the tracer movement in the previous tests (figs. 2 and 3), the tracer movement (fig. 4) in the saline wedge indicates less landward (left) migration. This indicates that the tidal fluctuation acts as a mixing mechanism between the two miscible fluids and that the fresh-water flow seaward (right) transports the diluted saline water back to the sea.

SUMMARY

The model studies were undertaken to investigate the intricacies of flow in a two-fluid system such as that which occurs in a coastal aquifer. The three flow conditions modeled were: (1) without tidal in-

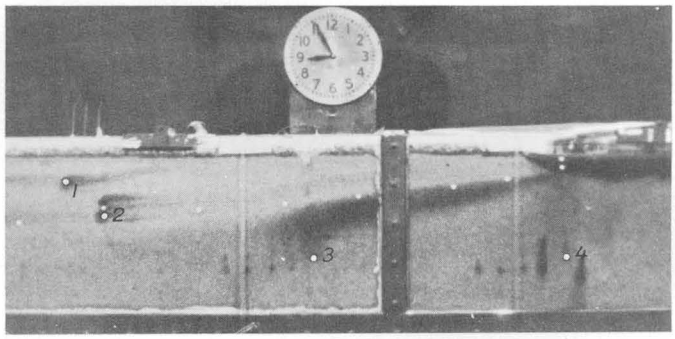

FIGURE 4.—Photograph of tracer movement through salt-water zone when the fresh-water flow seaward and tidal amplitude were increased 50 percent over previous model conditions. (See figs. 2 and 3.) Position of tracer in photograph is 40 hours after tracer injection began. Fluid movement in a landward direction is to the left and in a seaward direction is to the right.

fluence, (2) with tidal influence, and (3) with an increase in fresh-water flow seaward combined with an increase in tidal amplitude. The studies give good visual documentation—through time-lapse color movies—of the manner in which the cyclic flow of salt water occurs. This cyclic flow involves salt water that enters the aquifer through the floor of the sea, moves inland to become progressively diluted with fresh water, and then moves back to the sea as it is swept up in the seaward flow of fresh water. The cyclic flow of salt water was observed in all three of the modeled flow conditions. It appears to be markedly increased, however, by the introduction of tidal fluctuations in the salt-water body. The phenomenon is important because the continuous return to the sea of part of the inland flow of salt water tends to minimize the extent to which salt water occupies the aquifer.

REFERENCES

Cooper, H. H., Jr., 1959, A hypothesis concerning the dynamic balance of fresh water and salt water in a coastal aquifer: Jour. Geophys. Research, v. 64, no. 4, p. 461–467.

Cooper, H. H., Jr., Kohout, F. A., Henry, H. R., and Glover, R. E., 1964, Sea water in coastal aquifers: U.S. Geol. Survey Water-Supply Paper 1613–C, 84 p.

Henry, H. R., 1959, Salt intrusion into fresh-water aquifers: Jour. Geophys. Research, v. 64, no. 11, p. 1911–1919.

Kohout, F. A., 1960, Cyclic flow of salt water in the Biscayne aquifer of the Miami area, Florida: Internat. Assoc. Sci. Hydrology, Comm. Subterrannean Waters Pub. 52, p. 440–448.

Rumer, R. R., Jr., and Harleman, R. F., 1963, Intruded salt-water wedge in porous media: Jour. Hydraulics Div., Am. Soc. Civil Engineers, v. 89, no. Hy. 6, p. 193–220.

MOVEMENT AND DISPERSION OF FLUORESCENT DYE IN THE DUWAMISH RIVER ESTUARY, WASHINGTON

By J. R. WILLIAMS, Tacoma, Wash.

Work done in cooperation with the Municipality of Metropolitan Seattle

Abstract.—Rhodamine B was introduced 13.1 miles above the Duwamish River mouth on a falling tide, with a discharge of about 700 cfs, and dye concentrations were measured continuously for 67 hours at sites 5.4 and 8.3 miles downstream from the point of release. Times of travel to the 2 sites were 5 hours 2 minutes and 18 hours 40 minutes, respectively. Dye concentrations and traveltimes for all but the first peak at the upstream site were affected by tide. The dispersion coefficient at the downstream site (200 to 400 sq ft/sec) was considerably larger than that at the upstream site (about 100 sq ft/sec) because of the tidal action.

The Duwamish River, which flows into Puget Sound at Seattle, Wash. (fig. 1), has been used in the past to carry sewage and other waste products to the sea, and probably will be given greater loads to carry in the future. Because of complex problems concerning the time of travel and dispersion of a pollutant in a tidal estuary, the U.S. Geological Survey conducted a fluorescent-dye test in the Duwamish River estuary in October 1964 to obtain data for use in studying these problems. In the Duwamish River estuary, the area influenced by salt or brackish water from Puget Sound varies considerably with tide stage and river discharge. During this study, the saline wedge extended about 6 miles upstream from the mouth of the river at low tide; and it extended about 10 miles upstream at high tide.

For this test, rhodamine B was used as the tracer, and two Turner model III fluorometers were used to detect and record continuous traces of the dye concentration in the estuary. The fluorometers were installed at East Marginal Way and 16th Ave. South (fig. 1). Multiparameter monitors that give a continuous record of water quality are also installed at these sites.

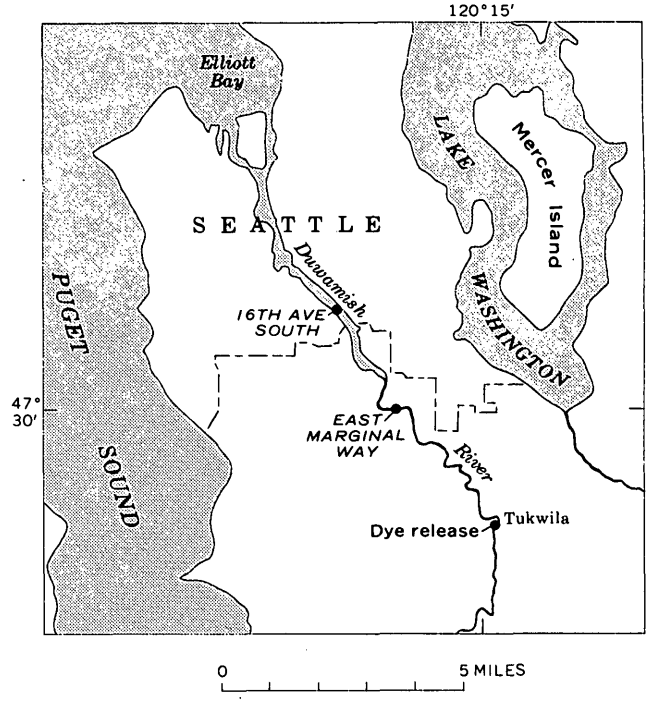

FIGURE 1.—Duwamish River and vicinity.

The monitors employ submersible pumps with intakes 3 feet below water surface at midstream, and these pumps were used to force water through the fluorometers for this test.

At 2100 hours on October 26, 1964, 48 pounds of rhodamine-B dye was introduced into the Duwamish River at the highway crossing at Tukwila, Wash., about 13 miles upstream from the mouth. The 48 pounds of dye was divided into 4 equal parts, so that the total amount could be released at the same instant from 4 locations in the river cross section, thereby

approximating a line source. The dye consists of 40 percent rhodamine by weight in an acetic acid–methanol solution, and it has very nearly the same specific gravity as water. A greater volume of dye was used for this test than would normally be used for studies in a 13-mile reach, to insure detection at the lower site in the estuary after several tide cycles.

For this test, the dye was released immediately after high tide, so that its travel from the release point to East Marginal Way (5.4 miles) would not be slowed by an incoming tide. The discharge at the point of injection, the Green River at Tukwila (the Green River becomes the Duwamish River about a mile downstream from Tukwila station), dropped more or less steadily from 700 cubic feet per second at the time of the dye release to 675 cfs when the test was ended, 67 hours later. Figure 2 shows the tide stages at 16th Ave. South, and the time distribution of dye concentrations at East Marginal Way and 16th Ave. South for the 67 hours of the test. Time differences between tidal stages at various sites in the study reach are considered insignificant.

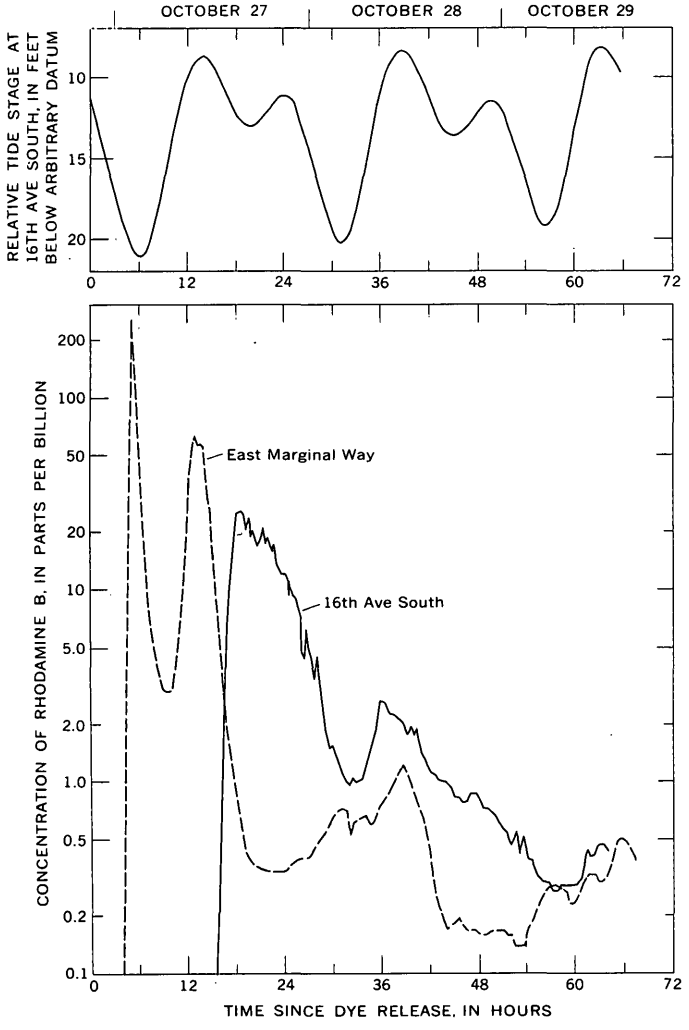

FIGURE 2.—Concentration of rhodamine B at East Marginal Way and 16th Ave. South, and hydrograph of tide stage at 16th Ave. South during the 67-hour test.

During an outgoing tide, when streamflow is seaward, the dye cloud takes a characteristic shape. The longitudinal concentration curve has a steeper slope on the downstream side (front) than on the upstream side (tail). As the dye cloud moves downstream, its base length increases and the peak concentration decreases, owing to dispersion.

When the tide changes and the flow reverses, the longitudinal profile of the dye cloud is changed because the front of the cloud is slowed, then stopped, by the incoming tide, while the tail still is being moved downstream by the flow of the river. Continued action of the incoming tide causes a flow reversal, after which the cloud moves back upstream. Thus, at any particular site the cloud will be detected on its way downstream on an outgoing tide, and it will be detected again as it is brought upstream by the incoming tide. Under some conditions, however, the incoming tide will bring back upstream past an observation point only part of the tail that was associated with the downstream passage before the tide changes again. The resulting concentration hydrograph for the upstream movement shows a peak that does not represent a true maximum concentration of the dye in the river.

RESULTS AT EAST MARGINAL WAY

Figure 3 shows the shape of the first recorded dye-distribution curve at East Marginal Way, 5.4 miles (28,350 feet) downstream from the site of dye release. The graph, based on fluorometer readings, shows that the dye was first detected about 4½ hours after release, and that the concentration rose rapidly to a peak of 242 parts per billion at 5 hours 2 minutes of elapsed time. After this, the concentration dropped at a slower rate than it had risen until it reached 3 ppb at 9½ hours. The shape of time-concentration curve is characteristic of dye clouds in a normal river.

Before the dye concentration reached zero at East Marginal Way (fig. 2), the tide changed, and brought the dye cloud back upstream past the site. The time-concentration distribution recorded after the change in tide is shown in figure 4. The graph shows that the dye cloud started to move upstream beyond East Marginal Way between 10 and 11 hours after the dye release, and that the concentration gradually rose to a maximum of 62 ppb after 12 hours 55 minutes of elapsed time. The concentration then dropped, and 25 minutes later began to rise to another peak of

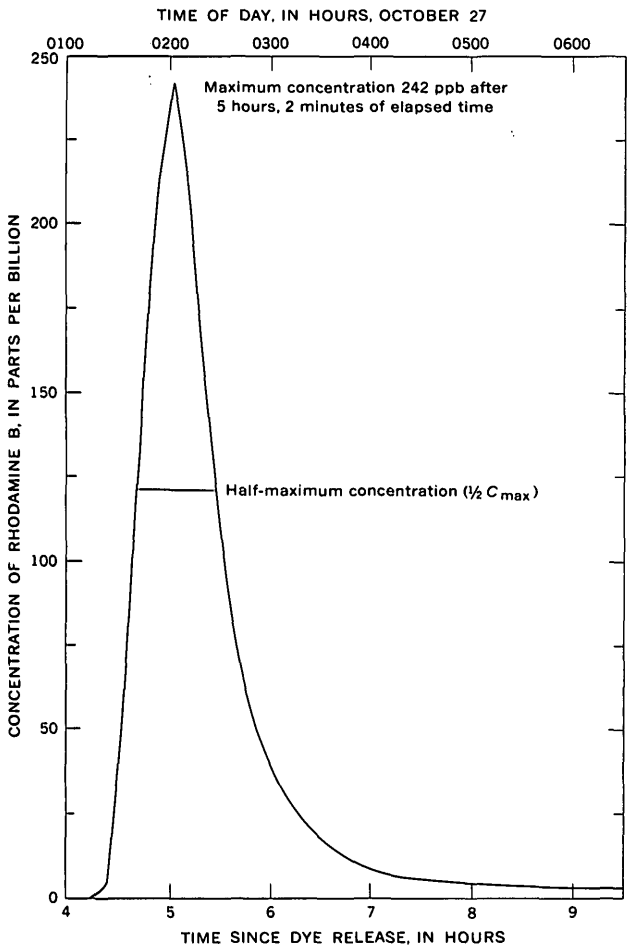

FIGURE 3.—Concentration of rhodamine B during first passage of dye at East Marginal Way during the period from 4 to 9½ hours after dye release.

58 ppb. The dye concentration subsequently dropped slowly, and leveled off at 2 to 3 ppb after 17 hours total elapsed time.

The two peaks, which are the second and third peaks to pass this site, can be explained as follows: The dye cloud first passed East Marginal Way in a downstream direction during the period between 4½ and 9½ hours after release and gave the peak shown in figure 3. After the cloud had traveled downstream from East Marginal Way but had not yet reached 16th Ave. South, the direction of the tide changed (fig. 2) and the incoming tide brought the most concentrated part of the dye cloud back upstream past East Marginal Way. Before the entire cloud had traveled upstream past the station, however, the tide reversed again. This reversal caused the most concentrated part of the cloud (now only 58 ppb because of dispersion) to pass East Marginal Way once more, this time in a downstream direction. As the tide continued to ebb, the concentration decreased slowly.

The rising and falling limbs of the time-concentration curve (fig. 4) have approximately the same shape, and appear to resemble the limbs of a normal distribution curve. After the first tide reversal, the long tail of the cloud no longer followed the more concentrated part, but preceded it. During the following ebb tide, both the peak and tail passed East Marginal Way again, but in a downstream direction.

The time-concentration curve at East Marginal Way shows that two additional significant dye-concentration peaks occurred about 38 and 65 hours after dye release (fig. 2). These peaks coincide approximately with times of high slack tide, as did the peaks that passed East Marginal Way at and shortly after 13 hours of elapsed time. Although the two concentrations were only 1.2 and 0.5 ppb, they appear to be definite increases in concentration. However, they probably represent only parts of the dye-cloud tail passing the station, rather than maximum concentrations in a cloud profile.

In addition to the peaks at 38 and 65 hours, definite peaks that bear no relationship to high slack tide occurred at about 31 and 57 hours elapsed time. Rather, they coincide with ebb slack, and may be due to the fact that the pump intake, which is a constant 3 feet below the water surface, approaches the channel bottom during low tide. This may result in more than the normal amount of particulate matter being pumped through the fluorometer. Because rhodamine-B dye can be adsorbed by organic and inorganic particulate matter in the river, the rise in concentrations recorded during the low tides may result from adsorbed—rather than dissolved—dye.

At the end of 42 hours, the concentration of dye at East Marginal Way decreased to 0.5 ppb, and at no time beyond 42 hours did the concentration exceed that amount.

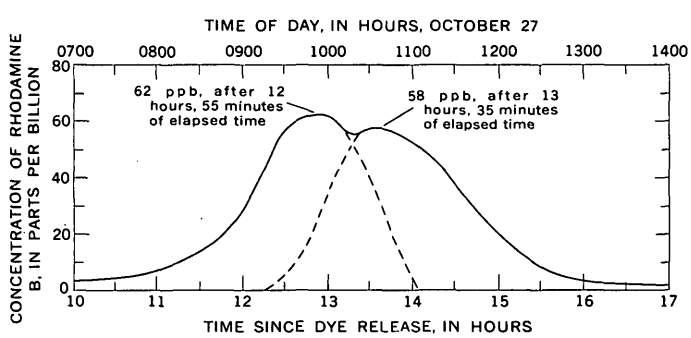

FIGURE 4.—Concentration of rhodamine B at East Marginal Way during the period from 10 to 17 hours after dye release.

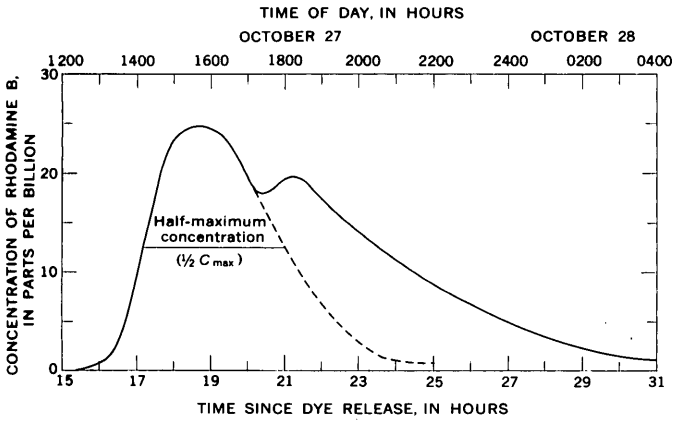

FIGURE 5.—Concentration of rhodamine B at 16th Ave. South during the period from 15 to 31 hours after dye release.

RESULTS AT 16th AVE. SOUTH

At 16th Ave. South, 8.3 miles downstream from the point of release, the dye cloud was first detected 15 hours 20 minutes after release, and the concentration rose to a peak of 26 ppb after 18 hours 40 minutes (fig. 5). The concentration distribution was highly skewed, and showed a subpeak of 19 ppb after 21 hours 10 minutes elapsed time. This subpeak doubtless resulted from a reversal of the outgoing tide. The peak and subpeak represent maximum concentrations in the dye cloud. Their interpretation with regard to tide reversals is similar to that for the second and third peaks at East Marginal Way.

After 54 hours, the dye concentration dropped below 0.5 ppb (fig. 2). At 16th Ave. South a somewhat greater time was required for the dye concentration to fall below 0.5 ppb than at East Marginal Way. Although not shown, the points that define the time-concentration curve for 16th Ave. South scatter more than those for East Marginal Way. This erratic behavior may result from incomplete mixing of the dyed river water with salt water. The effect is more evident at this downstream site because the ratio of salt water to fresh water is higher than at East Marginal Way.

DISPERSION COEFFICIENTS

A dispersion coefficient is used to describe quantitatively the rate of dispersion in a natural stream. Computation of the longitudinal dispersion coefficient requires knowledge of the mean velocity of a slug of water through a given distance, which in this study is known accurately for only the first dye passage at East Marginal Way. Because the distribution of the concentration-time data for that passage is skewed, the standard deviation for use in computing the dispersion coefficient was obtained by fitting a Pearson type-III distribution to the data (Godfrey and Frederick, 1963). Assuming a constant velocity under the given conditions of tide and river flow, a bulk longitudinal dispersion coefficient (K) of 113 square feet per second has been computed by the formula $K=\frac{\sigma^2 x^2}{2t^3}$, in which σ is the standard deviation of the time-concentration curve, x is the distance from point of injection, and t is the time from injection.

The same field data have been used to estimate the dispersion coefficient at East Marginal Way by a method suggested by Yotsukura (U.S. Geol. Survey, written commun., 1965), which involves the application of Taylor's formula (1954):

$$K=\frac{X_{½}^2}{16t_p \ln 2},$$

where t_p is the time to peak after the dye release, ln 2 is the natural logarithm of 2 (equal to 0.693), and $X_{½}$ is the distance the dye traveled during the time period ($t_{½}$) between the rising and falling limbs of the distribution at half the maximum concentration ($½C_{max}$). Calculation of the distance $X_{½}$ requires an estimate of the mean velocity of flow (V). The mean velocity within the reach between the point of dye release at Tukwila and the station at East Marginal Way during the period from zero time to 5 hours 2 minutes—the time of arrival of the first concentration peak—is estimated at about 1.6 feet per second. The time period $t_{½}$, measured from figure 3, is 0.79 hour, or 2,850 seconds. The distance $X_{½}$ is then $Vt_{½}=(1.6)\ (2{,}850)=4{,}560$ feet. Substituting the values in Taylor's formula, the dispersion coefficient is:

$$K=\frac{(4{,}560)^2}{(16)\ (18{,}000)\ (0.693)}=104 \text{ sq ft/sec.}$$

The two dispersion coefficients—113 and 104 sq ft/sec—agree closely. However, because of the limitations in accuracy of the experiment, the coefficient probably should be reported no closer than about a hundred square feet per second.

A dispersion coefficient based on data for 16th Ave. South was similarly estimated. Because of tidal effect, the falling limb could not be used to compute the coefficient. However, a hypothetical limb was constructed to represent the concentration recession in the absence of tidal effects. This limb is shown in figure 5 as a dashed line. The time $t_{½}$ at ½ C_{max} is about 3.8 hours, and the mean velocity is estimated as 0.87 fps, based on the time between the second peak of figure 4 and the first peak of figure 5. Taylor's formula then yields a K of about 190 sq ft/sec, using a t_p of 18.5 hours.

Using a modification of Taylor's formula:

$$K=\frac{1}{16 \ln 2} \cdot \frac{(X''_{\frac{1}{2}})^2-(X'_{\frac{1}{2}})^2}{t''_p-t'_p},$$

where $X'_{\frac{1}{2}}$ and t'_p are the values at East Marginal Way and $X''_{\frac{1}{2}}$ and t''_p are values at 16th Ave. South, K is 397 sq ft/sec.

The computations indicate that the dispersion coefficient at 16th Ave. South probably was 200 to 400 sq ft/sec, which is fairly high compared to that for ordinary streams. The tidal action undoubtedly contributed to the greater-than-normal dispersion.

REFERENCES

Godfrey, R. G., and Frederick, B. J., 1963, Dispersion in natural streams: U.S. Geol. Survey open-file report, 75 p.

Taylor, G. I., 1954, Dispersion of matter in turbulent flow through a pipe: Royal Soc. London Proc., ser. A, v. 223, p. 446–468.

AN INSTRUMENT FOR MEASURING pH VALUES IN HIGH-PRESSURE ENVIRONMENTS

By J. L. KUNKLER, F. C. KOOPMAN, and F. A. SWENSON,
Santa Fe, N. Mex., Albuquerque, N. Mex., Denver, Colo.

Abstract.—The design, development, and laboratory tests of an instrument capable of measuring pH values in submerged aqueous environments are described. The electrodes are designed with pressure-compensating features and have withstood external pressures of 400 pounds per square inch without damage or malfunctions. The accuracy of pH measurements with these electrodes is probably equivalent to that with conventional electrodes. When finally developed the pH electrodes will be secured to a sonde containing a preamplifier. The sonde will be used to log pH values of water in wells and will be designed to operate with conventional well-logging equipment.

The data for many studies of high-temperature and high-pressure systems are based mostly on chemical theory or laboratory experiments. Confidence in the conclusions of these studies could be strengthened with field data. This paper describes an instrument that can provide field pH data for empirical studies of some high-pressure geochemical systems. The instrument, still in the experimental development stage and code-named UNELAN for Underwater Electrometric Analyzer, was designed to measure the pH of water in wells at pressures of up to at least 1,000 pounds per square inch.

The instrument consists of a reference electrode, glass electrode, and thermistor probe securely attached to a 1¾-inch-diameter sonde that contains a recorder preamplifier. The sonde maintains electrical continuity with a recorder located near the wellhead by means of a three-conductor steel-reinforced transmission cable. It is raised and lowered in the well by a winch, thus allowing continuous monitoring of pH values. Although specifically designed for use in investigations of limestone hydrology, it should have wide geochemical application also.

Design and construction began in January 1964 and continued intermittently until February 1965. Professor Roy D. Caton, of the University of New Mexico, assisted the writers in this study.

ELECTRODES

Description

A reference electrode and a glass electrode (patents pending) were designed and constructed (fig. 1) as described below.

The head (*A*) of the reference electrode is a Teflon plug with a silver wire through it and is sealed with epoxy. A high-pressure electrical jack is soldered to the end of the wire at the top of the head. The other end of the silver wire is wound in a spiral and electroplated with silver chloride to form a silver-silver chloride half cell.

The electrolyte reservoir is a piece of latex surgical tubing (*B*) attached to the Teflon head and base (*C*) by rubber compression rings. A hole drilled through the base permits flow of the electrolyte from the filling tube (*D*), a section of rubber tubing. The filling tube is connected by a flanged glass connector (*E*) to the plug holder (*F*), a short length of rubber tubing containing a plug of porous glass rod (*G*).

The reservoir of the reference electrode is filled with electrolyte, usually a solution of saturated potassium chloride, by inverting the electrode assembly, removing the connector and plug holder from the filling tube, and inserting the tip of a plastic filling bottle into the filling tube. The reservoir is filled and then purged of air by alternately squeezing and relaxing the pressure on the filling bottle (see filling procedure, fig. 1). When the reservoir is purged and filled, the filling tube is pinched, the connector and plug holder are inserted into the filling tube, and the electrode is reinverted as shown in the figure-1 sketch of the assembled and filled electrode.

The glass electrode is similarly composed of a Teflon head (*H*), with a silver wire through it and is sealed with epoxy. A high-pressure electrical plug is soldered on the end of the wire at the top of the head. The other end of the silver wire is electroplated with silver chloride to form a silver-silver chloride

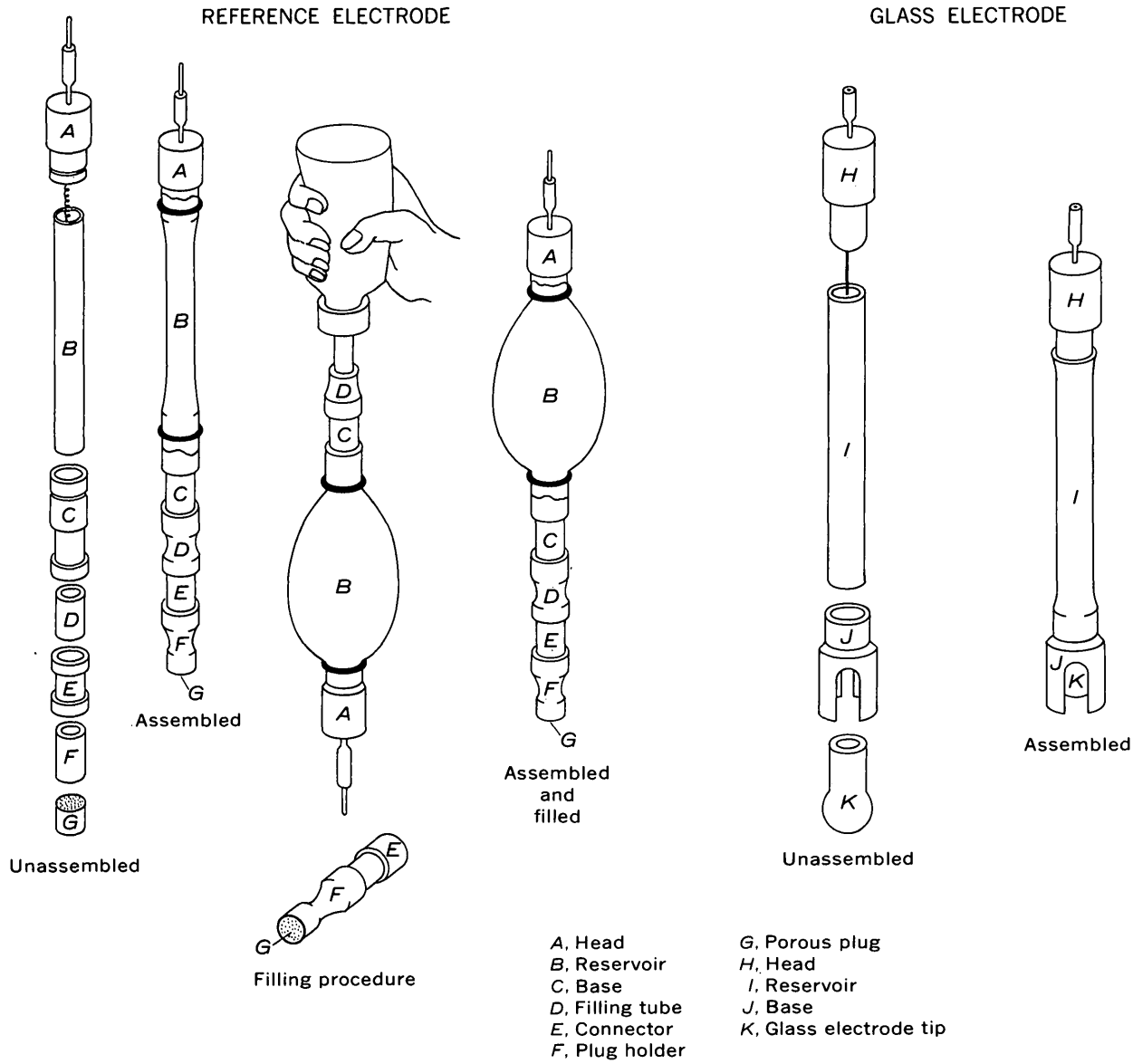

FIGURE 1.—Sketches of reference and glass electrode assemblies.

half cell. The reservoir (I) is a piece of flexible Teflon tube. The base (J) is a Teflon plug drilled to receive the neck of a conventional glass electrode tip (K).

The glass electrode is assembled by cementing the glass tip and reservoir wall to the base. The reservoir is filled with a suitable buffer, usually a solution of potassium chloride and potassium phthalate, and the head is cemented to the top of the reservoir wall.

Pressure compensation

Environmental pressure changes affect the response of pH electrodes by varying the rate of flow of electrolyte from the reference electrode to the liquid being measured and by creating strains within the glass electrode tip. The present electrode design nullifies these effects.

The pressure effect on the reference electrode is nil because the flexible reservoir maintains a nearly constant ratio of internal to external pressure, irrespective of environmental pressure changes. Moreover, the internal pressure is always higher than the external pressure because of the force exerted on the electrolyte by the distended flexible walls of the reservoir as they try to regain their original shape. A higher internal pressure assures unidirectional flow of electrolyte from the reservoir out into the liquid being measured, a necessary condition for proper functioning of the reference electrode. The rate of flow is controlled in

241-334 O—67——17

part by the thickness and permeability of the porous plug at the bottom, and although it has not been determined, it is estimated to be only a few milliliters per day. The loss of electrolyte does not appreciably decrease the internal pressure of the reservoir unless the electrode is used for several days without refilling. The pressure effect upon the glass electrode is also nil because the flexible Teflon reservoir wall tends to equalize the pressure across the glass tip.

Pressure tests

The electrodes described in this paper have been tested many times in a laboratory pressure-tank assembly (fig. 2) that is pressurized with compressed nitrogen. The pressure-tank tests are more rigorous than field tests because pressures rise and decline at more rapid rates. The test solution was usually one of the buffer solutions developed by the National Bureau of Standards and described by Bates (1964); however, tap water was used for some tests. Most pressure tests were made with the electrodes partly submerged as shown in figure 2; however, some tests were made with the electrodes fully submerged. Table 1 gives the pH data from a typical pressure test in which tap water (pH 7.65 at the laboratory atmospheric pressure) was used as a test solution.

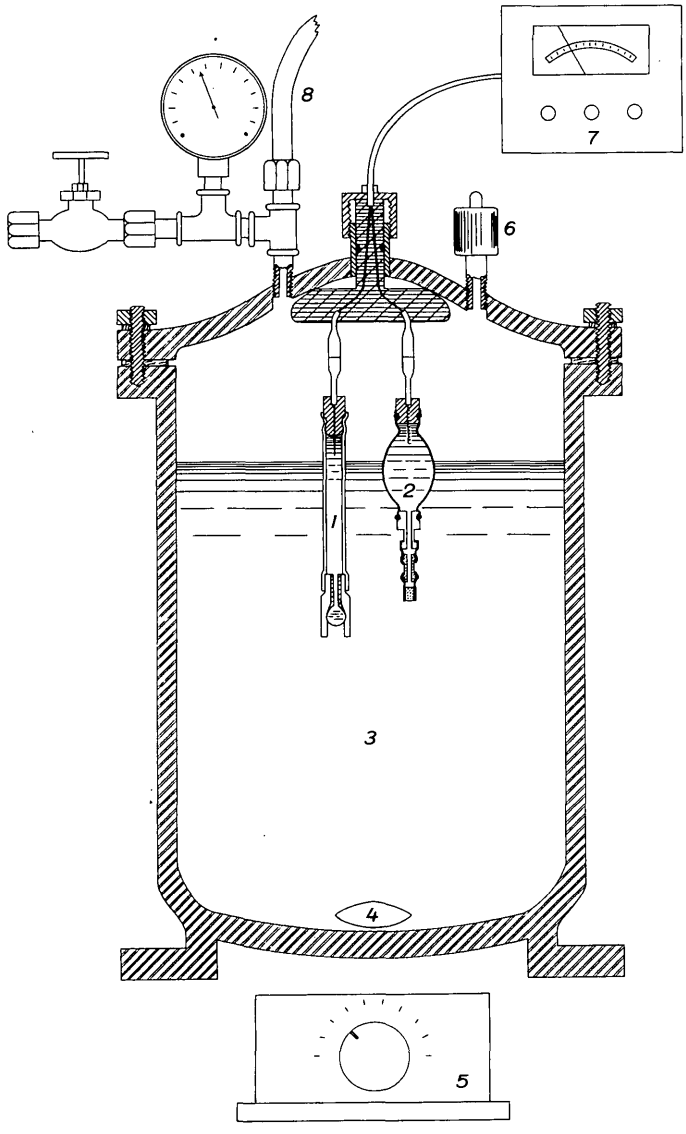

1. Glass electrode
2. Reference electrode
3. Test solution
4. Stirring magnet
5. Stirring motor
6. Relief valve
7. pH meter
8. Gas hose

FIGURE 2.—Pressure-tank assembly.

TABLE 1.—*Data from a typical pressure test of the new pH-measuring instrument*

Pressure (psi)	pH	Pressure (psi)	pH
12	7.65	325	7.65
75	7.70	285	7.67
200	7.65	200	7.67
300	7.66	80	7.71
400	7.65	12	7.70

Accuracy

The accuracy of pH measurements made with the experimental electrodes varied with the type, age, and physical condition of the glass electrode being used. The pH values were never measured directly but were calculated from the electromotive force (emf) or electrical potential measured with standard buffer solutions of pH 4.01 and pH 6.86 at 25°C. The emf of the pH electrode cell should change by 168–169 millivolts when these buffers are interchanged at room temperature.

At least 30 electrodes were built during this study. Those electrodes that were functional usually showed a difference of values of 166–169 millivolts in measurements with standard buffers of pH 4.01 and 6.86, a sensitivity that compares favorably with that of new conventional electrodes.

The results of two pressure tests are shown in figure 3. These data were traced from a recorder chart that monitored the pH during the tests. The variations in pH may be due to imperfections in the electrodes or to electrical noise in the test circuit. The maximum variation from the true pH is less than 0.1 pH unit.

ELECTRICAL EQUIPMENT

The electrical resistance of most glass electrodes measured during this study ranged between 25 and 50 megohms. Two consequences of the high internal resistance of the glass electrode are:

1. The impedance of the electrodes must be matched to that of the meter or recorder through the transmission cables; the matching is accomplished by a specially designed isolation amplifier.

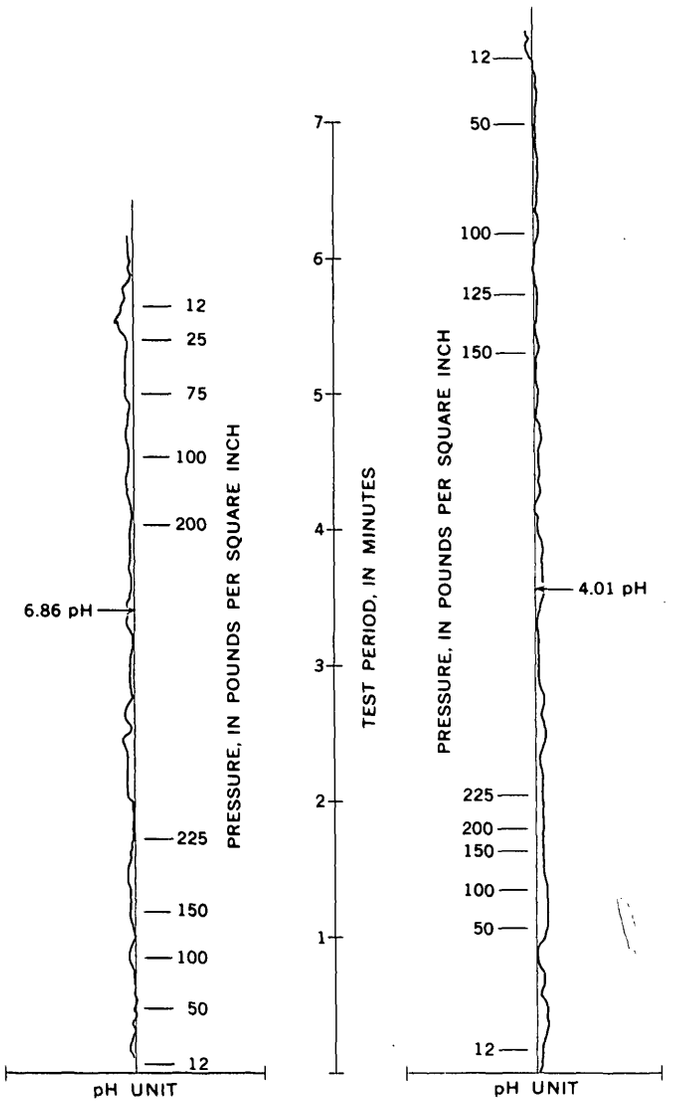

FIGURE 3.—Traces from a recorder chart, showing variations in pH of selected pressures.

2. The coupling between the electrodes and the amplifier must be well insulated and as short as possible to prevent power leakage.

Conventional pH electrodes are coupled to a pH meter, which contains an amplifier, by leads which are ordinarily only a few inches long. If the leads are much longer than about 18 inches, a preamplifier must be placed in the circuit to boost the power of the pH signal. UNELAN was designed to operate with about 4,000 feet of transmission cable; hence a preamplifier was needed.

The preamplifier used in this instrument was constructed of solid-state components to minimize the size and power requirements and to avoid the drift characteristic of vacuum tubes. The preamplifier was fitted into a sonde with an inside diameter of 1⅝ inches, and it was powered by four small nickel-cadmium batteries. The electrodes and a thermistor probe were rigidly attached to the base of the sonde; the thermistor probe transmitted an electrical signal proportional to the water temperature.

The pH and temperature signals were transmitted to a recorder located near the wellhead through a cable wound on a power winch. UNELAN has been field tested several times. It was cumbersome to operate and probably did not provide reliable data because of the difficulty of adequately insulating the electrical system from ground potential. Changes in construction of the preamplifier would allow coupling with a conventional logging truck and grounding of the critical part of the electrical system.

REFERENCE

Bates, R. G., 1964, Determination of pH, theory and practice: New York, John Wiley and Sons, Inc., p. 95–130.

USE OF DIGITAL RECORDERS WITH POND GAGES FOR MEASURING STORM RUNOFF

By JOHN E. McCALL, Trenton, N.J.

Work done in cooperation with the
New Jersey State Department of Agriculture, Soil Conservation Committee

Abstract.—New technology was developed and tested to solve the difficult problem of measuring peak-runoff rates from small drainage areas. A water-stage recorder with binary-coded paper-tape punching mechanism was adapted for measurement of runoff volumes stored in a 16-acre pond during storm events. This unattended-station technique has wide application to remedy a long-existing deficiency in the national stream-gaging network—namely, the lack of sufficient data on peak flows from small watersheds.

An automatic digital water-stage recorder with a 5-minute punching interval has been successfully used with a pond gage to compute (1) daily mean pond outflow, (2) outflow from the pond at 5-minute intervals, (3) inflow to the pond at 15-minute intervals, and (4) average evaporation rate from the pond surface during hot, dry periods of several days' duration.

The gaging station was established in 1962 on 16-acre Baldwin Lake near Pennington, N.J., draining 2.52 square miles, to study sediment load and trap efficiency. A 5-minute-interval digital recorder was used experimentally to enable automatic data reduction by digital computer.

The potential importance of the pond gage has long been recognized. The principal barrier to accurate direct measurement of peak-runoff rates from small areas, those of 1 or 2 square miles or less, has been the practical difficulty of getting there in time and working fast enough to measure these flashy streams. The pond gage is a form of direct volumetric measurement of runoff rates; its use allows a stream gager more time to reach the site and obtain the high-stage measurements. If there is no outflow during a given storm, the pond gage does not require any current-meter measurements for calibration. The techniques were carefully and completely described by Sloss (1963).

COMPUTATION OF DATA FOR LOUISIANA PONDS

The Louisiana system, described by Sloss, was based on accurate surveys of the capacity of a pond at different levels and use of a Stevens water-stage recorder operating on expanded time and gage-height scales. A gage-height scale of 10:12 and time scale of 9.6 inches per day were enlarged 3-fold by photostating the chart for periods of storm runoff to further facilitate accurate determination of rate of rise per unit time. Readings were taken to thousandths of a foot at 2½-minute intervals to determine inflow by the simple formula:

$$\text{Inflow} = \text{outflow} \pm \text{rate of change of storage } (I = O \pm \Delta S).$$

Factors affecting accuracy, such as intake lag, surface distortions and waves on the pond, direct rainfall on the pond, evaporation, bank-storage and seepage losses, were found to be relatively small and could to some extent be compensated. Sloss concluded that peak inflow could be computed within 2 percent and the whole storm hydrograph within 10 percent.

The biggest problems in the Louisiana technique are the amount of work involved and difficulty of achieving accuracy in picking off gage readings at precise time intervals, even on the expanded charts. Both the computational labor and the errors of timing are effectively reduced by the use of the digital punch recorder described by Wells (1960) and Carter and others (1963). The digital recorder can easily be regulated to keep time within 10 minutes per week or within 0.3 second in a 5-minute punching interval.

Furthermore, the personal element in reading the gage height is removed by the automatic punch. Admittedly, the figure punched may be as much as 0.005 foot high or low at each successive punch, giving a maximum error of 0.01 foot during the cycle simply because the standard Fischer and Porter instrument records only to the nearest hundredth of a foot. This probably could be refined by modifications in the instrument design, but experience on this project indicates that it is practical to minimize such error by mathematical and graphical averaging of the final inflow-discharge figures as printed out by the digital computer.

DIGITAL DATA FOR BALDWIN LAKE

On Baldwin Lake, with 700,000 square feet of surface area at normal pool level, a change of 0.01 foot in level in 5 minutes is equal to a net inflow or outflow of 23 cubic feet per second. Typically, the computer print-out sheet shows sudden increases of 23 cfs in the inflow column about every third or fourth 5-minute period as the storm runoff begins (table 1). Later the computed inflow may increase 23 cfs every 5 minutes until outflow discharge also begins to become significant, at which time the successive increments of computed inflow start increasing by 24 cfs each 5 minutes. This occurs because the outflow increases 1 cfs per hundredth rise in this range of gage heights and $I=O\pm\Delta S$.

To smooth out these abrupt steps the computed inflow figures for 3 successive 5-minute periods were averaged and plotted at the middle of the period. Thus, the averaged computer figures were computed and plotted at 1045, 1100, etc. (fig. 1). This still left some stepping in the plotted points, so further smoothing was accomplished graphically by drawing a line of best fit through the plotted points. While this may seem an incongruous mixture of modern computer technology with old-fashioned averaging methods, it must be remembered that there is no cumulative error as long as the pond capacity and outflow rating are accurately known. Furthermore, the manual processes are simple and quickly done for 3 or 4 storms each year.

A system of moving averages or some logical sequential averaging could undoubtedly be programmed on the computer without graphical plotting, especially as the items of special interest near the peak-inflow rate tend to smooth out even at 5-minute intervals. If many pond gages are operated, such an improvement would be in order to eliminate need for manual averaging and plotting.

The outflow hydrograph can be plotted directly from the computer print-out sheet at 5- , 15- , 30- , or 60-minute time intervals, with no computations or smoothing required. Likewise, the daily mean outflow is directly available from the computer on the standard print-out sheet used for conventional streamflow stations. These latter two items are all that are required for sediment and trap-efficiency studies; so the inflow hydrograph and peak-inflow rate information may be regarded as an inexpensive bonus in the Baldwin Lake installation.

TABLE 1.—*Excerpts from computer print-out sheet for pond gage for December 6, 1962*

[15-minute average inflow was added manually]

Time of day (hr)	Gage height (ft)	Outflow (cfs)	Pond storage rate (cfs)	Inflow (cfs)	Average inflow for 15-min intervals (cfs)
1025	0948	0002	0000	0002	
1030	0948	0002	0000	0002	2
1035	0948	0002	0000	0002	
1040	0948	0002	0000	0002	
1045	0949	0002	0023	0025	10
1050	0949	0002	0000	0002	
1055	0949	0002	0000	0002	
1100	0949	0002	0000	0002	10
1105	0950	0002	0023	0025	
1110	0951	0003	0023	0026	
1115	0952	0003	0023	0026	18
1120	0952	0003	0000	0003	
1125	0953	0003	0023	0026	
1130	0953	0003	0000	0003	19
1135	0954	0004	0023	0027	
1140	0956	0004	0048	0052	
1145	0956	0004	0000	0004	28
1150	0957	0005	0024	0029	
1155	0959	0006	0048	0054	
1200	0961	0007	0048	0055	47
1205	0962	0008	0024	0032	
1210	0964	0009	0048	0057	
1215	0967	0011	0073	0084	84
1220	0971	0014	0097	0111	

EVALUATION OF HYDROLOGIC FACTORS RELATED TO RUNOFF DATA

Another bonus is the ability to compute average evaporation rates during selected periods in summer when inflow and outflow were negligible and no precipitation fell. The pond is underlain by dense and relatively impermeable sandstone and shale, part of the Brunswick Formation of Triassic age (Vecchioli and Palmer, 1962). Observations during dam construction and areal ground-water studies indicate that bank storage and leakage are minor and ground-water inflow is negligible except during very wet weather. At the lower stages of the pond in late summer, little or no vegetation grows in or near the water. Thus the lowering of the pond level during several hot, dry

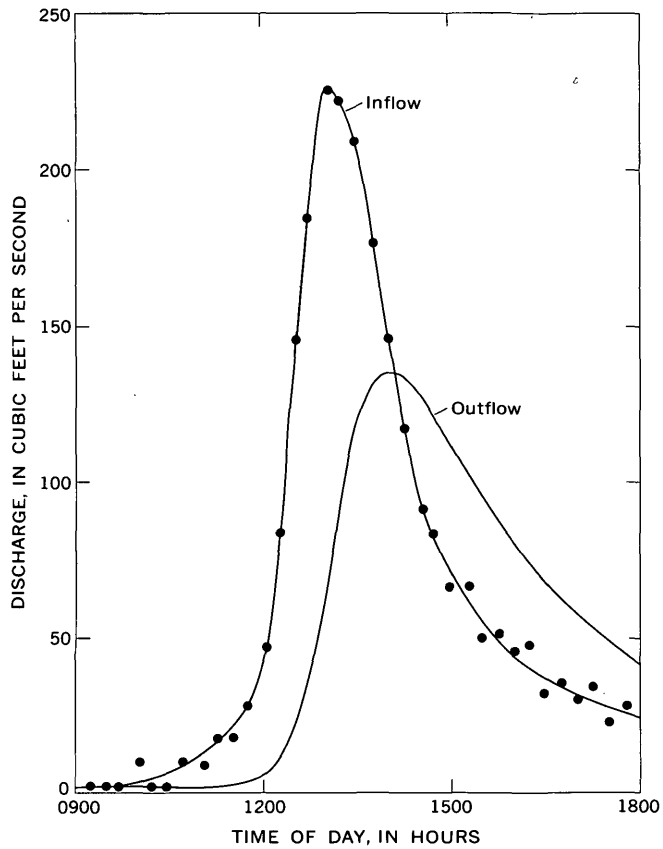

FIGURE 1.—Typical storm hydrograph for Baldwin Lake, near Pennington, N.J.

days, as recorded by the digital recorder, may be regarded as nearly all evaporation; transpiration or other losses cause very little lowering. Calculations show that evaporation did not exceed 0.6-inch per day on the pond, equivalent to an average rate of 0.5 cfs for the day or perhaps a maximum rate of 1 cfs in the hottest part of the day. This confirms the assumption that calculated inflow rates during storms need not be corrected for evaporation even in the hottest weather and probably errors from this source are less than 0.1 percent under heavy storm conditions.

On the Louisiana ponds Sloss operated a rain gage, which recorded on the same chart as the pond gage by means of a Stevens Duplex recorder. Rainfall could also be recorded on a digital-type instrument. Heavy rainfall of 1.44 inches per hour directly on the pond would register as a rise of 0.01 foot in 5 minutes or an apparent inflow of 24 cfs to Baldwin Lake. If inflow is desired at the upper end of a single-inlet pond, then direct rainfall should be subtracted from the rate of rise of the pond, and drainage area should be measured to the single inlet. Because at Baldwin Lake the drainage area and all flow computations were taken at the dam, no adjustment was made for the 100-percent runoff from direct rainfall on the pond. This could increase the peak-flow rate about 2 percent for a winter storm or 5 percent for a summer storm over the natural land runoff that would have occurred if no pond were present. Such differences are minor and the record is correct for today's conditions.

At Baldwin Lake the pond surface area is 1 percent of the total drainage area. Because the rise in pond level seldom exceeds 20 inches before outflow equals inflow, only about 0.20-inch runoff from the basin is in temporary storage at that time. This peak level (and peak-outflow rate) usually occurs 1 to 2 hours after the peak-inflow rate (fig. 1). The amount of runoff in temporary storage and the lag time for peak outflow could be increased by adding flashboards on one or two sides of the rectangular drop-outlet. Flashboards would, however, increase the amount of lake-level fluctuations, so this modification of the outlet has not been made. Moreover, modification is not required because Baldwin Lake is close to the Survey office, and excellent calibration of the outlet has been possible. If the station were remotely located, or if the outflow were large in relation to the changes in pond storage at the time of peak inflow, such a constriction of the outlet capacity would be desirable.

Sloss tested the pond-gage technique in Louisiana with ponds ranging from 10.3 to 87.1 acres in surface area. The drainage areas for these ponds ranged from 108 to 658 acres and the ratio of total drainage area to pond area ranged from 7.5:1 to 40:1. The Baldwin Lake ratio of 100:1 is a significant extension of the conditions under which the pond-gage technique has been successfully tested. However, the principal conclusion reached on this project is that the automatic digital recorder can be successfully adapted for use with a pond gage. Also, important savings in labor can be achieved with this instrument and digital-computation methods. Accuracy seems equal or better than with graphical chart recording and manual data-reduction and computation processes.

In summary, it has been found that pond gages equipped with digital recorders are a useful tool in hydrologic data collection and research. The pond gage offers a unique and inexpensive means of obtaining peak-inflow hydrographs, as well as peak-runoff data, for small drainage areas. The rapidly growing number of ponds in most regions and the need for hydrologic data on them make the technique one that will be both widely applicable and very useful.

REFERENCES

Carter, R. W., chm., and others, 1963, Automation of streamflow records: U.S. Geol. Survey Circ. 474.

Sloss, Raymond, 1963, Use of ponds to measure rates of storm runoff in Louisiana: U.S. Geol. Survey open-file report.

Vecchioli, John, and Palmer, M. M., 1962, Ground-water resources of Mercer County, New Jersey: New Jersey Dept. Conserv. and Econ. Devel., Div. Water Policy and Supply, Spec. Rept. 19.

Wells, J. V. B., 1960, Change in the streamflow data collection program of USGS: Am. Water Works Assoc. Jour., v. 52, p. 735–741.

ELECTRO-OPTICAL CALIBRATOR FOR CAMERA SHUTTERS

By THOMAS O. DANDO, Washington, D.C.

Abstract.—An electro-optical calibrator for camera shutters has been designed and built by the U.S. Geological Survey for testing cameras used by private firms on Geological Survey contracts. This new shutter calibrator photographically records the shutter action as shown on an oscilloscope and provides a precise measure of the effective exposure time for any setting of the shutter. Knowledge of the performance to be expected from his camera will enable the contractor to obtain better mapping photographs.

Almost all the aerial photographs needed for topographic mapping by the U.S. Geological Survey are obtained under contract from private firms. All cameras that are to be used under these contracts must first be tested and calibrated by the Survey. One of the series of tests involves the shutters. For this test, the Geological Survey has designed and constructed a shutter calibrator that is used to determine the total open time, the efficiency, and the effective exposure time of a shutter.

The calibrator consists principally of an oscilloscope-camera combination that provides a measurable photographic record of the shutter action of a camera being tested. Figure 1 is a schematic diagram of the equipment system. The 75-watt floodlight is powered by rectified and filtered 110-volt line current. The light beam is directed through the lens, shutter, and cone assembly (of the aerial camera being tested) to a photoelectric cell. When the shutter is tripped, the light that it admits strikes the photoelectric cell causing it to conduct a current which is fed to the vertical deflection plates of the oscilloscope. The charge on the plates deflects the traversing cathode beam an amount proportional to the amount of light striking the cell. Consequently, the moving spot of light on the screen of the cathode-ray tube (CRT) in the oscilloscope is deflected. The duration of the deflection corresponds to the exposure time. The current to the floodlight must be rectified and filtered because the photocell is so sensitive that it would pick up a phase ripple if the bulb filament were powered directly by the alternating-current source.

Besides deflecting the moving spot vertically, the output of the photocell also triggers horizontal left-to-right movement of the spot. The rate at which the spot sweeps across the CRT screen can be adjusted so that the entire shutter action, from opening to closing, is contained in a single trace. This action is recorded photographically by a camera mounted in front of the CRT screen. No synchronization of the shutters of the two cameras is necessary; the shutter of the recording camera remains open, but the film remains unexposed until the sweep movement of the spot is triggered, illuminating the CRT screen.

The calibrator also has a stable audiofrequency signal generator and an electronic frequency counter. The audiofrequency signal is fed to the intensity ("Z") amplifier of the oscilloscope. On the negative half of each cycle, the negative bias on the CRT grid represses the beam of cathode rays and, as a result, intermittenly blanks out the trace on the screen. The input frequency is selected so that the trace across the CRT screen will consist of a series of short, discrete dashes, as shown on the representation of the recording-camera photograph in figure 1.

To provide a base line for the response curve from which to measure the amount of deflection, a trace can be triggered deliberately with a pulse too small to produce any deflection of the beam.

TOTAL OPEN TIME

Each dash of the trace represents one cycle of the audiofrequency wave. Since the frequency is known, a dash also represents a time unit for each complete cycle according to the relationship $t=1/f$, where t is the duration of one cycle and f is the frequency of the

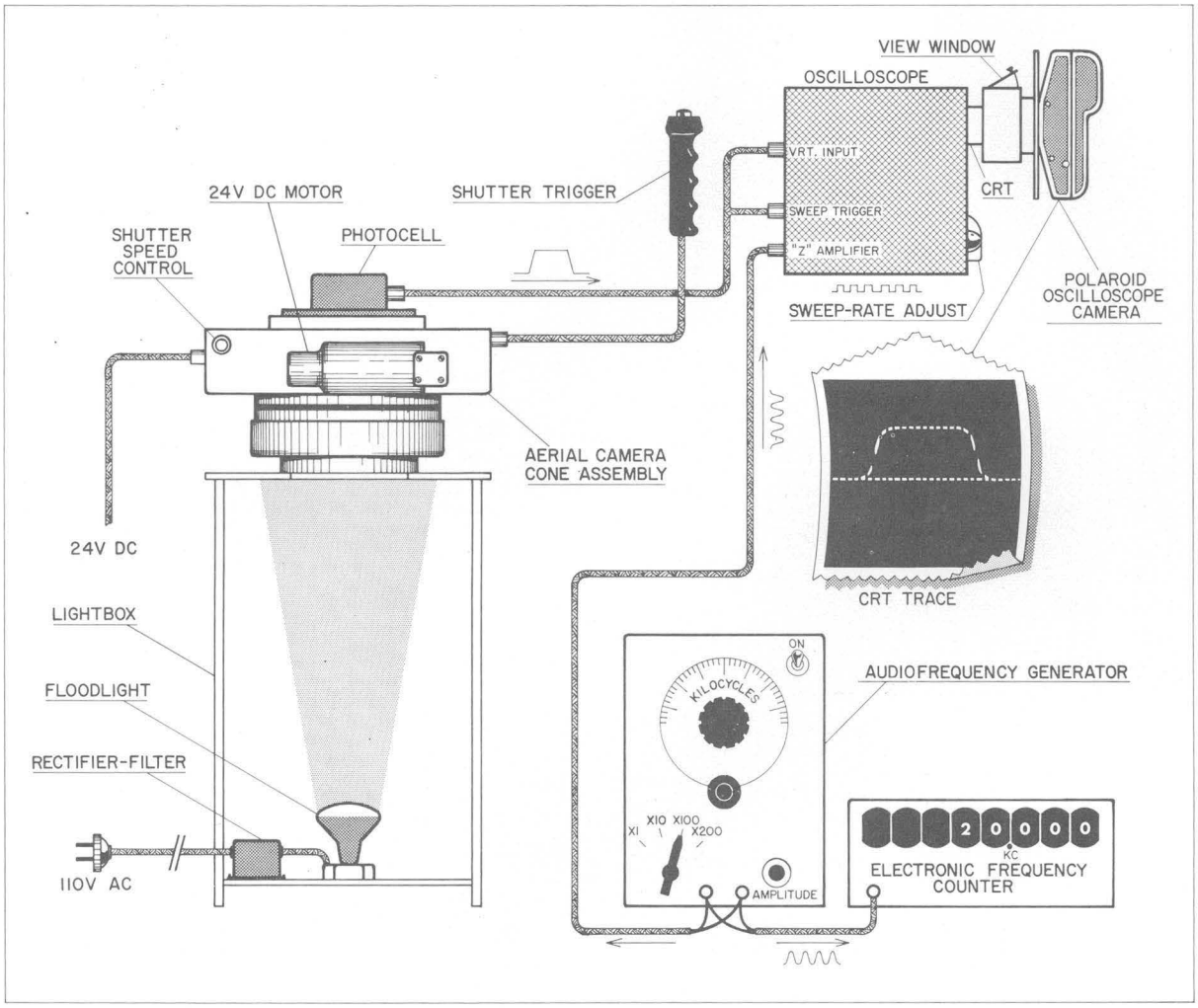

FIGURE 1.—Calibration-equipment system complete with audiofrequency generator and counter.

wave. Total open time, t_o, is obtained by multiplying the number of dashes, N, from shutter opening to closing by the value of t, so that $t_o=Nt$. For greater accuracy, the frequency (f) is read from the counter rather than from the frequency-setting dial on the generator.

Figure 2 shows a set of three calibration photographs for a camera being tested at nominal shutter speed setting of 1/700 second. The dashes in the top exposure were made by a 20-kilocycle signal. Counting the number of dashes, N, from where the shutter opened at point a to where it closed at point d, either along the base or along the curve, and multiplying by the dash time, t, gives the total open time, t_o.

$$t_o=N_{ad}t.$$

Then, as $t=1/f$,

$$t_o=N_{ad}/f.$$

In this example,

$$t_o=33.5/20\times10^3=1/597 \text{ sec.}$$

EFFICIENCY

Efficiency, E, is the ratio of light passed by a shutter to that passed by a theoretically perfect shutter. A perfect shutter would respond instantaneously; that is, it would go from full-closed to full-open (or vice versa) in zero time. The area under the curve (fig. 2) represents the amount of light passed.

The actual rate of opening and closing is represented by the slopes of the lines forming the sides of the trapezoid. The efficiency, E, can be calculated as the area of the trapezoid divided by the area of a rectangle

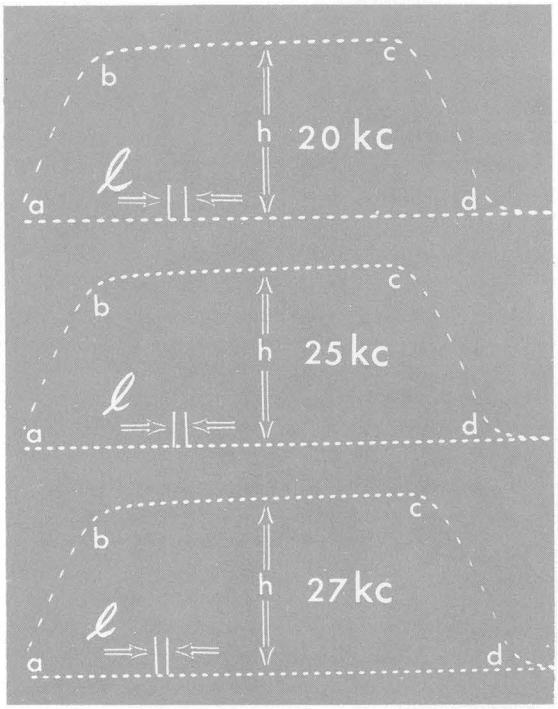

a, Starting point of shutter opening action.
b, Full-open point.
c, Starting point of shutter closure action.
d, Full-closure point.
h, Amplitude of deflection trace.
l, Length of a complete cycle.

FIGURE 2.—Oscillograms from an aerial camera with a nominal shutter-speed setting of 1/700 second. From top to bottom, t_o=1/597 sec, 1/602 sec, and 1/607 sec, respectively. The frequencies of the currents applied to the "Z" amplifier and the CRT grid are indicated.

formed by an ideal shutter having the same total open time. Mathematically, the efficiency is

$$E=\frac{N_{ab}hl/2+N_{bc}hl+N_{cd}hl/2}{N_{ad}hl},$$

where h is the amplitude of the deflection, and l is the length of each complete cycle of the audiofrequency signal. Since h and l are common to all terms and therefore cancel, the equation reduces to

$$E=\frac{N_{ab}/2+N_{bc}+N_{cd}/2}{N_{ad}}.$$

Thus the amplitude, h, of the curve and the length, l, of each cycle need not be considered. Again referring to the top exposure of figure 2, the efficiency is

$$E=\frac{6/2+21+6.5/2}{33.5}=0.813.$$

EFFECTIVE EXPOSURE TIME

Effective exposure time, t_e, is defined as efficiency multiplied by total open time, or, $t_e=Et_o$. For the top exposure of figure 2, then,

$$t_e=0.813\times 1/597=1/734 \text{ sec.}$$

Similarly, the effective exposure times for the middle and bottom exposures are 1/728 and 1/744 sec, indicating a consistency of measurement of about ± 1 percent.

The equation for the efficiency is valid only if the shape of the curve representing shutter action approximates a trapezoid. If the response curve deviates seriously from the trapezoidal form, indicating erratic action, a solution for t_e can be obtained by using a planimeter to determine the area under the curve and applying this value in the formula

$$t_e=\frac{\text{area under the curve}}{\text{maximum ordinate of curve}\times l\times N_{ad}(N_{ad}/f)}.$$

The entire calibration procedure is repeated for all shutter-speed settings because the performance of a shutter may vary widely at different speeds. Figure 3 shows the action of a shutter found to be defective at low speeds, as indicated by the wide variation in t_o for successive traces at the same speed setting. From visual inspection of the oscillographs alone, the camera could be rejected for erratic shutter performance. As a result of these tests, the manufacturer redesigned the shutter.

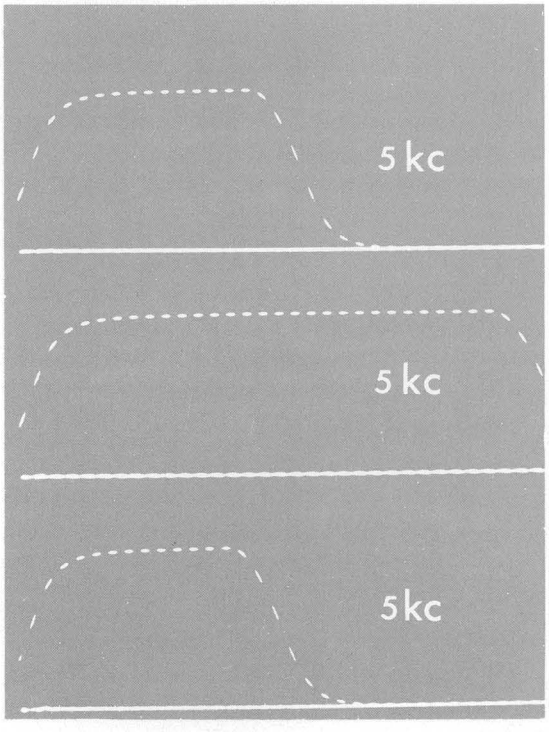

FIGURE 3.—Oscillograms from an aerial camera with a nominal shutter-speed setting of 1/120 second. The oscillograms were made with an applied pulse frequency of 5 kc. Note the erratic performance of the shutter.

SUBJECT INDEX

[For major headings such as "Economic geology," "Geophysics," "Paleontology," see under State names or refer to table of contents]

AUTHOR INDEX

○